RADIOACTIVITY IN THE ENVIRONMENT • VOLUME 3
Series Editor: M.S. Baxter

RADIOACTIVE FALLOUT AFTER NUCLEAR EXPLOSIONS AND ACCIDENTS

by

YU. A. IZRAEL

ELSEVIER

RADIOACTIVE FALLOUT AFTER NUCLEAR EXPLOSIONS AND ACCIDENTS

RADIOACTIVITY IN THE ENVIRONMENT

A companion series to the Journal of Environmental Radioactivity

Series Editor
M.S. Baxter
Ampfield House
Clachan Seil
Argyll, Scotland, UK

Volume 1: Plutonium in the Environment
(A. Kudo, Editor)

Volume 2: Interactions of Microorganisms with Radionuclides
(F.R. Livens and M. Keith-Roach, Editors)

Volume 3: Radioactive Fallout after Nuclear Explosions and Accidents
(Yu.A. Izrael, Author)

RADIOACTIVE FALLOUT AFTER NUCLEAR EXPLOSIONS AND ACCIDENTS

(Translated from the original Russian Work)

By

Yuri A. Izrael

Russian Academy of Sciences, Russian Federal Service for Hydrometeorology and Environmental Monitoring, Institute of Global Climate and Ecology
Glebovskaya str., 20b, Moscow, 107258, Russian Federation

Editor of English Translation
M.S. Baxter

ELSEVIER
2002
AMSTERDAM – BOSTON – LONDON – NEW YORK – OXFORD – PARIS
SAN DIEGO – SAN FRANCISCO – SINGAPORE – SYDNEY – TOKYO

Ю.А. Израэль

РАДИОАКТИВНЫЕ ВЫПАДЕНИЯ ПОСЛЕ ЯДЕРНЫХ ВЗРЫВОВ И АВАРИЙ

«ПРОГРЕСС-ПОГОДА»

Санкт-Петербург
1996

ELSEVIER SCIENCE Ltd
The Boulevard, Langford Lane
Kidlington, Oxford OX5 1GB, UK

© 2002 Elsevier Science Ltd. All rights reserved.

This work is protected under copyright by Elsevier Science, and the following terms and conditions apply to its use:

Photocopying
Single photocopies of single chapters may be made for personal use as allowed by national copyright laws. Permission of the Publisher and payment of a fee is required for all other photocopying, including multiple or systematic copying, copying for advertising or promotional purposes, resale, and all forms of document delivery. Special rates are available for educational institutions that wish to make photocopies for non-profit educational classroom use.

Permissions may be sought directly from Elsevier Science Global Rights Department, PO Box 800, Oxford OX5 1DX, UK; phone: (+44) 1865 843830, fax: (+44) 1865 853333, e-mail: permissions@elsevier.co.uk. You may also contact Global Rights directly through Elsevier's home page (http://www.elsevier.com), by selecting 'Obtaining Permissions'.

In the USA, users may clear permissions and make payments through the Copyright Clearance Center, Inc., 222 Rosewood Drive, Danvers, MA 01923, USA; phone: (+1) (978) 7508400, fax: (+1) (978) 7504744, and in the UK through the Copyright Licensing Agency Rapid Clearance Service (CLARCS), 90 Tottenham Court Road, London W1P 0LP, UK; phone: (+44) 207 631 5555; fax: (+44) 207 631 5500. Other countries may have a local reprographic rights agency for payments.

Derivative Works
Tables of contents may be reproduced for internal circulation, but permission of Elsevier Science is required for external resale or distribution of such material.
Permission of the Publisher is required for all other derivative works, including compilations and translations.

Electronic Storage or Usage
Permission of the Publisher is required to store or use electronically any material contained in this work, including any chapter or part of a chapter.

Except as outlined above, no part of this work may be reproduced, stored in a retrieval system or transmitted in any form or by any means, electronic, mechanical, photocopying, recording or otherwise, without prior written permission of the Publisher.
Address permissions requests to: Elsevier Science Global Rights Department, at the mail, fax and e-mail addresses noted above.

Notice
No responsibility is assumed by the Publisher for any injury and/or damage to persons or property as a matter of products liability, negligence or otherwise, or from any use or operation of any methods, products, instructions or ideas contained in the material herein. Because of rapid advances in the medical sciences, in particular, independent verification of diagnoses and drug dosages should be made.

First edition 2002

Library of Congress Cataloging in Publication Data
A catalog record from the Library of Congress has been applied for.

British Library Cataloguing in Publication Data
A catalogue record from the British Library has been applied for.

This book is a translation of a book by the Author originally published in Russian, with substantial revisions and a new final chapter written by the Author. Translated from Russian by O.V. Glushko (chapters 1, 5, 6) and N.A. Zaitseva (all other chapters).

ISBN: 0-08-043855-5

⊗ The paper used in this publication meets the requirements of ANSI/NISO Z39.48-1992 (Permanence of Paper).

Printed in The Netherlands.

This Page Intentionally Left Blank

Summary

The results of many years of study of radioactive fallout from atmospheric and underground nuclear explosions and accidents are summarized in this book.

The formation of radioactive aerosol particles, the composition of radionuclides and their fractionation in nuclear explosions conducted under various conditions are analyzed. Much attention is also given to the meteorological aspects of fallout, the modeling of the transport of radioactivity, the reconstruction and retrospective analysis of the initial radiation patterns from nuclear explosions/accidents and the analysis of radiation exposure dose rates to populations.

A considerable section of the book is devoted to long-term studies of radioactive fallout following the Chernobyl accident and special attention is given to the problems of restoration and remediation of lands contaminated as a result of nuclear accidents/explosions.

The book is based on material obtained directly by the author or through his participation in cooperative programs; in addition, a vast amount of material of Soviet (Russian) research and that of foreign authors is summarized. An English translation of an earlier Russian-language version of this book has been supplemented here by recent results that have been published during the past 5–6 years as well as material from special symposia and conferences. A new final chapter on remediation of contaminated sites has been added.

The book is intended for various specialists—geophysicists, ecologists, health experts and inspectors, as well as those who are concerned with radioactive contamination of natural environments.

This Page Intentionally Left Blank

Preface

From the time the very first nuclear weapon tests were conducted (in 1945 in the USA and in 1949 in the USSR), it became evident that the resulting radioactive contamination of the earth's surface was a serious issue. Further, it became clear that this radioactive contamination of the environment presented a danger to populations living outside the immediate vicinity of the nuclear test sites. Thus, on a number of islands in the Pacific Ocean (USA tests) and in regions contiguous with the Semipalatinsk site (USSR tests), the local populations were exposed to nuclear radiation. Nuclear tests conducted at ground level are particularly dangerous from the point of view of this radioactive contamination.

In the early 1960's, global radioactive fallout increased over vast territories of the earth. This arose from the deposition of the longer-lived radioactive products of powerful nuclear explosions that had been injected into the stratosphere. Since the signing, in 1963, of the treaty on the prohibition of nuclear weapons tests in the atmosphere, in space and under water, the quantities of both local and global radioactive fallout have decreased substantially. However, not all countries adhere(d) to the treaty. Further, underground nuclear explosions were still carried out and when venting of the explosions occurred, radioactive material was released to the atmosphere.

In the early 1970's, international discussions took place with regard to the possible exploitation of the energy created by underground nuclear explosions for peaceful purposes, such as for the creation of water channels, improving the output of gas and oil recovery and in the mining of minerals. Although many specialists emphasized the positive aspects of the use of underground nuclear explosions for peaceful purposes, it became more and more evident that the radioactive contamination of natural environments was a decisive factor in the rejection of this approach.

In the second half of the 20th century, several significant nuclear accidents occurred, e.g., at the nuclear power station in Windscale (Great Britain), at two nuclear enterprises in the Southern Urals (USSR) and at the nuclear power station at Three-Mile-Island (USA). On April 26, 1986, the largest accident occurred at the Chernobyl nuclear power station (NPS) in the Ukraine, resulting in vast territories being contaminated with radioactivity, about 135 thousand people being obliged to evacuate their homes and workplaces and hundreds of thousands of others being exposed to radiation.

Thus these events of the past 50 years have heralded the new nuclear era for humanity and have resulted in significant increases in the surface contamination of our planet by radioactivity. The additional radiation dose to the population from this nuclear radiation is comparable to that from the natural radiation background and in some regions it exceeds the background values.

Although populations, especially those residing near nuclear test sites, have always expressed their anxiety with respect to increased levels of radiation, the Chernobyl accident resulted in a new wave of such anxiety. People have become interested not only in the

levels of the radiation that arise directly after a test or an accident but also in the long-term radiation hazards from the fallout of long-lived radioactive products of explosions and accidents, as well as the long-term effects of small radiation doses on human beings.

A new problem has arisen with respect to the need to conduct retrospective analysis of the immediate radiation situation that existed after a past nuclear explosion and/or nuclear accident. This problem has arisen not only for zones contaminated after nuclear accidents such as those at the Chernobyl NPS or in the Southern Urals but also for zones more distant from the sources of contamination. Thus, in the Altai Territory, the program for the Altai–Semipalatinsk test site, aimed at an assessment of the radioactive products that impacted on the population after the first (1949) and subsequent nuclear explosions in the Semipalatinsk region, has been underway for several years. In Russia, similar problems have arisen in the Novosibirsk region, in the Republics of Gorny Altai and Tuva and in the Arctic regions associated with the Novaya Zemlya test site. During recent years, the International RADTEST Project (within the framework of SCOPE) was carried out with the objective of assessing the radiation conditions following nuclear explosions conducted in different countries. In addition, the program endeavored to assess the effects on human health.

To achieve successful solutions to the problems resulting from local, distant and global radioactive fallout after nuclear explosions and accidents and to achieve successful retrospective analyses of the radiation conditions from recent observations, we need to know the following:

- the distribution of the exposure dose rate in the atmosphere and in a country,
- the distribution of radionuclides in natural environments and the nuclide composition of the radioactive fallout,
- the features of formation of the aerosol particle-carriers of the radioactivity and of the nuclide distribution of the particles of different sizes formed under different conditions,
- the processes involved in the migration of radioactive products in different zones and environments,
- the external and internal effects of nuclear radiation on human beings.

In addition, to construct models that are capable of predicting the radioactive contamination of the environment under possible future explosion and accident scenarios (as well as for retrospective analyses from current observations), a knowledge of the source of the radioactivity, its structure and size, the meteorological situation prevailing at the site and time of the event and, subsequently, the dynamics of formation of the contamination in various environments are all required.

This monograph is devoted to a number of these problems, namely, to studies of the radioactive fallout composition, the formation of the aerosol particles that transport the radioactive products and to the analysis of the external radiation doses resulting from nuclear explosions and/or accidents. Problems of restoration and rehabilitation of contaminated land areas are also touched upon in the monograph. To solve such problems one requires knowledge of the mobility of radionuclides, an understanding of their uptake by plants, their transportation within the food chain and finally their uptake by animal and/or human organisms.

A number of publications have been drawn upon in the writing of this monograph, viz. "Isotope composition of radioactive fallout" (Izrael, 1973), "Peaceful nuclear explosions and the environment" (Izrael, 1974) and the book (in Russian) "Chernobyl: radioactive contamination of natural environments" (Izrael, 1990). "Radioactive fallout after nuclear explosions and accidents" (Izrael, 1996a) was also used extensively and includes numerous data from investigations of nuclear explosions and atomic accidents in the USSR over the past 40 years. Much of the basic data on the nuclear explosions of the 1950's–70's, and those on the Chernobyl accident in April 1986, are unique and are, as yet, unpublished. In 2000, several books summarizing the results of the RADTEST project were published but the problems treated in this book were discussed only to a moderate degree. Extensive data obtained at nuclear accidents, e.g., the Chernobyl accident, have been included in this publication. Some of the data were presented at two recent international conferences held in Moscow, viz. "Radioactivity after Nuclear Explosions and Accidents", Moscow, 24–26 April, 2000, and "Radiation Legacy of the 20th Century: Environmental Restoration", Moscow, 30 October–3 November, 2000.

The first four chapters of the book are devoted to a description of the processes determining, and an analysis of the available data on, the radioactive fallout nuclide composition from atmospheric (Chapters 1 and 2) and underground (Chapters 3 and 4) nuclear explosions, while Chapter 5 relates to nuclear accidents. Approaches to the reconstruction of former radioactive patterns are described in Chapter 6 and the analysis of radiation dose rates and the methodological basis of aerial gamma-ray surveys of radiological patterns following nuclear explosions and accidents are given in the Chapter 7. Chapter 8 deals with the remediation of contaminated areas and the mobility of radionuclides.

In conclusion, the author expresses his deep gratitude to all of his colleagues with whom he has been fortunate to work in this field and for the opportunity to have been able to obtain absolutely new information, sometimes under extremely complicated and non-trivial situations.

The author hopes that the book will be useful to specialists working in this field, as well as to a wider readership of those who follow nuclear matters.

The author expresses his deep gratitude to Dr. Nina Zaitseva who translated the major part of the text and kindly helped him in editing the final text in English. He also wishes to thank translator O. V. Glushko, typist A. V. Gromova and assistant S. V. Gontarev for their hard work and dedication in the preparation of this book.

This Page Intentionally Left Blank

Contents

Summary vii

Preface ix

Professor Yuri A. Izrael—A Biographic Summary of the Author xvii

Glossary of Definitions and Units xxi

Chapter 1. Fractionation of Radionuclides in Atmospheric Nuclear Explosions. Radioactive Aerosol Particles 1

1. Major Processes Influencing the Character of Radioactive Contamination after a Tropospheric Nuclear Explosion 1
2. Temperature Regime in the Fireball of a Tropospheric Nuclear Explosion 3
3. Formation of Particle-carriers of Radioactivity. Role of Thermodynamic Conditions in the Fireball 7
4. Radioactive Products from Nuclear Explosions 12
5. Thermophysical Properties and Radioactive Transformations of Major Explosion Products 26
6. Activation of Particles 35
7. Characteristic Features of Fractionation of Radioactive Products from Tropospheric Nuclear Explosions 52
8. Quantitative Estimation of Fractionation Effects 57
9. Conclusion 61

Chapter 2. Basic Features of Radioactive Particle Formation and Radionuclide Fractionation in Underground Nuclear Explosions 63

1. Development of an Underground Nuclear Explosion 63
2. Release of Radioactivity into the Atmosphere and Formation of a Cloud and Base Surge in an Underground Nuclear Explosion 71
3. Characteristic Features of Radioactive Particles from an Underground Nuclear Explosion 75
4. Fractionation of Nuclides in the Radioactive Particles Produced by Underground Nuclear Explosions 80
5. Interpretation of Data on Fractionation. Scheme of Particle Activation in Underground Explosions 87

Chapter 3. Radionuclide Composition of Radioactive Fallout from Tropospheric Nuclear Explosions. Meteorological Aspects of Fractionation **93**

1. Meteorological Aspects of Fractionation 93
2. Radionuclide Composition of Fallout Near Ground-Zero Following Atmospheric and Surface Explosions 97
3. Global and Long-Distance Fallout 102

Chapter 4. Radioactive Fallout from Underground Nuclear Explosions **119**

1. Characteristics of Major Cratering Explosions 120
2. Radioactive Cloud 123
3. Radioactive Contamination in the Bulk Zone and the Cloud Pattern 125
4. Radionuclide Composition of the Fallout from an Underground Explosion 135
5. Prediction of the Radioactive Contamination of Surrounding Land after an Underground Nuclear Explosion 140

Chapter 5. Terrestrial Contamination from Chernobyl and Other Nuclear Power Station Accidents and its Radionuclide Composition **149**

1. Dynamics of Radioactivity Release and the Conditions of Radioactive Aerosol Particle Formation from the Chernobyl Accident 150
2. Characteristic Features of Radioactive Aerosol Particles Produced by the Chernobyl Accident and Their Radionuclide Composition 153
3. Terrestrial Contamination from the Chernobyl Accident 156
4. Radionuclide Composition of the Terrestrial Contamination from the Chernobyl Accident 163
5. Analysis and Reconstruction of the Source of Radioactivity Release from the Chernobyl Accident 178
6. Modeling of Close-in Radioactive Deposition (Fallout) from the Chernobyl NPS Accident 200
7. Characteristic Features of Radioactive Contamination from Various Nuclear Accidents 205

Chapter 6. Reconstruction of Contamination on the Old Patterns from Nuclear Explosions and Accidents **213**

1. The Problems Associated with the Reconstruction of Terrestrial Contamination Distributions 213
2. Terrestrial Contamination after the Chernobyl NPS and Other Accidents 215
3. Reconstruction of Terrestrial Contamination from Nuclear Explosions 217

Chapter 7. Gamma-Radiation Field Above the Fallout Patterns of a Nuclear Explosion **231**

1. Calculation of the Surface γ-Radiation Exposure Dose Rate 231
2. Influence of Natural Environmental Conditions on the Surface γ-Field 233
3. Aerial γ-survey. Determination of the Total Surface Density of the Terrestrial Contamination from the Measured Dose Rate 236
4. Aerial γ-survey. Estimation of the Surface Density of the Terrestrial Contamination by Individual Nuclides 239

Chapter 8. Remediation of Contaminated Areas. Rehabilitation of Areas Subjected to Radioactive Contamination and Mobility of Radionuclides **243**

1. Fractionation 244
2. Radionuclide Mobility after Nuclear Explosions and Accidents 245
3. Solubility and Biological Accessibility 246
4. Radioactive Contamination of Vegetation and Experimental Data on the Uptake of Radionuclides by Humans and Animals 251
5. Problems of Rehabilitation of Contaminated Areas. Agricultural Radioecology 252
6. Practical Measures for the Restoration of Contaminated Territories 257

References **263**

Subject Index **275**

This Page Intentionally Left Blank

Professor Yuri A. Izrael—A Biographic Summary of the Author

Academician Professor Yuri A. Izrael is one of Russia's and indeed the world's top names in the environmental and nuclear sciences. As the most senior scientist involved in the monitoring, behavioural and assessment studies at and around the previously secret nuclear weapon tests of the former Soviet Union and at the Chernobyl and other nuclear accidents, Professor Izrael has a wealth of unique knowledge and experience of the science of these sites of special scientific interest. Indeed, he has himself pioneered much of that science.

The scientific career of Yuri A. Izrael, Doctor of Sciences (Physics and Mathematics), Professor and Member of the Russian Academy of Sciences as well as of a number of other academies, has been devoted to nuclear and environmental sciences, meteorology and climatology. Graduating in 1953 from the Central Asian State University, he worked, at first, in the Geophysical Institute and then in the Institute of Applied Geophysics of the USSR Academy of Sciences, where he progressed from junior scientist to Institute Director (1969). He defended his Ph.D. (1963) and D.Sc. (1969) theses (in the fields of physical and mathematical sciences).

Since the beginning of his scientific career, Professor Izrael specialized particularly on the meteorological aspects of both radioactive contamination and chemical pollution of the natural environment. He became one of the first scientists to personally obtain and analyze extensive experimental data on the dispersal and behaviour of radioactive products after nuclear weapon tests (1954–1974), participating in investigations after accidents at nuclear power installations (1957–1986), after the Chernobyl nuclear accident (1986–1996), and on transport of chemical products during operations of different enterprises (1963–1996). This experience permitted Professor Izrael to encourage and play his own part in the development, and then improvement, of transport models for both conservative and chemically active admixtures in the atmosphere and thus to develop methods of predicting the pollution of natural environments.

And thus the author's investigations carried out since 1954 were amongst the first to apply meteorology to atomic energy and indeed he created a new direction in Soviet meteorology, i.e., the study of the consequences of radioactive fallout after nuclear explosions and accidents. These works combined the potential of meteorology for solving problems of the environment with his wide understanding of ecology resulting in elaboration of methods for calculation and analysis of the transportation and effects of pollutants over trans-boundary distances.

In 1969–1973, Professor Izrael headed the Institute of Applied Geophysics and, in 1978, he also created a Laboratory of Environment Monitoring and Climate. By 1990, this Laboratory's development and excellent performance was recognized by the establishment of the Institute of Global Climate and Ecology. Since the very beginning, Professor Izrael has served as Director of both organizations. In the latter, he has developed new concepts

of complex monitoring of the environment involving the wide use of hydrometeorological information. He has also carried out investigations of the planet's climate system and ozone layer under extreme conditions in the case of global nuclear impacts (nuclear winter).

Professor Izrael worked as the First Deputy Head and then Head of the Main Department of the Hydrometeorological Service, USSR Council of Ministers (1970–1978), and from 1978 until 1991 he headed the USSR State Committee on Hydrometeorology and Control of the Natural Environment. In 1974, Professor Izrael was elected a member of the World Meteorological Organization (WMO) Executive Committee and at the VIIth WMO Congress (1975–1987) as WMO Vice-President. He served in the latter capacity for 12 years and in the former for 18 years. In 1978, he participated in the formulation of the new concept of the World Climate Program and has since participated very actively in its development and improvement, especially in its data collecting aspects and in formulation of its "Impact" scientific component. Beginning in 1989, Professor Izrael has also worked actively in the new scientific organization, the International Panel on Climate Change (IPCC), which, in accordance with a UN proposal, was organized by WMO and UNEP to investigate climate change and its effect upon the environment, economics and human health. He is now its Vice-chairman. He has, in collaboration with a number of scientists, written several books on climate, three of which have been translated into English and published in the USA and Great Britain. In 1992, he was awarded the prize and gold medal of the International Meteorological Organization.

His investigations in the field of the radioactive contamination of natural environments allowed Professor Izrael to formulate a basis for ecological monitoring of the Earth. His book "Ecology and Control of the Environment" was awarded the Sukachev gold medal of the USSR Academy of Sciences (1983) for outstanding work in the field of ecology. This book was published in both English and German languages.

In April 1986, in the former USSR, the largest nuclear accident ever, at the Chernobyl atomic power station, occurred and it was Professor Izrael who directed the work of helicopters and aircraft which carried out the dosimetric and gamma-spectrometric surveys as well as, in general, overseeing the whole programme for estimating radiation conditions around the site and on studying the movement of polluted air masses. Together with specialists of his institute, he developed improved models of radionuclide diffusion in the atmosphere after the Chernobyl accident based on the models used previously for the aftermath of nuclear explosions and accidents. These results were published widely. Later on, he headed the work on mapping the post-Chernobyl radioactive contamination over Europe in general. Under his directorship and participation, two important atlases (one for Europe, the second for Russia, Ukraine and Belorussia) were published, making it essentially easier to resolve the problems related to the consequences of the Chernobyl accident. For this activity, he was, in 1990, awarded the Gold Medal (for Chernobyl) of the "Ettore Majorana" (Italy) International Centre and, in 1992, he received the prestigious UN-UNEP Sasakawa Environmental Prize. He was also awarded some state orders and prizes.

The author is a Member of the International Academy of Astronautics, an Honorary Member of the Hungarian Meteorological Society, a full Member of the Russian Academy of Sciences and a full member and now President of the Russian Academy of Ecology. He has won many national and international awards for distinguished science and has

presented keynote lectures in the plenary sessions of many international conferences. In 1999, he was elected a member of the International Union of Radioecologists. He is also Chief Editor of the Russian "Meteorology and Hydrology" Journal which was the unique scientific meteorological journal in the Soviet Union and is so now in the Russian Federation.

This book, then, aims to bring to the English-language literature, for the first time, a specialized monograph by this most distinguished of scientists, on the theory, based on his unique experience of, the monitoring, understanding, modeling and assessment of nuclear fallout from weapons tests and accidents. In so doing, this book should be useful both to peers who have perhaps studied similar sites outside the former "iron curtain" and most importantly to the younger generation of scientists worldwide, who can hopefully learn much about the results of phenomena which were extremely important in the 20th century but will not, we all hope, be repeated.

This Page Intentionally Left Blank

Glossary of Definitions and Units

A *dose* of radiation is determined as the energy of ionizing radiation absorbed by unit mass of a medium being exposed to that radiation. The following definitions of doses of ionizing radiation which reflect features of the energy transfer to a substance, with consideration of the properties of the radiation and the substance irradiated, are widely used in dosimetry (both the obsolete special units and new units of the SI system).

The *absorbed dose*, D, is the energy transferred by ionizing radiation to a substance in some elementary volume, divided by the mass of substance in this volume. The unit of absorbed dose is the rad (rad is the abbreviation for "radiation absorbed dose"), equal to an energy of 100 erg or 10^{-7} Joule absorbed by one gram of a substance (100 erg/g $= 10^{-2}$ J/kg). In the SI system, the unit of absorbed dose is the Gray (Gy). 1 Gy = 1 Joule per kg (J/kg). 1 Gy = 100 rad. The rad can serve as the unit of absorbed dose of any type of irradiation in any medium. However, difficulties of direct measurement in different substances and especially in biological tissue stimulated specialists in dosimetry to measure the absorbed dose in an equivalent medium in which measurements are possible (in the given case, this is a tissue-equivalent medium, e.g., air).

The *exposure dose* (*exposure*) is a dose stemming from absorption of ionizing radiation by the air. It corresponds to the total charge of ions of the same sign appearing in the air after complete slowing down of all the secondary electrons which were generated by the photons in a small air volume, divided by the air mass in the same volume. The unit *Roentgen* is used for measurements of exposure dose. It is measured by the ionization in the air using ionizing chambers or other air-equivalent instruments. The Roentgen, R, is a unit of absorbed dose in air of X-radiation or γ-radiation such that the corpuscular emission (i.e., electrons) associated with this dose generates in 0.0012930 g of air mass (at 0 °C temperature and a pressure of 1013 hPa) ions carrying a charge of one electrostatic unit (e.s.u.) of electricity.

Hence the absorbed dose expresses the absorbed energy of the irradiation, while the exposure dose expresses the energy transferred to the charged particles. They are equal to one another only under conditions of electron equilibrium (balance), i.e., under conditions when the absorbed energy of the irradiation in some volume of a medium is equal to the total kinetic energy of the ionizing particles formed within the same volume.

The generation of one pair of ions (p.i.) in air needs, on average, the expenditure of 34 eV of energy (within the 10 keV–3 MeV radiation energy range). One electrostatic unit of charge corresponds to $1 : 4.8 \times 10^{-10} = 2.08 \times 10^{9}$ p.i., from which the energy equivalent of the Roentgen is equal $2.08 \times 10^{9} \times 34 = 7.07 \times 10^{10}$ eV $= 0.114$ erg (per cm^3 of air). In this case, 1 g of air absorbs 88 erg or 5.39×10^{13} eV.

The Roentgen is a special unit of the exposure dose. 1 R = 0.258 mC/kg. In the SI system, the Roentgen is measured in C/kg units. Note that all definitions of the Roentgen include the work of ionization which is determined by experiment, on average

being 34 eV per pair of ions. This leads to the energy equivalent of the Roentgen being approximately 88 erg/g [1]. With this energy equivalent (88 erg/g) for air, 1 rad = 1.136 R and 1 R = 0.88 rad. The energy spent by electrons or X-radiation in formation of one pair of ions has been estimated by different authors for different ranges of energy of X-radiation, γ-radiation and electrons within the interval 33.4–34.2 eV [4] and these can lead to slightly different equivalents of the Roentgen. For example, paper [3] presents a value of 87.3 erg/g.

To determine the energy absorbed by a biological tissue, a unit called the "*tissue Roentgen*" or the *physical equivalent of the Roentgen* was used earlier (one "tissue Roentgen" is equal in value to the energy absorbed by tissue at a point with a measured exposure dose of 1 Roentgen). One "tissue Roentgen" corresponded to an absorbed energy of 93 erg/g of tissue [5].

When determining a value for the biological effect on a tissue or organ caused by different types of nuclear radiation (i.e., the ultimate hazard to human health), it was found that, for the same absorbed dose from different radiation types, the damage can be rather different and distinct. This led to the necessity to introduce the concept of the *equivalent dose*. The equivalent dose, H, is the absorbed dose, D, in a tissue multiplied by an average coefficient for the *quality factor*, k (a weighting coefficient), of the ionizing radiation in a given volume of biological tissue, i.e., $H = Dk$ (for X-, γ- and β-radiation, $k = 1.0$, while for α-radiation, $k = 20$). The special unit for the equivalent dose is the rem. The rem is a unit of absorbed dose, expressed in rads (100 erg/g), multiplied by the quality factor of the radiation. In the SI system, 1 rem = 10^{-2} Sievert.

Sometimes one can find in the literature the unit "*Roentgen-equivalent-man*" [2]. In this case, the energy equivalent for the X-, γ- and β-radiation amounts to 88 erg/g [1]. In the Russian literature, the term "*biological equivalent of Roentgen*" (ber) exists with the energy equivalent 88 erg/g [5]. In the SI system, the unit of equivalent radiation dose is the Sievert, Sv. 1 Sv = 1 J/kg with the quality factor of the radiation equal to 1.0. Under this condition, 1 Sv = 1 Gy or 100 rad.

The *effective dose* is a dose corresponding to the sum of the products of the equivalent doses in all organs and tissues of a body multiplied by corresponding weighting coefficients for the same organs and tissues (it is used for biological purposes). In the SI system, the unit of effective dose is the Sievert.

Below we indicate some additional important definitions and units:

- A *dose rate* is the rate (possible or real) of absorption of the dose per unit time, for example: Roentgen/hour ($\mathrm{R\,hr^{-1}}$, $\mathrm{mR\,hr^{-1}}$, $\mu\mathrm{R\,hr^{-1}}$); Sievert/hour ($\mathrm{Sv\,hr^{-1}}$), $\mathrm{cSv\,hr^{-1}} = 1\ \mathrm{R\,hr^{-1}}$, etc. A Roentgen/hour is an energy of 88 erg/g absorbed by the air during 1 hour in the course of formation of the charges of ionizing particles, as determined for the Roentgen (see above).
- The *activity*, A, of a radioactive substance is the number of spontaneous nuclear transformations, $\mathrm{d}N$, in this material in a small time interval $\mathrm{d}t$, divided by this interval, $A = \mathrm{d}N/\mathrm{d}t$.
- The *density of radioactive contamination* of a (land or other) surface is the value of activity per unit area of the surface (for example, $\mathrm{Curie/km^2}$, $\mathrm{kBq/m^2}$, etc.).

At a level of 1 m from an ideal flat isotropic source with a contamination density of 1 $\mathrm{Ci/km^2}$ of gamma-radiating radionuclides ($^{137}\mathrm{Cs}$ + $^{137\mathrm{m}}\mathrm{Ba}$), a field of radiation is

Table 1
Comparison of irradiation dose and activity units (older and SI systems)

	New name and notation	The same in other SI units	Old special unit and its notation	Conversion factor	Inverse conversion factor
Exposure dose	–	C/kg	Roentgen (R)	1 C/kg ~ 3876 R	1 R = 88 erg/g
Absorbed dose	Gray (Gy)	J/kg	rad (rad)	1 Gy = 100 rad	1 rad = 10^{-2} Gy
Equivalent dose	Sievert (Sv)	J/kg	rem (rem)	1 Sv = 100 rem	1 rem = 10^{-2} Sv
Activity	Becquerel (Bq)	s^{-1}	Curie (Ci)	1 Bq = 2.7×10^{-11} Ci	1 Ci = 3.7×10^{10} Bq
Density of radioactive contamination	Becquerel/m^2 (derivative unit)	$s^{-1}\,m^{-2}$	Curie/m^2 (Ci/m^2)	1 Bq/m^2 = 2.7×10^{-11} Ci/m^2	1 Ci/m^2 = 3.7×10^{10} Bq/m^2 = 3.7×10^{7} kBq/m^2
Concentration of radioactive contamination	Becquerel/m^3	$s^{-1}\,m^{-3}$	Curie m^{-3} (Ci/m^3)	1 Bq/m^3 = 2.7×10^{-11} Ci/m^3	1 Ci/m^3 = 3.7×10^{10} Bq/m^3

created with a dose rate of 10 μR/hr (micro-Roentgens per hour) or (in SI units) above a contamination density of 1 kBq/m^2, the corresponding absorbed dose rate amounts to 23.8 nGy/hr.

Units of activity

The Curie is a special unit of activity, Ci. 1 Ci = 3.7×10^{10} nuclear transformations (decays) per second.

The Becquerel, Bq (in the SI system) is one nuclear transformation (decay) per second or 0.027 nCi.

For tritium: 1 tritium unit (TU) (tritium ratio TR) is the unit of tritium concentration, i.e., 1 atom of tritium per 10^{18} atoms of hydrogen, 1 TU is equal to an activity of 0.118 Bq/kg of water.

When carrying out a radiometric survey in a radioactive fallout zone, the most used units (or their fractional values), in both the early and SI systems, are as shown in Table 2.

We present here such a detailed description of the definitions and units used in dosimetry over the last 50 years in order to explain how these definitions and units have been used in this book, how they should be correctly understood and what units should be used, bearing in mind the problem of the new units introduced with the SI system. It is necessary to emphasize that this book is the generalization of a large body of material accumulated on radioactive fallout over a period of more than 50 years (since 1949, in fact). Many real data were obtained at explosions and accidents of the 1950's and 1960's and these are now absolutely unique (i.e., were only once published in special reports or papers). So, the units used were related to this period. Whether we can now recalculate these data and present them in new units, for instance in the SI units, is a great question?

Table 2

Parameter	Obsolete units	New SI units
Exposure dose	Roentgen (R), mR, μR	
Exposure dose rate	R/hr, R/s, mR/hr, μR/hr, mR/s	
Absorbed dose	rad, mrad, μrad	Gy, cGy = 1 rad, nGy
Absorbed dose rate	rad/hr, mrad/s, mrad/hr, μrad/hr, mrad/s	Gy/hr, cGy/hr, Gy/year
Equivalent dose	rem, mrem	Sv, cSv = 1 rem
Equivalent dose rate	rem/hr, rem/s, mrem/hr	Sv/hr, cSv/hr, Sv/year
Activity	Ci, mCi, μCi, nCi	1 Bq, kBq, MBq
Density of radioactive contamination	Ci/km^2, Ci/m^2, mCi/km^2, $\mu Ci/m^2$	1 Bq/m^2, kBq/m^2, MBq/km^2
Concentration of radioactive contamination	Ci/km^3, Ci/m^3, mCi/km^3, $\mu Ci/cm^3$, nCi/cm^3, pCi/cm^3	1 Bq/m^3, kBq/m^3, Bq/cm^3, kBq/m^3

Note: c is centi (10^{-2}), m is milli (10^{-3}), μ is micro (10^{-6}), n is nano (10^{-9}), p is pico (10^{-12}), k is kilo (10^3), M is mega (10^6). Other abbreviations used later in this book are: G is giga (10^9), T is tera (10^{12}), P is peta (10^{15}) and E is exa (10^{18}).

It is also necessary to note that this book is a physical and geophysical book on radioactive fallout. It is very useful for biologists as well but it is not a biological book; this is why we have rarely used here units like rem or biological equivalent of Roentgen, though at the present time, the most-used units for evaluating doses and dose rates (as well as for estimating external dose on a land site and internal dose to man) are the SI system units, i.e., Sievert, which is the biological equivalent of the absorbed dose in rad units.

In the 1950's–1960's, the main unit used in dosimetry was the Roentgen (R) or mR, μR (to measure doses), and R/hour, mR/hour, μR/hour to measure dose rates. The Roentgen unit is a very convenient unit for a measurement as, in this case, the exposure dose can be measured directly by an ionizing chamber (via the electric charge) or any other instrument with an air-equivalent sensor calibrated by the ionizing chamber (these instruments were called Roentgen-meters). An important and historic example of such measurements was the dose rate measurement mission immediately after the Chernobyl accident. A large official group of specialists (headed by the author) measured the dosimetric characteristics in the area using air-equivalent Roentgen-meters. But many geologists (and the scientific community at large) had "Crystal" (or "SRP") instruments in which the detector of the radiation was a NaI(Tl) scintillator, i.e., obviously non-air-equivalent but sensitive to the gamma-radiation for geological survey work. Having been calibrated for a single source of gamma-radiation (^{60}Co or ^{137}Cs), this equipment showed similar data to the air-equivalent instrument during measurement of point sources at a close distance. However, in the case of land contamination (when intense scattered "soft" radiation appeared) the "Crystal" instrument showed an excessive "dose" (2–4 times larger) and this caused many misunderstandings (the dose measured by the population at large exceeded by several times that obtained by the official survey). In this case, a special decision of the State Commission, headed by the President of the USSR Academy of Sciences, academician A. P. Alexandrov (a famous specialist in the field of nuclear energy), was needed in order to solve this problem quickly and supporting the use of the air-equivalent instruments.

In the context of the above, therefore, we should note here that the primary data on doses and dose rates presented in this book in maps and tables and in the text itself are given first in the form in which they were actually obtained so that we could avoid the introduction of errors in the process of conversion of the units used into those in the SI system. This is why we retain in the book the primary dose notation in Roentgens, the dose rates in R/hr, R/year, mR/hr, μR/hr, etc. and in some sections we use the units "rad" and "rem". When doing this, we indicate that 1 Roentgen = 0.88 rad (1 rad = 1.136 R) and, when converting into the SI system, 1 rem = 0.01 Sv = 1 cSv; 1 rad = 0.01 Gy; 1 Gy = 100 rad (if $k = 1.0$). In tables which present values of activity, the data have generally been converted from Curie units into Becquerels (Bq, kBq, MBq, etc.).

In most cases throughout the book, however, in order to make the data and the scientific content as intelligible as possible to both young and old, we have either provided handy conversion factors in the relevant places or we have presented the data in both systems of units, the secondary data in parentheses. We hope that you will now be able to follow the story without too much confusion!

References

[1] Aglintsev, K. K. (1957). *Dosimetry of Ionizing Irradiation* (503 p.). Moscow: State Publ. of Techn.-Theoret. Literature.

[2] Rahn, F. J., Adamantiades, A. G., Kenton, J. E., & Braun, Ch. (1984). *A Guide to Nuclear Power Technology* (752 p.). New York: Willey.

[3] Warner, S. F. & Kirchmann, R. J. C. (Eds.) (2000). *Nuclear Test Explosions, SCOPE-59* (269 p.). Chichester.

[4] Eger, R. (1961). *Dosimetry and Protection against Irradiation* (translated from German) (211 p.). Moscow: State Publisher of Literature in the Field of Atomic Science and Engineering.

[5] Ivanov, V. I. (1970). *Dosimetry* (392 p.). Moscow: Atomizdat.

This Page Intentionally Left Blank

Chapter 1

FRACTIONATION OF RADIONUCLIDES IN ATMOSPHERIC NUCLEAR EXPLOSIONS. RADIOACTIVE AEROSOL PARTICLES

Contents

1. Major Processes Influencing the Character of Radioactive Contamination after a Tropospheric Nuclear Explosion 1
2. Temperature Regime in the Fireball of a Tropospheric Nuclear Explosion 3
3. Formation of Particle-carriers of Radioactivity. Role of Thermodynamic Conditions in the Fireball 7
4. Radioactive Products from Nuclear Explosions 12
5. Thermophysical Properties and Radioactive Transformations of Major Explosion Products 26
6. Activation of Particles 35
7. Characteristic Features of Fractionation of Radioactive Products from Tropospheric Nuclear Explosions 52
8. Quantitative Estimation of Fractionation Effects 57
9. Conclusion 61

1. Major Processes Influencing the Character of Radioactive Contamination after a Tropospheric Nuclear Explosion

The ensuing contamination of the environment by radioactivity following a tropospheric nuclear explosion results from the spread of the explosion's radioactive products in the atmosphere and their subsequent deposition on the surrounding areas. The radioactive products are formed, either as a result of the nuclear fission or fusion of the fuel or by the interaction between the neutrons generated by the explosion and the device material (including the fuel) and the environment. They are also composed of radionuclides (tritium, uranium and plutonium isotopes, etc.) that were originally contained in the device itself before the explosion, as well as their transformation products.

The scale of the radioactive contamination of the environment is a product of the amount of radioactive products released into the atmosphere by the explosion and the degree to which they are dissipated in the atmosphere. The processes that occur during the first few seconds after an explosion essentially control the characteristics of the radioactive contamination (and its nuclide composition). These processes depend, in turn, upon the nature of the environment where the explosion is conducted and the parameters of the explosion itself. Prevailing meteorological conditions influence only the degree and character of the dissipation of the explosion products, i.e., their concentration, but the qualitative composition of the products depends largely on the abovementioned processes.

Of most importance (from the point of view of radioactive contamination of the environment) are the explosions conducted in the atmosphere, as well as some types of underground and underwater explosions. Atmospheric explosions can be at ground level

(at the earth's surface), near-surface level (at low elevation), in the air (at an elevation exceeding the fireball radius) and in the upper atmosphere (stratosphere) and/or in space. Ground and underground cratering explosions are of primary importance from the point of view of land contamination. A characteristic feature of this list of explosions is the localization of the radioactive products within a clearly bounded region (e.g., the fireball after an atmospheric explosion and the cavity after an underground explosion) within the first seconds after the explosion. During this time period, the distribution and fixing of the radioactive products take place in the inert environmental material located in the immediate area of the detonation. This can give rise to the possibility of further spread of the different radionuclides within the environment either as separate atoms/molecules or combined with particle-carriers generated from inert material.

A complicated assemblage of physical and chemical processes, occurring from the first few seconds after the explosion both in the fireball and the cloud simultaneously with the transformation of the radioactive nuclei of the explosion products, exert a major influence on the radionuclide composition of the various materials (particles, molecular groups). This can lead to fractionation of the radioactive products.

The radionuclide fractionation starts when the evaporated matter condenses, resulting in the selective capture of isotopes of certain elements by the liquid phase at the time of radioactive particle generation. This arises because the different products (or their oxides) have different saturated vapor pressures at the same temperature and nuclides belonging to the same mass chain at different stages of particle generation can as a consequence occur in the form of different chemical elements with different properties as a result of radioactive transformation. The most refractory elements are condensed within liquid particles of the ground, or any other local, material and are distributed within these particles, while the more volatile elements condense later, often after solidification of these particles. It would appear reasonable that the large particles that leave the radioactive cloud earlier than the small ones would thus be enriched in refractory nuclides, whereas the smaller particles would be enriched in volatile species (or by those having gaseous or volatile precursors in a transformation chain). In this connection, it is obvious that radioactive contamination of the environment will be largely controlled by the nuclear and physico-chemical processes occurring in the fireball or explosion cavity, as well as by the amount and properties of the environmental material in this zone (or situated at its boundary). Below we consider the processes which determine the radioactive contamination from an atmospheric explosion, this chapter being based on a similar section (written in Russian only) contained in the book "Isotopic composition of radioactive fallout" (Izrael, 1973). Underground explosions are discussed in the next chapter.

To arrive at a quantitative estimation of the fractionation of different radionuclides and the activation of particles within the ongoing complexity of physico-chemical and nuclear processes taking place in a nuclear explosion, the factors of primary importance to be considered are the temperature regime within the fireball, the types of explosion products and inert material, the thermodynamic conditions in the explosion zone and the thermal/physical properties of the material involved in this zone.

2. Temperature Regime in the Fireball of a Tropospheric Nuclear Explosion

As a result of the rapid and enormous energy release within a limited space during a nuclear explosion, the neighboring matter is heated to a temperature exceeding millions of degrees and a "hydrodynamic front" that is formed at the boundary of the heated zone moves from the explosion center outwards with a velocity of hundreds of kilometers per second. In the initial stages, energy transfer takes place faster through irradiation than through linear transfer by the moving mass. However, as the temperature drops, the irradiation flux falls and energy transfer by this mechanism diminishes. By approximately one millisecond after the explosion, a shock wave crosses the irradiation front ("hydrodynamic separation" takes place). At this moment, the outer part of the sphere consists of luminous heated air and the fireball appears. The fireball increases in size due to the intense irradiation and the material flying apart. The surrounding air becomes entrained and these processes lead to a temperature drop. The inner part of the fireball is practically isothermal with the luminous air screening the inner isothermal sphere. Several milliseconds later, the minimum temperature is recorded at the surface of the fireball (about 2000 K). After the shock wave front becomes transparent for irradiation of the isothermal sphere, the effective temperature of the fireball itself rises to 7000–8000 K (the second and final maximum) and then falls as a function of time (at that moment the temperature outside and that of the isothermal sphere are the same) the temperature drop being best described by a power or exponential function (Glesston, 1966; Storebo, 1964). According to Freiling (1965), using Hillendal's calculations, the rate of fireball cooling as a function of time t or temperature T after the second maximum can be written as

$$-\frac{dT}{dt} = 776W^{0.10}t^{-1.34} \approx 3 \times 10^{-11}W^{-0.3}T^4, \tag{1.1}$$

where W is the explosive yield, in kilotons (kt).

Equation (1.1) describes the rate of cooling mainly due to the radiation process at a temperature exceeding 2000 K. At lower temperatures, the cooling rate is influenced considerably by other processes, especially the entrainment of cooler air. Storebo (1964) calculated the temperature change in a fireball and the radioactive cloud at the initial stage of its generation in an atmospheric nuclear explosion. In his study, in addition to radiation, he took into account the process of mixing of the contents of the fireball with the ambient air, and heating due to nuclear radiation absorption, as well as the dissociation energy release. Unfortunately, since the rate of air incursion into the fireball is unknown, Storebo conducted calculations for rates from 1 to 10 m/s. Figure 1.1 shows the temporal changes in the fireball temperature, calculated from Hillendal's formulae (curve 1), and also the changes in the cloud temperature from the time when its temperature was equal to 2000 K to the time of cloud stabilization (8–10 minutes after the explosion) as calculated by Storebo for air entrainment rates of 1, 3 and 10 m/s (curves 2, 3 and 4, respectively) and an explosion of 20 kt.

On average, for an explosion of 20 kt (for $t > 4$ s, curve 5),

$$T(t) = 4000t^{-0.588} \quad (t < 40 \text{ s}), \tag{1.2}$$

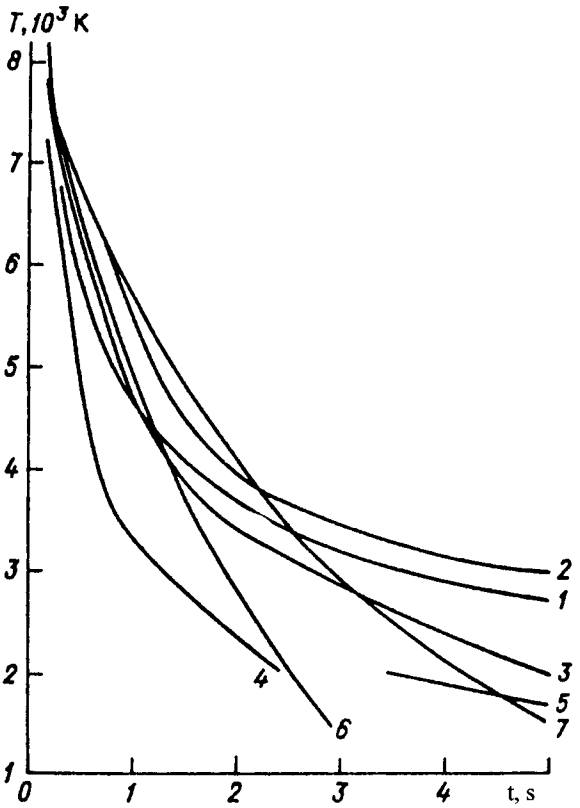

Fig. 1.1. Change of temperature (T) in a fireball as a function of time t.

$$T(t) = 2183t^{-0.374} \quad (t > 40 \text{ s}). \tag{1.3}$$

In these calculations, it was assumed that the cloud had a toroidal shape and that the temperature in the inner part of the toroid can decrease more slowly than described by formulae (1.2) and (1.3). For comparison, Fig. 1.1 also shows the relationship between the fireball temperature and time, as obtained using the suggestions of Glesston (1966) (curve 6) and Lavrenchic (1965) (curve 7). It follows from the figure that values of $T(t)$ obtained by these authors essentially differ from one another. This observation may be explained by the fact that the authors, in carrying out their calculations, did not take into account all the processes occurring in the fireball. Because of a lack of reliable experimental data, many of the suggestions of the authors are probably unjustified or rather approximate. We believe Storebo's study (1964) to be the most relevant since it takes into account a large variety of processes occurring in the fireball. However, it too has considerable uncertainty associated with the rates of air entrainment into the fireball. Later we will use the curve obtained by Storebo for an entrainment rate of 3 m/s (curve 3). It should be noted that virtually none of the authors mentioned took into account the role of inert material in calculating the temperature variation of the fireball apart from

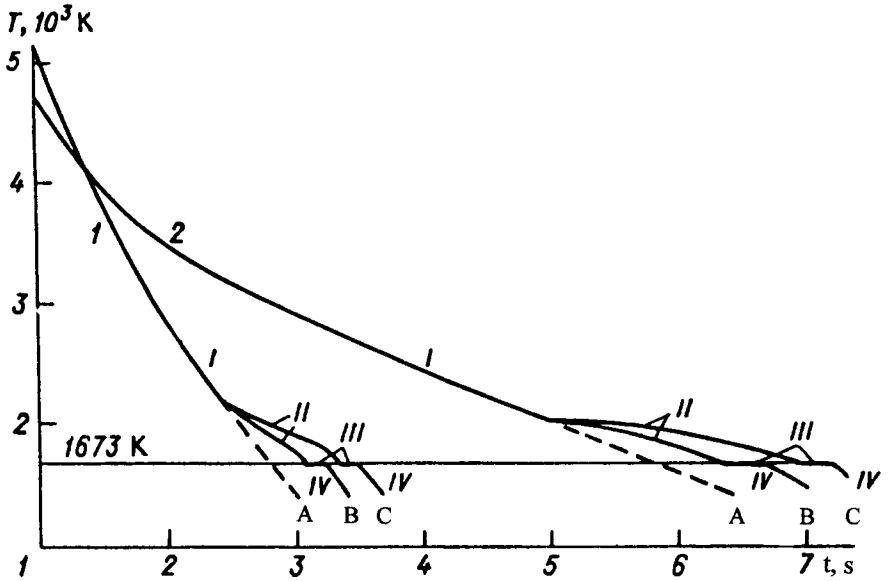

Fig. 1.2. Change in temperature T in the fireball with time t for a ground-level explosion.

an indication in Storebo (1964) that, if the fireball from a 20 kt explosion contained 1 t of iron then the temperature drop would be delayed by 0.016 s due to liquid iron oxide formation.

An effort has been made by the author to take into account the influence of inert material involved in the fireball upon the change in temperature, with factors such as heat capacity, heat of evaporation and melting, and dissociation energy being considered. It is essential, in ground-level explosions, where a considerable amount of earth is incorporated into the fireball that this factor be considered. Figure 1.2 shows the change in temperature with time $T(t)$ during a ground-level nuclear explosion when these factors are taken into account. The presence of inert material slightly decreases the temperature in the fireball and delays the time that temperatures in the range 1700–3000 K exist in the fireball. This range is of primary importance in calculations of radionuclide fractionation. The author (1973) calculated the delay period in the temperature drop due to incorporation of inert material.

In Fig. 1.2, curve 1 corresponds to curve 6 in Fig. 1.1 and curve 2 to curve 3. In the sections marked I of curves 1 and 2, the existence of inert material practically does not influence the temperature regime of the fireball. In sections II, the temperature change is simularly caused by condensation, calculated using 25 t of earth per kt of explosive yield—curve B, and by the release of dissociation energy—curve C. In sections III, the effect of the release of the ground melting heat on the temperature change is shown (calculated using 200 t of melted ground per kt). In sections IV, we can see that the influence of inert material (as well as on section I) is practically negligible.

The delay period, τ_{del}, calculated by the author (1973) for the temperature regime of the fireball, as shown by curves 6 and 3 in Fig. 1.1, amounts to 0.6 and 1.6 s (when $W = 20$ kt), and the period for particle solidification after the explosion (when $T_1 = 1673$ K) is equal to

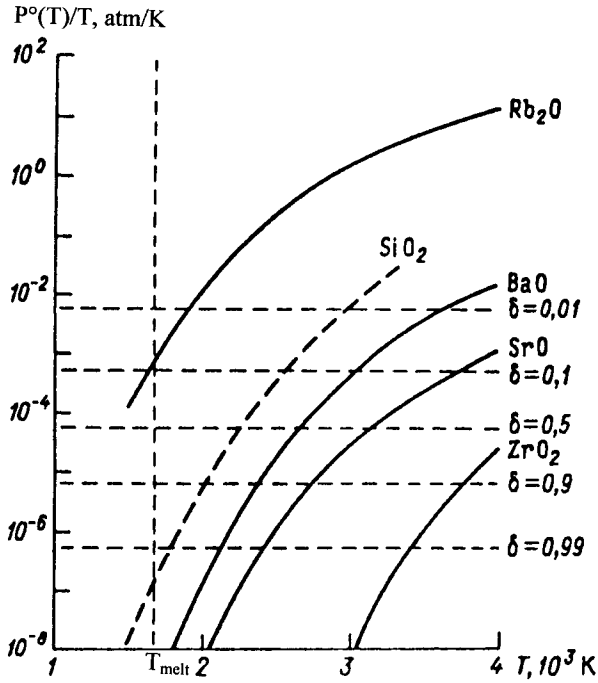

Fig. 1.3. The relationship between saturated vapor pressure $P_i^0(T)/T$ and temperature T for refractory elements.

3.5 and 7.2 s, respectively. (This is close to the value of $t_1 = 6$ s, calculated by Miller for a ground explosion of 25 kt as reported by Freiling et al. (1964).)

When calculating the following values were used at $T \approx 2000$ K: $\varepsilon_{evap} = \varepsilon_{dis} \approx 2000$ cal/g, $\varepsilon_{melt} = 92$ cal/g (ε_{evap}, ε_{dis} and ε_{melt} are latent heats of evaporation, dissociation and melting of ground material), $c_p^g \approx 0.15$ cal/(g °C) (Johnson, 1959), specific heat capacity of ground, $c_p^a \approx 0.3$ cal/(g °C) (Onufriev, 1967); $L_{evap}(t)$, rate of evaporation (condensation) of the ground mass, was obtained by differentiation of the function

$$\frac{M_{evap}}{M_{evap} + M_{melt}} \cdot \frac{\mu_{gr} P_{gr}^0(T) V}{RT}, \tag{1.4}$$

where M_{evap} and M_{melt} are the amounts of evaporated and melted ground-derived material, $M_{evap}/(M_{evap} + M_{melt}) = 1/9$; μ_{gr} is the relative molecular mass of the ground material (for $SiO_2 \approx 60$), V is the fireball volume at the moment of particle solidification; R is the gas constant; $P_{gr}^0(T)$ is the relation between the saturated vapor pressure of SiO_2 over liquid SiO and T (also taking dissociation and SiO into account). The relation $P_{gr}^0(T)/T$ is presented in Fig. 1.3 on the basis of reference book data (Glushko, 1962) for SiO_2.

The calculations did not consider the heat inertia of ground particles (it was suggested that $v(t) = v'(t)$) but this did not change significantly the value of τ_{del}. This problem is discussed in Section 1.3.

If the volume within which the ground condensation takes place is smaller than that of the fireball, the delay time will not change. The delay will not be related to the fireball as a whole, however, but only to the indicated volume ("screening" which Storebo discussed in 1964 will occur).

3. Formation of Particle-carriers of Radioactivity. Role of Thermodynamic Conditions in the Fireball

Immediately after generation, a fireball begins to rise mainly by Archimedean forces as a result of the differences in density between the inside and outside of the fireball. Rotational circulatory movement appears very quickly in the rising mass of heated gas under frictional forces (Onufriev, 1967). The volume takes on the form of a toroid, within which the air rotates around a horizontal circular axis line and a circulating flow appears outside. As a result, an element of the vortical circle is affected by Zhukovsky's force, directed perpendicularly to the velocity of the elementary circular movement. The circle is thus slightly stretched under this force. Over several seconds, a maximum rise velocity is reached and then the velocity decreases. Due to intensive mixing of the cloud content with the surrounding cool air, the angular velocity of gas rotation decreases, resulting in the reduction of the outer flow circulation.

If the explosion is carried out near the earth's surface, the upper ground layer evaporates and fuses under the heat and the air layer is warmed due to the radiation, thus promoting the appearance of an ascending flow at the epicenter. In addition to the glowing air and atmospheric moisture, the fireball, and then the cloud, contain evaporated (or fused) material of the nuclear charge and the surrounding earth, the latter comprising crushed grains or clusters of the original ground material.

As the temperature of the fireball and cloud falls, the evaporated explosion products begin to condense, generating radioactive particles in air explosions. When ground and near-surface explosions are conducted, the activation of fused/melted ground particles begins at this stage. After atmospheric explosions, the particles appear from formation of nuclei with ensuing condensation (some authors assume simultaneous coagulation). In the first case, the particle size-distribution has an exponential character (Izrael, 1973); in the second case, the distribution is log-normal (Stewart, 1956). As a rule, the sizes of particles from air explosions do not exceed 10–25 μm, and their mean sizes are fractions of μm (Stewart, 1956; Freiling, 1962). The highly active particles exceeding 1–2 μm formed in an air explosion are almost always exceptionally spherical in shape (Freiling and Kay, 1966; Benson et al., 1965a; Crocker et al., 1966), typical solidified drops. The particle composition is a mixture of ferrous oxides (the main component), aluminum, uranium and plutonium. Studies by Benson et al. (1965a) indicate that the relationship between particle activities and their sizes (for particles larger than 2 μm) is a power one, with an index of about 3.0. This clearly indicates that the activity is evenly distributed over the volume of particles from atmospheric explosions (at constant activity concentration).

Particles from ground explosions consist of a glass-like material resulting from the melting/fusing of silicate minerals, when such materials constitute the major constituents

of the underlying earth. In this case, two types of particles are formed: spherical (or drop-shaped) and those of irregular shape (angular), formed at the periphery of the fireball as a result of the fusion of individual grains of soil or ground. Both types of particles are up to 2–3 mm in diameter (Adams, 1960; Freiling, 1962). Radioactive particles are distributed more or less evenly in the spherical particles over their volumes or thick volumetric layer. According to Adams (1960), an "inactive" core constitutes 10–30% of the volume of large particles (with diameter of 0.5–2 mm). Radioactive particles are distributed in the thin surface layer of large angular particles. The amount of such particles is insignificant.

The size distribution of the activity of particles for a ground (and underground) explosion can be expressed by the log-normal law, therefore

$$N(d_1, d_2) = \frac{1}{\sigma\sqrt{2\pi}} \int_{\log d_1}^{\log d_2} \exp\left[\frac{(\log d - \log \bar{d})^2}{2\sigma^2}\right] \mathrm{d}(\log d), \tag{1.5}$$

where $N(d_1, d_2)$ is the fraction of activity associated with particles of d_1 to d_2 in diameter; $\bar{d}$ and σ are the distribution parameters.

It is characteristic that the distribution of particle activity by size does not depend on the explosion yield of a given type, but depends more on the nature of the earth for a ground-level explosion or for those underground explosions that produce craters (Anderson, 1957). Hence, it follows that elementary grains of ground material (or their clusters) constitute the basis of the radioactive particles, the size-distribution of the former being slightly different for different ground types (Garkusha, 1954). Thus, in formula (1.5) for local fallout after ground explosions for solid soils of the Nevada type, $\log \bar{d} = 2.053$ and $\sigma = 0.732$, and for a coral substrate $\log \bar{d} = 2.209$ and $\sigma = 0.424$ (Stewart, 1956).

Radioactive particles are also characterized by a normal logarithmic mass-distribution (Storebo, 1964) and surface-distribution. Figure 1.4 shows the integral mass (M) and volume (V) distribution according to particle size (Freiling, 1962). The relationships between surface area (S) and particle activity (A) as a function of size are also presented. These latter data are taken from a study by Kellog (1957).

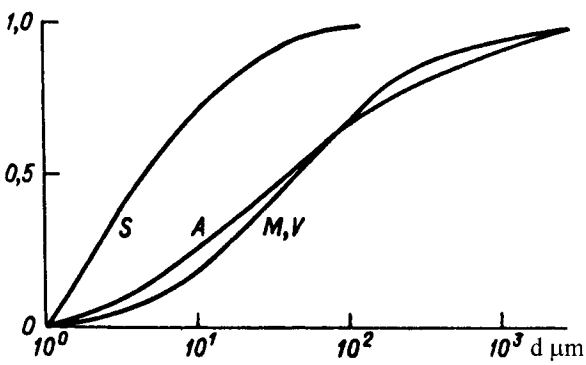

Fig. 1.4. Integral distributions of mass, volume, surface area and activity as functions of the size of radioactive particle.

The particle surface area distribution $S(d)$ can be derived from the mass distribution $M(d)$ using the relationship:

$$S(d) = \frac{6M(d)}{\rho d}, \tag{1.6}$$

where ρ is the density of the particles, equal to about 2.5 g/cm^3.

In a study by Petrov and Pressman (1962), based on examination of the spread of the admixed particles with a non-uniform deposition rate ω (or by size r, where r is the radius), and an instantaneous point-source release, the authors proposed the distribution to be a two parameter function (gamma-distribution):

$$N(\omega) = \frac{a^{n+1}}{\Gamma(n+1)}\omega^n e^{-a^\omega}, \tag{1.7}$$

where a and n are the distribution parameters and Γ is the gamma-function. $N(\omega)$ or $N(r)$, as obtained from experimental data, is well approximated by this formula. Thus the distribution of the particle activity $N(r)$ in their sizes, as presented by Izrael (1973), can be shown as a relationship of this type, n being equal to 2 and $a = 0.06$ (Izrael, 1965).

The transition of the radioactive products of the explosion to particles of inert material, i.e., the particle activation (and finally, the character of the radioactive particle distribution), is determined by the thermo-physical properties of all the constituents and the thermodynamic conditions in the fireball. As indicated above, inert material incorporated into the fireball influences the thermal regime of the fireball.

In a ground-level nuclear explosion, about 5000 t of earth per kt of explosive yield are released into the atmosphere (Freiling, 1962) and, of that quantity, 180–200 t are fused (Izrael, 1973). From 1.5 to 25 t per kt are evaporated (Izrael, 1973). The last figure was arrived at through analogy with an underground nuclear explosion where up to 50–70 t of ground-derived material per kt are evaporated and by assuming about half of this value for a ground-level explosion. The comparatively small amount of evaporated earth can be explained by the low evaporation rate of SiO_2 and the short duration of the high temperatures in the fireball.

The material involved in the fireball is mixed within the volume formed as a result of the whirling motion in the generated toroid. A column of partially evaporated molten earth (the column's diameter can be considered to be approximately equal to the diameter of the explosion crater) passes through the fireball (cloud) center and then starts its circulation around the vortex ring axis. The linear speed of the particles increases with distance from the axis and then decreases on contact with the ambient air masses. The maximum linear speed (for an axial circle radius a) can be obtained from the equation

$$v = \Gamma_0/2\pi\alpha, \tag{1.8}$$

where, according to Onufriev (1967), the circulation of the external flow, Γ_0, is calculated using the equation

$$\Gamma_0 = \gamma_0 R\sqrt{Rg}, \tag{1.9}$$

Here $\gamma_0 = 0.26\sqrt{(1-\xi)\sqrt{\xi}}/[\alpha(1+\xi)]$, ξ being the ratio between the air densities inside and outside the toroid; α is an entrainment coefficient for the turbulent mixing and is equal to 0.03–0.08 (Abramovich, 1948). When $\xi = 0.1$ and $\alpha = 0.055$, $\gamma_0 = 0.55$.

Assuming the fireball volumes from air and ground explosions to be equal and that $R_M = 89\sqrt[3]{2W}$ (Izrael, 1973) for a ground explosion, we obtain (in m/s)

$$v = 5.3\, W^{0.16} \quad \text{(if } W \text{ is expressed in kt).} \tag{1.10}$$

This indicates that, at the moment of particle solidification, and taking into account the volume expansion due to gravitational settling of the particles, the volume of earth involved will constitute only 10–20% of the fireball volume. This part of the volume is the zone of contact between the evaporated explosion products and the liquid particle-carriers. In this case, the vapor phase volume V_v can be considered to be equal to 0.2 of the fireball volume V_f.

We can also assume that the evaporated explosion products are distributed rather quickly (within hundredths of a second) throughout the fireball due to the high rates and free pathways of the molecules. In this situation, therefore, the vapor-phase volume can be considered to be equal to that of the fireball. Although the material involved occupies a relatively small space (10–20% of the total volume of the fireball), in this case, the evaporated explosion products (being in molecular form) can freely come into contact with the material. The rates of particle formation (due to Brownian motion) are not high and particles larger than several fractions of a micron in size can be considered to be trapped in the immediate vicinity of their origin (Glesston, 1966). As mentioned above, particle transport due to turbulent mixing can be ignored.

When the fireball temperature exceeds the boiling point of the particle-carriers (2500–3000 K), equilibrium between the liquid and vapor phases (at a pressure of 1 atm) is unattainable. However, thermodynamic equilibrium could be reached if the fireball temperature drops below the indicated value. The author considered the conditions for attainment of equilibrium and what temperature difference between the fireball and liquid particles is possible (Izrael, 1973). With the continuing drop in the fireball temperature, the liquid particle temperature will always be delayed with respect to the vapor phase temperature due to final heat conductivity considerations. Such "lags" ($\tau_{0\,av,c}$) of the mean temperatures at the centers of particles $T_{av,c}$ of different radii with respect to fireball temperatures have been calculated (Izrael, 1973). For sections I, II and III of curves 1 and 2 (see Fig. 1.2)

$$\tau_{0\,av,c} = \frac{T_{av,c}(t) - kt}{k}, \tag{1.11}$$

where k characterizes the fireball cooling rate. For curve 2, τ_{0c} is 1.4×10^{-3} s for section I and particles with diameter $d = 200$ μm, 3.5×10^{-2} s for $d = 1000$ μm and 0.14 s for $d = 2000$ μm (the contribution of the latter to the total mass of the particles is about 5% and in terms of activity it is even smaller).

As an example, Fig. 1.5 shows the changes in temperature with time at the centers of particles of diameter 2000 μm (curve 2) and a fireball from $W = 20$ kt (curve 1 or curve 2 in

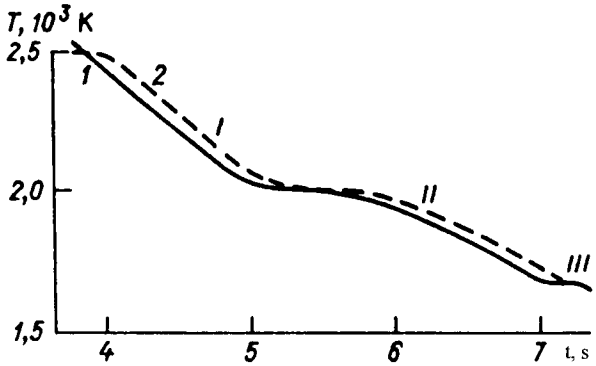

Fig. 1.5. Change in temperature (T) with time (t) in the centers of particles of diameter 2000 μm.

Fig. 1.2). Thermodynamic equilibrium is attainable even for such particles at sections III. The maximum value of $\tau_{0\max}$ (for the particle centers) can be obtained from a simple relationship

$$\tau_{0\max} = \frac{r_0^2}{6k}. \tag{1.12}$$

This is found to be very low for the majority of particles. One should also take into account the thermal inertia of the particles relative to the ambient gaseous medium. Cooling of the particles within the range 2500–1400 °C was taken into account for both the radiation and heat conductivity of the medium. Rough calculations showed that the temperature lag of particles of diameter 100 μm is about 0.1 s behind the fireball temperature within the range indicated.

So, although the "liquid–vapor" state is very close to equilibrium in the fireball at $T_{\text{mel}} \leqslant T \leqslant T_{\text{boil}}$, in the strict sense, the thermodynamic equilibrium can only be attained in the fireball at a time corresponding to section III of the curve reflecting the fireball thermal regime. As already stated, for the majority of particles, the deviation from equilibrium between the vapor and liquid phases is negligible for all the time intervals within the temperature range between the boiling and melting points of the particulate matter. In calculating the condensation rate (assuming equilibrium) we will obtain an overestimation if we use curve 1 (see Fig. 1.5) and an underestimation if we use curve 2. Finding the mean value of these data will yield a value closer to the truth and the difference between them will represent the maximum error. Equilibrium conditions are best fulfilled for explosions of high yields.

To examine the total amount of material capable of being transferred into particles (liquid phase) before their solidification, one can use both curves 1 and 2 (see Fig. 1.5). In this case, the following relationship applies:

$$\tau_{0\max} \leqslant \Delta t_{\text{III}},$$

where Δt_{III} is the length of sections III (see Figs. 1.2 and 1.5). In this situation, only the degree of nuclide penetration into the particles will vary slightly.

When calculating the condensation rate and the total amount of condensed phase at thermodynamic equilibrium for a one-component "liquid–vapor" system, one should take into account the fact that, at any moment, the value of the partial pressure of the vapor of any substance must be equal to that of the saturated vapor:

$$P_i = n_i^0 \frac{RT}{V_v}, \tag{1.13}$$

where n_i^0 is the number of moles in volume V_v of the vapor phase, R is the gas constant and T is the absolute temperature.

The vapor pressure of the ith component, as described by Raoult's law for a two-component system (i, j are the components), is:

$$P_i = \frac{n_i}{n_i + n_j} P_i^0, \tag{1.14}$$

where P_i^0 is the vapor pressure above the one-component liquid (i); and n_i and n_j are numbers of moles of the ith and jth components in the solution. Combining formulae (1.13) and (1.14)

$$\frac{n_i^0}{n_i} = \frac{P_i^0 V_i}{(n_i + n_j) RT} \tag{1.15}$$

one can calculate the ratio between the amounts of the ith component material in the vapor and liquid phases.

4. Radioactive Products from Nuclear Explosions

During a nuclear explosion of 1 kt yield, 1.45×10^{23} nuclei fission events take place and 4.19×10^{19} ergs of energy are released (Izrael, 1973; Leypunsky et al., 1959). With every fission event, an average of 2.5 neutrons (^{235}U fission) or 3.0 neutrons (^{239}Pu fission) are released with an average energy of about 2.0 MeV and a most probable energy of 0.8 MeV (Yampolsky, 1961). In an energy release of 200 MeV, 7.2–8.4 MeV is instantaneous γ-radiation (Izrael, 1973; Leypunsky et al., 1959) and about 13 MeV is β- and γ-radiation from fission products (Izrael, 1973; Goldstein, 1961).

In thermonuclear or hydrogen bombs (Bethe, 1950; Ridenour, 1950), a fusion of light nuclei takes place with an accompanying substantial energy release. The inclusion of ^{238}U into the thermonuclear bomb case significantly amplifies its effect, because the neutron surplus is used for ^{238}U fission. An explosive device, consisting of a thermonuclear bomb (with an atomic "fuse") enveloped by a ^{238}U case, was named a "fission–fusion–fission" bomb. Early publications that mentioned the possible use of such a scheme in a bomb date back to 1955 (Rotblat, 1955; Lapp, 1955; Libby, 1953). About 80% of the total energy of such a bomb can be released in the ^{238}U fission reaction with fast neutrons (Rotblat, 1955).

The fission and total yields of atmospheric nuclear tests conducted by different countries are summarized below (from UNSCEAR, 1982):

Country	Fission (Mt)	Total (Mt)
USA	72.1	138.6
Former USSR	110.9	357.5
UK	10.6	16.7
France	10.9	11.9
China	12.7	20.7
Total	217.2	545.4

The yield of thermonuclear weapons tested together with the "fission–fusion–fission" varieties covers a wide range from hundreds of thousands to tens of millions of tons of trinitrotoluene (TNT) (Telegadas, 1959; EC, 1963; Hardy, 1964; Mikhailov, 1996). Only two long-lived radioactive nuclides are generated during thermonuclear reactions: tritium ^{3}H and, possibly, ^{7}Be (Magata, 1963; Drevinsly et al., 1964; Schumann and Storppler, 1963). The tritium generated in significant quantities during a thermonuclear explosion (or that which was initially contained in the charge) is not a γ-emitter and has a β-energy equal to 18 keV.

Fission products of heavy nuclei are the basis of the radioactive contamination of the atmospheric and terrestrial environments. An exception is the near-surface or underground explosion of a very "pure" bomb. In this case, the main contributors to the γ-activity are the radionuclides generated by neutron activation of ground (rock) elements ("induced activity") (Lane, 1962; Essington et al., 1965; Batzel, 1960).

The first study describing time variations in the composition of a fission product mixture is that of Way and Wigner (1948). They described the changes with time in the activity mixture by the empirical formula

$$A(t) = A_0 t^{-n}, \tag{1.16}$$

where A_0, $A(t)$ are the activities of the product mixture at the initial time t_0 (e.g., $t_0 = 1$ s, 1 hr, ...) and a subsequent time t. The index n in formula (1.16) can slightly vary with time and has an average value of $n \approx 1.2$.

The decay rate for an instantaneous fission product mixture of ^{233}U, ^{235}U, ^{239}Pu, as well as the activity of each radioactive nuclide have been calculated on the basis of the known fission yields and nuclide decay schemes (Essington et al., 1965; Hunter and Ballou, 1951; Maly et al., 1957; Grechuskina, 1964; Low and Bjornerstedt, 1958; Bjornerstedt, 1959; Zysin et al., 1963). The resulting data are presented in our study (Izrael and Stukin, 1967). The fission product mixture was examined as the sum of the individual fission products and the contribution of conversion electrons was not considered. Grechushkina (1964) has described the activities of individual nuclides for periods ranging from 1 hr to 100 years for 5 types of fission ($^{235}U_{n_{therm}}$, $^{235}U_{n_{fis}}$, $^{239}Pu_{n_{fis}}$, $^{238}U_{n_{fis}}$, $^{238}U_{n_{14\,MeV}}$) (in numbers of decays per minute per 10^4 fissions). The relationship between the total β-activity and time

Table 1.1
The relationship between β- and γ-activities of fission debris and mixture age after a 1 kt explosion

Mixture age	β-activity (decay/s)		γ-activity (MeV/s)			
	$^{235}U_{n_{fis}}$ [a]	$^{239}Pu_{n_{fis}}$ [a]	$^{235}U_{n_{fis}}$ [b]	$^{235}U_{n_{fis}}$ [c]	$^{239}Pu_{n_{fis}}$ [b]	$^{239}Pu_{n_{fis}}$ [c]
1 hr	1.6×10^{19}	1.47×10^{19}	1.73×10^{19}	1.65×10^{19}	1.46×10^{19}	1.44×10^{19}
2 hr	6.6×10^{18}	5.92×10^{18}	6.94×10^{18}	7.72×10^{18}	5.93×10^{18}	6.62×10^{18}
5 hr	2.23×10^{18}	1.93×10^{18}	1.77×10^{18}	2.03×10^{18}	1.44×10^{18}	1.7×10^{18}
10 hr	1.09×10^{18}	1.0×10^{18}	6.96×10^{17}	7.6×10^{17}	5.95×10^{17}	6.88×10^{17}
1 day	4.16×10^{17}	4.2×10^{17}	2.38×10^{17}	2.53×10^{17}	2.21×10^{17}	2.45×10^{17}
2 days	1.73×10^{17}	1.93×10^{17}	9.31×10^{16}	9.7×10^{16}	9.49×10^{16}	1.02×10^{17}
5 days	6.14×10^{16}	7.42×10^{16}	3.25×10^{16}	3.12×10^{16}	3.91×10^{16}	3.65×10^{16}
10 days	3.05×10^{16}	3.24×10^{16}	1.65×10^{16}	1.56×10^{16}	1.74×10^{16}	1.7×10^{16}
20 days	1.49×10^{16}	1.43×10^{16}	7.65×10^{15}	–	7.33×10^{15}	–
30 days	9.44×10^{15}	8.72×10^{15}	4.65×10^{15}	4.45×10^{15}	4.32×10^{15}	4.14×10^{15}
70 days	3.65×10^{15}	3.26×10^{15}	1.42×10^{15}	–	1.3×10^{15}	–
100 days	–	–	–	8.97×10^{14}	–	8.05×10^{14}
150 days	1.46×10^{15}	1.39×10^{15}	5.41×10^{14}	–	4.84×10^{14}	–
1 year	3.24×10^{14}	4.33×10^{14}	6.87×10^{13}	6.38×10^{13}	7.68×10^{13}	7.22×10^{13}
1.5 years	1.72×10^{14}	2.65×10^{14}	1.65×10^{13}	–	2.97×10^{13}	–
2 years	1.16×10^{14}	1.83×10^{14}	7.8×10^{12}	–	1.83×10^{13}	–
3 years	6.6×10^{13}	9.9×10^{13}	4.85×10^{12}	5.18×10^{12}	1.04×10^{13}	1.05×10^{13}
5 years	3.22×10^{13}	3.65×10^{13}	4.57×10^{12}	–	5.05×10^{12}	–
10 years	1.65×10^{13}	1.25×10^{13}	2.85×10^{12}	3.09×10^{12}	2.9×10^{12}	3.14×10^{12}
15 years	1.27×10^{13}	9.27×10^{12}	2.52×10^{12}	–	2.49×10^{12}	–
30 years	8.33×10^{12}	5.79×10^{12}	1.77×10^{12}	1.84×10^{12}	1.76×10^{12}	1.82×10^{12}

[a] Grechushkina (1964). [b] Izrael and Stukin (1967). [c] Bjornersted (1960).

has been calculated from the data of Grechushkina (1964) and is presented in Table 1.1 for a 1 kt explosion yield.

Taking into account the data of Bethe (1950), one would expect that the time-dependence of the β-activity (as well as the yield of β-decays per fission) could differ from that shown in Table 1.1 by 10–20% and perhaps more depending on the times and fission types. The change with time in the composition of the fission product mixture resulting from the fission of ^{235}U by thermal neutrons ($U_{n_{therm}}$) corresponds closely to the experimental data of Essington et al. (1965), Batzel (1960), Way and Wigner (1946) and Mostovaya (1961).

Calculation of the γ-radiation for a debris mixture for an explosion is much more complicated. In addition to the above uncertainties, there are additional errors arising from insufficient knowledge of the decay schemes of the nucleus under consideration. The integral characteristics of the γ-radiation emanating from fission debris mixtures were calculated on the basis of the β-activity data for various time intervals following the explosion (Grechushkina, 1964) and the associated characteristics of the γ-radiation from the individual nuclides. Figure 1.6 (Izrael and Stukin, 1967) presents the calculated relationship between the γ-radiation intensity and time for the mixture of fission products from a 1 kt atomic explosion for two fission types: $^{235}U_{n_{fis}}$ and $^{239}Pu_{n_{fis}}$. From a comparison of the curves in Fig. 1.6 it can be seen that the γ-radiation intensity differs by less than 20% for the period 1 hr to 1 year; however, the results differ by more than a

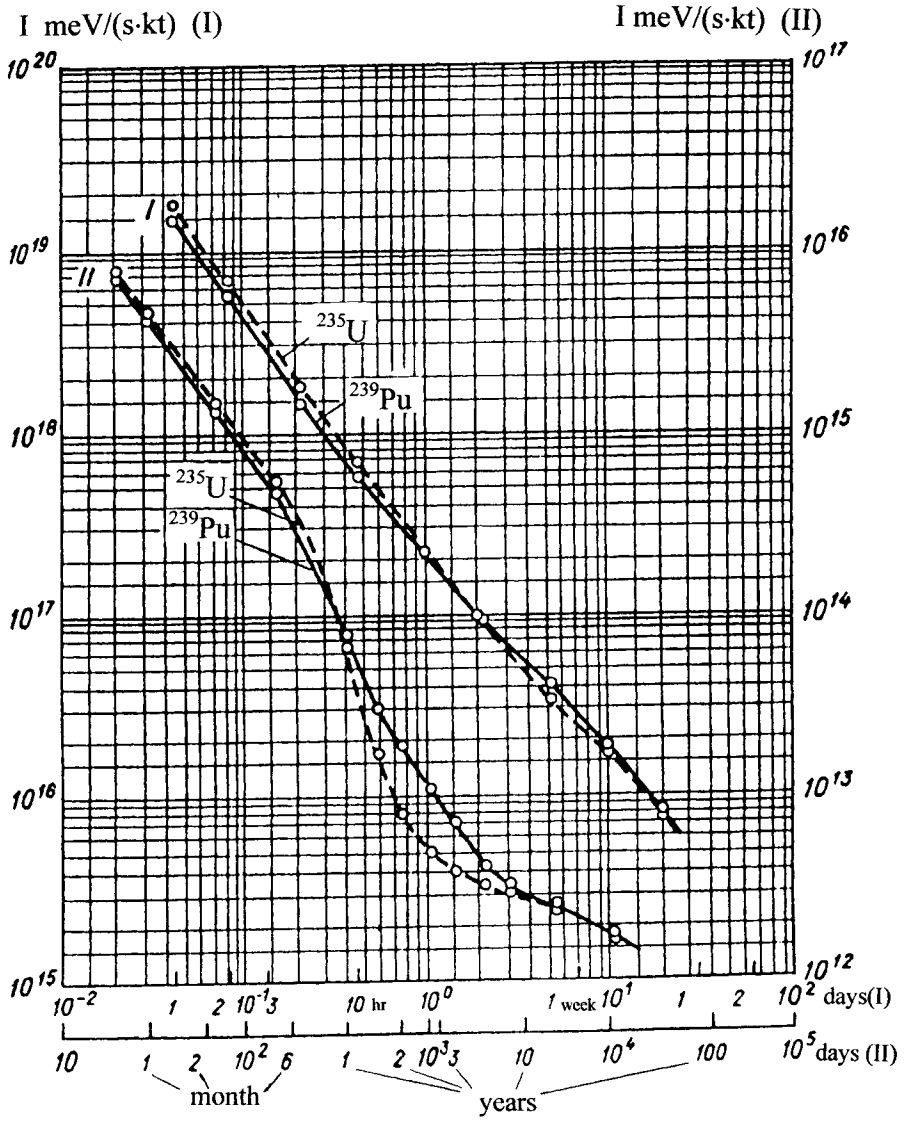

Fig. 1.6. The relationship between γ-radiation intensity and the age of the mixture of fission debris resulting from a 1 kt atomic explosion for two fission types: $^{235}U_{n_{fis}}$ and $^{239}Pu_{n_{fis}}$.

factor of two at 2 years. This divergence is related to the essentially different ^{106}Ru yields for the two fission types. In Fig. 1.7a, a curve is presented of the total dose rate variation with time that results from the fission of ^{238}U by thermonuclear neutrons (results are for a height of 1 m above an infinite plane contaminated evenly with a density of 10^4 fissions per cm^2). Fig. 1.7b shows the changes in the relative contributions of individual products of ^{238}U fission by thermonuclear neutrons to the total dose rate as a function of time (Freiling

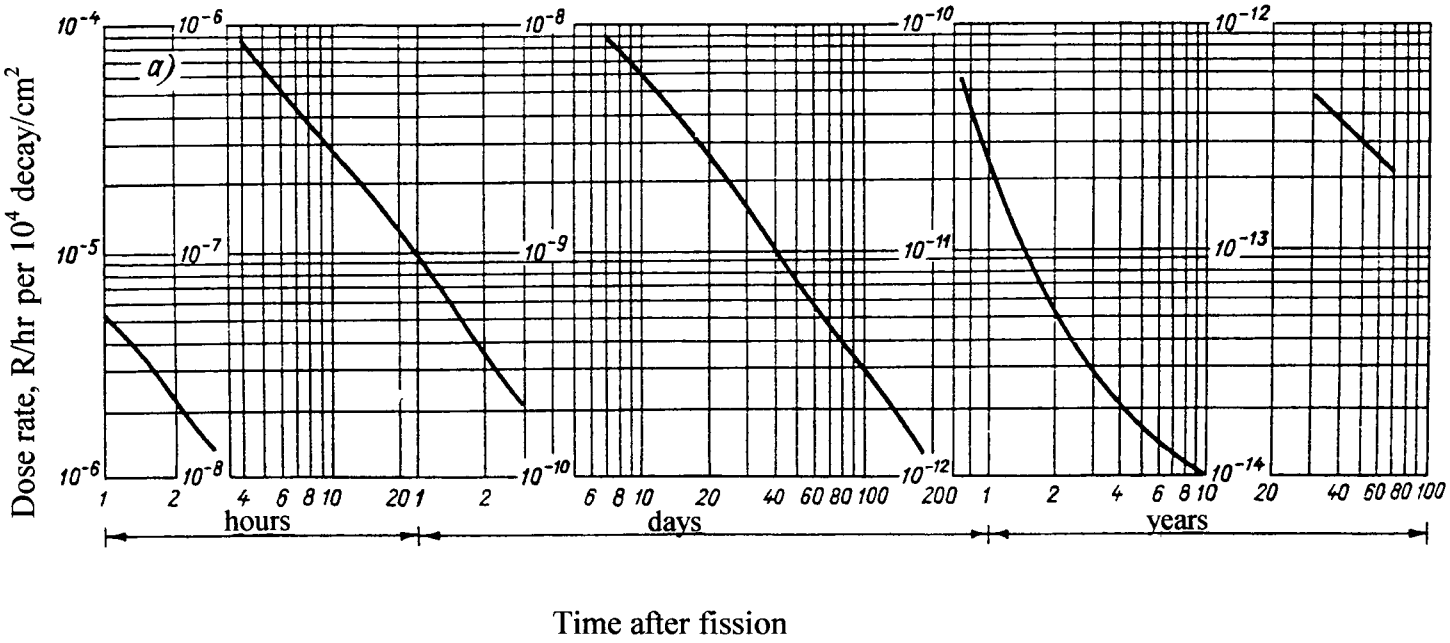

Fig. 1.7 (a) Variations of the total dose rate with time following the fission of ^{238}U by thermonuclear neutrons.

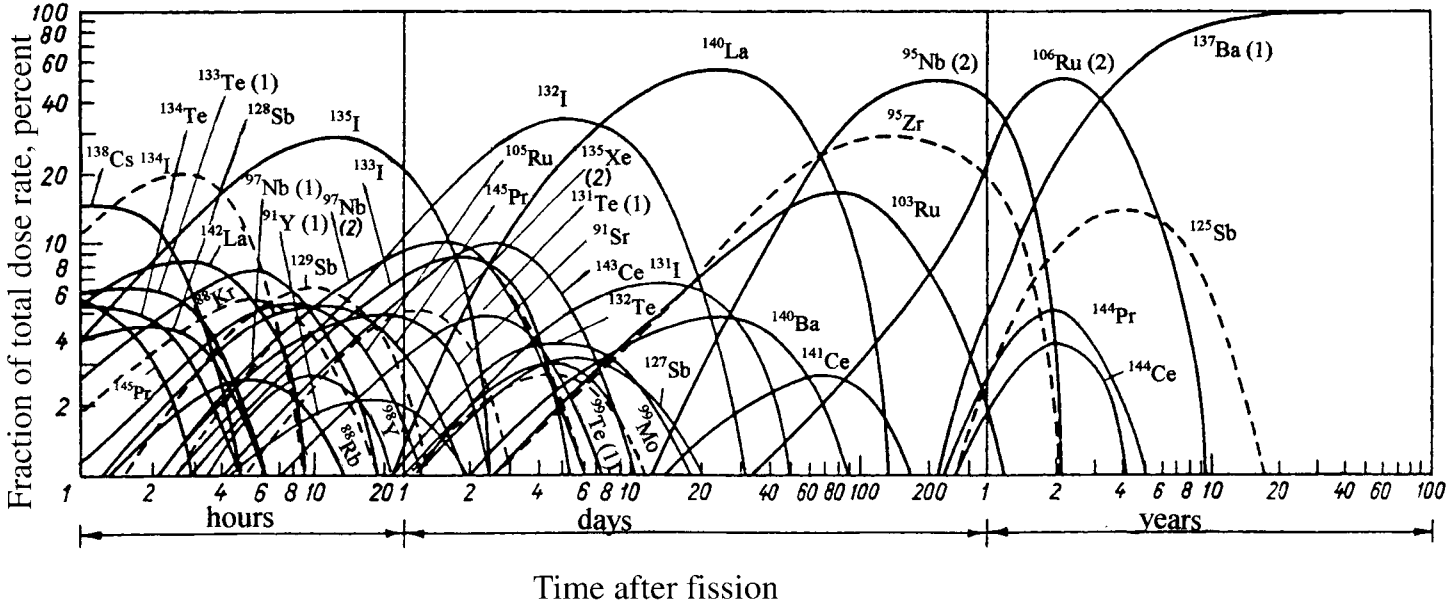

Fig. 1.7 (Continued) (b) The relative contribution of individual fission products to the total dose rate for ^{238}U fission by thermonuclear neutrons.

Table 1.2
Changes in n-index value in Eq. (1.17) with age of ^{239}Pu and ^{235}U fission product mixture

Age	$^{239}Pu_{n_{fis}}$	$^{235}U_{n_{fis}}$
2 hr	1.31	1.32
5 hr	1.43	1.43
10 hr	1.39	1.40
1 day	1.32	1.35
5 days	1.24	1.31
20 days	1.23	1.25
70 days	1.26	1.27
150 days	1.26	1.27
1 year	1.34	1.37

et al., 1968). On the assumption that the γ-radiation intensity drops according to a power law, analogous to that of the total β-activity decrease, this change can be represented by:

$$\frac{I}{I_0} = \left(\frac{T_0}{T}\right)^n. \tag{1.17}$$

Assuming $T_0 = 1$ hr, one can determine the index n for different ages. Table 1.2 presents the values of n for both fission types.

In the presence of large quantities of a volatile component and following the resulting fractionation, the experimental curves and the value of n in Eq. (1.17) can differ significantly from those shown here, especially for fission products of age up to 10–20 days. Variations in the ratio of volatile to bound components for the iodine isotopes (^{134}I, ^{135}I, ^{133}I and ^{131}I), for example, can exert a substantial influence on the character of the curves and the index n. (It follows from Fig. 1.7b that these isotopes are the dominant radionuclides in the fission debris mixture during the early period from the first hour up to 10 days.)

On the basis of tables found in Grechushkina (1964), the numerical intensity of γ-quanta was calculated as a function of time and expressed as the number of quanta per second per kt fission (Table 1.3). This relationship is similar in form to that for the energy intensity:

$$\frac{N_\gamma}{N_{\gamma_0}} = \left(\frac{T_0}{T}\right)^n. \tag{1.18}$$

The index in Eqs. (1.16), (1.17) and (1.18) depends weakly on whether it is the temporal variation in total β-activity or the numerical and energy intensity of the γ-radiation from the fission debris mixture that is under consideration.

Such values as the average energy of γ-quanta, E_{av} (MeV per quantum), the mean quantum yield v (the number of quanta per decay), the mean γ-radiation yield (MeV/decay), corresponding to the total quantity of fission debris for a given age, are frequently needed in calculations. Figure 1.8 shows the time variations in the mean energy (MeV/decay) and the average quantum yield (quanta/decay) for two fission types $^{235}U_{n_{fis}}$

Table 1.3
The relationship between numerical intensity of γ-radiation from fission debris nuclide mixture and its age, quantum/(s kt)

Mixture age	$^{239}Pu_{n_{fis}}$	$^{235}U_{n_{fis}}$
1 hr	1.9×10^{19}	1.7×10^{19}
2 hr	7.63×10^{18}	6.93×10^{18}
5 hr	2.05×10^{18}	1.82×10^{18}
10 hr	9.36×10^{17}	8.81×10^{17}
1 day	4.08×10^{17}	4.05×10^{17}
2 days	1.83×10^{17}	1.97×10^{17}
5 days	6.7×10^{16}	8.3×10^{16}
10 days	3.01×10^{16}	3.37×10^{16}
20 days	1.2×10^{16}	1.22×10^{16}
30 days	6.94×10^{15}	6.81×10^{15}
70 days	2.23×10^{15}	2.16×10^{15}
150 days	8.22×10^{14}	7.75×10^{14}
1 year	1.1×10^{14}	1.29×10^{14}
1.5 year	3.4×10^{13}	5.71×10^{13}
2 years	1.87×10^{13}	3.69×10^{13}
3 years	1.06×10^{13}	2.06×10^{13}
5 years	7.87×10^{12}	9.15×10^{12}
10 years	4.39×10^{12}	4.58×10^{12}
15 years	3.82×10^{12}	3.82×10^{12}
30 years	2.68×10^{12}	2.66×10^{12}

(curve 1) and $^{239}Pu_{n_{fis}}$ (curve 2). It should be noted that these values were calculated taking into account only those nuclides for which the decay schemes are known for mixtures of all ages. It can be seen in Fig. 1.8 that the mean energy of the γ-radiation from the fission product mixture does not exceed 0.9 MeV/decay (reaching a maximum value of 0.9 MeV 2 hours after fission). It reaches minima of about 0.4 MeV after 2–5 days and 2–3 years. The deviations in the time–mean energy relationship were essentially insignificant for the two types of fission.

The mean quantum yield of the mixture varies with age more widely: thus at $T = 1$ hr it is equal to nearly 1.25, with about 0.2 quantum/decay for an age of about 2 years.

In addition to the overall characteristics of the fission debris mixture, we have calculated the differential γ-spectra (the so-called line spectra) for ^{238}U fission by neutrons of energy 14 MeV (Izrael and Stukin, 1967). The chosen age range was from 2 days to 1 year. A choice of the fission reaction ($^{238}U_{n_{14\,MeV}}$) for the calculations was related to the fact that the probability of symmetrical fission drastically increases at a neutron energy of 14 MeV. The nuclides whose lines appear in the line spectra during the fission reaction ($^{238}U_{n_{14\,MeV}}$) will thus not be present significantly in the spectra of other fission reactions. As an illustration, Fig. 1.9 shows the calculated spectra for $t = 30$ days. They are presented for two energy ranges: (1) from 0 to 400 keV (the second range is "soft") and (2) from 0 to 2000 keV (the 1st range is "hard"). The chosen ranges correspond approximately to those where the fission debris spectra are under experimental investigation.

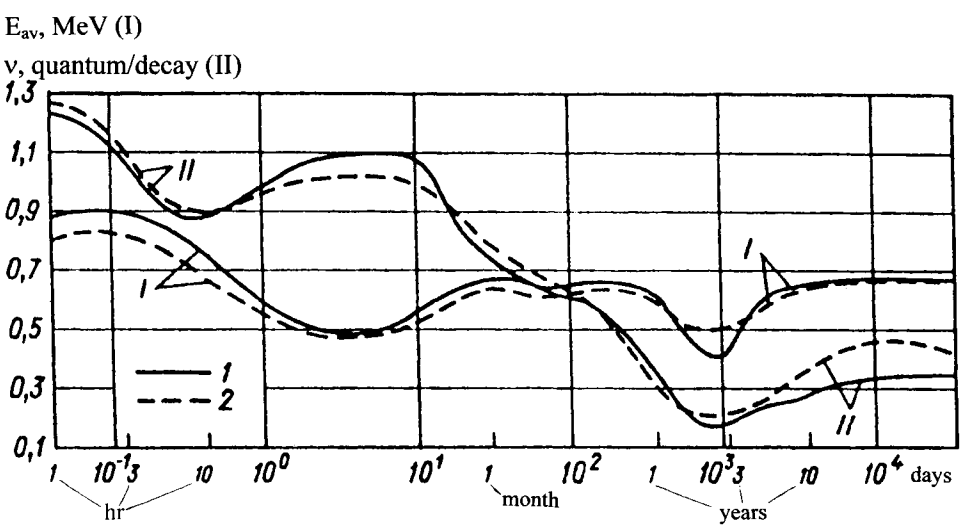

Fig. 1.8. Time-dependence of the mean energy E_{av} and the mean quantum yield v for fission product γ-radiation for two fission types: $^{235}U_{n_{fis}}$ (I) and $^{239}Pu_{n_{fis}}$ (II).

Up to the present, we have dealt only with the fission debris from a nuclear explosion. During an explosion, however (especially a thermonuclear one), a considerable amount of activity can originate from the interactions between the neutrons and the environmental materials around and the construction materials in the bomb. In these situations, the induced activity depends on the flux of released neutrons, the respective compositions of the immediate environment and the bomb construction materials, as well as on the energy fluxes and spatial distribution of the neutrons. Thus the radionuclides produced in these ways can be subdivided into three groups, i.e., those resulting from the interactions of neutrons from the explosion:

1. With elements of the charge itself;
2. With elements used in the construction of the bomb;
3. That escape from the bomb with environmental elements from the air, water, ground, etc.

Among the main nuclides of the first group are ^{239}Np ($T_{1/2}$ = 23 days) and ^{237}U ($T_{1/2}$ = 6.7 days) (Mather, 1956; Lapp, 1959). ^{239}Np, with a γ-radiation line of 106 keV, is formed according to the reactions

$$^{238}U(n, \gamma)^{239}U, \tag{1.19}$$

$$^{239}U \rightarrow ^{239}Np + \beta^{-}. \tag{1.20}$$

^{237}U, with a mean energy γ-radiation line of about 0.1 MeV, is formed through ^{238}U

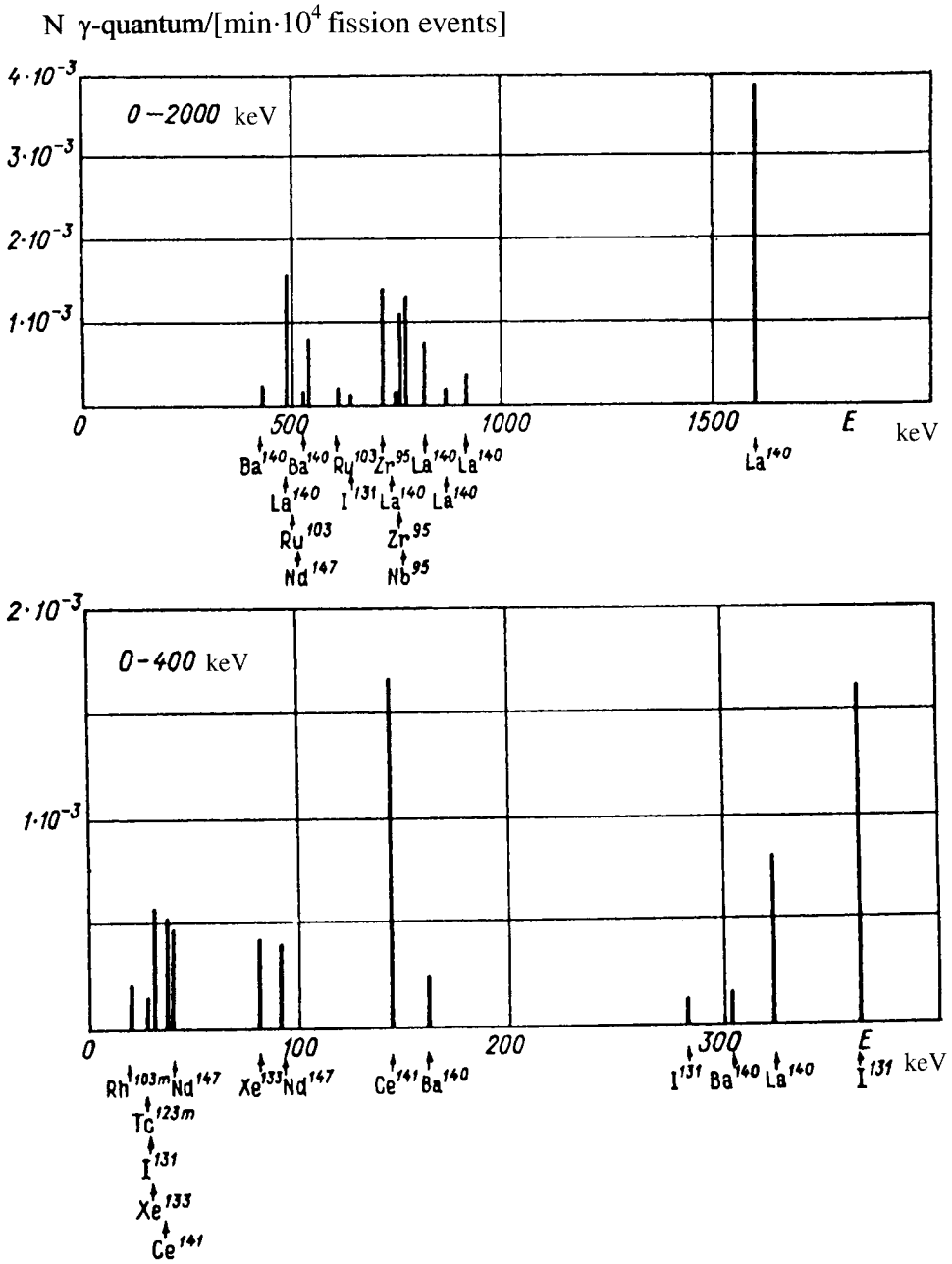

Fig. 1.9. Line spectrum of γ-radiation from a 30-day-old fission product mixture (within the ranges 0–2000 and 0–400 keV).

bombardment by high energy neutrons according to the reaction

$$^{238}U(n, 2n)^{237}U \tag{1.21}$$

(the reaction threshold is about 5.9 MeV (Arnold, 1958)).

It follows from these reactions (1.19)–(1.21) that the presence of ^{238}U included in the charge is a necessary precondition for the appearance of ^{239}Np and ^{237}U in the explosion products. Thus, in the explosion of an atomic bomb containing a ^{235}U–^{238}U mixture, some ^{239}Np can be generated. The ^{237}U isotope, however, appears only in negligible amounts because of the high reaction threshold (1.21). In a thermonuclear bomb, many more neutrons are released per unit of energy than in an atomic bomb explosion (Yampolsky, 1961; Emeljanov, 1958). Hence, a greater amount of induced radioactivity is generated by the neutron flux. Elements with higher atomic number can thus appear in such a bomb as a result of the effects of the powerful high-energy neutron flux on fissionable materials (Chiorso et al., 1955; Izrael et al., 1996; Cameron, 1959). If ^{238}U is added to the bomb case to intensify the explosive yield (the "fission–fusion–fission" bomb), larger amounts of ^{239}Np and ^{237}U are formed (Lapp, 1959). The ^{239}Np content (by activity) in the radioactive products of such a weapon can reach as much as 50–65% of the total activity at 3–4 days after the explosion (Lapp, 1959).

The presence of the radionuclide ^{237}U amongst the explosion products uniquely determines the occurrence of a thermonuclear reaction, because this isotope is formed from ^{238}U according to the above reaction (1.21), of threshold about 5.9 MeV. The presence of ^{237}U in the products of the explosion was first mentioned in early publications (Nishiwaki, 1954) that described the results of radiochemical and radiometric analyses of particles deposited on Japanese fishing vessels (so-called "Bikini ash") after the "Bravo" explosion at Bikini Atoll on 1 March, 1954.

The presence of considerable amounts of the radioactive nuclides ^{239}Np and ^{237}U in the explosion products of the "fission–fusion–fission" type bomb distinguishes them from those of the simple fission debris mixture ($^{235}U_{n_{therm}}$). Izrael et al. (1994) have analyzed in detail the possible formation of different transuranic radionuclides (including plutonium isotopes) and their occurrence in radioactive fallout as a result of thermonuclear explosions. Special attention was given to the long-lived radionuclide ^{241}Am that had been detected experimentally in fallout (this nuclide was also found in lesser activities in the central zone after the Chernobyl accident, see Chapter 5).

In an explosion of the "fission–fusion–fission" type, minor amounts of the ^{240}U isotope are formed (Zysin, 1963; US Atomic Energy Congress, 1959). In this case, the ^{238}U nucleus has to capture two neutrons. Other transuranium elements are formed in negligible amounts, e.g., ^{255}Es and ^{255}Fm (Chiorso et al., 1955; Cameron, 1959). In this situation, the ^{238}U nucleus has to capture 17 neutrons. According to the available publications (Telegadas, 1959; EC, 1963; Hardy et al., 1964; US Atomic Energy Congress, 1959), all the weapons of high yield that were detonated prior to 1958 were based on the "fission–fusion–fission" reaction. No "pure" thermonuclear bombs of high yield were mentioned for this period. Estimates of the ratio between the fission product yields of the "fission–fusion–fission" weapons and the atomic bombs (per unit of power) were 0.5, 0.66 and 0.8 (Dunning, 1959; Lapp, 1959).

According to Yampolsky (1961), the total yield for all nuclear weapons exploded during the period from 1945 to 1958 was equal to approximately 170 Mt with nearly 92 Mt of this total being attributable to fission. The ratio fission yield/total yield can therefore be taken to be about 0.5 for the explosions of this period. The total yield of nuclear weapons tested during the period 1959–1962 was 510 Mt, 190 Mt of which was attributable to fission reactions. Thus the above-mentioned coefficient decreased to about 0.37 (US Atomic Energy Congress, 1959; Hardy et al., 1964). There are some data that suggest that in 1961, during the period when the USSR conducted very large tests, this coefficient was further reduced to 0.04.

The induced activity resulting from the interaction between neutrons and the construction elements of a bomb can be relatively large. In addition, it is obvious that the neutron flux inside a bomb is sufficient, especially in a thermonuclear explosion, that the (n, 2n) reaction with its relatively high threshold can contribute significantly. Investigators have obtained extensive data on the induced activities which can be attributed to this second group of interactions. The induced nuclides include: ^{60}Co (Cameron, 1959; Nishiwaki, 1954; US Atomic Energy Congress, 1959; Mamuro and Matsumani 1965; Salter, 1965; Krieger and Groche, 1960; Krieger, 1965; Strom et al., 1958; Weiss and Shipman, 1957); ^{57}Co, ^{58}Co (Strom et.al., 1958); ^{59}Fe (Batzel, 1960; Japan Society for the Promotion of Science, 1956); ^{55}Fe (US Atomic Energy Congress, 1959); ^{54}Mn (Essington et al., 1965; Batzel, 1960; Mamuro and Matsunami, 1965; Gaglione and Ravera, 1964; Gustafson, et al., 1964; Johnson et al., 1966); ^{65}Zn (Krieger and Groche, 1960; US Atomic Energy Congress, 1959); ^{88}Y (Essington et al., 1965); ^{185}W, ^{181}W, ^{187}W, ^{188}Re (Lane, 1962; Essington et al., 1965; Godt, 1961; Kurchatov et al., 1962; Kauranen, 1964) and two isomers of ^{102}Rh (Essington et al., 1965; Gustafson et al., 1964; Kalkstein, 1962; UNSCEAR, 1962; Yunge, 1965), as well as ^{152}Eu and ^{154}Eu which result from a fission reaction and the interaction between neutrons and soil elements (Izrael et al., 1994b). W and Rh isotopes were formed as a result of the activation of elements specifically introduced into the bomb casing during the series of American explosions named "Hardtack". They were used, probably, as tracers to identify the products of individual explosions. There is also mention of the use of the nuclides ^{124}Sb, ^{109}Cd and ^{113m}Cd as tracers (Salter, 1965; Kalkstein et al., 1965). It is also reasonable to expect that ^{58}Ni, ^{62}Ni, ^{93}Nb, ^{165}Ho, ^{191}Ir and the short-lived ^{56}Mn, ^{24}Na, ^{31}Si, ^{28}Al (see Fig. 1.10) are amongst the induced activity products.

The radionuclides resulting from the interaction between the neutrons outside the bomb casing with the environmental elements are considered in the third group. The environment itself can be the air (in atmospheric explosions); construction materials of a tower (for explosions on towers); water (in near-water and underwater explosions); and especially the ground in near-surface, ground-level and underground explosions. When the escaped neutrons interact with atoms of the air, a negligible amount of induced activity is formed, constituting less than 1% of the total fission debris activity at 1–2 hours after the explosion, and composed mainly of the short-lived isotope ^{41}Ar and a small amount of long-lived ^{14}C (Abramovich, 1948; Nydal et al., 1963, 1965).

For explosions conducted near ground or at the sea water surface, the amount of induced activity is greater and is formed as a result of the interaction between the neutrons and the surface elements (ground or water). According to the calculations of Leipunskii et

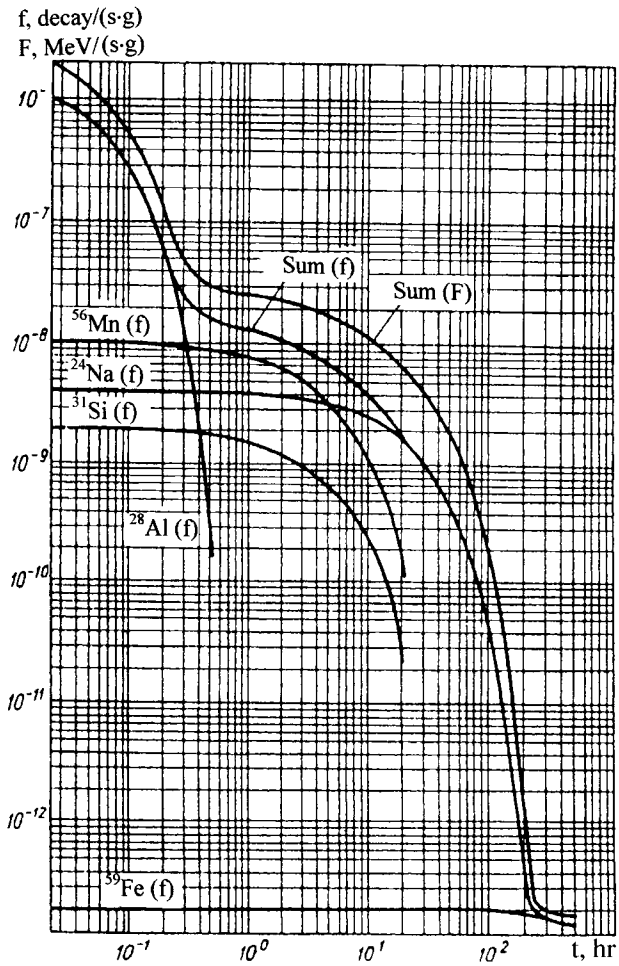

Fig. 1.10. Temporal variations in the induced activities of ground material irradiated by unit neutron flux (n_{therm}).

al. (1959), Batzel (1960) and Nishita (1965), the most important elements in the generation of induced activity in the surface material are: aluminum, silicon, sodium, manganese, iron and cobalt (in the ground); and chlorine, sodium, magnesium and bromine (in sea water).

The induced activity in ground material $A(t)$ [decay/(s cm^3)] at time t after irradiation is described by the relationship:

$$A(t) = \rho\Psi \sum_i \sum_j 10^{-24} \alpha_j N_i \sigma_{aj} \lambda_j e^{-\lambda_j t}, \tag{1.22}$$

the induced γ-activity (the amount of γ-radiation, MeV/(s cm^3) being characterized by a

similar relationship:

$$A_\gamma(t) = \rho\Psi \sum_i \sum_j 10^{-24} \alpha_j N_i \sigma_{aj} E_j \lambda_j e^{-\lambda_j t}. \tag{1.23}$$

Here, ρ is the density of the surface medium, in g/cm^3; Ψ is the flux of neutrons at the activation point for the whole period of irradiation, in neutron/cm^2; α_j is the fraction of the jth isotope in the mixture of the ith element isotopes; N_i is the number of atoms of the ith element in 1 g of the ground material; σ_{aj} is the microscopic cross-section of neutron capture of the jth isotope, in barns; λ_j is the decay constant of the nuclide resulting from the jth isotope activation, s^{-1}; E_j is the total energy of γ-radiation per disintegration of the radioactive nuclide resulting from activation of the jth isotope of the ith element, in MeV/decay. Let us denote f as the activity concentration of 1 g of the ground material (decay/(s g)) that has been irradiated by the neutron flux (neutron/cm^2) for a time t; F is the energy emitted per second as γ-radiation by 1 g of the material irradiated by the neutron flux, in MeV/(s g). Then,

$$f(t) = \frac{A(t)}{\rho\Psi}, \qquad F(t) = \frac{\sigma_\gamma(t)}{\rho\Psi}. \tag{1.24}$$

Figure 1.10 shows the relationships $f(t)$ and $F(t)$ for ground material of average composition for $0.03 \leqslant t \leqslant 500$ hr (by average composition is meant the global average surface soil composition (Garkusha, 1954)). Curves are shown of the time variations of the activities of individual nuclides constituting the major part of the total activity concentration f (for the ground material).

As seen in Fig. 1.10, the induced activity of the ground material (γ-activity) is largely due to the following radionuclides:

^{28}Al	from 0 to 15 min,
^{56}Mn and ^{24}Na	from 15 min to 200 hr,
^{59}Fe	after 300 hr.

At 100–300 days after the explosion, the radionuclide ^{60}Co begins to contribute considerably to the induced activity (Essington et al., 1965; Batzel, 1960). The contribution of different chemical elements varies so much among soil types that the activity concentration f and γ-activity F will differ markedly from those shown in Fig. 1.10 from soil to soil. Table 1.4 presents the chemical composition of the most widespread soil types (Garkusha, 1954).

The second half of Table 1.4 presents the calculated correction factors $k_i(t)$ relative to the data from Fig. 1.10 for different soil types and time intervals, i.e.,

$$k_i(t) = \frac{f_i(t)}{f_{\text{av}}(t)}, \tag{1.25}$$

where $f_i(t)$ corresponds to the ith soil type, and $f_{\text{av}}(t)$ represents the average soil composition. It follows from Table 1.4 that the activity concentration (or γ-activity) values

Table 1.4
Correction factors for determination of induced activity in soils of different types

Soil type	Elemental content (%)				Correction factor		
	Si	Al	Fe	Na	0–15 min	10–200 hr	>200 hr
Chernozem	20.7	8.37	3.16	0.58	1.12	0.22	0.75
Podzolic	32.5	7.93	2.16	1.90	1.06	0.8	0.52
Highly podzolic loam	36.1	4.19	1.93	1.26	0.6	0.53	0.48
Desert–steppe gray soils	27.9	5.92	3.64	1.86	0.8	0.77	0.87
Dark chesnut	30.8	7.88	3.06	0.83	1.06	0.35	0.73
Desert zone	32.0	6.90	2.2	1.3	0.93	0.54	0.52
Tundra					0.18	0.84	
Average composition	26.0	7.45	4.2	2.4	1.0	1.0	1.4

vary slightly between different soil types, on average by not more than a factor of 1.5–2. Other radionuclides can appear in other soils, e.g., ^{45}Ca (in explosions at a coral atoll) and ^{35}S (Nishiwaki, 1954); however, these cases are not typical. Measurements of fallout samples and air samples taken from the near-surface atmosphere confirm the presence of induced activities. In addition to ^{60}Co, ^{59}Fe and ^{55}Fe, belonging to the third group, the nuclides ^{46}Sc (Essington et al., 1965; Krieger, 1965), ^{24}Na (Karlslow, 1964), ^{134}Cs, ^{152}Eu and ^{154}Eu (Izrael et al., 1994b; Krieger, 1965) have been mentioned in various publications. They, too, can be attributed to this group.

It should be mentioned that only a minor fraction of the neutrons absorbed by the ground participate in the activation process. This is determined by the ratio of the sum of effective cross-sections of activation to that of the effective capture cross-sections of neutrons in the soil. For the average elemental content of the earth's crust (for dry soil), this ratio is roughly equal to 0.15 (Leipunsky, 1959); the higher the moisture content, the lower this value.

The salt content in seawater is practically constant all over the globe. In the open ocean it is about 35 g per kg of water (Alekin, 1952); the content of major ions is also relatively uniform. Thus in the oceans there are 10.7 g of Na^+, 1.3 g of Mg^{2+} and 19.3 g of Cl^- per kg of water. Thus, for the early period (during the first 2 hours), ^{38}Cl and ^{24}Na can contribute substantially to the induced activity for a marine explosion.

5. Thermophysical Properties and Radioactive Transformations of Major Explosion Products

To describe the process of transition of evaporated products to the liquid phase and the activation of particle-carriers, it is essential to know the form of the elements/nuclides at the different stages of particle formation, as well as their thermophysical properties. As a rule, it is radioactive fission products that are converted into the nuclides in question following a series of radioactive transformations, the products subsequently falling out on to the surrounding land. Radionuclides belonging to any mass chain (isobars) can thus be transformed into elements with quite different chemical properties:

$$
\begin{array}{l}
\qquad\qquad\qquad\qquad\quad {}_{36}Kr^{88} + n \\
\qquad\qquad\qquad\qquad\quad \nearrow \\
\qquad\qquad\qquad\qquad\quad 2.8\ \text{hr} \\
{}_{35}Br^{89} \xrightarrow[4.4\ \text{s}]{} {}_{36}Kr^{89} \xrightarrow[3.2\ \text{min}]{} {}_{37}Rb^{89} \xrightarrow[15.4\ \text{min}]{} {}_{38}Sr^{89} \xrightarrow[50.5\ \text{day}]{} {}_{39}Y^{89}
\end{array}
\tag{1.26}
$$

As an example, we can see that the first member of this particular chain is a volatile element (bromine), the second is an inert gas (krypton), the third is a relatively volatile element (rubidium) and the fourth is refractory (strontium). If, before solidification of the fused particles, the mass chain cited above were represented in the fireball mainly by krypton-89, it is obvious that strontium-89 would be practically absent inside such particles. Thus, to be able to calculate the radionuclide transformations within the particles of all members of the chains to which the most important radionuclides belong (from the viewpoint of radioactive contamination), it is necessary to have a complete knowledge of the nuclear constants, e.g., independent yields and half-lives, etc. for the mass chains 89–93, 95, 97, 99, 103, 105, 106, 125, 131–133, 135, 137 140, 141, 143, 144, 147, 149 and 151. Radionuclides belonging to these chains contribute the majority of the activity of the mixture of fission debris for the period from 1 day to 10 years after the explosion (Grechushkina, 1964). To obtain the independent yields of individual radionuclides in the chain for which experimental data are not available (they are not available for many radionuclides!), Grechushkina and Izrael (1965) used a method, proposed in a study by Wahl et al. (1962), who assumed that the distribution of independent yields over the chain members as a function of the atomic number (charge) is governed by Gauss' law, viz.,

$$p'(Z) = (c\pi)^{1/2} \exp\left[-\frac{(Z - Z_p)^2}{c}\right], \tag{1.27}$$

where $p'(Z)$ is the independent yield from fission of a nucleus with charge Z (the yield of the whole mass chain is taken to be equal to 1, or 100%); $c \approx 2(\sigma^2 + 1/12)$; σ^2 is the mean square deviation (assumed to be the same for all the chains); $\sigma = 0.62 \pm 0.06$; hence, $c = 0.94 \pm 0.15$; Z_p is some effective value of charge corresponding to the Gauss' curve maximum. Wahl et al. (1962) have published the Z_p values for different members of the chain. On the basis of these Z_p values, the independent yields were calculated for all the chain members of mass numbers shown above. The calculation was carried out using the equation:

$$p'(Z) = 58.2 \exp\left[-\frac{(Z - Z_p)^2}{0.94}\right] \tag{1.28}$$

(if $p'(Z)$ is expressed in %). The values of the independent yields obtained from the calculations agree closely with the known experimental results (Goldstein, 1961). It was also assumed here that the distribution of independent yields over Z in the mass chains, calculated in the case of ^{235}U fission by thermal neutrons, is applicable to fission products resulting from nuclear explosions, i.e., for fission neutrons and neutrons of 14 MeV energy.

Clearly, the absolute values of the independent yields $a(Z)$ will vary for different types of fission, if the accumulated yields "b" are not the same, because

$$a(Z) = bp'(Z). \tag{1.29}$$

Half-life values for individual radionuclides, as given by Zysin et al. (1963), Katcoff (1960) and Stehn (1960), have been used. Table 1.5 presents the mass chains listed above. It shows the mass chain number, Z_p values, the directions of the radioactive transformation (by arrows), the half-life periods for each chain member and the calculated independent yields (in brackets). In addition, the table presents absolute values of the accumulated fission yields for different types of fission. Using these values and Eq. (1.29), it is an easy matter to calculate the absolute values of the independent yields for all the radionuclides and types of fission.

All the chains in Table 1.5 are subdivided into three columns. Column 3 contains radionuclides in the form of volatile elements; column 5 those in the form of refractory elements and column 4 those in an intermediate form. Elements that are certainly not condensed in the fireball at the moment of particle solidification ($T = 1673$ K) were classified as volatile (krypton, xenon, iodine and bromine). Strontium, yttrium, zirconium, niobium, barium, lanthanum, cerium, neodymium, praseodymium and promethium were classified as the refractory elements. Their boiling points are so high that their condensation (or that of their oxides) will certainly be entirely completed at the time of particle solidification. The remaining elements, the boiling points of which (or their oxides) are relatively close to the solidification point of the particles, were conditionally assigned to the intermediate group of elements, e.g., rubidium (Rb_2O), cesium (Cs_2O), molybdenum (MoO_3), rhodium, ruthenium (RuO_4), technetium, antimony, tin (SnO_2) and tellurium (TeO_2). It is assumed that, at a temperature exceeding the solidification point of the particle materials (1673 K), the rubidium occurs in the form of Rb_2O, cesium as Cs_2O, molybdenum as MoO_3, tin as SnO_2 and tellurium as TeO_2. Ruthenium's state in the fireball is unknown although it is known that ruthenium tetroxide decomposes at 106 °C (Zvyagintsev et al., 1965). In calculations we assumed about 10% of the ruthenium was in the RuO_4 form (in so doing, we used experimental data on ^{106}Ru fractionation).

A part $\delta_{liq}(T)$ of the ith element, transformed into a condensed phase at a temperature T in the fireball (if an equilibrium between the liquid and vapor phases exists), can be calculated from the relationship (see Eq. (1.15))

$$\delta_{liq}(T) = \frac{n_i}{n_i + n_i^0} = \left[1 + \frac{P_i^0(T)V_v}{(n_i + n_j)RT}\right]^{-1} \approx \left[1 + \frac{P_i^0(T)V_v}{Tn_jR}\right]^{-1}. \tag{1.30}$$

The amount of condensed explosion products (n_i) is negligible compared to the amount of fused ground/earth (n_j): $n_i + n_j \approx n_j$.

In Eq. (1.30), $P_i^0(T)$ is the saturated vapor pressure of a pure component at temperature T, V_v is the vapor phase volume; n_j is the number of moles of melted ground. Figures 1.3 and 1.11 demonstrate the relationships between $P_i^0(T)/T$ and T, compiled from different studies for a number of the most important elements (Glushko, 1962; Freiling, 1962; Freiling and Kay, 1966; Chirkin, 1968). These relationships are presented

Table 1.5
Mass chains of the main fission products

Number of the mass chain	Z_p	Volatile	Intermediate	Refractory	Accumulated yield		
					$^{235}U_{n_{fis}}$	$^{239}Pu_{n_{fis}}$	$^{238}U_{n\,14\ MeV}$
89	35.42	2.8 hr $^{88}_{36}Kr + n$ ↗ 4.4 s* $^{89}_{35}Br$ (48.2)** ⟶ 3.2 m $^{89}_{36}Kr$ (40.7)	⟶ 15.4 m $^{89}_{37}Rb$ (4.1) ⟶	50.5 d $^{89}_{38}Sr$ (0.05) ⟶ ⟶ stable $^{89}_{39}Y$	4.15	1.44	2.49
90	35.84	3.2 m $^{89}_{36}Kr + n$ ↗ 1.6 s $^{90}_{35}Br$ (27.5) ⟶ 33 s $^{90}_{36}Kr$ (56.7)	⟶ 2.7 m $^{90}_{37}Rb$ (13.9) ⟶	28 y $^{90}_{38}Sr$ (0.41) ⟶	4.38	2.23	2.91
91	36.32	10 s $^{91}_{36}Kr$ (50.5)	⟶ 72 s $^{91}_{37}Rb$ (35.6) ⟶	9.7 hr $^{91}_{38}Sr$ (2.9) → 0.6 → 50 m $^{91m}_{39}Y$ ↓ 9.7 hr $^{91}_{38}Sr$ (2.9) → 0.4 → 57.5 d $^{91}_{39}Y$	5.27	2.69	3.32
92	36.81	3.0 s $^{92}_{36}Kr$ (31.0)	⟶ 5.3 s $^{92}_{37}Rb$ (56) ⟶	2.7 hr $^{92}_{38}Sr$ (1.3) ⟶ ⟶ 3.6 hr $^{92}_{39}Y$ ⟶	5.26	3.21	3.73

Table 1.5 — Continued

Number of the mass chain	Z_p	Volatile	Intermediate	Refractory	Accumulated yield		
					$^{235}U_{n_{fis}}$	$^{239}Pu_{n_{fis}}$	$^{238}U_{n_{14\ MeV}}$
93	37.4	2.2 s $^{93}_{36}Kr$ (7.2)	$\longrightarrow$ 5.6 s $^{93}_{37}Rb$ $\longrightarrow$ (49.1)	7.54 m $^{93}_{38}Sr$ $\longrightarrow$ (39.7) $\longrightarrow$ 10.3 hr $^{93}_{39}Y$ $\longrightarrow$ (4.0) 1.5×10^6 y $^{93}_{40}Zr$	5.38	3.64	4.05
95	38.4	short $^{95}_{36}Kr$ (0.1)	$\longrightarrow$ 2 s $^{95}_{37}Rb$ $\longrightarrow$ (7.2)	40 s $^{95}_{38}Sr$ $\longrightarrow$ (49.1) $\longrightarrow$ 10 m $^{95}_{39}Y$ $\longrightarrow$ (39.7) $\longrightarrow$ 65 d $^{95}_{40}Zr$ $\longrightarrow$ (3.8) $\longrightarrow$ 35 d $^{95}_{41}Nb$ (1.2)	6.72	5.12	4.69
97		short $^{97}_{36}Kr$	$\longrightarrow$ short $^{97}_{37}Rb$ $\longrightarrow$	short $^{97}_{38}Sr$ $\longrightarrow$ $\longrightarrow$ short $^{97}_{39}Y$ $\longrightarrow$ $\longrightarrow$ 17 hr $^{97}_{40}Zr$ (97)	6.51	5.05	5.52
99	39.5		2.1×10^5 y $^{99}_{43}Tc$ $\longleftarrow$ $\longleftarrow$ 66.5 hr $^{99}_{42}Mo$ $\longleftarrow$ (0.2)	2.4 m $^{99}_{41}Nb$ $\longleftarrow$ (5.3) $\longleftarrow$ 33 s $^{99}_{40}Zr$ (44.6)	6.10	5.73	5.81

Table 1.5 — Continued

Number of the mass chain	Z_p	Volatile	Intermediate	Refractory	Accumulated yield		
					$^{235}U_{n_{fis}}$	$^{239}Pu_{n_{fis}}$	$^{238}U_{n_{14\ MeV}}$
102			stable $^{102}_{44}Ru$ ⟵ 206 d $^{102}_{45}Rh$				
103	41.42		stable $^{103}_{45}Rh$ ⟵ ⟵ 57 m $^{103m}_{45}Rh$ (~0) ⟵ 39.4 d $^{103}_{44}Ru$ (0.05) ⟵ 1.2 m $^{103}_{43}Tc$ (4.1)		3.97	6.25	4.89
105	41.8		45 s $^{105m}_{45}Rh$ (0); 4.4 hr $^{105}_{44}Ru$ (0.34) ⟵ 10 m $^{105}_{43}Tc$ (12.6); 36 hr $^{105}_{45}Rh$	⟵ 2 m $^{105}_{42}Mo$ (55.8)	1.02	4.68	3.53
106			stable $^{106}_{46}Pd$ ⟵ 30 s $^{106}_{45}Rh$ ⟵ ⟵ 1.01 y $^{106}_{44}Ru$		0.47	6.17	3.11
125	49.5		stable $^{125}_{52}Te$ ⟵ 58 d $^{125m}_{52}Te$; 2.0 y $^{125}_{51}Sb$ (5.3); 9.4 m $^{125}_{50}Sn$; 9.7 d $^{125m}_{50}Sn$ (44.6)		0.123	0.257	1.00

Table 1.5 — Continued

Number of the mass chain	Z_p	Volatile	Intermediate	Refractory	Accumulated yield		
					$^{235}U_{n_{fis}}$	$^{239}Pu_{n_{fis}}$	$^{238}U_{n_{14\ MeV}}$
131	50.77	← 8.05 d $^{131}_{53}$I (0.3)	30 hr $^{131m}_{52}$Te; 0.8 → 25 m $^{131}_{52}$Te (11.6); 23 m $^{131}_{51}$Sb (55) ← 3.4 m $^{131}_{50}$Sn (31)		3.11	4.85	4.26
132	51.26	stable $^{132}_{54}$Xe (~0) ← 2.3 hr $^{132}_{53}$I (2.3) ←	77 hr $^{132}_{52}$Te (32.5) ← 2.1 m $^{132}_{51}$Sb (54.2) ← 2.2 m $^{132}_{50}$Sn (10.8) ←		4.44	6.32	4.89
133	51.46	← 5.27 d $^{133}_{54}$Xe (~0) ← 20.8 hr $^{133}_{53}$I (4.7) ←	63 m $^{133m}_{52}$Te → 2 m $^{133}_{52}$Te (42.7); 4.1 m $^{133}_{51}$Sb (46.2)		1.76	1.81	0.31
135	52.4	15.3 m $^{135m}_{54}$Xe; 6.7 hr $^{135}_{53}$I (39.7) ←; → 9.2 hr $^{135}_{54}$Xe (4.0)	24 s $^{135}_{52}$Te (49.1) ← 24 s $^{135}_{51}$Sb (7.2)				

Table 1.5 — Continued

Number of the mass chain	Z_p	Volatile	Intermediate	Refractory	Accumulated yield		
					$^{235}U_{n_{fis}}$	$^{239}Pu_{n_{fis}}$	$^{238}U_{n_{14\ MeV}}$
136			12.9 d $^{136}_{55}Cs$ (100) $\longrightarrow$	stable $^{136}_{56}Ba$	6.2×10^{-3}	0.083	
		stable $^{136}_{54}Xe$ (48) $\longleftarrow$ 86 s $^{136}_{53}I$ (52)	13 d $^{136}_{55}Cs \longrightarrow$	stable $^{136}_{56}Ba$	6.44	6.65	
137	53.26	$^{138}_{54}Xe + n$ ↗ 24.4 s $^{137}_{53}I$ (54.2) $\longrightarrow$ 3.9 m $^{137}_{54}Xe$ (32.5) $\longrightarrow$	30 y $^{137}_{55}Cs$ (2.32) ↘ ↗	2.3 m $^{137m}_{56}Ba$ ↓ stable $^{137}_{56}Ba$	6.18	6.14	5.71
140	54.34	1.5 s $^{140}_{53}I$ (8.5) $\longrightarrow$ 16 s $^{140}_{54}Xe$ (51.5)	$\longrightarrow$ 66 s $^{140}_{55}Cs$ (36.6) $\longrightarrow$	12 d $^{140}_{56}Ba$ (3.1) $\longrightarrow$ 40.2 hr $^{140}_{57}La$ (0.3) $\longrightarrow$	5.79	4. 95	4.69
141	54.97	1.7 s $^{141}_{54}Xe$ (21.4)	$\longrightarrow$ 25 s $^{141}_{55}Cs$ (58.2)	18 m $^{141}_{56}Ba$ (18.8) $\longrightarrow$ 3.7 hr $^{141}_{57}La$ (0.73) $\longrightarrow$ 33 d $^{141}_{58}Ce \longrightarrow$	5.29	4.65	4.45
143	55.92	1 s $^{143}_{54}Xe$ (1.2)	$\longrightarrow$ 1 s $^{143}_{55}Cs \longrightarrow$ (23.7)	13 s $^{143}_{56}Ba$ (55) $\longrightarrow$ 19 m $^{143}_{57}La$ (16) $\longrightarrow$ 33 hr $^{143}_{58}Ce$ (3.0) $\longrightarrow$ 13.7 d $^{143}_{59}Pr \longrightarrow$ (1.0)	5.18	4.85	3.74

Table 1.5 — Continued

Number of the mass chain	Z_p	Volatile	Intermediate	Refractory	Accumulated yield		
					$^{235}U_{n_{fis}}$	$^{239}Pu_{n_{fis}}$	$^{238}U_{n_{14\ MeV}}$
144	56.40	short $^{144}_{54}Xe$ (0.2)	$\longrightarrow$ 1.5 s $^{144}_{55}Cs$ $\longrightarrow$ (2.7)	3.5 s $^{144}_{56}Ba$ $\longrightarrow$ (49.1)	4.76	3.66	3.32
				$\longrightarrow$ 15 s $^{144}_{57}La$ $\longrightarrow$ (39.7)			
				$\longrightarrow$ 290 d $^{144}_{58}Ce$ $\longrightarrow$ (3.8)			
147				2.64 y $^{147}_{61}Pm$ $\longleftarrow$	3.24	2.52	2.07
				$\longleftarrow$ 11.3 d $^{147}_{60}Nd$ $\longleftarrow$			
				$\longleftarrow$ 12 m $^{147}_{59}Pr$ $\longleftarrow$			
				$\longleftarrow$ 1.2 m $^{147}_{58}Ce$ $\longleftarrow$			
149				$\longleftarrow$ 54 hr $^{149}_{61}Pm$ $\longleftarrow$ (13)	1.17	1.88	1.32
				$\longleftarrow$ 2 hr $^{149}_{60}Nd$ (87)			
151				$\longleftarrow$ 93 y $^{151}_{62}Sm$ $\longleftarrow$	0.46	1.29	0.83
				$\longleftarrow$ 27.5 hr $^{151}_{61}Pm$ $\longleftarrow$ (10)			
				$\longleftarrow$ 12 m $^{151}_{60}Nd$ (90)			

*Half-life.

**Calculated independent yield.

s — second, m — minute, hr — hour, d — day, y — year.

Note: This table includes the mass chains of the fission products that contain the most important radionuclides (from the viewpoint of radioactive contamination of the environment). In addition, the isobars are shown in each mass chain as they allow better understanding of the transformations and behaviour of these radionuclides in the biosphere.

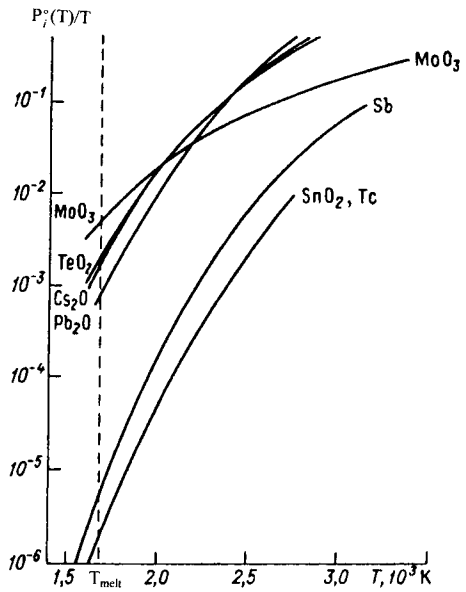

Fig. 1.11. Relationship between saturated vapor pressure $P_i^0(T)/T$ and T for the intermediate group elements.

for both the elements and their oxides (it is assumed that the elements will occur as oxides (although other compounds are possible, e.g., with nitrogen) in atmospheric explosions if they do not decompose at the given temperature).

It is assumed that, under the conditions of thermodynamic equilibrium in the fireball, the molten and condensed phases are the unified phase that is in equilibrium with the vapor phase. The vapor phase, like the condensed part, consists of a mixture of rocks, construction materials that formed the nuclear charge and radioactive explosion products. It is also assumed that the vapor phase is an ideal gas mixture and that the molten soil does not enter into chemical reactions with products of the explosion.

6. Activation of Particles

Activation of particles starts in the fireball or the nuclear explosion cloud either when particle nuclei are formed in the atmospheric explosion or when the most refractory nuclides are condensed on liquid particles of the ground/earth-derived materials that have been incorporated into the fireball. The first stage of activation is completed by the time of particle solidification. At this stage, the nuclides penetrate the particles and spread within. In the second stage (from the moment of solidification to the fallout of particles from the cloud), the nuclides are distributed on the surfaces of particles. Rotblat (1955) has shown that in any explosion a uniform distribution of each nuclide is observed on the particle surfaces despite their sizes. This fact has been proven in our model experiments (Izrael et al., 1968).

Activation of particles by refractory nuclides (zirconium, lanthanum, yttrium, strontium, etc.) occurs at temperatures above that of the boiling ground/earth-derived matter (2500–3000 °C), i.e., under conditions far from equilibrium (at normal pressure, the temperature of the particles cannot exceed the boiling point of the material). Under such conditions, condensation is fast and it can be assumed that the condensation factor is close to unity. At temperatures between 2500 and 1400 °C (from the boiling point to the ground particle solidification temperature) during the condensation, thermodynamic equilibrium is possible (or conditions close to equilibrium, as was shown in Section 1.5) between liquid (particle) and gaseous (evaporated ground and explosion product) phases. The condensation factor can essentially differ from unity for the temperature range indicated. When equilibrium is achieved, the ratio between the ith nuclide atoms in the gaseous and liquid phases is controlled by the saturated vapor pressure in the given volume at the given temperature and pressure.

In atmospheric explosions, the processes of coagulation (Stewart, 1956) and agglomeration (Lavrenchik, 1965; Adams et al., 1960) can become significant for the formation and activation of particles. However, in ground explosions, they are of much less importance because the assumption can be made that the overwhelming majority of particles results from direct condensation of gaseous products on the huge number of ground particles that are involved in the fireball. Let us consider a nominal (20 kt) ground explosion as an illustration. According to the saturated vapor pressure and the fireball temperature, the condensation of evaporated ground will take place within the 0.8–2.6 s time interval and will be most intense in the range 1.2–1.8 s (3500–4100 K), assuming that the vapor phase occupies a volume of 0.05 of the fireball. If this volume exceeds 0.05 of the fireball, the temperature interval will be shifted toward lower temperatures. This matter can either be condensed on the incorporated inert material (the surface area of the melted particles of the disintegrated (crushed) ground will be about 4×10^{12} cm^2 in the nominal explosion) or form condensation nuclei with radius $r = r_m \sqrt[3]{t}$, where r_m is the median size (for a nominal air explosion this is 10^{-5} cm (Stewart, 1956)). At this particle size, for $t = 10^{-2}$ s, $r = 2 \times 10^{-6}$ cm, the SiO_2 vapor partial pressure above, taking into account the Thomson effect, will be equal to 1.10 (the surface tension coefficient being 10^{-1} N/m (100 din/cm) for SiO_2 (Stewart, 1956)). This effect will hamper condensation on small particles, causing a lag or delay of 0.05–0.1 s that is compensated for by the prolongation of condensation on to larger particles due to thermal inertia (0.1 s). The surface area of small particles originating in the first-hundredth of a second is equal to about 10^9 cm^2, i.e., less than 0.1% of the total surface area of the incorporated particles (in the ground explosion).

Radioactive product condensation, even if it continues during the period when condensation nuclei have been formed but not yet captured by larger particles, occurs mainly on the particles of incorporated material. Supposing that, for the first second (when about a half of the evaporated ground/earth is condensed), half of the condensation nuclei will be preserved and their size will grow to 2×10^{-5} cm, their total surface area will increase but the flux of molecules condensing on to the small particles will constitute no more than 30% of the total flux.

Although the time for particle activation is rather long (greater than several tenths of a second), almost the same concentration of condensation products has had time to be incorporated in the small particles and in the upper layers of the large particles. Apparently,

the volume of small particles (weighing about 0.1 t per kt explosion yield) is much smaller than the volume of the upper layers of large particles, where the diffusion of molecules of explosion products has occurred. If the depth of the molecular penetration is assumed to be $\xi = 10$ μm (see Section 1.5), the upper layer volume will be larger by nearly three orders of magnitude than that of the small particles and the fraction of the nuclides condensed on the particles formed (10^{-5} cm) will be substantially less than 1% of the total amount.

Let us consider a possible scheme for activation of particles.[1] In this scheme, the following assumptions are made:

- Changes in the fireball temperature are governed by the regime described in Section 1.2; the temperature within the fireball is uniform;
- The pressure in the fireball is 1 atm;
- The period to achieve the particle solidification temperature is controlled by the temperature regime of the fireball, taking into account the inertial effects described above;
- The distribution of radioactive products (the vapor phase) and incorporated inert material is uniform within the fireball (either over the whole volume or over a fraction constituting 20% of its volume);
- The maximum radius (in m) is $89\sqrt[3]{W}$ for a fireball in an atmospheric explosion and $89\sqrt[3]{2W}$ for a fireball in a ground level explosion (Izrael, 1973); their volumes are the same because the fireball from a ground explosion is hemispherical, the radius indicated corresponding to the time of solidification of particles;
- The amount of ground melted in a ground-level explosion and coming into contact with the radioactivity is about 200 t per kt of explosive yield (Glesston, 1966; Freiling, 1962);
- The distribution of the total mass (and, consequently, of volume and area) as well as the activity according to the sizes of melted (and then solidified) particles is described by a log-normal relationship;
- Most of the elements are present as oxides in the fireball, excluding those whose oxides are decomposed (or cannot be formed) at such temperatures;
- The ground is an ideal carrier and does not enter into chemical reactions with the explosion products (Freiling, 1962);
- The maximum amount of ground evaporated in a ground level explosion is half of that evaporated by an underground explosion, i.e., 25 t per kt yield;
- All radioactive explosion products are initially present in the evaporated state in the fireball.

In developing the scheme of particle activation, two main problems need to be solved:

(i) Which radioactive nuclides will be involved in the activation at the first stage (before particle solidification) and which at the next stage and to what extent?
(ii) How are the different radionuclides distributed over the volumes and on the surfaces of particles of various sizes?

[1] The scheme of particle activation fractionation presented here was developed by the author in 1965 (Izrael, 1965).

Before arriving at a solution to the second question, a comprehensive answer to the first is required. To calculate roughly the amount of a radionuclide penetrating the particles (the fraction of the nuclides belonging to the ith mass chain and penetrating the particles is denoted as F_i (the analogous value for an individual nuclide being F_{Zi}), we can assume that all isotopes of the elements with boiling temperatures T_b higher than the melting temperature of the ground T_l, can penetrate the particles. The concept of this calculation was presented by the author (Izrael, 1965), while some data are given in (Grechushkina and Izrael, 1965). More detailed results were published in 1973 (Izrael, 1973). Such an approach is valid for isotopes of elements for which $T_b \gg T_l$.

It is the straightforward to obtain F_{Zi} values for different elements using Eq. (1.30) and assuming that:

$$F_{Zi} = \delta_l^Z(T_l). \tag{1.31}$$

Clearly then,

$$F_i(T_l) = \sum_Z p_i(Z, T_l) F_{Zi}(T_l), \tag{1.32}$$

where $p_i(Z, T_l)$ is the isobar share in nuclei with atomic number Z in the ith mass chain for the particular isobar at the time of particle solidification (at temperature T_l). The time when particle solidification happens can be derived from the curves of the fireball temperature decrease taking into account inertial effects; $p_i'(Z, t)$—see formula (1.28). $p_i(Z, t)$ can be calculated using the following equations:

$$p_i(Z, t) = p_i'(Z)\mathrm{e}^{-\lambda_Z t},$$

$$p_i(Z+1, t) = p_i'(Z)\lambda_Z\left(\frac{\mathrm{e}^{-\lambda_Z t}}{\lambda_{Z+1} - \lambda_Z} + \frac{\mathrm{e}^{-\lambda_{Z+1} t}}{\lambda_Z - \lambda_{Z+1}}\right) + p_i'(Z+1)\mathrm{e}^{-\lambda_{Z+1} t}. \tag{1.33}$$

Figure 1.12(a–d) presents changes in $p_i(Z, t)$ for nuclides of the most important mass chains belonging to the intermediate, refractory and volatile groups. The figure shows curves for each intermediate nuclide and, in the case of the refractory species, the curve reflects their sum but is indicated by one of the most important or well-known nuclides. Figure 1.12d shows $p_i(Z, t)$ for the volatile nuclides including those whose precursors were refractory or intermediate species; the curves are given for the sum of the volatile nuclides.

Table 1.6 presents F_{Zi} values (at $T_l = 1673$ K) calculated assuming that, at the time of particle solidification, the vapor phase volume occupied either the whole fireball volume ($\varepsilon = V_v/V_{fb} = 1$) or 0.5, 0.2 or 0.1 of its space.

Figure 1.13 shows the relationships $F_i(t)$ for different chains (when $\varepsilon = 1$). Calculations of $F_i(t)$ values (when $\varepsilon = 0.2$) show that the values are quite similar for all chains except for those with numbers 89, 90 and 137.

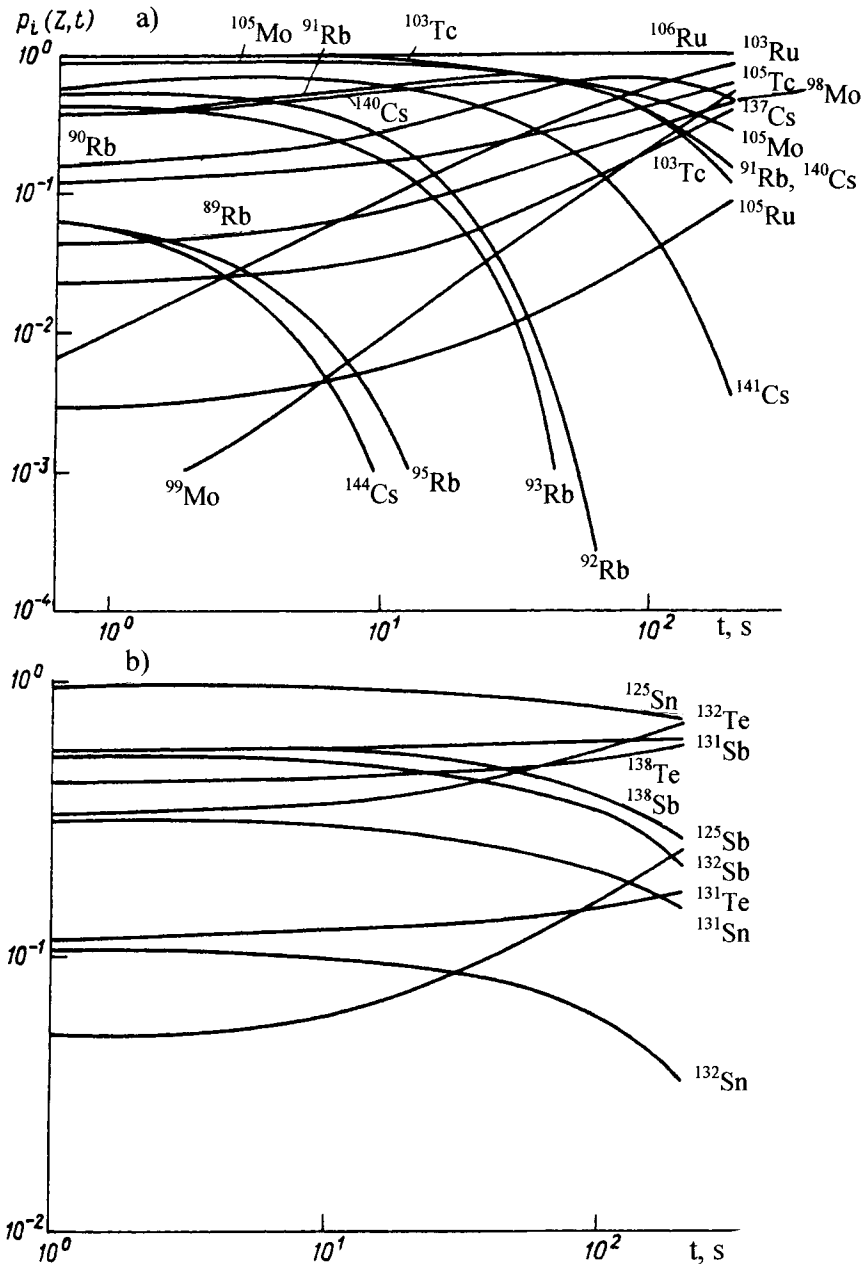

Fig. 1.12. Change in $p_i(Z,t)$ for the intermediate (a, b) elements.

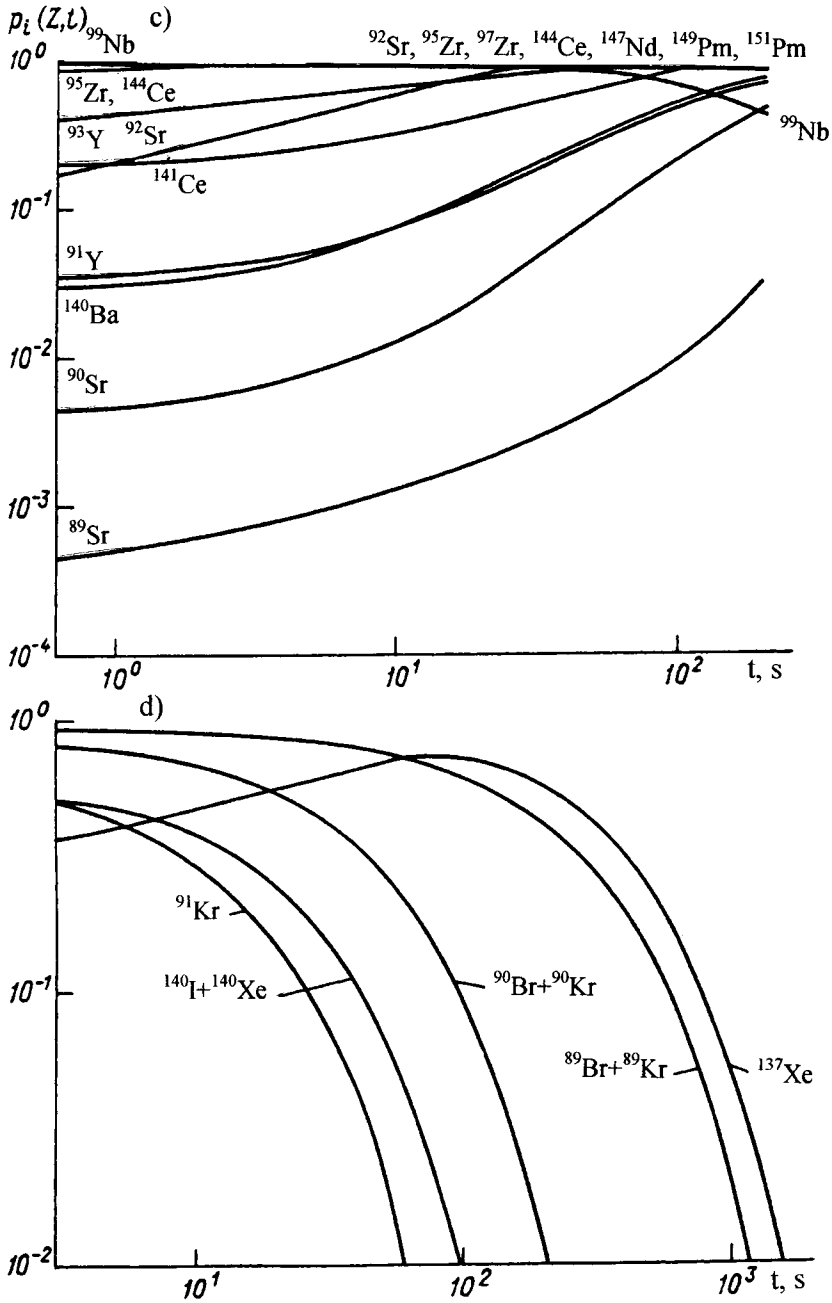

Fig. 1.12 (Continued) Change in $p_i(Z,t)$ for the refractory (c) and volatile (d) elements.

Table 1.6
F_{Z_i} values (%) for nuclides in the form of different elements and different volumes of the vapor phase

ε	MoO_3	TeO_2	Cs_2O	Rb_2O	Sb	SnO_2, Te
1.0	1.82	4.4	5.5	11.3	94.9	98.2
0.5	3.6	8.6	10.4	20.4	97	99
0.2	8.5	19	21.6	39	99	99.6
0.1	15.7	31.9	36.9	56.2	100	100

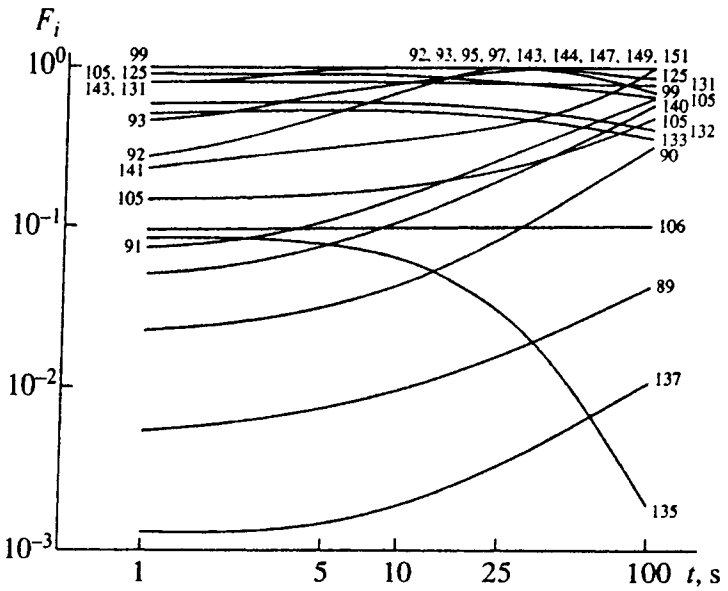

Fig. 1.13. Time-change in the fraction of the ith mass chain nuclei, transformed into SiO_2 condensed phase.

Additionally,

$$F_i(t) = \frac{Q_i^{\mathrm{v}}(t)}{Q_i(t)}, \tag{1.34}$$

i.e., the ratio between the activity of the ith nuclide penetrating the particle and the total activity of this nuclide at time t.

Fractionation effects are proportional to $\sqrt{F_i}$ and are shown in the relationship between $\sqrt{F_i}$ and t in Fig. 1.14.

To conduct detailed calculations of the fractionation effect, one should know the fraction of the total activity of radionuclides that penetrates the particles (or the γ-activity for different time periods). The fraction of the total activity is determined by the formula:

$$\eta(t, t_1) = \frac{\sum_k Y_k \lambda_k \mathrm{e}^{-\lambda_k t} F_k(t_1)}{\sum_k Y_k \lambda_k \mathrm{e}^{-\lambda_k t}}. \tag{1.35}$$

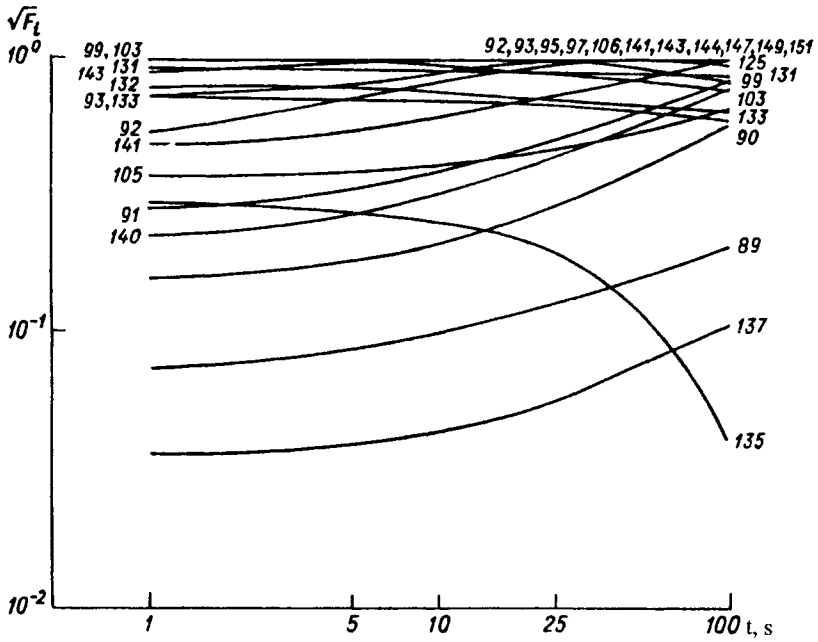

Fig. 1.14. The time-dependence of $\sqrt{F_i}$.

The γ-activity contribution is

$$\eta_\gamma(t, t_1) = \frac{\sum_k \sum_Z Y_k \lambda_k e^{-\lambda_k t} p_i(Z, t_1) F_{Zi}(t_1) E_{Zk}}{\sum_k \sum_Z Y_k \lambda_k e^{-\lambda_k t} p_i(Z, t_1) E_{Zk}}, \tag{1.36}$$

where E_{Zk} is the γ-radiation intensity of decay for each isotope (Z) in the kth mass chain, MeV/decay; Y_k is the yield of the given chain from fission; λ_k is the decay constant.

Figure 1.15 shows the relationships between values of $\eta(t, t_1)$, $\eta_\gamma(t, t_1)$ and t_1 in different types of fission: ^{235}U, n_{fis} (curve I); ^{239}Pu, n_{fis} (curve II), and ^{238}U, $n_{14\,MeV}$ (curve III) at t equal to 1 and 10 days after the explosion and ε equal to 1 and 0.2.

An estimate of the distribution of refractory and intermediate nuclides by particle volumes and those of intermediate and volatile nuclides by surfaces (at the second stage of activation) can be made as follows. Initially, we consider the activation of particles under conditions far removed from equilibrium. It is known from kinetic theory (Lavrenchik, 1965) that the number of ith element molecules occupying a unit area of any surface in unit time is defined by the expression:

$$J_i = \frac{n_i \bar{v}_i}{4}, \tag{1.37}$$

where $\bar{v}_i$ is the mean velocity of the molecules, equal to $\sqrt{8kT/(\pi m_i)}$; n_i is the concentration of molecules; m_i is their mass. Note, e.g., that in the fireball ($T = 2000$ K),

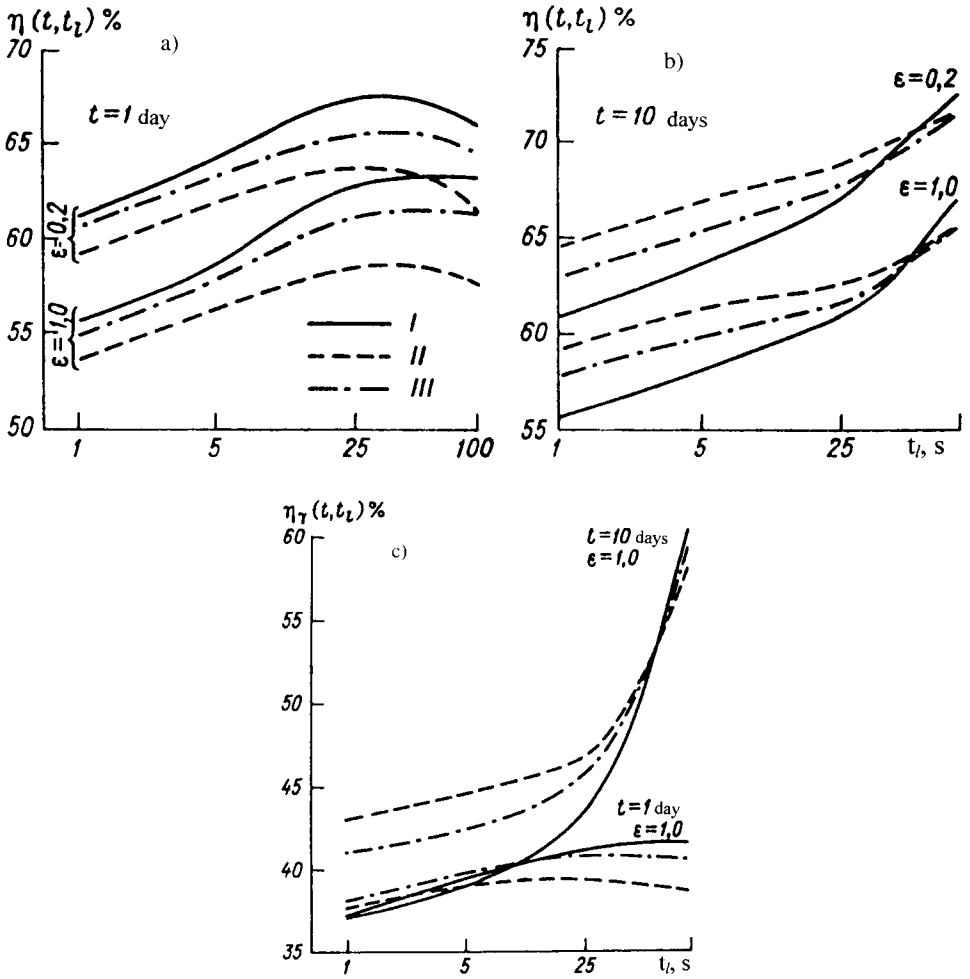

Fig. 1.15. The relationship between the total activity (a, b) and γ-activity (c) of a non-fractionated mixture of fission debris at various times t in melted SiO_2 and at time t_l after melt solidification.

$\bar{v}_i$ is about 7×10^4 cm/s for rubidium and strontium and about 6×10^4 cm/s for cesium. According to the Fuchsian equation, the condensation rate for one particle (of size r greater than 1 μm) can be written as:

$$h = \alpha S \frac{n_i \bar{v}_i}{4} \frac{r + \lambda}{\alpha l r^2 + r + \lambda}. \tag{1.38}$$

Here, α is a condensation coefficient (fraction of condensable molecules), S is the particle-surface area; $l = (\bar{v}_i/4)/D$, where D is a diffusion coefficient. According to the data of Lavrenchik (1965) for strontium, D is equal to 0.25 cm^2/s in air at $T \approx 2000$ K; according

to Storebo (1964), it is 2–3 cm^2/s; λ is the free pathway length ≈ 0.1 μm for the molecule under normal conditions.

If there is no re-evaporation and we can assume that first order kinetics apply, then the condensation rate S on the surface of all the particles will be described by the formula (for $r \gg \lambda$)

$$-\frac{dn_i}{dt} = \alpha n_i \frac{\bar{v}_i S}{4V_v(\alpha l r + 1)}, \tag{1.39}$$

where V_v is the vapor phase volume from which the condensation proceeds. Hence,

$$n_i = n_i^0 e^{-t/t_v}, \tag{1.40}$$

where n_i^0 is the initial concentration,

$$t_v = \frac{4V_v(\alpha l r + 1)}{\alpha \bar{v}_i S} \tag{1.41}$$

is the mean time of the molecule's existence in the vapor phase (α does not change during the activation, i.e., $\alpha =$ constant).

If α is so small that $\alpha l r \ll 1$, then

$$t_v = \frac{4V_v}{\alpha \bar{v}_i S}. \tag{1.42}$$

Assuming in the ground explosion[2] that $\log \bar{d} = 2.0$, $\sigma = 0.76$ (Izrael, 1973; Johnson et al., 1959), $M_{melt} = 2 \times 10^8 W_2$, $V_{fireball} = \frac{2}{3}\pi(89\sqrt[3]{2W})^3 \times 10^6$ $cm^3 \approx 2.9 \times 10^{12} W$ cm^3 using Eqs. (1.41) and (1.42), we find that, for $V_v = V_{fb}$, $t_v = 10^{-2}$ s; for $V_v < V_{fb}$, t_v is still smaller. Obviously, volume V_d from which the molecules diffuse for a time t_v will be close to V_v:

$$V_d = N\frac{4}{3}\pi\left(\sqrt{2Dt_v}\right)^3, \tag{1.43}$$

where

$$N \approx M_{melt} W \Big/ \rho \frac{4}{3}\pi r_m^3.$$

Assuming $D \approx 1$ cm^2/s, $t_v = 10^{-2}$ s, $W = 1$ kt, $M_{melt} = 200$ t/kg, $\rho = 2.5$ g/cm^3, $r_m = 5 \times 10^{-3}$ cm, we obtain $V_d = 1.8 \times 10^{12}$ cm^3, which is close to V_v when $W = 1$ kt. As has been noted, t_v is the period of existence of the molecules in the vapor phase under conditions far from equilibrium ($\alpha < 1$). Under conditions close to equilibrium ($\alpha = 1$) and for the same time, collisions between molecules and particles certainly take place; however, it is not certain that the molecules are captured.

[2] It is accepted here that the fireball volume in a ground explosion is one half that in an air explosion.

After the refractory and intermediate nuclides condense on to the liquid particles, they begin to diffuse into the particles. To estimate roughly the mean depth $\bar{\xi}^2$ of penetration of the ith nuclide into a particle, Einstein's equation can be used:

$$\bar{\xi}^2 = 2D_i t, \tag{1.44}$$

where D_i is the diffusion coefficient for the molecules of the element of the ith nuclide for the form in which it occurs in the fused rock. More accurate calculations (Lavrenchik, 1965), based on the use of thermal conductivity formulae to estimate the diffusion of material into spherical particles (calculated for a sphere with a given heat flux on the surface (Carslow and Eger, 1964)), lead to the conclusion that the concentration of molecules diffusing in the layer $\sqrt{\bar{\xi}^2}$ does not differ from the average by more than 30 per cent. Thus, the use of Eq. (1.44) is quite reasonable for approximate calculations.

In general, the volumetric contamination $\bar{\sigma}_v$ (averaged per particle) varies. Three cases are possible (in contamination):

1. When constant values of σ_v' are fulfilled. This case exists only for particles of small size (e.g., in atmospheric explosions or when the activation period t_a is long, as in very powerful explosions).
2. Fast activation (a characteristic feature of low yield explosions and the most refractory nuclides); here the nuclide flux through the particle surface is constant and does not depend on the particle size.
3. The most common case which occurs during particle activation when the volumetric concentration σ_v' of the contaminated layer of particles tends towards homogeneity as the nuclides diffuse into the particles, $\bar{\sigma}_v$ tending to become constant. It occurs because initially a quantity of molecules proportional to the surface area of the particles penetrates into the layer of $\sqrt{\bar{\xi}^2}$ thickness (see formulae (1.38)), resulting in a different concentration of molecules in the upper layer (the concentration being higher with smaller particles). In turn, this leads to a rise in vapor pressure in the vapor phase of a soluble component (Akopyan, 1955) above the smaller particles and to faster condensation on the larger ones. Thomson's effect (the increase in saturated vapor pressure above small particles) caused by surface curvature of particles larger than 0.1 μm in size can be considered, in this situation, to be negligible (Yunge, 1965).

The third case is intermediate between the first and second. The particle-size distributions of the total volume of particles $V(r)$ and of the volume containing the ith nuclide (at the moment t_l of particle solidification) are slightly different. Apparently,

$$V_i(r, t_l) = V(r)\chi_i(r, t_l), \tag{1.45}$$

where

$$\chi_i(r, t_l) = \frac{\frac{4}{3}\pi\{r^3 - [r - r_0(t_0, t_l)]^3\}}{\frac{4}{3}\pi r^3} = \frac{3r_0}{r} - \frac{3r_0^2}{r^2} + \frac{r_0^3}{r^3}, \tag{1.46}$$

$$r_0(t_0, t_l) = \left[\int_{t_0}^{t_l} D_i(t)\,\mathrm{d}t\right]^{1/2} \tag{1.47}$$

(when $r_0 \geqslant r$, $\chi_i(r, t_1) = 1$); t_0 is the initial time of activation; we will attribute t_0 to the time of the maximum condensation rate, because the ith nuclide condensation is prolonged.

The third case is the most typical for the intermediate group nuclides, which penetrate entirely or partially inside the particles at a temperature close to that of particle solidification. The following relationships have been calculated

$$V_i'(r, t_1) = \frac{V_i(r, t_1)}{\int_0^\infty V_i(r, t_1)\,\mathrm{d}r} \tag{1.48}$$

for the following radionuclides (the most important from the point of view of contamination): ^{89}Sr, ^{90}Sr, ^{95}Zr, ^{103}Ru, ^{131}I, ^{132}Te, ^{137}Cs and ^{140}Ba. During activation, these nuclides (see Figs. 1.2, 1.3, 1.11 and Table 1.5) are present in the condensed phase mainly as rubidium (^{89}Sr and ^{90}Sr), strontium, yttrium (^{95}Zr), antimony and tellurium (^{131}I and ^{132}Te), cesium and barium (^{137}Cs and ^{140}Ba). Time t_0 corresponds to the time when the following temperatures are attained: 3150 K for strontium, 2670 K for barium, 1870 K for antimony, 1673 K for rubidium and cesium (the ground-melting temperature). In a 20 kt explosion, the activation times are, respectively, 4.0, 3.3, 1.3 and 0.3 s (see curve 3 in Fig. 1.1).

$D_i(t)$ values at different temperatures have been presented in a number of studies (Lavrenchik, 1965; Musikhin and Esin, 1962) for sodium, calcium, niobium and antimony. Later it will be seen that $D_i(t)$ for rubidium and cesium coincides with $D_i(t)$ for sodium, and that for barium, strontium, yttrium, tellurium and tin with the $D_i(t)$ for calcium and antimony.

Figure 1.16 shows the relationships for the above listed nuclides at $t_1 = 7$ s (for a yield of $\sim$ 20–30 kt); V_1' corresponds to ^{95}Zr, V_2'—to the nuclides ^{103}Ru, ^{131}I and ^{132}Te, and V_3'—to the nuclides ^{89}Sr, ^{90}Sr and ^{137}Cs. $V(d)$, taken from a study by Freiling (1962), is governed by a normal logarithmic relationship for a median size of particles equal to 100 μm and a mean square deviation for $\sigma = 0.76$. For comparison, the figure also portrays the relationships between $V'(d)$ and $S'(d)$ (see below).

As to the nuclides that are in the form of elements essentially different in their chemical properties during the activation of particles, it is necessary to take into account the accumulation rate of the element that condenses most rapidly at the given time. Thus, in calculating V_i' for ^{140}Ba, we need to take into account changes in the ^{140}BaO concentration in the fireball during the activation due to two processes, viz. the accumulation of decomposed ^{140}Cs and the condensation process. If the condensation of newly formed ^{140}BaO is rapid enough (compared to the whole activation period), one could surmise that the concentration σ_{V_i}' in the layer adjacent to the surface of the given particle, at each subsequent moment t^*, is defined by the equation

$$\sigma_{V_i}' = \int_0^{t^*} \frac{v_i(t)}{V_i(t^* - t)}\,\mathrm{d}t, \tag{1.49}$$

where $v_i(t)$ is the rate of ^{140}Ba accumulation from ^{140}Cs; V_i is the volume of the given layer.

After solidification, the second stage of particle activation begins; the radionuclides which had not condensed before particle solidification are deposited on the surface.

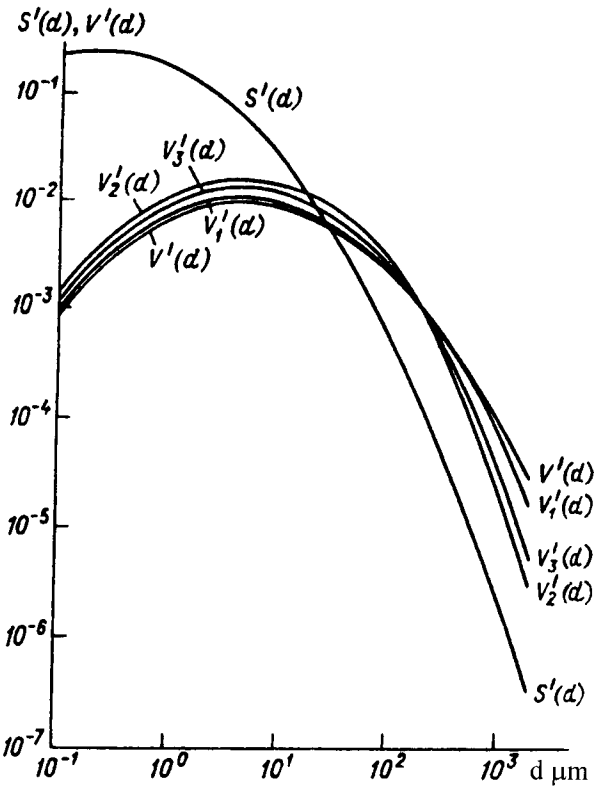

Fig. 1.16. The relationship between the contaminated layer volume and particle size (for different nuclides).

Here, an assumption can be made that any nuclide depositing on the particle surface will be deposited with a constant surface concentration not related to the particle size. As indicated above, model laboratory investigations (described below) confirmed this assumption (Izrael et al., 1968). The area of sub-micron particles was believed to be already relatively small for $t > t_1$.

Given that the average period a molecule spends in the vapor phase is not long and that the condensation coefficient on a solid surface is practically equal to unity (for nuclides which begin to condense before solidification), such nuclides (belonging to the intermediate group) will be condensed several tenths of a second (or several seconds) after particle solidification. Further, the refractory or intermediate nuclides, resulting from volatile species, will condense on the surface of particles inside the fireball or cloud (e.g., ^{89}Rb resulting from ^{89}Kr decay). The condensation coefficients of such nuclides are also considered to be equal to unity (within the same time interval). They will continue to condense on the particles until the latter are deposited from the cloud (under gravity).

Evaporation can also take place of the volatile nuclide particles that are formed from the refractory ones deposited on to the particle surface (e.g., ^{133}I and ^{133}X formed from ^{133}Te).

One should take into account, however, that, if the iodine evaporation occurs from fallout particles deposited on land, terrestrial contamination by iodine can remain due to the secondary uptake of the iodine (e.g., by plants). These secondary effects are not discussed here.

The activity distribution of the ith mass chain nuclides on particle surfaces can be described by the following equation (for any time t) for the chains where element transformations (resulting from radioactive decay) follow the scheme: volatile–intermediate–refractory elements (e.g., for chains with numbers 89–93, 97–144):

$$N_i^{\mathrm{S}}(r,t) = Q_i(t)S'(r)\left\{\sum_Z p_i^{\mathrm{in}}(t_1,Z)\left[1 - F_{Zi}(t_1)\right] + \int_{t_1}^{t} v_i(t')f(r,t)\,\mathrm{d}t\right\}$$

$$= Q_i(t)S'(r)G^{\mathrm{S}}(r,t,t_1). \tag{1.50}$$

The index "in" refers to intermediate elements; $v_i(t')$ is the rate of formation of non-volatile nuclides from the volatile ones (index "v $\rightarrow$ r"); $v_i(t') = \mathrm{d}p_i^{\mathrm{v}\rightarrow\mathrm{r}}(t,Z)/\mathrm{d}t$; $f(r,t)$ is the fraction of particles of size r and smaller remaining in the cloud at time t. If within the time interval under consideration (t,t_1), the accumulation $p_i^{\mathrm{v}}(Z,t)$ has already ceased and changes with time for the volatile isotopes are influenced only by its decay, then $v_i(t) = p_i^{\mathrm{v}\rightarrow\mathrm{r}}(t_1)\lambda_i \mathrm{e}^{-\lambda_i(t-t_1)}$; $S'(r) = S(r)/\int_0^\infty S(r)\,\mathrm{d}r$; $Q_i(t)$ is the total activity of the ith nuclide for period t.

Figure 1.17 shows the relationship $f(r,t)$ for particles of 30–500 μm in radius (i.e., the particles from near-fallout) for explosions of 20 kt and 1 Mt yields. This relationship was calculated assuming that the particles and radionuclides are concentrated in the upper part of the cloud (see Section 1.3). It is here that, according to experimental data, the major portion of the activity of the cloud is concentrated (Ferber, 1965). The deposition rate of the particles was calculated according to Stokes' law (corrections being made for particles exceeding 100–150 μm in size) for heights of 7–12 km above sea level (the cloud height for explosions of the yields cited). Particles were taken to be spherical with a density of 2.5 g/cm^3. The cloud thickness was taken to be 2–3 and 6–8 km (Kellog and Rapp, 1957) for explosions of 20 kt and 1 Mt, respectively.

The total surface contamination of particles σ_{S}, equal to the ratio $N^{\mathrm{S}}(r)/S(r)$ for nuclides having comparatively long-lived volatile precursors, depends therefore on particle size. Because gravitational deposition of particles occurs from the cloud, the types of particles remaining at the second stage must be taken into consideration. For the chains where the element transformation is preceded by the scheme "refractory–intermediate–volatile" (e.g., for mass chains with numbers 131–135), the formula for $N^{\mathrm{S}}(r,t)$ will take the form

$$N_i^{\mathrm{S}}(r,t) = Q_i(t)S'(r)\sum_Z\left[1 - F_{Zi}(t_1)\right]\left[p_i^{\mathrm{in}}(t_1,Z) - p^{\mathrm{v}}(t,Z) + p^{\mathrm{v}}(t_1,Z)\right]$$

$$= Q_i(t)S'(r)G^{\mathrm{S}}(t,t_1). \tag{1.51}$$

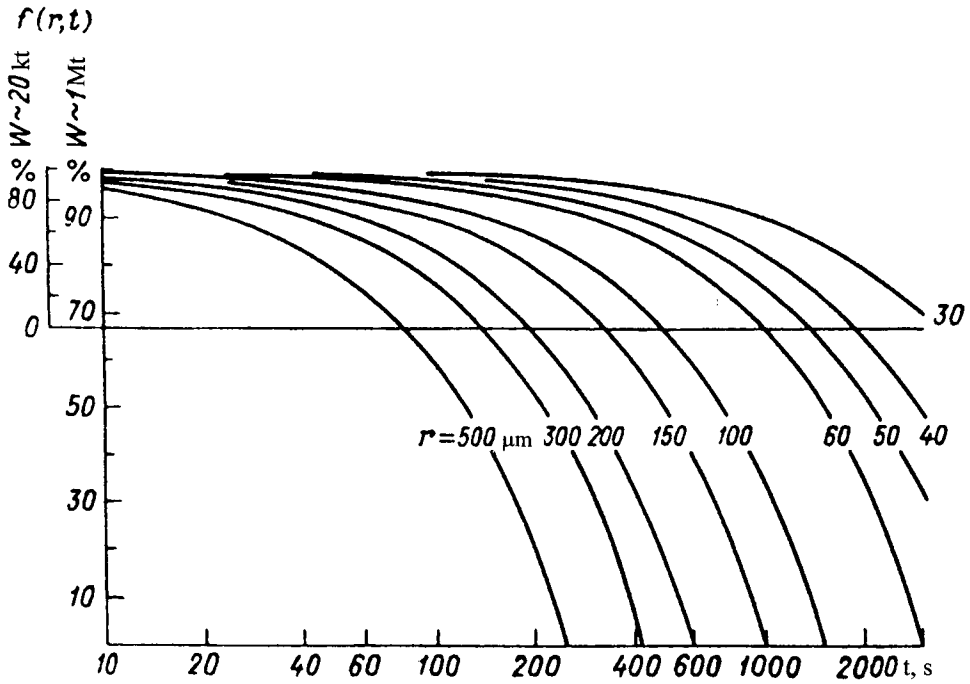

Fig. 1.17. The relationship $f(r, t)$ for smaller particles remaining in the cloud at time t.

At moment t_0 when the amount of iodine isotopes transformed into xenon is negligible in mass chains 131–135, and if iodine evaporation from the particles can be ignored, then the following approximation can be made:

$$G^{S}(t, t_1) = \sum_{Z} \left[1 - F_{Zi}(t_1)\right]\left[p_i^{in}(t_1, Z) - p^{v}(t, Z) + p^{v}(t_1, Z)\right] \approx 1 - F_i(t_1). \tag{1.52}$$

The same approximation is valid for mass chain 103. Using the obtained equations, one can determine the character of the relationship between the activity of individual particles and their sizes $a_i(r)$. Thus,

$$a_i(r) = \frac{N_i(r)}{n(r)} = \frac{N_i^{V}(r) + N_i^{S}(r)}{n(r)}, \tag{1.53}$$

where $n(r) = 3V(r)/4\pi r^3$ is the size distribution of the particles.

As to the general (the third) case of intermediate contamination,

$$N_i^{V}(r) = V(r)\chi_i(r)\sigma_V', \tag{1.54}$$

$$N_i^{S}(r) = S(r)\sigma_S, \tag{1.55}$$

where

$$S(r) = \frac{3V(r)}{r}.$$

Hence,

$$a_i(r) = 4\pi\sigma'_V\left[r^2\left(r_0 + \frac{\sigma_S}{\sigma'_V}\right) - rr_0^2 + \frac{r_0^3}{3}\right], \tag{1.56}$$

where σ_S = constant, σ'_V = constant for a given explosion (if σ_S variations are negligible due to deposition of particles from the cloud). Thus the relationship $a_i(r)$ is intermediate between a quadratic and cubic one for each nuclide (as well as for their sum). It follows from Eq. (1.56) that, when $r_0 \to 0$ (or $\sigma'_V = 0$), the relationship $a_i(r)$ becomes quadratic and that, when $r = r_0$, it is cubic. Apparently in the case when equilibrium does not exist, the relationship $a_i(r)$ is intermediate between quadratic and cubic. The relationship $a_i(r)$ is close to quadratic even for refractory nuclides (when $\sigma_S = 0$) and large particles (corresponding to the close-in pattern). When $r_0 \geqslant 10$ μm and 100 μm $< r <$ 1000 μm, $a_i(d)$ is approximately equal to d^n, for refractory nuclides where $n = 2.1$. In this case, the relationship $a_\Sigma(r)$ also should be intermediate between quadratic and cubic for the sum of the nuclides. The different situations were confirmed by Loborev et al. (1994) from the data on six explosions carried out at the Semipalatinsk Test Site in 1953–1961 (Fig. 1.18). This figure shows that the values for n range between 2 and 3 for cases (a)–(d), for case (e) it is close to 2.0, and for case (f) it is nearly 3.0.

To verify the calculations of particle activation and fractionation effects, some modeling experiments of nuclear explosion particles were conducted in the laboratory (Izrael et al., 1968). Of primary importance was a verification of the assumption that the refractory nuclides were distributed over the particle volume and the volatile ones only on the surface. For this purpose, σ_S was determined for particles of various sizes for the same activation period. Conditions under which radioactive particles were formed in a nuclear explosion were reproduced in the laboratory. Radioactive particles were obtained which simulate those formed in ground explosions. Two methods were used to obtain such particles:

1. Particles were generated using a coal-graphite resistance furnace. A well-stirred mixture of finely-crushed coal (80–90%) and graphite (10–20%) was used to fill the space between two flameproof tubes made of quartz glass. Copper, river sand and phosphorus were used as the particle-carriers and crushed material of the carrier and nuclide was mixed as flameproof particles of 0.1–0.5 mm size in a ratio of 1 : 10. The mixture obtained in this manner was placed in the inner tube of the furnace and heated for about 1 min. The current varied from 20 to 60 A (voltage was 220 V) during the experiments and the maximum temperature attained in the operating volume was about 2000 °C.
2. In this experiment, the particles were generated in a high temperature plasma using an induction plasma burner at atmospheric pressure. A mixture of quartz-sand grains or other material and the nuclide chosen for the investigation was injected through a fine aperture along the plasma axis. The maximum temperature of the plasma reached

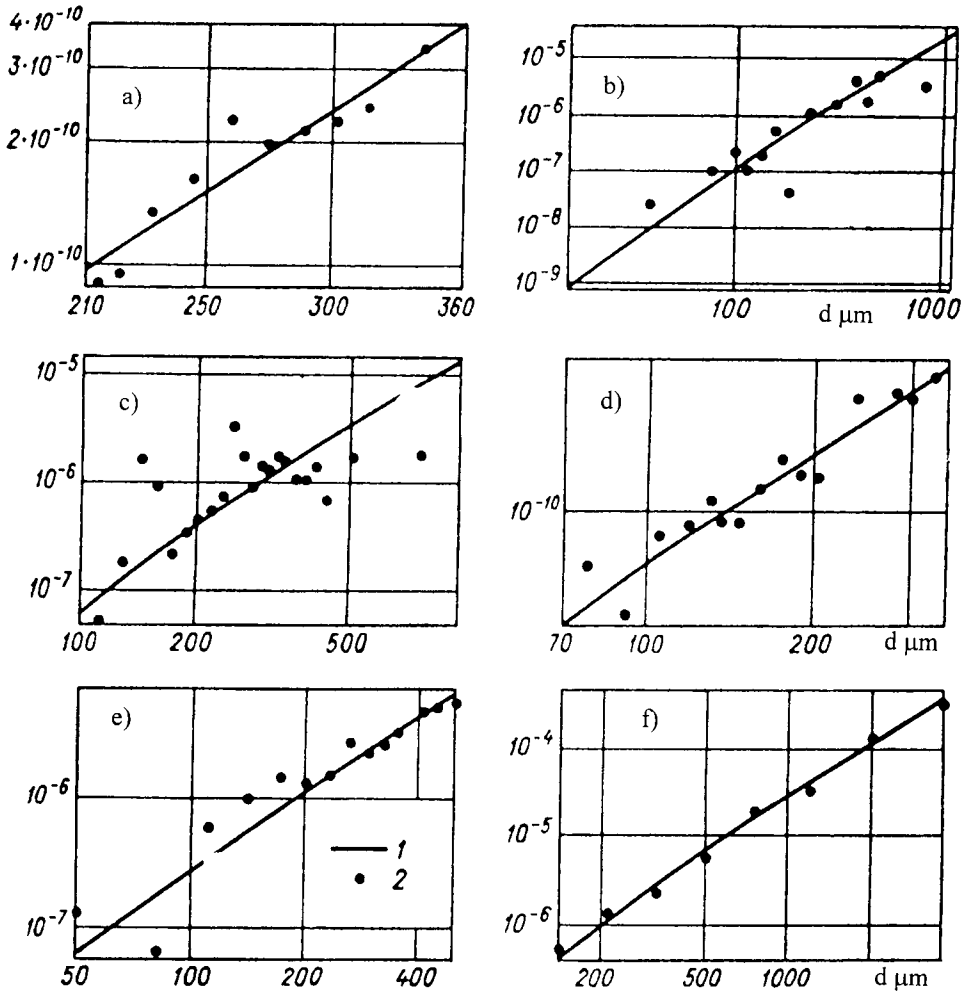

Fig. 1.18. The beta-activity–size relationship of particles in different experiments: (a) 12 August 1953; (b) 29 July 1955; (c) 25 March 1956 and (d) 24 August 1956, all trends three or more years after the explosion; (e) 24 August 1956, trend within three hours of the explosion; (f) 24 September 1961. 1 — calculated; 2 — experimental data.

12000 °C, the atmosphere consisting of oxygen or inert gases. The molten particles cooled rapidly as they descended and did not stick together in the air or inert gas receiver ($h \approx 1$ m). Electric arc and coal resistor furnaces can also be used to produce the particles.

Radioactive particles produced in these ways were examined carefully. Their shape, colour, structure and specific weight were investigated, as well as the relationship between the activity of the particles and their size. The relationship between surface concentration of nuclides and particle size was calculated. On the basis of their appearance and structure

it was difficult to distinguish between these particles and those formed in ground-level nuclear explosions. All were of spherical shape (or close to it); as to the structure and colour, the particles varied from light and glassy to black and opaque with bright surfaces. The structure and colour of the model particles were determined by the mineralogical composition of the initial ground particles.

During the experiments made in the coal-graphite furnace, the activity–size relationship of the particles was investigated. Copper ($T_{mel} = 1080$ °C) was chosen as the material for the particle-carriers and ^{35}S and ^{76}As were the radionuclides (with boiling points of 450 °C and 600 °C, respectively). The relationship between the mean specific surface activity σ_S for ^{35}S and ^{76}As in the particles and their size was examined (Izrael et al., 1968) over the range 150–1600 μm (64 particles with ^{76}As and 339 with ^{35}S). It was found that the activity σ_S essentially did not depend on the size of the particles within this range (mean square deviation for the average value was 18%). Thus, under these experimental conditions for particle generation, the earlier assumption re. the surface concentrations of volatile nuclides in particles of various sizes appears to be valid. Analogous experiments were also carried out for quartz sand.

7. Characteristic Features of Fractionation of Radioactive Products from Tropospheric Nuclear Explosions

At the present time, extensive sets of experimental and theoretical data are available (Freiling, 1961, 1962, 1966; Lavrenchik, 1965; Izrael and Stukin, 1967; Izrael, 1965; Grechushkina and Izrael, 1965) to enable estimation of the characteristic features of radionuclide fractionation in nuclear explosions, to develop schemes for the quantitative estimation of fractionation effects and hence to predict the radionuclide composition of terrestrial contamination resulting from nuclear explosions. The data do not allow us to make even a rough prediction of the terrestrial contamination by individual nuclides without the necessary systematization and compilation of the above-mentioned schemes. Freiling's studies (1961, 1962) were the first major publications devoted to the fractionation of nuclides. Freiling described the main features of fractionation in surface and air explosions. However, his studies did not allow us to estimate quantitatively the fractionation on contaminated land at different distances from an explosion. The author and his colleagues have made a number of attempts to compensate for this deficiency (Izrael, 1965, 1968; Izrael and Stukin, 1967; Grechushkina and Izrael, 1965) and we present here a scheme for the quantitative estimation of fractionation factors in explosions of different types and yields and for particles of various sizes.

It is known that the fractionation factor $f_{i,j}$ can be specified as a number, by which the ratio between two nuclides varies as a result of any processes after their generation. In this case, it signifies the ith nuclide fractionation relative to the jth one:

$$f_{i,j}(t,r) = \frac{n_i(t,r)}{n_j(t,r)} : \frac{n_i(t)_T}{n_j(t)_T}, \tag{1.57}$$

where $n_i(t,r)$ and $n_j(t,r)$ are nuclide activities determined by the experiment. They belong respectively to the ith and jth mass chains in a particle (or a group of particles);

r is their size at time t after an explosion. $n_i(t)_T / n_j(t)_T$ is the theoretical ratio (at a time t) between the activities of the same nuclides (or the number of nuclei) formed in the explosion.

Thus,

$$\frac{n_i(t)_T}{n_j(t)_T} = \frac{Y_i \lambda_i e^{-\lambda_i t}}{Y_j \lambda_i e^{-\lambda_i t}}, \tag{1.58}$$

where Y_i / Y_j is the ratio between numbers of nuclei of the ith and jth nuclides at formation (in the case of their formation from fission—the ratio between the accumulated yields); λ_i, λ_j are the radioactive decay constants. The fractionation factors can be greater or less than unity besides varying over a wide range. In Freiling (1961), the nuclides ^{95}Zr and ^{89}Sr were chosen as the basic nuclei i, j for the calculation of fractionation factors. This choice was connected to the fact that their ratio is a sensitive function of fractionation, because there is a relatively long-lived volatile nuclide in the chain with mass number 89 (^{89}Kr with half-life of 3.2 min) and the chain with mass number 95 essentially contains no volatile parents. Additionally, both nuclides belong to the "peak" products, i.e., they are formed in relatively abundant quantities. The choice of ^{95}Zr and ^{89}Sr is also appropriate because fractionation of this pair of nuclides is at a maximum. It was found that the value of $f_{95,89}$, calculated on the basis of different samples, varied five-fold for an explosion of 1 Mt yield; twenty fold for an explosive yield below 1 Mt at the surface of a deep bay; twelve-fold for a 1 Mt surface detonation on a shoal and hundred-fold for an explosion conducted on a coral atoll surface (Freiling, 1961). The range of values for $f_{95,89}$ is among the highest for listed ground nuclear explosions.

The value of $f_{i,j}$ is a complicated function of the type and yield of the explosion, the surface characteristics, location and time of sampling, the size and type of radioactive particles in the probe, etc. The calculation of the fractionation factor of a nuclide relative to another, e.g., to ^{95}Zr, is performed through a correlation of the values of $f_{95,89}$ and $f_{i,89}$, obtained for different samples from the same explosion. In conducting this correlation, it should be realized that the regression line gradient characterizes the mean fractionation factor of the nuclide in question relative to ^{95}Zr. Figure 1.19 shows the correlations of various nuclides (on a logarithmic scale) for an underground cratering explosion (Izrael et al., 1970a,b). It follows from the figure that the ith nuclide fractionation is characterized by two values—the tangent of the angle of inclination b_i ($b_i = \tan\alpha$) of the regression line and the value of the ordinate a_i when $\log f_{95,89} = 0$ (the value of the "cut-off"). Figure 1.20 presents the analogous correlation graphs of fractionation factors in an atmospheric nuclear explosion (Freiling, 1963).

If we suppose that the ^{95}Zr is distributed only over the volume of a particle if $a(r) \sim r^{N_i}$, N_i being equal to 3.0, and ^{89}Sr only on the surface ($N_i = 2.0$), it was shown by Freiling (1963) that a logarithmic correlation exists between $f_{i,89}$ and $f_{95,89}$ as follows:

$$\log f_{i,89} = a_i + b_i \log f_{95,89}, \tag{1.59}$$

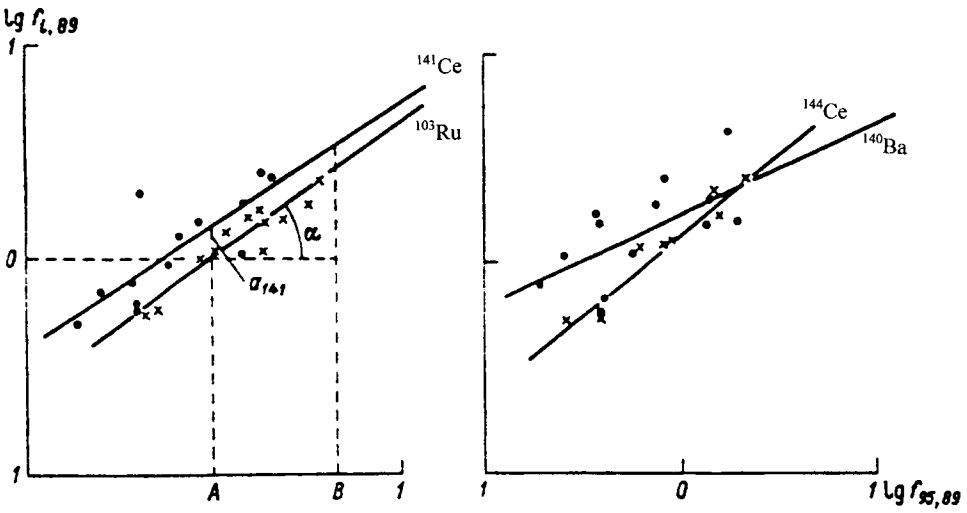

Fig. 1.19. Correlation graphs of the fractionation factors for various nuclides as determined in the fallout pattern from the Sary-Uzen, 1003 explosion.

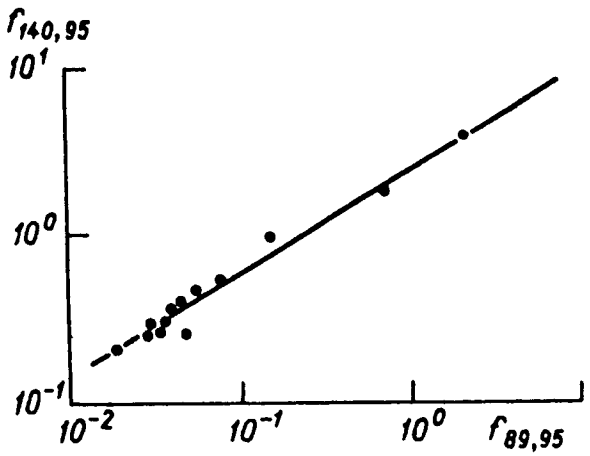

Fig. 1.20. Illustrative correlation graph of fractionation factors in an atmospheric nuclear explosion.

where a_i is the value of "cut-off", b_i is the tangent of the angle of inclination of the regression line. The same study showed that $b_i = N_i - 2$, and

$$a_i = \frac{b_i(1 - b_i)\sigma^2}{4.6} \neq 1. \tag{1.60}$$

Here σ^2 is the mean square deviation in the logarithmic distribution of activity or mass of the radioactive particles by size. The value of a_i attains its maximum when $b_i = 0.5$ and is equal to $e^{\sigma^2/8}$ (Freiling, 1963).

The depicted regularities allow the development of a simplified semi-empirical prediction model for the fractionation effects. If b_i characterizes the angle of the regression line (logarithmic correlation), then the distribution of the ith nuclide activity by particle size will be characterized by the logarithmic distribution with the median diameter as obtained from the formula $\bar{d}e^{(b_i-1)\sigma^2}$, where σ^2 is the mean square deviation. Here $\bar{d}$ and σ^2 are parameters of the normal logarithmic distribution of the radioactive-particle masses with size. Undoubtedly such a prediction is approximate because b_i values vary in different contaminated zones, e.g., in the cloud—as numerous experimental data have shown (Freiling, 1961). However, such an approach seems to be quite simple.

It is also evident from these statements that a single-valued relationship must exist between n_i, b_i and F_i. The tangent of the angle of inclination of the regression line can be obtained, e.g., from the graphs in Figs. 1.19 and 1.20

$$b_i = \tan\alpha = \frac{\log(f_{i,j})_a - \log(f_{i,j})_b}{\log(f_{k,j})_a - \log(f_{k,j})_b} = \frac{\log\frac{(f_{i,j})_a}{(f_{i,j})_b}}{\log\frac{(f_{k,j})_a}{(f_{k,j})_b}} = \frac{\log\left[\left(\frac{n_i}{n_j}\right)_a : \left(\frac{n_i}{n_j}\right)_b\right]}{\log\left[\left(\frac{n_k}{n_j}\right)_a : \left(\frac{n_i}{n_j}\right)_b\right]}. \tag{1.61}$$

From Eq. (1.61) it follows that the value of b_i does not depend on the type of fission (ratios Y_i/Y_j and Y_k/Y_j were cancelled); b_i does vary for different nuclides (i, j) and is dependent on the nuclide (the kth nuclide), with which each pair of fractionating nuclides is being correlated. In this connection, b_i should then be written with the threefold index b_{ijk}. It is clear also that b_i and a_i depend on the size distribution of particles ($b_i = N_i - 2$).

It follows from the graph in Fig. 1.19 that

$$Y_0 = \log a_i = \log f_{i,j} - b_{ijk}\log f_{k,j} \rightarrow a_i = \frac{f_{i,j}}{f_{k,j}^{b_{ijk}}}. \tag{1.62}$$

Hence,

$$a_i = \frac{n_i Y_k^{b_{ijk}} n_j^{b_{ijk}-1}}{n_k^{b_{ijk}} Y_i Y^{b_{ijk}-1}}. \tag{1.63}$$

In the general case, the value of the "cut-off" varies for different (i, j) nuclides and depends on the type of fission and the nuclide (k) chosen as the reference. Since, in practice, different nuclides are used as the reference nuclides and since the parameters of the regression equation for fractionation factors depend on the type of reference nuclides, Izrael (1973) has developed formulae that relate the fractionation factors to different reference nuclides.

The values of the tangents of the angles of inclination of the regression line (in the logarithmic correlations of different nuclides of samples taken from contaminated areas following high yield atmospheric explosions (Freiling, 1961)) are shown in Table 1.7.

Table 1.7
The values of $\tan\alpha$ at correlation for different nuclides after atmospheric explosions

Nuclide	$\tan\alpha$
^{90}Sr	0.32
^{99}Mo	0.11
^{132}Te	0.60
^{137}Cs	−0.06
^{140}Ba	0.43
^{144}Ce	0.94
^{237}U	1.04
^{239}Np	1.05

Note that the inclination essentially does not depend on the environment. The values for the "cut-off" a_i oscillate around unity.

The experimental results presented in Table 1.7 show that fractionation depends, to a significant degree, on the existence of volatile precursors in the decay chain. Freiling (1961) has developed the relationship between $\tan\alpha$ and the fraction of refractory elements F_i in the mass chains of particles that are in the condensed phase at the time of their solidification. This relationship can be described by the equation

$$\log f_{i,89} = \sqrt{F_i} \log f_{95,89}. \tag{1.64}$$

Results of $\sqrt{F_i}(t)$ are presented in Fig. 1.14 and in (Izrael, 1974). In low yield explosions, the fractionation effect is more clearly pronounced (Kroker et al., 1965). This latter study presents some data on the relationship between fractionation factors and particle sizes. Studies by Freiling and Kay (1966), Edwarson et al. (1959), Mamuro et al. (1963b, 1965a) and Gaziev et al. (1965) are devoted to the fractionation of radionuclides in atmospheric explosions. As a rule, the range of values of $f_{95,89}$ is smaller in atmospheric explosions than in surface ones; however, in individual cases, it can reach values of 500–900 (Freiling and Kay, 1966). The latter authors concluded that the following groupings of nuclides became fractionated in practically the same manner in an atmospheric explosion as in a surface detonation; ^{237}U, ^{239}Np and ^{240}U; ^{111}Ag and ^{115}Cd; ^{95}Zr and ^{97}Zr; ^{153}Sm, ^{156}Eu and ^{161}Tb. Zr isotopes did not fractionate relative to those of rare-earth metals; and the behaviors of ^{137}Cs, ^{89}Sr and ^{90}Sr were practically identical.

Freiling (1962) arrived at a series of nuclides arranged in order of the increase of their refractory properties (taking into account their precursors) as follows: ^{137}Cs, ^{89}Sr, ^{90}Sr, ^{136}Cs, ^{115}Cd, ^{111}Ag, ^{140}Ba, ^{91}Y, ^{141}Ce, ^{99}Mo, Ru, rare-earth isotopes, Zr.

Freiling and Kay (1966) also demonstrated the correlation between the thermodynamic properties of the elements and the parameters of nuclide fractionation. It is notable that substantial "inverse" fractionation was not observed experimentally in atmospheric explosions (Edwarson et al., 1959; Mamuro et al., 1963b, 1965a; Gaziev et al., 1965), a feature that is characteristic of distant fallout from surface explosions. The reason is that the fraction of the activity situated on large hot particles is generally not significant and the mass balance is essentially not disturbed for nuclides located on very thin particles.

Fractionation in underwater and near-surface water explosions (when the thickness of the water layer is considerable) approaches that in an atmospheric explosion (Adams et al., 1960; Freiling, 1961). The reason is that, in such explosions, most of the activity is contained in small spherical particles that are generated from the construction materials of the nuclear charge, in much the same way as in atmospheric explosions (Adams et al., 1960).

8. Quantitative Estimation of Fractionation Effects

As shown previously, fractionation factors can vary over a wide range even for samples taken near each other (in space and time). In the development of a scheme for the quantitative estimation of fractionation effects, we have to visualize average fractionation factors $f_{i,j}(t,r)$ for particles of the given size. The values of this factor when correlated with factors $f_{k,j}(t,r)$ obtained for other samples (and the same range of particle sizes) can be considered to correspond to the regression line of a correlation graph. The mean value

$$f_{k,j}(t,r) = \frac{\bar{n}_i(r,t)}{\bar{n}_j(r,t)} : \frac{n_i(t)_T}{n_j(t)_T}$$

corresponds to the specific value $f_{i,j}(t,r)$. In this case, one can write:

$$\frac{\bar{n}_i(r,t)}{\bar{n}_j(r,t)} = \frac{N_i(r,t)}{N_j(r,t)} = \frac{N_i^{\mathrm{V}}(r,t) + N_i^{\mathrm{S}}(r,t)}{N_j^{\mathrm{V}}(r,t) + N_j^{\mathrm{S}}(r,t)}, \tag{1.65}$$

where $N_i^{\mathrm{V}}(r,t)$, $N_i^{\mathrm{S}}(r,t)$ and $N_i(r,t)$ are functions of the distribution density of the volumetric, surface and total activities of the ith nuclide (or the total mixture of nuclides) for $N^{\mathrm{V}}(r,t)$, $N^{\mathrm{S}}(r,t)$ and $N(r,t)$ with particle sizes at time t, $\int_0^\infty N_i(r,t)\,\mathrm{d}t = Q_i(t)$ being the total activity of the ith nuclide at time t. Thus,

$$f_{i,j}(r,t) = \frac{Y_j\lambda_j \mathrm{e}^{-\lambda_j t}[N_i^{\mathrm{V}}(r,t) + N_i^{\mathrm{S}}(r,t)]}{Y_i\lambda_i \mathrm{e}^{-\lambda_i t}[N_j^{\mathrm{V}}(r,t) + N_j^{\mathrm{S}}(r,t)]}. \tag{1.66}$$

It is possible to write a number of relationships that are valid for the activation schemes considered in Section 1.5 of this chapter (Izrael, 1973), viz.:

1. For a case when volumetric contamination of particles is constant ($\bar{\sigma}_V = \mathrm{const}$)

$$N_i^{\mathrm{V}}(r) = V(r)\bar{\sigma}_{V_i}, \tag{1.67}$$

where

$$\bar{\sigma}_{V_i} = \frac{Q_i^{\mathrm{V}}(t)}{\int_0^\infty V(r)\,\mathrm{d}r}.$$

2. For a case of fast activation when the nuclide flux through the surface of the particles is constant

$$N_i^{\mathrm{V}}(r) = \beta S(r), \tag{1.68}$$

where

$$\beta = \frac{Q_i^{\mathrm{V}}(t)}{\int_0^\infty S(r)\,\mathrm{d}r}.$$

3. The most common case where the volume concentration in a layer of diffused nuclides has become homogeneous ($\sigma'_V = \text{const}$)

$$N_i^{\mathrm{V}}(r) = V(r)\chi_i(r)\sigma'_{V_i}, \tag{1.69}$$

where $\chi_i(r)$ is determined by Eq. (1.46)

$$Q'_{V_i} = \frac{Q_i^{\mathrm{V}}(t)}{\int_0^\infty V(r)\chi_i(r)\,\mathrm{d}r}. \tag{1.70}$$

It is also possible to write for the first two cases:

$$N_i^{\mathrm{V}}(r) = \frac{Y_i\lambda_i \mathrm{e}^{-\lambda_i t}F_i}{\sum_k Y_k\lambda_k \mathrm{e}^{-\lambda_k t}F_k} N^{\mathrm{V}}(r). \tag{1.71}$$

For any nuclide $Q_i^{\mathrm{V}} = Q_i F_i$; for the refractory ones $F_i = 1$ and $Q_i^{\mathrm{V}} = Q_i$.

Similarly,

$$N_i^{\mathrm{S}}(r) = HS(r), \tag{1.72}$$

where $H = Q_i^{\mathrm{S}}(t)/\int_0^\infty S(r)\,\mathrm{d}r$ and

$$\begin{aligned} Q_i^{\mathrm{S}}(t) &= Q_i(t)\left\{\sum_Z [1 - F_Z(t_1)]\left[p_i^{\mathrm{in}}(t_{1,Z}) - p_i^{\mathrm{v}}(Z,t) + p_i^{\mathrm{v}}(Z,t_1)\right]\right. \\ &\qquad \left. + \int_{t_1}^{t} V_i(t) f(r,t)\,\mathrm{d}t\right\} \\ &= Q_i(t) G_i^{\mathrm{S}}(r,t). \end{aligned} \tag{1.73}$$

For refractory nuclides, $Q_i^{\mathrm{S}} = 0$ and $N_i^{\mathrm{S}} = 0$. In Eqs. (1.67)–(1.73), $Q_i^{\mathrm{V}}(t)$ and $Q_i^{\mathrm{S}}(t)$ are the total amounts of activity of the ith nuclide that (i) penetrate the particles and (ii) deposit on their surfaces: $Q_i(t) = Q_i^{\mathrm{V}} + Q_i^{\mathrm{S}}$.

Substituting the obtained values of $N_{i,j}^{\mathrm{V}}$ and $N_{i,j}^{\mathrm{S}}$ into Eq. (1.66), one can derive the final equation for $f_{i,j}(r)$. Assuming the ith nuclide fractionation to be calculated relative to a

refractory species (e.g., ^{95}Zr), we obtain the following equation for the most common case:

$$f_{i,95}(r,t,t_1) = \frac{Y_{95}\lambda_{95}e^{-\lambda_{95}t}}{Y_i\lambda_i e^{-\lambda_i t}} \frac{V_i'(r,t_1)Q_i^{\mathrm{V}}(t,t_1) + S'(r)Q_i^{\mathrm{S}}(t,t_1)}{V_{95}'(r,t)Q_{95}(t)}$$

$$= \frac{V_i'(t_1,r)F_i(t_1) + S'(r)G_i^{\mathrm{S}}(t,t_1,r)}{V_{95}'}, \tag{1.74}$$

where

$$V_i'(r) = \frac{V(r)\chi_i(r)}{\int_0^\infty V(r)\chi_i(r)\,\mathrm{d}r}.$$

The relationships for $V_i'(r,t_1)$, $F_i(t_1)$, $S'(r)$ and $G_i^{\mathrm{S}}(r,t)$ are presented in the previous paragraphs.

Figure 1.21 shows the relationships between the fractionation factors $f_{i,95}$ and particle size (within the size range typical of a close-in pattern from a surface explosion) for the most important radionuclides, viz. ^{131}I, ^{132}Te, ^{89}Sr, ^{90}Sr, ^{103}Ru, ^{140}Ba and ^{137}Cs, at times t_1 equal to 7 and 40 s. For the nuclides ^{97}Zr, ^{99}Mo, ^{143}Pr, ^{144}Ce and ^{147}Nd, the value of $f_{i,95} = 1$.

A simplified way to calculate the fractionation factors for spherical particles ("hot" particles larger than 2 μm in size) in atmospheric explosions has been described in Izrael (1965). Here, we can consider $\sigma_{\overline{V}'} = \text{const}$. The feasibility of this approach was demonstrated (Izrael, 1968) using, as an example, one of the American atmospheric devices exploded during the "Dominic" test series in 1961 (explosion A, for details see Benson et al. (1965b)).

The value of the relationship between the ^{140}Ba fractionation factor and particle size (relative to ^{95}Zr) for particles 3 μm $\leqslant d \leqslant$ 20 μm is the following:

$$f_{140,95}(d) = 0.57\,d^{-0.78}. \tag{1.75}$$

A similar theoretical dependence was shown to apply by Izrael (1965),

$$F_{140,95}(d) \approx F_i + (1 - F_i)\frac{\eta}{d}, \tag{1.76}$$

where $\eta \approx 0.5$ (see formula (1.35)).

Integrated fractionation factors can be calculated in the following way for different contamination zones, e.g., portions of a deposition pattern, in the cloud, etc.:

$$f_{i,j}^{\mathrm{int}}(r_1,r_2,t_1) = \frac{\int_{r_1}^{r_2} N_i(r,t_1)\,\mathrm{d}r}{\int_{r_1}^{r_2} N_j(r,t_1)\,\mathrm{d}r} : \frac{Q_i}{Q_j}$$

$$= \frac{F_i(t_1)\int_{r_1}^{r_2} V_i'(r,t_1)\,\mathrm{d}r + \int_{r_1}^{r_2} G_i^{\mathrm{S}}(r,t)S'(r)\,\mathrm{d}r}{\int_{r_1}^{r_2} V_{95}'(r)\,\mathrm{d}r}. \tag{1.77}$$

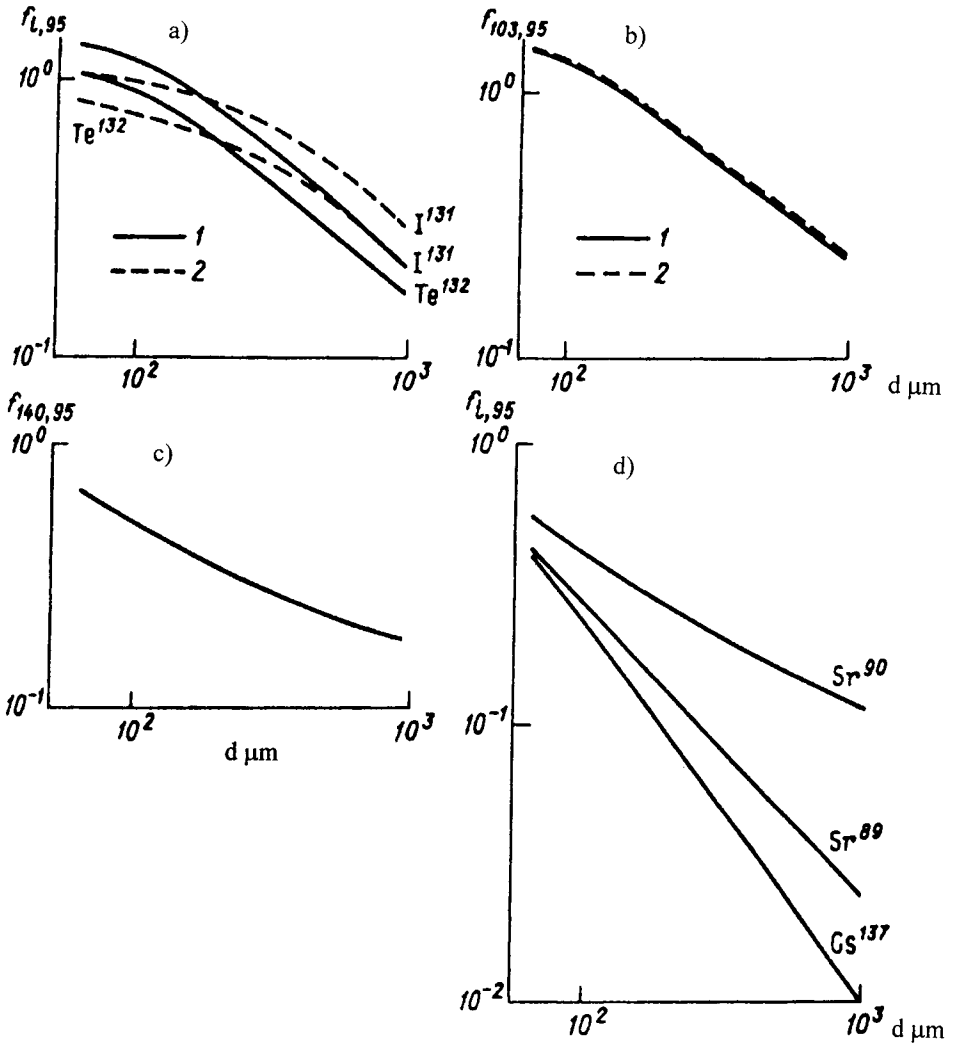

Fig. 1.21. The relationship between the fractionation factors for ^{131}I, ^{132}Te (a), ^{103}Ru (b), ^{140}Ba (c), ^{89}Sr, ^{90}Sr and ^{137}Cs (d) and particle size at various t_1 and ε. (a) $t_1 = 7$ s (1), $t_1 = 40$ s, $\varepsilon = 1$ (2); (b) $t_1 = 7$ s, $\varepsilon = 1$ (1); $\varepsilon = 0.2$ (2); (c) $t_1 = 7$ s, $\varepsilon = 0.1$; (d) $t_1 = 40$ s, $\varepsilon = 1$.

The numerator of the last equation is that part of the activity of the given nuclide associated with particles within the size range (r_1, r_2). Apparently, the ith nuclide activity fraction $\delta_i(r, t, t_1)$ associated with particles of size exceeding r, is described by the equation

$$\delta_i(r, t, t_1) = F_i(t_1) \int_r^\infty V_i'(r, t_1)\, dr + \int_r^\infty G_i^S(r, t) S'(r)\, dr. \tag{1.78}$$

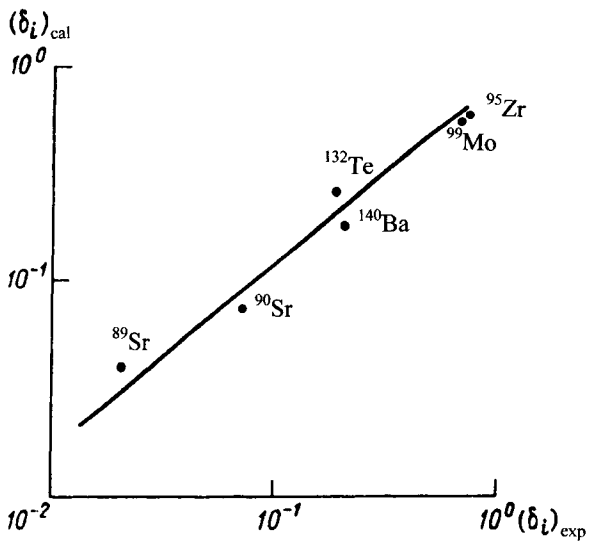

Fig. 1.22. Correlation between the calculated and experimental values for the fractions of the nuclides occurring in the close-in deposition pattern of a low-yield surface nuclear explosion.

Figure 1.22 shows the correlation between the calculated $(\delta_i)_c$ and the experimental $(\delta_i)_e$ values for several nuclides. The experimental data $(\delta_i)_e$ for particles exceeding 90 μm in size (mean diameter) were taken from the work of Freiling et al. (1965) for the close-in pattern of the American low-yield explosion "Small-Boy". It is clear from the graph that the experimental and calculated values are in good agreement with each other.

9. Conclusion

This chapter has reviewed the processes in atmospheric (ground and air) nuclear explosions, i.e., in the fireball and nuclear cloud of the explosion, which determine the behaviour of the product radionuclides during their propagation through the natural environment. The generation of radioactive aerosol particles in atmospheric explosions, the activation of these particles and the behaviour of the different radionuclides have been discussed in detail.

Both the theory and experimental data on radionuclide fractionation during the process of the generation and activation of radioactive aerosol particles have been presented. Differential fractionation of the radionuclides is conditioned by the fact that, depending on their positions in the mass decay chains, they are produced as different chemical elements of differing volatility. Thus, in activation, even radioactive isotopes (for instance, ^{89}Sr and ^{90}Sr) can be incorporated into particles of various size since their predecessors, specifically ^{89}Kr and ^{90}Kr, have different decay half-lives and, at the moment of solidification of the aerosol particles, they can be either in the form of the volatile chemical element krypton or already in the form of the refractory chemical element strontium. This

determines the size distribution of their sizes and finally the character of the distribution of the different radionuclides in the atmosphere, the rate of their fallout in particles onto the earth's surface, the features of their migration and penetration into soils, plants (vegetation), animals and humans, i.e., their mobility in the natural environment and their biological accessibilty.

Subsequent chapters present the essential characteristics of radionuclide fractionation in other categories of nuclear explosion, especially in those underground, as well as in different accident situations (in reactors, waste storage systems, etc.). The conditions of radionuclide generation in these different source-terms (different temperatures, materials of radioactive particles and fragments) determine the varying character of nuclide fractionation. Those discussions emphasized in the book highlight the fact that radionuclide fractionation is the most important characteristic of the radioactive contamination of the atmosphere and in fallout; it is one that determines the subsequent distribution of the product radionuclides in space and time and hence their mobility and biological availability in the environment and biosphere.

Chapter 2

BASIC FEATURES OF RADIOACTIVE PARTICLE FORMATION AND RADIONUCLIDE FRACTIONATION IN UNDERGROUND NUCLEAR EXPLOSIONS

Contents

1. Development of an Underground Nuclear Explosion 63
2. Release of Radioactivity into the Atmosphere and Formation of a Cloud and Base Surge in an Underground Nuclear Explosion 71
3. Characteristic Features of Radioactive Particles from an Underground Nuclear Explosion 75
4. Fractionation of Nuclides in the Radioactive Particles Produced by Underground Nuclear Explosions 80
5. Interpretation of Data on Fractionation. Scheme of Particle Activation in Underground Explosions 87

In an underground explosion, the radioactive particles that constitute the fallout on surrounding areas are essentially different from those produced in an atmospheric explosion. It is because of the different formation conditions for both the particles and the radioactive fallout that the nuclide compositions of both can also differ so markedly between underground and surface and atmospheric explosions. The reasons behind these features are undoubtedly the huge volumes of ground that are involved in the explosion process and the different thermodynamic conditions that prevail in the various stages of the explosion both underground and after venting to the atmosphere. Thus, in an underground explosion, the formation of the particle-carriers of the radioactive products proceeds under conditions that are essentially different from those that exist in an atmospheric explosion.

1. Development of an Underground Nuclear Explosion

The most complicated processes that take place in an underground explosion are those that ultimately determine the distribution of radioactivity in terrestrial rocks, its potential release into the atmosphere and its ultimate deposition onto the surrounding land.

When an underground explosion occurs at a large depth h ($h \gg R$, where R is the radius of the cavity from the explosion), the radioactive products remain buried in the immediate zone of the explosion, i.e., in the region of the explosion cavity. Only a small portion of the isotopes of the inert gases and the most volatile elements (for example, iodine) can escape into the atmosphere through fissures in the rock (Izrael, 1970a). At lesser depths ($h \sim R$), a larger fraction of the products escapes into the atmosphere and the escape flux is more intensive. At still less depth ($h < R$), venting of the cavity occurs, resulting in huge volumes of the earth and significant quantities of the radioactive products, refractory elements among them, being ejected into the atmosphere. In this type of explosion, i.e.,

one in which a crater is formed, significant quantities of earth are also ejected into the atmosphere and a zone of remaining rubble is created. A cylindrical central dust column is produced and its upper part is the main cloud reaching altitudes of several kilometers; the descent of this significant quantity of rock fragments results in a powerful base surge reaching altitudes up to 1000 m.

The main cloud and that of the base surge move downward with the wind and contain radioactive products, the majority of them being absorbed on ground particles. At varying distances from ground zero, these particles, whose sizes range rather widely, fall out due to gravity and constitute the radioactive contamination of the area. In some explosions, instead of a crater, a hill of bulked earth can be formed (e.g., in the American explosion "Sulky" (Nordyke, 1970) or the USSR's "Crystal" explosion in Yakutia on 2nd October 1974, at a distance of 90 km NE of Aikhal settlement (Mikhailov, 1996). Such explosions can be used for earth-moving purposes. Thus, in an underground nuclear explosion, the volume and composition of the radioactive products reaching the atmosphere and thus resulting in contamination of the environment are determined largely by the mechanics of the explosion.

The conditions for the formation of particles of radioactive fallout in an underground nuclear explosion differ essentially from those that prevail in a surface or atmospheric detonation. The particle character, their distribution over land and the radionuclide composition of the fallout from such explosions can be quite different. In some regions, where temperatures are high and the radionuclides are intermixed with molten ground and then disintegrated into fine pieces, the conditions for radioactive particle formation can be somewhat similar. Differences can arise in the specific thermodynamic conditions as a result of the explosion's impact on the environment and these can influence particle formation. The successive stages of an underground explosion have been described in a number of publications, e.g., (i) the formation of a symmetrical cavity in a contained (camouflet) explosion (without venting) under the action of the shock wave and the gas pressure (Dokuchaev, 1963; Butkovich, 1965); and (ii) the development and venting of a cavity in a rather shallow explosion due to ground movement occurring during the phase of gas acceleration (Dokuchaev, 1963; Teller et al., 1968; Knox, 1965; Morokhov, 1970). Laboratory modeling experiments of such explosions have been described by Rodionov (1970). There are, however, practically no data on the temperature regime within the cavity of an underground nuclear cratering explosion. This information is necessary to gain an understanding of the processes of radioactive particle formation, the loss of radioactive products to the atmosphere and the fractionation of nuclides in the explosion. Izrael (1966) has endeavored to perform relevant calculations and to estimate the influence of the temperature regime upon fractionation of the radionuclides. The successive stages in the development of an underground nuclear explosion and their influence on the radioactive contamination of the natural environment are described in the following pages.

In an underground explosion, the energy exchange between the gaseous explosion products and the surrounding ground generates a disturbance leading to the formation of a contained cavity. It is generally known that Hopkinson's law of geometrical similarity, derived under weak explosion conditions, is not applicable to powerful chemical and nuclear explosions (Dokuchaev, 1963). The deviations are due to the influence of gravity on the geometry of the crater cavity that forms in high-yield explosions conducted at great

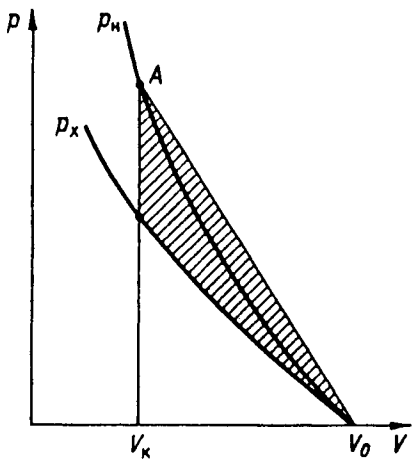

Fig. 2.1. pV-diagram for the shock compression of original cold materials (p_H is the shock adiabatic curve, p_x is the curve for cold compression).

depth. This, and the essential differences between real rocks and "ideal" ground, make for still greater difficulties in determining the influence of the explosion's mechanical action, and, consequently, of the radioactivity released to the atmosphere for a given yield and depth of detonation.

An underground explosion generates a powerful shock wave that results in the ground behind the front of the wave becoming heated and propelled towards the outer regions. A large part of the energy generated in the explosion is consumed in the melting and evaporation of hard rock located near to the explosion's epicenter. In the first microsecond, the gas attains a temperature higher than 10^6 K and a pressure of 10^7 atm. Under the peak pressure p_v and a shock wave of about 1 Mb in a medium of tuff, the rock evaporates (it melts under 0.4 Mb) (Johnson et al., 1959). For other ground materials, p_v is 0.75 Mb for alluvial deposits, 1.81 Mb for granite and 0.84 Mb for rock salt (Higgins and Butkovich, 1967). Thus, in the American underground explosion "Rainier", of 1.7 kt yield, the tuff evaporated within a radius of 2.3 m and melted within a radius of 3.3 m (Johnson and Higgins, 1959). The shock wave spreads away from the site of the explosion, crushing and breaking the rock before it gradually decays and is transformed into an elastic wave.

A rarefaction wave is reflected simultaneously with the gaseous products in the cavity. The explosion cavity sharply increases in size at the outset and then pulsates (like a gas bubble in water). The pulsation following the expansion is rather insignificant in amplitude and only takes place in this first phase. Penny has characterized this motion as "oscillationless" (see Chadwick, 1966). The elasticity-plastic model of the cavity formation under the contained explosion is described in detail in the work of Butkovich (1965).

The quantity of the heat energy transferred by the shock wave to a substance that has undergone shock compression can be determined from the pV-diagram (Fig. 2.1), in which the curves for both adiabatic cold compression $p_x(V)$ and shock compression $p_H(V)$ are plotted (Zeldovich and Raizer, 1966). In this case (a body with zero initial temperature is assumed to simplify calculations), the heat energy is equal to the difference between the

total internal energy that is numerically equal to an area of a triangle bounded by V_0, V_k and the point A on the shock curve, corresponding to V_k. The elastic energy $\varepsilon_x = \int_{V_k}^{V_0} p_x(v)\,dV$, is numerically equal to the area of a curvilinear triangle bounded by V_0, V_k, and a section of the cold compression adiabatic curve between V_0 and V_k. The area in the figure that is numerically equal to the heat energy of the substance that has undergone the shock compression is shaded.

Thus, for example, in the "Rainier" underground nuclear explosion, about 27% of the energy instantaneously released was heat energy (if the energies of the momentary neutrons and gamma-quanta are included, it is about 30%); 65–68% of the energy was consumed in the destruction, crushing and displacement of the rocks and about 5% in the formation of seismic waves. The quantity of earth evaporated amounts to about 50 t per kt of explosion yield (Johnson et al., 1959; UCRL, 1960). The spherical cavity of a contained explosion reaches its maximum size at the end of the initial phases in several hundredths or tenths of a second (in the "Rainier" explosion in 80 ms), depending on the pressure generated by the evaporated material. The pressure inside the cavity is determined by the physical characteristics of the rocks and the lithostatic pressure. At that time, the cavity walls are covered with melted rock (about 10 cm thick) amounting to 500–600 t per kt of explosion yield (Teller et al., 1968; Johnson et al., 1959). A sharp rise in temperature then occurs outside the cavity boundaries. This causes the release of volatile substances that were generated under the high temperatures. Water can also be transformed into vapor outside the cavity but, in practice, it is contained within the cavity in quantities corresponding to those generated by the molten and evaporated earth.

Higgins and Butkovich (1967) have shown that the cavity radius depends on the explosion yield and the depth of burial but not on the rock's composition. It is clear, however, that there should be a relationship between the cavity radius and the solidity and water content of the surrounding rock material. Sadovsky (1971) has cast some doubt, however, on the existence of a relationship between the size of the cavity and the depth of burial.

In the following expression, the constant C characterizes this relationship between the cavity radius R, the explosion yield W and the depth of burial h (Nordyke, 1970):

$$C = \frac{R}{W^{1/3}}(\rho h)^{1/3\gamma}, \tag{2.1}$$

where ρ is the rock density, γ is the Poisson coefficient, taken to be 4/3. The value of C changes somewhat but not by more than 20% from one rock to another (tuff, alluvial material, granite and rock salt (halite) and by not more than 7% from one explosion to another if both are carried out in similar rocks).

If in Eq. (2.1), $W^{1/3}$ is replaced by the expression $W[(V_1 + V_2 + V_3)^{1/3}]/V_1$, where V_1, V_2, V_3 are the volumes of evaporated earth, water vapor and other volatile components (e.g., CO_2 and CO), if the volume of the ground evaporated is unity, then the constant C will exhibit reduced scattering for different rocks and different explosions. The problem with Eq. (2.1) is that only the evaporated earth (which is proportional to W) is considered, while the water content of the rocks and the presence of volatile components are ignored. Attempts to take into account the influence of rock water content upon the radius of a

Table 2.1
Values of constants in equation defining cavity size for a contained explosion in different rocks

Rock	Approximate composition	$\alpha = (1/3)\gamma$	ρ (g/cm^3)	C	Number of explosions
Granite	SiO_2+1% H_2O	0.324	2.7	103	2
Tuff	SiO_2+15% H_2O	0.292	1.9	97	11
Alluvium	SiO_2+12% H_2O	0.296	1.9	89	30
Rock-salt (halite)	–	0.311	2.3	96	2
Dolomite	–	0.329	2.3	89	1

cavity have been reported by Higgins and Butkovich (1967). On the basis of substantial experimental material (data on 46 nuclear explosions were used), it was shown that this influence could be taken into account if one were to introduce a dependence of the index of adiabatic expansion γ on the water content of the rock. It was also shown here that the cavity radius R did not depend (within the accuracy of the measurements) on the characteristics of the rock strength.

The magnitude of the constant C in the equation

$$R = C\frac{W^{1/3}}{(\rho h)^{1/4}} \tag{2.2}$$

which takes into consideration the water content of the rock, can be defined by the relationship

$$C = \left[\frac{3(\gamma' - 1)p_V^{1/(\gamma-1)}}{4\pi g^{1/\gamma}}\right]^{1/3}, \tag{2.3}$$

where $(\gamma' - 1)$ is a constant of proportionality linking the energy E with the quantity $p_V V_V$ for the ground that is evaporated (Higgins, 1967)

$$p_V V_V = (\gamma' - 1)E. \tag{2.4}$$

For rocks with different water content, the values of C are presented in Table 2.1.

Olsen (1967) has presented some calculations of the changes in pressure and temperature within the cavity of a contained explosion from the time when the cavity ceases to expand to the time of water vapor condensation. The experimental data used in the paper were obtained from an explosion of 6.5 kt yield. The character of the curve derived from the experimental data was similar to that of the calculated curve and the coefficients were ascertained on the basis of "experience". According to the calculations, water vapor condensation for the explosion (Olsen, 1967) began 6.6 min after time zero with a pressure of 11.7 bar and a temperature > 460 K. The high temperature in the cavity resides for a relatively long time as the thermal conductivity of the rocks outside the cavity is not high. For example, in the "Rainier" explosion, the temperature of about 1400 °C continued for 0.5–2 min and then stayed at 80 °C for longer than 5 months after the explosion (Johnson,

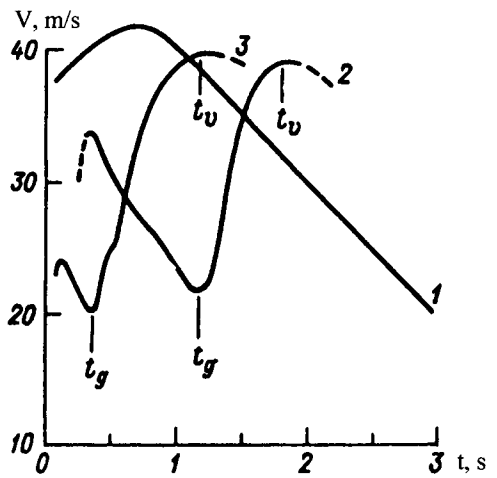

Fig. 2.2. The relationship between the vertical velocities of surface particles located at the epicenter of an underground explosion and time following an underground explosion: 1 — "Danny-Boy" $E = 0.42$ kt, basalt; 2 — "Sedan", alluvial material, $E = 100$ kt; 3 — "Schooner", alluvial material, $E = 0.5$ kt.

1959). In the "Gnome" explosion, 12 days after time zero, the temperature in the free part of the cavity exceeded 100 °C and in the debris zone it varied from 50 to 650 °C (Nifontov, 1965).

When an explosion takes place near the earth's surface, the compression shock wave is reflected from the surface in several tens of milliseconds (provided that the burial depth is at least several hundreds of meters for certain types of rock) and the wave of rarefaction spreads throughout the ground (Stratton, 1965). At a certain depth, the amplitude of the wave of rarefaction exceeds that of the wave of compression and the medium is broken under this tension; the surface layer of the rocks is separated and the underlying layers at some depth are crushed. Gases in the cavity continue to expand. Before the cavity vents, they give an additional acceleration to the overlying layers of rock at time t_g (Fig. 2.2) before emerging from the rock into the atmosphere at time t_v. The depth of rocks where this acceleration occurs can change markedly depending on the explosion depth (Johnson et al., 1959) and the type of rocks. The venting of gases may not always be synchronized with the gas acceleration. This phenomenon was observed first in explosions carried out in loose rocks where the shock wave is attenuated more sharply than in hard rocks and secondly in materials such as alluvial deposits and tuff, etc. where there is a considerable amount of water present which results in vapors with low temperatures of condensation (Knox, 1965; Toman, 1970; Izrael et al., 1970a). This acceleration can also be essential in explosions in rocks where significant volumes of volatile or gaseous substances are generated at the high temperatures.

A release of incandescent gases occurs at time t as the gas acceleration proceeds, i.e., within several tenths of a second or in several seconds after an explosion at a scaled depth of 40–60 m/km$^{1/3.4}$ (Johnson and Higgins, 1965; Izrael et al., 1970a).The gas release proceeds simultaneously with the destruction of the cupola and its transformation into a multitude of flying fragments. It reaches its maximum velocity when the pressure within the cavity

exceeds the lithostatic pressure arising from the overburden or, in the extreme case, when it is equal to atmosphere pressure (Dokuchaev et al., 1963). In the first situation, a significant portion of the energy is carried away with the outsurge of vapors and explosion products.

In the Soviet explosion "Sary-Uzen 1003" (Izrael et al., 1970b), conducted at a scaled depth of approximately 48 m/kt$^{1/3.4}$ in sandstone, the gas acceleration phase was clearly measurable 0.25 s after the explosion. At this time, the lifting speed at the cupola surface (a height of 7 m) reached 60–70 m/s. In 0.4 s after the explosion (with the cupola height now at 19 m), a visible outburst of gases took place, resulting in the formation of a spherical plume on the cupola top. The gas release proceeded at a velocity of 170 m/s. A bright luminescence, observed on the plume surface, stopped 1.5 s after the explosion. During the lifting process, the cupola gradually took on a cylindrical shape. In this detonation, the maximum height attained by heaving rocks was 190 m with a diameter of 240 m, all occurring within 6 s after the explosion. An effort to calculate the geometry of the cavity during the gas acceleration phase and of the funnel after the explosion and the ground release was made by Knox (1965) for the "Scooter" chemical explosion. The configuration of the cavity above the center of the explosion and the topography of the free surface during the gas acceleration phase were determined using Newton's second law of thermodynamics as the basis of the calculation of acceleration of elementary ground volumes (masses), corrected for frictional forces.

A more perfect method of calculating the dimensions of the cavity, funnel and ground bulk, taking medium property into account, has been proposed in Terhune et al. (1970) and Cherry (1967). Using data on medium properties obtained in the laboratory made it possible for these authors to calculate the parameters of funnel formation in a number of explosions where ground ejection occurred. On the basis of various calculations, one can conclude that the methods described by Teller et al. (1968), Morokhov (1970) and Cherry (1967) would indeed allow an accurate description of the geometry of the cavity and the funnel to be made if the yield, depth of the charge and the medium properties are known.

The temperature regime in the cavity of an underground explosion is of great importance for the calculation of particle activation and height of cloud lifting. Izrael (1966) has calculated the temperature regime in a cavity using information on the development and venting of the cavity resulting from an underground explosion of 100 kt yield at a scaled depth of 50 m/kt$^{1/3.4}$ conducted in alluvial material (explosion of the "Sedan" type). The water content in the rock was taken to be 10%. The initial radius of the cavity (the lower part of a hemisphere) was calculated on the basis of a one-dimensional hydrodynamic elasticity–plasticity model of rock behavior in an explosion (Butkovich, 1965). The configuration of the cavity as it developed and vented was calculated according to the scheme presented by Knox (1965). Certain assumptions, described in Knox (1965), Johnson et al. (1959), Johnson and Higgins (1965) were made, viz.:

a) about half of the explosion energy (32–47%) is consumed by rock heating and melting;
b) the melting and heating of the ground and, as a result, the generation of water vapor in the process take place mainly within the space of the initial cavity (at time t_c);
c) the temperature and pressure at all points within the cavity are uniform;

d) the temperature of melting the rock is 1500 °C; if water constitutes 15% of the rock, then the specific enthalpy for the molten state is 700 cal/g, while for the vapor state at about 3000 °C it is 3000 cal/g.

It was also assumed that thermodynamic equilibrium existed in the "melted rock–gas" system in the cavity. Calculations revealed that $\sim 6 \times 10^4$ t of the rock would be melted and 6×10^3 t of water evaporated. Given the number of assumptions indicated, only rough estimates of these parameters can be calculated. No account is taken of the many real conditions that remain uncertain or even undefined. Nevertheless, such estimates can sometimes lead to useful conclusions.

At the moment of venting, the cavity volume, as calculated on the basis of data taken from Knox (1965), was 1.1×10^7 m^3 and, at the time of fragmentation through gas acceleration, the rock fragments were calculated to occupy a volume of approximately 1.8×10^7 m^3 (V_{max}) and to have risen to a maximum height of 130–150 m. The temperature regime within the cavity was calculated assuming that during the time interval Δt the gas expanded in an adiabatic manner ($p_c V$ = constant), but then immediately thereafter, due to the heat influx from the molten earth, it heated up to the temperature of the latter. According to data from Ryabinin (1959), within the range of temperatures and pressures under consideration, the ratio of the water vapor heat capacities $\gamma = C_p/C_v = 1.2$. As shown by Vorgaphnik (1963) for the most common gases at temperatures of 1400–1500 °C and pressures up to several atmospheres, the γ values range from 1.16 to 1.20 for carbon monoxide, water vapor and carbon bisulphide and are about 1.30 for nitrogen and oxygen, suggesting that for these gases they are almost the same. The pressure in the cavity, as calculated, amounted to about 5 bars, taking into consideration the thermal expansion at the time t_v of venting. It was found that the energy input required by the cavity gas during its adiabatic expansion for successive time intervals Δt from the initial volume V_c to the maximum V_{max} was significantly less than the energy released on solidification of the molten rock. Since, during the cavity expansion up to the volume V_{max}, the heat losses due to emission and heat conductivity are not significant, the temperature of the incandescent gases does not drop below 1500 °C in this example. It is quite probable that this feature of the temperature regime was not taken into account when predictions were made of the height of the ensuing cloud for the "Sedan" explosion. It was obviously assumed that the temperature of the gases would be significantly lower at the time of their escape. This seems to be the only explanation why the predicted cloud height (1200 m) turned out to be almost four times lower than the actual height (Johnson et al., 1959).

It is interesting to consider the effects that could arise when the gas temperature and the melting point temperature of the rock are the same at about 1500 °C. To do this, we estimate, for the general case, the ratio between the heat A_1, released by the melted rock within the cavity of the explosion during its solidification (due to the specific heat), and the work A_2, accomplished by the gases of the cavity during their expansion from the initial volume V_c to the final volume (at the moment of venting). We take the temperature in the initial volume of the cavity to be higher than that of the molten rock. We also assume

that the temperature of the rock has already fallen but that the heat released during the solidification of the rock has not yet been consumed. Thus, for isothermal processes,

$$\frac{A_1}{A_2} = \frac{Q\alpha}{(Q\alpha_2/\mu_2 + Q\alpha_3/\mu_3)RT \ln(V_{\max}/V_c)}, \tag{2.5}$$

where α is the heat of rock melting (about 90 cal/g); $(Q\alpha_2/\mu_2 + Q\alpha_3/\mu_3)$ is the quantity of gas moles in the cavity (per unit of explosion yield); $V_{\max} \approx (2/3)\pi h^3$ is the cavity volume at the time of maximum expansion (lifting); V_c is the cavity volume at time t_c. Consequently, when the water content in the earth is as much as 25% (by mass) and the explosion depth is 200 m below the scaled depth of 50 m/kt$^{1/3.4}$, under the equilibrium conditions existing between liquid (molten earth) and vapor phases at the time of cavity venting, the temperature of the incandescent gases does not drop below that of the molten ground (1400–1500 °C). At the moment (the volume is V_c) the temperature in the cavity reaches more than 1400 °C and the cavity vents with a pressure greater than one atmosphere (Knox, 1965), the gas temperature at venting is equal to the temperature of the molten ground and, if the rock is significantly more liquid, it can even exceed the ground melting temperature such as occurred in the "Sary-Uzen 1003" test (Izrael et al., 1970b).

Hence, despite the imperfect nature of a number of the assumptions (for example, incomplete equilibrium between liquid (melted ground) and vapor phases), we can see that, in the most frequent cases observed in practice (a rock water content up to 10–12%), by the time of venting the temperature in the cavity does not drop below that of the melting ground. In the "Sary-Uzen 1003" explosion, the temperature of the illuminated area on the cupola surface where the gas escape took place actually reached 1900–2100 °C. This conclusion is extremely important for explaining the effects of nuclide fractionation and in calculations of the radioactive cloud height in underground cratering explosions.

2. Release of Radioactivity into the Atmosphere and Formation of a Cloud and Base Surge in an Underground Nuclear Explosion

In an explosion where there is ejection of earth into the atmosphere after cavity venting, the incandescent gases begin to rise. According to calculations made by Izrael (1966), the velocity of ascent of the gas bubble is controlled by Archimedean forces and will exceed that of the rock ascent in 4–5 s after the time of the explosion (up to 100 kt yields). The final separation of the gas bubble takes place after the rock fragments fall. It is then that a significant fraction of the gases inside the cavity escapes (i.e., 6–14 s after the explosion) and cloud formation begins. In underground cratering explosions, the cloud ascent happens in a way similar to that from surface atmospheric explosions because the cloud's initial temperature corresponds to that of rock melting, i.e., $\sim$ 1500 °C. The change in temperature within the cloud with time is also generally similar to that in an atmospheric explosion. Stabilization of the cloud, i.e., when its temperature becomes equal to the ambient temperature, occurs only after several minutes after the explosion. Thus, in the "Sedan" explosion, the cloud stabilized after 5 minutes when it reached a height of 4000–4500 m.

Unlike an atmospheric explosion, an underground cratering explosion results in a huge quantity of dust and ground particles being contained in the cloud, especially in the lower section, and this hampers the heat emission from the cloud. After several tens of seconds from the time of the explosion, a base surge begins to be generated. The surge overtakes the lower part of the bubble of hot gases and promotes the long-term retention of the great heat. According to the calculations of Izrael (1966), the base surge and the lower part of the cloud represent a zone where the temperature is sustained at a level not lower than that of the molten ground (about 1500 °C) for a relatively long time (not less than 5–10 s for explosions of 1–2 kt yield and 6–14 s for those of 100 kt yield). It is quite possible that this time could be even longer since there is a dense layer of fine ground particles that descends more slowly than the rock fragments and which could sustain the conditions required to maintain the high temperatures within the zone.

At the "Sary-Uzen 1003" explosion, the base surge propagated over a volume of 600 m in diameter for 35–40 s. Like the cloud, the maximum height of the dust column, of diameter 120 m, was 300 m (Izrael et al., 1970b). The atmospheric inversion layer in existence at the time limited any further ascent.

The geometric dimensions of the main cloud and of the base surge depend on the total yield of the explosion and the rock characteristics in the immediate locale, as well as the depth of the charge and the meteorological conditions prevailing at the time of cloud formation. For underground explosions that take place in rocks that are similar in composition, the relationships between the dimensions of the cloud and the base surge resemble one another despite any yield differences. The development of both high-yield "Sedan" (Ferber, 1965) and "Sary-Uzen 1003" (Izrael et al., 1970b) explosions was actually the same.

The dependence of the geometric dimensions of the cloud and the base surge on the yield of underground explosions in alluvial materials has been determined by Knox (1965) on the basis of both chemical and nuclear explosions. In a group explosion, when individual charges are placed at an optimal distance so as to form a channel, cloud heights and the base surge will not actually differ from those in a single explosion (Knox, 1965). As already indicated, when cavity venting and funnel formation take place in underground nuclear explosions that are carried out near to the earth's surface, the radioactive products penetrate into the atmosphere and contaminate the environment. The degree of contamination of the atmosphere and the surrounding land after an explosion is controlled by the following factors:

(1) the total quantity of radioactivity generated by the explosion;
(2) the fraction of radioactivity released into the atmosphere;
(3) the characteristics of the radioactive particles at different depths in the different rocks;
(4) the degree of dilution of the radioactive products in the atmosphere via meteorological factors.

As noted above, when an explosion is performed near the earth's surface, at a scaled depth $\bar{h} = h/W^{1/3.4}$, of less than 60–80 m/kt$^{1/3.4}$, venting of the cavity can take place which is then followed by the ejection of radioactive products into the atmosphere. The depth from which the "primary" ejection of radioactive products into the atmosphere can

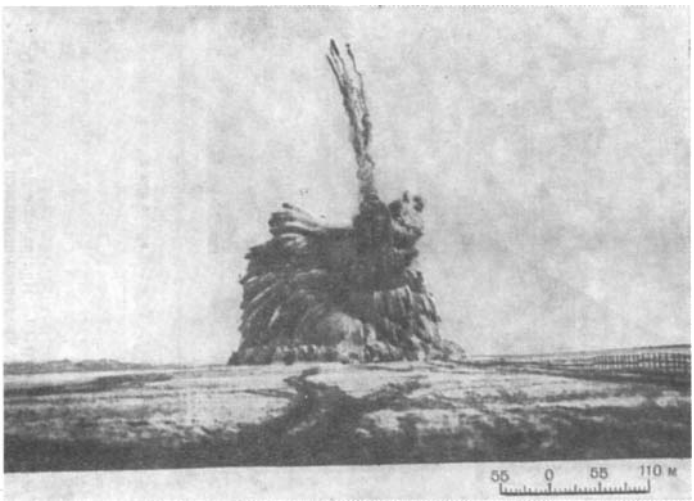

Photograph of dome formation and gas breakthrough at the "Sary-Uzen 1003" explosion at $T = 6.3$ s.

take place depends on the water content and the quantities of volatile substances in the rock, its strength characteristics, etc. An exact boundary dividing contained explosions and those that produce craters cannot be fully defined. For example, the majority of cratering explosions were performed at depths of less than 55 m/kt$^{1/3.4}$ (see Table 4.1). At the same time, a number of explosions performed at a depth of 70–80 m/kt$^{1/3.4}$ were contained (Higgins, 1970). However, the "Blanca" explosion at $\bar{h} = 90$ m/kt$^{1/3.4}$ resulted in an ejection of radioactive products into the atmosphere (Knox, 1965).

In a cratering explosion, a lifting of the ground dome (cupola) takes place and this precedes the gas outburst. During this heaving, the dome gradually takes on a cylindrical form. After the outburst into the atmosphere occurs, the incandescent gases begin to rise, thus forming the radioactive cloud. An underground explosion is followed by the formation of a powerful base surge and a central dust column (see photo).

Within the temperature regime described above, the rock that is melted inside the cavity captures the radioactive products and is later broken into fragments; individual slag-like formations and smaller particles of irregular form can result. Assuming that activation of the particles begins in the cavity when the melted ground is still not broken up and thermodynamic equilibrium still exists, one might expect that the radioactive products would be regularly distributed over the entire volume. With the temperature close to 1500 °C, the particles of the original earth can be fused or slightly softened and can bind the refractory nuclides very tightly. In such particles, the radioactive products are concentrated in the outer layers. Volatile nuclides will be deposited on the surfaces of the particles that remain in the cloud or the base surge after cooling (similar to the processes in an atmospheric explosion). This has been confirmed by experimental data obtained at the the "Sary-Uzen 1003", "Sedan" and "Schooner" explosions (Izrael et al., 1970b; Lane, 1962).

Following an underground explosion, the melted ground and the radioactive particles from the high-temperature zone form the first source of radioactive contamination of the

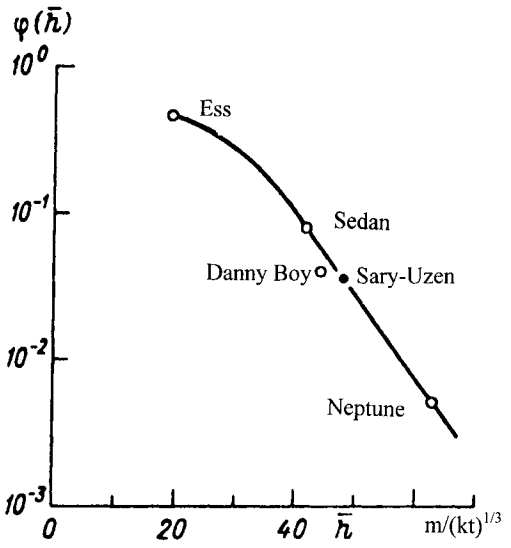

Fig. 2.3. Dependence of the fraction of total radioactivity deposited near to ground zero on the scaled depth of the underground explosion.

land. The products that are filtered through the layer of ground material forming the disintegrating cupola and those that settle on the finer particles in the cloud form the second source. These are mainly products having gaseous of rather volatile precursors in the radioactive decay chains. Their composition and quantity depend on the period of existence of the filter layer as well as on its thickness and its degree of breakdown, i.e., ultimately on the yield and scaled depth of the explosion. The total quantity of refractory products entering the cloud for explosions conducted at a scaled depth of 40–50 m/kt$^{1/3.4}$ is negligible (tenth of a per cent or less) while the fraction of the nuclides having gaseous precursors that enters the cloud is 10% and more (12% for ^{137}Cs in "Danny-Boy" according to Bonner and Miskel (1965)).

The magnitude of atmospheric and terrestrial radioactive contamination following an underground nuclear explosion is basically determined by the total quantity of radioactivity released by the explosion, the fraction that enters the atmosphere and by the degree of dilution in the atmosphere. In addition, the character of the contamination depends on the geometry of the contamination source (i.e., the cloud and the base surge) and the distribution of radionuclides in the cloud on the various sizes of particles and hence on radionuclide fractionation. The total amount of radioactivity generated is defined by the quantity of fission debris as well as by the induced activity resulting from the interaction of the neutrons of the explosion with the construction materials of the explosive device and the nuclei of the elements composing the rocks in the immediate zone of the explosion. The characteristics of these radioactive products are described in Chapters 1 and 3. Problems concerning the distribution of nuclide activity over the particles and the fractionation of these are presented in Chapter 1 and in the following paragraphs. Here, we dwell on the component of the radioactive products ejected by the underground explosions into the atmosphere.

A number of attempts have been made, using experimental data, to derive the relationship between the fraction of total activity φ released into the atmosphere or deposited near ground zero and the scaled depth, $\bar{h}$, of an explosion. In some papers, the scaled depths were expressed in m/kt$^{1/3}$ while in others in m/kt$^{1/3.4}$. In Nordyke and Wray (1964), the fraction of the total activity φ was expressed as a function of the ratio of the explosion depth to that of the visible funnel. The use of this expression has been found to be unsuitable. Using the function $\varphi(\bar{h})$ where the depth $\bar{h}$ is expressed in m/kt$^{1/3}$ (Fig. 2.3) probably corresponds better to the experimental data, although, as already mentioned, the law of geometric similarity is not fulfilled in nuclear explosions.

There is no description in the literature of the function $\varphi_i(\bar{h})$ for individual nuclides. However, we believe that such functions can be useful and will not depend on the time of measurement. Clearly, the quantity of volatile nuclides, or those having gaseous precursors, that escape into the atmosphere should be greater than the quantities of refractory nuclides that escape (for the same detonation depth). As already mentioned, even in completely contained explosions, only negligible quantities of volatile products escape into the atmosphere through rock fissures (e.g., inert gases, iodine and those having volatile precursors).

In addition to the factor of scaled depth for an explosion, part of the radioactive products that are released to the atmosphere apparently depends on rock composition (the content of water and volatile products) as well as on its strength characteristics. Thus, for example, in an excavative explosion in hard dry rocks, the fraction of radioactivity released into the atmosphere amounts to $\sim 5\%$ and, for such an explosion in loose moist rock, it can be as much as 30% (Ferber, 1965).

3. Characteristic Features of Radioactive Particles from an Underground Nuclear Explosion

All radioactive particles generated by underground explosions and released into the atmosphere can be subdivided into two main types according to the location and temperature conditions of their formation. Particles of the first type are generated from the disintegration of melted rock and activated in the explosion cavity at high temperatures. In such particles, the activation products are usually homogeneously by distributed. Particles of the second type are fragments of relatively cold rock that are fractured well above the depth of the cavity. Such particles are homogeneously activated over their entire surface or only over a thin volumetric surface layer.

Very soon after an explosion (in tens of seconds up to several minutes), the radioactive products are distributed between the main cloud, the cloud of the base surge and the zone of funnel and the ground itself. Within the main cloud and that of the base surge, the distribution of the radioactive products is continuously changing due to the fallout of the larger particles and the activation of the remaining particles by products having relatively long-lived gaseous precursors. To predict the fallout's potential radionuclide composition we need to know the distribution of radioactivity on the particles of different sizes and their spatial distribution in the main cloud and that of the base surge. To estimate the radioactivity distribution over all particles we need to add the activities of the main cloud

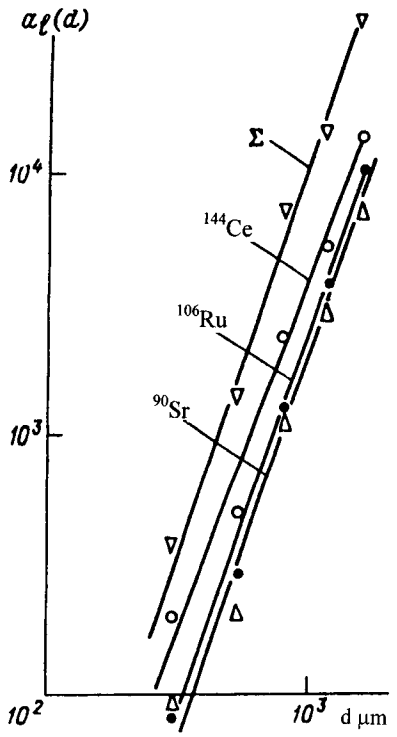

Fig. 2.4. Dependence of activity on particle size for different nuclides in particles of the first type.

to those of the cloud of the base surge and of the fallout already formed and then distribute the activity over all existing particles (present or available).

Larger slag-like particles, influenced by gravity, and many finer particles, entrained by the huge volume of falling neutral rock mass, are distributed over the funnel periphery and in the ground bulk. Already, in less than several minutes, no larger particles remain in the main cloud and that of the base surge. For example, by 12 minutes after the "Schooner" explosion, no particles of diameter larger than 177 μm were found (Heft et al., 1971). The basic features and regularities of the distribution of different types of particles were investigated for the "Sary-Uzen 1003" and "Chagan 1004" explosions and for the small yield devices "Telkem-1" and "Telkem-2" (Izrael et al., 1970a).

Radioactive particles in the cloud of underground explosions have mainly irregular forms, spherical particles being rarely observed (Izrael et al., 1970a; 1970b). Their structures are also different, being slag-like and porous, "sugar-like" and glass-like. The size distribution of the radioactive aerosols in the cloud, observed at different times following an explosion (from 0.3 to 4.0 hr), is satisfactorily approximated by a normal logarithmic function with about 90% of the particles having diameters of less than 0.5 μm. The distribution of particle activities with size also follows a normal logarithmic function but, in this case, it provides a less accurate description. The median diameter of the particles (in this latter relationship) is approximately 2 μm at any given time (Izrael et al., 1970b). Figure 2.4 shows the distributions of total activity of the particles with size $a_l(d)$ in the

clouds from various explosions. It is seen here that the carriers of radioactivity for the very small-yield devices "Telkem-1" and "Telkem-2" are all finer than those for the "Sary-Uzen 1003" and "Chagan 1004" explosions (Izrael et al., 1970a).

Immediately after an explosion, the cloud still contains radioactive particles that are subsequently deposited in the near zone. Thus, in one sample taken 3 s after an explosion, about 80% of the activity was on particles larger than 10 μm, while only 1% was on particles smaller than 0.5 μm. As already noted, all explosion particles can be divided into two types. Fallout particles, in particular, can be classified in this way because of their distinctive size range.

Particles of the glass-like structure, formed from the melted rock, can be assigned to the first type of particle (Izrael, 1970a). These have irregular forms with a great number of gas inclusions. The density of these particles (1.8–2.3 g/cm^3) is 1.1–1.7 times less than that of the initial neutral rock from the place of the explosion. In appearance, the particles resemble fragments of a broken glass from light to dark in color. Rarely observed are those particles that are typical of surface explosions, having a regular spherical form, transparent and dark with a shiny surface, or drop-like in nature.

Heft et al. (1971) distinguished two varieties among the slag-like particles of the first type, viz. (i) black, shiny particles like the mineral obsidian and having the largest content of refractory nuclides, and (ii) transparent, glass-like particles having frequent inclusions of a black material. The authors believe that the former particles were formed from the melted rock adjoining the inner surface of the cavity. The fact that one can find, among these slag-like particles, those of molten rock originally melted rock, having different properties, from different parts of the cavity and apparently not completely mixed, confirms the other observation that particles of this type, having the same size, can exhibit activities that differ by up to 4 orders of magnitude (Izrael et al., 1970b).

Particles of the second type are formed from relatively cold rock crushed by the explosion, which determines their form and appearance. Other particles, fused at their surfaces, can also be attributed to this type. Conglomerates, consisting of particles of the same or different varieties, are also among these particles.

In addition to the two main types, several sub-types of particles can be separated. Thus, four sub-types of particles were identified in the first classification proposed by Izrael et al. (1970b). Five subtypes can now be identified—three within the first major type and two within the second. The following belong to the first type of particles: (1) dark bright particles (like obsidian) formed from the melted rock associated with the inner part of the cavity, (2) transparent glass-like particles with irregular forms, and (3) glass-like particles of regular spherical or drop-like form. Amongst the second type are: (1) particles whose appearance and density do not differ from those of the rock crushed by the explosion and (2) particles of crushed rock, fused at the surface. Investigations of the activities of the different particles have revealed that the activity of the first type of particles is significantly greater than that of the second type (Izrael et al., 1970a).

Layer-by-layer etching of the particles with hydrofluoric acid has shown that the activity (total and of individual nuclides) is distributed practically uniformly for particles of the first type while, in those of the second, it is distributed over the surface or in thin surface layers. It was shown by Izrael et al. (1970a) that the surface layers of the second type particles

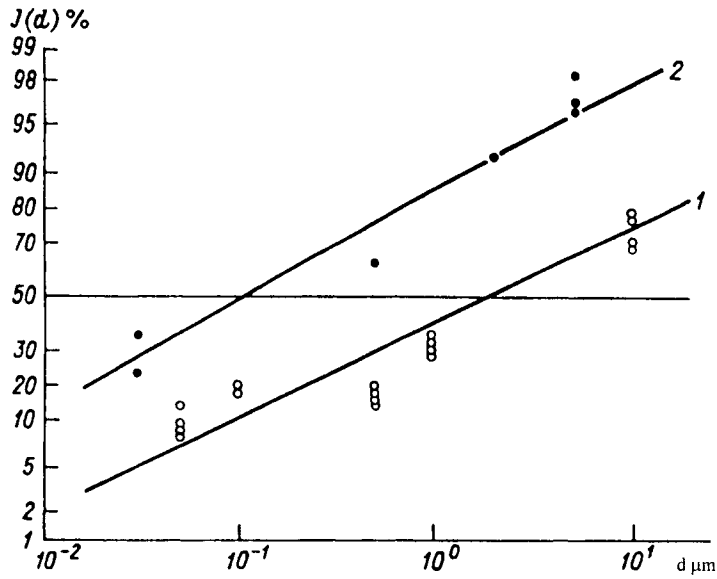

Fig. 2.5. Distribution of particle activity as a function of size for various explosive yields.

(constituting about 5% by weight), contain up to 25–30% of the activity; and up to 50–100% of the activity when the weight attains 10% of the total, while in particles of the first type the activity concentration is practically constant overall. A similar result is obtained from studies of the dependence of the total and individual nuclide activity on the particulate size distribution; the relationship is close to being cubic for first type particles. In this case, the particles are depleted in light/volatile nuclides and those that have gaseous precursors.

The activity of the particles can be expressed as an exponential function of their size by $a(d) \approx d^n$ (Izrael et al., 1970b) (for atmospheric nuclear explosions). Here, $n = 2.7$–3.0 for the first type of particles, and $n \approx 1.9$ for the second type. For the former, the cubic dependence of the particle activity on size is valid for individual radionuclides as well (Fig. 2.5). Data obtained at the "Sedan" explosion show similar results (Lane, 1969). Izrael and Kazakov (1970) have found that the size distribution of particles of the first and second sub-types is described by a logarithmic function and that other distribution parameters, e.g., the median diameter and the degree of dispersion, are different for different fallout zones and vary with distance. The dependence of the particle activity on size is also logarithmic (see Fig. 2.6).

Heft et al. (1971) have attempted to determine the particle size distribution for different radionuclides after the "Schooner" explosion. The distributions and particle activities were examined individually for the cloud, the base surge and the fallout. Activities were determined in the melted rock and on the surfaces of particles of rock from immediately above the cavity. The distribution was determined first for ^{147}Nd (considered to be totally distributed in the melted rock) and for ^{181}W that is distributed mainly on particles of the second type but which is also present in the melted rock. Twelve minutes after the explosion, the typical value of the atom ratio ^{181}W/^{147}Nd in the cloud was $(1.6–1.7) \times 10^4$

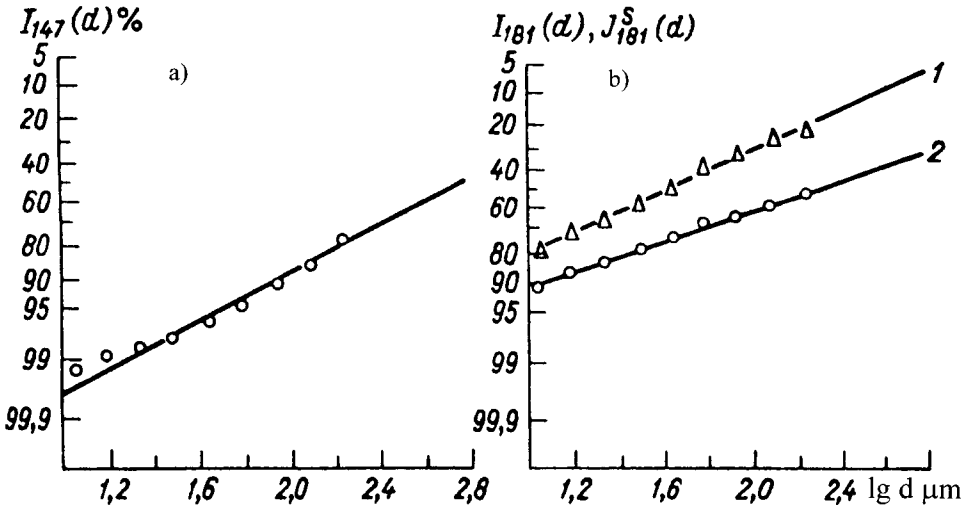

Fig. 2.6. Change in the activities of (a) ^{147}Nd and (b) ^{181}W associated with particle sizes greater than d (integral distribution of activity of ^{147}Nd and ^{181}W over the particle sizes): (a) $I_{147}(d)$; $\log\bar{d} = 2.785 \pm 0.648$, $\bar{d} = 609.5$ μm; (b) 1) $J^{\nu}_{181}(d)$; $\log\bar{d} = 1.640 \pm 0.704$, $\bar{d} = 43.7$ μm; 2) $I_{181}(d)$; $\log\bar{d} = 2.322 \pm 0.972$, $\bar{d} = 210$ μm.

and in the base surge it amounted to 2.7×10^4. After 3–4 hr, this ratio increased in the cloud to $(9–16) \times 10^4$. In the bulk ground and the fallout pattern, the ratio $^{181}W/^{147}Nd$ increased from 1.5×10^3 (150–180 m) to $(1.0–1.4) \times 10^4$ (1000 m) and then decreased slightly with distance. The average (representative) value for the bulk ground was taken to be 2.37×10^3.

The distribution of the particles in the size range 11–177 μm was also studied (at 12 minutes after the explosion, particles greater than 177 μm were already absent from the cloud and particles smaller than 11 μm had a descent velocity comparable to that of atmospheric vertical motions). The activity of ^{147}Nd obtained for different groups of particle sizes within this range was summed and distributed over the bulk ground, the cloud and the cloud of the base surge. The size distribution of the ^{147}Nd activity over all particles was expressed by the logarithmic function:

$$\Phi_{147}(Z) = \frac{1}{\sigma_{147}\sqrt{2\pi}} \exp\left[-\left(\frac{\log\bar{d}_{147} - \log d}{\sigma_{147}\sqrt{2}}\right)^2\right]. \tag{2.6}$$

Here, $\Phi_{147}(Z)$ is the probability that ^{147}Nd is present in particles whose sizes range from Z to $(Z + dZ)$, where $Z = \log d$ (d is the particle diameter) and the logarithm of the particle median size $\log d_{147} = 2.785$, while the distribution dispersion factor $\sigma_{147} = 0.648$. The median size of the particles was approximately equal to 610 μm. The distribution indicated is obviously valid not only for ^{147}Nd but also for all refractory products of the explosion.

Figure 2.6a shows the change of $I_{147}(d)$, the integral size distribution of particle activity for the fraction of ^{147}Nd associated with particles possessing a size greater than the

indicated (d). For ^{181}W $\log d_{181} = 2.322$, $\sigma_{181} = 0.972$ and the median diameter was 210 μm. Integral distribution of $I_{181}(d)$ and $J^s_{181}(d)$ is shown in Fig. 2.6b (Heft et al., 1971).

4. Fractionation of Nuclides in the Radioactive Particles Produced by Underground Nuclear Explosions

Because of the varied origins of the different particle types as well as the different conditions of their activation, the particulate radionuclide composition of explosion products is variable. The nuclides formed in the explosion are also fractionated due to different thermal conditions that exist at the time of their formation, the conditions of their activation and the different rates of passage of the particles through active zones.

In an underground nuclear explosion, the process of fractionation is extremely complicated and the coefficients of fractionation are very scattered, more so than in atmospheric nuclear explosions. Our knowledge of the fractionation processes makes it possible, however, to estimate the nuclide composition of the radioactive fallout, to predict it and, in addition, to develop an idea of the processes that cause activation of the molten and crushed rock and the formation of the particles constituting the ensuing fallout.

Let us consider the fractionation effects for the different particle types. Analysis of experimental data shows that the radioactive products in the particles of the explosion cloud differ substantially from those in a non-fractionated mixture of the explosion products. Table 2.2 presents the fractionation coefficients for certain individual nuclides compared to the refractory species ^{99}Mo and ^{147}Nd (or ^{95}Zr) that are weakly fractionated (Izrael et al., 1970b; Heft et al., 1971; Izrael et al., 1970a; Miskel, 1966; Bonner and Miskel, 1965). Analysis of the data in Table 2.2 and the known parameters of the explosions mentioned above allows the following conclusions to be made with respect to the fractionation of the radioactive products in the explosion cloud:

1. The radioactive products are significantly depleted in the nuclides of refractory elements and are enriched in those having gaseous precursors.

2. The degree of enrichment of these nuclides correlates with the half-lives of their precursors. The fractionation coefficients for all nuclides (with respect to the refractory nuclides) decrease in magnitude according to the following sequence: ^{144}Ce, ^{95}Zr, ^{131}I, ^{103}Ru, ^{141}Ce, ^{92}Sr, ^{140}Ba, ^{91}Y, ^{139}Ba, ^{90}Sr, ^{137}Cs, ^{89}Sr and ^{138}Cs.

3. There is a weak dependence of the fractionation coefficients on the scaled depth of the explosion. The lowest fractionation coefficients were recorded for the radioactive products from the cloud of the "Chagan 1004" explosion where cavity venting was greatest and a very distinct cloud was formed. The same was observed in the cloud of the "Palanquin" explosion where the radioactive products escaped easily into the atmosphere through a ground fissure. The highest fractionation coefficients were noted in the "Telkem-2" and "Sulky" explosions where no radioactive clouds were produced.

4. With lower explosion yields, there is a tendency for the fractionation coefficients to be higher (for example, in the "Danny Boy" explosion as compared to the "Sary-Uzen 1003" explosion). In the clouds of small yield explosions (e.g., "Sulky", "Telkem-1",

Table 2.2
The fractionation coefficients for particles in a radioactive cloud after different underground cratering nuclear explosions

Name of explosion	Time of sampling	^{89}Sr	^{90}Sr	^{91}Y	^{103}Ru	^{131}I	^{137}Cs	^{140}Ba	^{141}Ce
Palanquin[1]		2	–	–	–	–	0.4	0.5	0.6
Sary-Uzen, 1003[2]	3–5 s	0.004	–	0.3	0.8–1.3	0.02	0.1	0.4	0.6–1.1
Chagan, 1004[2]	0.25–1.1 hr	35	11	12	7.1	9.6	25	12	4.3
Sary-Uzen, 1003[2]	1.5–2.4 hr	48–93	–	13–26	3.4–5.4	0.2–1.2	19–35	25–37	4.9–5.3
Danny Boy[1]	15 min	236	137	45	–	–	212	54	567
Danny Boy[1]	2.3 hr	754	421	130	–	–	755	155	11
Schooner[1]	3 hr	–	–	–	6.8–11.3	–	–	–	–
Telkem-1, 2308[2]		8.3×10^3		3.7×10^3	97	43	5.3×10^3	3.3×10^3	2.3×10^2
Telkem-2, 2305–2307[2]	5 min–2.4 hr	1.4×10^4	6.5×10^3	6.1×10^3	72	23	1.4×10^4	5.6×10^3	6.1×10^2
Sulky[1]		10^5	–	–	–	–	7×10^2	10^4	7×10^2

Note: 1 — refers to coefficient of enrichment with respect to ^{147}Nd; 2 — coefficient of enrichment with respect to ^{99}Mo.

"Telkem-2"), the fractionation coefficients for nuclides having volatile precursors are much larger than for those in the clouds of middle or high yield explosions.

5. As the time of sampling lengthens, the fractionation coefficients sharply increase due to the increased presence of nuclides of volatile elements or those having volatile precursors, corresponding to more particles of smaller and finer sizes.

Samples taken from the cloud several hours after an explosion are strongly enriched in nuclides with gaseous precursors, i.e., the radionuclide composition of the cloud which travels over long distances is represented by a collection of the following species: ^{89}Sr, ^{90}Sr + ^{90}Y, ^{91}Sr + ^{91}Y, ^{137}Cs, ^{140}Ba, ^{103}Ru and ^{141}Ce, the latter two being present in smaller quantities. Samples with such a radionuclide composition are not found in either the near zone or in the pattern from the dust column. At the same time, samples taken during the first seconds after the explosion are very similar in their nuclide composition to those of the slag and the earth taken from regions of the funnel and the ground bulk. Studies of the composition of individual particle fractions taken from the same sample have shown that the fractionation coefficients of the radionuclides change insignificantly over a wide range of particle sizes (from 0.05 to 10 μm) and for individual nuclides the distribution of activity over the particle fractions is similar to that of the total activity.

Following the former USSR explosions at "Sary-Uzen 1003", "Chagan 1004", "Telkem-1" and "Telkem-2" some studies were undertaken of the nuclide composition of particles taken from other contaminated zones, along with the effects of fractionation (Izrael et al., 1970a). It was found that the radionuclide compositions of different types of particles were dissimilar. Particles of the first type were significantly depleted in the volatile species (iodine-131, tellurium-132) and those nuclides having gaseous precursors (strontium-89, barium-140). In contrast, particles of the second type were enriched in the nuclides from these groups. Particles from two different size fractions of each type (400–600 μm and smaller than 50 μm) also differed in their nuclide composition, with those smaller than 50 μm being enriched in highly volatile nuclides.

The biological accessibility of the radioactive particles is drastically different for each particle type. About 12% of the activity of type-one particles can become available while, for the second type, up to 60–80% is available in aqueous media. On the basis of this study and measurements of ground samples after the "Sary-Uzen 1003" and "Chagan 1004" explosions, over a distance up to 50 km from the site of the explosion, we could establish that:

(i) Pieces of the slag taken from the explosion funnel were depleted in nuclides having volatile precursors.
(ii) For the whole zone close to the epicenter, the nuclide composition was typical of the slag fragments. The depletion of the nuclides was less distinct in these materials. However, on the lee side, samples were enriched in these nuclides, even though to a minor degree.

After the "Sary-Uzen 1003", "Chagan 1004", "Telkem-1" and "Telkem-2" explosions, in the ground bulk area the average fractionation coefficient of all radionuclides, except those having comparatively long-lived gaseous precursors (^{89}Sr, ^{90}Sr, ^{137}Cs, ^{140}Ba), was close to unity. The epicenter zone of the explosion was depleted in ^{89}Sr, ^{90}Sr, ^{137}Cs and ^{140}Ba nuclides. For ^{89}Sr, ^{90}Sr and ^{137}Cs, the average coefficient of fractionation lay

Table 2.3
Coefficients of nuclide fractionation relative to ^{95}Zr in different zones of the "Sary-Uzen, 1003" and "Chagan, 1004" explosions

Zone	^{91}Y	^{140}Ba	^{103}Ru	^{144}Ce
"Sary-Uzen, 1003" explosion				
Bulk ground	0.83	0.85	1.2	1.3
Cloud pattern	1.90	2.2	0.90	1.1
Base surge pattern	2.3	3.5	0.84	0.93
"Chagan, 1004" explosion				
Bulk ground	–	0.67	1.3	–
Cloud pattern	0.85	1.15	0.93	0.85
Base surge pattern	2.7	1.3	1.3	0.8

between 0.2 and 0.5 and for ^{140}Ba it was within the range 0.7–1.0. For the ground pattern, a rather insignificant increase in the relative content of the volatile nuclides, or those having volatile precursors, with distance from the epicenter was a typical finding. The fractionation coefficients in first type particles in the ground pattern for ^{90}Sr (with respect to ^{95}Zr) were approximately 0.2, and for ^{106}Ru about 0.5–0.7.

The radionuclides with gaseous precursors were enriched in the base surge fallout when compared with the cloud pattern and the ground bulk zone. Table 2.3 shows the average coefficients of fractionation for the ground bulk zone, in fallout from the cloud of the base surge and in the cloud pattern after the "Sary-Uzen 1003" and "Chagan 1004" explosions. On the basis of these data, it is clear that there is enrichment of particles of the volatile species in fallout in comparison with the fallout in the cloud pattern. It should be recalled that particles in the far zone of the fallout would contain significant quantities of nuclides with volatile precursors.

Analysis of soil samples taken from the region of the Chagan "atomic lake" (explosion 1004) showed, during later years, increased concentrations of radionuclides that are the products of activation of soil components, ^{60}Co, ^{152}Eu, ^{154}Eu. A good correlation was also found between the concentrations of ^{239}Pu and ^{241}Am; ^{90}Sr and ^{137}Cs; and ^{60}Co and isotopes of europium. The ratio $A^{239}Pu/A^{241}Am$ was $\sim$ 1.4–4.0 (in other places up to 10); $A^{90}Sr/A^{137}Cs \sim 0.6$–2.0 and $A^{152}Eu/A^{154}Eu \sim 1.4$–1.8 (in other places up to 6–20). It is of interest to note that ^{207}Bi is present among these other radionuclides (it correlates more with ^{137}Cs than with ^{60}Co). It is possible that ^{207}Bi is linked to material forming the charge of the weapon. ^{207}Bi is accumulated in plants and its concentration reaches 400 Bq/kg in the vegetation around the lake (Kadyrzhanov et al., 2000).

To determine the character of nuclide fractionation in any of the zones of radioactive contamination, graphs of the correlation of the fractionation coefficients of nuclides i with respect to ^{89}Sr and those of the fractionation coefficients for ^{95}Zr with respect to ^{89}Sr for the samples from the ground fallout pattern were prepared. The slope of the regression line characterizes the fractionation coefficient of the ith nuclide with respect to ^{95}Zr for the whole of the contamination zone. Figures 2.7 and 2.8 show the correlation graphs for two explosions, "Sary-Uzen 1003" and "Danny Boy". The magnitudes of $b_{i,95,89}$ for the "Danny Boy" explosion were derived on the basis of the correlation between

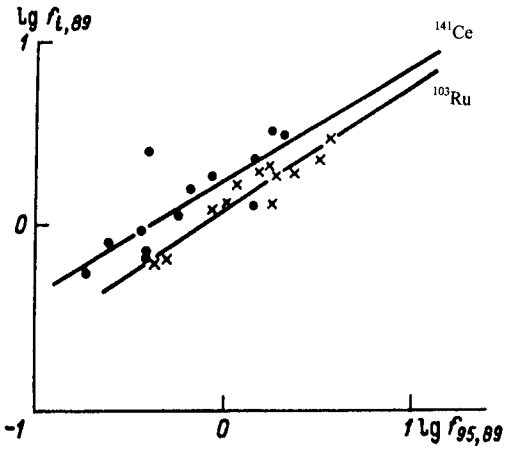

Fig. 2.7. Correlation graphs for two nuclides after the "Sary-Uzen 1003" explosion.

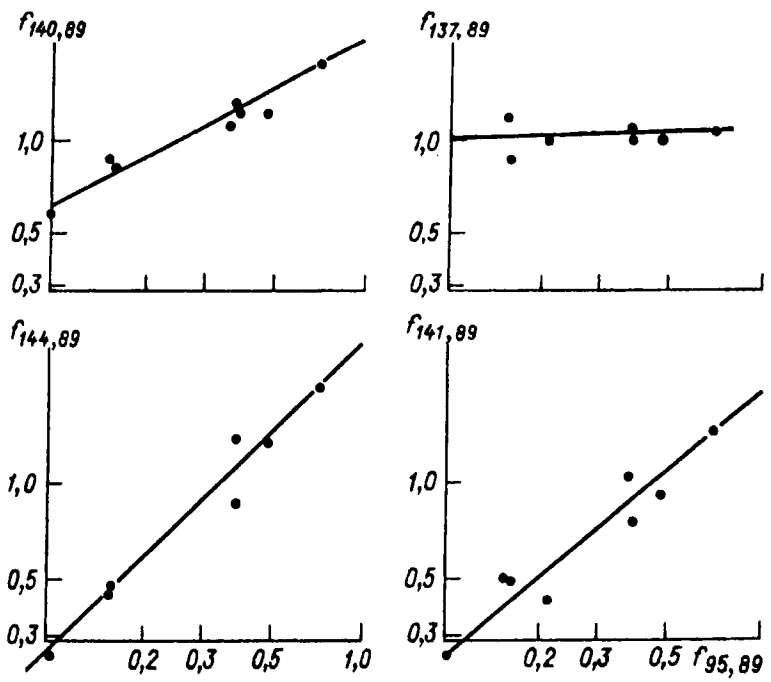

Fig. 2.8. Correlation graphs of the fractionation coefficients for different nuclides in the ground fallout pattern from the "Danny Boy" underground explosion.

the fractionation coefficients described by Izrael (1974). Tangents of the slopes of the regression line for the "Sary-Uzen 1003" explosion and the two American explosions ("Sedan" and "Danny Boy"), taken from papers by Izrael et al. (1970a), Bonner and Miskel

Table 2.4
Tangents of angles of the regression lines for correlation of the fractionation coefficients for some underground explosions

Radionuclide	Explosion		
	Sary-Uzen	Sedan	Danny Boy
^{91}Y	0.46	0.56	
^{95}Zr	1.0	1.0	1.0
^{99}Mo	0.96	0.96	0.90
^{103}Ru	0.63	0.50	
^{106}Ru	0.56	0.42	
^{131}I	0.60	0.44	
^{132}Te	0.75	0.57	
^{137}Cs	0.04	0.01	
^{140}Ba	0.38	0.52	0.54
^{141}Ce	0.62	0.77	0.84
^{144}Ce	0.93	0.83	1.0

(1965) and Kroker et al. (1965), are presented in Table 2.4. The magnitudes of $b_{i,95,89}$ for the ground bulk after the "Sary-Uzen 1003" explosion (Izrael, 1974) were also determined.

It was observed that the slope of the regression line was smaller for the fallout pattern than for the bulk zone. The tangents of the slopes of the regression lines $b_{i,95,89}$ for the various nuclides can be arranged sequentially as follows (in order of increasing slope and decreasing fractionation relative to ^{95}Zr): ^{137}Cs, $^{89}Sr < {}^{90}Sr < {}^{140}Ba$, ^{91}Y, ^{103}Ru, $^{131}I < {}^{132}Te < {}^{136}Cs < {}^{141}Ce < {}^{144}Ce < {}^{99}Mo$, ^{95}Zr. Commas divide nuclides that differ only slightly. This sequence practically coincides with a similar sequence for the decrease in nuclide volatility (see earlier). In the zones of the funnel and the bulk ground, there is only weak fractionation of the nuclides. The average coefficients of fractionation for all radionuclides, except those having relatively long-lived gaseous precursors (^{89}Sr, ^{90}Sr, ^{137}Cs, ^{140}Ba), are close to unity (with respect to ^{95}Zr). The average coefficients of fractionation after "Telkem-1", "Telkem-2", and "Chagan 1004" tests (Izrael et al., 1970a) are within the ranges 0.67–1.1 for ^{140}Ba, 0.27–0.61 for ^{90}Sr, 0.38–0.51 for ^{137}Cs and 0.20–0.47 for ^{89}Sr. The maximum scatter of the nuclide fractionation coefficients $f_{95,89}$ that can characterize the fractionation in a given zone did not exceed one order of magnitude in the close-in pattern for "Sary-Uzen 1003", while for the bulk it was $\sim$ 3–4 times. The scattering of the fractionation coefficients of other nuclide pairs was smaller than the values indicated.

The base fallout zone was enriched in radionuclides with gaseous precursors as compared to the zone of the cloud pattern and especially the bulk ground. This effect was particularly evident in the "Chagan 1004" experiment where the base surge and explosion cloud patterns were separated as a result of the meteorological conditions at the time (Izrael et al., 1970a). The fractionation coefficients of ^{89}Sr and ^{91}Y in relation to ^{95}Zr amounted, respectively, to 3.1 and 2.5 in the base surge fallout zone and 0.3 and 0.8 in the cloud pattern.

As already mentioned, fractionation in the close-in pattern of the radioactive cloud was not great and changed little along its length. For explosions where there was no clear division between where the cloud and the base surge occurs, the fractionation (and the coefficient of scattering) increased and, when the explosions were very small, it can become

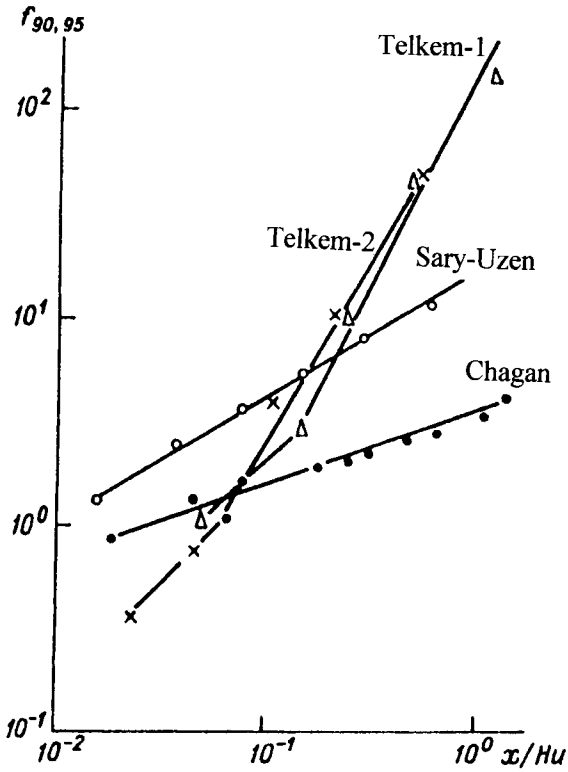

Fig. 2.9. Changes of the fractionation coefficients $f_{90,95}$ with the relative distance x/Hu for different explosions (x is the distance along the axis, H is the cloud height and u is the wind velocity).

essentially zero. Thus, in "Chagan 1004", the radioactive products in the near-zone were weakly fractionated; throughout the area of fallout, along its axis, the fractionation coefficient of ^{90}Sr relative to ^{95}Zr remained within the range of 1.0 to 4.0; in "Sary-Uzen 1003", the nuclide fractionation was substantially higher; thus, for example, the fractionation coefficient changed over the range 1–10, while in "Telkem-1" and "Telkem-2" the coefficients changed from less than 1 to values in the hundreds (Fig. 2.9) (Izrael et al., 1970a). Long-distance fallout is characterized by rather significant coefficients of the fractionation.

Results of studies of the nuclide composition of, and fractionation in, particles after the "Schooner" underground explosion are described by Heft et al. (1971). In this U.S. explosion, which was partially vented, the particles of different slag formations, both black and shiny ones and transparent glass-like pieces with black particles embedded within, were investigated. The first particles were highly enriched in refractory nuclides and they were obviously generated in the inner part of the molten rock within the cavity. Samples of such particles (p) were used as the basis for normalizing the nuclide ratios found in other particles or samples. The ratios were determined relative to the content of the most

refractory nuclide ^{147}Nd in the sample, i.e., the ratios N^A/N^{147} were determined and normalized for the ith sample:

$$X^A = \frac{(N^A/N^{147})_i}{(N^A/N^{147})_p}. \tag{2.7}$$

For the refractory nuclides ^{144}Ce, ^{99}Mo, ^{54}Mn and ^{88}Y, $X^A = 1.00$. The nuclide ratio resulting from activation of one element, e.g., $^{181}W/^{187}W$, is invariant as well.

Changes of the value of X^A for samples taken at different times in the cloud and in the base surge and in samples of fallout were extremely large. It was especially clear from a comparison of samples taken from different zones, i.e., in the cloud, the base surge and in the fallout pattern, that the X^A values differed by factors of ten to several hundreds. This is explained by the fact that all of the samples contained a mixture of particles that were formed from both the molten rock and from fractured material located originally in the area immediately above the cavity.

As a tracer of the particles formed from the crushed, but not molten, rock, the nuclide ^{103}Ru was used. It is a volatile species but without volatile (gaseous) precursors. As the X^A values change greatly from one sample to another, the ratio $(X^A - 1)/(X^{103} - 1)$ will remain practically invariant. It was shown by Heft et al. (1971) that X_0^A, the integral of the X^A value, is

$$X_0^A = \frac{N_0^A/N_0^{147}}{(N^A/N^{147})_p} = 1 + N_S^A/N_c^A. \tag{2.8}$$

The ratio N_S^A/N_c^A is an important characteristic that presents the ratio of the number of atoms deposited on the particle surfaces (mainly those formed from destroyed rock) to those enclosed within the slag formations and the glass-like particles formed from the molten rock. The values for $(X^A - 1)/(X^{103} - 1)$, X_0^A and N_S^A/N_c^A for different radionuclides, as found after the "Schooner" explosion (Heft et al., 1971), are presented in Table 2.5.

5. Interpretation of Data on Fractionation. Scheme of Particle Activation in Underground Explosions

Using a number of theoretical and experimental results and data on the fractionation of the nuclides in radioactive particles, we have endeavored to build a possible scheme for the formation and activation of the particles as they are produced in underground cratering nuclear explosions. This allows us to predict the nuclide composition of the radioactive fallout in different zones after such explosions. From Table 2.5 it is clear that, despite the great differences between the yields of the "Sary-Uzen 1003", "Danny Boy" and "Sedan" explosions, the tangents of the slopes of the regression lines for different nuclides that characterize the integral fractionation coefficients in the close-in fallout pattern, are much the same for these explosions.

Table 2.5
Average values of $(X^A - 1)/(X^{103} - 1)$, X_0^A and N_S^A/N_c^A for different radionuclides after the "Schooner" explosion (Heft et al., 1971)

Radionuclide	$(X^A - 1)/(X^{103} - 1)$	X_0^A	N_S^A/N_c^A
^{137}Cs	10.56	16.65 ± 1.78	15.65 ± 1.78
^{132}Te	6.91 ± 0.61	11.21 ± 0.90	10.21 ± 0.90
^{203}Pb	5.50 ± 0.68	9.13 ± 1.00	8.13 ± 1.00
^{196}Au	3.06 ± 0.50	5.52 ± 0.74	4.52 ± 0.74
^{181}W	2.61 ± 0.27	4.86 ± 0.40	3.86 ± 0.40
^{74}As	2.29 ± 0.93	4.38 ± 1.38	3.38 ± 1.38
^{131}I	1.56 ± 0.15	3.30 ± 0.22	2.30 ± 0.22
^{103}Ru	1.0	2.48 ± 0.10	1.48 ± 0.10
^{110}Ag	0.702 ± 0.220	2.04 ± 0.32	1.04 ± 0.32
^{140}Ba	0.427	1.63 ± 0.062	0.63 ± 0.062
^{134}Cs	0.306 ± 0.090	1.452 ± 0.133	0.452 ± 0.133
^{136}Cs	0.276 ± 0.068	1.408 ± 0.100	0.408 ± 0.100
^{24}Na	0.154 ± 0.065	1.228 ± 0.096	0.228 ± 0.096
^{141}Ce	0.102 ± 0.011	1.151 ± 0.016	0.151 ± 0.016
^{57}Co	0.018 ± 0.004	1.027 ± 0.006	0.027 ± 0.006
Refractory radionuclides		1.0	0

In a similar way to Freiling (1961), we take $\tan(\alpha) = \sqrt{F_i}$, where F_i is the fraction of refractory nuclides in each mass chain, for the given radionuclide. We can then determine an effective time t_{ef} corresponding to the moment of particle solidification, under typical conditions, for ground explosions because the dependence of F_i on t for such conditions is known (Izrael, 1969). The average value of t_{ef} obtained in this way for the above explosions (for different nuclides) amounts to ~ 40 s. Therefore, the fractionation occurring in the close-in fallout pattern after an underground explosion virtually coincides with that after a surface explosion. Note that the formation of particles from the molten ground material in underground explosions obviously takes place quicker and this implies that, under high pressure and temperature, the solution of gases in the molten ground material becomes possible.

It is of interest to analyze the data on activation of the molten rock and to compare these with ^{134}Cs results, as was performed by Heft et al. (1971). ^{136}Cs, a product of the fission process, forms without any volatile precursor and immediately after an explosion it is present in the cavity only in the gaseous state. On the other hand, the ^{134}Cs is a product of the activation of a small part of the nuclear fuel and the rock by neutrons from the explosion. At the beginning, it is in a partly evaporated and partly molten state. A comparison of the data indicates that, for these two isotopes, the values of N_S and N_c are the same within the limits of error. Therefore, by the time of the gas outburst (for the "Schooner" detonation, 1.75 s), equilibrium must have been reached between the gaseous and liquid phases. In their calculations Heft et al. (1971) used Henry's law to carry out theoretical calculations of the phase separation. From Henry's law, the mass of gas that is weakly dissolved in a certain liquid at a given temperature is proportional to the partial pressure of the gas (true for gases that do not enter into any chemical reactions with

the solvent). For ideal gases and dilute solutions, Henry's law gives an indication of the dependence of the partial pressure of an element A on temperature:

$$P_A = \frac{G_A}{G_S} K^A \exp\left[-\left(\frac{\Delta H^A}{RT}\right)\right], \tag{2.9}$$

where G_A is the mass of the element A that is condensed; G_S is the mass of the solvent S; K^A is the equilibrium constant for the reaction; ΔH^A is the enthalpy of the reaction; R is the gas constant; T is the temperature, K.

Results of the measurement of the pressure of cesium vapors over a diluted cesium solution in a molten $CaO{\cdot}Al_2O_3{\cdot}SiO_2$ mixture are presented in Heft et al. (1971). The results follow Henry's law for the reaction

$$Cs^+_{solution} + X^-_{solution} \rightleftarrows CsX_{gas}, \tag{2.10}$$

in which the X^- concentration in the liquid silicate is significantly greater than the Cs^+ concentration. In this work, the constants $K^{136} = 4.06 \times 10^6$ and $\Delta H^{136} = 79$ kcal/mol were determined.

The second relationship between the partial pressure of ^{136}Cs and its concentration in the molten silicate rock was derived on the assumption that ^{136}Cs behaves in the cavity of the "Schooner" explosion as an ideal gas, in which case:

$$P_{Cs} = \frac{N_S^{136}}{6.02 \times 10^{23}} \frac{T}{273} \frac{22400}{V} \times 10^6 \tag{2.11}$$

(P_{Cs} is expressed in atmospheres and V is the cavity volume in m^3).

In addition,

$$G_{Cs} = \frac{136 N_c^{136}}{6.02 \times 10^{23}} \tag{2.12}$$

(G_{Cs} is expressed in g). Hence, it follows that

$$\frac{P_{Cs}}{G_{Cs}/G_S} = \frac{N_S^{136}}{N_c^{136}} \frac{T}{V} G_S \cdot 6.03 \times 10^{-7}, \tag{2.13}$$

where G_S is the molten rock mass in grams.

When Eqs. (2.9) and (2.13) are combined for $P_{Cs}/(G_{Cs}/G_S)$ and then solved for N_S^{136}/N_c^{136}, we obtain

$$\frac{N_S^{136}}{N_c^{136}} = \frac{1.66 \times 10^2 V K^{136} \exp(-\Delta H^{136}/RT)}{T G_S}. \tag{2.14}$$

The cavity volume V in the "Schooner" explosion has been estimated as 1.9×10^6 m^3 at the moment of ventilation, with a gas temperature at outburst $T \geqslant 2875$ K, $G_S = 1.4 \times 10^{10}$ g (i.e., 350 t of the molten rock and 70 t of the evaporated rock per 1 kt of the explosion). Hence, the calculated value

$$\frac{N_S^{136}}{N_c^{136}} \geqslant 0.290. \tag{2.15}$$

In the opinion of different authors, this represents a lower limit since lower limits for the value of V were used in the calculation. This can exert essential influence on the final results. It is true that, by the moment of venting (1.7–2.0 s), the cavity volume, as determined from calculations by Knox and Terhune (1965), amounted to 1.1×10^7 m^3 for an explosion of 100 kt. When it was recalculated for the yield of the "Schooner" detonation, the volume obtained was approximately 3.3×10^6 m^3, i.e., 1.7 times larger than the volume used by Heft et al. (1971). Then the ratio

$$\frac{N_S^{136}}{N_c^{136}} = 0.5. \tag{2.16}$$

Values of the quotient N_S^{136}/N_c^{136} determined experimentally were 0.408 ± 0.100. This calculational approach can also be used for other nuclides.

If we generalize the most interesting results and draw up a scheme for the activation of the rock and for the formation of the radioactive particles in underground explosions, we arrive at the following conclusions.

In the first place, our theoretical calculations have shown that, for a long time (5–14 s) in the cavity, as well as in the lower part of the cloud, a temperature of rock solidification of 1500 °C holds "relatively" steady (see Section 2.1 in Izrael (1966)) but, 1–2 s after the explosion, the temperature reaches 2000 °C. In reality, in the "Sary-Uzen 1003" explosion, the gas temperature at the moment of venting and later (1 s after the explosion) was 1900–2000 °C and, in the "Schooner" explosion, at approximately 2 s after the explosion, it was 2600 °C.

Further, the interpretation of data on fractionation for different underground explosions (Izrael et al., 1970b) shows that activation of the particles (mainly molten) proceeds in such a way and under such conditions that the effects of fractionation are much the same as in high yield ground explosions where solidification occurs roughly 40 s after the explosion. This can be possible only when, in underground explosions, under the prevailing high pressures and temperatures, a significant fraction of the volatile products and inert gases turns out to be in a dissolved state (i.e., at the time when the crushing of the now solidified, molten rock into separate fragments occurs (Izrael et al., 1970b)).

On the basis of analysis of data on activation of molten rock for the nuclides ^{136}Cs and ^{134}Cs (the first is a fission product, formed at the explosion center, and the second a product of induced activity, formed in partially evaporated and molten rock as well as, to a small extent, in the fuel material), it becomes clear that, in the "Schooner" explosion, at least by the time of venting (1.75 s), an equilibrium distribution of these isotopes between the gaseous phase of the cavity and the molten rock was attained (Heft et al., 1971). It follows also (Izrael et al., 1970b) that radioactive products do not mixed homogeneously in the molten rock, the quantity of which in the cavity amounts to 350–600 t/kt, while that of the evaporated rock is 50–70 t/kt.

Analysis of the "Schooner" data has shown that, by the time of formation of the particles (or at their time of solidification), all refractory products were present in the molten rock, and also about 80–90% of the ^{24}Na and ^{141}Ce, as well as $\sim$ 70% of the partly "intermediate" ^{134}Cs and ^{136}Cs, 40% of the ^{103}Ru and only about 10% of the ^{132}Te and

6% of the ^{137}Cs. In this context, we believe that the scheme of activation of the rock and the formation of radioactive particles in an underground explosion is as follows:

1. A powerful shock wave develops in an underground explosion with the general motion being directed outwards. Behind the shock front, the ground is heated and, at some distance, the ground evaporates and, further on, it melts. Under the pressure generated by the gaseous substances (evaporated rock, gaseous products of rock decomposition and water vapor), the spherical cavity increases in size until the time when the pressure is balanced by the lithostatic pressure (obviously this equilibrium is not reached in an explosion where venting occurs). The walls of the cavity are covered with the molten rock.

After the passing of the shock wave front, the gaseous products remain in the cavity. This is confirmed by the observation that the cavity radius, within a contained explosion, as well as the occurrence of venting in a cratering explosion, are undoubtedly dependent on the water content of the rock and on the quantity of gases formed through rock decomposition (Terhune et al., 1970). A certain proportionality was found between these effects and the content of water and gases. It is probable that only a fraction of the radioactive products of an explosion that are evaporated can find its way into the molten rock as a result of the shock wave action.

2. During the cavity expansion, there is extensive evaporation of water vapor as well as gas emission from the molten rock; so-called "boiling" takes place. This results in the formation of slag and pumice concretions. The gaseous inclusions reduce the rock's density by 10–30%, a fact that is only possible if there is evaporation of a larger part of the mass, namely, water and volatile products. Radioactive volatile products amount to only a negligible part of this volume. During the "boiling" phase, significant quantities of small particles are released into the cavity (as in the bursting of bubbles in sea water (Yunge, 1965)).

3. For a relatively long time, the temperature in the cavity, at least until it reaches its maximum volume in a contained explosion, remains high and does not drop below that of the condensation temperature for evaporated rock. By this time, only the refractory radioactive products of the explosion, or a large fraction of them, are condensed in the rock. When the cavity reaches its maximum volume, if it is a cratering explosion, the temperature drops sharply and a large amount (50–70 t/kt) of the evaporated earth condenses. The condensation takes place on the cavity walls and on particles of the rock that enter the cavity. Accumulations of molecules composed of the rock elements can also be generated. Intensive mixing obviously takes place in the cavity. At this moment, the cavity interior resembles the fireball that follows an atmospheric explosion. The high pressure, however, remains within the cavity. During this period, the refractory products are completely absorbed on the particles and molecular aggregations and, in accordance with Henry's law, the volatile and gaseous products of the explosion, including the inert gases (xenon and krypton), can also be absorbed. The volume of vapors, based on a water content of 10% (35–60 t/kt) and given the high pressure in the cavity of about 10^4 m^3/kt, is significantly greater than that of the condensed rock (about 25–35 m^3 at 50–70 t/kt). The amount of inert gases dissolved in these particles can obviously constitute only a small fraction or, at most, several per cent. Thus, for example, the coefficient of solubility is 0.035 (Freiling et al., 1965) when helium is dissolved in liquid glass at a temperature of 1200–1480 °C but can reach 0.46 for other inert gases in the case of ground explosions. This corresponds to the dissolution of about 0.2% of the inert gases. We believe, however, that, under the specific

conditions that exist in the cavity of an underground nuclear explosion, this coefficient of solubility can increase. This is confirmed by the data of Heft et al. (1971), where a value of 6% dissolution was estimated for ^{137}Cs (which exists in the form of an isotope of xenon, ^{137}Xe, during the cavity expansion). Turbulent motion arises in the cavity and this results in the particles and molecular aggregations coming into contact with the cavity walls where they are entrapped and form the most active layer of contiguous rock dust. This has been confirmed in a number of observations (Izrael et al., 1970b; Heft et al., 1971).

4. When the cavity expands to the point of the bursting/venting, the gas temperature does not drop immediately below 1500 °C, i.e., the temperature at which the molten rock solidifies (Izrael, 1966). After the "Sary-Uzen 1003" and "Chagan 1004" explosions and the "Schooner" detonation, the temperature of the escaping gases even exceeded this value (at the bursting of "Chagan 1004", a bright glow was observed). What is more, after the upper part of the cavity is broken, the temperature will not drop below 1500 °C until the cold rock comes into the lower part of the broken cavity. This requires a time of 6–14 s. Throughout this time interval, activation of the particles formed from the molten rock continues over the volume of cooling volatile products as well as the non-volatile products formed from their gaseous precursors as a result of decomposition. During this period, the emission of gaseous substances from the particles can also take place since the pressure sharply decreases.

5. At the time the cavity vents, the melted rock is broken into fragments and mixes with the colder rock destroyed by the explosion in the zone above the cavity. It comes into collision with a huge quantity of pieces and particles of this rock. The rock (still molten or already solidified) is broken and disintegrated by these particles of cold rock. At the same time, some particles of the cold crushed rock can, for a short period, enter the high-temperature regions of the escaping candescent gases and, as a result, be fused from the surface inwards. Simultaneously, the absorption of more volatile products (in accordance with their physical and chemical properties) takes place on the surfaces of the particles of the cold rock and solidified fragments of the molten rock.

6. When mixing with the huge mass of crushed rock (not less than 10^5 t/kt), the temperature of the gases and the particles that have left the cavity zone drop sharply. Large fragments of the rock and particles quickly fall back down into the funnel and thus form the zone of the ground bulk. Entrained with them are large radioactive slag formations and smaller particles that are distributed on the surfaces of the funnel walls and ground bulk material (Izrael et al., 1970a).

Comparatively small particles remain in the cloud and continue to be activated by the products of decay of the inert gas nuclides. Activation of the particles by the ^{137}Cs and ^{89}Sr can take place for longer than 10 minutes (the half-lives of ^{137}Xe and ^{89}Kr are 3.9 min and 3.2 min, respectively). By this time, no large particles exist in the cloud and these radionuclides are spread out with the small particles over great distances, forming the basis of the long-range fallout of radioactivity.

Chapter 3

RADIONUCLIDE COMPOSITION OF RADIOACTIVE FALLOUT FROM TROPOSPHERIC NUCLEAR EXPLOSIONS. METEOROLOGICAL ASPECTS OF FRACTIONATION

Contents

1. Meteorological Aspects of Fractionation 93
2. Radionuclide Composition of Fallout Near Ground-Zero Following Atmospheric and Surface Explosions 97
3. Global and Long-Distance Fallout 102
   - 3.1. Global Fallout 102
   - 3.2. Long-Distance Fallout 111
   - 3.3. Tritium Fallout in a Distant Fallout Zone 118

The character of radioactive fallout depositing on the earth's surface depends on the nature of the source of radioactivity (its intensity, geometry, etc.), together with the prevailing environmental meteorological conditions. This strongly depends also on the landscape features. The direction of transport and the downwind distribution of the radioactive fallout depend on the wind velocity and direction while the degree of dispersion depends on atmospheric stratification, turbulence, etc. Although these factors are evident, it is not always possible to evaluate them quantitatively. It is less obvious that the radionuclide composition of the fallout and, consequently, the effects of fractionation also depend on meteorological phenomena.

Using the known data on the character of radionuclide fractionation on aerosol particles from nuclear explosions, the influence of meteorological conditions on fractionation of nuclides and their redistribution on land and in the atmosphere is examined in the following sections.

1. Meteorological Aspects of Fractionation

Meteorological aspects of fractionation are discussed here on the basis of experimental data for two types of nuclear explosions, viz. (i) tropospheric tests and (ii) underground tests that lead to craters being formed and ground material being ejected.

As already noted in Chapters 1 and 2, the distribution of radioactive products inside the cloud after a nuclear explosion is extremely irregular. Nuclides occur on particle-carriers of different types and sizes and, at the moment of cloud formation and stabilization, they are transported upwards to different levels in the cloud. In atmospheric explosions, one should expect the greatest activity to be at the top and center inside the cloud because of the effects of the cloud's toroidal motion. It is likely that weakly activated ground particles will be at the cloud base and in its lower and peripheral parts. Such a distribution was actually found by Ferber (1965) where less than 1% of the total activity was observed in

the cloud base and 60% was present in the center and upper parts of the cloud (at elevations greater than 80% of the cloud's top height). In an underground nuclear explosion where there is cratering and subsequent ejection of material, these differences in activity and in the distribution of particles between the major cloud and that of the base surge are more evident. The major cloud contains radioactive particles derived from the molten rocks and activated over the whole volume (the first type). The cloud of the base surge contains particles produced by activation of colder ground particles (the second type). The upper part of the cloud supposedly contains mainly particles that are activated by products of the radioactive decay of inert gases. Nuclide fractionation and the composition of separate parts of the cloud change continuously due to the settling and separation of the heavier particles. By the time the cloud stabilizes, the slag-like formations and the largest particles have fallen out in the zone of the crater and bulk ground.

If the wind does not change in the vertical direction, the fallout from different parts of the cloud proceeds as summarized and we obtain an averaged radionuclide composition in the fallout. With increasing distance from the explosion, fractionation differences are observed due to the fallout of particles of differing sizes. In an underground explosion, where the fallout pattern from the cloud of the base surge is wider than that from the major cloud, a decrease of first-type particles is seen as one moves away transversally from the axis of the fallout pattern. Izrael et al. (1970a) made such an observation in the data from the "Sary-Uzen 1003" explosion.

In the situation where the wind changes direction along the vertical axis, particles of the same size from different parts of the cloud may form contaminated areas on the earth's surface and give rise to different radioactive fallout patterns. For example, after an atmospheric explosion, there are fallout patterns from the stem and the cloud, while in underground tests there are patterns from the major cloud and the cloud of the base surge. Thus, in the "Chagan 1004" and "Schooner" explosions, the trajectories of major cloud movement and that of the base surge were obviously different (Izrael et al., 1970a; Krey and Freid, 1965), resulting in fallout compositions in these zones that were quite different.[1] After the "Small Boy" surface explosion of low yield, a wind gradient was observed at heights of 3000 and 4800 m (Krey and Freid, 1965). At its upper level, the cloud had greater speed than that its lower part. Further on, the cloud was broken. The contents of ^{90}Sr, ^{95}Zr and ^{137}Cs in fallout samples at 1000 km in a southerly direction from the explosion's epicenter actually increased after 12 hr when this slower cloud arrived at levels below 3000 m. The amounts of ^{140}Ba slightly decreased in this direction. In this case, the observed fractionation in the fallout took place because of the influence of the meteorological conditions.

From the data presented in Table 2.3 for underground explosions, one can see that the fallout in the zone of the base surge when compared to that in the cloud pattern, and especially that in the ground bulk zone, is enriched in radionuclides with gaseous precursors. This effect manifested itself particularly in the "Chagan 1004" experiment when, under the influence of the meteorological conditions, the patterns from the cloud of the base surge

[1] After the Chernobyl accident (although it was not a nuclear explosion as such but the emission and presence of radioactive particles in a cloud and a cloud stem), more than ten radioactive patterns having different radionuclide compositions were formed in the 60-km near-zone due to the prolonged nature of the source (several days) in parallel with changing meteorology (see Chapter 5).

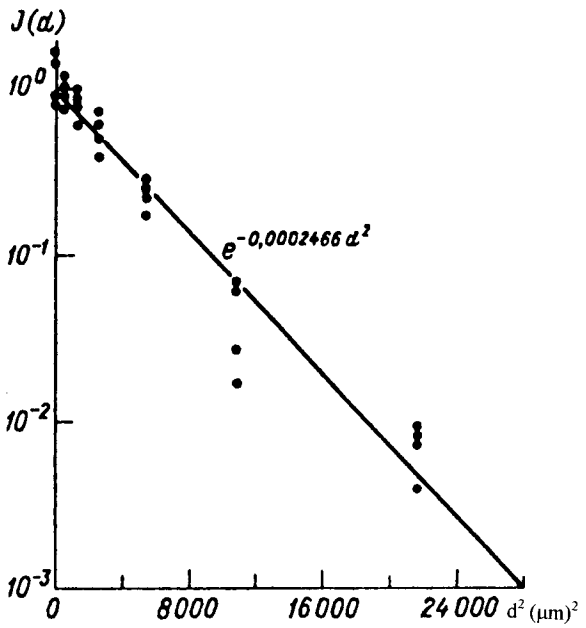

Fig. 3.1. The particle-size distribution of ^{181}W and ^{147}Nd in the major cloud and the base surge.

and those of the major cloud of the explosion were obviously separated. After the "Sedan" explosion, due to the wind velocity gradient at heights of 3000 m and 5000 m, a break-up of the initial cloud took place. The cloud at higher altitudes moved slightly northwards with a greater velocity than the cloud at lower levels (Krey and Freid, 1965).

To estimate the radionuclide composition of the fallout and especially to predict quantitatively the density of the fallout of individual nuclides on the surrounding land, knowledge is required of the distribution of the radionuclides within and between different parts of the cloud as well as of the size-distribution of these nuclides in the different types of particles present in the cloud. Data on the particle-size distribution of ^{181}W and ^{147}Nd activities in air (within the major cloud and in the cloud of the base surge) are presented in a paper by Heft et al. (1971) and are shown in Fig. 3.1.

It is assumed by Knox (1965) that, after an underground explosion, 80% of the gamma-activity of F_c is contained in the major cloud, while only 20% is in the cloud of the base surge. It is also supposed that a radioactive substance settling from the major cloud is divided between two normal logarithmic particle-size distributions: $w_{m}(1)F_c$ with parameter $\ln \bar{r}_{m(1)}$ and standard deviation $\sigma_{m(1)}$ and $w_{m}(2)F_c$ with parameter $\ln \bar{r}_{m(2)}$, and standard deviation $\sigma_{m(2)}$. A portion of the radioactive particles with the first distribution is uniformly distributed over the whole volume of the major cloud and a fraction of the particles with the second distribution is equally distributed but, this time, only in the lower part of the major cloud, i.e., that which occupies 1/5 of the total volume. A similar separation of the mass of the radioactive substances according to the first and second distributions and volume is assumed also for the cloud of the base surge.

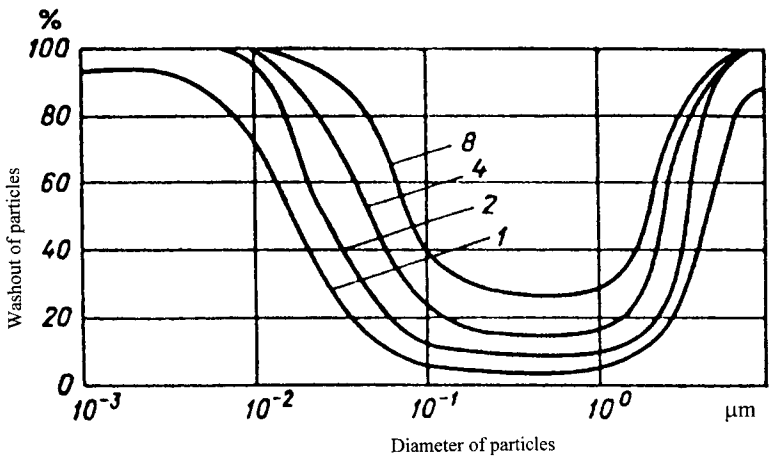

Fig. 3.2. The washout (%) of different sizes of aerosol particles (in the troposphere) at a rainfall intensity of 2.5 mm/hr and raindrop diameter of 20 μm. The effect of rain duration is indicated by the numbered (hours) curves.

When making attempts to calculate the radioactive fallout and the effects of nuclide fractionation accurately, the approach must take account of the physical features of an explosion and the prevailing meteorological conditions. Other meteorological processes, such as the unequal washout of particles of different sizes from the atmosphere, can influence the fractionation of radioactive products during the fallout process onto the earth's surface as well as the fallout intensity.

Large size particles fall mainly due to gravitational deposition. Particles with settling rates comparable to the vertical motions in the atmosphere (i.e., those of less than 10–12 μm) are deposited on the earth's surface either through collision with the surface under the influence of the turbulent motion of the air masses (dry deposition) or through washout by atmospheric precipitation (moist or wet deposition). For global fallout, the dry deposition amounts, on average, to 15–20% (Pavlotskaya et al., 1970) and can be characterized by an effective rate of deposition (ratio of the rate of fallout accumulation to the concentration of the radioactive products in a near-ground air layer) of about 1 cm/s. For instance, in the southern USSR, in 1963, the mean annual value for dry precipitation was 0.7 cm/s and for wet deposition 1.1 cm/s (Makhon'ko, 1971) (no tests of nuclear weapons were carried out in this year).

The rate of particle washout by atmospheric precipitation essentially depends on the sizes of particles in the atmosphere as well as on precipitation type and intensity. Quantities of wet fallout most commonly increase with increasing precipitation, although fine drizzling rains wash out the radioactive particles more efficiently. The calculated efficiency of washout of aerosol particles from the atmosphere is shown in Fig. 3.2 as a function of particle size. One can see that there is a sharp decrease of the washout coefficient for particles of size 0.1–1.0 μm. This feature explains the differences in washout by precipitation for individual nuclides.

Table 3.1
Degree of radioactive product transition into water (in 100 days) after an underground nuclear explosion (A) and the ratio (in activity) between particles of the 1st and 2nd types (B) in different contamination zones

Contaminated zone	A (%)	B (%)
Cloud pattern		
Base surge	17	2.1
Main	4.3	10
Zone of combined fallout	12	3.4
Ground rubble	3.4	–

The more important radionuclides in global fallout can be placed in the following sequence according to their washout intensity (Makhon'ko, 1971): (^{95}Zr, ^{144}Ce) > ^{90}Sr > ^{137}Cs (^{106}Ru, ^{89}Sr) > ^{125}Sb. The sequence is influenced by the dispersion of the particles to which different nuclides are attached. Thus, in atmospheric explosions, larger particles are enriched in ^{140}Ba, while smaller ones are enriched in ^{89}Sr and ^{90}Sr. It was probably due to this factor that, in the spring of 1963, the ^{140}Ba/^{90}Sr ratio in rainwater increased, relative to 1962, at a rate that was higher than the change in the ^{89}Sr/^{90}Sr ratio (Kuroda et al., 1965).

Kalkstein et al. (1965) has also described the fast decrease of the ^{140}Ba/^{90}Sr ratio in the troposphere by more rapid washout of the larger particles. It was noted also by Mamuro et al. (1963a), Gaziev (1965) and Gaziev et al. (1965) that, at the beginning of a rain shower, the radionuclide composition of rain samples differs from the overall average composition because of the early washout of larger particles. Storebo (1960a,b) has described this fractionation as taking place on the windward side of mountains. Changes in the particle sizes of global fallout, and hence in the rate of their washout from the atmosphere, can be caused by their coagulation with natural aerosols (Gaziev et al., 1965). During the process of washout, a fraction of the radionuclides can also become dissolved in the water. This can explain the increased migration and biological accessibility of a given nuclide.

As indicated previously, nuclides on the surfaces of particles are more easily transferred into solution. In this connection, after an underground explosion, particles of the second type are the most subject to leaching. Consequently, the greatest possibility of dissolution of the radioactive products is observed in the fallout zone of the base surge. Table 3.1 presents the amounts of dissolution in water for samples taken from the different fallout zones of the "Chagan 1004" explosion (Izrael et al., 1970a).

2. Radionuclide Composition of Fallout Near Ground-Zero Following Atmospheric and Surface Explosions

Radioactive fallout from nuclear explosions is usually subdivided into: (i) local/close (first tens to several hundreds of kilometers from the explosion site and having particle sizes larger than 50 μm), (ii) long-range (up to distances of several thousands of kilometers) (iii) intermediate tropospheric (lasting for one-two weeks) and (iv) global or stratospheric (lasting for many weeks, months and even years).

Table 3.2
Integral coefficients of fractionation (for the close-in fallout pattern) of different nuclides after surface nuclear explosions ($\bar{h} = 0$)

Nuclide	Integral coefficients*			
	Of fractionation for the close-in pattern		Of leaching (%)	
	$t_l = 7$ s	$t_l = 40$ s	$t_l = 7$ s	$t_l = 40$ s
^{95}Zr	1.0	1.0	0	0
^{99}Mo	1.0	1.0	0	0
^{103}Ru	0.61	0.73	0.06	0.03
^{106}Ru	0.14	–	–	–
^{89}Sr	0.06	0.10	0.95	0.79
^{90}Sr	0.10	0.23	0.87	0.43
^{131}I	0.55	0.77	0.03	0.03
^{132}Te	0.43	0.53	0.08	0.09
^{137}Cs	0.04	0.08	0.96	0.94
^{140}Ba	0.37	–	0.23	–
^{144}Ce	1.0	1.0	0	0

*With respect to refractory point nuclides.

Andryushin et al. (1996) have described the distribution of radioactive fallout from an explosion in 1949 (USSR) using measurements of γ-radiation fluxes. The curve of the dose-rate variation with distance indicated a sharp increase (up to 14 R/hr; $\approx$ 140 mGy/hr) at a distance of about 100 km from the epicenter (near the village of Dolon). (At this stage, we remind the reader about our definitions of units of radioactivity and dosimetry in the introductory Glossary—it might be useful to re-read that section now!) Nearer to the epicenter, from 20 to 90 km, it was from 9 to 11 R/hr ($\approx$ 90 to 110 mGy/hr), while beyond 200 km it corresponded 3 R/hr ($\approx$ 300 mGy/hr). It was stated by the authors that the γ-radiation dose rate in the Altai region gradually diminished with distance from the explosion's epicenter up to 1000 km. Such a distribution was confirmed by later investigations.

The radionuclide composition of local fallout is determined by the degree of dispersion of the particle-carriers that are, as a rule, formed from completely molten particles of surrounding rock. The fractionation of the radionuclides in such particles has been considered in detail in Chapter 1.

Now the area of the fallout pattern from the 1953 explosions at the Semipalatinsk Test Site amounted to $\sim$ 250 km^2, with a contamination level by ^{137}Cs of 1–2 Ci/km^2 (35–70 GBq/km^2) and a further area of $\sim$ 25 km^2 with a contamination level of 2–5 Ci/km^2 (70–185 GBq/km^2). A flux/dose rate up to 1400 mR/hr ($\approx$ 14 mGy/hr) from ^{137}Cs covered an area of about 0.5%. The total amount of ^{137}Cs in the territory of the former Semipalatinsk test site amounts to $\sim$ 3 kCi (110 TBq) or 8% of the total quantity released from the ground explosions, while for ^{90}Sr it is $\sim$ 2.5 kCi (92 TBq) (or somewhat less than 10% of the total quantity (Dubasov and Tukhvatulin, 2000)).

Average coefficients of fractionation for a zone of local fallout can be calculated by averaging the values of $f_{ij}(d)$ within the limits of d change that we are interested in (e.g., for local fallout as a whole, up to particle diameters of 50–100 μm). Table 3.2 shows

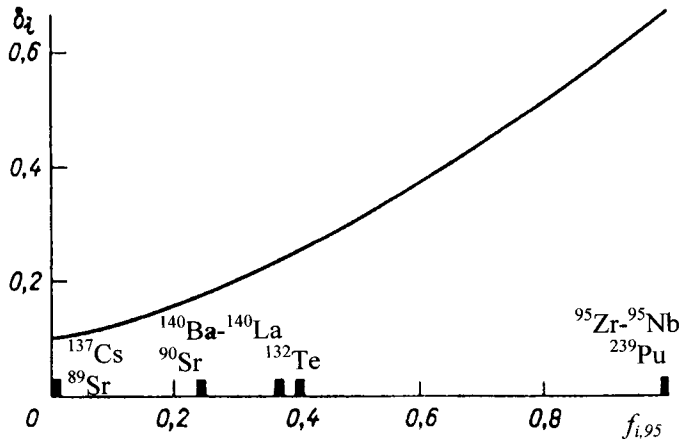

Fig. 3.3. Changes in contributions of the activities of different nuclides in local fallout.

Table 3.3
Fraction of the total activity in the close-in fallout pattern after a number of atmospheric nuclear explosions in the USA

Explosion	W (kt)	$\bar{h}$	Fraction in the fallout activity (%)			^{90}Sr/^{89}Sr nuclide ratio in the fallout
			Sum of radionuclides	^{89}Sr	^{90}Sr	
			Tower explosions			
Fizeau	11.1	0.67	6.7	0.45	1.59	3.54
Galileo	11.4	0.66	10.4	0.80	2.82	3.52
Boltzmann	11.5	0.65	24.5	1.80	6.33	3.52
Shasta	16.5	0.35	21.7	2.05	7.18	3.49
Diablo	17.0	0.58	16.6	1.22	4.27	3.50
Whitney	18.5	0.56	16.1	1.61	5.65	3.50
Smoky	44.0	0.60	19.6	1.70	5.97	3.51
			Near-ground (balloon) explosions*			
Wilson	10.3	0.69	0.91	0.04		
Newton	12.0	1.95	0.10	0.04		
Priscilla	36.6	0.63	2.12	0.13		
Hood	74.3	1.07	0.17	0.008		

*From a list of the balloon explosions, these four were selected on the basis of $\bar{h}$ being less than or close to unity.

the average coefficients of fractionation f_{ij} calculated in this way for the close-in fallout pattern of surface detonations of differing yields, i.e., $t_1 = 7$ s and $t_1 = 40$ s (Izrael, 1973). The change of part of the activity for different nuclides δ_i in local fallout is shown in Fig. 3.3, as taken from the data of Freiling et al. (1965). This curve practically coincides with the results of our own calculations. A part of the radioactivity of the ith radionuclide, equal to $1 - \delta_i$, accordingly, is intermediate (long-distance) and global fallout.

Table 3.3 shows the fraction of the radioactivity of ^{89}Sr and ^{90}Sr found in the close-in fallout from 1 min to 2 hr after several tower and near-ground (balloon) explosions of

Table 3.4
Comparison between the radionuclide distribution in fallout predicted by a semi-empirical method for a ground explosion with that obtained on the basis of analysis of the nuclear fragments (Freiling et al., 1968)

Radionuclide	Predicted distribution			Fraction in the cloud 24 hr after a high-yield explosion on a coral surface	Distribution for a low-yield explosion on a silicate surface		
	Local	Intermediate*	Global		Local	Intermediate†	Global
^{137}Cs	0.1	0.1	0.8	0.36 ± 0.36	0.00	0.22	0.78
^{89}Sr	0.1	0.1	0.8		0.02	0.24	0.74
^{90}Sr	0.15	0.1	0.75	0.11 ± 0.11	0.07	0.24	0.69
^{140}Ba–^{140}La	0.25	0.1	0.65		0.20	0.26	0.54
^{132}Te	0.25	0.1	0.65		0.18	0.26	0.56
^{95}Zr–^{95}Nb	0.65	0.1	0.25		0.72	0.19	0.09
^{99}Mo (coral surface)	0.65	0.1	0.25	0.02 ± 0.02	0.72	0.19	0.09

*Particles with diameters of 25–50 μm are assigned to the intermediate fallout.
†Particles with diameters from 18 μm to about 90 μm are assigned to the intermediate fallout.

the American "Plumbob" series performed in 1957. For all explosions, the scaled height $\bar{h} = h/\sqrt[3]{W}$ (ratio of explosion altitude to fireball radius) was less than or close to unity.

The percentage of the total activity in the close-in fallout after the tower explosions was 10–25% (sum of all nuclides), including 0.5–2% for ^{89}Sr and 1.5–7.2% for ^{90}Sr. Apparently these explosions are closer to ground explosions than near-surface blasts. On the basis of our calculations (see Chapter 1), the values of δ_{89} and δ_{90} for a ground explosion of small and medium yield should be 2.5 and 7%, respectively. Based on the data presented by Freiling et al. (1965), theoretically they are 10 and 15% but according to experimental data they are 2 and 7% (see Table 3.4). Attention is drawn to the constant values of the ratio between ^{90}Sr and ^{89}Sr in the close-in fallout pattern of these explosions (Lavrenchik, 1965; Johnson et al., 1959). This finding agrees well with our calculated values (Izrael, 1973).

The close-in fallout pattern of a balloon explosion falls off (for $\bar{h} \sim 1.0$) drastically with increase in explosion altitude (for total activity to 0.1–2% and for ^{89}Sr activity to 0.008–0.13%). A comparison between the radionuclide mix in fallout predicted by the semi-empirical method used by Freiling et al. (1965) with that obtained from an analysis of the nuclear fragments is presented in Table 3.4.

It is interesting to note that the slopes of the regression lines as well as the intercepts in a logarithmic plot of the fractionation coefficients for ^{140}Ba relative to ^{89}Sr (representing the data obtained for particles collected on filters and individual particles from two high yield atmospheric explosions in the Dominic series (USA, 1961)) are comparable (within limits of error) to plots of the same parameters for a 1 Mt yield test on a coral surface and three other types of near-water explosions (Benson et al., 1965).

Explosions carried out by the USA in the Pacific on barges are of special importance. If the water layer thickness under the barge is not taken into account, it becomes impossible to consider such explosions as being close to atmospheric or ground blasts. However, it is clear that, as the water layer increases, these explosions approach atmospheric tests, judging from the quantity of radioactivity seen in the close-in fallout pattern. In this

connection, the large particles of local fallout are depleted in volatile nuclides (or those having gaseous and volatile predecessors). To achieve a mass balance of these nuclides, the small particles that are deposited at significant distances from the explosion (intermediate and global fallout) should be enriched in the same nuclides and, conversely, should be depleted in more volatile species. Thus, if in local fallout $f_{89,95} \ll 1$, then in long-range fallout, $f_{89,95} \gg 1$ (a process sometimes termed inverse fractionation).

Several authors have noted such inverse fractionation after ground explosions (Krey and Freid, 1965; Mamuro et al., 1965a; Kuroda et al., 1965). Thus, the results from long-distance fallout measurements, at a distance of 1000 km after the "Small Boy" low-yield ground explosion (Krey and Freid, 1965) are characterized by a noticeable fractionation of ^{90}Sr and ^{137}Cs. If the particles are depleted in nuclides such as ^{140}Ba, ^{141}Ce, ^{103}Ru and ^{91}Y, relative to ^{95}Zr, then coefficients of fractionation for ^{90}Sr and ^{137}Cs of, on average, 12.4 and 7.2, respectively, confirm this inverse fractionation.

The effects of inverse fractionation have been observed in other studies also (Mamuro, 1966) at several hundred kms after a surface explosion. Coefficients of fractionation of ^{103}Ru (relative to ^{95}Zr) have been found to be in the range 10–60, and 4–13 for ^{131}I in the most active particles. In probes of the "filter" and the rain, the fractionation effect was weak, fractionation coefficients ranging from 2.0 to 2.5, while in rain studies, at still greater distance, they were 0.6–0.8. ^{239}Np, which contributed 70% of the total activity after 3 days, and ^{237}U were observed in these particles. No inverse fractionation has been observed in atmospheric explosions (see Chapter 1).

An example of an atmospheric explosion performed at low elevation is one that was detonated near the town of Totsk in the Orenburg region of the former USSR on 14 September, 1954. The explosion, which had a yield of 40 kt, was detonated 350 m above the surface and the fireball did not touch the ground. The cloud reached an altitude of 15 km in 7 minutes. Radionuclides were traced up to a distance of about 210 km. In 1996–1999, the radiation situation was characterized by levels in the zone of the epicenter of about 9–16 mR/hr ($\approx$ 90–160 μGy/hr) due to ^{152}Eu (total quantity is 0.2 Ci (7 GBq)) and ^{60}Co. The average value for ^{137}Cs amounted to 65.8 mCi/km^2 (2.43 GBq/km^2, close to global background values). Maximum deposition values in the fallout pattern reached about 15 mCi/km^2 (555 MBq/km^2), with a density of contamination of 44.2 mCi/km^2 (1.63 GBq/km^2) for ^{90}Sr and 4.4 mCi/km^2 (163 MBq/km^2) for $^{239+240}$Pu. The activity ratios are ^{90}Sr/^{137}Cs = 0.7 and $^{239+240}$Pu/^{137}Cs = 0.07. These data indicate that there was no "radioactive" fallout pattern of fission products after this explosion (Trifonov and Dubasov, 2000).

In local fallout, in addition to fission products, induced nuclides can be also observed. The long-lived radionuclides of neutron-induced activity ^{46}Sc, ^{134}Cs, ^{152}Eu, ^{152}Eu, ^{154}Eu and ^{60}Co were present in soil collected at the Nevada test site in July 1957. Long-lived activation products ^{152}Eu, ^{154}Eu and ^{155}Eu were also found, in the close-in patterns, even 35–45 years after the explosions conducted at the Semipalatinsk Test Site (apparently they can be formed as a result both of the fission process and of activation by neutrons). For the most part, the significant neutron-activation products are radionuclides of the refractory elements. Some relatively volatile nuclides can, however, be present (for instance, ^{134}Cs (Heft et al., 1971)). Nuclides such as ^{57}Co, ^{58}Co, ^{55}Fe, ^{24}Na, ^{54}Mn, ^{65}Zn, ^{185}W, ^{181}W, ^{102}Rh, ^{124}Sb, ^{109}Cd and ^{113m}Cd were described for particles from the nuclear detonation

(Izrael and Stukin, 1967). These particular species were produced as a result of the interaction between the neutrons of the explosion with nuclei of the device's charge or with the ground. Several nuclides were obviously formed through activation of elements specially introduced into the bomb's shell for use as tracers of specific processes.

3. Global and Long-Distance Fallout

As already noted, long-distance and "intermediate" fallout (particles of size 50 to 10 μm and smaller) and global fallout constitute the boundary limits beyond the close-in fallout pattern. Each type of fallout is highly distinctive. These categories are formed from highly dispersed particles (sizes in units and fractions of μm) that are thrown up into the higher altitudes of the atmosphere following a high-yield nuclear explosion. They result in extensive contamination within given latitude bands around the whole globe. Long-distance fallout is formed from the highly dispersed particles that are, as a rule, limited to the troposphere (some fallout from the stratosphere is not entirely excluded). Long-distance fallout occurs over periods of several days; global fallout takes place over many weeks, months or even years after an explosion. Many monographs and articles have been devoted to global radioactive fallout. Some contain serious analyses of the meteorological aspects of the global transport of radionuclides in the atmosphere, e.g., "Radioactive isotopes and the global transportation in the atmosphere" (Karol, 1972). Several interesting recent international conferences have discussed global and regional contamination, not only from nuclear explosions and accidents but also from continuous discharges from the nuclear industry, e.g., Conferences on the Radioactive Contamination of the Arctic (1993, 1995, 1997, 1999) and on "Radioactivity after Nuclear Explosions and Accidents" held in Moscow in April, 2000.

A characteristic feature of long-distance fallout is the relationship that exists between its composition and the source of the contamination, a feature often traceable over many hundreds and thousands of kilometers from the explosion site. A second global fallout feature is the mixing that occurs in the stratosphere of particles and products from different explosions. Thus global fallout results from the deposition of highly dispersed particles from one or more series of powerful explosions. Intermediate fallout is an initial phase of global fallout and is, as a rule, difficult to identify with any specific explosion. Below we present a description of global fallout, observed everywhere throughout the globe, especially in the 1960s, and which was considered to pose a significant radiation threat. The growth of testing slowed substantially after the Moscow Treaty on the Prohibition of Nuclear Weapons Tests in the Atmosphere, Space and Underwater was signed in 1963 (only China and France continued to test explosions in the atmosphere after that time). The data on global fallout relate, as a rule, to the 1960s, i.e., the time of their maximum intensity and when data on specific fractionation in global and long-distance fallout were collected. In the following, we present data on long-distance fallout from a series of high-yield tests conducted in the atmosphere in 1961 at the Novaya Zemlya Test Site.

3.1. *Global Fallout*

The most important radionuclides in global fallout are undoubtedly ^{90}Sr and ^{137}Cs, because of their long half-lives, association with particles of submicron sizes and radiation

hazard, and, to a lesser degree, tritium. The observed distribution of ^{90}Sr and ^{137}Cs in global contamination is determined by a number of factors, the most important being:

- the character of the nuclear weapons' tests (power and type, i.e., atmospheric, underground, etc.);
- the primary importance of tests conducted in the northern hemisphere;
- the general systematics of the atmospheric circulation;
- the features of climatic and synoptic conditions for different regions.

In accordance with the data of the UN Scientific Committee on the Effects of Atomic Radiation (UNSCEAR, 1962), from the beginning of testing until 1963, 0.71 EBq (19.3 MCi) of ^{90}Sr and 1.22 EBq (33 MCi) of ^{137}Cs were injected into the atmosphere. Subsequent tests have contributed significantly less. If this amount were to be uniformly spread over the earth's surface, then by 1970 the following average levels of contamination should have been observed: for ^{90}Sr, 1.15 GBq/km^2 (31 mCi/km^2) and, for ^{137}Cs, 1.97 GBq/km^2 (53 mCi/km^2). Because of the above factors, the actual levels of contamination were quite different in some places.

The ^{90}Sr distribution in soils has been investigated systematically. Pavlotskaya et al. (1970) and List et al. (1965) have presented reviews of the data. The most detailed information on the levels of global contamination relates to the period 1963–1964. Before 1963, the quantity of ^{90}Sr in soils increased rapidly. By 1964, a large part of the ^{90}Sr released into the atmosphere had returned to the earth's surface. According to the estimates of List et al. (1968), approximately 370 PBq (10 MCi) of ^{90}Sr had fallen out by then. Following the prohibition of atmospheric nuclear explosions in the USA and USSR, the ^{90}Sr fallout on land was essentially balanced by the decreases due to radioactive decay and river transport to the seas and oceans. This effect is illustrated in the data on average levels of contamination of the former USSR territory in different years:

Year	1963	1964	1965	1966	1967	1968	1969
Inventory (GBq/km^2)	1.63	2.07	2.00	1.96	1.63	1.59	1.59
(1 GBq/km$^2 \approx$ 27 mCi/km^2)							

A map of the global contamination of the earth's surface by ^{90}Sr at the end of 1963/beginning of 1964 is presented in Fig. 3.4. The results of List et al. (1965), supplemented with information on contamination levels in the former USSR from Pavlotskaya et al. (1970) and Morokhov et al. (1970a), were used. This map is rather sketchy and reflects only the most general features of the ^{90}Sr contamination. Thus, for instance, specific studies of ^{90}Sr fallout show some hot-spot regions of increased contamination that are still present. These are in the Mediterranean basin, Japanese Islands, North-East USA, the Pacific shore of the USA, etc. These regions are not highlighted on the map. It is clear from Fig. 3.4 that the most typical feature of the ^{90}Sr distribution is the sharp distinction in pollution levels between the northern and southern hemispheres. Rough estimates show that the ^{90}Sr inventory in the northern hemisphere is almost five times larger than that in the southern hemisphere.

The latitudinal effect in the contamination distribution is also noted in both hemispheres. Maximum levels are found in regions where the majority of the tests were performed, i.e.,

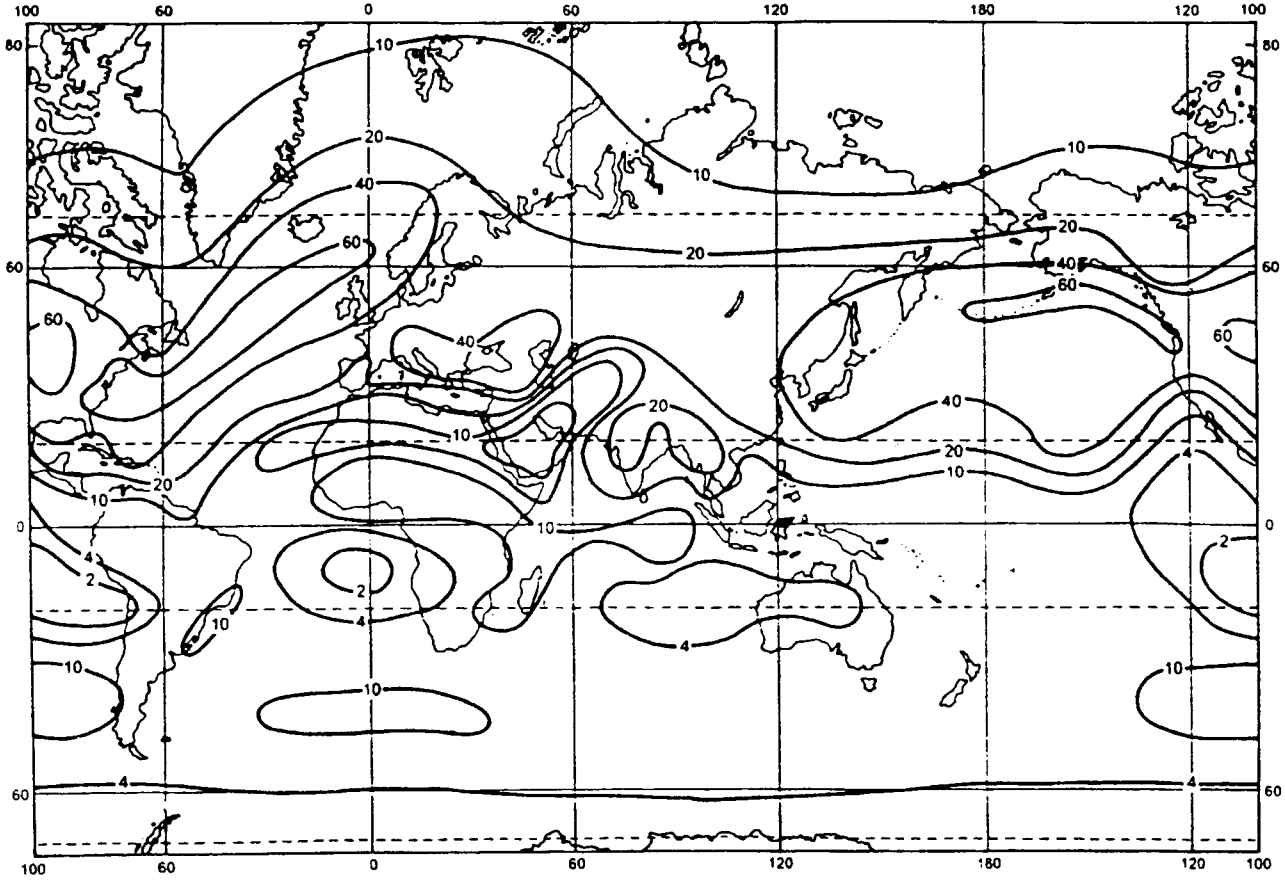

Fig. 3.4. Inventory of ^{90}Sr (mCi/km^2) in soil for the period 1963–1964 (1 mCi/km^2 = 37 MBq/km^2).

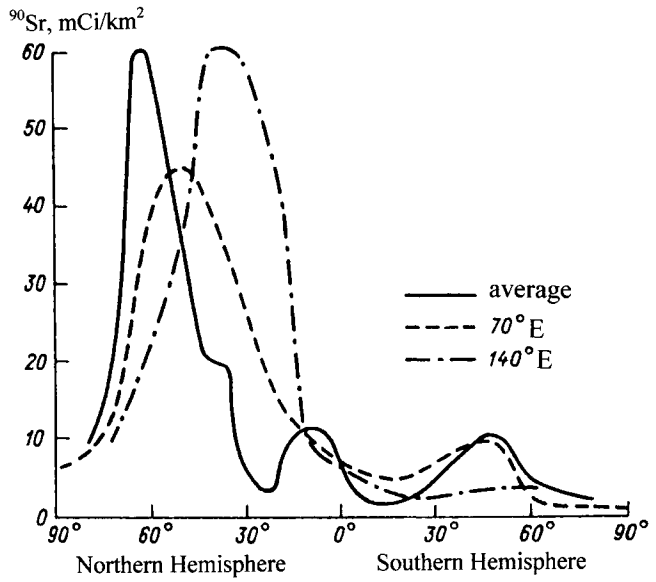

Fig. 3.5. Latitudinal distribution of ^{90}Sr (mCi/km^2) in soils in 1963–1964 (1 mCi/km^2 = 37 MBq/km^2).

in the middle latitudes. Here, in the northern hemisphere, the average fallout is six times greater than in the equatorial zone. The averaged latitudinal curve constructed from the data of List et al. (1965) is given in Fig. 3.5. Specific cross-sections along the 70° E and 140° E meridians are shown also. It is seen from the graphs that the latitudinal variations along these meridians are quite different. Calculations show that, in 1963, in the latitude band from 20 to 70° N, the average amount of ^{90}Sr that had accumulated was about 1.48 GBq/km^2 (40 mCi/km^2).

The contamination characteristics for several countries (average, minimum and maximum levels) are shown in Table 3.5 (Pavlotskaya et al., 1970). The average levels of contamination differ dramatically even for neighboring countries such as Denmark and Poland. Overall, the irregularity and spottiness of the contamination are typical features of global fallout.

Data on global contamination by ^{137}Cs are less available than for ^{90}Sr (except in the former USSR where airborne gamma-surveys were carried out for ^{137}Cs over the entire territory (Boltneva et al., 1977)). We believe that the most reliable way to estimate ^{137}Cs contamination is to use measurements of the activity ratio between ^{90}Sr and ^{137}Cs. Thus, for example, the average data on ^{137}Cs contamination levels and its relationship to ^{90}Sr for the former USSR territory during the period 1963–1969 were:

Year	1963	1964	1965	1966	1967	1968	1969
^{137}Cs (GBq/km^2)‡	3.18	3.59	4.00	3.22	3.11	3.11	3.18
^{137}Cs/^{90}Sr	1.95	1.73	1.93	1.64	1.91	1.95	2.0

‡1 GBq/km^2 ≈ 27 mCi/km^2.

Table 3.5
The ^{90}Sr burden (mCi/km^2) in different countries in 1963

Country	Density of contamination‡		
	Average	Minimum	Maximum
		Northern Hemisphere	
Denmark	40.6	26.0	48.0
Canada	37.4	15.9	62.5
Norway	33.8	18.0	51.8
Poland (1964)	27.1	20.0	40.0
USSR	44	9.6	67.2*
30–40° N	50	–	–
40–50	45	–	–
50–60	44	–	–
60–70	35	–	–
Alaska	47.6	12.4	73.4
Hawaiian Islands	15.8	8.2	23.0
France	27.4	22.3	31.3
Japan	49.7	48.8	50.8
		Southern Hemisphere	
Australia	6.2	3.4	12.0
New Zealand	11.6	6.4	16.9
Chile	3.2	0.5	4.5

‡1 mCi/km^2 = 37 MBq/km^2.
*According to the data of Boltneva et al. (1977), maximal values reach 175 and larger.

For the first few years after 1963, the ratio $^{137}Cs/^{90}Sr$ changed from 1.65 to 2.0 (USA and Europe included). The average value for the ratio was 1.85. Variations in the $^{137}Cs/^{90}Sr$ ratio are mainly caused by fluctuations of these nuclides in fallout and by different removal rates from upper soil horizons. The effect of these factors can be seen in the data for different latitude zones of the former USSR (Pavlotskaya, 1970):

Latitude (° N)	^{137}Cs (GBq/km^2)‡	$^{137}Cs/^{90}Sr$
30–40	3.51	1.9
40–50	3.51	2.1
50–60	3.44	1.7
60–70	2.22	1.9
Average	3.18	1.95

‡1 GBq/km^2 ≈ 27 mCi/km^2.

Based on the above data, we believe that a relatively satisfactory estimate of global contamination of the earth's surface by ^{137}Cs can be obtained from a map of the ^{90}Sr distribution. For the latitude band 20 to 70° N, the average accumulation of ^{90}Sr was estimated in 1963 to be 40 mCi/km^2 (1.48 GBq/km^2). Using 1.85 as the mean value of the ratio $^{137}Cs/^{90}Sr$, we obtain an estimate of 74 mCi/km^2 (2.74 MBq/km^2) for the ^{137}Cs inventory within this zone. As noted above, detailed monitoring information on the

actual distribution of the global fallout of ^{137}Cs is available only for the former USSR where detailed aerial gamma-surveys were carried out at the end of the 1960s (Boltneva et al., 1977). Procedures used to carry out such surveys and the methods employed in the interpretation of the results are presented in Boltneva et al. (1977) and in Kogan et al. (1969). Distances between survey transects averaged about 50 km, reaching 100 km in some cases. Along the routes, the average concentrations of radionuclides were determined usually over distances of about 10 km length. The flight altitude was 25–30 m and hence the readings obtained characterized an under-lying band of 100–200 m width, with an area of about 1 km^2. The reproducibility of the determination of ^{137}Cs deposition, taking navigational uncertainty into account, was not worse than 10%. At a level of contamination of about 100 mCi/km^2, i.e., 3.7 GBq/km^2, the accuracy of the ^{137}Cs estimate was approximately 20%.

Figure 3.6 presents a map, for the end of the 1960s, of the contamination of the former USSR by global fallout from nuclear explosions. The contamination levels fall mainly within the range 50–175 mCi/km^2 (1.85 to 6.48 GBq/km^2) with an average accumulation of ^{137}Cs of 90 mCi/km^2 (3.33 GBq/km^2) (Boltneva et al., 1977). A number of regularities in the spatial distribution of the ^{137}Cs contamination were found, i.e., that geographical conditions (landscape) and climate influenced the distribution. This is visible in the data:

1. Contamination levels are closely related to precipitation. Comparison of a map of contamination with that of precipitation shows the isoline patterns to be very similar. A zone of maximum contamination occurs in northerly parts of the European USSR territory with a ^{137}Cs level of 150–175 mCi/km^2 (5.55–6.48 GBq/km^2) corresponding to zones of precipitation of up to 600–700 mm/yr. Reduction of the ^{137}Cs levels to the north of this zone to 50–75 mCi/km^2 (2.78–3.23 GBq/km^2) is connected to a decrease in annual precipitation, near the Barents Sea, down to 300 mm. A band of low ^{137}Cs contamination of 50–75 mCi/km^2 (2.78–3.23 GBq/km^2) spreads along the southern boundary of the survey. This is the zone of deserts and semi-deserts of Kazakhstan where the precipitation is $\sim$ 100–200 mm/yr together with a dry zone near the Black Sea with annual precipitation less than 400 mm.

2. Contamination levels increase with proximity to the mountains: the Carpathians, the Crimea, the Caucasus, Tien Shan, the Urals, Sayan and East Siberia. Zones of increased moisture levels coincide with these mountain systems and the piedmont areas.

3. Generally, the latitudinal zonality is a common characteristic of the contamination levels. Actually, all local zones are stretched along a latitude.

4. Attention is drawn to the rather complicated character of the ^{137}Cs contamination patterns within a region, with the existence of numerous local zones where the levels are very distinct from adjacent regions. To a certain degree, a similar spottiness can also be seen on the precipitation map. However, the spottiness is conditioned also by the landscape features.

The distribution of the dose rate from the ^{137}Cs γ-radiation (at a height of 1 m) over the former USSR is shown in Fig. 3.7. When calculating the dose rate, it was assumed that, on virgin land sites, ^{137}Cs decreased exponentially with depth. In 1972, the depth coefficient was 0.6 ± 0.2 cm^2/g. Using this value of the coefficient, the dose rate P at a height of 1 m was found to be related to ^{137}Cs inventory q, as follows: P ($\mu R/hr$) $= 6.5 \times 10^{-3}$ q

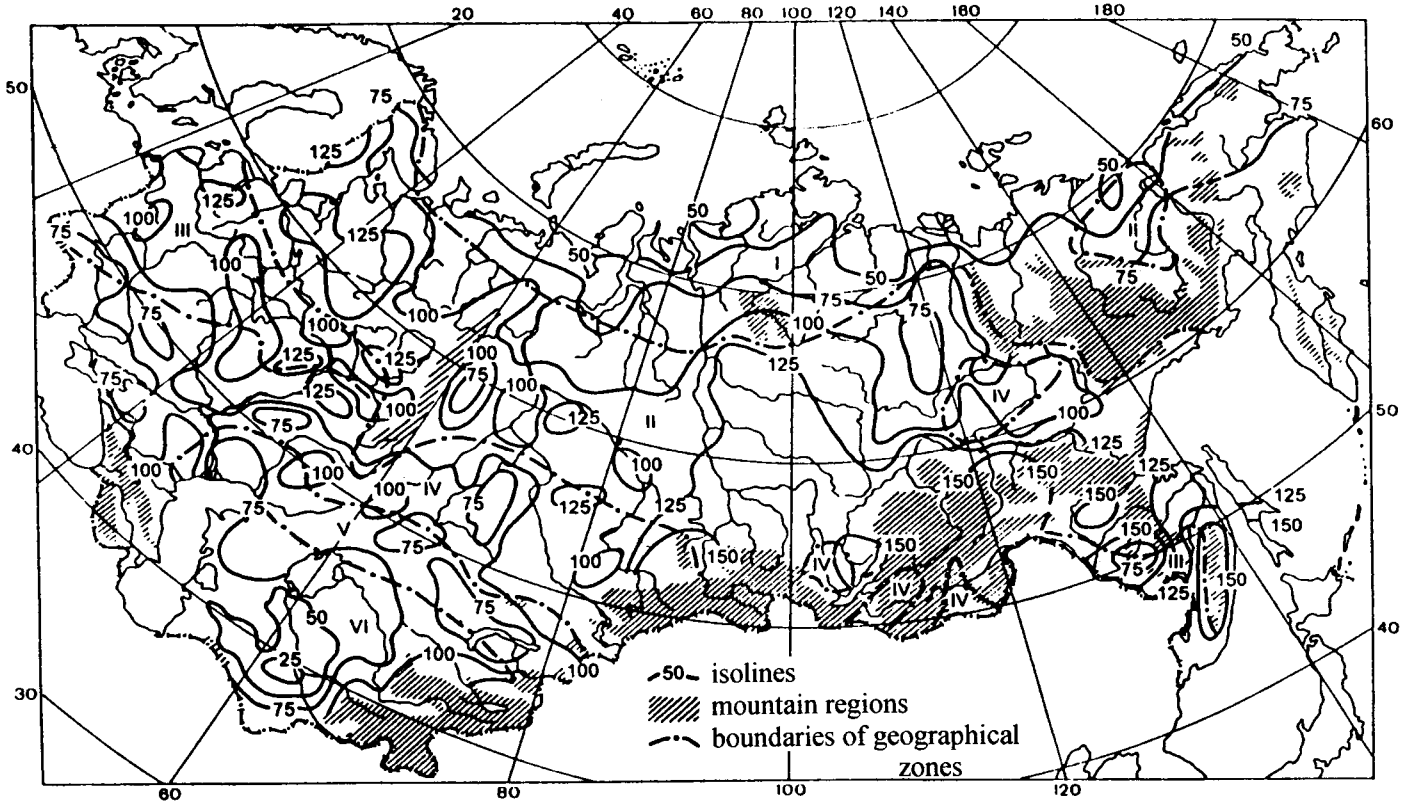

Fig. 3.6. Distribution of the ^{137}Cs accumulated on USSR territory by the end of the 1960s, in mCi/km^2 (1 mCi/km^2 = 37 MBq/km^2). I — tundra and forest-tundra; II — coniferous forest; III — mixed forest; IV — forest-steppe and steppe; V — semi-desert; VI — desert.

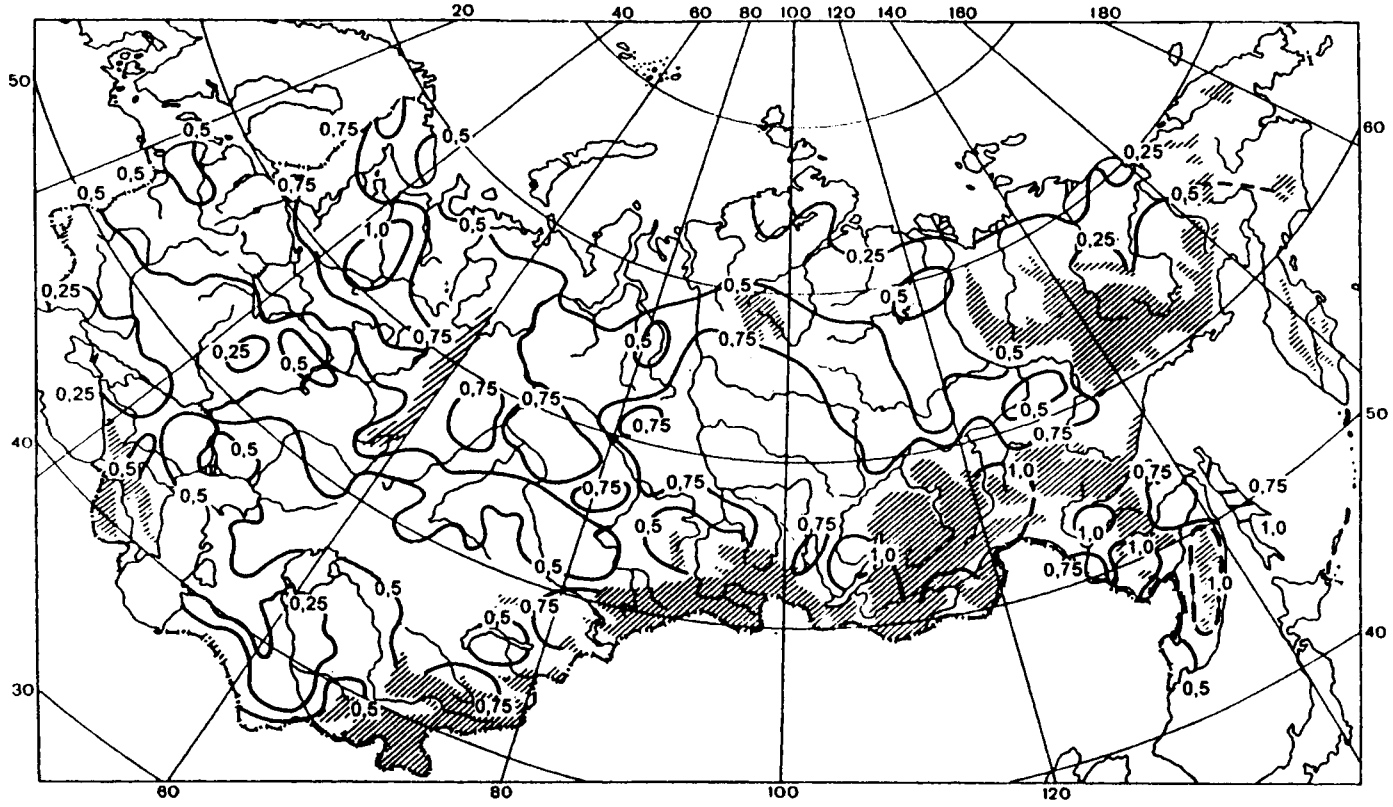

Fig. 3.7. The dose rate of γ-radiation (μR/hr) at a height of 1 m (1974 survey). See caption of Fig. 3.6 (1 μR/hr ≈ 10 nGy/hr).

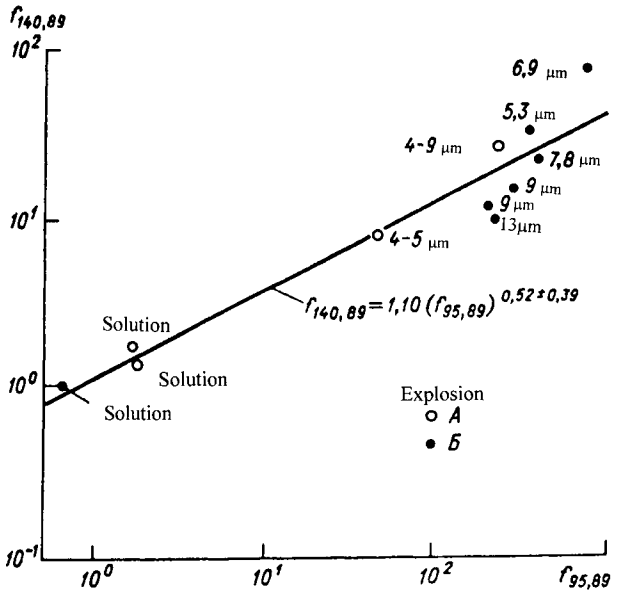

Fig. 3.8. Graph of the logarithmic correlation of the fractionation factors for ^{140}Ba following atmospheric explosions.

(mCi/km^2), which in SI units becomes approximately: P (nGy/hr) $= 1.757 \times 10^{-3}$ q (MBq/km^2). Because of fluctuations in the depth coefficient, variations in the dose rate amount to $\pm 15\%$.

There are certain differences between the maps of ^{137}Cs accumulation and dose-rate related mainly to the fact that on arable lands ^{137}Cs is transported to greater depths in the ploughed layer. Therefore, in regions of intensive agricultural development, the average dose level turns out to be smaller. The overall range of dose-rate levels is 0.10 to 1.24 μR/hr ($\approx$ 1–12 nGy/hr).

With regard to tritium, by the beginning of 1964, it was estimated by Tetcher et al. (1965) that the total amount of tritium that had reached the earth's surface as a result of nuclear explosions was 44–96 kg (approximately 15.5–34.0 EBq; 420–920 MCi). The stratospheric inventory at this time was estimated to be 124–172 kg and hence the total amount of tritium on the globe was ~168 kg (59.2 EBq; 1.6 GCi).

We now present the characteristics of fractionation of different nuclides in global and long-distance fallout. The radionuclide compositions of particles of size 2.5–25 μm produced from atmospheric explosions (typical of semi-global fallout) and at time-periods of 9, 42 and 145 days, were presented by Benson et al. (1965a). A graph from that paper, of the logarithmic correlation of ^{140}Ba fractionation (with respect to ^{89}Sr) for such particles, is shown in Fig. 3.8. In the same work, the conclusion is drawn that curves of the logarithmic correlation of particle fractionation for high-yield atmospheric explosions actually coincide with similar curves of $f_{140,89}$ and $f_{95,89}$ for explosions on coral surfaces and near-water explosions. Values of $f_{i,95}$ for radioactive particles of global fallout collected in Japan in 1961–1962 are presented in papers by Mamuro et al. (1963b, 1965a). For particles of size

~10 μm, the values of $f_{103,95}$ are close to zero (with respect to the refractory nuclide ^{95}Zr), i.e., ^{103}Ru is actually absent in such particles. Values of $f_{(141+144),95}$ are within the range 0.25–0.7, in good agreement with the data of Edvardson et al. (1959) for particles collected in 1957–1958 over Sweden. They do not contradict the results obtained by Gaziev et al. (1965) for particles collected in the Moscow suburbs in autumn 1962.

It is interesting that, for smaller particles, the values of $f_{103,95}$ apparently increase. So, for the dust probes taken over Japan in 1961–1962 that contained particles containing very fine size fractions, the $f_{103,95}$ values were in the range 0.45–0.55, with one value of 0.95; values of $f_{(141+144),95}$ reached 0.85–1.0 while, for $f_{237,95}$ and $f_{239,95}$, they were equal to 1.0 (Mamuro et al., 1963b; 1965a). The values of $f_{140,95}$ for individual particles were 0.02–0.12; for ^{239}Np, they were within the range 0.05–0.35, while, for ^{237}U, they were in the range 0–0.45.

For 43 particles collected in Japan in September 1962, the fractionation coefficients were as follows (with respect to refractory nuclides):

Nuclide	^{90}Sr	^{89}Sr	$^{141}Ce + {}^{144}Ce$	^{103}Ru
Fractionation factor	0.35–0.40	0.006–0.01	0.15–0.30	$\ll 0.1$

(the first figures correspond to data from a group of more active particles). Particles with sizes up to 20 μm were found in fallout in Japan (Mamuro et al., 1965a).

Because the time of transfer of fallout from the stratosphere is relatively long, its radionuclide composition is determined largely by the content of relatively long-lived species. The half-life for the removal of aerosol products from the stratosphere, after the 1961–1962 test series in the northern hemisphere, was from several months to a year, while the half-life for the removal of products from the upper atmosphere above 21 km was several years (Friedlander et al., 1968). Thus we find that it is the nuclides ^{90}Sr, ^{137}Cs, ^{144}Ce, $^{95}Zr + {}^{95}Nb$ that are present in global fallout together with ^{54}Mn and some other "tracer" products (for instance, ^{109}Cd, ^{113m}Cd and ^{102}Rh (Kalkstein et al., 1965)).

Hot particles of size about 10 μm are at the upper limit of the particle size distribution and are removed faster. Global fallout arose mainly from atmospheric explosions and hence there was never any well-pronounced inverse fractionation in particles of this type of fallout (for the reasons explained in Chapter 1). In global fallout, it is also found that the sizes of particles in which ^{137}Cs predominates are smaller than those in which ^{144}Ce is bound. Coarsely-dispersed fractions of the aerosol are also enriched in $^{95}Zr + {}^{95}Nb$ and ^{185}W, while the highly dispersed ones are enriched in ^{90}Sr and others. This results in different removal rates from the atmosphere for different radionuclides (Gaziev et al., 1965).

3.2. *Long-Distance Fallout*

During a period of intense nuclear testing, it is rather difficult to follow the long-distance fallout pattern, extending over thousands of kilometers from an individual explosion, because the ensuing patterns from many explosions are superimposed on one another over these great distances. However, after 1963, it was possible to follow the distant but distinctive fallout patterns from certain individual underground nuclear explosions that released debris to the atmosphere. Such patterns are described in the work of Krey and Freid (1965), Kalkstein et al. (1965) and Izrael (1971).

Of particular interest was the "Schooner" underground nuclear explosion detonated in 1968 at the Nevada test site in the USA. After this explosion, the fallout could be traced across the Atlantic, into Western Europe and then into the USSR (Izrael et al., 1970b). A unique feature of this explosion was the presence in the fallout of the relatively short-lived radionuclides ^{181}W and ^{185}W. Several years earlier, a series of powerful type-one test explosions was performed in autumn 1961 at the Novaya Zemlya test site in an attempt to measure unique fallout patterns at great distance. These tests proved to be extremely important. Both geometrically and geographically, these fallout patterns at several thousands of kilometers away from the test site retained the features of the close-in patterns of fallout for high-altitude atmospheric explosions (for example, in the distributions of maximum contamination). These explosions were high-yield (up to tens of megatons) and were performed at relatively high altitude (3–5 km). However, their fallout patterns were similar to the close-in pattern for high air explosions but on a much larger scale. The fallout patterns had fairly clear boundaries, and no significant fractionation of the ruthenium isotopes with respect to $^{95}Zr + {}^{95}Nb$ was observed. Below we describe, in more detail, the results of the investigations carried out on these patterns from this 1961 series (Izrael at al., 1995).

It is known (Dubasov et al., 2000) that explosions performed at this test site were mainly high-yield high-altitude nuclear explosions in the atmosphere and, at a later time, underground nuclear blasts. And, though the high altitude explosions (at a height of 3–5 km) did not result in large-scale local contamination of the land around the test site (cf. the contamination at the Semipalatinsk Test Site), they could cause radioactive fallout, low in intensity, over rather vast territories outside the boundaries of the test site because of the displacement of the contamination maxima along the axes of the fallout pattern in the case of high altitude, high-yield explosions. Below are the actual data on radioactive contamination of the former USSR after the autumn (1961) series of high-yield tests at Novaya Zemlya. In this series, more than 10 nuclear devices in the megaton range (Dubasov et al., 2000) were exploded and, on 23 and 30 October 1961, some of the highest yield devices ever tested in the world, viz. 25 and 55–60 Mt (Dubasov et al., 1994), larger than 10 and 50 Mt (Machta et al., 1962), and 50 Mt (Mikhailov, 1996) were exploded there. Radioactive clouds from all of these explosions rose to great altitudes, traveling mainly in a southeasterly direction toward continental USSR.

A survey of the USSR territory, aimed at determination of the limits and degrees of contamination caused by the radioactive fallout products of these explosions, was carried out in April 1962 during the course of the special expedition organized by the author with colleagues from the Institute of Applied Physics (Izrael et al., 1995). The IL-14 (Iljushin-14) aircraft used for this survey was equipped with instrumentation for the onboard performance of continuous gamma-surveys of the terrain together with measurements of the gamma-radiation spectrum. The sensitivity of this instrumentation permitted changes of 0.3–0.5 μR/hr ($\approx$ 3–5 nGy/hr) in the gamma-field level to be measured at the flight altitude of 100 m. Since the gamma-field from the explosion products could at times during this survey be lower than the sensitivity threshold of the gamma-survey system, a sample of the deposited radioactivity was always taken, for calibration, at the points where the aircraft landed (if it were snow, a sample of the complete thickness of the covering was taken). The amount of detail in the survey obviously depended on the degree of sampling that was, in turn, determined by the spacing of the aerodrome network. For the territory surveyed, all

available airports used as landing sites were also used for sample collection (there being relatively few suitable, at this time of year, for the landing of aircraft such as the IL-14). The snow probes were taken at 21 points, each from an area of (2×2) m^2 over the whole depth of the snow cover (see Table 3.6 and Fig. 3.8).

Fallout after the explosions performed in October 1961 was observed over a significant part of the Soviet Union during the period after the stable snow cover was formed, which, as a rule, remains until the end of April–May (Hydrometeoizdat., 1960) (see Table 3.6). To ensure that we sampled only the fallout from the explosions that we were interested in, i.e., without any admixture of fragments from explosions of previous years, we took samples only in those regions where the snow cover could not melt. The samples were analyzed in the laboratory after the survey was over.

The survey was carried from 5 to 15 April, 1962 and covered the territory of the USSR from approximately 38 to 130° E longitude and from 52 to 74° N latitude.

Analyses of the liquid samples were carried out from 20 to 25 May 1962 using a NaI (Tl) gamma-scintillation spectrometer. The spectrometer was calibrated using a ^{137}Cs aqueous solution while the background was determined when the counting vial was filled with distilled water. The geometry was controlled during both the calibration and the measurements with a primary standard. Two peaks in the region of energies 0.5 and 0.75 MeV were evident in the spectra. We would emphasize that, on the whole, no peak corresponding to ^{137}Cs was found in the samples and therefore there was no strong enrichment of this radionuclide in these samples.

At the time of sample measurement (May 25, 1962), approximately 200 days after the explosion, the principle gamma-emitters in the mixture were $^{95}Zr + {}^{95}Nb$ (0.756; 0.724 and 0.764 MeV) and ^{103}Ru (0.495 MeV). More than 80% of the total gamma-activity of the mixture is composed of these two radionuclides (see Fig. 1.7). The activities of the given nuclides were calculated from the areas of the peaks and then estimates were made of the density of the contamination at the sites where the snow samples were taken. If the site was "representative", i.e., the density of contamination was typical of a large surrounding area, then an average density for the surface contamination around the sampling site was determined. The accuracy of the approach is determined by the accuracy of the sample analysis as well as by the representativeness of the sampling site. Errors in analysis were less than 20%, while sampling errors, estimated by statistical means, are believed to be better than 30%.

A map of contamination constructed from the data of Table 3.6 is presented in Fig. 3.9. Isolines of the density of contamination by $^{95}Zr + {}^{95}Nb$ (250, 200, 150, 100 and 50 mCi/km^2 (9.25, 7.40, 5.55, 3.70 and 1.85 GBq/km^2)) for the time of the measurements, i.e., end of May 1962, are drawn schematically on the map. When analyzing the map, one can conclude that there are two separate regions of contamination and that each of these has a different fallout pattern. One pattern is to the south, while the other has a southeasterly extension. At the end of May 1962, the maximum values for contamination by $^{95}Zr + {}^{95}Nb$ were revealed to be (i) ~ 210 mCi/km^2 (~ 7.77 GBq/km^2) (at Vorkuta) in the southerly pattern and (ii) ~ 300 mCi/km^2 (~ 11.1 GBq/km^2) in the south-east sector (at Volochanka and Taimyr). A comparison of the areas of the two peaks in each spectrum allows a calculation of the activity ratio of $^{95}Zr + {}^{95}Nb$ to ^{103}Ru to be made and the average ratio is 4.8.

Table 3.6
Sampling locations and dates

Sample No.	Location of sampling	Coordinates		Date			Activity (Ci/km^2)*	
		North latitude	East longitude	Formation of stable snow cover	Early snow disappearance	Sampling	$^{95}Zr + {}^{95}Nb$	^{103}Ru
1	Cherepovets	59°08′	37°55′	21 November	1 April	5 April	0.055	–
2	Syktyvkar	61°40′	50°50′	1 November	11 April	5 April	0.08	0.01165
3	Vorkuta	67°02′	64°02′	11 October	21 May	6 April	0.21	0.045
4	Amderma	69°46′	61°40′	21 October	24 May	6 April	0.078	–
5	Dikson	73°31′	80°30′	1 October	June	6 April	0.047	–
6	Tareya	73°16′	90°08′	21 September	21 May	7 April	0.13	0.0325
7	Khatanga	71°57′	102°28′	6 October	21 May	7 April	0.104	–
8	M. Kosisty	73°40′	109°45′	1 October	21 May	7 April	0.05	0.007
9	Tiksi	71°38′	128°50′	21 September	25 May	8 April	0.042	0.0084
10	Zhigansk	66°46′	123°20′	1 October	11 May	8 April	0.138	0.036
11	Yakutsk	62°02′	129°45′	11 October	1 May	8 April	0.037	–
12	Olekminsk	60°23′	120°26′	11 October	21 April	9 April	0.152	0.035
13	Kirensk	57°47′	108°08′	11 October	11 April	9 April	0.048	0.0106
14	Irkutsk	52°17′	104°19′	1 November	1 April	10 April	0.020	–
15	Eniseisk	58°27′	92°12′	21 October	15 April	11 April	0.078	–
16	Podkamennaya Tunguska	61°36′	90°06′	11 October	21 April	12 April	0.069	–
17	Turukhansk	65°48′	87°57′	1 October	10 May	12 April	0.034	–
18	Dudinka	69°24′	86°12′	21 September	16 May	12 April	0.040	0.023
19–25	Volochanka (in layers)	70°58′	94°35′	21 September	21 May	12 April	0.297 (sum over layers)	–
26	Norilsk	69°18′	88°02′	21 September	16 May	13 April	0.018	
27	M. Kamenny	68°26′	73°35′	11 October	21 May	13 April	0.095	–

*1 Ci/km^2 = 37 GBq/km^2.

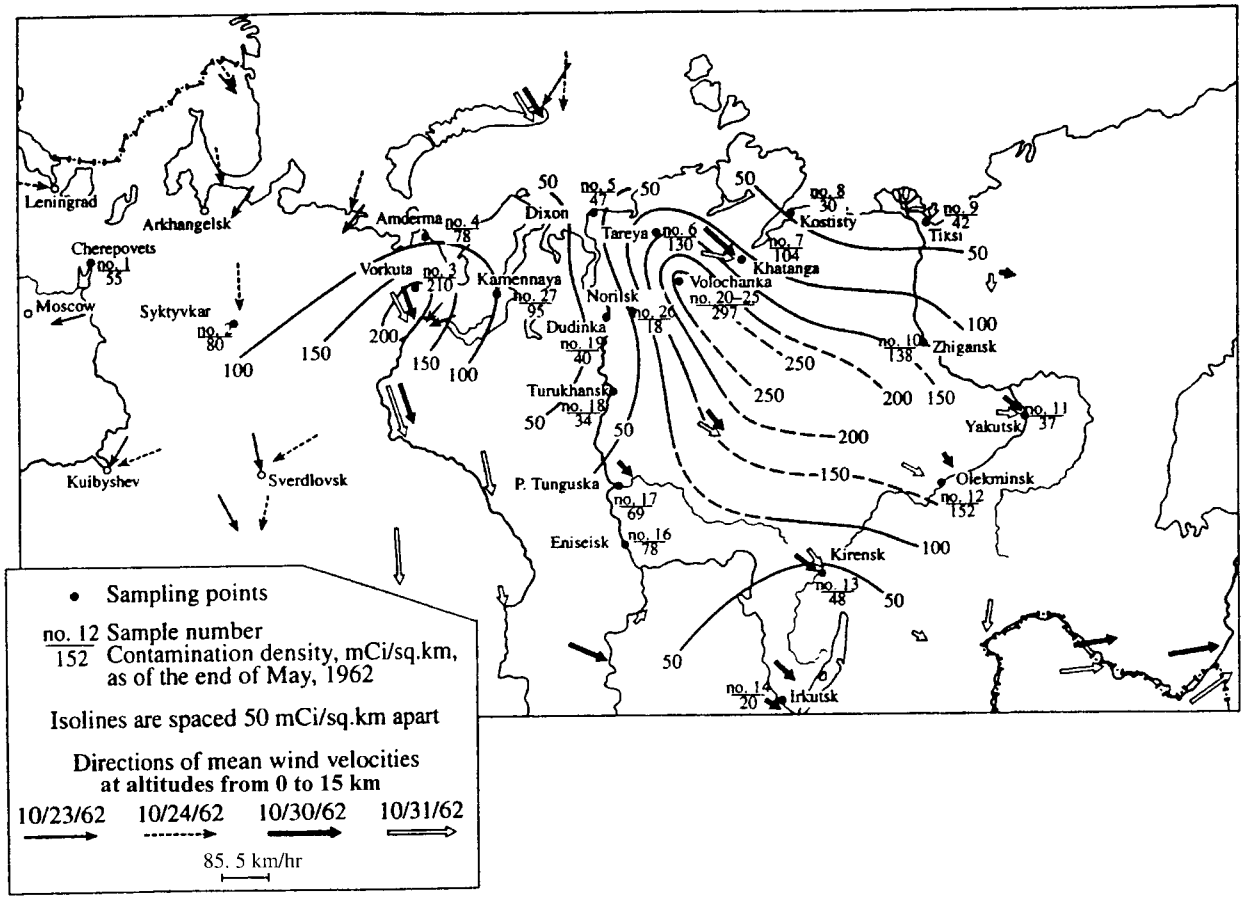

Fig. 3.9. Distant fallout patterns from a series of powerful atmospheric nuclear explosions conducted in 1961 (survey of 1962).

At the time of measurement, the total density of contamination exceeded that by $^{95}Zr + {}^{95}Nb$ by a factor of 3–3.5 (Grechushkina, 1964). The calculation shows that, for a $^{95}Zr + {}^{95}Nb$ contamination density of 0.3 Ci/km^2 (11.1 GBq/km^2), the γ-radiation dose rate of at a height of 100 m, without considering screening by snow, amounted to 0.9 μR/hr (≈ 9 nGy/hr). The snow cover reduced this level several times (by not less than three times in regions with the highest contamination). Thus, 6 months after the explosion, the gamma-field from the contamination at the height of flight was 0.3 μR/hr (≈ 3 nGy/hr). This level is such that it could not be measured confidently using the aircraft instruments at our disposal because of the fluctuations in background gamma-radiation that occur naturally.

Calculations made by the method of Izrael and Stukin (1967), for 1 day after the explosion, indicate that the gamma radiation levels amounted to 1.5–1.8 mR/hr (≈ 15–18 μGy/hr) in the zone of maximum contamination at the earth's surface.

In the 1962 report, synoptic maps relating to the dates of the largest explosions (23 and 30 October 1961) and the subsequent days were examined. Average values of the wind velocity and direction in the layer from the earth's surface to an altitude of 16 km were calculated for that period. These data are plotted in Fig. 3.9. The agreement of both fallout patterns with the meteorological conditions during the period of their formation is very clear. This allows us to postulate that the radioactive patterns were most probably generated from these very high-yield nuclear explosions in October 1961. Here again, however, the proviso must be added that other explosions in the autumn of 1961 could have influenced the contamination of this area and so further analysis is required. Nevertheless, this determination of contamination density, by means of the analyses of snow samples, turns out to have been the only way to determine the order of the contamination levels and the resulting external doses over such a large area after the series of weapons tests conducted at the Novaya Zemlya Test Site in autumn 1961.

In summary then, on the basis of the above survey carried out in April 1962, it was possible to distinguish at least two vast zones of radioactive contamination, the first in the west from the Urals (southwards) and the second on the Taimyr and in Central Siberia (directed toward the south-east). Both zones had areas of maximum contamination that were still evident far from the epicenters of the explosions.

In April 1962, the maximum contamination of lands over the continental territory of the Soviet Union as a result of the autumn 1961 test series (maximum estimates) amounted to:

Total activity	Up to 1000 mCi/km^2 (37 GBq/km^2)
$^{95}Zr + {}^{95}Nb$	300 mCi/km^2 (11.1 GBq/km^2)
^{103}Ru	55 mCi/km^2 (2.0 GBq/km^2)

The dose from the external gamma-radiation (ignoring screening by the snow cover) at the point of the maximum contamination (from the fallout time of about 1 day after the explosion until complete decay) amounted to about 0.2–0.3 R (≈ 2–3 mGy), in Zhigansk 0.1–0.15 R (≈ 1–1.5 mGy) and less than 0.1 R (1.0 mGy) in Yakutsk.

Within the same context of long-distance fallout, we can examine the radioactive fallout that occurred after the explosion at Bikini Atoll (USA) and which spread over hundreds and thousands of kilometers in the Pacific Ocean (IAEA, 1998c).

In much the same manner as in ground explosions, in situations following an underground explosion where partial ejection into the atmosphere takes place, "inverse"

Table 3.7
Relative contents of nuclides (percentages) in a distant zone of the explosion cloud

Nuclide	Calculated	Air samples	Fallout samples
^{89}Sr	40	43	18
^{90}Sr ($+^{90}Y$)	0.35	0.25	0.2
^{95}Zr	–	0	0
^{91}Y	–	3.4	2.8
^{103}Ru	–	4.0	2.9
^{106}Ru	–	0.9	0.8
^{137}Cs	0.3	0.8	0.45
^{140}Ba	24	24	33
^{140}La	28	24	33
^{141}Ce	–	0	4.9
^{144}Ce	–	0	0.8
^{99}Mo	–	0.4	1.0

fractionation is observed in the distant fallout. This is unlike the situation after purely atmospheric explosions. It was shown by Bonner and Miskel (1965) that, in the cloud from an underground nuclear explosion, the coefficients of enrichment of the volatile nuclides (with respect to ^{140}Ba) reach fairly high values. On the basis that those products still present in the cloud several hours after an explosion will become part of distant fallout (up to several thousand kilometers from the explosion site), estimates have been made of the radionuclide composition of this category of fallout (Izrael, 1968). In this case, a fraction of the ith nuclide in distant fallout will be

$$\alpha_i = \frac{a_i c_i}{\sum_i a_i c_i},$$

where α_i is the fraction of the ith nuclide in the non-fractionated mixture of explosion products; c_i is the coefficient of enrichment of the ith nuclide. Values of α_i, obtained in this way (Izrael, 1968) are in good agreement with the experimental values (see Table 3.7).

In Table 3.7, data are presented on the nuclide composition of the products collected on air filter samples with other results from the "Sedan" fallout collected at distances of about 1000 km from the explosion site. These were taken from the work of Krey and Freid (1968) and relate to five stations, are averaged over seven samples and are corrected to 15 days after the explosion when only the products outlined in the table remained in the mixture.

It is seen in Table 3.7 that ^{89}Sr and ^{140}Ba constitute the main portion of the activity in the distant fallout 5–15 days after the explosion. For external exposure, the main contributors to dose to the population living in the distant fallout zone will be ^{140}Ba (^{140}La) and ^{137}Cs, while for internal dose ^{89}Sr and especially ^{90}Sr will be the main contributors.

Table 3.7 shows also that the nuclide composition of the air samples does not completely agree with that of the fallout samples. This occurs because of the differing fractionation of the nuclides in particles of different sizes occurring in both dry and wet fallout. As this takes place, the effect can be slightly different in dry and wet fallout because the washout efficiencies of particles of different sizes in the atmosphere differ between precipitation and dry fallout.

Table 3.8
Tritium fallout from the "Chagan 1004" explosion (1965)

Distance from the explosion site (km)	Period of precipitation collection	Tritium concentration in the precipitation (TU)	Tritium fallout (mCi/km^2)
200	D + 2 to D + 14 (12 days)	29000 ± 1500	945
450	D + 1 to D + 13 (12 days)	8400 ± 1200	500
500	D + 10 (1 day)	11500 ± 1200	90
500*	D + 10 (1 day)	10500 ± 200	82
500†	D + 2 to D + 13 (11 days)	5300 ± 1000	42
500	D + 3 to D + 10 (7 days)	3600 ± 1000	60
550	D + 6 to D + 14 (8 days)	8800 ± 1250	240
1800	D + 5 (1 day)	12900 ± 1500	20
3300	D + 3 to D + 10 (7 days)	4700 ± 1000	45
550‡	Period of explosion	2000 ± 1000	14
4000‡	The same	1000 ± 1000	10

*Second sample.
†Third sample.
‡Background samples taken outside the fallout zone.
1 mCi/km^2 = 37 MBq/km^2.

3.3. *Tritium Fallout in a Distant Fallout Zone*

Tritium concentration variations at large distances from an explosion site constitute another important feature of considerations of distant global fallout. The mechanism of tritium fallout onto the earth's surface in global fallout is still not well studied. We may assume, however, that when precipitation occurs, the tritium fallout in a distant zone is not markedly different from the fallout of other volatile nuclides in the nuclear explosion products (e.g., ^{89}Sr and ^{90}Sr, ^{137}Cs, ^{140}Ba, etc.). It is known that when fallout occurs with precipitation (wet fallout), it results in a greater radioactive contamination of the earth's surface relative to dry fallout.

Tritium fallout in precipitation in a distant fallout zone was examined after the Chagan, 1004 underground cratering explosion. The data are presented in Table 3.8 (Izrael, 1971) where it should be noted that not all samples correspond to the axial position in the fallout pattern. Levels of tritium contamination did not exceed 1 Ci/km^2 (37 GBq/km^2) at distances exceeding 200 km from the explosion site. If we consider all possible ways by which tritium can enter an organism, then in this case the maximum exposure dose to the population did not exceed 1.5 mrad/yr ($\approx$ 15 μSv/yr) at 1 Ci/km^2 (37 GBq/km^2).

Chapter 4

RADIOACTIVE FALLOUT FROM UNDERGROUND NUCLEAR EXPLOSIONS

Contents

1. Characteristics of Major Cratering Explosions 120
   - I. High- or Medium-Yield Explosions 120
   - II. Low-Yield Explosions 120
   - III. Explosions of Very Low Yield 121
   - IV. Group Explosions 121
2. Radioactive Cloud 123
3. Radioactive Contamination in the Bulk Zone and the Cloud Pattern 125
4. Radionuclide Composition of the Fallout from an Underground Explosion 135
5. Prediction of the Radioactive Contamination of Surrounding Land after an Underground Nuclear Explosion 140
   - 5.1. Prediction of Close-in Fallout 141

In underground nuclear explosions where there is an ejection of surrounding materials into the atmosphere (a cratering explosion), some of the radioactive products that are formed are carried upwards with the rocks and then returned to the crater or the immediate vicinity through gravitational settling. A fraction associated with the relatively small ground particles can be transported by the wind over large distances away from the explosion site. When the products are spread in the atmosphere and precipitate or settle out, a number of "activity zones" and other features can be recognized (Izrael, 1974) as follows:

(i) in the atmosphere:
   (a) the radioactive cloud contains radioactive particles with a rather wide range of sizes and gaseous radioactive products; its height can range from several hundred meters to several kilometers according to the explosion yield and it can spread over great distances;
   (b) the base surge cloud rises to altitudes that are significantly lower than the cloud (i.e., up to 100–1000 m);

(ii) on the surrounding land:
   (a) the crater zone (several tens or hundreds of meters for an explosion of 1–100 kt yield) and the ground around the crater (up to a radius of 1 km);
   (b) the close-in fallout zone formed by the fallout of the largest particles from the cloud and base surge; this near-zone is limited to the first few hours (5–10 hr) of fallout from the radioactive cloud and the base surge;
   (c) the long-distance fallout zone that occurs after the close-in fallout and then lasts for several days after the explosion.

1. Characteristics of Major Cratering Explosions

Investigations of these zones were carried out on tests performed in both the Soviet Union and the United States of America (more than ten explosions). All explosions performed in the USSR were designed to study the peaceful uses of underground nuclear explosions.

I. High- or Medium-Yield Explosions

1. The "Chagan 1004" borehole test of January 15, 1965 in USSR had a yield of 100–150 kt and was carried out in aqueous sandstone mixed with coal-clay shale at a depth of 175 m. The loss of groundmass through fusion amounted to 7%. The crater formed as a result of the blast had a diameter on the surface of 400–430 m, a depth of about 100 m and a volume greater than 6×10^6 m^3 that was afterwards filled with water. A cloud, together with the base surge, rose from the explosion (Kedrovsky, 1970; Mikhailov, 1996).

2. The "Sedan" explosion (July 6, 1962; USA) of about 100 kt yield was carried out at a depth of 193 m in alluvial deposits. A crater was formed after the explosion, approximately 400 m in diameter and about 100 m in depth. A cloud and a powerful base surge were also formed at the explosion (Toman, 1970).

3. "Schooner" (December 8, 1968; USA) had a 35 kt yield and was performed at a depth of 108 m in tuff formations: the first layer of the tuff was composed of dry rocks, the second of porous rocks with a water content of 8–10%; the third contained up to 20–38% of water and the fourth layer was similar to the first. A cloud and powerful base surge were formed at the explosion. The volume of the crater was 1.74×10^6 m^3; its diameter was 130 m and its depth 63.4 m. Ground rubble that accumulated around the crater had a height of 13.4 m (Toman, 1970).

II. Low-Yield Explosions

4. The "Cabriolet" explosion (January 26, 1968; USA), with a 2.3 kt yield, was performed at a depth of 52 m in a stratified rhyolite. The crater formed by the explosion had a volume of 137×10^3 m^3, a radius of 55 m and a depth of 36 m. The height of the rubble ridge was 9.4 m (Toman, 1970).

5. The "Sary-Uzen" explosion (borehole 1003; October 14, 1965; USSR) was of 1.1 kt yield and was performed at a depth of 48 m in fractured sandstone. The amount of rock lost due to melting and evaporation was ~5.4%, while the moisture content was 0.8% by mass. A crater with a diameter of 110 m was formed, its maximum depth reaching 31 m (Izrael et al., 1970b).

6. The "Danny-Boy" explosion (March 5, 1962; USA), of 0.42 kt yield, was carried out at a depth of 33.5 m in dry basalt. A crater 19 m deep of 33 m radius was formed. The crater volume amounted to 27.5×10^3 m^3 (Toman, 1970; Nordyke and Wray, 1964).

In the case of the low-yield explosions (4 and 5), no noticeable separation of the cloud and the base surge was observed and with "Danny-Boy" no cloud was formed.

III. Explosions of Very Low Yield

7. The "Telkem-1" explosion (borehole T-I; October 21, 1968; USSR) had a yield of 0.24 kt and was performed at a depth of 31.4 m in a sandstone that contained large amounts of organic compounds. The loss of material through melting, etc. was 13%. The crater, 21 m in depth, had a diameter of 70 m. The height of the ground rubble crest reached 8–10 m (Mikhailov, 1996).

8. The "Sulky" Explosion (USA, 1964) of 0.088 kt yield was performed at a depth of 27.4 m in dry basalt. No crater appeared but a hill of broken rock, with a height of 6.3 m, was formed at the site (Toman, 1970).

Except for dust formation, no distinctive cloud or base surge was observed for these very low-yield explosions.

IV. Group Explosions

9. The "Buggy" explosion (March 12, 1968; USA) consisted of five charges, each of 1.1 kt yield, arranged in a horizontal line. The test was performed at a depth of 41.2 m in stratified basalt. It resulted in the formation of a hollow trench 260.6 m long, 19.8 m deep and 77.4 m wide, with a relatively even base. The ground rubble had a maximum height of 12.4 m at the sides and 4.37 m at the ends of the trench (Toman, 1970).

10. The "Telkem-2" explosion (borehole T-II; November 12, 1968; USSR) consisted of a simultaneous explosion of three charges each of 0.24 kt placed on the same line at a distance of 1.3 m between charges. The yield and depth for each was similar and corresponded to the characteristics of the "Telkem-1" explosion (item 7 above). The gas-content of the rocks (aleurolite, porphyrite, gritstone) amounted to only 3%. A trench 20 m deep, 142 m long and 64 m wide was formed after the explosion with the rubble height reaching 18 m on its sides and 6–7 m at the ends (Mikhailov, 1996).

11. The "Taiga" explosion ("Kanal"; March 23, 1971; USSR) was carried out at a depth of 128 m, using three equal charges of 15 kt yield; a channel profile, i.e., a trench, was formed as a result of the explosion.

Table 4.1 presents a summary of the basic data for the above explosions. We should also mention two other explosions, data for which were published later by Dubasov and Takhuvatulin (2000) and Myasnikov et al. (2000) and Adushkin and Spivak (2000). One of these, "Lasurite", of ~2 kt yield, was detonated on December 7, 1974 in the USSR at the Semipalatinsk Test Site in borehole P-1 at a depth of 75 m. With this explosion, because of the presence of a ground fault along the mountain slope, a dam-like ridge resulted and a release of radioactivity was recorded. The second explosion, "Crystal" (included

Table 4.1
Basic data on experimental cratering nuclear explosions. From US Department of Energy (1994); Mikhailov (1996); Izrael et al. (1970a) & (1970b); Kedrovsky (1970); Toman (1970)

No.	Explosion name	Country	Date D/M/Y	Yield (kt)	Explosion depth (m)	Scaled depth ($m/kt^{1/3.4}$)	Height of cloud or dust formation (m)	Amount of substance precipitated (t) (from energy release)	Amount of radioactivity precipitated on pattern (%)
					I. High- or medium-yield				
1	Chagan, 1004	USSR	15/01/65	140	175	41	4800		20
2	Sedan	USA	06/07/62	100	193	50	3600–4200	1200–1400	4–17
3	Schooner	USA	08/12/68	35	108	39	4000	340	
					II. Low-yield				
4	Cabriolet	USA	26/01/68	2.3	52	41	120	7	
5	Sary-Uzen, 1003	USSR	14/10/65	1.1	48	48	300	35	3.5
6	Danny Boy	USA	05/03/62	0.42	33.5	43.2	300	17–30	4–7
7	Crystal	USSR	02/10/74	1.7	98	85			~1.0
					III. Very low-yield				
8	Telkem-1, 2308	USSR	21/10/68	0.24	31.4	51	200	0.4	0.2
9	Sulky	USA	18/12/64	0.088	27.4	56	–	–	–
					IV. Group explosions				
10	Buggy (A, B, C, D, E)	USA	12/03/68	1.1 × 5	41.2	41.2	660		
11	Telkem-2 (2305–2307)	USSR	12/11/68	0.24 × 3	31.4	51	450	1.8	0.3
12	Taiga/Kanal (1B, 2B, 3B)	USSR	23/03/71	15 × 3	128	39.4			

in Table 4.1) was performed on October 2, 1974 in the USSR at Yakutia, located 90 km NE of Aikhal. The depth of the test was 98 m and its yield was 1.7 kt. The heavy loosened rocks from this explosion created a dam and a tailing pond at the site.

We should note here two nuclear explosions which were carried out in rather deep boreholes but, due to emergencies, partial releases of the radioactive products into the atmosphere occurred. One of those was the "Kraton-3" explosion in Yakutia (24.08.1978); its yield was 22 kt performed at a depth of 577 m. The gases and aerosols escaped and formed a fallout pattern up to 31 km long (the calculated integral dose was 0.5 ber ($\approx$ 4.4 mSv)). The second was the "Globus-L" explosion (Ivanovo region, 19.09.1971) of 2.3 kt yield at a depth of 615 m. At 17 min after the explosion, a gas–water plume burst out through the borehole (Myasnikov et al., 2000).

2. Radioactive Cloud

To understand the character of the radioactive fallout and its radionuclide composition, a brief description of its formation in an explosion is useful. As a rule, in a "cratering" explosion, a cloud is formed, the elevation of which depends on the yield and the scaled depth of the explosion as well as on the water content and the volatile products in the rocks. In the "Sedan" explosion, the cloud reached an altitude higher than 5 km (Krey and Freid, 1965), while in the "Sary-Uzen 1003" explosion it reached only about 300 m (Kedrovsky et al., 1970) and in "Danny-Boy", carried out in dry basalt from which no cloud was formed, only a dust column was observed (Nordyke and Wray, 1964).

Several hours after an explosion, the dose rate within the cloud can amount to $\sim$1 R/hr ($\sim$10 mGy/hr), even when the explosion is small. Thus, at "Sary-Uzen 1003", the radiation level reached 0.82 R/hr ($\approx$8.2 mGy/hr) 107 min after the explosion. The inventory of gamma-emitters contained within the cloud 15–70 min after the explosion amounted to approximately 1% of the original quantity (corrected for decay).

A typical feature of an underground explosion is the initiation of a base surge whose radial propagation for some time after the explosion does not seem to be dependent on the meteorological conditions. In "Chagan 1004", the base surge diameter actually reached a height of 500–750 m and had a diameter of 5000 m at 1.5 minutes. Further on, the cloud and the base surge propagate with the wind, being scattered by the action of horizontal turbulent diffusion, and, as a result, their horizontal dimensions increase. If the increase in height is small, then the γ-radiation dose at ground level from a passing cloud D_{cl} can be significant and many times greater than the dose from the radiation that is deposited D_{pat}. Thus, following the "Sary-Uzen 1003" explosion, the ratio $D_{\mathrm{cl}}/D_{\mathrm{pat}}$, increased outwards from the epicenter from a value of 0.5 to 24 at distances from 8 to 50 km, respectively. After "Telkem-1" and "Telkem-2", this ratio ranged from 53–150 over a distance of 0.4–50 km. After "Sedan" and "Chagan 1004", the clouds passed at great altitude and hence the γ-radiation dose emanating from the cloud was significantly smaller compared to that on the ground (Izrael, 1974).

Radioactive particles in the cloud are mainly irregular in form. The composition of the particles that are dispersed by the cloud changes with time. In several seconds after the "Sary-Uzen 1003" explosion, for example, the fraction of particles of diameter smaller

Table 4.2
Coefficients of enrichment of different nuclides in the cloud and bulk ground after the "Sary-Uzen 1003" explosion (relative to ^{95}Zr)

Time of sampling (after explosion)	Location of sampling and distance	^{144}Ce	^{141}Ce	^{103}Ru	^{131}I	^{140}Ba	^{117}Cs	^{89}Sr
3 s	The dust column above the epicenter	0.89	1.07	0.8	0.96	0.79	0.25	1.10
1.5 hr	The cloud, $R = 70$ km	0.89	4.9	3.35	0.175	37.4	34.8	39.3
–	The bulk ground	0.94	1.6	0.34	0.42	0.83	0.226	0.176

Table 4.3
Coefficients of enrichment of different nuclides in the cloud from the "Danny Boy" explosion (relative to ^{95}Zr)

Nuclide	Time of sampling (after the explosion) (min)			
	8	15	47	138
^{89}Sr	142	196	357	377
^{90}Sr	90	114	200	211
^{91}Y	32	37	64	65
^{137}Cs	125	177	354	377
^{140}Ba	38	45	76	78
^{141}Ce	4.6	4.7	6.8	5.5
^{144}Ce	1.0	1.0	1.1	1.9

than 0.5 μm did not exceed 1%, with 80% of the total radioactivity on particles larger than 10 μm. This distribution changed so rapidly that, after only 0.3 hr, approximately 90% of the radioactivity was held on particles smaller than 0.5 μm. The distribution of particles and their activity can be satisfactorily described by a normal logarithmic expression, the median diameter in the distribution being 2 μm at 0.3–0.4 hr after the "Sary-Uzen 1003" explosion.

The nuclide composition of the aerosol samples taken after the "Sary-Uzen 1003" explosion was rather typical of the cloud as a whole. Table 4.2 presents analytical results for several typical samples taken from the dust column several seconds after the explosion and from the cloud as it moved away from the explosion's epicenter to a distance of 70 km. Table 4.3 presents coefficients of enrichment for a number of nuclides in the cloud at different time-intervals after the "Danny-Boy" explosion (relative to the refractory nuclide ^{95}Zr) (Bonner and Miskel, 1985).

When analyzing the Table 4.2 data, one can see that the samples taken from the dust column several seconds after the explosion are depleted in volatile nuclides and those having volatile and gaseous precursors.

Tables 4.2 and 4.3 show that samples taken from the cloud at several tens of minutes after an explosion are strongly enriched with radionuclides having gaseous precursors and that the coefficient of enrichment increases with time. Actually, the radioactive composition of the cloud that spreads over long distances (hundreds and thousands of kilometers) reflects a mixture of the following radionuclides: ^{89}Sr, ^{90}Sr, ^{91}Y, ^{137}Cs, ^{140}Ba and ^{103}Ru, with ^{141}Ce being present in smaller amounts. This is confirmed by the composition of the near-surface

Table 4.4
Coefficients of enrichment of different nuclides in the clouds of different explosions (relative to ^{90}Mo)

Radionuclide	Palanquin	"Chagan" $\bar{h} = 41$ (m/kt$^{1/3.4}$)	"Danny Boy" $\bar{h} = 43.2$ (m/kt$^{1/3.4}$)	"Sary-Uzen" $\bar{h} = 48$ (m/kt$^{1/3.4}$)	"Telkem-2" $\bar{h} = 51$ (m/kt$^{1/3.4}$)	"Sulky" $\bar{h} = 56$ (m/kt$^{1/3.4}$)
^{89}Sr	4.0	35	150	100	1.4×10^4	3×10^5
^{137}Cs	1.0	25	25	23	1.4×10^4	2×10^5
^{140}Ba	1.3	12	15	29	5.6×10^3	3×10^4
^{141}Ce	1.5	4.3	5.0	5.1	6.1×10^3	2×10^3

air-filter samples taken at a distance of about 1000 m after the "Sedan" explosion by Krey and Freid (1965).

Nuclide	^{89}Sr	^{90}Sr	^{91}Y	^{103}Ru	^{106}Ru	^{137}Cs	^{140}Ba
Coefficient of enrichment	122	51	8.2	5.5	15	178	18

One can see from the data presented here that, for most of the nuclides analyzed in the near-ground air samples, the coefficients of enrichment (with respect to ^{95}Zr) are close to the values found in the cloud for the same species in the first hour after the explosion. Note that samples with such compositions are not found either in the close-in zone or in the fallout pattern of the dust column. At the same time, samples taken from the dust column during the first seconds after the explosion are very similar in their radionuclide composition to the ground samples taken from the area of the crater and the bulk ground. For comparison, the results of the nuclide analysis of the ground rubble samples are given in Table 4.2.

Table 4.4 presents the enrichment coefficients (relative to the refractory isotope ^{99}Mo) for a number of nuclides that were isolated from the cloud generated by a number of cratering explosions (Izrael et al., 1970a; Bonner and Miskel, 1965; Miskel, 1966). These explosions led to the creation of domes within the ground and these had essentially different "filtering" properties. After the "Sulky" and "Crystal" explosions, the dome was not actually destroyed but only a "negative" crater was formed, i.e., a hill of heaped ground or "retarc". In the case of the "Palanquin" explosion, the radioactive products easily found their way into the atmosphere through holes/fissures in the underground rock formations.

With the "Sary-Uzen 1003", "Chagan 1004", "Danny-Boy" and "Telkem-2" explosions, well-defined craters were formed and the higher "filtering" capacities at increased depths were related to increases in the coefficients of enrichment. Especially large coefficients of enrichment after the "Telkem-2" and "Sulky" explosions merit attention. These were low-yield explosions so, because of their ground domes, they had more effective "filters" than the higher yield explosions.

3. Radioactive Contamination in the Bulk Zone and the Cloud Pattern

When radioactive particles descend from the cloud and from the base surge, the surrounding land becomes contaminated in the region of the crater and the bulk ground

as well as along the trajectory of both the cloud and base surge. Precipitating particles from the base surge contaminate the ground also on the windward side of the crater. The principal characteristics of the terrestrial contamination are the following: (i) the distribution of the radiation levels on the ground; (ii) the fraction of the total amount of radioactive products deposited in the near-fallout pattern and in the zone of bulk ground and (iii) the temporal changes of the radiation levels on the ground. A fourth characteristic is the distribution of the radioactive products with depth in the zone of the bulk ground.

Investigations of the distribution of radioactivity on land were carried out by means of aircraft gamma-surveys after a series of underground nuclear explosions carried out by the USSR and USA. Additional data were gathered from ground-level gamma-surveys as well as from laboratory analyses of samples collected in contaminated regions, particularly ground rubble zones (Izrael et al., 1970a; Nordyke and Wray, 1964; Izrael and Stukin, 1967). Radiation levels measured at different times after a given explosion were normalized to a common time.

Aircraft roentgenometric gamma-surveys performed after the "Sary-Uzen 1003" and "Chagan 1004" explosions and others were carried out by successive flights along radial routes over the ground rubble zone and by flights across their axes when surveying fallout patterns (Izrael et al., 1970a). Aerial gamma-surveys, performed using aircraft or helicopters, are effective methods for the determination of the fallout outlines and radioactivity distributions that are needed to determine general radioactive conditions and the external doses from environmental radiation. Such surveys of fallout patterns, along with supplementary investigations of the radioactive products in the fallout pattern, complement a whole complex of investigations of radiation conditions.

Isolines of the intensities of the γ-radiation dose reduced to a height of 1 m were drawn on the basis of such measurements. Reduction was carried out using an "altitude" curve derived from data on the radiation levels measured at different times and heights over a fixed area within a ground fallout pattern (this curve is close to the theoretical one that depends on the initial energy of the gamma-emitters). When recalculating the radiation levels within the bulk ground zone, as measured from an aircraft or helicopter, the volumetric 4π character of an emitter was taken into account. Reduction to the given time was made using a curve obtained from successive measurements of the radiation levels above the fallout pattern (this curve is an exponential function with the exponent $n = -1.3$). The inventory of radioactive products in a fallout pattern was estimated from the energy release of the explosion products deposited on the ground (see Chapter 7).

To assess the overall radiation level, measured distributions were averaged along the fallout pattern axis and in the direction across the axis. The following quantity was then determined

$$Q_{\text{pat}} = \int_R \int_l P(R, l)\, \mathrm{d}R\, \mathrm{d}l, \tag{4.1}$$

where Q_{pat} is the quantity of radioactive substances in the fallout pattern, $P \cdot \text{km}^2/\text{hr}$; $P(R, l)$ is the dose rate at height $h = 1$ m, R/hr (remembering that 1 R/hr is approximately 10 mGy/h in current S.I. units—see introductory Glossary on units); R is distance along the pattern axis, km; l is a distance across the pattern axis, km. The total inventory of radioactive substances deposited in the fallout pattern was calculated in units of energy, based on

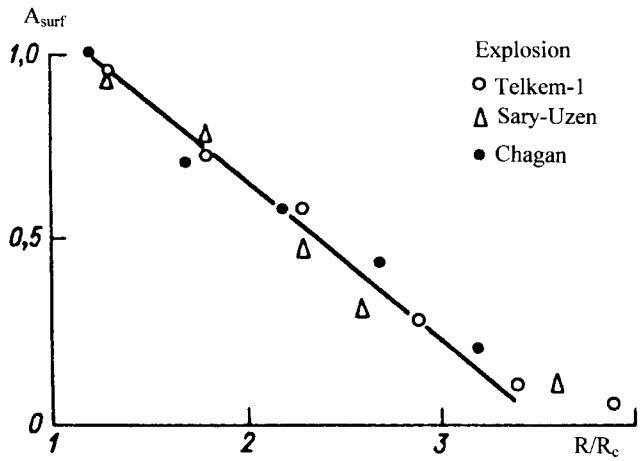

Fig. 4.1. Dependence of the average density of contamination in the surface layer of bulk ground on distance from the epicenter for different explosions (R is distance from the epicenter; R_c is the crater radius).

the assumption that 1 $P \cdot km^2/hr$ corresponds to an energy release in the explosion products of 2.86×10^{15} MeV/s (the influence of ground roughness was taken into account—see Chapter 7). The fraction of γ-radioactive products deposited in the fallout pattern was compared to the total inventory of radioactive products Q (MeV/s) formed in the explosion at a given time (the contribution of induced activity was carefully taken into account).

When calculating the total amount of substance deposited in the ground rubble zone, the distribution of radioactivity with depth was taken into account, i.e., the calculation was performed using an average radioactivity concentration for the total rubble obtained from either laboratory measurements of samples or aerial surveys, but with the introduction of a correction factor for depth variation.

It was determined that, for all three explosions "Sary-Uzen 1003", "Chagan 1004" and "Telkem-1" (Izrael et al., 1970a), the maximum specific density of contamination of the surface layer lay within the epicentral zone of the bulk ridge and that the activity concentrations decreased steadily with distance from the ridge. At a distance of three crater radii from the limits of the displaced rocks, the surface density of contamination, averaged over all directions, was 2.5–3 times less than on the bulk ridge. The change in the average density of contamination in the bulk ground surface layer for the "Sary-Uzen 1003", "Chagan 1004" and "Telkem-1" explosions as a function of distance (expressed in crater radii) is shown in Fig. 4.1. It can be seen that, for all of the above experiments, the character of the distribution of radioactive products in the surface layer of the bulk ground is practically the same.

The activity concentration of surface samples taken from the internal zone of the crater of the "Sary-Uzen 1003" explosion decreases sharply from the bulk ridge towards the epicenter of the explosion. On average, the activity concentrations in samples collected at distances of 10–20 m from the epicenter are 4–5 times smaller than in samples taken from the rubble ridge. Radioactive products in the bulk ground occur in a relatively thin

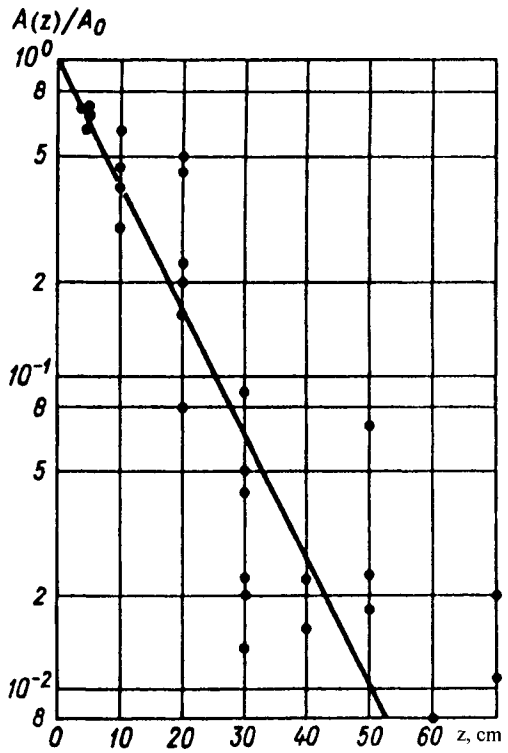

Fig. 4.2. Dependence of the ground beta-activity concentration on depth in the bulk ground for the "Chagan 1004" explosion.

surface layer. The variation of activity concentration of the bulk ground with depth $A(z)$ is satisfactorily approximated by the exponential relationship

$$A(z) = A_0 e^{-mz}, \tag{4.2}$$

where A_0 is the beta-activity concentration in a thin surface layer of the rubble. The value of the coefficient m was 0.066 cm^{-1} for the "Sary-Uzen 1003" explosion and 0.088 cm^{-1} for the "Chagan 1004" explosion. A graph of the variation in beta-activity versus depth in the bulk ground for the "Chagan 1004" explosion is shown in Fig. 4.2 (Izrael et al., 1970a).

The total amounts of some nuclides present in the ground rubble of the "Sary-Uzen 1003" and "Chagan 1004" explosions are given in Table 4.5. The results take into account the distribution of the radioactive products with depth in the rubble. Data on the total nuclide inventory in the bulk ground of the "Sary-Uzen 1003" explosion as presented by Izrael et al. (1970b) were lower than during the "Chagan 1004" explosion (Izrael et al., 1970a).

One can see from the table that the ground rubble contains about half of all the refractory nuclides formed. The quantities of species having volatile precursors are less because of

Table 4.5
Amounts of radionuclides in the bulk ground (% total)

Nuclide	Explosion	
	"Sary-Uzen 1003"	"Chagan 1004"
^{95}Zr	39	49
^{106}Ru	55	54
^{103}Ru	45	63
^{141}Ce	40	62
^{144}Ce	49	–
^{140}Ba	34	32
^{137}Cs	15	25
^{89}Sr	9	23
^{90}Sr	11	30

their redistribution during rock-breaking and cracking and their increased release into the atmosphere.

The radioactive fallout from the base surge results in the formation of a circular zone of contamination around the crater at distances of up to several kilometers. Figure 4.3 shows isolines of dose yields for the epicenter zone, the bulk ground and the circular contamination from the base surge following the "Sary-Uzen 1003" explosion (Izrael et al., 1970a), "Danny-Boy" (Nordyke and Wray, 1964) and the group explosion "Telkem-2" (Izrael et al., 1970a). One can see that the characteristics of contamination in these zones are similar. Similar contamination patterns were observed for the epicentral zone after other cratering explosions (e.g., "Sedan").

A characteristic of the surface contamination in the cloud fallout pattern after an underground explosion is that it is generally similar to that for a ground explosion. In the situation where there is no change in wind direction with height, a band of contamination extends windwards. Figure 4.4 shows the dose-rate isolines for the cloud pattern after the "Sary-Uzen 1003" explosion. In one day after the explosion, the 5 μR/hr isoline had extended outwards to about 300 km.

Maps of the patterns formed after the "Danny-Boy", "Cabriolet", "Buggy" (Tewes, 1969), "Sary-Uzen 1003" (Izrael et al., 1970b) and "Sedan" (Martin, 1965) explosions are presented in Figs. 4.4, 4.5 and 4.6. In the context of the latter (Fig. 4.6), a change in wind direction at a specific height resulted in an increase in the relative width of the pattern. The distribution of radiation levels along the axis of the pattern and the change in $I(R) = \int P(R, l)\,\mathrm{d}l$ with distance after explosion "Sary-Uzen 1003" are shown in Fig. 4.7(b). The distribution predicted for the contamination density of the land by ^{137}Cs, 36 years after the "Chagan 1004" explosion, is shown in Fig. 4.8.

The distributions of radiation levels along the axis of the fallout pattern for different cratering explosions have similar characteristics and can be satisfactorily described by the exponential function $P(R) \sim R^{-n}$ with an average value for $n = 2.0$ (derived by analysis of data from "Sedan", "Sary-Uzen 1003", "Danny-Boy" and "Neptune" explosions (Izrael et al., 1970a). After the "Chagan 1004", "Cabriolet" and "Buggy" explosions, these

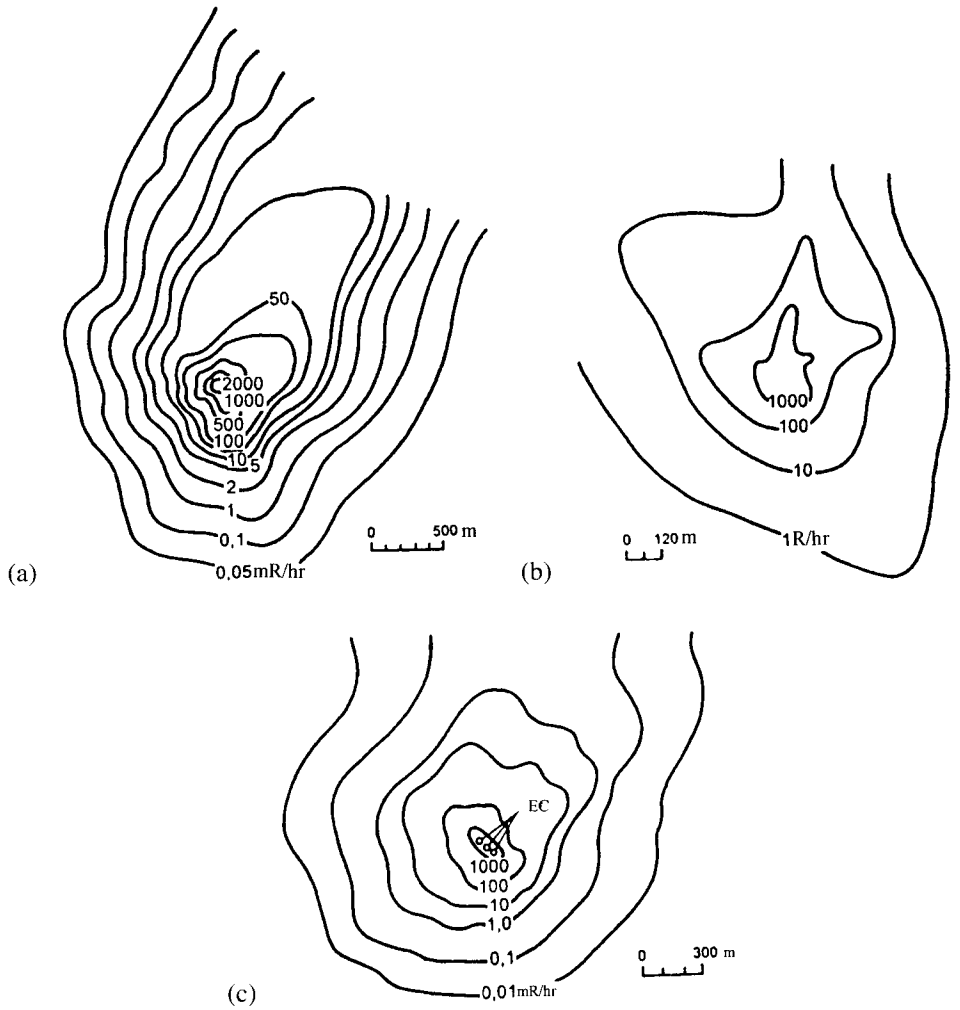

Fig. 4.3. Distribution of the gamma-radiation dose rates in the epicentral zone (a) 5 days after the "Sary-Uzen 1003" explosion; (b) one hour after "Danny-Boy" and (c) 17 days after the "Telkem-2" group explosion.

similarities in character of the change in radiation levels along the fallout pattern axis were observed (Izrael et al., 1970a; Tewes, 1969).

The amount of fallout radioactivity deposited outside the boundaries of the bulk ground amounted to 3.5% of the total amount produced in the "Sary-Uzen 1003" explosion.

Table 4.1 presents the main characteristics of the USSR and USA explosions that resulted in the production of craters and a fallout deposition pattern. It should be noted that, after the 2.3 kt yield "Cabriolet" explosion, the radioactive fallout products were present in the equivalent of 7 t of debris (Tewes, 1969), with a further 2 t present in the cloud. This result was obtained by integration of the radioactivity in the fallout pattern debris that gave rise to a dose rate of 18 R/hr (≈180 mGy/hr) per square mile one hour after the explosion.

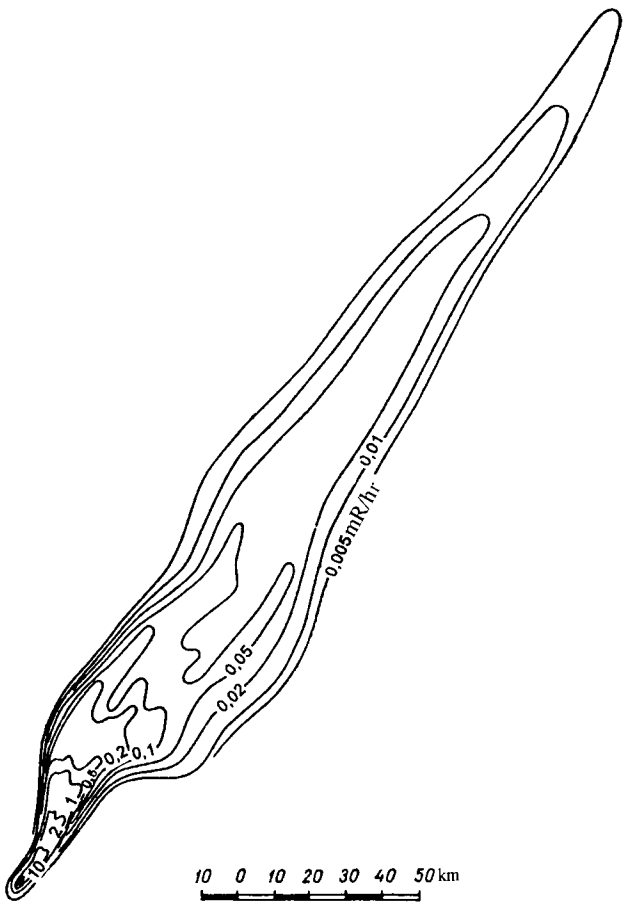

Fig. 4.4. Distribution of the gamma radiation dose rate in the fallout pattern one day after the "Sary-Uzen 1003" explosion.

It is known that fallout resulting from the fission of 1 kt of an explosive, collected over an area of 1 square mile, creates a dose rate of 3.38 kR/hr (33.8 Gy/hr) 1 hr after the explosion at a height of 1 m above the earth's surface. When the earth's surface roughness and screening factor were taken into account, a correction factor of 0.75 had to be applied. After the "Buggy" explosion, composed of five charges each of 1 kt yield placed in a line, the equivalent of 35 t of fallout debris was calculated based on the measured dose rate of 90 R/hr per square mile at time $H + 1$. An additional 5 t of the debris were in the cloud. For reference purposes, it is interesting to note that 1 t of debris corresponds to approximately 5.5×10^{-2} g of actual fission debris by mass or 1.73×10^{16} MeV/s 1 hr after the explosion.

It is interesting to consider how a group explosion influences the configuration of the contamination zones and the fraction of radioactivity settling in the near-fallout pattern. In fact, after a group explosion, the close-in fallout pattern is similar in its configuration and characteristics to that of a single explosion, as shown in Fig. 4.9 for "Telkem-2".

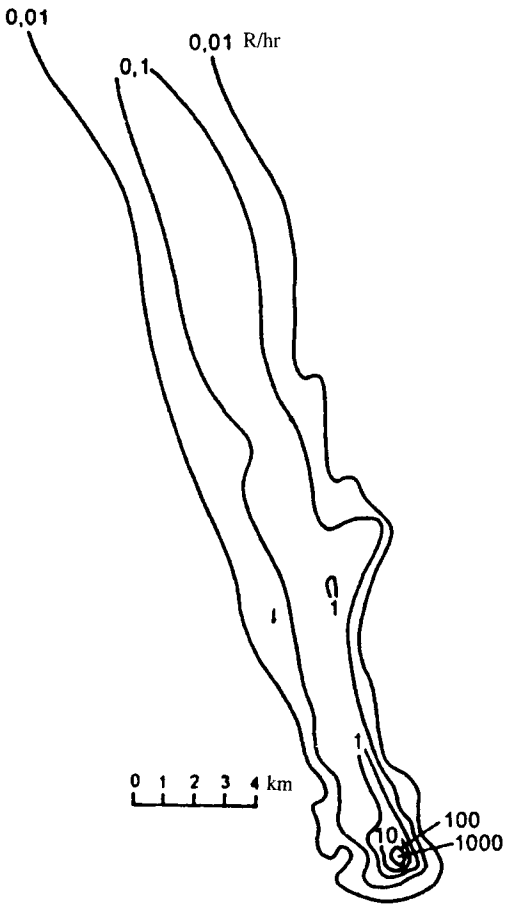

Fig. 4.5. Distribution of the gamma-radiation dose rate in the fallout pattern one hour after the "Danny-Boy" explosion.

Let us compare the characteristics of the terrestrial contamination after the "Telkem-1" (single) and "Telkem-2" (group) explosions. The relative amounts of radioactive products in the zones of the epicenter and the bulk ground (up to 1 km from the epicenter) represented 2.2% and 2.5% for "Telkem-1" and "Telkem-2", respectively. Quantities of the products in the fallout pattern (0.2–2.5 km) amounted to 0.2% and 0.3%, respectively. Thus, the "Telkem-2" group explosion did not result in any increase in the relative quantities of radioactive products deposited on the surrounding land.

The fallout of particle-carriers of radioactivity that have different sizes and shapes is the cause of radioactive contamination of the nearby land surfaces. Near the epicenter, the fallout of slag formations of size greater than 1 cm is rather common, while in the fallout pattern the particle sizes are substantially smaller at ~1 mm. In accordance with the classification proposed by Izrael et al. (1970b), radioactive particles on the surface after an explosion such as "Sary-Uzen 1003" can be conditionally divided into four types:

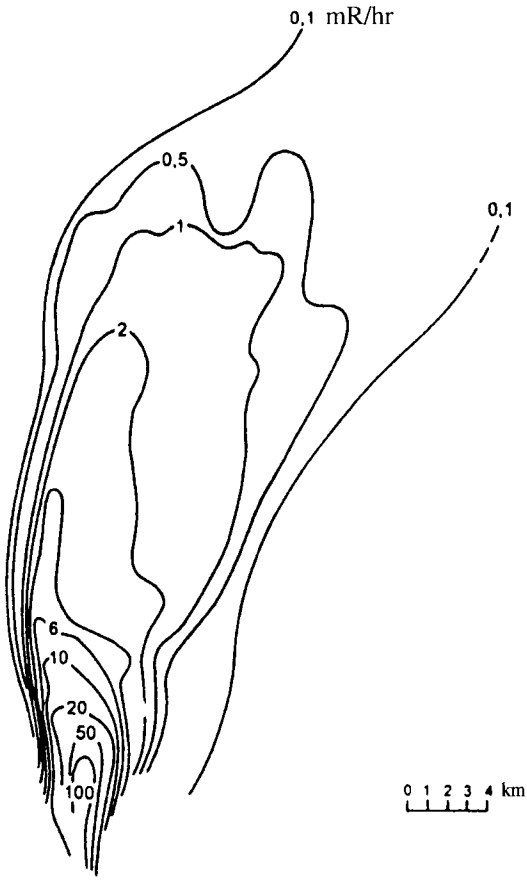

Fig. 4.6. Distribution of the gamma-radiation dose rate in the fallout pattern one hour after the "Sedan" explosion.

(i) Melted particles with irregular forms, mainly transparent and glass-like. The radioactivity A in such particles is distributed uniformly over their volumes and their dependence on size is determined by the exponential function $A(d) \sim d^n$ where $n \approx 2.7$–3.0.
(ii) Particles with irregular forms that were not completely melted. In these particles, the activity decreases from the surface to the center.
(iii) Particles that do not differ in their appearance from the neutral broken rock. Contamination of these particles is only on the surface ($n \approx 1.9$).
(iv) These are rare in occurrence and consist of melted particles, spherical or drop-like in form and similar to those formed in ground explosions (Izrael, 1970).

For the first type, the relationship between the particle radioactivity for individual nuclides and particle size is close to being cubic. The size distribution of particle activities deposited in fallout on the surrounding land is approximated by a normal logarithmic expression.

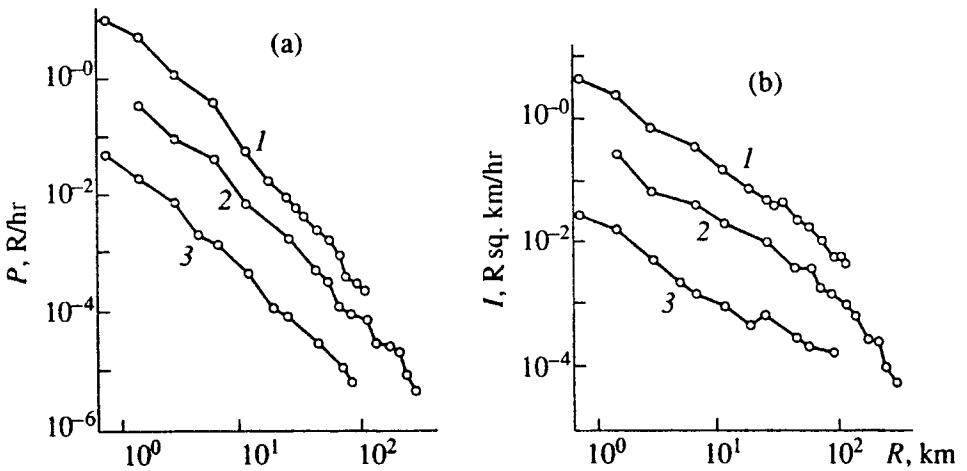

Fig. 4.7. Dependence of the gamma-radiation dose rates along the axis of the fallout pattern (a) and integral quantity of radioactivity I (b) on distance R after the "Sary-Uzen 1003" explosion (1 — at 5 hours, 2 — at 24 hr, 3 — at 15 days after the explosion).

In addition to the products of fission, there are nuclides formed through induced activity, as mentioned in earlier sections. As noted, significant quantities of these induced activities were observed in near-surface air filter samples after the "Sedan" explosion. Isotopes of tungsten were found in distant fallout from the "Schooner" explosion (Izrael, 1970). The contribution of induced radionuclides to the total gamma-activity of the samples after the "Sary-Uzen 1003" explosion was insignificant. But 1000 days after that explosion, the dose in the crater zone due to the induced activity (mainly ^{60}Co) comprised 50–60%, while after the "Chagan 1004" explosion it constituted up to 90%.

When the formation of radioactive contamination in the crater zones, bulk ground and cloud pattern is finished, some products belonging to a refractory or intermediate group of nuclides can decay into volatile nuclides or those of inert gases. For instance, in the mass decay chain ^{133}Sb... $\rightarrow$ ^{133}Cs (Izrael, 1970a), relatively particulate and short-lived ^{133}Sb ($T_{1/2} = 4.1$ min) and ^{133m}Te ($T_{1/2} = 52$ min) present in the fallout decay into the volatile ^{133}I ($T_{1/2} = 20.8$ hrs) and gaseous ^{133m}Xe ($T_{1/2} = 2.3$ days) and ^{133}Xe ($T_{1/2} = 5.27$ days). These radionuclides can escape from the particles and spread in a downwind direction as a stream of radioactive gases and volatile nuclides. It is evident that the isotopes of the inert gases (^{85}Kr, ^{85m}Kr, ^{87}Kr, ^{88}Kr, ^{133}Xe, ^{135}Xe, ^{133m}Xe, ^{138}Xe) and daughter products ^{88}Rb, ^{138}Cs and isotopes of iodine (^{131}I, ^{133}I, ^{134}I, ^{135}I) can be present. Gamma-spectrometric investigations of samples taken in the gas stream several hours after the "Sary-Uzen 1003" explosion revealed that the radioactivity of the gases was practically entirely attributable to a collection of xenon isotopes (^{133}Xe, ^{135}Xe). Throughout the investigation, the measured quantities of these isotopes were in close agreement with the calculated values obtained for a non-fractionated mixture of the isotopes. The iodine isotopes (^{131}I and ^{133}I) were also present but in quantities that were lower by factors of approximately 10^3–10^4 in activity terms. On other days, the upper edge of the stream rose to 900 m altitude. In 4 hr, the radiation levels at a height of 50 m amounted to 2 mR/hr ($\approx$20 μGy/hr) at a distance of

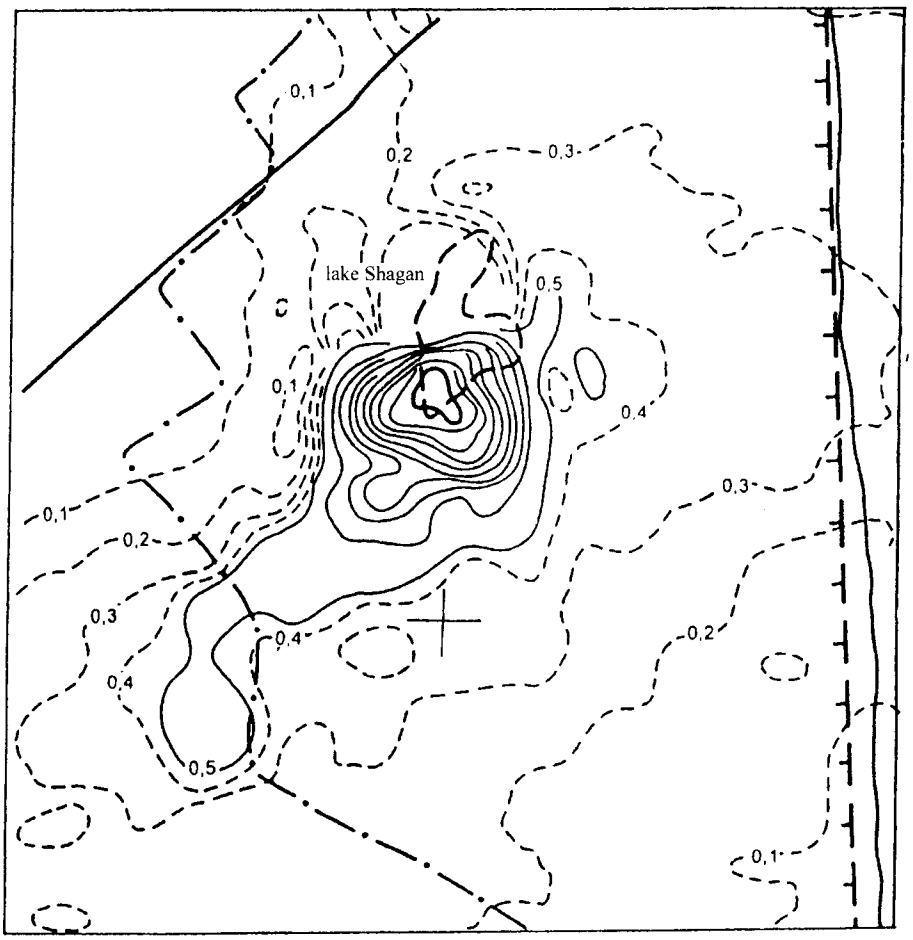

Fig. 4.8. Distribution of contamination density of the surrounding land by ^{137}Cs 36 years after the "Chagan 1004" explosion (1991 survey).

15 km from the epicenter. To quantify the total inventory of gases released, it is noted that, 74 hr after the explosion, the discharge of radioactive gases was equal to 1.26 kCi/hr (46.62 TBq/hr) (Izrael et al., 1970b).

4. Radionuclide Composition of the Fallout from an Underground Explosion

The identification and qualitative determination of the fission products ^{140}Ba, ^{141}Ce, ^{144}Ce, ^{132}Te, ^{99}Mo, ^{131}I, ^{103}Ru, ^{106}Ru, ^{95}Zr, ^{137}Cs, ^{89}Sr and ^{90}Sr and the activation products ^{60}Co, ^{134}Cs, ^{54}Mn, ^{59}Fe and ^{46}Sc for the "Chagan 1004" explosion and ^{60}Co for the "Sary-Uzen 1003", "Telkem-1" and "Telkem-2" explosions were made from measurements of the nuclide composition of samples taken after the underground

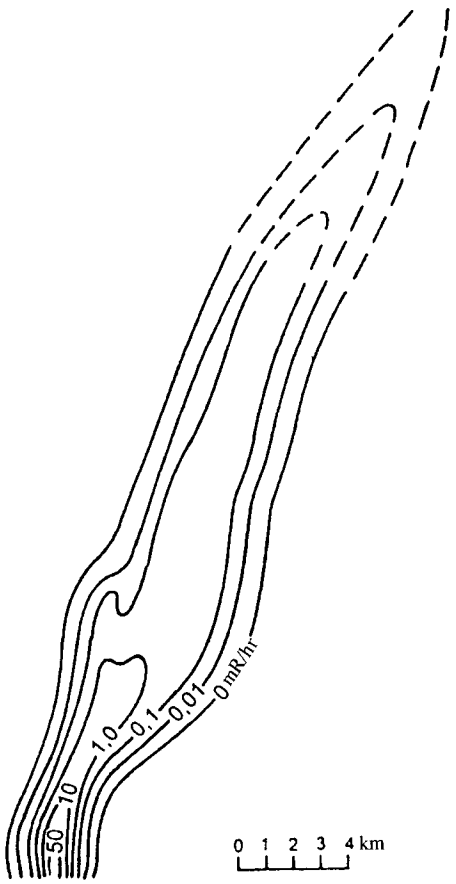

Fig. 4.9. Distribution of the gamma-radiation dose rate in the fallout pattern 1 day after the "Telkem-2" explosion.

explosions. It should be noted that the contribution of ^{60}Co to the dose rate in the epicentral zones of the "Sary-Uzen 1003" and "Chagan 1004" explosions was rather high. At 1000 days after the explosions, it was 50–60 and 85–90%, respectively (Izrael et al., 1970a; Izrael, 1973).

The relationships that exist between the nuclides in the fallout from an underground explosion essentially depend on the character of the particles that constitute the fallout (see Chapter 2) and on the nature of their sources in different parts of the main cloud and the base surge cloud. There is a group of fission fragments in ground bulk zones and in the close-in fallout pattern that it is largely composed of slag formations and particles of the first type, which essentially exhibit no fractionation. The base fallout zone, in contrast to the cloud pattern and especially to the ground bulk zone, is considerably enriched in radionuclides having gaseous precursors. Analysis of the data allows us to conclude that the largest fraction of all radionuclides (except the most volatile ones) formed in an underground cratering explosion is present in the epicentral zone of the explosion (the

crater and ground rubble) and in the close-in fallout pattern. In this near-fallout pattern, the relative quantity of all the radionuclides practically coincides with the relative quantity of total activity (about 20% for the "Chagan 1004" explosion and about 4% for the "Sary-Uzen 1003" explosion).

It should be noted that the depletion in the bulk ground of nuclides that have relatively long-lived gaseous precursors was apparently related to the fact that a significant amount of them can be present in the crushed rock zone immediately adjacent to the crater and in the cloud of the explosion. Data obtained from the analyses of samples taken from exploratory holes drilled in the epicentral zone of the "Sary-Uzen 1003" explosion showed that about 40% of the total ^{137}Cs formed in the explosion was found in the crushed rock zone. About 30% of the ^{89}Sr was found in distant fallout from the radioactive cloud. It was also found that the distribution of different nuclides in the near-pattern depends, first and foremost, on the explosion's characteristics, particularly its yield and depth. Among other factors, the distribution is explained by the fact that the enrichment of nuclides with volatile or gaseous precursors is greater in the cloud after low-yield explosions or at a large scaled depth. So, for instance, after the low-yield explosions "Telkem-1" and "Telkem-2" (especially after "Telkem-2"), no fissures were observed in the ground, while after the "Chagan 1004" explosion there were obvious holes through which the radioactive products could be easily transported away. For small explosions, the "absorption capacity" of the rocks per unit volume, and consequently per unit of yield, is larger at the time of break-through than for higher yield explosions since the ratio of this "absorption capacity" increases with increasing volume. In this connection, it is interesting to compare the distribution of different radionuclides in the close-in fallout patterns of different underground explosions. To illustrate this, the distribution of ^{131}I measured at given distances and integrated over the whole width of the fallout pattern (per unit section of pattern length) $\int \sigma_{131}(x)\,dy$ after different explosions is shown in Fig. 4.10 versus the scaled distance x/Hv (x is the distance, H is the cloud altitude and v is the average wind speed from the upper edge of the cloud down to the earth's surface). It has been shown by Izrael et al. (1970a) that the slopes of the curves of this relationship found for the "Sary-Uzen 1003" and "Chagan 1004" explosions do not really differ and that the differences in the curves of total activity for individual nuclides are insignificant.

The distributions of radioactive products in the close-in patterns after the "Telkem-1" and "Telkem-2" explosions (two low-yield explosions where there was no breaking up of the cloud, the dust column and base surge) are sharply different from those observed after the "Chagan 1004" and "Sary-Uzen 1003" explosions. For "Telkem-2", the density of contamination by refractory nuclides (^{95}Zr) and by those species having no gaseous precursors (^{103}Ru and ^{131}I) varied with distance in a more extreme fashion than for the "Sary-Uzen 1003" and "Chagan 1004" explosions. As for the distribution of nuclides such as ^{89}Sr and ^{90}Sr that have relatively long-lived gaseous precursors, this is described in a more complex manner and is characterized by two sections corresponding to two different zones of fallout. The first zone is dependent on yield and the second exhibits a maximum in the relationship. Analysis of the composition of the radioactive particles dispersed in the fallout has shown that the first zone contained relatively large particles, while the second zone was characterized by the presence of very fine particles, the sizes of the latter being significantly less than 10 μm. It had been suggested by Izrael et al. (1970a) that the first

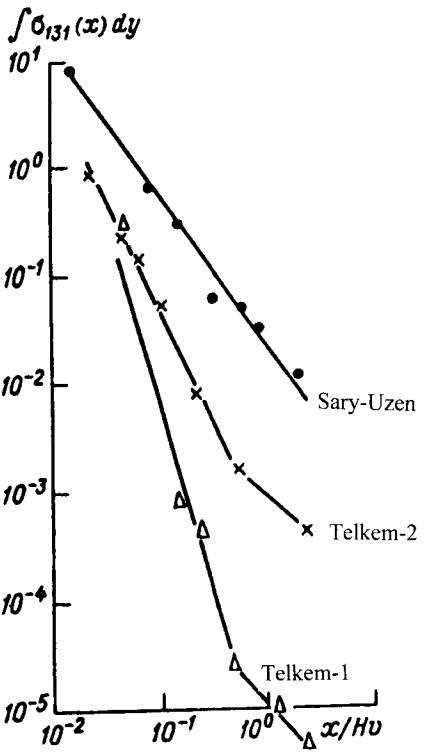

Fig. 4.10. Dependence of the integrated amount of ^{131}I on distance along the fallout axis for different underground explosions.

zone was formed due to kinematic deposition while the second zone could apparently be explained by diffusive deposition of fine particles enriched with volatile nuclides. This difference is particularly important for low-yield explosions where the main cloud and that of the base surge are not divided. These features broadly define the radionuclide composition of such a fallout pattern.

After the "Chagan 1004" explosion, the radioactive products in the close-in fallout pattern were weakly fractionated. Suffice to note that the fractionation coefficient of ^{90}Sr relative to ^{95}Zr over the whole area of the pattern (along its axis) changed from 1 to 4. After the "Sary-Uzen 1003" explosion, the fractionation was more pronounced. For ^{90}Sr, the fractionation factors varied from 1 to 10, while in the "Telkem-1" and "Telkem-2" experiments these coefficients ranged from tenths to hundreds of units.

The above regularities have been confirmed in the results of studies of the composition and fractionation of radioactive fallout from the "Schooner" explosion. For large particles (500 to 104 μm) taken from the fallout pattern, the fractionation effect for ^{131}I and ^{132}Te relative to the slag formations was 4 times and, for particles smaller than 500 μm, it was 12 times for ^{131}I and 50 times for ^{132}Te. Overall, the nuclide composition in the close-in fallout pattern changed insignificantly.

Table 4.6
Fractionation factors and the abundance (%) of different nuclides in the total activity of the fallout (at a given distance)

Nuclide	Fractionation factor	Fraction (%)
^{89}Sr	21	31
^{90}Sr	14	0.12
^{91}Y	2.7	4.5
^{95}Zr	–	About 0
^{103}Ru	1.6	5.2
^{106}Ru	5.2	1.1
^{137}Cs	40	0.65
^{140}Ba (+^{140}La)	4.6	47
^{141}Ce	2.5	9.2
^{144}Ce	3.4	1.1

Changes in isotopic relationships take place essentially in the cloud within a time period from 15 min to 3 hr after the detonation and thus appear in the pattern of distant fallout at distances of thousands of kilometers from the site. Here, the fallout is greatly enriched with the nuclides having gaseous precursors (^{140}Ba, ^{90}Sr, ^{89}Sr, ^{137}Cs, ^{91}Y) and the relative contribution of these nuclides depends on the half-lives of the precursors. The largest fractionation coefficients should be expected for ^{89}Sr and ^{137}Cs. This was confirmed by the data of Krey and Freid (1965) for the fractionation coefficients relative to ^{99}Mo for samples of distant fallout from the "Sedan" explosion (~1000 km from the explosion site, at a time of 2.5 days after the explosion). Table 4.6 shows the average nuclide composition of the radioactive fallout at nine stations. The major part of the activity was composed of ^{140}Ba(+ ^{140}La), ^{89}Sr, ^{91}Y, ^{103}Ru and ^{141}Ce (at time of the fallout formation).

Comparison of nuclide activities in the filter samples and in the fallout shows a significant enrichment in the filter samples for the ^{89}Sr, ^{90}Sr, ^{137}Cs and ^{140}Ba (approximately 4–6 times) due to the greater efficiency of the filters for the fine particles. The opposite tendency was noted for ^{141}Ce and ^{144}Ce, these isotopes being principally associated with the larger particles in samples of fallout and being practically absent from the highly dispersed fine fractions found in the filters. The fraction of the total activity of the isotopes formed in the test and which are precipitated in the distant fallout pattern after an underground explosion is insignificant. After the "Telkem-1" and "Sary-Uzen 1003" explosions, it amounted to 0.45 and 0.66%, respectively (Izrael and Petrov, 1970).

It follows from the experimental data that the main components of a sample of distant radioactive fallout are ^{89}Sr, ^{140}Ba and ^{91}Y. Approximately ten days after an explosion, the fraction attributable to these nuclides amounts to more than 80% of total activity. The samples are very highly enriched with the ^{90}Sr and ^{137}Cs and the activity of species such as ^{132}Te, ^{103}Ru and ^{141}Ce amounts to only a few percent of the total activity. It should be noted also that the ratio between the basic components in fallout, e.g., ^{140}Ba and ^{89}Sr, changes with distance from the explosion site. If the theoretical ratio of the ^{89}Sr activity to that of ^{140}Ba is taken as unity at time zero, then in the close-in fallout at an explosion site at a given time it is close to 0.1–0.2 and in a distant zone it can reach 4–5. If we take the ratio $^{89}Sr/^{140}Ba = 1$ as the average for the whole pattern of a distant fallout explosion, then

a fraction of the nuclides ^{89}Sr and $^{140}Ba + {}^{140}La$, falling in the distant pattern and making up the main contribution to the activity, will amount respectively to 20–40 and 2.5–5% of the total quantities of the given nuclide(s) formed in the explosion. It is therefore clear that it is mainly the nuclides of volatile elements (or those having gaseous precursors) that are present in distant fallout.

The relatively volatile nuclides of induced activity (for instance, the tungsten isotopes) can also contribute to the fallout. Significant quantities of these can exist, even in those situations where the amounts of other products of the explosion have become insignificant. This feature is characteristic of the explosions conducted by the USA and intended for industrial use (Namburger, 1970). An example is the "Schooner" underground cratering explosion performed in the USA in December 1968 at the Nevada test site. The spread of fresh radioactive products, e.g., the tungsten isotopes, was observed over a large area after this explosion. Thus Izrael (1970) has presented some gamma-spectra for air filter samples collected in the Moscow suburbs. They were taken from within the air mass whose trajectory could be traced back to the time when the "Schooner" explosion was detonated. A comparison of the data for a time before the radioactivity appeared with those during the period 13–21 December indicated that the 59 keV line appeared in the air samples taken after 13 December. The half-life of the radioactive products in these samples, determined from the rates of decrease of the line intensity, turned out to be approximately 140 days, i.e., the data confirmed the presence of ^{181}W in these samples. ^{195}W was also identified in these samples. The $^{195}W/^{181}W$ activity ratio at the time of the explosion varied in different samples from 0.9 to 4.6, with an average value of 2.7 ± 0.6. Obviously, the isotopes ^{181}W and ^{185}W were the products of neutron activation in the explosion.

5. Prediction of the Radioactive Contamination of Surrounding Land after an Underground Nuclear Explosion

In the context of the possible uses of underground explosions for industrial and construction purposes, there is considerable pressure on scientists to predict the environmental contamination that results from such explosions, particularly to predict the contamination following cratering explosions. Several zones can be identified for which the prediction of contamination should be carried out particularly thoroughly. They are as follows:

(1) zones of the crater (funnel) and bulk ground where further work involving human participation may be implemented after the explosion (e.g., change of the ground bulk form, etc.),
(2) zone of close-in fallout where the radiation levels are significant and can be hazardous for humans,
(3) zone of long-distance fallout where irradiation is not great but which can impact on a large number of individuals.

If the conditions for an explosion are properly chosen, the potential dangers from contamination can be minimized; hence the need to make accurate predictions of potential contamination. In the following, we consider various prediction schemes for close-in fallout and the distant spreading of radioactive products that occurs after underground nuclear cratering explosions.

5.1. *Prediction of Close-in Fallout*

Radioactive contamination of the external environment depends on the quantity of radioactivity, q, formed in an explosion, the fraction of these products, $\varphi(\bar{h})$, that penetrates into the atmosphere, and the meteorological conditions that determine the degree of dilution of these products in the atmosphere. To predict the close-in fallout, one needs to know the geometry of the sources (i.e., the cloud and base surge), the functions describing the activity distribution throughout the source and the rates of particle descent. In addition, one should also know the dependence of the fractionation factors for different nuclides on particle size (Izrael, 1965). A model of the fallout can then be constructed on the basis of the above data. The work of Knox (1965) describes such a model that is similar to the dynamic model of fallout developed by Anderson (1961) for ground explosions.

The Anderson model assumed that the stabilized cloud consisted of a series of n superimposed round cylinders, each cylinder corresponding to a class (by size) of radioactive particles. It was presumed that particles of a given size are uniformly mixed within its particular cylinder. In turn, each cylinder was then divided into several disks, depending on explosive yield. The trajectory of each disk in the air was considered to be that of a particle whose size corresponds to the class of particles of a given cylinder. Thus, when particles corresponding to different particle classes fall out, the cylinders move away one from another.

The radiation levels for the "Jungle-U" (Nevada) underground nuclear explosion were predicted using this model. In this case, the cloud height and its geometry were taken to be the same as for the "Jungle-S" ground explosion of the same yield. It was clear that the "Jungle-U" explosion was performed at a shallow depth of 5.2 m (scaled depth of about 5 m/kt$^{1/3}$). It is possible that, in an underground explosion conducted at low depth, the close-in fallout could be greater than that from a surface explosion. The distribution of activity as a function of particle size was determined by the formula (see Chapter 1):

$$F(d_1, d_2) = \frac{1}{\sigma\sqrt{2\pi}} \int_{\beta_1}^{\beta_2} \exp\left[-\frac{(\beta - \bar{\beta})^2}{2\sigma^2}\right] \mathrm{d}\beta, \tag{4.3}$$

where F was the fraction of activity related to the class of particle of size d_1 to d_2; $\beta_1 = \log d_1$, $\beta_2 = \log d_2$, $\beta = \log d$. For the soils of Nevada, $\beta = 2.053$ and $\sigma = 0.732$. If the depth of the explosion is large, then one needs additional data on the radioactivity released into the atmosphere, on the geometries of the cloud and base surge, as well as accurate functions describing the activity distribution with particle size and rates of particulate descent.

According to Knox (1965), to predict the radioactive fallout one should know:

(i) the heights of the base and top and the radii of the main cloud and base surge at the time they stabilize,
(ii) the total fission equivalent of the explosion and the portion of the radioactive products ejected into the atmosphere and deposited in the close-in fallout pattern,
(iii) the size distribution of the radioactive particles in the cloud and base surge and the fraction of radioactivity within each of these features,

(iv) the velocity of particle descent,
(v) the forecast of spatial and temporal wind conditions within the layers through which the descending particles pass, and
(vi) the increase in the horizontal dimensions of the "disks" filled with radioactive products under the effect of horizontal turbulent diffusion.

Special graphs were used by Knox (1965) to forecast the linear dimensions R of the cloud and base surge for explosions in alluvial materials. They related the depth of the charge loading h to that of the crater diameter d and the explosive yield. It was assumed that 80% of the products ejected into the atmosphere were contained in the cloud, while 20% were in the base surge, and that the cloud content was in two parts. In the first component, the material was distributed in accordance with a logarithmic expression relating $W_{\mathrm{cl}\,1}$ and the parameters $\ln r_{\mathrm{cl}\,1}$ and $\sigma_{\mathrm{cl}\,1}$ (the standard deviation), while the second part occupied the lower 1/5th of the cloud volume. A similar distribution was assumed for the base surge. Numerical values for the parameters indicated were then selected using the findings of radioactive fallout after the "Sedan" and "Danny-Boy" explosions. Thus, for the upper part of the cloud, $W_{\mathrm{cl}\,1} = W_{\sigma 1} = 0.9$ (0.9), $\log r_{\mathrm{cl}\,1} = \log r_{\sigma 1} = 2.9$ (3.0) and $\sigma_{\mathrm{cl}\,1} = \sigma_{\sigma 1} = 0.69$ (0.69). No cloud was formed after the "Danny-Boy" explosion and all the data are related to the base surge. The above model was verified for other explosions, in particular, for the "Teapot-Ess" explosion, and gave satisfactory results. One can see from this information how much the forms and linear dimensions of the sources and the actual distributions of the particles differ for underground and ground explosions.

Taking into account some of the features of the close-in contamination pattern for a cratering underground explosion, it is possible to simplify the model. From the experimental data, it follows that the character of the radioactive product distribution in the close-in fallout pattern does not depend to a great extent on the scaled depth and yield of an explosion, i.e., there is a similarity in these distributions after different explosions. In the absence of wind sheer, it is then possible to ignore any of the complicated features of the source of radioactive fallout and to select some distribution function to describe the activities over a range of descent velocities for the N particles (by analogy with an atmospheric explosion) for all explosions, assuming that they originate in a point source. It is obvious that, within certain distance intervals, this function should correspond to the actual distribution of the products on the surrounding land. In such a case, according to Petrov and Pressman (1962), we can write the following expression for the surface concentration $k(R, l)$ of a mixture that spreads in a multi-directional sense from an instantaneous point source

$$k(R, l) = \frac{QN(Hv/R)Hv}{\sqrt{2\pi}\,\sigma_l(R)R^2} \exp\left[-\frac{l^2}{2\sigma_l^2(R)}\right], \tag{4.4}$$

where R, l are distances along and across the pattern axis, respectively; H is the height of the source; Q is the amount of substance in the source; $k(R, l)$ is the density distribution of the contamination; σ_l^2 is the dispersion of the distribution $k(R, l)$ in the direction of the

axis l; $w = Hv/R$ is the particle descent velocity; v is the average wind velocity within the layer from the source down to the earth's surface,

$$v = \frac{1}{H}\int_0^H u(d)\,\mathrm{d}h,$$

$u(h)$ is the wind velocity within the layer $\mathrm{d}h$.

Note that $k(R, l)$ is related to the dose rate by the relationship

$$P(R, l) = ck(R, l), \tag{4.5}$$

where c is a constant dependent on the units of measurement. Thus, for the pattern from an underground nuclear explosion, we can write

$$P(R, l) = \frac{mQ\varphi(\bar{h})HvN(Hv/R)}{\sqrt{2\pi}\,\sigma_l(R)R^2}\exp\left[-\frac{l^2}{2\sigma_l^2(R)}\right]. \tag{4.6}$$

Here, Q is the amount of substance formed after an explosion; $\varphi(\bar{h})$ is the fraction of the substance released into the atmosphere; m is a constant depending on the units of measurement.

The dispersion $\sigma_l(R)$ can be found from the equation

$$\sigma_l(R) = \frac{\int_{-\infty}^{+\infty} P(R, l)\,\mathrm{d}l}{\sqrt{2\pi}\,P(R, 0)}, \tag{4.7}$$

where $P(R, 0)$ is the dose yield along the fallout pattern axis. It is obvious that with increase in R then $\sigma_l(R)$ increases (the fallout pattern widens from the initial σ_0 as defined by the cloud size).

On the basis of the solution of the equation for turbulent diffusion, as proposed by Sutton (1947), values for σ_l can be written as

$$\sigma_l = c_l(vt)^{(2-n)/n}, \tag{4.8}$$

where c_l is the virtual coefficient of diffusion and n is an index of stability (dimensionless).

Equation (4.6) is appropriate for the calculation of the scattering of a cloud of radioactive products formed in the case of a short-time energy release in a reactor explosion, i.e., similar to that to be considered in Chapter 5. Later, a number of efforts were made to improve the models used to predict the contamination after atmospheric nuclear explosions (Loborev et al., 1994), the distant fallout from chemical pollution (e.g., acid rain, 1984) and, particularly important, the effects of major atomic accidents such as the Chernobyl incident (Izrael et al., 1989b; Sedunov et al., 1989; Izrael et al., 1990). Loborev and Sudakov (1994) compared the results of calculations made using the model (as proposed by the authors), on the distribution of activity along the axis of the radioactive fallout pattern, with the experimental data obtained for six atmospheric nuclear explosions performed at

the Semipalatinsk Test Site in 1953–1962. For "neutral" meteorological conditions (with a large temperature gradient) and a cloud height of 200–500 m, $c_l \approx 0.10$ and $n = 0.20$–0.25 (Fedorov, 1959); then, $\sigma_l = 0.1(vt)^{0.9} = 0.1R^{0.9}$. When calculating σ_l for a small R, one has to take into account the initial dispersion.

Izrael et al. (1970) have shown that the value $\sigma_l(R)$ for underground explosions is satisfactorily described by the equation

$$\sigma_l(R) = \sqrt{\sigma_0^2 + 0.01R^2}.$$

The initial dispersion σ_0^2 is related to the cloud's horizontal dimensions and corresponds to the radioactive product distribution in the fallout pattern in the crosswise direction at small distances from the explosion center. If we take $\sigma_l \approx 0.1R$, the distribution function $N(Hv/R) = N(w)$ can be written in the following form:

$$N(w) = \frac{0.1P(R,0)R^3\sqrt{2\pi}}{Q\varphi(h)Hv}, \tag{4.9}$$

i.e., if a map of the explosion's fallout pattern is known, then it is not difficult to determine $N(w)$.

The dependence of $\chi(w) = w^3N(w)$ on w for the "Sary-Uzen 1003", "Sedan", "Danny-Boy" and "Neptune" explosions is shown in Fig. 4.11 (Izrael et al., 1970b). In the given scale, $\chi(w)$ for all the explosions is more accurately expressed by a straight line of gradient -1.0, i.e., $N(w) \approx 1/w$. Hence,

$$P(R,0) \approx \frac{Q\varphi(\bar{h})}{R^2}. \tag{4.10}$$

As already stated, $N(w)$ does not depend on the cloud height, explosion yield or depth. It follows from formula (4.10) that the dose yield in close-in fallout is determined mainly by the quantity of radioactive products ejected into the atmosphere after the explosion.

In situations where the wind changes with altitude (for instance, explosions conducted in mountainous regions), one has to use either a linear vertical source or a volume source in the calculations. It is then necessary to know the vertical distribution of radioactive products in the source, especially for the lower sections where local winds may be important. Knox (1965) assumed in his calculations that the base-surge contained 20% of all products released into the atmosphere. In the case of group explosions placed in a line of length L (such explosions are promising in constructing roads and excavating channels), if there is a cross-wind, the dose of gamma-radiation from N explosions is calculated from the expression (Izrael et al., 1970b)

$$D_N\left(R, \frac{L}{2}\right) = ND_l(R,0)\sqrt{\frac{\pi}{2}} \cdot 2\frac{\sigma_l}{L}\Phi\left(\frac{L}{2\sigma_l}\right), \tag{4.11}$$

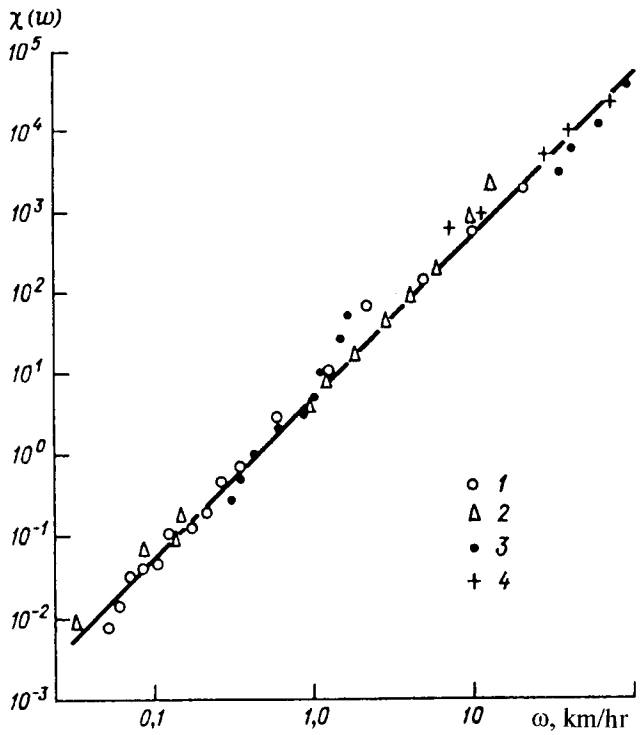

Fig. 4.11. Dependence of $\chi(w)$ for fallout patterns from different explosions. 1 — "Sary-Uzen 1003"; 2 — "Danny-Boy"; 3 — "Sedan", 4 — "Neptune" explosions.

where D_l is the dose from a single explosion and $\Phi(L/2\sigma_l)$ is an integral of probability. If $(L/2\sigma_l) < 1$ and the uncertainty is smaller than 17%, we can write

$$D_N\left(R, \frac{L}{2}\right) \approx N D_l(R, 0). \tag{4.12}$$

When deducing this formula, it was assumed that the fraction of the products ejected into the atmosphere after a group explosion is equal to the fraction from a single explosion and that there is no interaction between the clouds of different explosions. Actually, it was demonstrated, in certain chemical explosions where tracers were introduced, that this fraction increases by a factor of 2 but it certainly was not a linear function of the number of explosions (Knox, 1965). This fraction did not increase in a grouped underground nuclear explosion (Izrael et al., 1970a).

The above forecast scheme for close-in fallout can also be used to predict the radionuclide composition in the fallout pattern. In this case, Eq. (4.6) is now used to find the surface density of the contamination $k_i(R, l)$ by the ith nuclide. Instead of q, one should substitute q_i which is the quantity of a nuclide deposited in the close-in fallout pattern, and, instead of $N(w)$, $N_i(w)$ is substituted, this being the distribution function of the ith nuclide's activity over the particle descent velocities. In the case where the fractionation

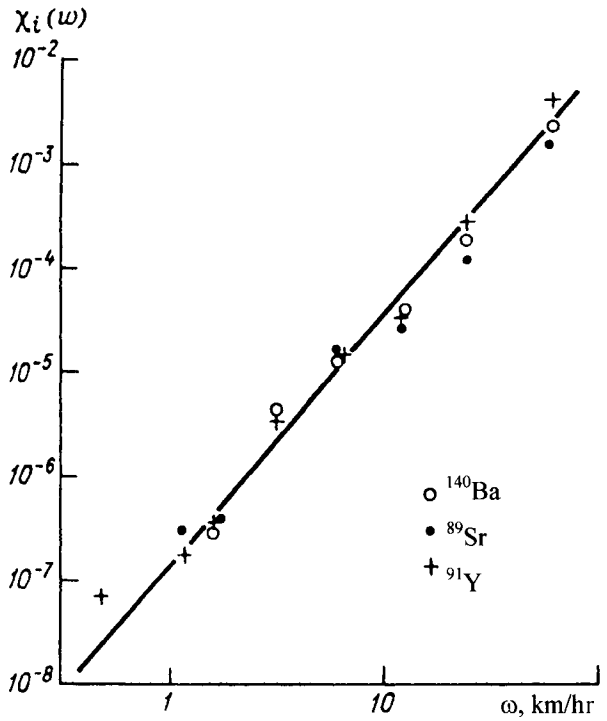

Fig. 4.12. Dependence $\chi_i(w)$ for different nuclides in the fallout pattern of the "Sary-Uzen 1003" underground nuclear explosion.

in the direction perpendicular to the fallout pattern axis is not very large, we can take σ_{l_i}, i.e., the dispersion across the axis for the ith nuclide, to be the same as for the sum of the nuclides. Having sufficient experimental data on the dependence of q_i and $N_i(w)$ on the explosion parameters, one can use the above-described scheme to predict the radionuclide composition of the radioactive fallout in the close-in fallout pattern.

As an example, the dependence $\chi_i(w) = w^3 N_i(w)$ for a number of nuclides from the "Sary-Uzen 1003" explosion is shown in Fig. 4.12. One can see from this figure that this dependence is similar to that of $\chi_i(w)$ for the fallout patterns from different explosions (see Fig. 4.11).

Since generally there are not sufficient experimental data on the nuclides of the radioactive fallout in close-in patterns, we try to calculate $k_i(r)$ or $k_i(w)$ using features of radionuclide fractionation in order to build a prediction scheme for the fallout when only the dependence of fractionation factors on particle size is known. For the sum of surface densities of contamination by different nuclides in the near-fallout zone, we can write (indices "e" will be related later to experimental values and "c" to the calculated or theoretical values):

$$\frac{\sum k_i^{\mathrm{e}}(r,t)}{k_{95}^{\mathrm{e}}(r,t)} = \frac{k_{\Sigma}^{\mathrm{e}}(r,t)}{k_{95}^{\mathrm{e}}(r,t)},$$

where k_i, k_{95}, k_Σ are the surface densities of contamination by the ith nuclide, ^{95}Zr and the sum of the fission products at a distance R_r from the explosion site. This distance corresponds to the point where fallout of particles of radius r occurs, at time t. We can also write

$$\frac{k_i^{\mathrm{c}}(t)}{k_{95}^{\mathrm{c}}(t)} = \frac{Y_i \lambda_i \, \mathrm{e}^{-\lambda_{95} t}}{Y_{95} \lambda_{95} \, \mathrm{e}^{-\lambda_{95} t}}, \tag{4.13}$$

where Y_i, Y_{95} are the yields of ith nuclide and ^{95}Zr at fission and λ_i, λ_{95} are their decay constants, respectively.

The fractionation factor can also, by definition (see Chapter 1), be written as

$$\frac{k_i^{\mathrm{e}}(r,t)}{k_{95}^{\mathrm{e}}(r,t)} : \frac{k_i^{\mathrm{c}}(t)}{k_{95}^{\mathrm{c}}(t)} = f_{i,95}(r,t). \tag{4.14}$$

And from Eqs. (4.13) and (4.14)

$$k_i^{\mathrm{e}}(r,t) = k_{95}^{\mathrm{e}}(r,t) \frac{Y_i \lambda_i \, \mathrm{e}^{-\lambda_i t}}{Y_{95} \lambda_{95} \, \mathrm{e}^{-\lambda_{95} t}} f_{i,95}(r,t). \tag{4.15}$$

Thus,

$$k_\Sigma^{\mathrm{e}}(r,t) = \sum k_i^{\mathrm{e}}(r,t) = \frac{k_{95}^{\mathrm{e}}(r,t)}{Y_{95} \lambda_{95} \, \mathrm{e}^{-\lambda_i t}} \sum_i Y_i \lambda_i \, \mathrm{e}^{-\lambda_i t} f_{i,95}(r,t), \tag{4.16}$$

$$\frac{k_i^{\mathrm{e}}(r,t)}{k_\Sigma^{\mathrm{e}}(r,t)} = \frac{Y_i \lambda_i \, \mathrm{e}^{-\lambda_i t} f_{i,95}(r,t)}{\sum_i Y_i \lambda_i \, \mathrm{e}^{-\lambda_i t} f_{i,95}(r,t)}. \tag{4.17}$$

Since, from formula (4.5),

$$k_\Sigma^{\mathrm{e}}(r,t) = \frac{1}{c} P^{\mathrm{e}}(R,t), \tag{4.18}$$

$$k_i^{\mathrm{e}}(r,t) = \frac{1}{m} P^{\mathrm{e}}(R_r,t) \frac{Y_i \lambda_i \, \mathrm{e}^{-\lambda_i t} f_{i,95}(r,t)}{\sum_i Y_i \lambda_i \, \mathrm{e}^{-\lambda_i t} f_{i,95}(r,t)}, \tag{4.19}$$

where $P^{\mathrm{e}}(R_r, l)$ is the dose rate near the earth's surface at point R_r, corresponding to the fallout of particles of average radius r at time t. k and m are constants depending on the units of measurements. Thus, if we know the relationships between the fractionation coefficients and particle size and also between the prediction scheme for the γ-radiation dose rate or the contamination density for the known sum of the radiation fragments, we can then calculate the expected density of the contamination by any nuclide i at a given point in the fallout pattern.

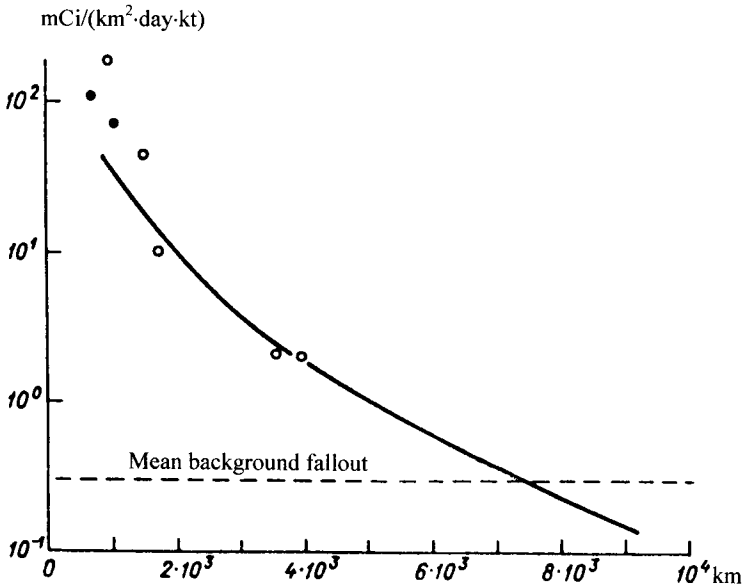

Fig. 4.13. Dependence of the density of radioactive fallout on distance for an explosion of 1 kt yield.

It is interesting that, if the change of fractionation in the direction perpendicular to the pattern axis is ignored, we can write

$$\frac{k_i(R_r,t)}{k_\Sigma(R_r,t)} = \frac{\int_l k_i(R_r,t)\,\mathrm{d}l}{\int_l k_\Sigma(R_r,t)\,\mathrm{d}l} = \frac{Q_i(t)N_i(r)}{Q(t)N(r)}, \tag{4.20}$$

and

$$\frac{Q_i N_i(r)}{QN(r)} = \frac{Y_i\lambda_i\,\mathrm{e}^{-\lambda_i t} f_{i,95}(r,t)}{\sum Y_i\lambda_i\,\mathrm{e}^{-\lambda_i t} f_{i,95}(r,t)}. \tag{4.21}$$

Thus, to make a predictive calculation, one should know either the dependence of $f_{i,95}(r,t)$ or $Q_i(t)$ and $N_i(r)$, or $Q_i(t)$ and $N_i(w)$. The fractionation coefficients can be obtained either through experiment or by calculation. Experience suggests that, in underground explosions, the fractionation in the close-in fallout zone is insignificant.

Note that in the case of admixture diffusion where there is air flow over a horizontal homogeneous surface has been considered by Izrael et al. (1970a) and Izrael (1973) in estimating the concentrations and densities of fallout of radioactive products at large distances (i.e., after several days of propagation). The curve representing the calculated change in the radioactive fallout density with increase in distance from the epicenter of an explosion of 1 kt yield under a wind velocity $v = 40$ km/hr, is shown in Fig. 4.13. Data points indicate the calculated values. Background values are related to 1960's information.

Chapter 5

TERRESTRIAL CONTAMINATION FROM CHERNOBYL AND OTHER NUCLEAR POWER STATION ACCIDENTS AND ITS RADIONUCLIDE COMPOSITION

Contents

1. Dynamics of Radioactivity Release and the Conditions of Radioactive Aerosol Particle Formation from the Chernobyl Accident 150
2. Characteristic Features of Radioactive Aerosol Particles Produced by the Chernobyl Accident and Their Radionuclide Composition 153
3. Terrestrial Contamination from the Chernobyl Accident 156
4. Radionuclide Composition of the Terrestrial Contamination from the Chernobyl Accident 163
5. Analysis and Reconstruction of the Source of Radioactivity Release from the Chernobyl Accident 178
6. Modeling of Close-in Radioactive Deposition (Fallout) from the Chernobyl NPS Accident 200
7. Characteristic Features of Radioactive Contamination from Various Nuclear Accidents 205
   - 7.1. Radionuclide Composition of Deposition in the Southern Urals Area 205
   - 7.2. Terrestrial Contamination from an Accident at the Siberian (Tomsk-7) Chemical Enterprise 208

Aerosol products that lead to radioactive fallout are not released in quantity during normal operation of nuclear power stations. According to studies carried out in many countries, nuclear reactors do, under normal operating conditions, release certain radioactive inert gases (^{41}Ar, ^{133}Xe, ^{85}Kr) to the atmosphere and, in some cases, insignificant amounts of tritium (^{3}H) and iodine (^{131}I). Some other nuclides have also been identified (for instance, ^{135}Xe, ^{14}C and ^{129}I) in routine gaseous releases. Up to 7.4–14.8 PBq/year (200–400 kCi/year) of gaseous products (relatively short-lived inert gas nuclides), up to 370 GBq/year (10 Ci/year) of aerosol products and 18.5 GBq/year (0.5 Ci/year) of radioactive iodine are actually released during trouble-free operations. Only very small quantities of aerosol products, including the iodine isotopes, find their way to the ground surface.

The occurrence of accidents at nuclear reactors and other types of nuclear installation is an important exception to this release scenario. Among the more notable accidents that have occurred at nuclear reactors are, in chronological order, (i) the Windscale accident in Great Britain in 1957, (ii) the Three-Mile-Island nuclear power station accident in the USA in 1983 and (iii) the world's largest accident, at the Chernobyl nuclear power station in the former USSR, in 1986. For comparison, the total releases of radioactivity from nuclear weapons tests and the largest accidents (in PBq at D + 3) are as follows:

Nuclide	Tests	Chernobyl (former USSR)	Windscale (UK)
^{137}Cs	1500*	89*	0.044
^{134}Cs		48	0.0011
^{90}Sr	1300*	7.4	0.00022
^{131}I	780000	1300	0.59

* rough estimates

(^{134}Cs is an "induced" nuclide generated by irradiation with reactor neutrons.)

1. Dynamics of Radioactivity Release and the Conditions of Radioactive Aerosol Particle Formation from the Chernobyl Accident

Unit IV of the Chernobyl nuclear power station (CNPS) was destroyed and a short-term release of accumulated radionuclides to the environment occurred as a result of the thermal explosion on April 26, 1986. During the nearly ten days that followed (up to May 6), a plume of gaseous and aerosol-associated radioactive products continued to escape into the atmosphere due to the high temperature generated by the burning graphite and by inner heating (Abagyan et al., 1986a,b). The data on the total radionuclide release from the reactor and a theoretical reconstruction of the source behavior during the accident are discussed in more detail in Section 5.5.

Naturally, the mechanism of aerosol particle formation and, as a consequence, the structure, composition and other characteristics of aerosol particles resulting from "nuclear" accidents differ considerably from those originating in nuclear explosions (see Chapters 1 and 3). These differences are the result of the quite different physical and chemical conditions of particle generation and the differences in the materials from which the particles are formed, etc.

The principal circumstances in which particle generation occurs in some of these different cases are:

(i) in a fireball from a nuclear explosion that incorporates ground material, resulting in fission products and induced activities,
(ii) in a chemical explosion in a container containing long-lived radioactive waste (the formation of the "Urals fallout pattern"),
(iii) in the destruction of a reactor by a non-nuclear explosion and the subsequent burning of graphite accompanied by radioactive particle formation (as occurred during the Chernobyl accident).

An important feature of the radioactivity released from nuclear weapons tests and power station accidents is its radionuclide composition. In nuclear explosions, in their initial phase, many average- and long-lived radionuclides (^{89}Sr, ^{90}Sr, ^{140}Ba, ^{137}Cs, etc.) that are important from a dose-delivery perspective are entirely present as short-lived nuclides of radioactive inert gases (^{137}Xe, ^{140}Xe, ^{89}Kr, ^{90}Kr, etc.). Under the conditions existing within the cooling fireball, it is this *in-situ* decay process that controls their distribution both on aerosol particles and, finally, at the ground surface. During a nuclear accident, the

great majority of the dose-forming radionuclides listed above have already accumulated and they behave as caesium, strontium, barium isotopes, etc. and not as inert gases.

The conditions of radioactive particle formation during the Chernobyl accident are discussed below. The following scheme for radioactivity release in the emergency was proposed by Sivintsev and Khrulev (1995). It includes four main stages:

- the 1st stage—a release related to the explosion in the reactor due to introduction of positive reactivity,
- the 2nd stage—a release connected with the burning of the graphite core in the reactor,
- the 3rd stage—a release due to increased temperatures in the fuel and fuel-containing materials as a result of the energy produced during radioactive decay of the accumulated fission products, and
- the 4th stage—a drastically diminished release as a result of stabilisation and the ensuing gradual temperature drop.

Different measures taken by the emergency unit can exert an influence on the release dynamics. Sivintsev and Khrulev (1995) assumed that the covering materials dropped by helicopters on to the building of the Chernobyl unit reduced the iodine and caesium release; however, we believe that it could have led to temperature rise in the 3rd stage. According to Sivintsev and Khrulev (1995), the temperature rose to 1800–2000 K during the 1st stage. At the beginning of the 1st stage, the heat-producing rods were destroyed and the fuel dispersed because of the thermal pressures created by fuel heating and fission product expansion in the low porosity materials of the fuel (a gaseous "explosion"). Almost immediately afterwards, a second gaseous explosion occurred as a result of penetration of the hot dispersed fuel into the heat-exchange material.

In the 2nd stage, the graphite-burning phase, it is believed that, along with the combustion products, the finely dispersed fuel particles that were incorporated in the graphite were released together with associated fission products into the explosion area of the reactor core. In the 3rd stage (May 2–5, 1986), an increase in radionuclide release occurred because of overheating of the fuel to $\approx$2500–2800 K due to radioactive decay of the fission products (we believe also that it was due to the effect of the "blanket" of covering material). By the end of this stage, in addition to the mass release of volatile products, the leakage of refractory elements such as Zr, Nb and Ce (together with fuel) could occur.

Presumably, aerosol contamination of the atmosphere can conditionally be subdivided into two main phases; the first being the particles released from the destroyed reactor in the first moments after the explosion(s) (partially fused glassy particles could be present here) and the second being the ejection of particles during the ongoing process of graphite burning and particle formation in the destroyed reactor zone from the condensation of gaseous volatile radioactive products. This second phase release in the form of a gaseous plume occurred mainly during the first ten days after the accident (including May 5, 1986) right up to the time of stabilisation and major drop in temperature.

Partially fused radioactive particles, analogous to those formed in nuclear explosions, were found. A considerable number of these particles were, however, fragile. They consisted of different materials; sometimes they were particles of "graphite ash" covered by radioactive products (Izrael et al., 1990), resulting largely from the thermodynamically

controlled processes that took place in the reactor after the accident. These problems are discussed in Abagyan et al. (1986a,b), Sivintsev and Khrulev (1995) and Khodakovsky et al. (1993).

The conditions of radioactive particle formation are of primary importance. According to Abagyan et al. (1986a), at the moment of the explosion(s), the fuel was heated up to a temperature of 1000–1800 K. Graphite burning and radioactive decay of fission products accelerated the heating of the reactor core. The fuel temperature then dropped through heat loss to the graphite stack and reactor construction materials. The dropping of material by helicopters (about 5000 t) during the period from April 28 to May 2 led to additional cooling and drop in temperature to 900 K, due to the reactions of dolomite decarbonization, clay dehydration and the melting and evaporation of lead. Later, however, a considerable temperature rise took place (up to 2300 K) because of the decreased penetrability of the barrier and reduced heat removal under the intense decay of radioactive products. After May 5, the temperature began to drop sharply and the intense escape of gaseous radioactive products from the destroyed reactor practically ceased; although some radioactive releases and outflows were recorded later, their magnitudes were substantially smaller.

Powers et al. (1987) produced the following evaluation of the fuel temperature. For release of the volatile elements (Cs, I), the temperature would have increased from 1200 to 1400 K between April 26 and May 5; for the elements of mean volatility (Ba, Ce), from 1800 to 2300 K and, for the refractory elements (Zr), from 2500 to 3000 K. But, as rightly pointed out by Abagyan et al. (1986a), such an approach is only valid when the aerosol particles are entirely condensation products. This is the case where the aerosol particles could result from mechanical release of dispersed fuel and other transformations. So, as the temperature increased and boron carbide (B_4C), lead, dolomite ($CaMg(CO_3)_2$), sand and clay were dropped onto the reactor from helicopters, a violent reaction from the formation of fuel carbides took place, e.g., producing uranium carbides and those of other elements (Pu, Zr, Fe, etc.), the oxides of which could be completely transformed into carbides over several days at the prevailing temperature of 2300 K. During the reaction between PuO_2 and graphite, Pu_2O_3 was formed as an intermediate compound ($T_{melt} = 2353$ K), its volatility being nearly one order of magnitude higher than that of PuO_2 (Khodakovsky et al., 1993). It seems likely that this led to a certain increase in concentrations of $^{239+240}Pu$ during the deposition of radioactive products from the accident outside the boundaries of the 30-km zone southwards (from the 5th to the 8th day after the accident). Carbon black/soot was also formed in the zone of graphite burning where there was a lack of oxygen. This could absorb considerable amounts of radioactivity onto its surfaces. The radioactive aerosols could be formed, therefore, by mechanical fragmentation of graphite and fuel debris by the flow of uprising gases and by condensation of volatile radioactive compounds from the gaseous phase. For example, the particular size-distribution of ^{103}Ru and ^{106}Ru particles can be explained by the existence of a highly volatile compound of this element—ruthenium tetroxide (Skitovich et al., 1993). This compound was absorbed from the gaseous phase as sub-micron inert particles of about 0.2 μm in diameter (an analogous effect was observed for the isotopes ^{137}Cs and ^{134}Cs).

Apparently, certain zones were formed in the reactor that exhibited considerably different oxidation–reduction conditions and differences in the forms of the solid and gaseous phases. With the complete consumption of oxygen and intense formation of fuel

carbides, elements such as Pu, Ba and Ce that normally form oxides were restored and hence their volatility increased. In contrast, on coming into contact with the oxygen of the air, the gaseous oxides of U, Ru, etc. could be formed along with aerosols resulting from the condensation of Cs, Ba–La, Ce, etc. vapors. It is suggested that the ejection of radioactive aerosols was significantly reduced by the dumping of materials onto the destroyed reactor from helicopters (Sivintsev and Khrulev, 1995).

2. Characteristic Features of Radioactive Aerosol Particles Produced by the Chernobyl Accident and Their Radionuclide Composition

Immediately after the Chernobyl accident, considerable amounts of highly active particles were detected, significantly contributing to the radioactive contamination. The particles were found (at distances of dozens of kilometers and beyond) in samples of materials such as leaves of trees, grass, etc. that have a certain air-filtering capacity (Izrael et al., 1990). Some dozens of highly active particles were often responsible for up to 90% of the total activity contained in soil section samples (taken from an area of about 150 cm^2).

As shown in Section 5.1, the conditions of radioactive particle production in the destroyed reactor at Chernobyl changed considerably during the ten day period of intensive release and radioactivity outflow to the atmosphere. In this connection, the particles detected at different distances and released from the reactor at different times could differ significantly both in their structure and in their radionuclide composition. This section therefore indicates some of the characteristic features of these highly active particles. It is likely that their description will permit us to understand better the radionuclide composition of the surface deposition in different zones following the Chernobyl accident.

In Section 3.8 of Izrael et al. (1990), the results of a study of the highly active particles sampled by gauze trays within the CNPS 60-km zone are presented (these particles arose from resuspension of surrounding dust). Particles were selected using autoradiography with a narrow-collimated radiation detector, followed by study of particle structure using a semiconductor gamma-spectrometer. As a rule, the highly active particles were detected either as "riders" on larger particles or in conglomerates of less active particles. Note that, since the period of resuspension before sampling was up to 3 years after the accident, the described conglomerates of particles were probably formed by the interactions between the primary particles and atmospheric or soil dust. Particles of active graphite ash/soot found in the above samples were easily destroyed by the slight touch of a needle, as were other particles of an irregular shape—probably those formed as a result of the production of fuel carbides.

The particles were divided into two groups on the basis of radionuclide composition. In the first group (probably formed during the primary or initial releases), the radionuclide composition was similar to the non-fractionated composition of fuel and fission fragments at the time of the accident. Particles depleted in the refractory products of the accident constituted the second group and these were probably formed during the period of graphite burning or heating after the inert material was dropped into the reactor. ^{137}Cs, ^{134}Cs and Ru isotopes and other volatile nuclides were significantly enriched in this latter source of

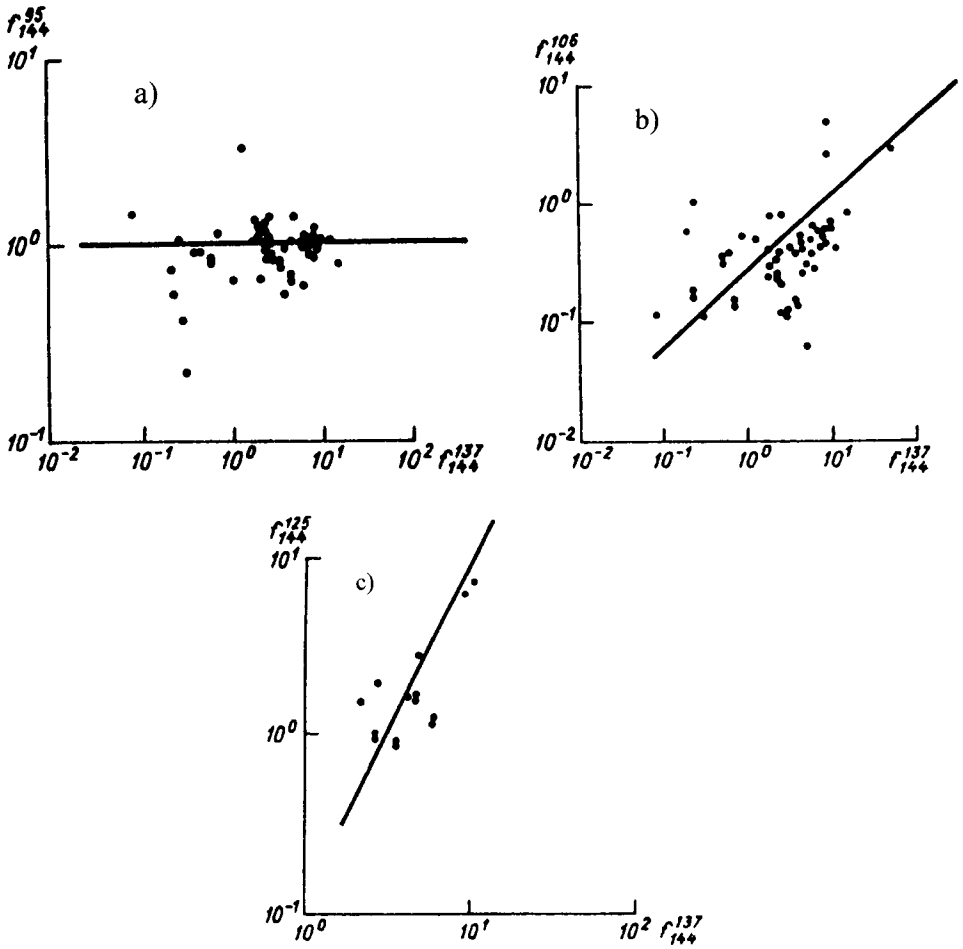

Fig. 5.1. Correlation between fractionation factors $f_{144}^{95}(f_{144}^{137})$ (a), $f_{144}^{106}(f_{144}^{137})$ (b) and $f_{144}^{125}(f_{144}^{137})$ (c) for "hot" particles sampled from soil in 1987–1988.

radioactivity. The Ru isotopes prevailed over radiocesium in some particles particularly those sampled in the "red" forest 1500 m from the reactor.

Figure 5.1 shows the correlations between the fractionation factors f_W for four pairs of radionuclides, with the $^{137}Cs/^{144}Ce$ pair being chosen as reference. For $^{95}Zr/^{144}Ce$, $^{106}Ru/^{144}Ce$ and $^{125}Sb/^{144}Ce$, the activity ratios f_W ("accumulated" releases) needed for calculations were taken at the time of the accident. The correlations found for the indicated fractionation factors are similar to those obtained for nuclear explosions. ^{95}Zr practically does not fractionate relative to ^{144}Ce, ^{106}Ru fractionation, on average, is similar to that of ^{137}Cs and ^{125}Sb exhibits an even higher volatility than ^{137}Cs (within the 60-km zone around the accident). The analysis of samples of radioactive aerosol particles, as presented by Gaziev et al. (1993), is of particular interest.

Table 5.1
Fractionation factors, $f_{i,144}$, of certain radionuclides in samples taken from the radioactive plume on 28th April and 6th May, 1986

Radionuclide	28 April	6 May
^{95}Zr	1.7	1.6
^{103}Ru	3.2	1.1
^{131}I	40	10
^{140}Ba	2.3	2.9
^{141}Ce	1.5	1.4
^{137}Cs	10	3.5

Table 5.1 lists the fractionation factors that were found in a typical air sample collected by an aircraft on April 28, 1986 from the plume of radioactive products issuing from the destroyed reactor. The fractionation factors were again normalized to ^{144}Ce. Theoretical ratios between the activity of the "accumulated" releases and that at the moment of the emergency release were taken from Izrael et al. (1990). The table shows considerable fractionation for ^{131}I and ^{137}Cs, with ^{103}Ru next in order. (Note: to arrive at the true value for the total iodine content, the experimental values (for the aerosol component) were multiplied by two.) Borisov et al. (1993) have analyzed the aerosol and gaseous products of the accident using sorption–filtering material so as to separate the two fractions. The sampling was conducted during the first half of May 1986, near the accident zone, as well as at distance (in the NE Atlantic). The results from the samples taken in the emergency zone showed that the radionuclides ^{95}Zr, ^{95}Nb, ^{134}Cs, ^{137}Cs, ^{140}Ba, ^{140}La, ^{141}Ce and ^{144}Ce were trapped almost entirely in the "aerosol" layer of the filter, while ^{103}Ru, ^{106}Ru, ^{131}I and ^{132}Te were found in the underlying, absorbing layers of the filter. The similarity of the ^{103}Ru and ^{106}Ru distributions in the filter suggests that they were present in the air as the same gaseous substance (Borisov et al., 1993), most likely as RuO_4. The abundances of gaseous compounds of Ru and Te reached 13 and 8%, respectively.

The iodine distribution in the absorption layers of the filter pointed to the fact that it was present as molecular iodine vapor. The gaseous forms of iodine sampled in the accident zone between the 8th and 19th of May, 1986 ranged from 30 to 90% in abundance. At the same time, the gaseous forms of ^{131}I amounted to 73–90% of the samples taken in the Atlantic.

From May 8–19th 1986, some sub-micron particles continued to be transported away from the reactor. Radioactive isotopes of Zr, Nb, La and Ce were found on particles of size 0.7 μm, with Ru, Fe and I on 0.4 μm particles. The fraction of gaseous iodine was 0.5–0.9. Already, by August 1986, aerosol particles in the air were being modified through their impact with the soil, vegetation, etc. The aerosol radioactivity concentration actually decreased much faster than can be accounted for by decay alone. Thus, for example, the secondary aerosol concentration of ^{137}Cs in the atmosphere fell by a factor of 12 over a period of 12 years. This is explained by the burial of cesium isotopes in the soil where they exist in strongly bounded chemical forms. The particle sizes for ^{137}Cs have since 1987 remained within the range 4–7 μm. Fires cause an increase in the aerosol concentration

of 1–2 orders of magnitude. During strong dust storms, the aerosol particles spread over distances of hundreds of kilometers (Budyko and Ogorodnikov, 2000).

Gaziev et al. (1993) have analyzed a number of radioactive particle samples collected using an aerosol impactor over the Chernobyl station zone from May 1986 until the end of 1987. The samples could contain products that have come directly from the reactor itself or, as the authors believe, products that have come mainly from the industrial site of the station and the adjacent territory over a distance not exceeding several kilometers. The sampled particles were divided into two groups: roughly dispersed aerosols with a median diameter of 40 μm and finely dispersed ones with a median diameter of 0.4–1.3 μm. The roughly dispersed fraction for ^{144}Ce comprised 85–100%, while, for ^{137}Cs, it increased from 40% in May–June 1986 up to 100% from April 1987 onwards. For ^{103}Ru, it changed from 10 to 100%. The characteristics of the ^{131}I aerosols were similar to those for ^{103}Ru and ^{140}La and the characteristics of the ^{95}Zr + ^{95}Nb aerosols were similar to those of ^{144}Ce.

It is interesting to note that the median diameter of the normal logarithmic distribution of particle sizes in the "close-in" radioactive fallout pattern (i.e., up to 100 km from the location of the Chernobyl accident) was 50 μm (Izrael et al., 1990).

Obviously, a detailed description of radioactive particles is needed to understand fully the processes involved in the radionuclide composition of deposited debris.

3. Terrestrial Contamination from the Chernobyl Accident

Terrestrial contamination by radioactive materials from the Chernobyl accident resulted from the fallout of debris from the radioactive cloud that occurred at the time of the primary release and from the plume of volatile radioactive products that was present in the area throughout the ten days after the accident. Considerable amounts of radioactive aerosol particles, including both refractory and volatile products, were blown into the atmosphere during the primary release. Highly dispersed aerosols were deposited on the earth's surface from the plume of volatile products. This process was particularly intensified by rainfall in the area and beyond.

From the first day of the accident, specialists in the field of chemical behaviour concentrated their attentions on the area within a radius of 10 km from the accident and experts from the State Committee for Hydrometeorology and Environmental Monitoring restricted their work to areas outside the limits of the zone and to the European regions of the former USSR. Representatives of other departments carried out gamma surveys of the radioactive contamination of the atmosphere and of the earth's surface using ground-based methods as well as aeroplanes and helicopters. The total number of aircraft equipped with roentgenometric, gamma-spectrometric and sampling instrumentation reached 10 during the initial period. The results of both the operational and long-term regular observations are given in Izrael et al. (1990; 1986) and Izrael (1996).

During the first few days, the gamma surveys of terrestrial contamination were impeded by the existence of the plume of contamination that changed continuously in space and time. Even as this occurred, maps of the radiation situation were compiled for both the earth's surface and the altitudes of the aircraft flights. Figure 5.2 shows one of the main plume fragments obtained from aircraft measurements on April 27, 1986.

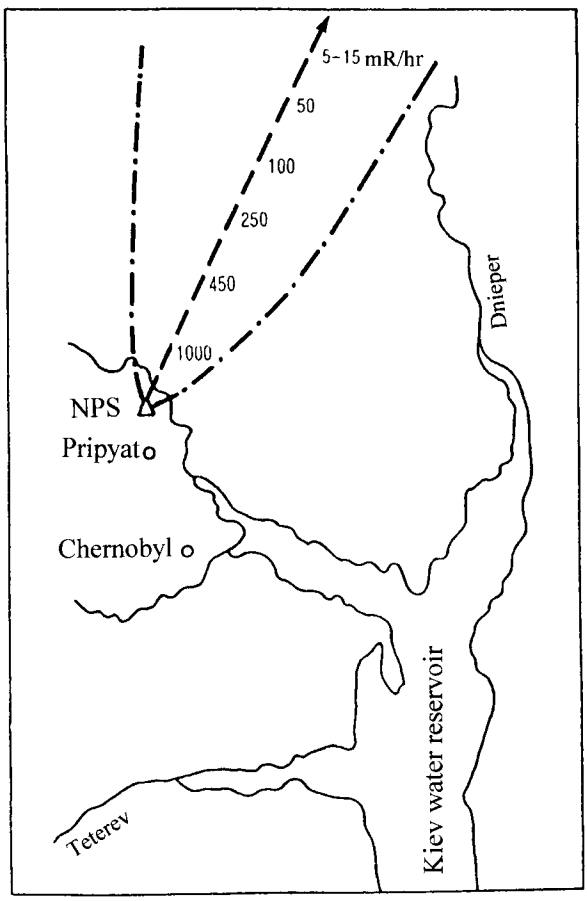

Fig. 5.2. Distribution of a plume of radioactive products at a height of 200 m on April 27, 1986. Gamma-radiation dose rate in mR/hr (1 mR/hr $\approx$ 10 μGy/hr).

Figure 5.3 shows the regional radiation situation obtained from aircraft measurements (height $h = 200$ m). Although some parts of the terrestrial contamination pattern could be distinguished, it was difficult to separate the terrestrial contamination from the atmospheric contamination.

The first detailed map of the close-in radiation pattern (isolines of exposure dose rate at a height of 1 m) for the terrestrial contamination existing at a distance up to 100 km from the accident site was compiled on May 1, 1986 and submitted to the Governmental Commission the following day. Such a presentation only became possible after the gamma-radiation contained in the plume and that in the terrestrial contamination became distinctly separated over the vast territory. Contamination continued to occur, however, especially in a southwards direction, even at later dates (Izrael et al., 1990).

During April–May 1986, gamma surveys of atmospheric and terrestrial contamination were carried out on a daily basis and at later dates on a regular basis, according to a

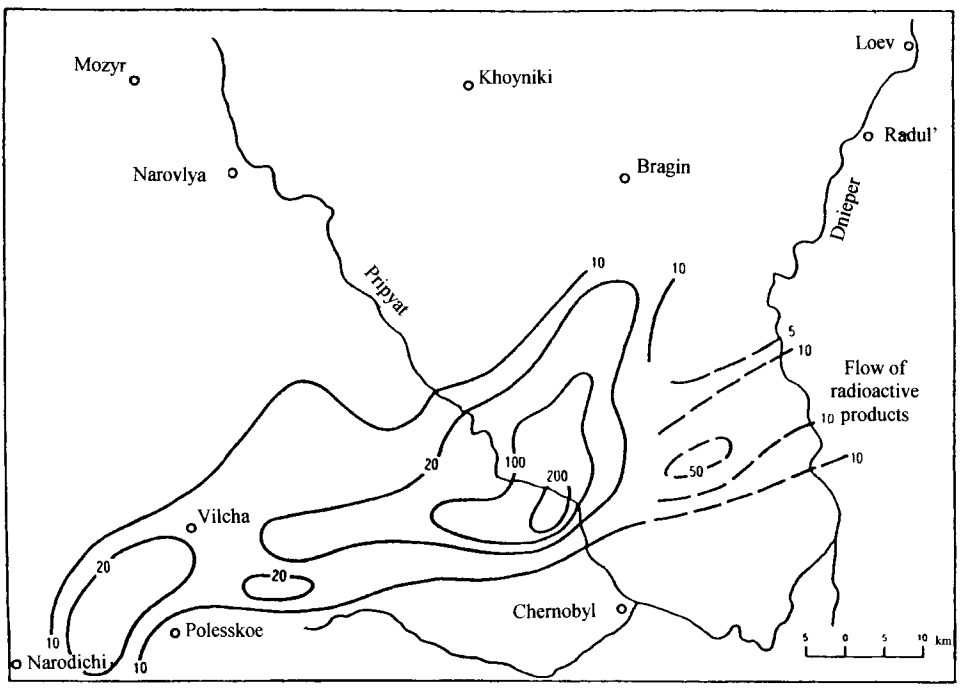

Fig. 5.3. Distribution of gamma-radiation dose rate (mR/hr) based on aircraft measurements at a height of 200 m on April 29, 1986 (1 mR/hr ≈ 10 μGy/hr).

prescribed schedule. On May 2, 1986, a decision was made to evacuate the population from the 30-km zone around the accident site because of the radiation situation on the ground and the continuing presence of a radioactive volatile plume from the destroyed reactor. Some time later, the population was evacuated from zones where the radiation levels were above 5 mR/hr (≈50 μGy/hr) as normalised to May 10, 1986 (this corresponds to a criterion of 10 rem (100 mSv) for the maximum admissible dose for the first year's exposure after the accident, as determined by the Ministry of Public Health of the USSR).

Figure 5.4 shows the dose rate map prepared from surveys conducted in early May (doses are normalised to May 10, 1986, the time when the plume of volatile radioactive products ceased to escape from the destroyed reactor (Izrael et al., 1990; 1986)). The western pattern is clearly pronounced on the map (isoline of 5 mR/hr (≈50 μGy/hr) on May 10, 1986 extending to 75–85 km from the accident site), as well as the southwestern and northern patterns (40–45 km long) and that to the south. The evacuation zone of complete restriction had an area of about 3000 km^2 and radiation levels above 20 mR/hr (≈200 μGy/hr) extended over an area of 1100 km^2 on May 10, 1986 (Izrael et al., 1990; Izrael et al., 1986). During the same time period, airborne gamma-surveys of the contaminated area over the whole European part of the USSR were conducted. These enabled us to single out newly contaminated zones and separate patterns of increased contamination (see Fig. 5.5) (Izrael et al., 1990; 1986).

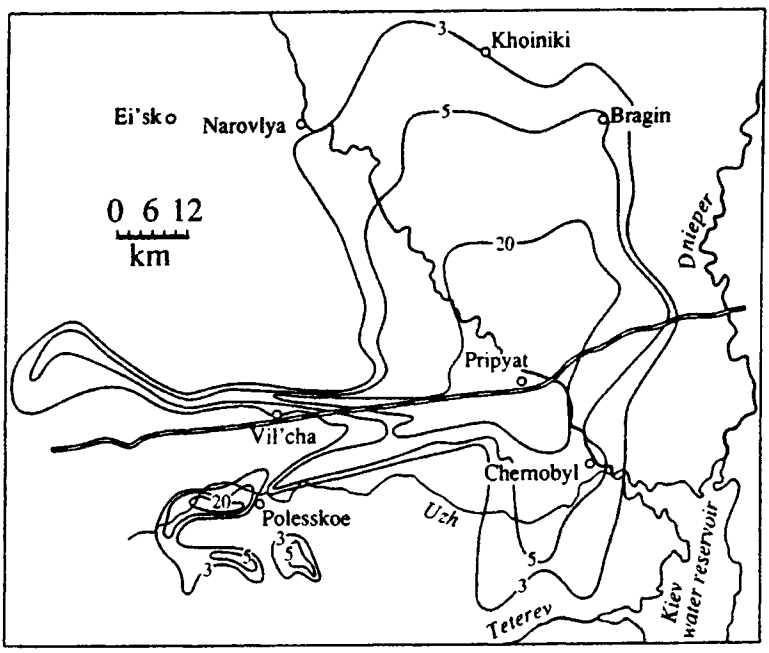

Fig. 5.4. Map of gamma-radiation dose rate (mR/hr) at a height of 1 m on May 10, 1986 (1 mR/hr $\approx$ 10 μGy/hr).

Apart from a central zone of high contamination, namely the "Gomel'–Mogilev–Bryansk" area that was easily distinguished on the map, another zone extended southwards–southwestwards from the accident site. The survey showed that an area with radiation levels above 0.2 mR/hr ($\approx$2 μGy/hr) covered more than 200×10^3 km^2 (Izrael, 1996b).

In parallel with the aerial surveys, extensive soil sampling was carried out in the contaminated areas, with laboratory analyses of individual radionuclides being made. Along with the airborne gamma-spectral measurements, these allowed us to compile the first maps of the radionuclide composition of the contaminated areas as soon as May–early June, 1986. Vast areas were contaminated in different directions as a result of the duration of the radioactive product release and the complicated meteorological conditions that followed the accident.

Figure 5.6 shows the temporal changes in energy release from the total inventory of radioactive products in the close-in pattern compared to the theoretical change in the energy release for the radioactive products in the reactor (operation time—1000 days) along with the calculated change in the energy release from the radioactive products in soil samples taken in the western and northern sectors of the close-in pattern (1–10 mR/hr; 1 mR/hr $\approx$10 μGy/hr).

Figure 5.7 presents the contours for radioactive contamination of the USSR at the 0.05 mR/hr ($\approx$0.5 μGy/hr) level as obtained from the aircraft gamma-surveys conducted during the first ten days of June 1986. The quantity of radioactive products deposited over the USSR territory generated approximately 1.2×10^8 (R/hr) m^2 [1.2 (MGy/hr) m^2] (i.e., the measured dose rate normalised to a height of 1 m) or 5.0×10^{17} MeV/s beyond the

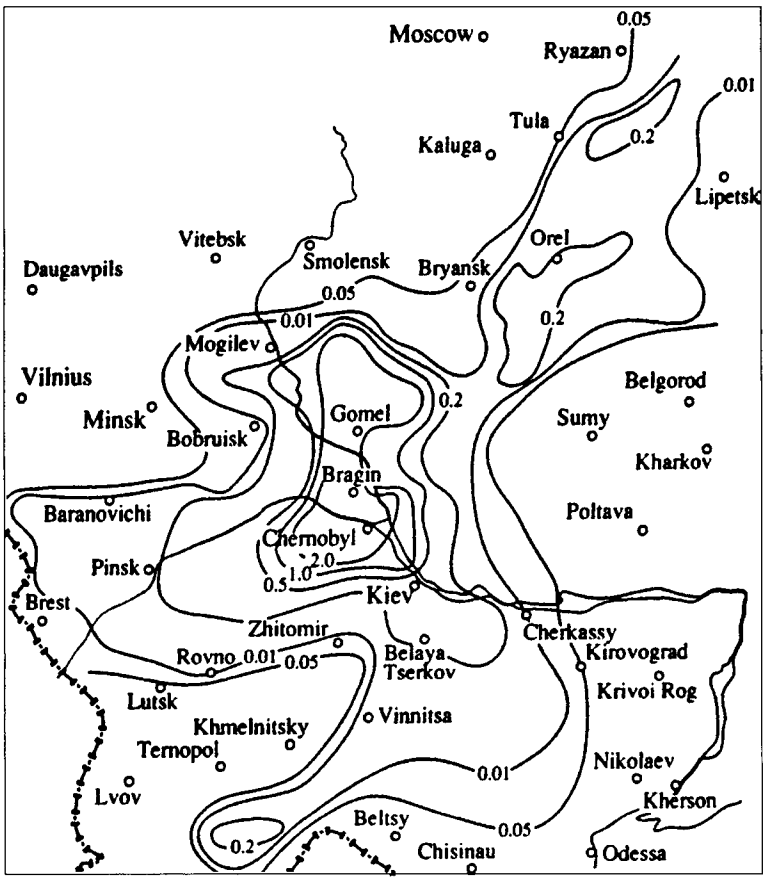

Fig. 5.5. Map of gamma-radiation dose rate (mR/hr) over the European sector of the USSR as determined by airborne gamma surveys from April 30 to May 7, 1986 (1 mR/hr ≈10 μGy/hr).

boundaries of the close-in fallout pattern. The total deposition was 9.0×10^{17} MeV/s in the close-in and distant zones (1.11–1.665 EBq (30–45 MCi) according to an average energy release per decay (MeV/decay) or 3.5–4.5% of the total theoretical energy release of the radioactive products in the reactor for the given period. According to Kolobashkin et al. (1983), 10 days after the reactor ceased to operate (i.e., May 5, 1986) the average energy yield was equal to 571 keV/decay (gamma-quanta); in this case, 9×10^{17} MeV/s corresponds to 1.57 EBq (42.6 MCi).

The quantity of radioactive products expressed in energy release units (MeV/s) and in integral units (R/hr) deposited in the close-in fallout pattern (outside the industrial site of the power station) is shown in Table 5.2. A detailed study of the dynamics of the temporal variations in areas with different exposure dose rates was performed using the results of the extensive airborne gamma-surveys of terrestrial contamination (Fig. 5.8).

As mentioned above, some radioactive contamination patterns were created on the ground surface after the CNPS accident, patterns which were characterised by different

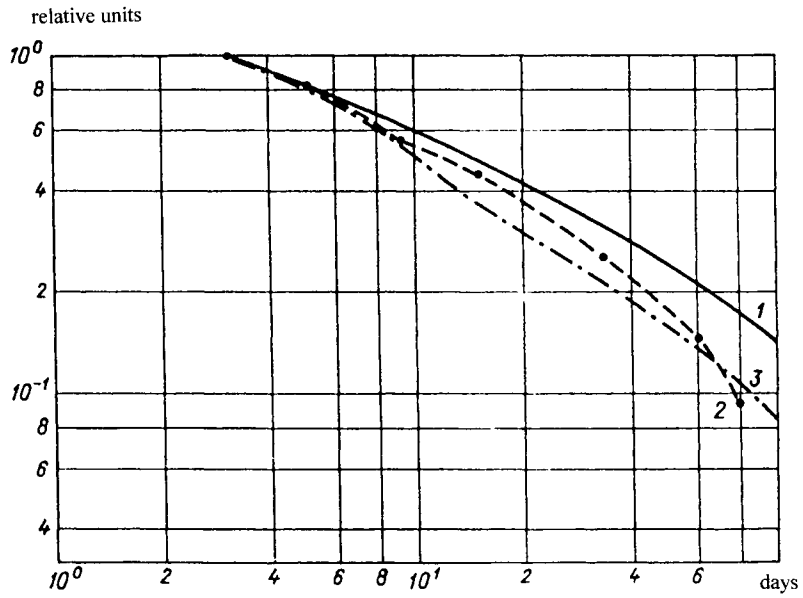

Fig. 5.6. Time-variation of the energy release from the radioactive products in the close-in fallout pattern: 1 — theoretical curve; 2 — total for the fallout pattern; 3 — the curve based on soil samples (from the northwest zone where radiation levels were 1–10 mR/hr (≈10–100 μGy/hr)).

Table 5.2
Total fallout radioactivity in close-in pattern (outside the industrial site), 1986

Date of survey of fallout pattern	Integral (R/hr) m^2 $h = 1$ m	Amount of radioactivity in the close-in fallout pattern (MeV/s)
29 April (D + 3)	1.75×10^8	7.3×10^{17}
1 May (D + 5)	1.45×10^8	6.1×10^{17}
5 May (D + 9)	9.9×10^7	4.1×10^{17}
10 May (D + 15)	7.9×10^7	3.3×10^{17}
29 May (D + 33)	4.4×10^7	1.8×10^{17}
26 June (D + 61)	2.5×10^7	1.1×10^{17}
13 July (D + 78)	1.65×10^7	6.6×10^{16}

radiation dose rate levels as a function of distance from the accident site; the rate of decrease of radiation levels was time-dependent and, in general, all of these features were associated with differences in the nuclide composition of the contamination (to be discussed in detail in Section 5.4). Figure 5.9 presents the change in these dose rates along the pattern's axis.

These studies of radioactive contamination demonstrated that contamination was extremely spotty, a spottiness related to features of the meteorological record such as the occurrence of heavy rains in some regions that enhanced the radionuclide deposition on the surface. This effect resulted in the formation of "caesium hotspots" in the territory of

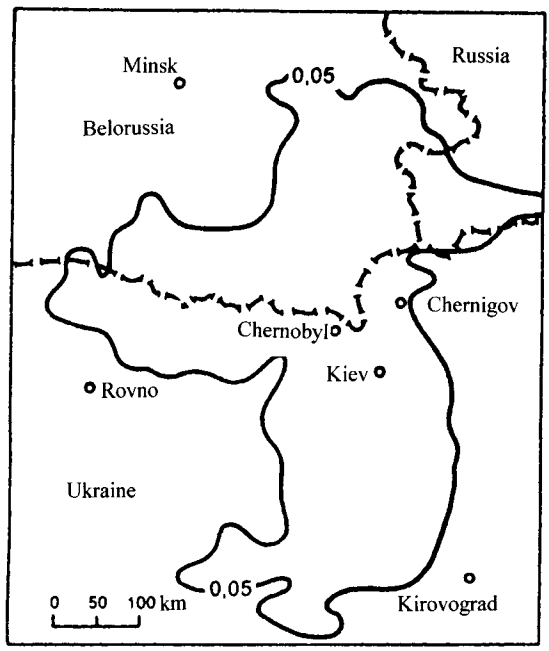

Fig. 5.7. Distribution of gamma-radiation dose rate along the 0.05 mR/hr (0.5 μGy/hr) isoline in the territory of the USSR on June 10, 1986.

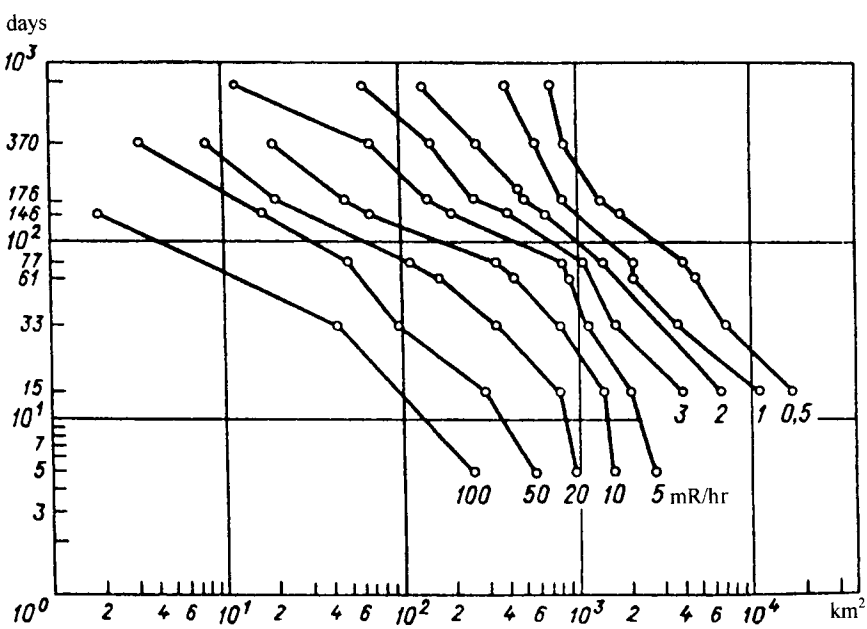

Fig. 5.8. Temporal change of the areas within specific dose rate isolines (based on airborne survey data).

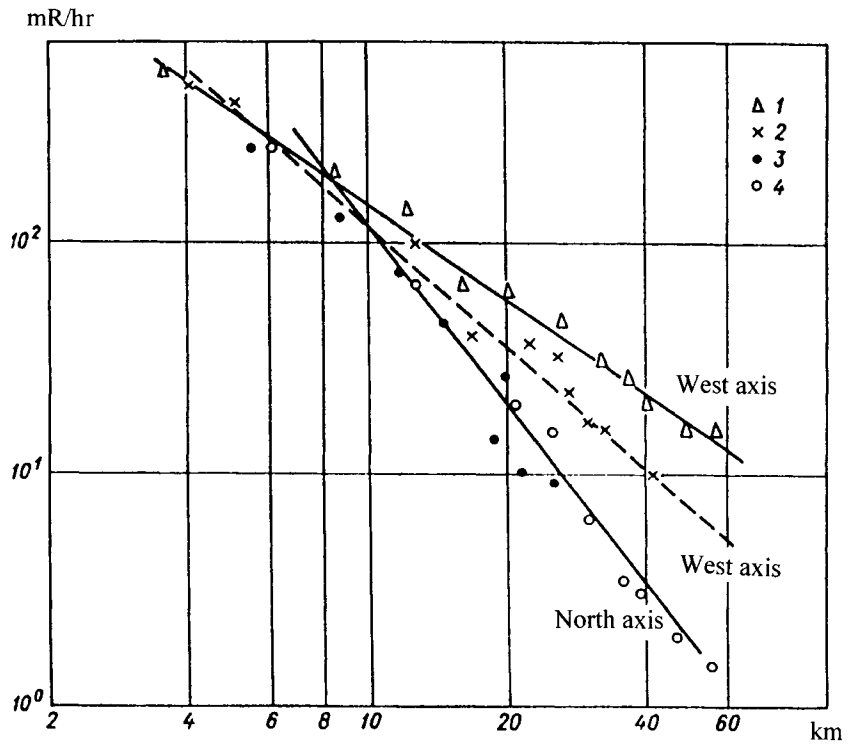

Fig. 5.9. Change in gamma-radiation dose rate (1 mR/hr ≈ 10 μGy/hr) (h = 1 m) along the fallout pattern axis. 1, 4 — survey from An-30 aircraft on May 29, 1986; 2, 3 — survey from Mi-8 helicopter, May 15, 1986.

Belarus (Gomel and Mogilev regions), in Russia (Bryansk, Tula regions) and in Austria, Germany, Italy and Sweden (Izrael et al., 1990; Hohenemser and Renn, 1988). Figure 5.10 shows the dependence of deposition on distance. The first line is for areas where there was precipitation, the other for areas where there was no precipitation. In these two cases, the intensity of contamination differed by more than an order of magnitude (at the same distance from the site). The quantities of radioactive materials deposited at considerable distances were more pronounced where there was precipitation (e.g., in Southern Bavaria) than in Kiev, where there was no precipitation during the generation of contaminated areas. During the process of pattern formation, features of landscape also play an essential role.

4. Radionuclide Composition of the Terrestrial Contamination from the Chernobyl Accident

As noted in previous sections, a cloud was formed during the initial phase of the releases from the Chernobyl NPS accident. The plume of gaseous and aerosol products continued to exist for a long period of time resulting in radioactive contamination on the ground. The unusual character of the contamination source with a continuing introduction of

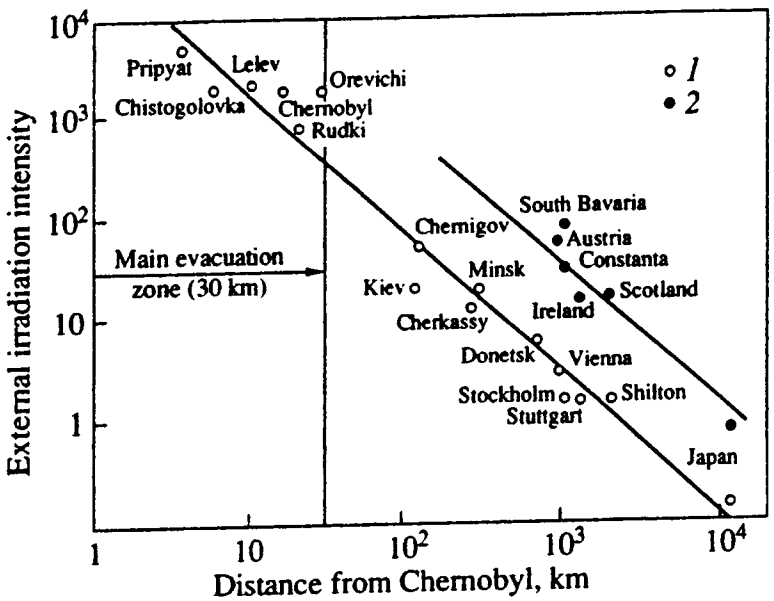

Fig. 5.10. Ground-surface gamma-radiation dose rates measured taking into account precipitation in the regions of radioactive deposition 7–10 days after the Chernobyl accident. The dose rates are measured in units of natural background, assumed to be 0.01 mR/hr (≈0.1 μGy/hr), and relate to the distance from Chernobyl, as $P(R) = (6.9 \times 10^4)R^{-1.4}$; 1 — no precipitation; 2 — precipitation.

new radioactive materials into the plume, in combination with unstable meteorological situations, in which the wind constantly changed direction, led to the formation of very complicated contamination zones (in terms of their structure and radionuclide composition) in the environment. The structural characteristics of the contamination zones and their gamma-ray fluxes have been considered in Section 5.3. Here we report details of the radionuclide composition of the contamination in the context of its spatial distribution on the surface.

The nuclide composition of the terrestrial contamination was determined by deploying aircraft and ground vehicles as well as by laboratory analyses of samples taken by ground teams. Aircraft measurements were carried out mainly with semiconductor gamma-spectrometric instruments. A full complex range of modern spectrometric and radiochemical methods was used for the laboratory analyses, making it possible to measure the gamma, beta and alpha radiation with high accuracy.

The first series of soil sampling was carried out on April 30, 1986 in directions westwards and southwards from the Chernobyl nuclear station (Izrael et al., 1987b). The subsequent soil sampling series were performed after taking into account the specific information on the radioactive fallout distribution gained from the aerial surveys. In the spectra that were measured during the days after the accident, gamma-lines of the following radionuclides were identified: ^{239}Np, ^{99}Mo (^{99}Tc), ^{132}Te, ^{131}I, ^{140}Ba, ^{140}La, ^{141}Ce, ^{103}Ru, ^{95}Zr, ^{95}Nb, ^{144}Ce, ^{106}Ru, ^{134}Cs and ^{137}Cs. ^{89}Sr, ^{90}Sr and ^{91}Y were identified via radiochemical analyses in the laboratory and measurements of the longer-lived alpha-

emitters ^{238}Pu, ^{239}Pu and ^{240}Pu were begun. Later ^{241}Am, ^{241}Cm and ^{242}Cm were identified, gamma-lines being one set of criteria used for ^{241}Am identification.

Examinations of the generalised radionuclide data for the period April 26–May 5, 1986 permitted the soil samples to be grouped into three sectors "South", "West" and "North" according to the distribution of the radioactive material. Also taking into consideration the radionuclide composition of the radioactive materials depositing on the earth's surface, along with the contamination density and the distance from the source, three zones were singled out within each sector in accordance with the gamma-ray fluxes at D + 15: (i) $P_\gamma \geqslant$ 10 mR/hr, i.e., $P_\gamma \geqslant 100$ μGy/hr, (ii) $2 \leqslant P_\gamma < 10$ mR/hr, i.e., $20 \leqslant P_\gamma < 100$ μGy/hr and (iii) $P_\gamma < 2$ mR/hr, i.e., $P_\gamma < 20$ μGy/hr. The identification of the zones to which any particular sample belonged was made on the basis of the dose rate P_γ at the sampling point at the time D + 15.

Table 5.3 presents the results of the nuclide analyses of the soil samples in the form of averages for each zone, with activity ratios $(A_i/A_{95})_0$ for April 26, 1986 and averaged σ_i/P_γ values for May 10, 1986, where σ_i is the ith nuclide's terrestrial contamination density. The table also shows averages for the zones' fractionation factors $f_{i,95} = (A_i/A_{95})_0/(Y_i/Y_{95})$, thereby characterising the variation in radionuclide composition in individual groups of samples as compared to the calculated theoretical composition. The data are normalized to ^{95}Zr, where Y_i is the ith radionuclide's production and Y_{95} that for ^{95}Zr in the reactor at the time of the accident.

Average values for the parameters $(A_i/A_{95})_0$ and (σ_i/P_γ) over groups of samples depended on both the direction from the contamination source and the level of ground contamination within each sector. The most significant characteristic of a radionuclide's behavior was the fractionation factor. The deviation of this factor from unity is indicative of the degree of radionuclide volatility compared to the refractory nuclide ^{95}Zr. The fractionation factor's variation with distance from the source was considered to be the most important characteristic when estimating radionuclide volatility. Accordingly, tellurium, iodine and caesium were found to be the most volatile radionuclides. The volatilities of the radionuclides in the contaminated zones under consideration were close to ^{95}Zr, i.e., they were fractionated only weakly relative to ^{95}Zr at a distance of 100 km from the source.

Based on the data on surface contamination density in various zones, alongside the dose rate values on D + 15, the activities for some radionuclides in the close-in zone of the fallout pattern were estimated (Table 5.4). The nuclides shown in Tables 5.3 and 5.4 can be subdivided into at least three groups based on their degree of fractionation (as will soon become evident, this characterises their volatility—the larger the fractionation factor of the ith nuclide relative to non-volatile ^{95}Zr, the higher the volatility of this radionuclide):

(i) radionuclides with high fractionation factors (^{137}Cs, ^{134}Cs, ^{132}Te, ^{131}Y, ^{125}Sb, ^{110m}Ag—the volatile nuclides);

(ii) radionuclides with low fractionation factors; however, their behaviour differed from that of ^{95}Zr at some sites (particularly, southwards), ^{140}Ba, ^{90}Sr, ^{91}Y, sometimes ^{103}Ru and ^{106}Ru;

(iii) radionuclides whose behaviour very closely resembled that of ^{95}Zr (the refractory nuclides)—^{141}Ce, ^{99}Mo, ^{239}Np, sometimes ^{103}Ru, ^{106}Ru, ^{90}Sr.

Table 5.3
Radionuclide composition of soils in contaminated area

Radionuclide	Zone I $P_\gamma \geqslant 10$ mR/hr			Zone II 2 mR/hr $\leqslant P_\gamma <$ 10 mR/hr			Zone III $P_\gamma <$ 2 mR/hr		
	A_i/A_{95}	$f_{i,95}$	σ_i/P_γ	A_i/A_{95}	$f_{i,95}$	σ_i/P_γ	A_i/A_{95}	$f_{i,95}$	σ_i/P_γ
				"South" sector					
^{239}Np	8.0	–	2.5	–	–	–	14	–	1.4
^{99}Mo	0.45	0.5	0.07	–	–	–	2.5	2.8	0.9
^{132}Te	1.4	1.9	1.1	0.9	1.2	0.8	1.3	1.8	0.8
^{131}I	0.6	1.0	4.0	0.6	1.0	5.0	2.0	3.3	8.0
^{140}Ba	0.8	0.8	9.0	0.9	1.0	13	1.0	1.0	8.0
^{141}Ce	1.1	1.2	18	1.1	1.2	25	1.0	1.0	13
^{103}Ru	0.7	0.7	13	0.7	0.7	17	0.8	0.7	10
^{89}Sr	0.2	0.4	5.0	1.6	3.0	6.0	1.2	2.5	16
^{91}Y	0.3	0.45	5.0	–	–	11	0.8	1.2	12
^{95}Zr	1.0	1.0	20	1.0	1.0	27	1.0	1.0	15
^{144}Ce	0.7	0.7	16	0.6	0.6	20	0.6	0.6	10
^{106}Ru	0.3	0.5	7.0	0.2	0.35	7.0	0.3	0.5	3.8
^{134}Cs	0.01	0.07	0.2	0.015	0.1	0.5	0.03	0.2	0.5
^{90}Sr	0.02	0.3	0.35	0.16	2.0	0.8	0.15	2.0	2.2
^{137}Cs	0.03	0.3	0.5	0.04	0.4	0.9	0.1	0.9	1.2
				"West" sector					
^{239}Np	6.0	–	1.7	9.0	–	2.0	5.0	–	0.9
^{99}Mo	1.4	1.6	1.0	1.4	1.6	0.3	1.5	1.7	0.3
^{132}Te	1.4	1.9	1.0	3.8	5.3	1.8	3.6	5.0	1.8
^{131}I	0.9	1.5	4.0	3.0	5.0	10	3.0	5.0	7.0
^{140}Ba	1.1	1.0	10	1.6	1.5	10	1.4	1.3	14
^{141}Ce	0.9	1.0	13	1.1	1.2	17	0.9	1.0	7.5
^{103}Ru	0.8	0.7	13	0.7	0.7	11	0.7	0.7	14
^{89}Sr	0.14	0.3	2.5	0.6	1.3	6.0	0.7	1.5	8.5
^{91}Y	0.2	0.3	4.0	0.6	0.9	9.0	0.9	1.4	11
^{95}Zr	1.0	1.0	20	1.0	1.0	19	1.0	1.0	20
^{144}Ce	0.6	0.6	11	0.7	0.7	15	0.6	0.6	7.0
^{106}Ru	0.25	0.4	5.0	0.3	0.5	6.2	0.2	0.35	2.6
^{134}Cs	0.02	0.13	0.4	0.14	0.9	1.5	0.13	0.9	1.7
^{90}Sr	0.02	0.3	0.3	0.03	0.4	0.4	0.1	1.3	1.6
^{137}Cs	0.5	0.5	1.0	0.2	1.8	2.1	0.2	1.8	2.7
				"North" sector					
^{239}Np	16	–	5.0	–	–	–	2.0	–	3.0
^{99}Mo	–	–	–	–	–	–		–	
^{132}Te	1.7	2.4	3.8	10	14	11	5.0	7.0	5.0
^{131}I	3.0	5.0	13	6.0	10	35	5.0	8.0	40
^{140}Ba	1.0	1.0	7.0	1.1	1.0	17	1.0	1.0	13
^{141}Ce	1.1	1.2	16	1.1	1.2	27	1.1	1.2	27
^{103}Ru	1.0	0.9	14	1.6	1.5	37	1.4	1.3	31
^{89}Sr	0.2	0.4	3.0	0.3	1.6	7.0	0.2	0.4	3.0
^{91}Y	0.3	0.45	4.5	0.5	0.8	9.0	0.1	0.15	2.0
^{95}Zr	1.0	1.0	14	1.0	1.0	30	1.0	1.0	30

Table 5.3 — Continued

Radionuclide	Zone I $P_\gamma \geqslant 10$ mR/hr			Zone II 2 mR/hr $\leqslant P_\gamma < 10$ mR/hr			Zone III $P_\gamma < 2$ mR/hr		
	A_i/A_{95}	$f_{i,95}$	σ_i/P_γ	A_i/A_{95}	$f_{i,95}$	σ_i/P_γ	A_i/A_{95}	$f_{i,95}$	σ_i/P_γ
^{144}Ce	0.65	0.7	12	0.6	0.6	21	0.7	0.7	22
^{106}Ru	0.3	0.5	6.0	0.4	0.7	11	0.3	0.5	9.0
^{134}Cs	0.1	0.7	1.5	0.18	1.2	5.0	0.13	0.9	4.0
^{90}Sr	0.02	0.3	0.4	0.03	0.4	0.9	0.02	0.3	0.6
^{137}Cs	0.2	1.8	3.5	0.3	2.7	9.4	0.03	2.7	7.8

Note. A_i/A_{95} is the ith radionuclide activity relative to the ^{95}Zr activity at the moment of the accident; $f_{i,95}$—fractionation factor; σ_i/P_γ—contamination density ratio to the dose rate at a height of 1 m on 10 May, 1986 (mCi/km^2/mR/hr). 1 mCi/km^2 = 37 mBq/km^2; 1 MR/hr $\approx$ 10 μGy/hr.

Table 5.4
Inventory of radionuclide activity in the close-in (up to 40 km) zone of the fallout pattern on D + 15

Radionuclide	Radionuclide activity (Ci)	Inventory of deposited radionuclide on D + 15 compared with total activity in the reactor
^{132}Te	2.5×10^6	5.0
^{131}I	1.3×10^6	5.1
^{140}Ba	9.1×10^5	1.4
^{141}Ce	1.7×10^6	1.7
^{103}Ru	1.5×10^6	1.4
^{89}Sr	6.2×10^5	1.2
^{91}Y	6.4×10^5	0.85
^{95}Zr	1.8×10^6	1.5
^{144}Ce	1.3×10^6	1.0
^{106}Ru	5.7×10^5	0.8
^{134}Cs	1.3×10^5	0.6
^{137}Cs	2.8×10^5	1.9
^{90}Sr	8.5×10^4	0.85
Total amount	1.1×10^7	Average 1.6

1 Ci = 37 GBq.

A clear and pronounced fractionation effect was noted within the so called "caesium hotspots" (to the north-east, i.e., Gomel, Mogilev, Bryansk, Tula regions) where the fractionation factors of ^{137}Cs, ^{134}Cs, ^{131}Y, ^{125}Sb and ^{110m}Ag reached the hundreds and above, relative to ^{95}Zr (Table 5.5). Evidently, these patterns, spaced at hundreds and even thousands of kilometres from the accident site, were formed when highly dispersed particles of volatile nuclides were distributed within the fallout zones during heavy rains. ^{103}Ru, ^{106}Ru and even ^{140}Ba behaved as volatile species relative to ^{95}Zr within these spots. Integration of the nuclides over the contaminated area within the limits of the close-in fallout pattern (up to 40 km from the accident site) gave the total inventories for these nuclides shown in Table 5.4.

Table 5.5
Averaged radionuclide composition of soil contamination and radionuclide fractionation within radiocesium fallout patterns

Radionuclide	Mogilev region, Krasnopolsky district		Gomel region, Vetkovsky district		Tulsk region, Plavsk	
	A_i/A_{95}	$f_{i,95}$	A_i/A_{95}	$f_{i,95}$	A_i/A_{95}	$f_{i,95}$
^{131}I	200	290	130	190		
^{140}Ba	15	15	10	10		
^{141}Ce	1.5	1.5	1.5	1.5		
^{103}Ru	36	36	18	18		
^{89}Sr	3.3	8.3	2.8	7.0		
^{110m}Ag	0.1	100	0.11	110	0.19	190
^{144}Ce	0.9	1.3	1.4	2.0	1.0	1.4
^{106}Ru	11	28	13	32	7.2	18
^{125}Sb	0.6	150	0.6	150	1.0	250
^{90}Sr	0.2	5.0	0.3	7.5		
^{137}Cs	21	370	9.2	170	14	250

Table 5.6
The external gamma-radiation dose on the terrain normalised to a dose rate of 1 mR/hr on D + 15 for certain parts of the radioactive fallout pattern, R

Sector	Zone	Dose from the total nuclide composition (R)		Dose from ^{137}Cs (R)	
		From D + 1 to 1 year	From 1 year to 50 years	From D + 1 to 1 year	From 1 year to 50 years
"North"	I	2.5	6.9	0.21	6.05
	II	2.5	8.3	0.25	7.2
	III	2.5	9.1	0.28	8.2
"South"	I	2.4	1.6	0.038	1.1
	II	2.1	1.9	0.049	1.4
	III	2.4	3.7	0.11	3.11
"West"	I	2.2	2.0	0.054	1.6
	II	2.3	5.7	0.16	4.8
	III	2.3	6.0	0.18	5.2

1 mR/hr ≈10 μGy/hr; 1 R ≈10 mGy.

In connection with calculations of dose rate and total exposure dose, the variability in the fractionation of the nuclides needs to be taken into account, particularly in the light of its magnitude and importance. An outline of such a calculation is shown below together with the results for different situations (Table 5.6).

To estimate the changes in gamma dose rate in different areas of the radioactive fallout footprint, the gamma-activity of the total inventory of radionuclides deposited on the earth's surface was calculated as a function of time. For each of the nine zones, an average for the segment's A_i/A_{95} ratio was assumed as a generalised characteristic of the

radionuclide composition. The dose rate, $P_\gamma(t)$, was assumed to be related to the energy release function, $\sum \varepsilon_i(t)$, of the total radionuclide inventory, as follows:

$$P_\gamma(t) = K \sum \varepsilon_i(t), \tag{5.1}$$

$$\varepsilon_i(t) = K_{\gamma i} \frac{\bar{A}_i}{A_{95}} e^{-\lambda_i t}, \tag{5.2}$$

where $K_{\gamma i}$ is the total ionisation gamma-constant of the ith radionuclide, $(R \cdot km^2)/(hr \cdot mCi)$; λ_i—decay constant, hr^{-1}; K—normalizing factor. Average $(\bar{A}_i/A_{95})_0$ ratios were also used to estimate the exposure dose of the external gamma-radiation by integrating expression (5.1) within the time intervals "1 day–1 year" and "1 year–50 years":

$$D(t_1, t_2) = \int_{t_1}^{t_2} P_\gamma(t)\, dt = K \sum \left(\frac{\bar{A}_i}{A_{95}} \right) K_{\gamma i} \int_{t_1}^{t_2} e^{-\lambda_i t}\, dt. \tag{5.3}$$

In this case, the normalisation factor K is selected to satisfy the condition $P_\gamma = 1$ mR/hr ($\approx$10 μGy/hr) at D + 15. The results of the calculations for the external dose are given in Table 5.6 (Izrael et al., 1987b). Fig. 5.11 shows the variations in dose rates (similarly normalised for different areas (Izrael et al., 1990).

In early June 1986, the first sketch maps of the terrestrial contamination by the nuclides ^{140}La, ^{103}Ru, $^{95}Zr + {}^{95}Nb$ at distances ranging up to hundreds of kilometres from the accident site were compiled (Izrael et al., 1987b). The survey was conducted by M.V. Nikiforov using gamma-spectrometers installed on aircraft (for ^{140}La, see Fig. 5.12). All the maps clearly show the northern (Mogilev–Gomel), western and south–south-western (between Cherkassy and Vinnitsa) deposition patterns separate from the central area. The highest contamination level on these maps (outside the 60-km zone) was observed for ^{103}Ru (370 GBq/km^2 (10 Ci/km^2) and above) and the lowest for Zr + ^{95}Nb.

The measurements of the terrestrial contamination by the most hazardous long-lived nuclides (^{137}Cs, ^{134}Cs, ^{90}Sr, $^{239+240}Pu$, etc.) were carried out to a high accuracy, including the ground-based measurements conducted over many years under the leadership of Stukin at reference points within the 60-km zone around the accident site. The ^{137}Cs inventory at the earth's surface was measured repeatedly from April 1986 over a vast area using both airborne gamma-surveys (over 40 surveys during the decade) and ground-based methods. As new analytical and statistical information became available, the data became more refined and the maps more detailed.

In 1998, an Atlas of ^{137}Cs and other radionuclide contamination in the Russian Federation, the Ukraine and Belarus (Izrael et al., 1998) and an Atlas of Chernobyl ^{137}Cs contamination over the whole of Europe (De Cort et al., 1998) were published. Figure 5.13 depicts the contamination over Europe while Fig. 5.14 presents maps of ^{137}Cs and ^{90}Sr terrestrial contamination over the European part of the former USSR in 1989 (Izrael, 1989; Izrael, 1990; Izrael, 1998). Figure 5.15 shows a map of ^{137}Cs fractionation relative to ^{144}Ce in the close-in zone. Table 5.7 presents areas of different contamination density over individual regions of the Russian Federation (Izrael et al., 1994a).

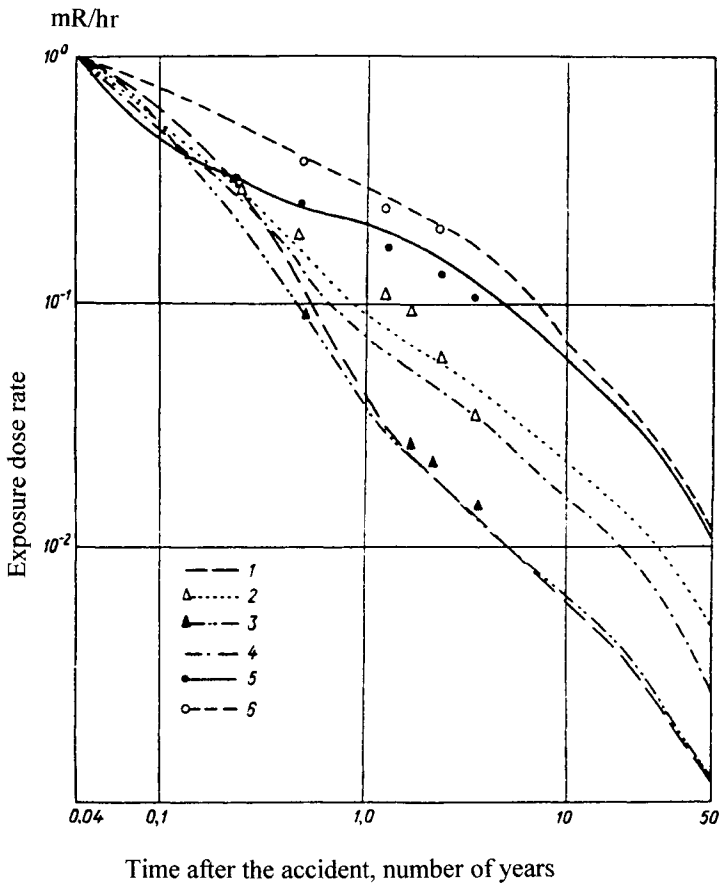

Fig. 5.11. Changes in external gamma-radiation dose rates from the Chernobyl deposition in some contaminated regions normalized to $P = 1$ mR/hr ($\approx$10 μGy/hr) 15 days after the accident (points are *in situ* measurement data). 1 — the initial composition; 2 — the north (Bragin); 3 — the south (Kiev); 4 — the west (Vilcha); 5 — caesium hotspots; 6 — the region south of Kiev.

The data on ^{239,240}Pu terrestrial contamination in 1986 and 1989 (Fig. 5.16) agree well, although Pu results for 1986 were relatively scarce. Analogous results were also obtained for ^{90}Sr. It was apparent from these data that the ^{239,240}Pu distribution was essentially limited to the restriction zone (to ~30 km). As to ^{90}Sr, the 3 Ci/km^2 (111 GBq/km^2) isoline (adopted as the maximum permissible value for the population in 1986) was insignificantly beyond the limits of the 30-km zone (see Fig. 5.14).

Data on the terrestrial contamination by ^{134}Cs, ^{137}Cs, ^{106}Ru, ^{90}Sr, ^{144}Ce, ^{238}Pu, $^{239+240}$Pu, ^{241}Am and ^{242}Cm within the 60-km zone around the Chernobyl NPS were included in the Atlas (Izrael et al., 1998). The $^{239+240}$Pu contamination in the close-in zone, compiled on the basis of its correlation with ^{144}Ce, is shown in Fig. 5.17. A map of the ^{90}Sr distribution in 1996, as presented in the Atlas (Izrael et al., 1998), is shown in Fig. 5.18,

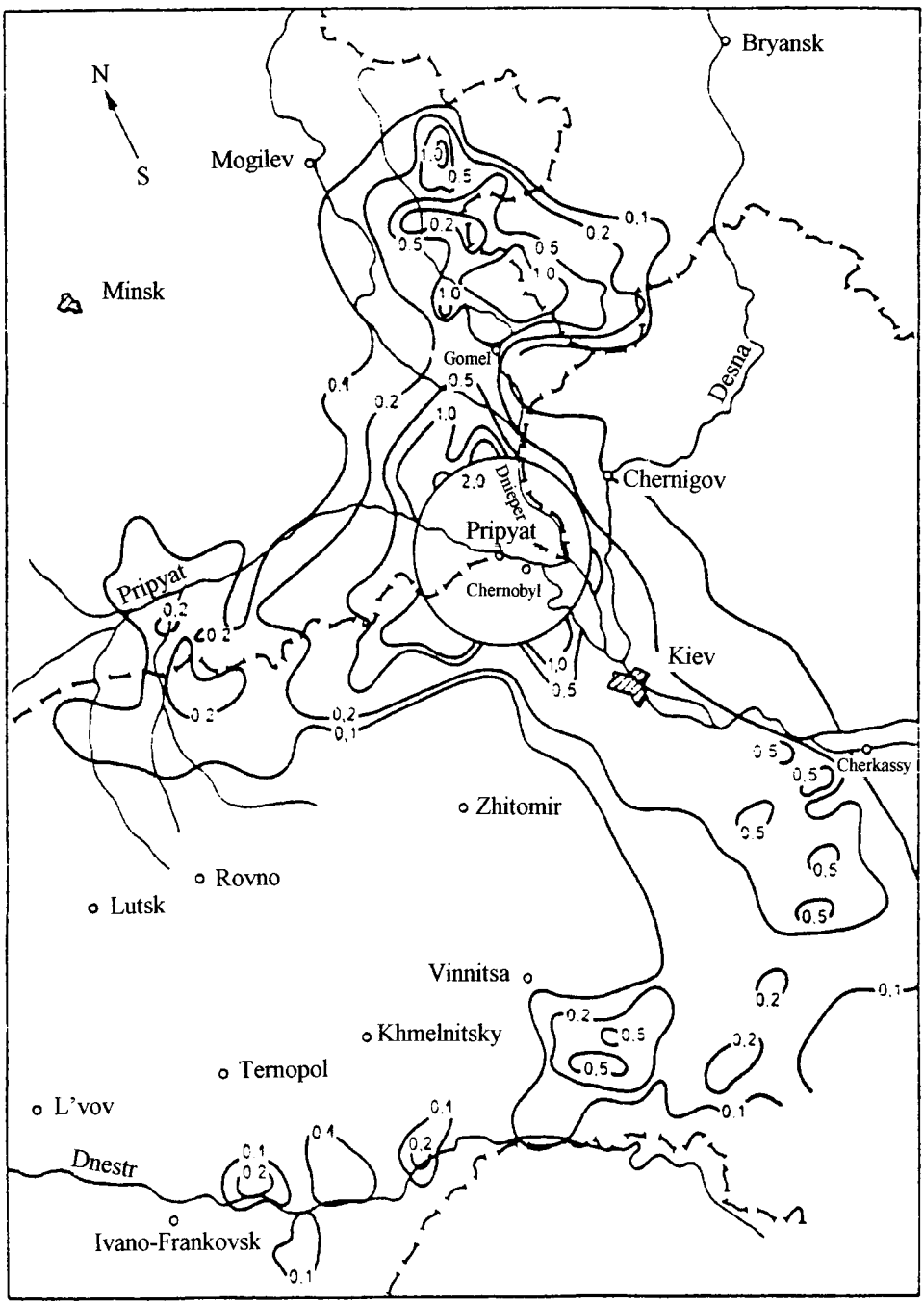

Fig. 5.12. Map of ^{140}La contamination, 2–12 June, 1986.

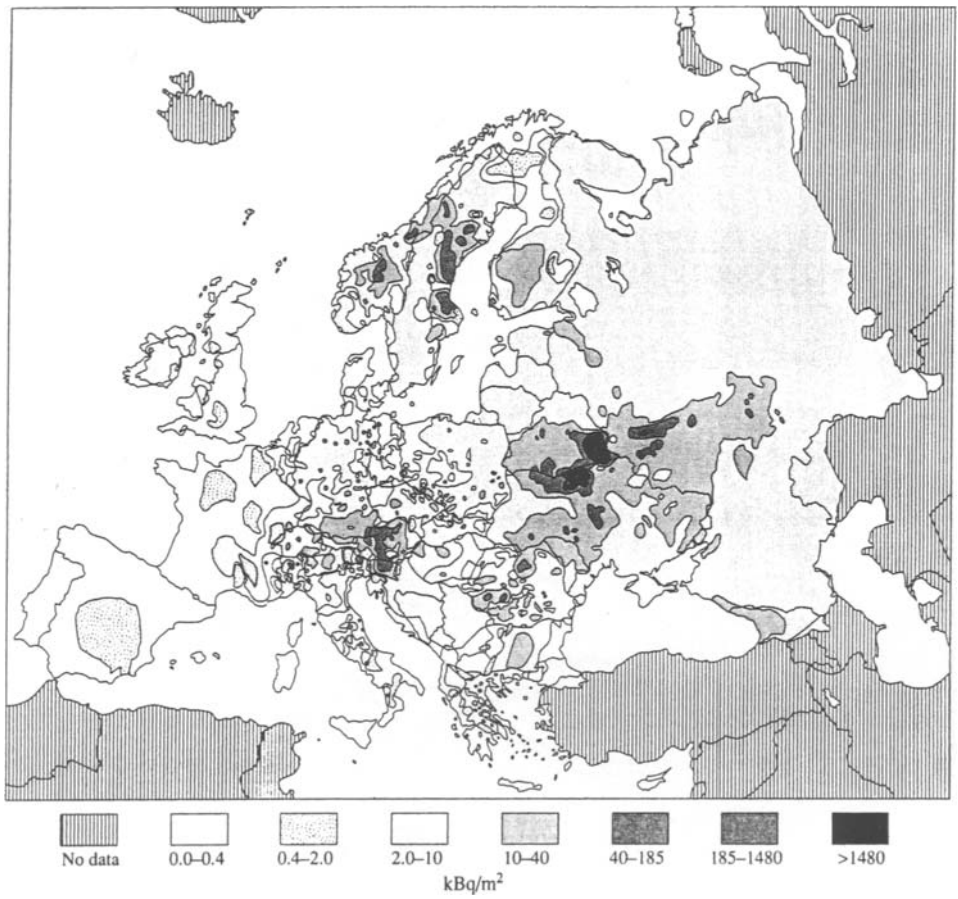

Fig. 5.13. ^{137}Cs contamination over Europe.

including the directions of the contaminated patterns after the Chernobyl accident. The dates of formation of the individual fallout patterns are also indicated.

As already noted, the alpha- and gamma-emitting ^{241}Am (which accumulates as a result of ^{241}Pu decay) was identified in the contaminated area in 1986. Figure 5.19 shows the ^{241}Am accumulation rate and the predicted variation with time of the total alpha-activity of the Chernobyl-derived radionuclides. An outline of ^{131}I terrestrial contamination (Fig. 5.20) was compiled on the basis of the meteorological data in the first days after the accident. Since ^{131}I is highly volatile, this map indicates only a potential fraction of the ^{131}I exposure of the population. Data from the reconstruction of the ^{131}I deposition density (Petkevich et al., 1994) yielded higher values.

From the map (Fig. 5.13) of the Chernobyl ^{137}Cs contamination over the whole of Europe, one can estimate the adjusted amount of Chernobyl ^{137}Cs that was deposited in 1986 to be about 1.72 MCi (63.64 PBq) (minus the ^{137}Cs from global fallout). From corrected and more precise data in the "Atlas of Caesium Deposition on Europe

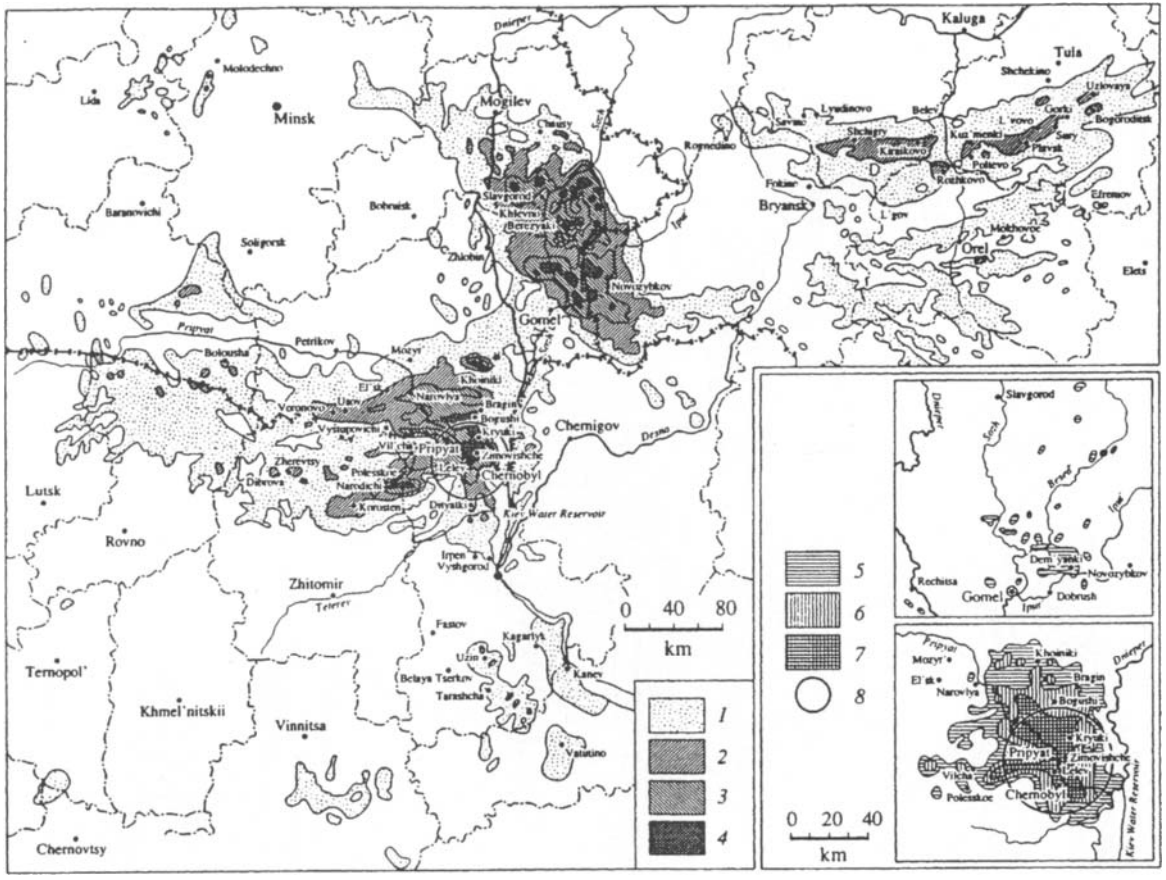

Fig. 5.14. ^{137}Cs (left) and ^{90}Sr (right) contamination over the former USSR, 1989. ^{137}Cs (Ci/km^2): 1, 1–5; 2, 5–15; 3, 15–40; 4, > 40. ^{90}Sr (Ci/km^2): 5, 1–2; 6, 2–3; 7, > 3 (8, 30 km boundary). (1 Ci/km^2 = 37 GBq/km^2.)

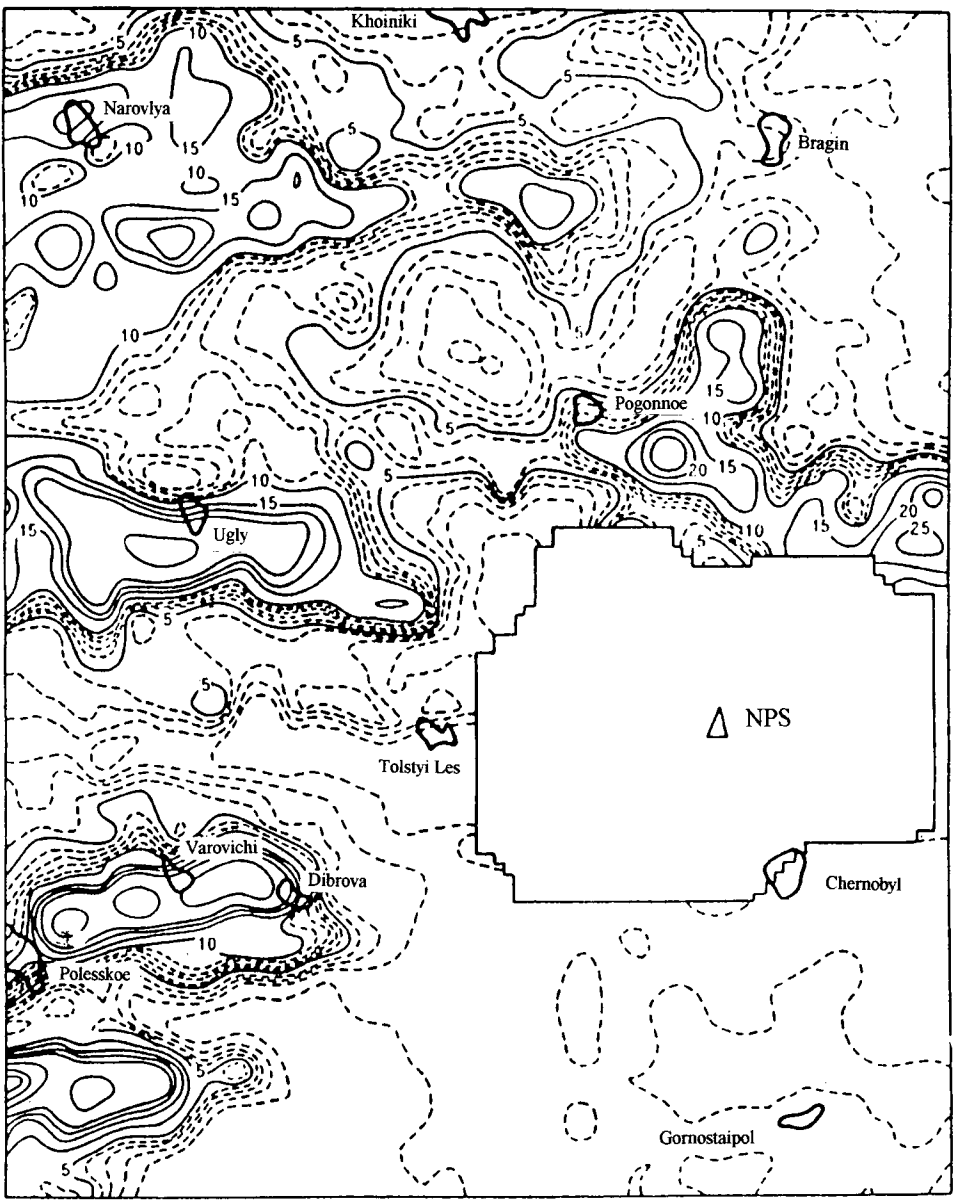

Fig. 5.15. Part of a sketch map of the distribution of the fractionation factor, f_{144}^{137}, including that within the 30-km zone (the survey scale is 1:500000).

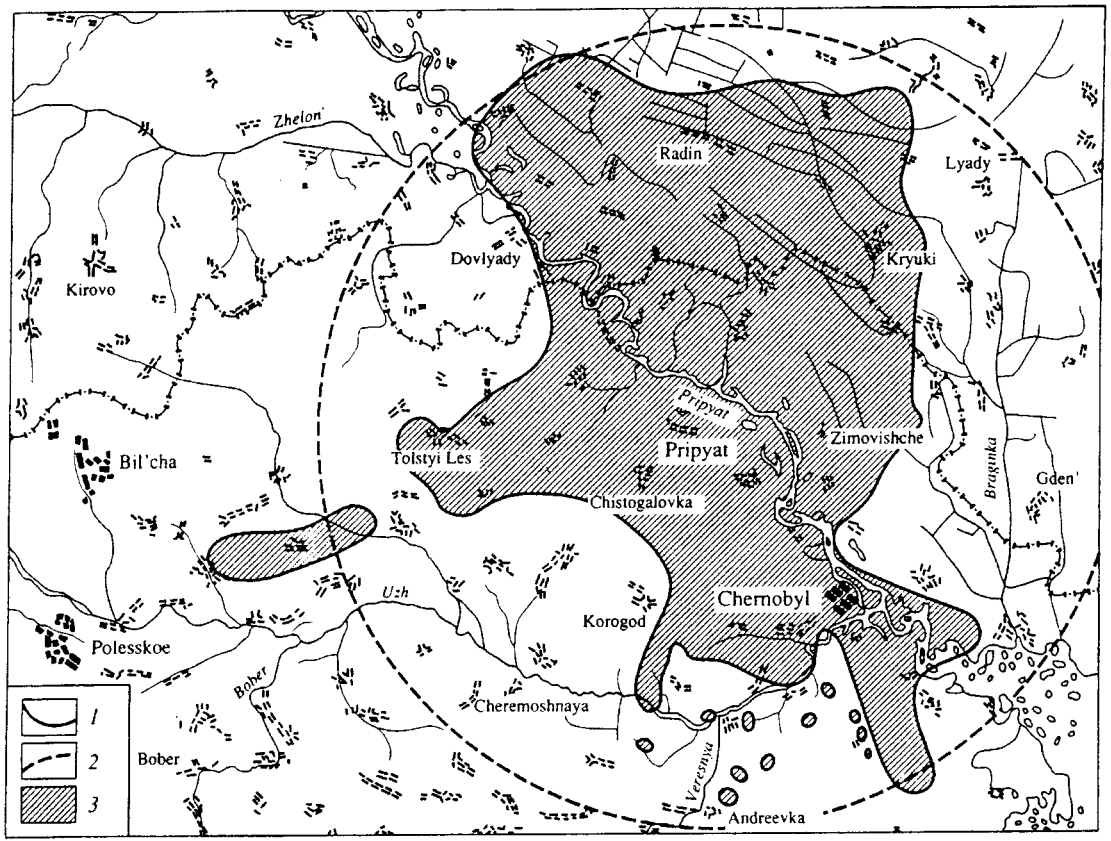

Fig. 5.16. $^{239+240}$Pu terrestrial contamination density, December 1989. 1 — isoline 0.1 Ci/km^2 (3.7 GBq/km^2); 2 — the 30-km zone boundary; 3 — the zone with contamination levels above 0.1 Ci/km^2.

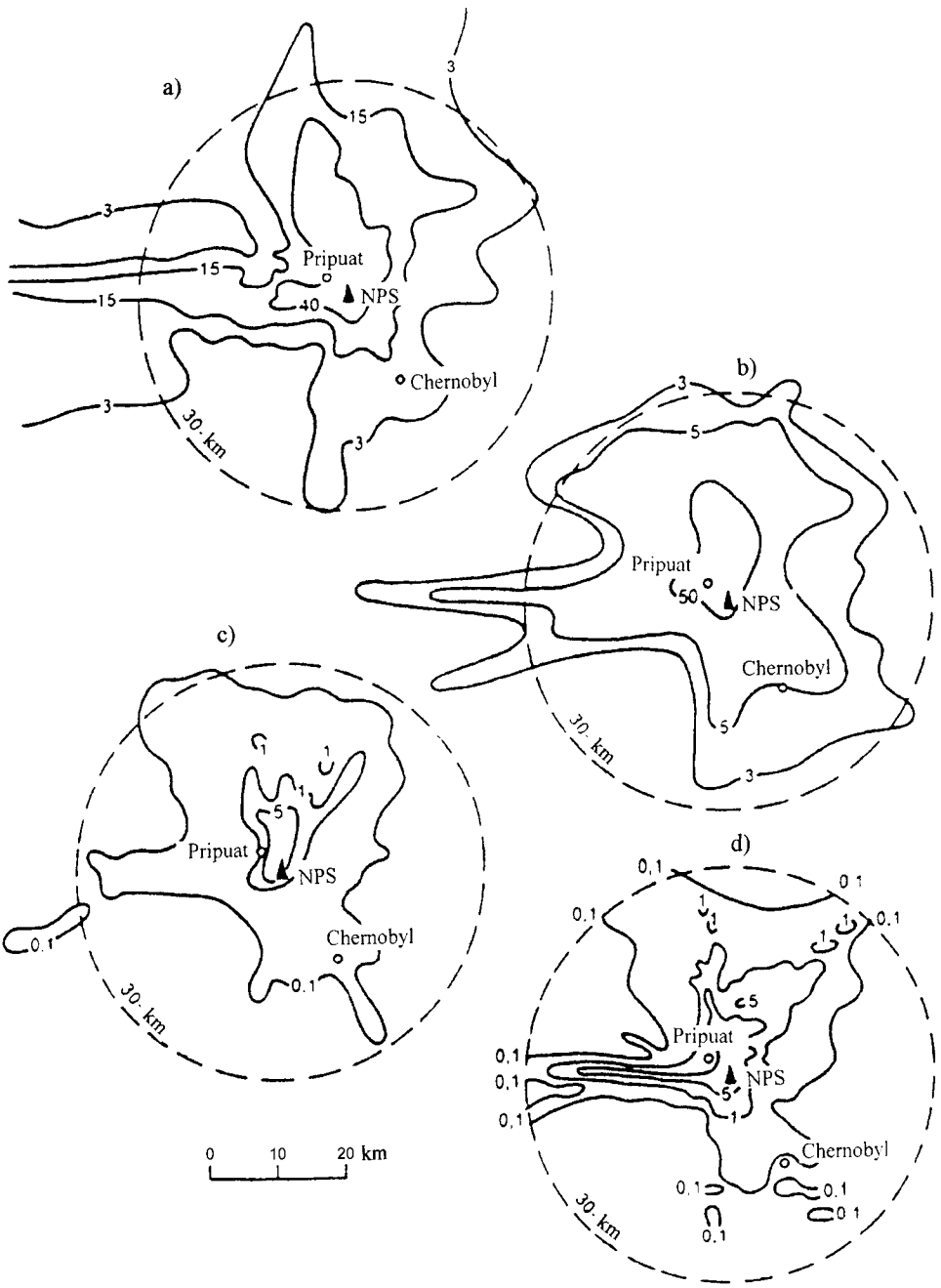

Fig. 5.17. Radioactive contamination (Ci/km^2) of the surrounding land by (a) ^{106}Ru, (b) ^{90}Sr and (c) $^{239+240}$Pu in the Chernobyl close-in zone from data from the reference network; also showing the calculated map of the contamination by $^{239+240}$Pu constructed from data on ^{144}Ce contamination (d) (1 Ci/km^2 = 37 GBq/km^2). (a), (b) — 1989; (c), (d) — 1990.

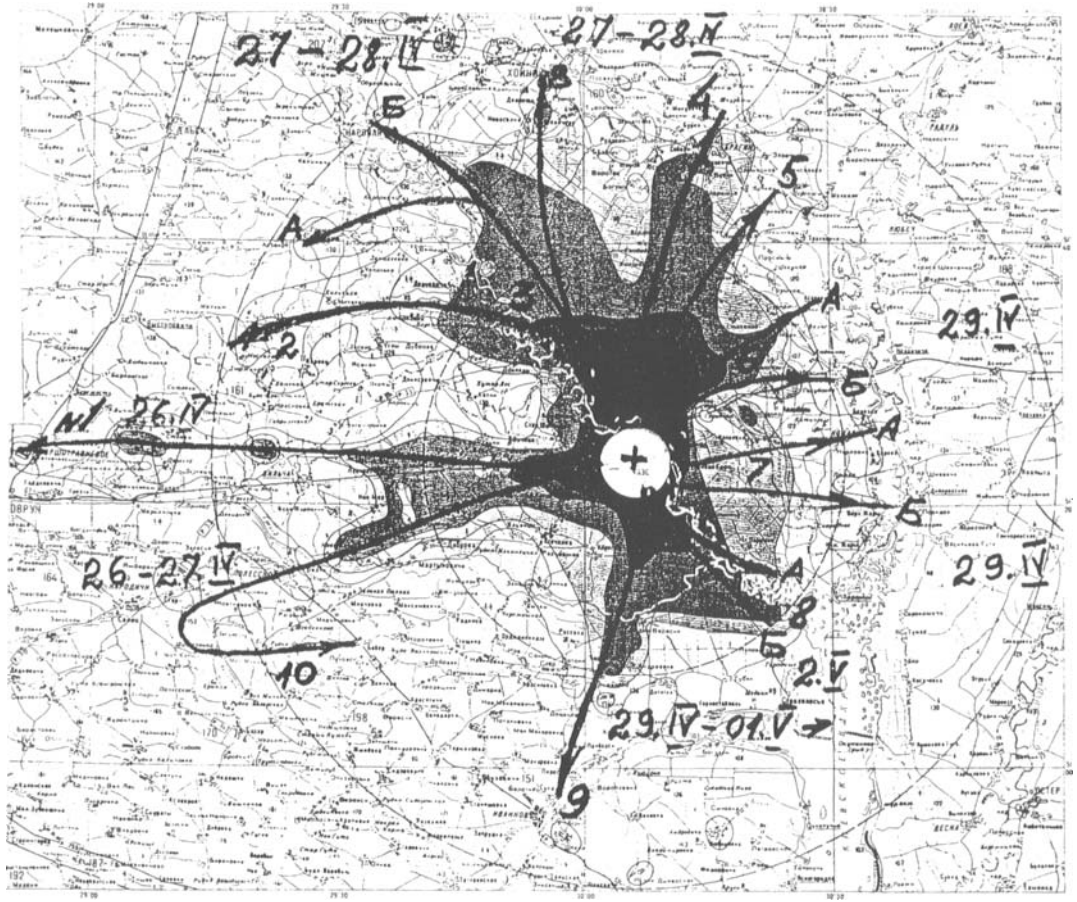

Fig. 5.18. Schematic map of radioactivity patterns in the 60-km close-in zone after the Chernobyl accident. Dates of pattern formation and outlines of the land contamination by ^{90}Sr are shown (black is > 3 Ci/km^2).

Table 5.7
Areas (km^2) within regions and republics of Russia with ^{137}Cs contamination levels above 1 Ci/km^2 (37 GBq/km^2), December 1993

Region/Republic	Area of region/republic (thousands of km^2)	Contamination level (Ci/km^2)			
		1–5	5–15	15–40	>40
Belgorod	27.1	1620	–	–	–
Bryansk	34.9	6750	2628	2130	310
Voronezh	52.4	1320	–	–	–
Kaluga	29.9	3500	1419	–	–
Kursk	29.8	1220	–	–	–
Lipetsk	24.1	1619	–	–	–
Leningrad	85.9	850	–	–	–
Nizhegorod	74.8	250	–	–	–
Orlov	24.7	8840	132	–	–
Penza	43.2	4130	–	–	–
Ryazan	39.6	5320	–	–	–
Saratov	100.2	150	–	–	–
Smolensk	49.8	100	–	–	–
Tambov	34.3	510	–	–	–
Tula	25.7	10320	1271	–	–
Ulyanov	37.3	1100	–	–	–
Mordovy	26.2	1900	–	–	–
Tatarstan	68.0	110	–	–	–
Chuvashy	18.0	80	–	–	–
Total		49760	5450	2130	310

1 $Ci/km^2 = 37$ GBq/km^2.

after the Chernobyl accident" (De Cort et al., 1998), the amounts of Chernobyl ^{137}Cs that were deposited in 1986 on the territories of individual countries (in PBq) were as follows: Russia—19.9, Belarus—15.0, Ukraine—12.0, Sweden—2.9, Austria—1.6, Finland—3.1, Norway—2.0, Estonia—0.05, Latvia—0.055, Lithuania—0.24, Moldova—0.34 (the aggregate total on the former USSR was 47.6 PBq or 1.29 MCi, see Table 5.7). These data, shown in Table 5.8 in the "Corrected data" column, are more accurate than the information obtained in the first year after the accident (Hohenemser and Renn, 1988).

The above data allowed accurate calculations to be made of the doses received by the population living in the contaminated zones and to take the necessary remedial actions during the initial phase after the accident and in the years that followed.

5. Analysis and Reconstruction of the Source of Radioactivity Release from the Chernobyl Accident

Data relating to the sources of the radioactivity released by nuclear explosions and accidents (e.g., source height, radioactivity amount, dynamics of radioactivity release) are needed to estimate the total scale of the resulting contamination. Meteorological information is also required for the preparation of forecasts of the radiological situation

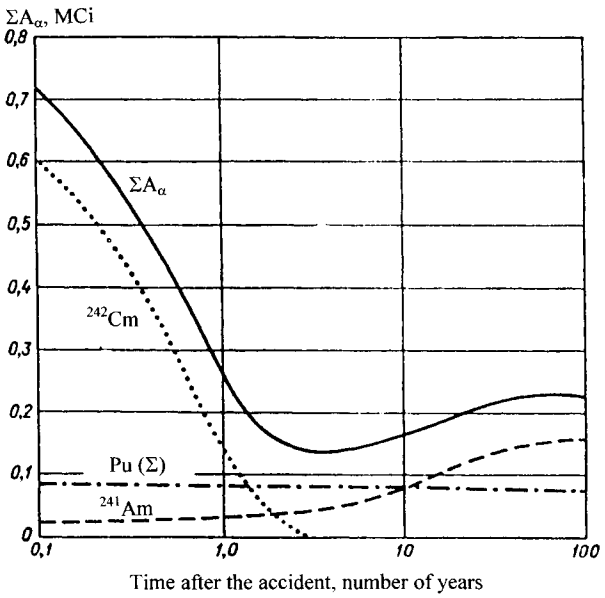

Fig. 5.19. Temporal variation of the total alpha-activity of the Chernobyl radionuclides (1 MCi = 37 PBq).

(i.e., the concentrations and density of contamination by specific radionuclides) both in the atmosphere and on the ground. As to underground nuclear explosions and atomic accidents, when the radioactivity can be released to the environment over a long period of time, information on the dynamics of release (e.g., of the total amounts and the particular radionuclides) as a function of time is of exceptional importance. It is especially important in the case of atomic accidents because the quantity of radioactivity released and its distribution with time are practically unknown during the initial stages and must be reconstructed mainly through a "reverse" approach, i.e., by integration of the amounts of radioactivity on the surface (and, to some degree, in the atmosphere) and taking the meteorological conditions into consideration. It is important to emphasize that information on the temporal distribution of the radioactivity released into the environment and on the typical features of transport for each radionuclide i (i.e., the function $q_i(t)$) are essential for the proper estimation of the external and internal dose rates to populations of humans and other living organisms in the aftermath of an atomic accident.

The total release of an individual ith radionuclide or the sum of all the radionuclides can be written as:

$$Q_\Sigma(t_\Phi) = \sum_i \int_{t_0}^{\infty} q_i(t) f(t_\Phi, t)\, \mathrm{d}t, \tag{5.4}$$

where $f(t_\Phi, t)$, the "recalculation" coefficient of radioactivity for the i-radionuclide from time t to some fixed time t_Φ, is the most important physical characteristic of the total scale of the accident. It does not, however, solve the problems concerning the real radiation

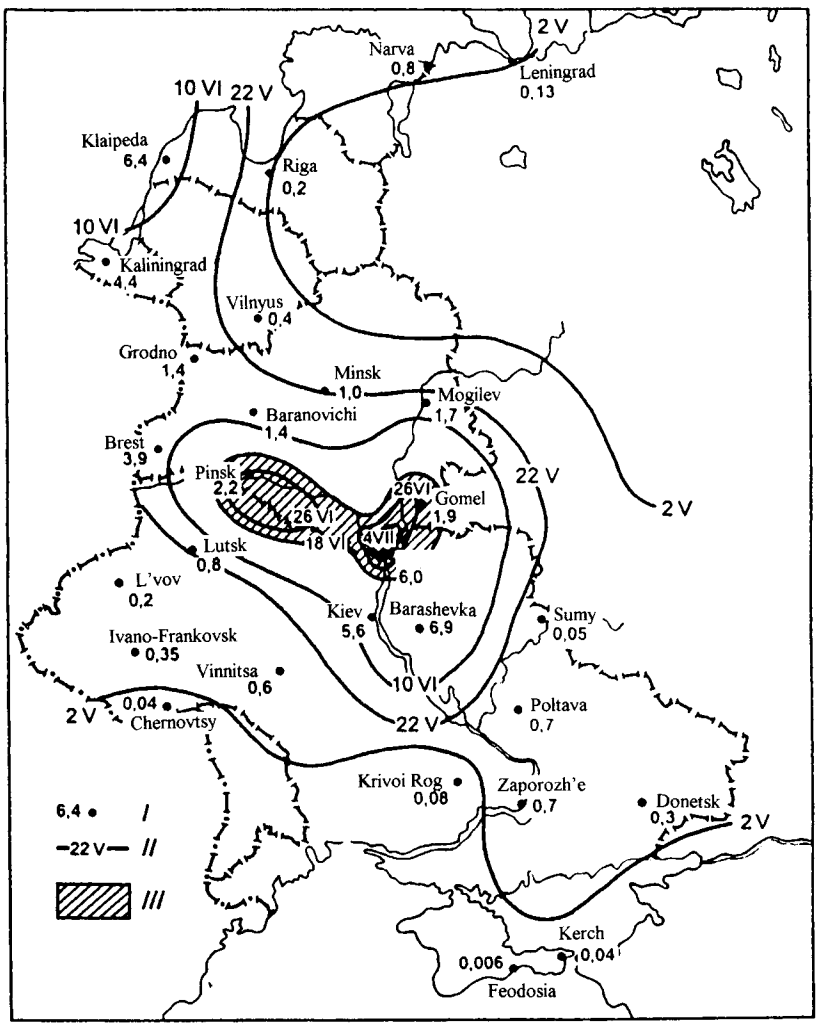

Fig. 5.20. Map of the terrestrial contamination by ^{131}I: I — ^{131}I content on 2 May, 1986; II — isolines showing the dates after which ^{131}I contamination would not exceed the 3.7 GBq/km^2 (0.1 Ci/km^2) level; III — the zone where ^{131}I content exceeded 370 GBq/km^2 (10 Ci/km^2) on 2 May, 1986.

situation and potential danger that may exist. A single and unique value for the total release $Q_\Sigma(t_\Phi)$ is not too informative or sufficiently practical when the actual situation is more complicated. Which time t_Φ should be taken for calculation of the total release if a considerable fraction of the total output is being released over a long period of time? Recalculation to $t = 0$ could produce overestimates. An analogous disadvantage, from the point of view of both overestimation and underestimation of the release, is inherent in the choice of any other particular time for the reconstruction. In addition, the distribution of

Table 5.8
^{137}Cs deposition (PBq) on individual countries after the Chernobyl accident of 1986

Country	Initial data (1988)*	Corrected data (1998)‡
Austria	1.10	1.6
Albania	0.39	
Belgium	0.019	0.01
Bulgaria	2.70	
Hungary	0.79	0.37
East Germany (GDR)	0.58	0.9
Greece	0.44	0.95
Denmark	0.05	0.087
Israel	0.005	
Ireland	0.25	0.35
Spain	0	
Italy	1.10	0.93
Canada	0.25	
China	0.54	
Kuwait	0.001	
Luxembourg	0.004	0.08
Netherlands	0.068	0.062
Norway	1.10	2.5
Poland	9.2	1.2
Romania	6.7	2.1
Great Britain	0.44	0.88
United States of America	0.28	
Turkey	1.80	1.0
West Germany (FRG)	1.60	1.0
Finland	1.90	3.8
France	0.83	0.93
Czechoslovakia	0.59	0.92
Switzerland	0.20	0.36
Sweden	3.4	3.5
Yugoslavia	6.1	
Japan	0.026	

*Hohenemser & Renn (1988).
‡De Cort et al. (1998) (Yu. A. Izrael, Scientific Direction).
1 PBq $\approx$ 27 kCi.

certain portions of the release can always take place in different geographical directions, e.g., if a share α of the release spreads southwards, then a $(1 - \alpha)$ share would not be included in the estimates of the radiation situation in this southerly zone, no matter what time was selected for the calculation.

Thus the total radioactivity release, its structure and composition should be estimated using a spectrum of characteristics that will provide maximum information on the:

- scale and character of the accident,
- potential hazard of the radioactive release for the human population and biota, and
- real hazard of the release.

To estimate the *real* hazard posed to the population and ecological systems, data are required, not only on the character and distribution of the products released but also on the spatial and temporal distributions of all the elements that are vulnerable to exposure, as well as data on the toxicity of the radiation, on the one hand, and the vulnerability of the exposed element (i.e., primarily man), on the other. In the case of abiotic components of the biosphere, we refer to the problems raised by their presence for the transport of the radioactivity and its effects on living organisms over long periods of time. To estimate the real danger of this factor, one can use the concept of ecological damage detection (Izrael, 1984). If we consider the effects on the biotic components of the biosphere, it will be apparent that the ecological damage will depend on the nature of the dose, the intensity of the radiation, the effects under consideration and the number and type of organisms exposed. It is valid to state that the magnitude of the effect upon a living component of the biosphere depends on the intensity of the factor that is influencing the biosphere (e.g., the concentration of a contaminating substance, the radiation intensity), the kind of biologically harmful influence ε (e.g., toxicity for the given population or ecosystem), whether it is a linear or non-linear effect, the quantity of organisms N_{nm} in the affected m-population of the n-ecosystem and the sensitivity K_m of the m-population in the ecosystem to the given effect. One should take into account the synergistic effects of all factors in the different environments.

In turn, the intensity of effect for any factor that varies in space and time (e.g., concentration of a contaminating substance and its toxicity $I_{il}(\mathbf{R}, t)$) is a function of the source $Q_i(R, t)$ and will depend on dissipation and transport, i.e., the hydrometeorological or physical characteristics of the environment. Thus

$$I_{il}(\mathbf{R}, t) = F(Q_i, v_{\mathbf{R}}, w_{\mathbf{R}}, v_Z, \ldots), \tag{5.5}$$

where v_R, w_R, v_Z are the wind speed, turbulent diffusion coefficient and gravitational deposition velocity, respectively.

In turn,

$$Q_i(\mathbf{R}, t) = \sum_j q_{ij}(\mathbf{R}, t), \tag{5.6}$$

where q_{ij} is the amount of the ith substance, released by individual j-sources. The $I_i(R)$ distribution essentially depends on the spatial distribution of the sources.

Estimating the degree of influence, it is suggested that the mechanisms involved in the transformation of the given i-class ingredient into another $(i + 1)$-class are well-known, as well as the changes involved in moving from one environment to another $(l \to l + 1)$:

$$I_{i+1,l} = \omega_i(t) I_{il}, \tag{5.7}$$

$$I_{i,1+1} = \mu_l(t) I_{il}, \tag{5.8}$$

where ω_i and μ_l are coefficients for the transformations and/or changes.

So the degree of influence A_n can be written in a general way for the n-ecosystem in a certain region

$$A_n = \int_{\mathbf{R}} \int_t \sum_m \sum_i \sum_l I_{il}(\mathbf{R}, t)\omega_i(t)\mu_l(t)C_{ilm}\varepsilon_{ilm}N_m K_m v_{i,l+k}\xi_{m,m+k}\,\mathrm{d}\mathbf{R}\,\mathrm{d}t, \tag{5.9}$$

where $v_{i,l+k}$ characterizes the effect of cumulative factors of the ith and $(i+k)$th (and any other) ingredient; $\xi_{m,m+k}$ is a coefficient which takes into account the cumulative influence upon the mth, $(m+k)$th (and any other) population of the given ecosystem; C_{ilm} is a geometric factor that takes into consideration the I-influence upon the given organism (a biosphere element) that is distributed in space and time. This factor takes into account the ratio between the distribution of the ith substance's concentration in the environment and the organisms of the mth population.

If A_n is estimated in absolute terms for the ecological damage to a given ecosystem, a coefficient K_m will be added to the equation that characterizes the significance (in some cases this could be the sensitivity or criticality) of the mth population in the given ecosystem, with $0 \leqslant K_m \leqslant 1$. When $K_m = 0$, this population is not significant for the ecosystem and can therefore be missed or replaced by another. In unique ecosystems, $K_m > 0$ for any population. K_m is equal to 1 for the most significant population (for example, humans).

Thus, the procedure that ranks the effects of specific accidental releases includes the following.

1. The general geometrical factors relating to the threat to the population and biota:
   - in a thick atmospheric layer (at height of release h[1]),
   - in the surface atmosphere,
   - terrestrial contamination (taking account of migration),
   - contamination of water bodies.
2. Factors relating to real contact:
   - with people and the biosphere—the need to know the spatial distribution of radionuclides and the affected organisms and their vulnerabilities (these can be different even for certain individuals of the same population, e.g., for man).
3. Factors relating to the duration and danger of the effect:
   - the radionuclide's half-life,
   - energy-release per decay and the type of nuclear radiation,
   - dissipation in the atmosphere,
   - migration in the aqueous environment,
   - migration in soil and biota,
   - coefficients of transition into other dangerous compounds and those of migration/transport to other natural environments.

[1] According to some data, h reached 3–7.5 km from Chernobyl.

The characteristic of the radioactive release from the accident is important but supplementary information is required to estimate the radiation situation beyond the reactor. Direct data on the radiation situation and radionuclide contamination must be known and can be obtained by direct measurements at specific sites. A decision has to be made as to which area is to be considered, viz. beyond the zone of the destroyed reactor; those zones beyond the protective cap of the NPS building, beyond the station site, the sanitary protective zone, etc.

As an example, it is noted that the radioactivity found beyond the destroyed body of the reactor from the accident at the Three-Mile-Island (TMI) station in the U.S. was (according to some data) larger than that from the Chernobyl NPS accident. However, the radioactivity found beyond the protective cap from the TMI accident was many orders of magnitude less than the radioactivity found beyond the Chernobyl NPS building.

So, let us examine the different possibilities to arrive at an estimate of the total or relative release of radioactivity from the Chernobyl accident, the accuracy of the data obtained as well as the scope and efficiency of their use. In calculations of the release/contamination, all aspects are examined in a traditional sense; correct units expressing the release (Bq, Ci); the time to which the release is normalized (the initial time, May 6, 1986, when the release from the destroyed reactor practically ended); the average radiation amounts and how they were determined; when summations are made, each part is corrected to the time of the release; the contribution of individual nuclides to the radiation dose; the amounts of radioactivity deposited in different directions, etc.

At present, there are many different estimates of both the total amount of radioactivity accumulated in the reactor at the time of the accident and the fraction of the activity released beyond the reactor (Abagyan et al., 1986a & b; Sivintsev and Khrulev, 1995; Izrael and Stukin, 1995; Sich, 1994; Bolsunovsky, 1995; Devell et al., 1996). Soviet experts carried out the first estimate of the radioactivity that escaped from the destroyed reactor and presented it to the international community via the IAEA (Abagyan et al., 1986a & b; Sivintsev and Khrulev, 1995) (see Tables 5.9 and 5.10). The latter authors, in turn, used three different approaches to answer this equation:

- estimates based on measurements of radiation levels (gamma) near the NPS;
- forecasts of the accidental release dynamics using a model of decay product release from the annealing of irradiated fuel, in particular, uranium–graphite fuel-rods;
- calculation of the fraction of released radionuclides and fuel from systematic measurements of exposure dose rates and the composition of radiation spectra at the surface.

Analyzing the initial information on the radiation situation, the data obtained before May 6, 1986 were considered the most reliable. Unfortunately, we need to note that, in the work of Sivintsev and Khrulev (1995), the authors did not use enough detailed data on the γ-radiation dose rate measurements (these specialists did not use the detailed maps of Roshydromet or their γ-spectrometric results). The meteorological situation was also not taken into account, as required, when the analysis was conducted. As a result, all of these approaches could lead to certain errors in estimations of the release from the reactor.

Table 5.9
Daily release, Q, of radioactive products into the atmosphere from the accident (excluding radioactive noble gases)*

Date	Time after the accident (days)	Q (MCi)‡
April		
26	0	12
27	1	4.0
28	2	3.4
29	3	2.6
30	4	2.0
May		
1	5	2.0
2	6	4.0
3	7	5.0
4	8	7.0
5	9	8.0
6	10	0.1
9	14	~ 0.01
23	28	20×10^{-6}

*Here and in Table 5.15, the error on the release estimate is ±50%. It is contributed to by errors in dosimetry (health monitoring instruments), radiometric measurements of the radionuclide composition of air and soil samples, as well as in averaging depositions over a large area.
‡Q values are normalized to 6 May 1986, taking into account radioactive decay. At the moment of the release on 26 April 1986, the activity was 20–22 MCi (740–814 PBq). The composition of the release is shown in Table 5.15. (1 MCi = 37 PBq).

In Sivintsev and Khrulev (1995), the activity on the lth day was calculated according to the relationship

$$Q = \sum_l \sum_m K_{ml} P_{ml} S_{ml},$$

where K_{ml} is the coefficient for the relationship between the exposure dose rate and activity concentration in the mth region (Ci km^{-2}/(R · hr)), P_{ml} is the mean exposure dose rate measured in the mth region (R/hr) and S_{ml} is the area of the region (km^2) with a mean exposure dose rate of P_{ml}.

The rate of deposition of the radionuclide release R (Ci/day) was estimated from the cumulative daily values, calculated from the relationship $R = Q_l - Q_{l-1}$, where Q_l, Q_{l-1} are the total activities of deposition for the lth day after the accident and for the previous $(l-1)$ day.

To estimate the amount of fuel and plutonium that escaped, the experimental data for the less volatile radionuclides (^{141}Ce, ^{144}Ce) in surface deposition samples were used, together with the calculated data on the cumulative amount of Pu in the reactor (as presented by E.V. Burlakov in July, 1986)—see Table 5.11.

Table 5.10
Estimation of the radionuclide composition of the release from the Chernobyl NPS accident

Nuclide*	Released activity (MCi)		% activity released from the reactor by 6 May, 1986 (%)
	26 April, 1986	6 May, 1986‡	
^{133}Xe	5	45	Possibly $\leqslant 100$
^{85m}Kr	0.15	–	Possibly $\leqslant 100$
^{85}Kr	–	0.9	Possibly $\leqslant 100$
^{131}I	4.5	7.3	20
^{132}Te	4	1.3	15
^{134}Cs	0.15	0.5	10
^{137}Cs	0.3	1.0	13
^{99}Mo	0.45	3.0	2.3
^{95}Zr	0.45	3.8	3.2
^{103}Ru	0.6	3.2	2.9
^{106}Ru	0.2	1.6	2.9
^{140}Ba	0.5	4.3	5.6
^{141}Ce	0.4	2.8	2.3
^{144}Ce	0.45	2.4	2.8
^{89}Sr	0.25	2.2	4.0
^{90}Sr	0.015	0.22	4.0
^{238}Pu	0.1×10^{-3}	0.8×10^{-3}	3.0
^{239}Pu	0.1×10^{-3}	0.7×10^{-3}	3.0
^{240}Pu	0.2×10^{-3}	1×10^{-3}	3.0
^{241}Pu	0.02	0.14	3.0
^{242}Pu	0.3×10^{-6}	2×10^{-6}	3.0
^{212}Cm	0.3×10^{-2}	2.1×10^{-2}	3.0
^{239}Np	2.7	1.2	3.2

*Data on the activities of the main radionuclides were obtained from radiometric analysis.
‡Total release up to 6 May 1986. 1 MCi = 37 PBq.

Table 5.11
Relative contribution of Pu-isotopes to alpha-activity

Degree of burn-up (mW·day/kg)	^{239}Pu	^{240}Pu	^{241}Pu	^{238}Pu	Activity (Ci)*	$\sum A_\alpha / A_{^{144}Ce}$
10.3	0.29	0.38	2×10^{-3}	0.32	8.5×10^4	10^{-3}

*1 MCi = 37 PBq.

Inasmuch as reactors of the Chernobyl type (RBMK—pressure tube reactors) use a continuous overcharge of fuel, the heat-producing rods (HPR) located within it are subject to burn-up and wide differences between individual radionuclides can be observed in measured samples. Generally, for the releases from the reactor, the radionuclide concentration was averaged and taken to be the composition typical of the mean production (10.3 MW/kg when operated over 640 days). The expected chemical forms and characteristic features of the process of fission product release from the overheated nuclear fuel were included in the considerations. In particular, volatile fission products

prevail in samples when $T \approx 2300$ K and at $T > 2300$–2400 K and the ratio between radionuclides becomes closer to those typical of fuel with common characteristics. An important consideration is that the release of fuel particles might occur. In addition to U and Pu, these could contain less volatile elements such as Ce. Thus, along with the extremely laborious measurements of Pu α-activity in samples, the data on Ce gamma-activity were used to assess the amount of Pu in the samples up to July 1986. The ratio between Pu alpha-activity and ^{144}Ce gamma-activity was assumed to be equal to 9×10^{-4} (close to 10^{-3}, see Table 5.11) in fuel of average composition.

From the results of specially designed experiments, the following observations were made with respect to element volatility and temperature T:

(i) Xe and Kr were the most volatile radioactive inert gases.
(ii) I and Te were volatile over almost the whole temperature range that typified the accident, i.e., at $T > 100$–200 °C.
(iii) Cs was volatile at $T > 800$–1000 °C. With increase in temperature, its volatility became closer to those of I and the radioactive inert gases.
(iv) Ba and Sr are elements with volatility close to, but less than, Cs (Ba is more volatile than Sr). Other elements are volatile at $T > 1700$ °C (the least volatile were Ce, Zr and Nb).
(v) Pu volatility is higher than U (insignificantly) but lower than Ce.

It was found that the first phase of the accident was characterized by an abundance of ^{131}I and a value of the coupling coefficient $K_{ml} = (1\ \text{R/hr})/(10^5\ \text{Ci/km}^2)$ while, at the end of the period under consideration, $K_{ml} = (1\ \text{R/hr})/(2 \times 10^5\ \text{Ci/km}^2)$. It was shown that the coefficient $K_\gamma(E_i) = 5.5 \times 10^5\ (\text{MeV/(s cm}^2))/(\text{R/hr})$ over the energy range $0.1\ \text{MeV} < E_i < 2\ \text{MeV}$.

Values of the fractionation factors K_f that characterize the relative enrichment or depletion of a particular radionuclide measured in a given sample compared to its mean content in the core were also used as one of the more important quantitative parameters. The following findings of primary importance became evident from the first experimental data and their interpretation:

(i) During the first stage explosion, the release of fuel heated to high temperatures took place in the solid phase, almost without UO_2 melting.
(ii) A significant share of volatile radionuclides means that the fuel release was comparatively insignificant.
(iii) During the third stage (May 5–10, 1986), repeated major releases of radioactivity were detected that were in accordance with the rate of heating of the damaged reactor (5–10 °C/hr). Predictions for iodine releases, carried out on May 1, were compared to the *in-situ* measurement results (Fig. 5.21). The radiation situation near the NPS was estimated from maps compiled by civil defense staff (some uncertainty could arise from these maps).

Table 5.12 presents a summary of the data on the activity releases and the fission product distributions at the site of the accident and beyond the limits of the power station during the first and late third stages.

Figure 5.22 shows the detailed daily release of radioactivity to the atmosphere (Sivintsev and Khrulev, 1995). It was proposed that further releases after May 6, 1986 caused by the

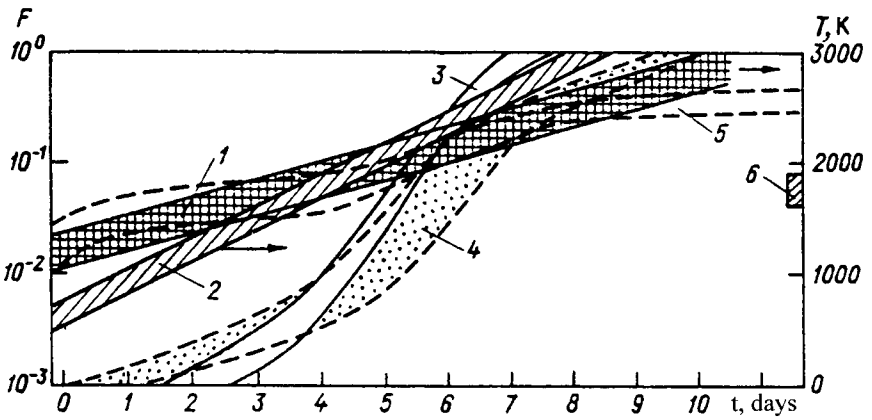

Fig. 5.21. Prediction of the iodine release compared to that actually recorded on April 26, 1986 (Sivintsev and Khrulev, 1995). 1, 2 — the rate of fuel heating, equal to 5 and 10 °C/hr, respectively; 3, 4 — the calculated release at heating rates of 5 and 10 °C/hr, respectively; 5 — the release from the reactor actually measured; 6 — effective fuel-temperature at the moment of explosion.

heating of construction materials by the fission products deposited on their surfaces did not result in much change in the total radiation situation on the ground (excluding the very local situation near to the NPS).

As a result of the investigations carried out by Yu.V. Sivintsev, A.A. Khrulev and O.Ya. Shakh, it was concluded that the total quantity of radioactivity released by the destroyed reactor (normalized to May 6, 1986) was 1.85 EBq (50 MCi) (or 3.5% of the accumulated activity). The very first estimate was made on May 20, 1986 by the author (see Izrael, 1996). This result practically coincides with the data obtained independently from a series of experiments and calculations (Izrael et al., 1990) (see below). V.A. Vetrov calculated the initial values of the ith radionuclide production in the destroyed reactor and the portion of the main nuclides released from the reactor using measurement data (Abagyan et al., 1986; Izrael et al., 1987; 1990) (see Table 5.13).

The values for the released radionuclides were calculated from direct measurement data for the total activity of the ith radionuclide in the radioactive products that escaped from the reactor during the first 10–12 days after the accident. These data were referred to calculated values of production Y_i.

Data on the radionuclide composition of deposition in the close-in zone (up to 10–20 km from the source), as obtained by direct measurement (IAEA, 1986; Izrael et al., 1987), were used in the analysis. It allowed us to make a very reliable and practical estimate of the ratios between the activities of the radionuclides and those of the most refractory elements (^{95}Zr or ^{144}Ce—A_i/A_{95} or A_i/A_{144}). The ratios $(A_i/A_{95})_0$ (see Table 5.13) were obtained from direct measurements of the radioactive deposition (the upper soil layer) in the close-in zone around the CNPS within a radius of 10–20 km from the source. It was assumed that fractionation effects manifested themselves relatively weakly in the close-in zone and that the $(A_i/A_{95})_0$ ratios were close to those at production Y_i/Y_{95}. Production parameters calculated in this way for each radionuclide are presented in Abagyan et al. (1986). The ratios obtained for Y_i/Y_{95} correspond best to the sum of the experimental and calculated

Table 5.12
Released activity and fission product distribution inside and outside the accident power unit at the first (26 April) and late third (6 May) stages, 1986 (Sivintsev & Khrulev, 1995)

Radionuclide	Released activity		Radionuclide activity						
			Inside the unit				Total (%)	Outside the unit	
			In fuel		In dump and constructions				
	Absolute (MCi)	Relative* (%)	Absolute (MCi)	Relative* (%)	Absolute (MCi)	Relative* (%)		Absolute (MCi)	Relative* (%)
	1st stage				End of 3rd stage				
Radioactive noble gases	10	<3	9	<20	1	2–3	<20	36	<80
Including:									
^{133}Xe	5	<4	9	<20	1	2–3	<20	35	<80
^{85m}Kr	0.15	1.5	–	–	–	–	–	–	<80
^{85}Kr	–	–	0.2	<20	0.015	2–3	<20	0.7	<80
Volatile fission products (excluding radiocaesium)	15	<2	<20	<20	<63	<63	83	17	17
Including:									
^{131}I	4.5	5	7.3	<20	22	<60	80	7.3	20
^{132}Te	4	4	2.4	<20	7.8	<65	85	1.8	15
Radiocaesium	1	1	4.6	<20	16	<70	90	2.3	10
Including:									
^{134}Cs	0.15	1	1	<20	3.5	<70	90	0.5	10
^{136}Cs			2.0	<20	7.2	<72	92	0.8	8
^{137}Cs	0.3	1	1.6	<20	5.4	<67	87	1.0	13
Refractory fission products	8–10	0.3–0.4	300–600	20–40	800–1100	57–78	<97	30	2–3
Including:									
^{90}Sr	0.016–0.02	0.3–0.4	1–1.5	20–30	3.7–4.2	66–76	<96	0.2	4
Actinides	0.25–0.3	0.3–0.4	70	<80	15–16	17–18	97–98	1.7–2.5	2–3

*The radionuclide activity in the RBMK on 26 April, 1986 was taken as 100%. 1 MCi = 37 PBq.

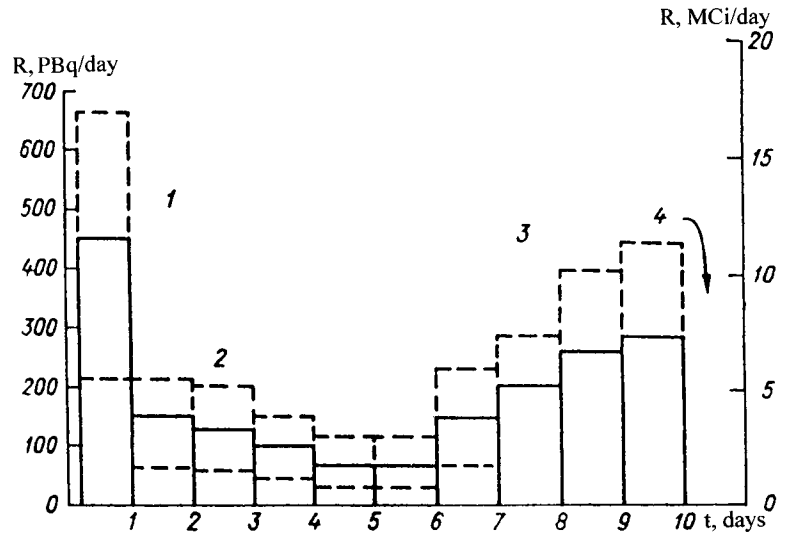

Fig. 5.22. Radionuclide release from the damaged unit of the NPS (Sivintsev and Khrulev, 1995). 1 — initial release; 2, 3 — periods of cooling and heating, respectively; 4 — sharp decline; the uncertainty range is shown by the dashed line.

Table 5.13
Parameters of the source of fission product release during the Chernobyl NPS accident

Radionuclide	$T_{1/2}$	Field measurements $(A_i/A_{95})_0$	Information for IAEA, 1986 (Abagyan et al., 1986a,b)				Adopted parameters	
			ΔA_{0i}* (MCi)	δ_i (%)	Y_i (MCi)	Y_i/Y_{95}	Y_i (MCi)	Y_i/Y_{95}
^{239}Np	2.35 days	10	23	3.2	720	5.5	1300	10
^{99}Mo	2.73 days	0.9	3.7	2.3	160	1.2	130	1.0
^{132}Te	3.27 days	1.1	11	15	73	0.56	120	0.9
^{131}I	8.04 days	0.8	17	20	85	0.65	90	0.7
^{140}Ba	12.6 days	1.0	7.3	5.6	130	1.0	130	1.0
^{141}Ce	32.5 days	1.0	3.5	2.3	150	1.2	130	1.0
^{103}Ru	39 days	1.0	3.8	2.9	130	1.0	130	1.0
^{89}Sr	51 days	0.3	2.5	4.0	62	0.48	52	0.4
^{91}Y	58.5 days	0.3					40	0.3
^{95}Zr	64 days	1.0	4.1	3.2	130	1.0	130	1.0
^{110m}Ag	250 days	0.001					0.13	0.001
^{144}Ce	284 days	0.7	2.4	2.8	86	0.66	90	0.7
^{106}Ru	368 days	0.4	1.6	2.9	55	0.42	52	0.4
^{134}Cs	2.07 years	0.03	0.5	10	5.0	0.04	4.0	0.03
^{125}Sb	2.7 years	0.004					0.5	0.004
^{90}Sr	28.5 years	0.03	0.22	4.0	5.5	0.04	5.2	0.04
^{137}Cs	30.2 years	0.05	1.0	13	7.7	0.06	7.2	0.055

*The total release of the ith radionuclide normalized from the ΔA_i value (for D + 10) to the moment of the accident. 1 MCi = 37 PBq.

Table 5.14
Characteristics of the source of the main transuranic elements in Unit IV of the Chernobyl NPS at the moment of the accident

Radionuclide	$T_{1/2}$	ΔA_{0i} (kCi) (Abagyan et al., 1986)	Y_i (MCi)	Y_i / Y_{144}
^{238}Pu	87.75 years	0.8	0.026	2.9×10^{-4}
^{239}Pu	24380 years	0.7	0.023	2.6×10^{-4}
^{240}Pu	6537 years	1.0	0.033	3.7×10^{-4}
^{241}Pu	14.5 years	140	4.6	5.1×10^{-2}
^{241}Am	432.8 years		0.024* (0.155)‡	2.7×10^{-4} (1.7×10^{-3})
^{242}Cm	163 days	21	0.7	7.8×10^{-3}
^{243}Cm	28.5 years		0.001*	1×10^{-5}
^{244}Cm	18.09 years		0.0026	3×10^{-5}
^{144}Ce	284 days	2400	86	1.0

*Calculation based on the data from Gaziev (1993).
‡ ^{241}Am accumulation resulting from ^{241}Pu decay in 50–70 years after the accident is shown in brackets.
1 kCi = 37 TBq; 1 MCi = 37 PBq.

data (the last column of Table 5.13), the absolute values of production Y_i being calculated by multiplying the accepted parameter Y_i / Y_{95} by the most reliable value for the production of ^{95}Zr, which was 4.81 EBq (130 MCi), as obtained from the data on the total release.

Without going into detail for each radionuclide, it is noted that the experimental ratios for the nuclides were used as additional criteria in arriving at acceptable ratios of production (see Table 5.13), namely: Ce $(A_{141}/A_{144})_0 = 1.4$; Ru $(A_{103}/A_{106})_0 = 2.6$; Cs $(A_{137}/A_{134})_0 = 1.8$ and Sr $(A_{89}/A_{90})_0 = 10$. As expected, these ratios were practically constant in soil, atmospheric aerosol particles, vegetation, etc. taken beyond the limits of the zone of local contamination, i.e., more than 5–10 km from the reactor.

In interpreting the Table 5.13 data, it is advisable to bear in mind that the estimates of the release ΔA_i (and, consequently, δ_i) have an associated uncertainty of ±50% (Abaygan et al., 1986). The data on the production of the long-lived transuranium elements (TUE) in the damaged reactor (Table 5.14) were obtained mainly from the activity values of individual radionuclides A_i in the release and the relative quantities of TUE produced (equal to 3%) (Abaygan et al., 1986).

Also using the data in Abaygan et al. (1986) on the dynamics of product release in reactor accidents, a histogram was compiled (Fig. 5.23, curve B) for the daily release of radioactive products, excluding radioactive noble gases (RNGs). The absolute values were obtained from the data for the source-term, as given for time D + 10 in Abaygan et al. (1986), corrected back to a specific time after the accident using the rate of decay of the sum of fission products and those of nuclear fuel activation (excluding the RNGs) in the pressure tube reactor RBMK-1000 (operating period 1000 days) for 10 days (Fig. 5.23, curve A). The correction factor for the decay was obtained from the accumulated total activity in the environment (Fig. 5.23, curve C) and the summation of the daily releases (taking into account the rate of decay of the sum of the radioactive products).

On D + 10, the sum of all RNGs released into the environment was about 2.22 EBq (60 MCi).

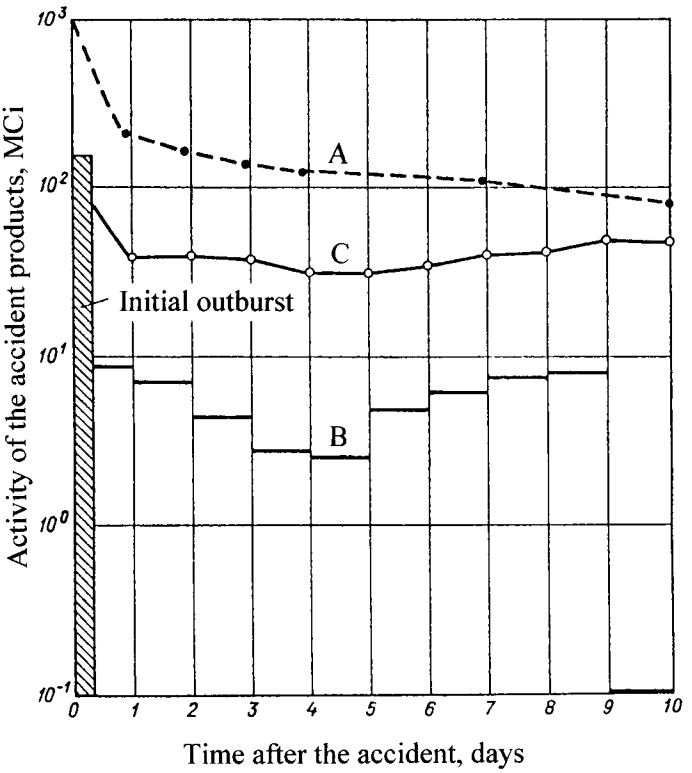

Fig. 5.23. The dynamics of the radioactive product release from the Chernobyl NPS accident (Izrael, 1990). A — total activity of the nuclear fuel of the RBMK-1000 reactor (relative units); B — daily release of fission and activation products (excluding RBG); C — accumulated total activity of accident products in the environment (RBG). 1 MCi = 37 PBq.

Table 5.15
Relative release of radionuclides to the atmosphere

Date	Sum of gamma-emitting products			Radionuclide	
	H = 1000 m	H = 500 m	Average	^{144}Ce	^{137}Cs
April, 1986					
26	0.17	0.17	0.17	0.19	0.1
27	0.29	0.25	0.27	0.28	0.3
28	0.29	0.29	0.29	0.30	0.4
29	0.14	0.15	0.14	0.12	0.18
30	0.11	0.14	0.13	0.11	0.02

The dynamics of the radionuclide release from the damaged reactor, under the changing meteorological conditions (Table 5.15 and Fig. 5.24) were reconstructed after examination of the radioactivity deposited in all directions of the contaminated zones (Izrael et al., 1990;

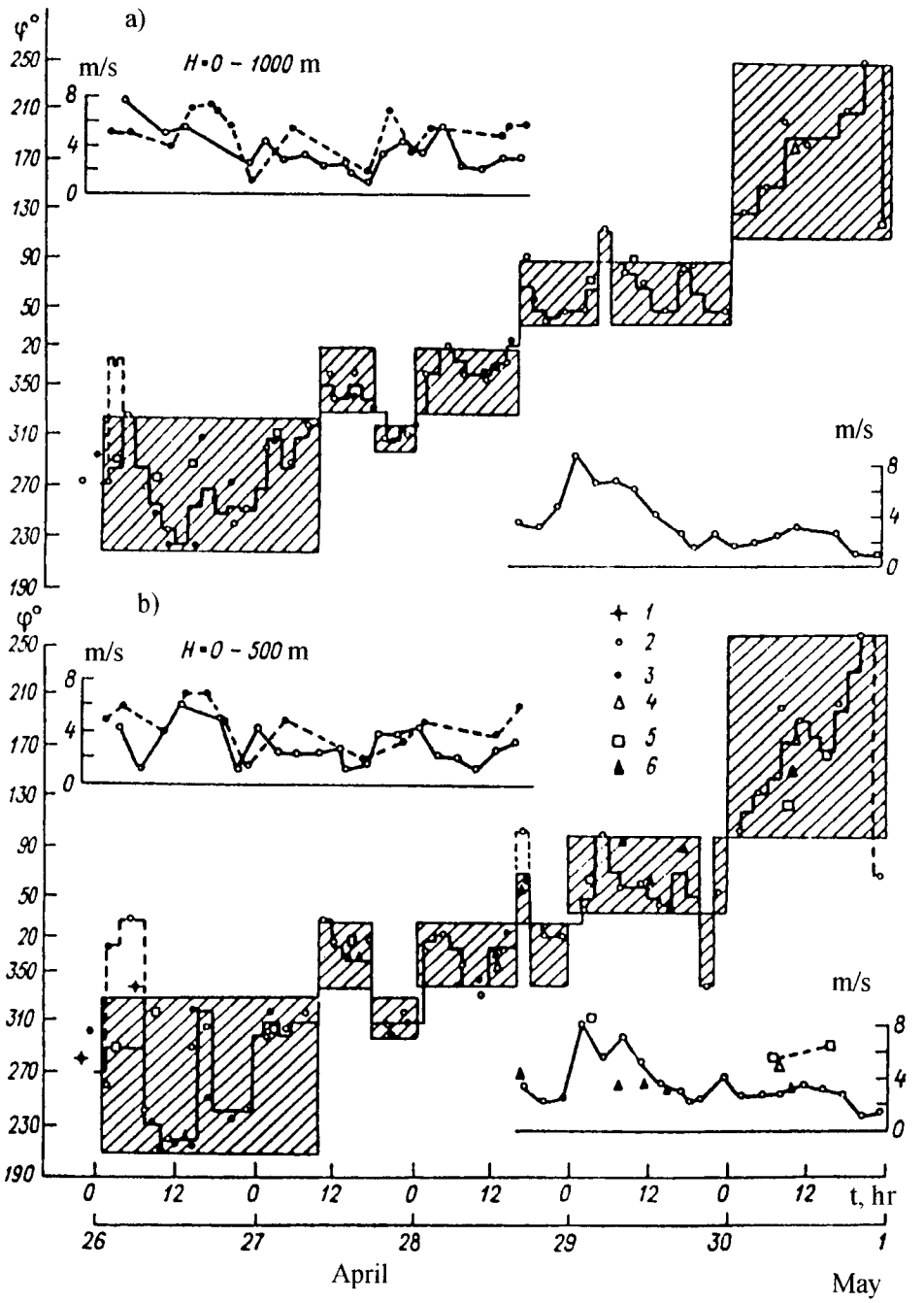

Fig. 5.24. Mean values of wind direction ($\varphi°$) and wind speed from April 26 to May 1, 1986 in the layers at (a) 0–1000 m and (b) 0–500 m in the area adjacent to the Chernobyl NPS. 1 — Kiev (radiosonde); 2 — Kiev (airport); 3 — Borispol; 4 — Mozyr; 5 — Gomel; 6 — Chernigov.

1987a & b; Izrael and Petrov, 1987). The technique for such calculations, which are the basis of modeling the terrestrial contamination in the close-in zone of the Chernobyl accident, is described in detail in Section 5.6.

In calculations of the total release, the question of to which time the release should be normalized is often discussed. Possible variants are:

- the initial time of the accident,
- summing over time,
- a particular time (e.g., the 10th day of the accident in the case of the Chernobyl accident),
- the end of the intense emissions of gaseous products during the accident,
- any other fixed time.

In my opinion, it is probably more useful to choose the variant that best describes the physical picture of the accident and provides the possibility of using it, on the one hand, to characterize the scale and typical features of the accident and, on the other, to characterize, calculate and forecast the real hazards posed for all living organisms.

Meanwhile, it is important to realize that, if the time chosen for normalization is very close to the initial time of the accident, the role of short-lived radionuclides (expressed in Bq or Ci) will increase considerably. Of course, their role should not be neglected, especially in estimating doses from the cloud or the gaseous effluent over the first hours (days). The overall danger from radiation effects, however, is characterized by the summation and type of all energy releases from radionuclides. In these circumstances, therefore, it is obvious that the estimate of a release in units of Bq or Ci does not characterize the danger objectively. The accompanying long-lived nuclides, even though they are present in significantly lower quantities of initial activity, can pose greater dangers than the short-lived activities. Good examples of long-lived radionuclides that can cause serious chronic (long-term) effects are ^{137}Cs, ^{90}Sr and $^{239}Pu + {}^{240}Pu$.

As a compromise, the estimation is often carried out for some period that characterizes the whole process of terrestrial contamination in different directions and at various distances. In the case of the Chernobyl accident, the times of D + 10 or D + 15 were chosen in many regions (i.e., 10 or 15 days after the accident). Let us consider the available data and estimates for the 10th day after the accident. First of all, if the works of Sivintsev and Khrulev (1995), Hohenemser and Renn (1988) and Devell et al. (1996) are examined, it is seen that the radionuclides were subdivided into groups of chemical elements to which their isotopes belong (although, not necessarily in an undisputable manner). Thus the elements were grouped into: inert gases, iodine isotopes, tellurium isotopes, caesium isotopes, volatile oxides, alkaline-earth elements, transuranium elements. The chemical properties and the volatility of the elements and their oxides in these groups and, consequently, the behavior of the radionuclides belonging to these groupings, vary significantly. Fractionation factors of these radionuclides vary, as do their ratios in air, aerosol particles and depositions at different distances from the site of the accident and in different directions. The quantities and fractions of these radionuclides deposited at different distances from the accident also vary.

Undoubtedly, it is important to take into account the distribution scale and hazard of individual radionuclides, as shown in Table 5.16. However, the following tables reflect an

Table 5.16
Main characteristics taken into account when estimating amounts and hazards of radionuclides in calculation of the total release (the total release is calculated as the sum of the individual radionuclides)

Type of classification		
Volatility	RNGs	Xe, Kr isotopes
	Volatile	^{131}I, ^{132}I, ^{132}Te, ^{137}Cs, ^{134}Cs, ^{106}Ru, ^{125}Sb
	Intermediate	^{140}Ba, ^{89}Sr, ^{90}Sr
	Refractory	^{144}Ce, ^{141}Ce, Zr + ^{95}Nb, ^{239,240}Pu, ^{239}Np
Radiation hazard	α-emitters	^{238}Pu, ^{239,240}Pu, ^{241}Am, ^{242}Cm, ^{244}Cm
	Specific effect on critical organs	^{131}I (thyroid gland)
Half-life	Short-lived	^{239}Np, ^{132}Te, ^{131}I, Ba + ^{140}La
	Intermediate	^{95}Zr, ^{103}Ru, ^{106}Ru, ^{89}Sr, ^{141}Ce, ^{144}Ce
	Long-lived	^{137}Cs, ^{134}Cs, ^{90}Sr, ^{241}Am
	Very long-lived	^{239}Pu, ^{240}Pu
Real hazard	Actual release of certain nuclides in relation to territory and direction of distribution, role of half-life, etc.	I period: ^{131}I, ^{239}Np, ^{132}Te, Ba + ^{140}La, etc. II period: ^{103}Ru, ^{106}Ru, ^{95}Zr, ^{89}Sr, ^{134}Cs III period: ^{90}Sr, ^{137}Cs, ^{239,240}Pu, ^{241}Am

attempt (in spite of lack of information) to classify the properties of various elements and radionuclides and present the most important data related to their deposition. To estimate the total release, normalized to May 6, 1986 (D + 10), we calculated the quantity of individual radionuclides belonging to certain groups, at different distances: (i) in the close-in zone (up to 40 km), (ii) in the distant zone (the territory of the former USSR outside the limits of the 40-km zone), and (iii) outside the European part of the Soviet Union (very long distances).

In our studies (Abagyan et al., 1986a & b; Izrael et al., 1986; Izrael, 1996a) presented at the conference of the IAEA Experts' Group in August 1986 and later published in a WMO report (January, 1987) and the periodical "Meteorology and Hydrology" (Izrael et al., 1994c) in February, 1987, data are presented from measurements of the radionuclide content in the close-in fallout zone (up to 40 km) created after the Chernobyl accident (see Table 5.4). It was pointed out that the total inventories of radionuclides (calculated at D + 15) were 407–444 PBq (11–12 MCi) (1.6% of the activity produced in the reactor) within the close-in fallout and 1147 PBq (31 MCi) over all the contaminated territory of the USSR. Further, it is obvious from Table 5.4 that, even in the close-in pattern, the fraction of the deposited radionuclides ^{132}Te, ^{131}I and ^{137}Cs is higher than the deposition of other radionuclides, viz. isotopes of the more refractory elements. Over the whole USSR territory, the total activity deposited was 2.8 times higher than that in the close-in pattern and for ^{137}Cs it was 3.2 times higher. In total, the ground deposition for radiocesium over the whole of Europe was 7–7.5 times higher than that in the close-in fallout zone. Using these values, we obtained estimates of the total release and the releases of individual radionuclides, normalized to D + 10 (Table 5.19).

Later, Devell et al. (1996) described their attempts to summarize the published material devoted to investigations of the release source characteristics during the Chernobyl accident in their paper entitled "One decade after Chernobyl" (8–12 April, 1996). Unfortunately, the study did not reflect the work of Soviet (Russian) scientists to a sufficient degree and dealt mainly with the results contained in the first reports that were presented to the IAEA (1986). It was emphasized in Devell et al. (1996) that different authors used various values for fuel burn-up (from 10 000 to 13 500 MW·day/t) to estimate the activity produced in the reactor at the time of the accident. Devell et al. (1996) presented in tabular form such calculations of the activity accumulation in the reactor. This table with some additions, viz. two columns of data, converted to Bq, that reflect our study (Izrael et al., 1990) and that of Gorbacheva et al. (1994), is shown as Table 5.17. Here some modified data are shown parenthetically, i.e., a possible initial error by Sich on ^{136}Cs accumulation is corrected (Sich, 1994). On the basis of data from Devell et al. (1996), it is believed that the estimates provided by Begichev et al. (1990) are the most reliable.

In examinations of the dynamics of the radioactivity release from the destroyed reactor, it has been pointed out (Buzulukov, 1993) that considerable releases of radioactivity took place 20–21 and 25–30 days after the accident occurred. However, it was noted that, on a relative scale, these releases did not add too much additional activity to that which had already been released. Attention should be paid, however, to the significant increases in radioactivity deposited in a number of areas to the north of Chernobyl, as recorded by Izrael et al. (1986).

As to the volatility of individual elements (and radionuclides), Devell et al. (1996) indicate the relative volatilities of Ba and Sr in their elementary state and of Ru, Mo and Te in their oxide forms. They also consider the serious possibility that fragmentation of the fuel rods into small pieces of fuel could have occurred during its cracking and oxidation from U to U_3O_8. They emphasize that the release of refractory products, such as Ce, Zr, Np and Pu (up to 3.5 $\pm$0.5% of the produced amount) was connected with such fragmentation. The short distances over which the majority of the fragments were scattered are related to this idea.

Table 5.18, taken from Devell et al. (1996), shows the fraction of the activity of individual radionuclides released from the destroyed reactor. It is noteworthy that the accuracy of these estimations depends on the absolute amounts of both the released activity and the radionuclides accumulated in the reactor. After numerous experimental determinations of ^{137}Cs, the most reliable of which were the integrations of ^{137}Cs contamination density as portrayed in the maps of the European Atlas compiled in early 1996, the total amount of Chernobyl ^{137}Cs deposited on the surface within all of Europe was about 63.64 PBq or 1.72 MCi. According to the data of Table 5.17 on the nuclide accumulations, it is obvious that this experimentally obtained value is equivalent to 22 to 30% of the amount of radiocesium accumulated in the reactor. The finding is highly dependent on the theoretical estimates of the amount of ^{137}Cs accumulated in the reactor, while the actual ^{137}Cs activity on the ground, which is the quantity used in the calculations of human exposure dose rates, is well-defined and does not depend on the calculations of specialists in the field of nuclear physics. This example shows the value of experimental information and their correct interpretation. On the whole, the data from Table 5.18 do not contradict the information presented above.

Table 5.17
Estimation of accumulated activities (Bq) of different radionuclides in the reactor at the moment of the accident (from different sources)

Radio-nuclide	Half-life	Abagyan et al. (1986); Warman (1987); IAEA (1986)	Izrael (1990)	Clough (from Devell et al., 1996)	Anttila (1987)	Kirchner & Noack (1988)	Little (from Devell et al., 1996)	Sich (1994)	Begichev et al. (1990)	Gorbacheva et al. (1994)
^{85}Kr	10.74 years	3.3×10^{16}	–	–	–	–	2.5×10^{16}	2.8×10^{16}	3.3×10^{16}	3.7×10^{16}
^{133}Xe	5.24 days	7.3×10^{18}	–	–	–	–	6.2×10^{18}	6.5×10^{18}	6.3×10^{18}	6.6×10^{18}
^{131}I	8.04 days	3.1×10^{18}	3.3×10^{18}	2.9×10^{18}	2.9×10^{18}	2.4×10^{18}	3.0×10^{18}	3.1×10^{18}	3.2×10^{18}	3.2×10^{18}
^{134}Cs	2.062 years	1.9×10^{17}	1.5×10^{17}	1.1×10^{17}	1.6×10^{17}	1.4×10^{17}	2.0×10^{17}	1.7×10^{17}	1.8×10^{17}	2.5×10^{17}
^{136}Cs	12.9 days	–	–	–	–	9.0×10^{16}	9.6×10^{16}	6.3×10^{18} (1.1×10^{17})	–	1.2×10^{17}
^{137}Cs	30.174 years	2.9×10^{17}	2.7×10^{17}	2.4×10^{17}	2.2×10^{17}	2.7×10^{17}	2.3×10^{17}	2.6×10^{17}	2.8×10^{17}	3.3×10^{17}
^{132}Te	78.2 hrs	3.3×10^{18}	4.4×10^{18}	4.1×10^{18}	4.4×10^{18}	4.4×10^{18}	4.1×10^{18}	4.5×10^{18}	2.7×10^{18}	4.3×10^{18}
^{89}Sr	50 days	2.3×10^{18}	1.9×10^{18}	3.6×10^{18}	4.0×10^{18}	3.2×10^{18}	3.0×10^{18}	4.0×10^{18}	2.3×10^{18}	3.4×10^{18}
^{90}Sr	28.5 years	2.0×10^{17}	1.9×10^{17}	2.0×10^{17}	1.8×10^{17}	2.0×10^{17}	1.7×10^{17}	2.3×10^{17}	2.0×10^{17}	2.5×10^{17}
^{140}Ba	12.8 days	5.3×10^{18}	4.9×10^{18}	5.8×10^{18}	5.6×10^{18}	5.5×10^{18}	5.4×10^{18}	6.1×10^{18}	4.8×10^{18}	5.7×10^{18}
^{95}Zr	63.98 days	–	4.9×10^{18}	5.8×10^{18}	–	5.3×10^{18}	5.1×10^{18}	5.8×10^{18}	5.6×10^{18}	5.7×10^{18}
^{99}Mo	2.73 days	7.3×10^{19} (7.3×10^{18})	4.9×10^{18}	5.5×10^{18}	5.7×10^{18}	–	5.2×10^{18}	6.1×10^{18}	4.8×10^{18}	–
^{103}Ru	39.4 days	5.0×10^{18}	4.9×10^{18}	4.3×10^{18}	4.0×10^{18}	4.6×10^{18}	4.5×10^{18}	3.8×10^{18}	4.8×10^{18}	4.8×10^{18}
^{106}Ru	368 days	2.0×10^{18}	1.9×10^{18}	8.9×10^{17}	7.9×10^{17}	1.1×10^{18}	1.2×10^{18}	8.6×10^{17}	2.1×10^{18}	1.5×10^{18}
^{141}Ce	32.5 days	5.6×10^{18}	4.9×10^{18}	5.6×10^{18}	5.4×10^{18}	–	5.1×10^{18}	5.6×10^{18}	5.6×10^{18}	4.9×10^{18}
^{144}Ce	284 days	3.2×10^{18}	3.3×10^{18}	3.9×10^{18}	3.4×10^{18}	3.8×10^{18}	3.4×10^{18}	3.9×10^{18}	3.3×10^{18}	4.4×10^{18}
^{238}Pu	86.4 years	1.0×10^{15}	9.6×10^{14}	–	–	7.3×10^{14}	1.6×10^{15}	1.3×10^{15}	1.0×10^{15}	1.3×10^{15}
^{239}Pu	24110 years	8.5×10^{14}	8.5×10^{14}	–	–	8.0×10^{14}	9.6×10^{14}	9.5×10^{14}	8.5×10^{14}	9.5×10^{14}
^{240}Pu	6553 years	1.2×10^{15}	1.2×10^{15}	–	–	1.6×10^{15}	1.6×0^{15}	1.5×10^{15}	1.2×10^{15}	1.5×10^{15}
^{241}Pu	14 years	1.7×10^{17}	1.7×10^{17}	–	–	1.9×10^{17}	1.8×10^{17}	1.8×10^{17}	1.7×10^{17}	1.8×10^{17}
^{239}Np	2.35 days	3.6×10^{18} (3.6×10^{19})	4.9×10^{19}	4.7×10^{19}	5.1×10^{16}	6.1×10^{19}	6.7×10^{19}	5.8×10^{19}	2.7×10^{19}	5.8×10^{19}
^{242}Cm	162 days	2.5×10^{16}	2.6×10^{16}	–	–	3.3×10^{16}	3.3×10^{16}	4.3×10^{16}	2.6×10^{16}	4.3×10^{16}

Note: numbers in brackets mean values corrected later (Devell et al., 1996).

Table 5.18
Percentage of individual radionuclides released from the destroyed reactor (Devell et al., 1996)

Radionuclide	Released (%)
^{85}Kr	100
^{133}Xe	100
^{131}I	50–60
^{132}Te	10–60
^{134}Cs	33 ± 10
^{137}Cs	33 ± 10
^{140}Ba	3.5–6
^{95}Zr	3.5
^{99}Mo	3.5–6
^{103}Ru	3.5–6
^{106}Ru	3.5–6
^{141}Ce	3.5
^{144}Ce	3.5
^{89}Sr	3.5–4.5
^{90}Sr	3.5–4.5
^{239}Np	3.5
^{238}Pu	3.5
^{239}Pu	3.5
^{240}Pu	3.5
^{241}Pu	3.5
^{242}Cm	3.5

Figures on ^{137}Cs in Table 5.18 ($33 \pm 10\%$) are the most crucial. The data on I (50–60%) are basically similar to those obtained by Sivintsev and Khrulev (1995), as discussed above. The data on ^{132}Te release (10–60%), however, are rather hard to interpret. Devell et al. (1996) consider that a figure of 10% is more realistic. The relative amounts of other slightly volatile and refractory elements (and their isotopes) are very close to our previous estimates and do not require further comment. The analysis of data from Table 5.18 shows that only a small fraction of the total release belongs to the group of highly volatile elements I, Te and Ce (without the inert gases).

If these radionuclide data are taken as the basis for calculation, it can be determined that, by the end of the release, the portion of all radionuclide activity released from the destroyed reactor was 4.4–5% (the radioactive inert gases and very short-lived isotopes were not considered here). Our initial estimate was 3.5%. The very first estimation carried out by us on May 20, 1986 yielded a figure of 5%, although at that time many people thought (and even now some still think) that the total, or almost the total, amount of activity accumulated in the destroyed reactor was released into the environment.

The apparent contradictions and differences between the amounts of radioactive products calculated as being beyond the limits of the reactor and those considered as being inside the destroyed reactor building are partially explained in physical terms by Devell et al. (1996) via the hypothesis that a flowing mixture of concrete in the core could have left the reactor chamber and then been cooled down in the bottom of the reactor vessel.

Table 5.19
Amounts of radionuclides (%) measured at different distances (Izrael, 1990)

Radionuclide	Close-in zone (up to 40 km)	Distant zone		Total (%)
		USSR territory	European territory	
I-nuclides	5.1			
^{137}Cs	3.8* (0.28)	8.0* (0.6)	14.0* (1.1)	26
^{132}Te	5.0			
Ru-nuclides	1.4			
Refractory	0.6–1.0			
The total radioactivity (averaged on 6 May, 1986)	1.6			3.5–5.0‡

*Percentages given on the assumption that the total amount of ^{137}Cs produced in the reactor was 7.6 MCi (the data in MCi are shown in brackets; 1 MCi = 37 PBq).
‡Evaluated data.

Table 5.20
Estimated release (%) of individual nuclides into the environment (from different studies)

	Abagyan et al. (1986)	Devell et al. (1996)	Hohenemser & Renn (1988)	Izrael (1990)	Sivintsev & Khrulev (1995)
Inert gases	100	100	100		80
I	20	50–60	20		25 (to 30)
Te	15	10–60*	15		19
Cs	13	33 ±10	12	26‡	9–14
Volatile oxides		3.5–6.0	3		
Alkali earths	4.0	3.5–4.5–6.0	5		4
Transuranics	3–3.2	3.5	3		2–3
Refractory	2.8–3.2	3.5			2–3
Total (averaged without inert gases) on 6 May, 1986	3.5			3.5–5.0	

*Devell et al. (1996) propose 60%.
‡Experimental data (see Table 5.19).

According to the data of Soviet researchers (Abagyan et al., 1986a & b), the total release from the reactor was 1.85 EBq (50 MCi) by May 6, 1986 (without inert gases). If this value is converted to the initial time of explosion or normalized by integrating over the whole period of the release, it will increase several times (e.g., according to our data (Izrael et al., 1990), the initial release was 3.7–4.4 EBq (100–120 MCi). However, such figures are of hardly any practical importance, especially in terms of the operating regime of the reactor which was far from normal even before the accident. It is therefore very difficult to calculate correctly the exact amount of the short-lived nuclides emitted.

The actual value of ^{137}Cs activity on the ground, needed for dose calculations, is defined rather well enough and does not depend on the theoretical estimates of the activity accumulated in the reactor.

Table 5.19 shows the amounts of individual radionuclides measured on the surface and Table 5.20 presents the estimated releases of certain radionuclides into the environment during the Chernobyl NPS accident. It follows from these tables that the data from the various studies coincide quite well (with the exception of the extreme theoretical data). The results in Tables 5.19 and 5.20 indicate that about 1.85 EBq (50 MCi) activity from all radionuclides was present in the environment on May 6, 1986 (a figure that has been mentioned above in a number of independent scientific studies). It suggests that figures presented in some sources, e.g., in Yablokov (1995) that the activity is 2–3 times greater than 50 MCi), are not correct.

6. Modeling of Close-in Radioactive Deposition (Fallout) from the Chernobyl NPS Accident

After the Chernobyl accident, a number of studies were published devoted to the modeling of radionuclide distributions in the atmosphere and the ensuing fallout onto the earth's surface at different times and over different regions. In Izrael et al. (1990) and Izrael and Petrov (1987), the deposition, over long periods of time, of the radioactive products released to the atmosphere were discussed. This deposition led to the residual contamination of the ground near to the CNPS ("near" here meaning at distances up to 100 km). A model was proposed to estimate the scale of the radiation danger within the area of the CNPS and to develop conditions that would ensure the safety of the population during this real accident (and indeed more generally after potential accidents). The approach described in Izrael and Petrov (1987) is briefly presented below. It takes into consideration the experience gained from other examples of contamination arising from radioactive sources.

For this model, information on the detailed characteristics of the source, including the height, the release dynamics and the dispersion characteristics of the cloud, etc. as well as data on the detailed behavior of the wind field over given time intervals, are required. Izrael et al. (1987) have formulated data on the radioactive contamination of the environment in the accident zone, as required for modeling. The most powerful plume of radioactive products from the damaged unit was observed during the first 2–3 days after the accident in the north and northeasterly directions. On the basis of aircraft data, the height of the plume was greater than 1200 m. The maximum radiation level around the CNPS was observed at an altitude of 600 m. On subsequent days, the height of the plume did not exceed 200–400 m.

Balloon observations on wind direction and velocity at the airports of Kiev, Mozyr, Gomel and Chernigov were used as the input meteorological information for the model, as well as radiosonde data obtained in Kiev from April 26 to May 1, 1986. Figure 5.24 shows the calculated values of the mean wind velocity and wind direction within the 0–500 m and 0–1000 m layers during the five days after the accident, data that were used to estimate particle transport in these atmospheric layers.

At the time of the accident, an instantaneous release of radioactive particles took place as a result of the explosion. It seems likely that they spread westwards and produced a long narrow belt of high radioactive contamination on the earth's surface. Then, on April 26

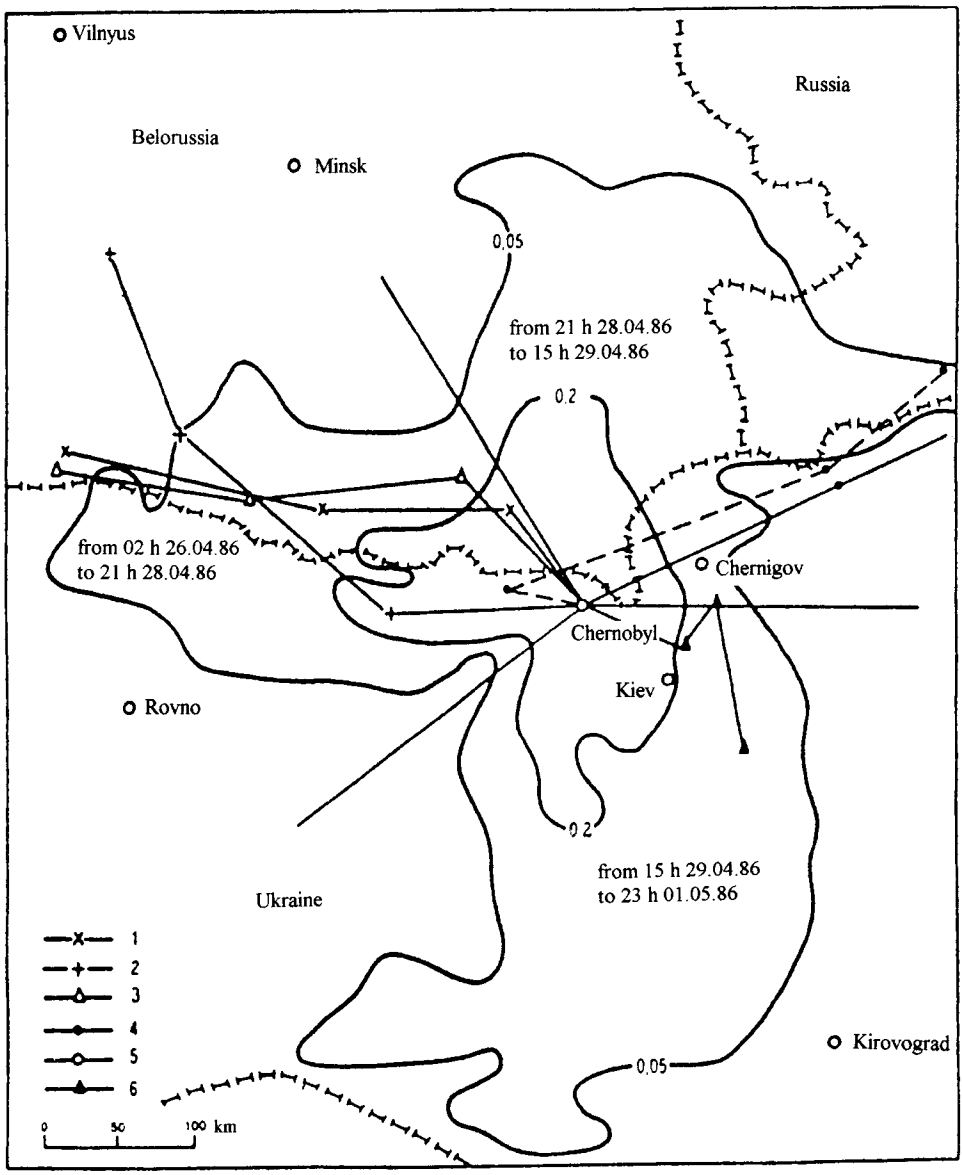

Fig. 5.25. Main sectors of particle distribution trajectories at the level of 925 hPa, as well as the gamma-field distribution in the area adjacent to the accident zone (isolines of 0.05 and 0.2 mR/hr, i.e., ≈0.5 and 2 μGy/hr) on June 10, 1986. 1 — from 3 a.m. on April 26; 2 — from 3 p.m. on April 26; 3 — from 3 a.m. on April 27; 4 — from 3 p.m. on April 28; 5 — from 3 a.m. on April 29 and 6 — from 3 p.m. on April 29.

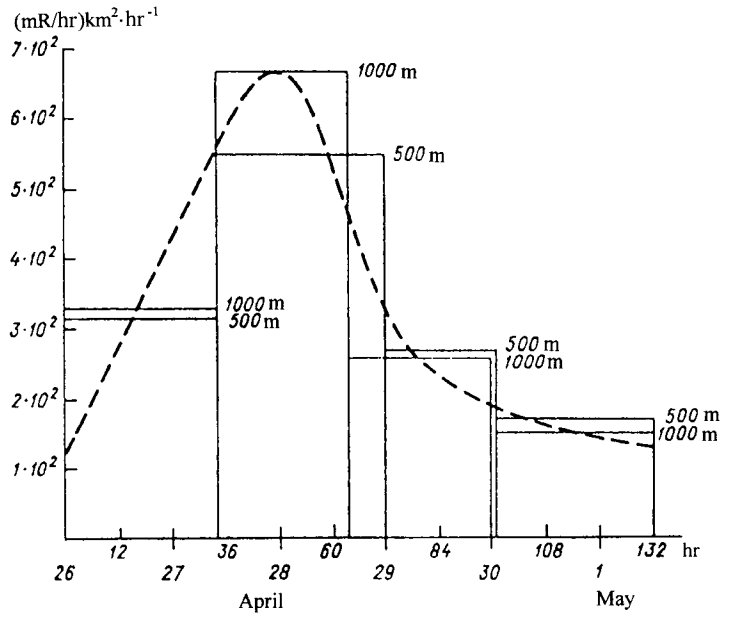

Fig. 5.26. Hourly releases of gamma-active materials into the atmosphere (deposited in the close-in fallout pattern).

and 27, the radioactive products of the plume were transported from the reactor zone southwestwards and northwestwards. On April 28–29, the transport direction changed again to the northeast, and, by April 30, to the southeast and south. Figure 5.25 shows the aerosol particle transport trajectories at an altitude of 700 m during specific time intervals after the accident, as well as the gamma-field distribution (the dose rate isoline of 0.05 mR/hr (≈0.5 μGy/hr) on June 10, 1986 in the area adjacent to the emergency zone. One can see that the contamination of this area comprised three tongues of radioactivity, extending west, north and southwards. An analogous contamination pattern is also apparent in the close-in zone.

So, on the basis of the currently available information on radioactive product release from the reactor, one can conclude that there were two independent sources of the radioactive aerosols, viz. the instantaneous release, resulting from the explosion that destroyed the reactor, and the longer-lived hot release from the reactor of the fission products that had accumulated in the fuel rods. The data on the daily release of radioactive substances into the atmosphere from the reactor zone are presented in Abaygan et al. (1986). For the first 4–5 days, relative variations in this release are closely approximated by the relationship:

$$Q(t) = 0.25\,e^{-0.28t}, \quad t = 0, 1, \ldots, 4 \text{ days}.$$

Radioactive deposition in the close-in zone came to an end after the first 4–5 days (except in the southern sector). The total amount of radioactivity in the fallout pattern corresponded to 4.4×10^4 mR·km²/hr at that particular time (Izrael et al., 1996). A histogram of

the calculated hourly releases of radioactive substances to the atmosphere that were subsequently deposited in the close-in fallout pattern is presented in Fig. 5.26. A dashed curve shows the relative variations in the hourly releases (from April 26 to May 1, 1986).

Taking into account the data and the ratios between the radioactive deposition density of a given radionuclide σ (Ci/km^2) and the dose rate P (mR/hr) for different sectors ("West", "North", "South"), as presented in Izrael et al. (1987), calculations were carried out on the relative and absolute releases of specific radionuclides to the atmosphere for the first five days after the accident.

The analysis of an air sample taken near the NPS on April 27 at a height of 400–600 m showed that hot particle sizes varied from units to dozens of micrometers in a background of numerous smaller particles. Since the more important initial data on particle size distributions were not available, the more readily available information on particle distributions within limited size ranges was employed, thereby allowing a description of the close-in radioactive fallout to be constructed. As in Izrael and Petrov (1975), the overall distribution of the total radioactivity on particles within specific size ranges in the close-in fallout pattern was approximated by a normal logarithmic relationship that included the distribution parameters such as the median diameter ξ of the particle and its standard deviation σ. Further, the upwards ejection of radioactive matter from the plant to a height H because of the existence of heat fluxes was represented as a continuous point source of a polydispersed mixture of radioactive particles to the atmosphere, the activity distribution on the particles being in accord with their size, as described by the normal logarithmic expression.

The amount of radioactive fallout reaching ground level from a thus-specified source of height H is subject to the kinetics of gravitational deposition of the particles, the temporal variations in the wind field and the process of horizontal diffusion. Trajectories of particle transport were calculated taking into consideration the time-distribution of wind speed and direction in the 0–500 m or 0–1000 m layers (see Fig. 5.24) in relation to the initial height of the source. Values of φ and v, wind direction and speed, respectively, for intermediate time intervals were interpolated.

The deposition time for particles of diameter δ (density of 2.5 g/cm^3) is a function of the source height H and the particle velocity, approximated by the relationship $w = 0.025(\delta - 22)$ km/hr for $\delta > 44$ μm; $w = 2.85 \times 10^{-4}\delta^2$ km/hr for $\delta < 44$ μm.

For monodispersed particle deposition subject to diffusion in the atmosphere, the contribution of the particles to a specified point on the surface is a function of their dispersion over the deposition time $t = H/w$. It is well known that, for a polydispersed mixture, the dissipation of the particles in the vertical plane and with the wind should not be taken into account (Patrov and Pressman, 1962). Horizontal diffusion in the atmosphere is described by the function (Izrael et al., 1970a):

$$F(r, l) = \frac{1}{2\pi\sigma_l^2} \exp\left[-\frac{r^2}{2\sigma_l^2}\right], \quad \sigma_l \approx 0.08\, l, \tag{5.10}$$

where r is the distance between the center of deposition of a portion of the monodispersed particle fraction and the point at which the deposition density is calculated. The distance

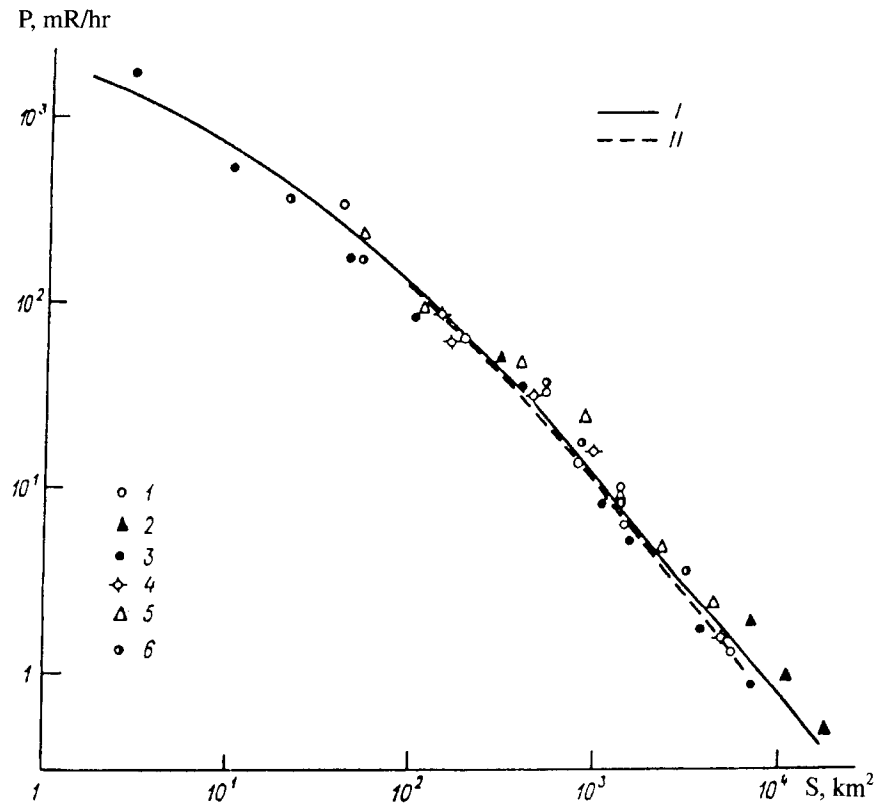

Fig. 5.27. The relationship between radioactive fallout area (in km^2) in the close-in pattern and dose rate isoline enclosing this area. The data were normalized to May 29, 1986. I — mean value obtained from measurement data; II — calculated results; 1–6 measured data on May 1 (1), May 11 (2), May 29 (3), June 26 (4), July 13 (5) and November 20 (6).

r and the horizontal path l of the particle before its deposition are controlled by the wind field variation with time (σ_l—dispersion (derivation)).

The radioactive fallout density on the surface from a source with constant capacity Q is described by the relationship:

$$P = \frac{0.434Q}{(2\pi)^{3/2}\sigma} \int_{\delta_1}^{\delta_2} \frac{1}{\delta} \exp\left\{\frac{[\lg(\delta/\xi)]^2}{2\sigma^2}\right\} \int_{t_1}^{t_2} \frac{1}{\sigma_l^2} \exp\left\{-\frac{r^2}{2\sigma_l^2}\right\} dt\, d\delta. \tag{5.11}$$

The non-stationary state of the source $Q(t)$ is taken into account using variations in its capacity and height within specified time intervals (t_1, t_2) and the summation of the calculated values of deposition densities obtained for these intervals.

The direct use of detailed maps of dose rate distributions to estimate the model parameters does involve some difficulties. In this connection, an integrated analysis of the results obtained from all airborne gamma-surveys was used. Figure 5.27 shows the relationship between the radioactive fallout in the close-in zone and the dose rate isolines

enclosing the area. The airborne gamma-survey data were normalized to the same time, namely May 29, 1986. Within the area contained by the isoline, the dose rate exceeds (or is equal to) that specified. Referring to Fig. 5.27, the results obtained from different surveys are very similar. An important problem then was to select values of ξ and σ for the normal logarithmic distribution such that the relationships between the radioactive fallout areas in the close-in zone (as calculated for the model and actual areas) and the dose rate isolines P are close to each other. This is quite feasible because the other initial parameters for the model (height, dynamics of radioactive product release and wind field variations with time) have been specified or are known. The values of ξ and σ were thus calculated numerically in order to obtain best agreement with the actual curve, as presented in Fig. 5.27, which was derived from the airborne gamma-surveys. Curve II shows the calculated relationship between S and P with the values of the parameters $\xi = 50$ μm and $\sigma = 25$.

Figure 5.28 shows the distribution of radiation levels in the close-in fallout pattern from the Chernobyl NPS accident on May 29, 1986, calculated using the model with the above parameters for the particle-size distribution of the gamma-active products along with specified initial data on the height, radioactivity release dynamics and temporal characteristics of the wind field. The actual distribution of radiation levels from the airborne gamma-survey data is also shown in Fig. 5.28 (Izrael et al., 1990).

During the calculations, the initial height of elevation of the ejected radioactive products was assumed to be 1000 m until 17 hours (p.m.) (Moscow time) on April 28, 1986 and 500 m thereafter. Wind directions for every two-hour period were obtained from a histogram (see Fig. 5.24).

For reference, we include Fig. 5.29 which shows the radiation levels in the close-in fallout pattern calculated for a hypothetical case in which there was an emergency and a release occurring on April 30 (i.e., with a shift of four days) with analogous dynamics for the radioactive products released into the atmosphere. In these calculations, the actual instrumental data on wind speed and direction for the area of the Chernobyl NPS from April 30 to May 4, 1986 were used. Early in May, more stable air-mass transport was observed in the area of the Chernobyl NPS in the southerly and southeastwards directions, which influenced contamination of the Kiev-city area.

7. Characteristic Features of Radioactive Contamination from Various Nuclear Accidents

7.1. *Radionuclide Composition of Deposition in the Southern Urals Area*

On September 29, 1957, one of the largest nuclear accidents took place at the "Mayak" atomic enterprise in the Southern Urals near Kyshtym town. A thermal explosion occurred in a depot where radioactive wastes were being stored, resulting in a release of a 77.7 PBq (2.1 MCi) mixture of medium- and long-lived radionuclides to the atmosphere. It was composed of the following: $^{90}Sr + {}^{90}Y$—5%, $^{144}Ce + {}^{144}Pr$—66%, $^{95}Zr + {}^{95}Nb$—24.9%, $^{106}Ru + {}^{106}Rh$—3.7% and ^{137}Cs—0.039% (Aleksakhin et al., 1993). The characteristic feature of the radioactive fallout was the extremely large deposit of long-lived ^{90}Sr. The fallout pattern was more than 100 km long and, according to certain data, covered an area

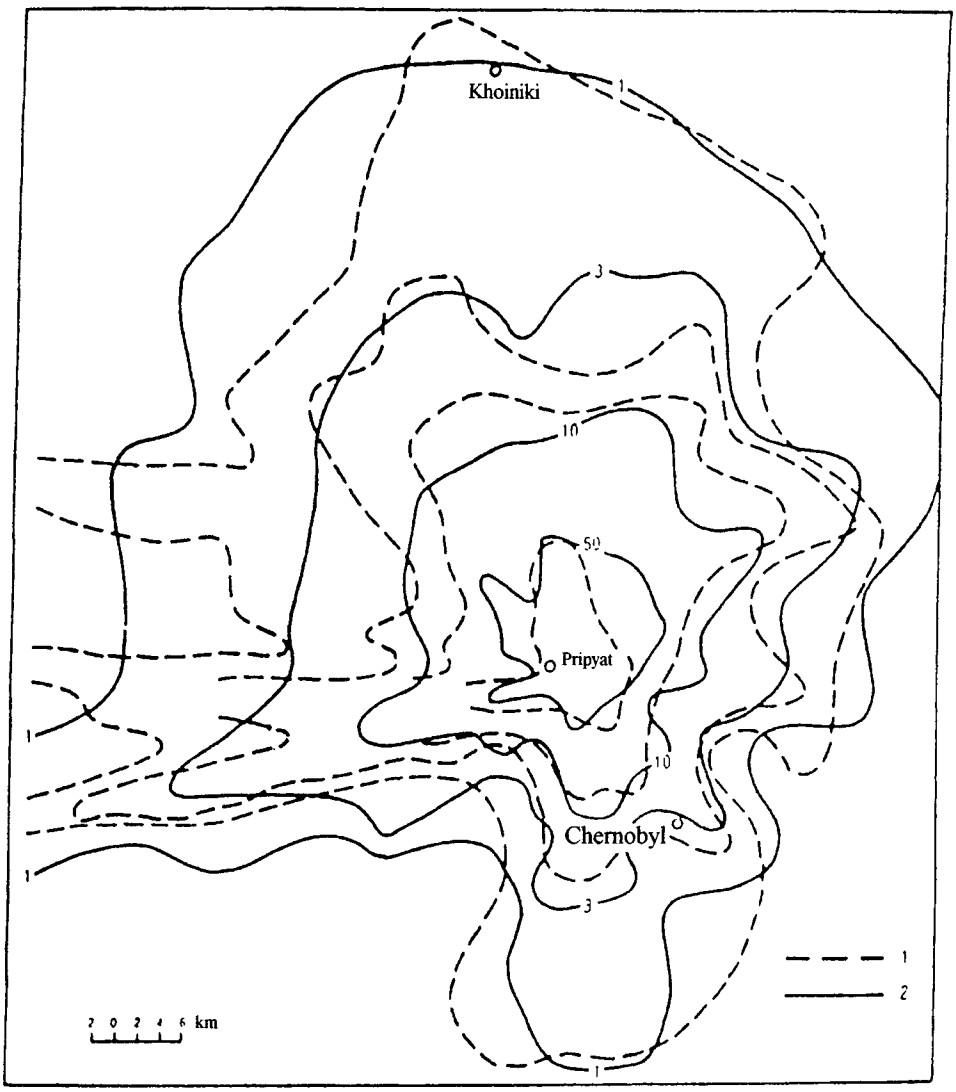

Fig. 5.28. Calculated (1) and measured (2) distribution of radiation levels (mR/hr) at the ground surface on May 29, 1986 (1 mR/hr $\approx$10 μGy/hr).

of 15 000 km^2 (Sokolov, 1993). Table 5.21 (Tikhomirov, 1993) shows the changes with time of the composition of the long-lived radionuclides in the fallout pattern. It is clear from Table 5.21 that, five years after the accident, more than 80% of the radioactivity was derived from ^{90}Sr. Apparently, this fact caused many radioecological consequences in the contaminated zone. Tikhomirov (1993) has described the vertical migration of ^{90}Sr and ^{137}Cs in grey forest soils within the area and found that the ^{90}Sr penetration in the soil was essentially faster than that of the ^{137}Cs.

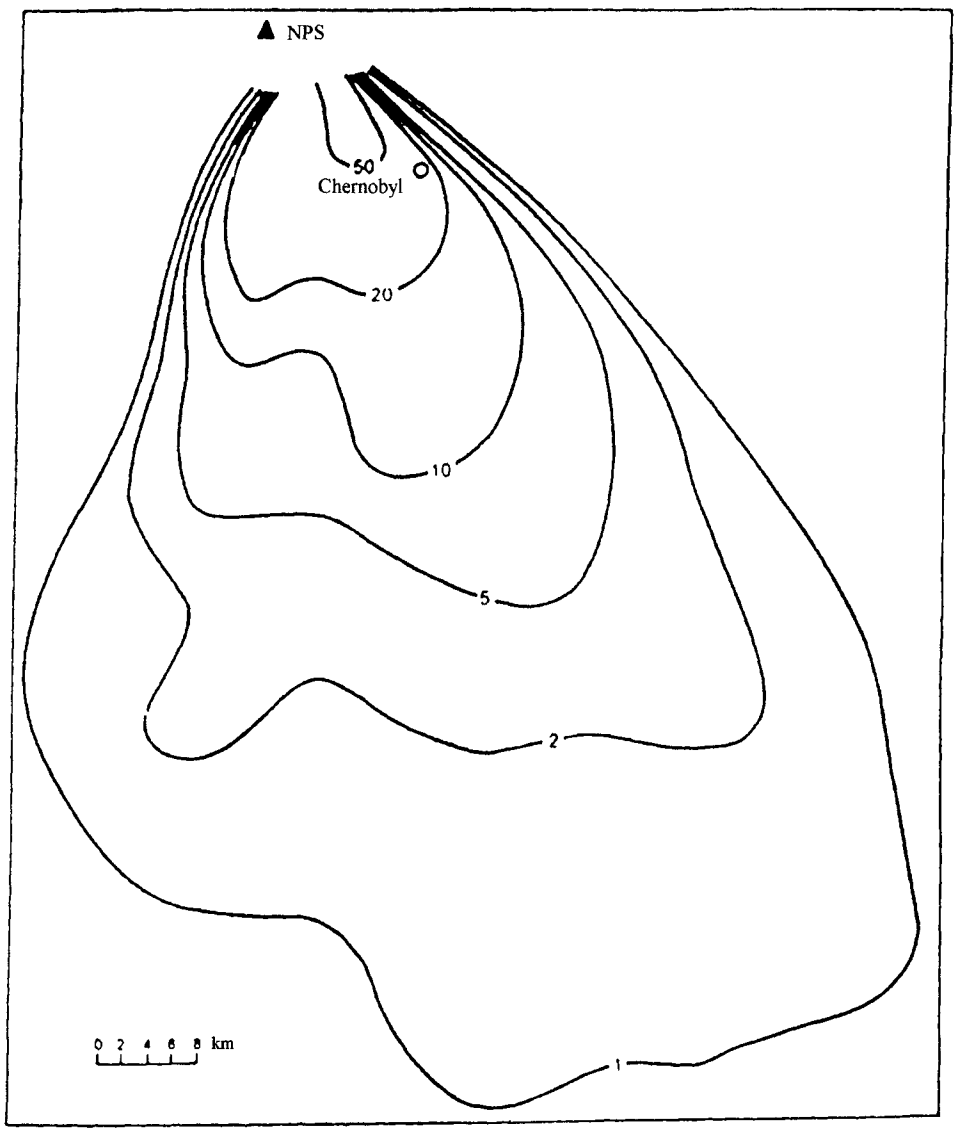

Fig. 5.29. Calculated surface distribution of radiation levels (mR/hr) from a hypothetical accident occurring on April 30, 1986 (1 mR/hr $\approx$10 μGy/hr).

Table 5.21
Contribution of long-lived radionuclides to the fallout pattern, % of total activity

Radio-nuclide	Half-life	1st October 1957	1st February 1958	1st July 1958	1st July 1959	1st July 1960	1st July 1961	1st July 1962
$^{144}Ce+$ ^{144}Pr	285 days	66.3	78.3	80.0	68.6	49.6	29.6	15.0
$^{90}Sr+$ ^{90}Y	28 years	5.15	8.4	12.3	26.0	45.6	66.6	82.7
$^{106}Ru+$ ^{106}Rh	1 year	3.45	4.6	4.9	5.3	4.8	3.8	2.3
$^{95}Zr+$ ^{95}Nb	65 days	25.1	9.0	2.8	0.1	0	0	0

Another significant re-release of radionuclides via the atmosphere occurred in the Southern Urals in 1967 near lake Karachay when a total of 22.2 PBq (0.6 MCi) of ^{137}Cs from mixed wastes was transported from the lake shore by exceptionally strong winds. Maps of the terrestrial contamination density of ^{137}Cs in the Southern Urals were compiled (from the two specific accidents) from the results of airborne gamma- and ground-based surveys conducted in 1991 and 1992 (Izrael et al., 1994c). The most detailed maps were made in 1996–1990. The main portion of the 1957 release spread north to northeastwards (Fig. 5.30), while that of 1967 spread in a northeasterly direction (Izrael et al., 1992).

7.2. *Terrestrial Contamination from an Accident at the Siberian (Tomsk-7) Chemical Enterprise*

This accident at the Siberian chemical enterprise (SCE) in Tomsk was essentially smaller in scale than those in the Urals. Izrael et al. (1993) have presented the results of several inspections (using airborne gamma-spectral surveys) of the areas contaminated by the radioactive products from the accident which occurred on April 6, 1993. The first detailed airborne gamma-survey of the territory was carried out on April 12–16, 1993. Ground-based measurements were conducted on the snow-covered area on April 12–15. As a result, a map was compiled of the gamma-radiation dose rate on April 12–13 (Fig. 5.31) and an energy yield of 4700 $\mu R \cdot km^2/hr$ was estimated from the radioactive products in the fallout pattern from the SCE boundary. The total inventory of radioactive products beyond the SCE site was estimated at 19.61–21.83 TBq (530–590 Ci). In the most contaminated central part of the pattern (where the contamination level was equal to or exceeded 300 μR/hr (≈3 μGy/hr), the accumulated gamma-radiation dose from the radionuclides ^{103}Ru, ^{106}Ru, ^{95}Zr and ^{95}Nb did not exceed 1 R (≈10 mGy) for the first year. In the following years, the gamma-radiation dose from the released radioactive products would not have been as high.

The main purpose of the second airborne gamma-spectrometry survey, conducted on June 18–19, 1993, was to estimate the spatial and temporal dynamics of the radioactive contamination pattern resulting from the release, including an estimation of the quantities of radioactive products washed off as a result of snow melting. The survey was carried out within the limits of the earlier fallout pattern, using the same tracks as on April 12–16, 1993. Figure 5.31 presents a comparison of the radioactive patterns obtained from the

Fig. 5.30. Contemporary soil contamination of the Southern Urals area by ^{90}Sr (Ci/km^2) from accidents at the "Mayak" nuclear production unit (1 Ci/km^2 = 37 GBq/km^2).

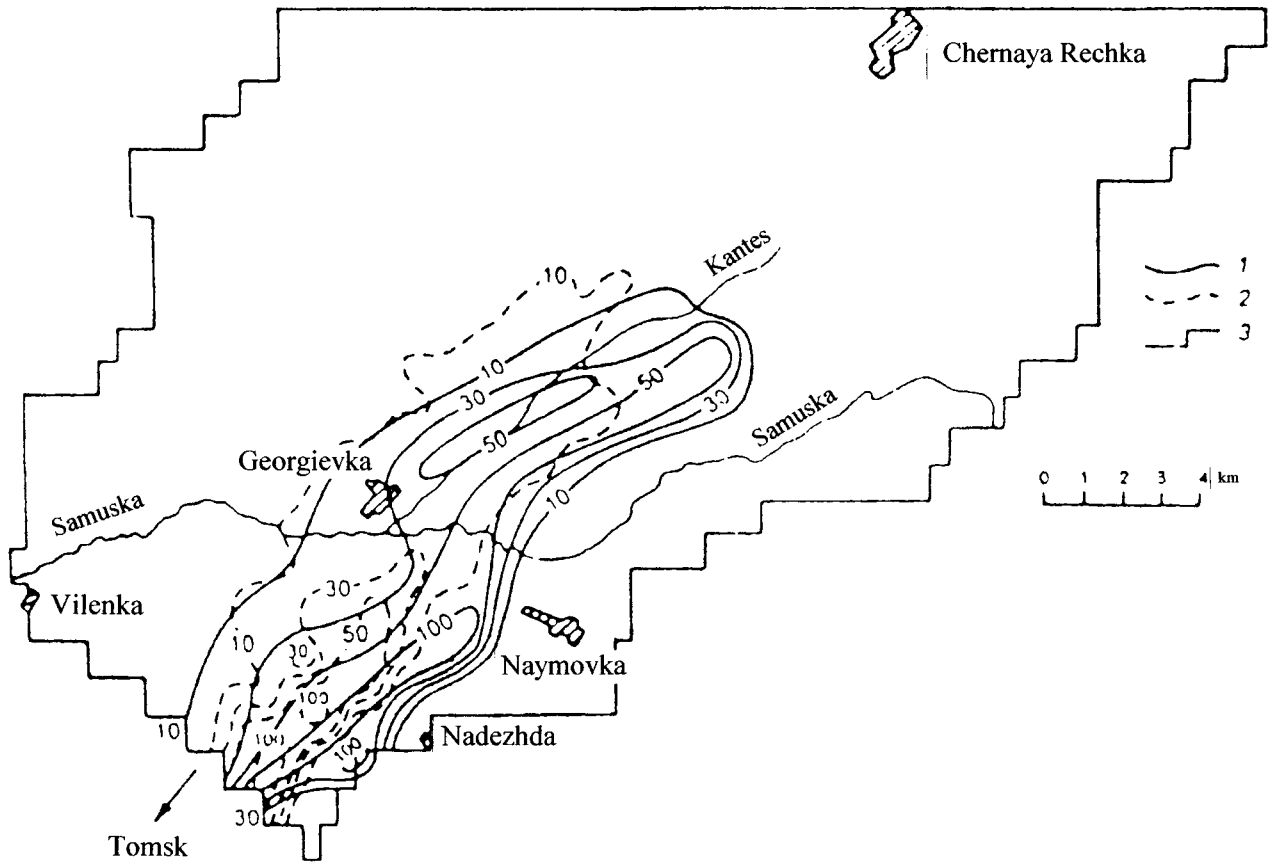

Fig. 5.31. Sketch map of the exposure gamma-dose rate distribution (μR/hr) on the surface as a result of the radionuclides deposited after the accident at the Tomsk-7 chemical enterprise on 6 April, 1993. 1 — survey of April 12–13; 2 — survey of June 18–19; 3 — the survey area boundary (1 μR/hr ≈ 10 nGy/hr).

two surveys, the first (curve I) and the second (curve II) within the 10 μR/hr (≈100 nGy/hr) isoline for the anthropogenic radionuclides (the contribution of the natural radionuclides was excluded by using the data on the natural radioactive elemental contents in the soil as measured in parallel with these surveys). The energy yield for the radioactive products within the fallout pattern was found to be 208 $\mu R \cdot km^2/hr$ for the period June 18–19 and the total quantity of radioactive products beyond the site of the enterprise was estimated at 8.32–9.25 TBq (225–250 Ci). As a result of radioactive decay, the initial amounts of anthropogenic radioactive products in the fallout pattern for April 12–13 had fallen by a factor of 2.35, with an energy yield of 2145 $\mu R \cdot km^2/hr$. As a result of the June 18–19 survey, it was found that the radioactive product wash-off by snow melting was relatively small—about 3%. At the same time, as Fig. 5.31 shows, the radioactive pattern traveled a distance of 1–2 km northwestwards during the two-month period from mid-April to mid-June.

This Page Intentionally Left Blank

Chapter 6

RECONSTRUCTION OF CONTAMINATION ON THE OLD PATTERNS FROM NUCLEAR EXPLOSIONS AND ACCIDENTS

Contents

1. The Problems Associated with the Reconstruction of Terrestrial Contamination Distributions 213
2. Terrestrial Contamination after the Chernobyl NPS and Other Accidents 215
3. Reconstruction of Terrestrial Contamination from Nuclear Explosions 217

The reconstruction of the characteristics and features of radioactive contamination that existed at an earlier time or, more importantly, at the time of its formation (i.e., the old patterns), using only recent or previously obtained data, is required for a number of reasons: (i) to provide a retrospective assessment of the dose rates to the population and ecosystems, (ii) to detail the character and scale of the contamination, (iii) to develop necessary measures aimed at mitigation or elimination of its consequences, and (iv) to identify the location and, in some cases, the parameters of the contamination source itself.

Meeting these objectives is not always easy because the parameters of the contamination source are often not known. The solutions are further complicated by the radionuclide fractionation that occurs during the release and distribution of the radioactivity.

1. The Problems Associated with the Reconstruction of Terrestrial Contamination Distributions

A number of reconstruction studies by Izrael et al. (1993b, 1994c, 2000a, b) have presented logical ways of solving the various problems associated with the spatio-temporal distributions of the contamination density $\sqrt{\sigma(x, y, t)}$ and the external gamma-radiation dose D arising from nuclear explosions or accidents. For a dose $D(x, y, t)$, the distribution may be expressed as follows (for any time interval (t_0, t_r) at the point that has location coordinates (x, y) for which the reconstruction is being conducted):

$$D(x, y, t_r) = \int_{t_0}^{t_r} P(x, y, t)\, dt, \tag{6.1}$$

where $P(x, y, t)$ is the spatio-temporal distribution of the external gamma-radiation dose rate.

If the terrain contamination density of the jth radionuclide $\sigma_j(x, y, t)$ is known at any time t, then the relationship for any time period of reconstruction t_r $(0 \leqslant t_r \leqslant t)$ is:

$$\sum_m \sigma_m(t_r) = \frac{1}{\delta_j(t_r)} \sigma_j(x, y, t)\, e^{\lambda_j(t-t_r)}, \tag{6.2}$$

where $\sigma_m(t_r)$ is the contamination density of the mth radionuclide at time t_r; λ_j is the decay constant of the jth radionuclide; $\delta_j(t_r)$ is the fraction of the jth radionuclide in the explosion product mixture at time t_r.

The exposure dose rate may be calculated from the expression:

$$P(t_r) = \sum_m K_m(t_r)\sigma_m(t_r) \approx K_\Sigma(t_r) \sum_m \sigma_m(t_r). \tag{6.3}$$

Here $K_m(t_r)$ and $K_\Sigma(t_r)$ are, respectively, scale coefficients relating the contamination density of the mth radionuclide and that of all radionuclides to the dose rate, which is usually calculated for a height of 1 m above the surface. Strictly speaking, the coefficient δ_j also depends on the coordinates (x, y) because of possible fractionation of the radionuclides. This is given special consideration in Chapter 1.

Assuming that the radioactivity source function is known for all nuclides at $t \geqslant 0$

$$q(h, t) = \sum_m q_m(h, t), \tag{6.4}$$

where $q_m(h, t)$ is the distribution at heights h and times t, of the mth radionuclide and assuming that the measurement results of the terrain contamination density at points (x_i, y_k) at times t_r are known, then:

$$\sigma_{ikn}(x_i, y_k, t_n) = \sum_m \sigma_m(x_i, y_k, t_n). \tag{6.5}$$

If archived data on wind velocity distribution are used, i.e., $\boldsymbol{V} = \boldsymbol{V}(x, y, h, t)$, one may obtain the corresponding relationship:

$$P(x, y, t) = L_1\big[q(h, t), \boldsymbol{V}, \sigma_{ikn}\big]. \tag{6.6}$$

When data on σ_{ikn} are not available, we face the problem of predictive calculations of the dose rate distribution with $q(h)$ and $\boldsymbol{V}$:

$$P(x, y, t) = L_2\big[q(h, t), \boldsymbol{V}\big] \tag{6.7}$$

for which numerous calculation schemes are known.

The operator L_1 may be obtained from the requirement of minimum deviation between the predicted distribution $P(x, y, t)$ and the observed values. This requirement may be written in the following way:

$$\sum_i \sum_k \big[P(x_i, y_k, t_n) - P_{ik}\big]^2 = \min, \tag{6.8}$$

i.e., it corresponds to the minimum sum of squared deviations between the calculated and observed values of the dose rate over the whole area of fallout.

As a rule, the main deviation arises from variations in wind direction, information on which is often absent. If the number of measurement points y_k is great enough at distances x_i and at individual cross-sections of the pattern, the following requirement is more convenient in practice and no less effective:

$$\sum_k \left[P(x_i, y_k, t_n) - P_{ik}\right]^2 = \min, \quad i = 1, 2, \ldots, l, \tag{6.9}$$

i.e., at each section, the sum of the squares of the deviations must be at a minimum. This approach may be used in two main types of reconstruction:

(i) When observational data are available (on a number of radionuclides and dose rates) in the present situation. The dose reconstruction is basically possible for certain time intervals.

(ii) When observational data are absent in the present situation (or data exist for 1–2 fission products only or the data are unreliable) with only some archived data on terrain contamination and meteorological situations being available. The reconstruction is then possible only in individual cases. In some cases, it is found to be unreliable and in others impossible.

Point source situations may have many different variants that can be analyzed in certain situations and for some contaminated areas. Examples are presented below.

2. Terrestrial Contamination after the Chernobyl NPS and Other Accidents

This example involves a situation for which voluminous information was available. As described earlier, regular ground observations and airborne γ-surveys from aircraft including helicopters produced a compilation of maps of land contamination (dose rates and contamination densities of different radionuclides) from the first days after the accident up to the present (see Abagyan et al., 1986a & b; Izrael et al., 1990; and Chapter 5). This data set enables us to restore the terrain contamination pattern for practically any time point and to calculate the external and internal doses for any required time interval.

Investigations of the close-in zone of the Chernobyl fallout pattern may be considered as typical examples of the reconstruction and estimation of former radioactive deposition fields. The zone was the most intensively examined and in geometric terms is represented here as a ring of outer radius 60 km and inner radius 5 km, both centered at Unit IV of the CNPS. This zone was repeatedly investigated using the airborne gamma-survey method with dosimeters mounted on aeroplanes and helicopters of different types. More than 40 such surveys were carried out over the first 3 years. The same zone (and much larger areas beyond) were examined using the airborne γ-spectral survey method in 1986 and 1987–1989. For this period, then, maps of radionuclide contamination by ^{140}La, ^{95}Zr, ^{95}Nb, ^{103}Ru, ^{106}Ru, ^{144}Ce, ^{134}Cs and ^{137}Cs were compiled, the latter being repeated many times (see Chapter 5).

A reference observation network for monitoring soil contamination and atmospheric deposition was thus established for this zone. The reference network, still operating today,

Table 6.1
Measured contamination density (Ci/km^2) for certain long-lived radionuclides in the Chernobyl accident fallout pattern (Izrael et al., 1994b)

Sample mass (kg)	^{137}Cs	^{134}Cs	^{125}Sb	^{154}Eu	^{241}Am	^{238}Pu	^{239}Pu, ^{240}Pu	^{90}Sr
2.55	1.7	0.058	0.01	0.0034	0.028	0.028	0.0028	0.076
2.83	1.5	0.051	0.016	< 0.002	< 0.002	< 0.002	< 0.002	0.22
2.59	1.24	0.041	0.019	0.0023	0.0023	0.0023	0.0031	0.062
1.85	1.16	0.039	0.011	0.0045	0.0022	0.0022	0.0028	0.11
2.17	1.88	0.064	0.21	0.0033	0.002	0.002	0.002	0.13
2.63	1.8	0.06	0.017	0.004	0.0024	0.0024	0.0032	0.096
2.73	1.18	0.037	0.01	0.0042	0.0025	0.0025	0.0025	0.067
3.01	1.64	0.063	0.013	0.0046	0.0037	0.0028	0.0037	0.092
2.60	2.36	0.089	0.018	0.0032	0.0024	0.0024	0.0024	0.015

1 Ci/km^2 = 37 GBq/km^2.

consists of a radial system of concrete posts 1 m high on which deposition collectors of standard size may be mounted for a given period. The reference network was established in 1987 and already in that year soil sampling was twice conducted there. During the years that followed, including 1991, soil sampling and analyses were performed once a year. Initially, the samples were examined only in the laboratory using semiconductor gamma-spectroscopic analyses. Soil contamination results were compiled for ^{137}Cs, ^{134}Cs, ^{95}Zr, ^{95}Nb, ^{144}Ce and ^{106}Ru for the CNPS close-in zone. In the following years, ^{90}Sr, ^{238}Pu, $^{239+240}$Pu, ^{241}Am, ^{242}Cm and ^{244}Cm were added to the radionuclide set following the introduction of radiochemical and alpha-spectrometric methods. The distributions of these radionuclides were published as maps in the Atlas (Izrael (Ed.), 1998).

This intensive system of measuring radionuclide contamination within the 5–60 km zone gave results for both the absolute and relative amounts of the radionuclides deposited in this zone with adequate certainty. It is clear that, using these data, it is possible to determine the required characteristics of the contamination and doses for given time intervals. More extensive areas were examined repeatedly, i.e., the whole European territory of the former Soviet Union as well as many European countries. At present, an atlas of radiocesium contamination of Europe (including the European part of Russia) has been published (De Cort et al., 1998), as well as a second on the radioactive contamination by individual radionuclides in the European part of Russia, the Ukraine and Belarus (Izrael (Ed.), 1998). The future picture of contamination of the areas that were subject to the effects of the accident is also of interest.

An example of the prediction of ^{137}Cs contamination over large areas of Russia is given in Izrael et al. (1998). As to the possibility of measuring long-lived radionuclides at considerable distances from the source, Table 6.1 shows the results obtained at distances of hundreds of kilometers from the site of the Chernobyl accident (Izrael et al., 1994b).

Radioactive contamination distributions at ground level after the accidents at the "Mayak" nuclear enterprise in Kyshtym in the Southern Urals and at the Siberian chemical plant at Tomsk were also studied carefully (see Chapter 5). A rough map of the accumulated ^{137}Cs in the South Urals fallout pattern is shown in Fig. 5.30, this having been compiled on the basis of regional airborne gamma-spectral survey data for ^{137}Cs collected

in 1991 and 1992. The main portion of the 1957 release spread northeastwards (upper branch), while that of the 1967 release was distributed along a eastnortheasterly line (lower branch). The data presented in the map show a general structure of radioactive hotspots over the area, i.e., around the accident site. Additional information on contamination of this region with ^{137}Cs and ^{90}Sr have been presented in Chapter 5.

The data from several airborne gamma-spectral surveys of the area contaminated by radioactive products from the accident at the Siberian chemical plant (SCP) in Tomsk on April 6, 1993 have allowed us to reconstruct the contamination situation existing at any given time and to extrapolate it to other periods (see Chapter 5).

3. Reconstruction of Terrestrial Contamination from Nuclear Explosions

The reconstruction of fallout patterns from nuclear explosions that were carried out many years ago is more complicated but no less important. The most difficult problems are the following:

- to determine the location of the fallout pattern on a particular territory (the inhabited areas and the persons exposed in the contaminated zone at the time),
- to estimate the dose rates at the time of fallout,
- to estimate the possible total external and internal doses to the population from the fallout pattern.

Possible approaches to these problems are demonstrated in these important examples.

Figures 6.1 and 6.2 (Izrael et al., 1994c) show the rough fallout patterns from a high-yield thermonuclear explosion that occurred in August, 1953 at the Semipalatinsk Test Site. In 1990–1991, aircraft surveys conducted by the "Aerogeophizika" enterprise (which belonged to the State Committee for Mineral Resources) clearly show the outline of the fallout pattern and its distribution at a distance of more than a hundred kilometers from the site of the explosion. On the basis of the contamination density data, obtained 40 years after the explosion, one may reconstruct the radionuclide composition and the contamination density at the time of deposition (isotopic fractionation and induced activities are not included). The dose rate P_1 one hour after the explosion can also be deduced and hence also the external exposure dose rate $D_{1-\infty} \approx 5P_1$, where $D_{1-\infty}$ is the accumulated dose for the period from one hour to infinity.

Artemjev et al. (2000) have presented similar distributions within the 120 km sector for the fallout from the thermo-nuclear explosion of August 12, 1953 along the axis from the epicenter. These data are of extreme importance since they allow determination of the ratio between the long-lived radionuclides in the given fallout pattern (not only for ^{137}Cs and ^{90}Sr) which is important in reconstructing the dose from "old" local patterns of this type. Attention is drawn to the slightly lower content (1.5–2.0 times) of ^{137}Cs in the fallout pattern obtained from the aerial gamma-survey data. This can be explained by distortion of the altitude correction coefficients arising from the significant roughness of the ground. The average ^{137}Cs/^{90}Sr activity ratio in the fallout pattern, of 2.0, is very close to the theoretical value in the fission reaction. The average activity ratio $^{239-240}$Pu/^{241}Am was 3.3. In this case, the calculated exposure dose is about 30 mGy (300 R) at a distance of 50 km from the

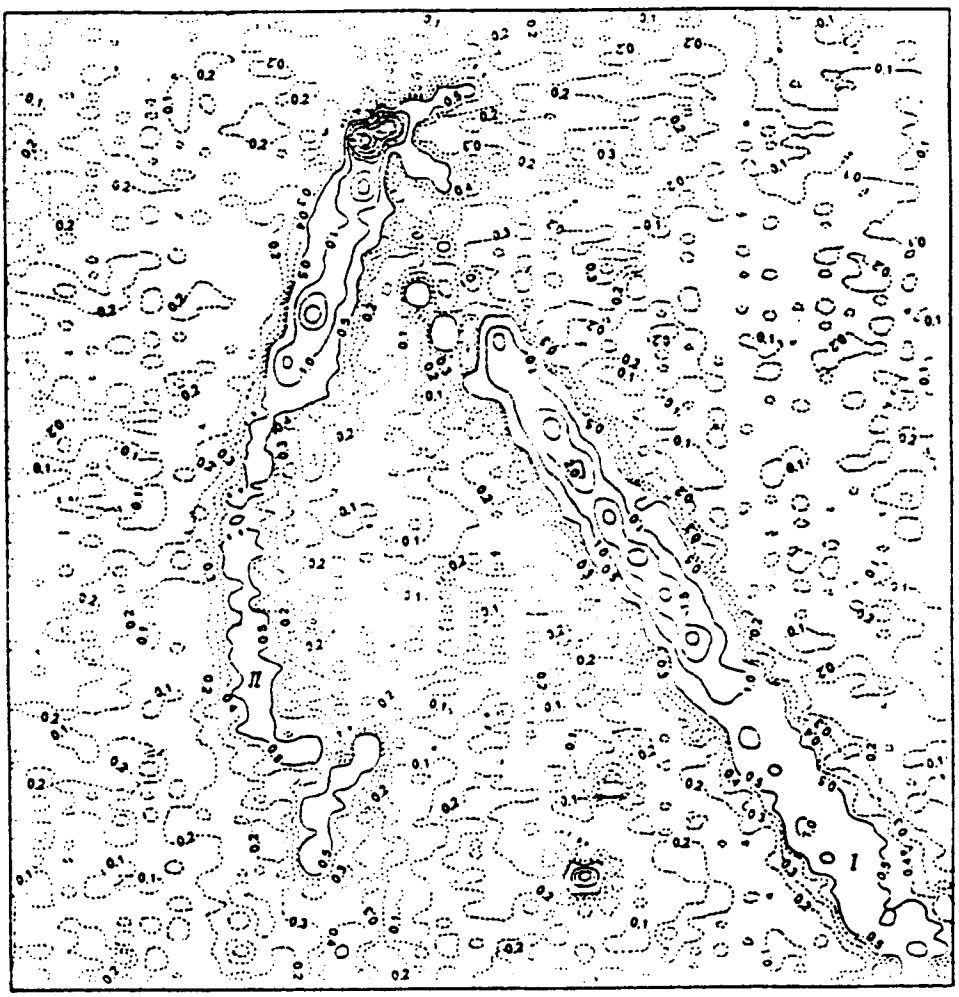

Fig. 6.1. Map of ^{137}Cs contamination at the Semipalatinsk Test Site (Ci/km^2) from the survey of 1991 — data collected by the state scientific production enterprise "Aerogeophizika" (see Izrael et al., 1994c) (1 Ci/km^2 = 37 GBq/km^2). I — the trace from the explosion in 1953; II — that from the explosion of 1951.

explosion. Undoubtedly this is approximate because, in some cases, the induced activity may contribute substantially as it did, for example, at the American "Sedan" explosion.

As we have seen in the above, the availability of basic activity data and the assurance that the given radionuclide is from the explosion under consideration are the governing factors in the calculation of doses and reconstruction of the initial fallout pattern. In this situation, we use the most reliable data on ^{137}Cs, because its fallout is closely connected to the fallout pattern outline that, in turn, is so dependent on the meteorological situation.

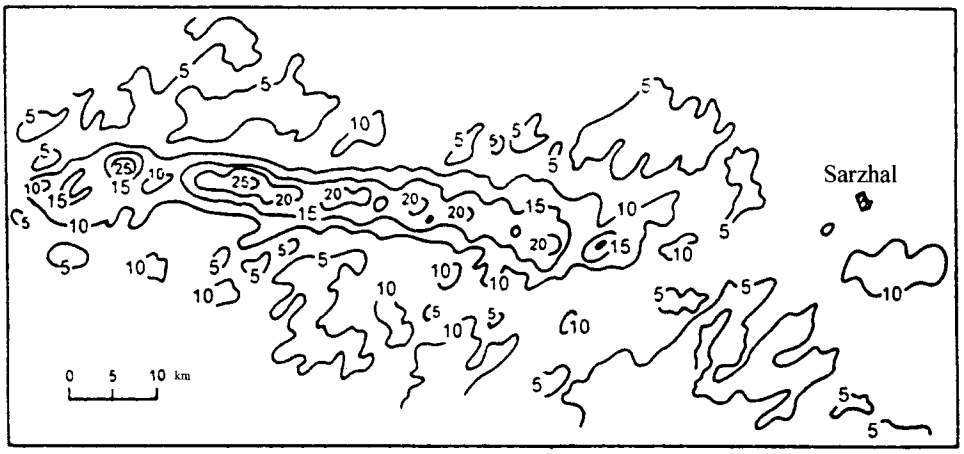

Fig. 6.2. Gamma-radiation exposure dose rates (μR/hr (≈ 10 nGy/hr)). Survey of 1991 — data from the state scientific production enterprise "Aerogeophizika" (Izrael et al., 1994c).

These examples demonstrate the feasibility of reconstructing a former radiation situation on the basis of the remnants of the activity patterns from a nuclear explosion. Additional material is presented as a map of the dose rates from the same survey (Fig. 6.2).

Let us now consider two complex situations in an example of reconstruction of a radioactive contamination distribution. A residual pattern (of dose-rate isolines) from the "Taiga" peaceful nuclear explosion exists at the boundary between the Perm' region of the Russian Federation and the Komi Republic (Fig. 6.3, Reshetov's data). Presumably, at present, the ^{60}Co contributes most significantly to the gamma-radiation dose rate and the ^{137}Cs contributes less so. In this situation, it would be impossible to reconstruct the dose from fission fragment activity at the explosion if the recent ratio between these radionuclides is not known. An analogous problem could arise for the residue from 1953 if it could only be examined in terms of the dose-rate isolines.

An example of an even more difficult reconstruction is that of the radioactive pattern and possible gamma-radiation doses in the Altai settlements that could be attributable to the first explosion of an atomic device at the Semipalatinsk Test Site in August 1949. Only individual spots with elevated ^{137}Cs contamination density (from 100 to 300 mCi/km^2, i.e., 3.7–11.1 GBq/km^2) can now be detected in the Altai (Fig. 6.4). In this situation, it is practically impossible to separate the ^{137}Cs deposition from a given explosion and the ^{137}Cs from global fallout if data are not available for any other radionuclide that was unique to the explosion of 1949. At present there is no clearly visible trace that can be attributed to the explosion of 1949 in the Altai. In this case, it is possible to model the travel of the contaminating air masses and the formation of the fallout pattern from data on the source as well as on the basis of the γ-radiation dose in the close-in zone and archived meteorological (and other) information; however, there are great uncertainties (Izrael et al., 1993b, 1994b, 1994c).

In reconstructions of exposure doses from old radioactivity patterns that were formed after the nuclear explosions decades ago, various approaches have been used, including:

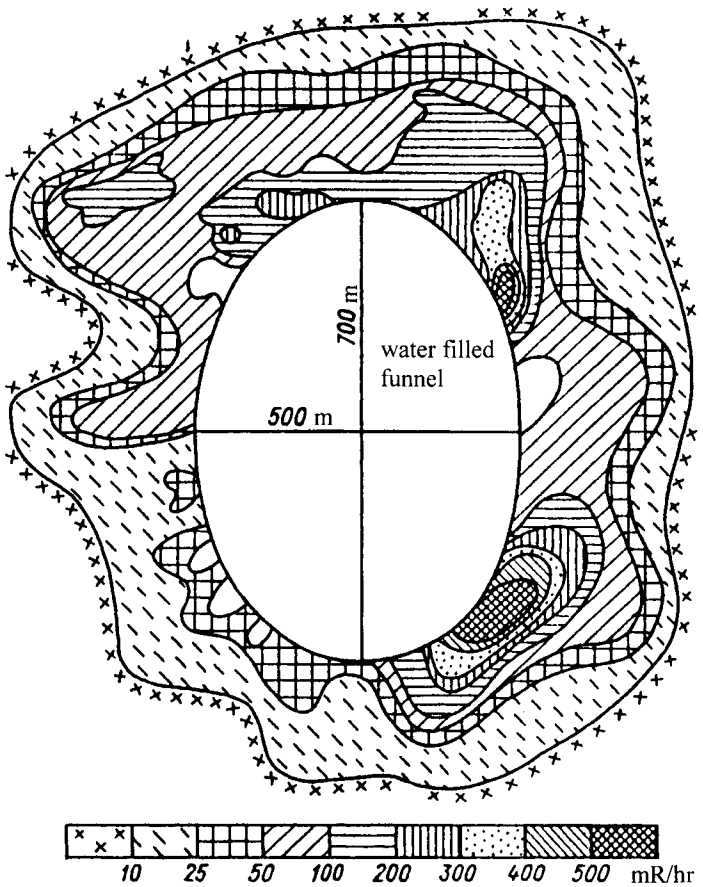

Fig. 6.3. Gamma-radiation dose rates in the region of the "Taiga" nuclear explosion. Survey of 1991 (Izrael et al., 1994c) (1 μR/hr ≈ 10 nGy/hr).

- the use of archived radiometric data;
- application of the numerous mathematical models that are available to construct fallout patterns from archived documents in areas where radiation data were not recorded immediately;
- the use of data on long-lived radionuclides, mainly ^{137}Cs and ^{90}Sr (based on the results from detailed airborne gamma-spectrometric surveys for determining ^{137}Cs, or soil sampling and laboratory analyses for ^{137}Cs and ^{90}Sr), with additional analyses of a small number of soil samples for ^{239}Pu and ^{240}Pu.

When performing this work, however, investigators have encountered significant difficulties in this approach, viz.:

- the lack of archived data on the radioactivity measurements and meteorological observations;

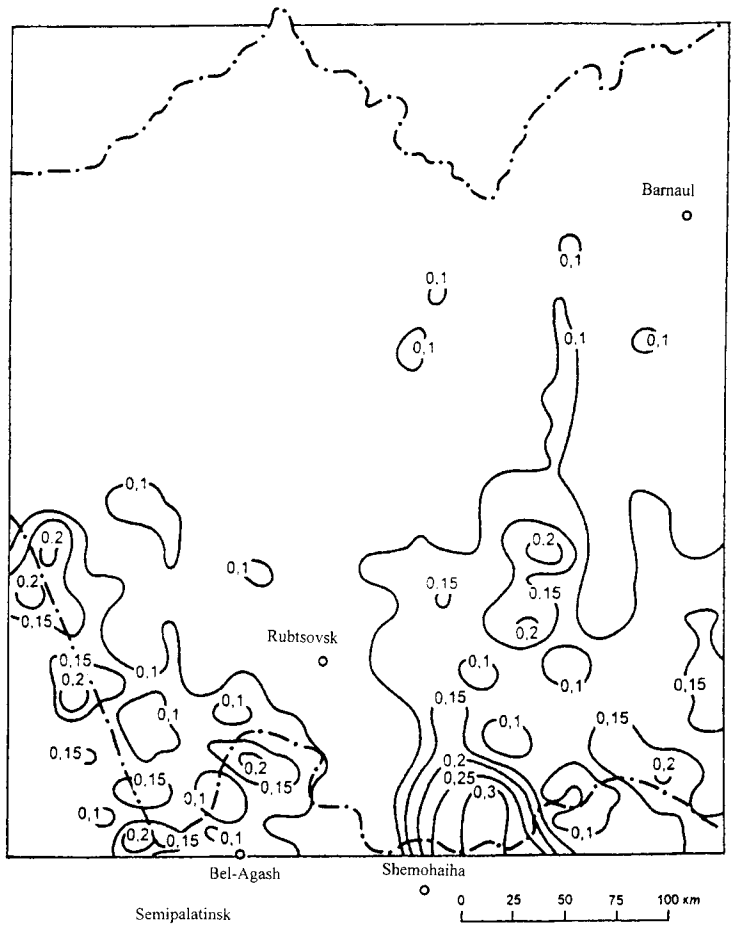

Fig. 6.4. Measurements of the ^{137}Cs contamination density (Ci/km^2) in the Altai territory in 1991 (Izrael et al., 1994c) (1 Ci/km^2 = 37 GBq/km^2).

- substantial deviations in the orientation of the "reconstructed" patterns due to inaccuracies in the meteorological data, source-term uncertainty, including explosion altitude and yield, as well as the size distribution of the radioactive particles;
- the presence of significant amounts of ^{137}Cs and ^{90}Sr of global fallout origin (and simultaneously layers of fallout patterns from several nuclear explosions).

These difficulties were the principal limitations to the proper reconstruction of exposure doses based on the radioactive patterns that remained many years after the nuclear explosions.

As previously noted, the currently measured ^{137}Cs contamination density in the Altai Region is 3.7–11.1 GBq/km^2 (100–300 mCi/km^2) (see Fig. 6.4). If it is assumed that the average contamination density from global fallout is 2.96 GBq/km^2 (80 mCi/km^2), then the remaining 0.74–8.14 GBq/km^2 (20–220 mCi/km^2) can be related to local nuclear

explosions and, primarily for the Altai Region, to the first nuclear explosion conducted in the USSR in August 1949 which gave rise to a cloud that moved towards the region. For specific locations in the area, however, the contamination could result not from a specific explosion, but solely or partially from global fallout, which had a range of values for ^{137}Cs from 0.37 to 14.80 GBq/km^2 (10–400 mCi/km^2) over the territory of the former Soviet Union. The higher values for global fallout were in the mountains and foothills, i.e., in zones of heavy precipitation. It is easy to calculate, for the above example, that the initial external dose associated with the nuclear explosion pattern, 50 years after the original fallout, will exceed the dose from global fallout by a factor of tens (short-lived radionuclides have essentially decayed away over this time period). The external-exposure dose from the global fallout will be below 0.5 R (rem) ($\leqslant$5 mSv), while for the above case (taking into account the decay of the short-lived radionuclides) it will be 25–30 R (rem) (250–300 mSv) for the nuclear explosion fallout pattern.

The meteorological situation, reconstructed from rather scanty archived information, does not permit the determination of the fallout outline or even its exact orientation with sufficient accuracy and measurements of only one radionuclide ^{137}Cs do not make it possible to separate, with any assurance, the local contamination from an "old" explosion against the background of global fallout.

To remove the existing uncertainties, one needs to find additional individual signals in the old radioactive fallout pattern which would allow its unique identification and permit the assessment of the dose rates from various radionuclides, but primarily ^{137}Cs, as well as the determination of the individual features of the fallout pattern for each explosion. This is especially important in the case where there is superposition of patterns from various explosions and a significant background of global fallout. Izrael et al. (1994b) proposed that such features could be:

(i) Aerosol-particle characteristics (each explosion features radioactive particles with individual characteristics); this is the principal difference between particles in local, and even some distant, fallout patterns and those in global fallout;

(ii) The radionuclide composition of these particles is also specific to each explosion and this is especially useful when these features are considered simultaneously with the changes in contamination characteristics at great distances from the source. It is difficult to single out individual particles and it is therefore expedient to identify the explosion by the ratio of characteristic radionuclides in soil samples.

For old nuclear explosion patterns, determinations of the maximum number of long-lived radionuclides and nuclide and isotopic ratios in particles and soil samples are necessary. Such a procedure is a complex but nevertheless feasible operation. These possibilities are considered below. For the purpose of comparison, global fallout samples should be treated in a similar way (in regions where "local" deposition certainly did not take place). As noted above, the radionuclide ratios obtained can be used to identify different fallout patterns and, subsequently, to reconstruct their essential characteristics.

A first approach used by Izrael et al. (1993b, 1994a) and others (Loborev et al., 1994) was based primarily on the measurement of ^{137}Cs and the utilization of dose-rate archives and meteorological data to reconstruct the fallout patterns of old nuclear explosions and accidents. Afterwards, the above methods were employed, including

Table 6.2
Long-lived radioactive products (half-life exceeding four years) in fission debris

Radionuclide	Products of thermal neutron fission of ^{235}U (Zysin et al., 1963)		Products of ^{239}Pu fission by fission-spectrum neutrons (Fleming, 1967)		Possibility of use as test indicator
	Half-life (years)	Yield (%)	Half-life (years)	Yield (%)	
^{79}Se	6×10^4	0.056	6.5×10^4	0.066	Possible
^{85}Kr	10.6	0.293	10.6	0.145	No
^{87}Rb	5×10^{10}	2.49		0.018	
^{90}Sr	28	5.77	28	2.14	Real
^{93}Zr	1.1×10^6	6.45	9.5×10^5	3.33	With difficulty
^{93m}Nb	12	6.45	3.7	3.33	Possible
^{99}Tc	2.1×10^5	6.06	2.1×10^5	6.10	
^{107}Pd	7×10^6	0.19	7×10^6	3.95	With difficulty
^{115}In	6×10^{14}	0.0097	6×10^{14}	0.064	No
^{121m}Sn	5	0.015	20	0.0004	Possible
^{126}Sn	2×10^5		2×10^5	0.075	
^{129}I	1.7×10^7	0.8	1.6×10^7	2.98	
^{135}Cs	2.6×10^6	6.41	2×10^6	6.56	With difficulty
^{137}Cs	30	6.15	30	6.83	Real
^{144}Nd	5×10^{15}		Stable	3.20	No
^{147}Sm	1.3×10^{11}	2.36	Stable	2.05	
^{151}Sm	80	0.44	90	0.884	Real
^{152}Eu	13.5	–			
^{154}Eu	16	–	16	0.0007	
^{155}Eu	4	0.033	1.7	0.249	

Note: A dash means the absence of data in the given literature source (Fleming, 1967) on the presence of ^{152}Eu and ^{154}Eu in fission debris. Stable means (according to Fleming, 1967) that the given radionuclide was considered to be non-radioactive.

searching for radioactive particles from the nuclear explosions, determining possible long-lived radionuclides so as to identify the fallout patterns and attempting to establish characteristic isotope and nuclide ratios for the various nuclear explosions. Radioactive patterns were found within some samples containing signals from two "old" nuclear explosions that had been conducted at the Semipalatinsk Test Site, namely the 20 kt nuclear (plutonium) tower explosion conducted on August 29, 1949 and the 430 kt thermonuclear tower explosion on August 12, 1953.

Melted, glassy particles some millimeters in diameter were found. Table 6.2 presents the long-lived radionuclides (with half-lives above 4 years) that result from nuclear fuel fission. Table 6.3 shows the radionuclides induced by nuclear-explosion neutrons on ground/soil fragments or on the explosion device itself (some radionuclides occur in both tables). Tables 6.2 and 6.3, therefore, illustrate the potential for use of a relatively large number of radionuclides in the identification of fallout patterns from earlier nuclear explosions.

Figure 6.5 presents the most typical reactions and variants of radioactive transformations of uranium and the transuranic radionuclides in the products of nuclear and thermonuclear explosions with nuclear fuels of various compositions.

Table 6.3
Long-lived radionuclides (of half-life exceeding four years) induced by nuclear-explosion neutrons

Radionuclide	Half-life (years)	Formation reaction	Possibility of use as test indicator
^{26}Al	7.3×10^5	$^{27}Al(n, 2n)$	Weak
^{36}Cl	3.01×10^5	$^{35}Cl(n, \gamma)$	
^{41}Ca	1.03×10^5	$^{40}Ca(n, \gamma)$	
^{59}Ni	7.6×10^4	$^{58}Ni(n, \gamma)$	Possible
^{60}Co	5.24	$^{59}Co(n, \gamma)$	Real
^{63}Ni	100	$^{62}Ni(n, \gamma)$	Possible
^{79}Se	6.0×10^4	$^{78}Se(n, \gamma)$	Weak
^{93}Zr	1.1×10^6	$^{92}Zr(n, \gamma)$	
^{93m}Nb	12	$^{93}Nb(n, n')$	Possible
^{94}Nb	2×10^4	$^{93}Nb(n, \gamma)$	
^{93}Mo	3500	$^{92}Mo(n, \gamma)$	
^{121m}Sn	5	$^{120}Sn(n, \gamma)$	
^{151}Sm	80	$^{150}Sm(n, \gamma)$	
^{150}Eu	36	$^{151}Eu(n, 2n)$	
^{152}Eu	13.5	$^{151}Eu(n, \gamma)$	
^{154}Eu	16	$^{153}Eu(n, 2n)$	Real
^{166m}Ho	1200	$^{153}Eu(n, \gamma)$	
^{178m}Hf	31	$^{165}Ho(n, \gamma)$	Possible
^{186m}Re	2×10^5	$^{177}Hf(n, \gamma)$	
^{192m}Ir	240	$^{185}Re(n, \gamma)$	Weak
^{193}Pt	60	$^{191}Ir(n, \gamma)$	Possible
^{205}Pb	1.5×10^7	$^{192}Pt(n, \gamma)$	
		$^{204}Pb(n, \gamma)$	Weak

Note: Half-life data mainly from Zysin et al. (1963).

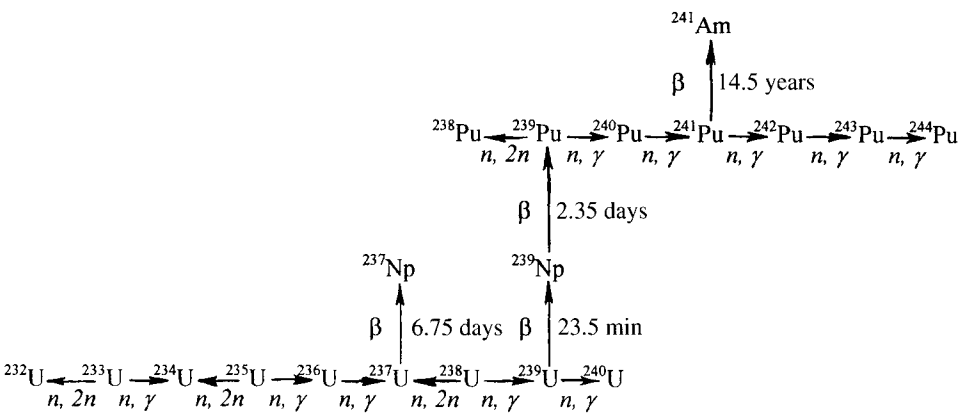

Fig. 6.5. The most typical reactions and transformations of uranium and the transuranic radionuclides leading to their appearance in the atmosphere after nuclear and thermonuclear explosions (Thomas and Perkins, 1975).

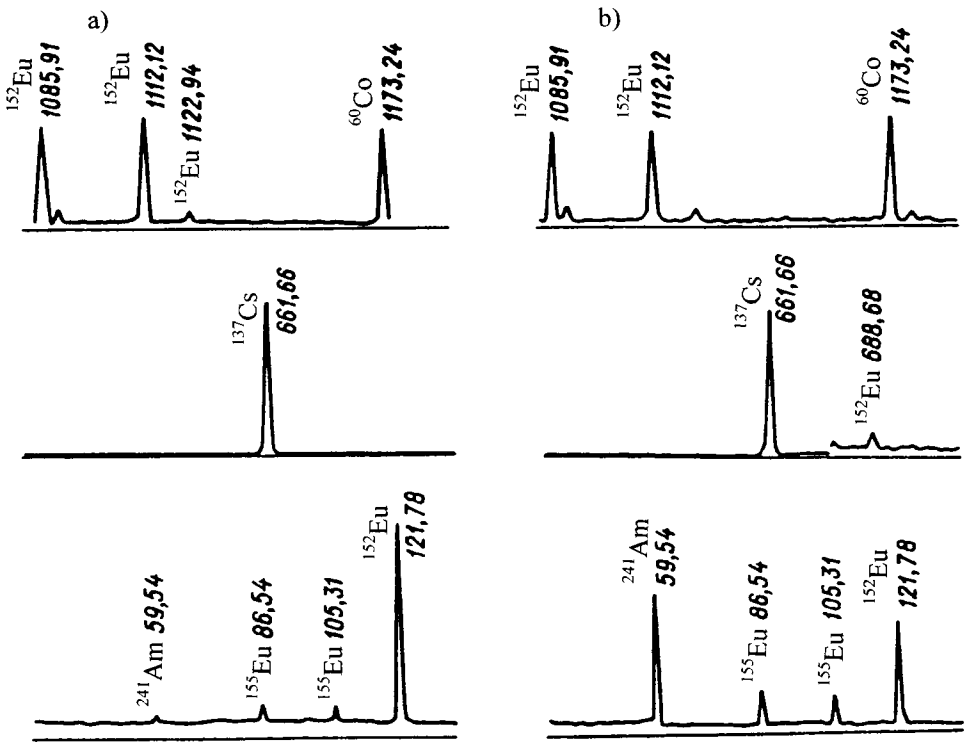

Fig. 6.6. Fragments of the semiconductor gamma-spectra of aerosol particles from the fallout from a nuclear explosion conducted on August 29, 1949 (a) and from a thermonuclear explosion conducted on August 12, 1965 (b). Measurements of 1994 (Izrael et al., 1994b). The radionuclide symbols and gamma-radiation energies (keV) are indicated above the peaks in the spectra.

Figure 6.6 shows the fragments of gamma spectra (measured using a semiconductor gamma spectrometer) of the large-size aerosol particles sampled in the fallout patterns of the 1949 and 1953 explosions. From the spectra, one can see the distinct gamma-lines of the following long-lived radionuclides: ^{137}Cs, ^{60}Co, ^{152}Eu, ^{154}Eu, ^{155}Eu and ^{241}Am. ^{60}Co is an induced product; ^{152}Eu and ^{154}Eu belong to both groups, induced and fission-fragment activities; ^{155}Eu belongs to the fission fragment group and ^{241}Am accumulates as a result of ^{241}Pu decay (see Fig. 6.6). It should be noted that ^{152}Eu and ^{154}Eu were found by us in aerosol particles as long ago as 1963.

As was expected, ^{241}Am was found in the particles, its relative amount being greater in particles from the 1953 explosion. A detailed study of the gamma-spectra shows that some of the lines are not yet identified. This could lead to an extension of the list of the long-lived radionuclides.

Tables 6.4 and 6.5 present the measured activities of various radionuclides in the particles (Bq/particle) as well as the ratios of the activity of the detected nuclide to that of ^{152}Eu in the particles and glassy slag in the explosion zone. One can see a relatively small

Table 6.4
Activities of different radionuclides (and their ratios) in particles from explosions in 1949 (the first four samples) and 1953 (latter four samples) at time of measurement (Bq/particle) (Izrael et al., 1994b)

Number of sample	^{60}Co	^{137}Cs	^{152}Eu	^{154}Eu	^{155}Eu
49P1	2.18×10^1	1.27×10^3	8.65×10^1	2.69	3.31×10^1
49P3	2.51	1.69×10^1	5.27×10^1	2.30	0.87
49P8	3.01	4.02×10^1	5.07×10^1	1.79	2.02
49P10	7.74	2.69×10^2	6.51×10^1	2.36	8.42
53P1	7.37	4.02×10^2	5.05×10^1	4.86	2.06×10^1
53P2	7.55	1.06×10^3	5.99×10^1	4.63	2.66×10^1
53P4	7.25	1.66×10^2	5.52×10^1	4.83	1.29×10^1
53P6	9.41	7.05×10^2	4.64×10^1	5.07	3.54×10^1
	^{241}Am	^{241}Am/^{152}Eu	^{154}Eu/^{152}Eu	^{137}Cs/^{152}Eu	^{60}Co/^{152}Eu
49P1	1.48×10^1	0.17	0.034	14.7	0.25
49P3	0.36	0.0068	0.044	0.32	0.048
49P8	1.12	0.022	0.035	0.79	0.059
49P10	4.00	0.061	0.036	4.13	0.12
53P1	1.72×10^2	0.43	0.096	7.96	0.15
53P2	1.48×10^2	0.14	0.077	1.78	0.13
53P4	9.90×10^1	0.60	0.088	3.01	0.13
53P6	2.78×10^2	5.99	0.11	15.2	0.20

1 Bq ≈ 27 pCi.

Table 6.5
Activities of different radionuclides and their ratios at the time of sample measurement (Bq/sample) in glassy-slag samples at ground zero (at epicenter of explosion) (Izrael et al., 1994b)

Number of sample	^{60}Co	^{137}Cs	^{152}Eu	^{154}Eu	^{155}Eu	^{60}Co/^{152}Eu	^{154}Eu/^{152}Eu
			Explosion of 29 August, 1949				
5	7.41×10^5	1.84×10^5	3.29×10^5	4.72×10^4	9.81×10^5	2.25	0.14
			Explosion of 12 August, 1953				
1	9.63×10^5	1.56×10^5	6.88×10^5	9.23×10^4	4.76×10^6	1.40	0.13
2	3.96×10^5	4.50×10^4	2.01×10^5	3.21×10^6	2.50×10^6	1.97	0.16

1 Bq ≈ 27 pCi.

spread in the numerical values of the ^{154}Eu and ^{60}Co radionuclide ratios of the particles and a larger (but typical) difference in the ^{137}Cs and ^{241}Am relative to ^{152}Eu.

The ratios of radionuclide activities obtained require further detailed analysis (with regard to possible fractionation) and the collection of more statistical data but it is already evident that the determination of long-lived nuclides in the particles (or samples) of the old patterns of nuclear explosions is a feasible and very informative way of characterizing these patterns.

Some questions and relevant problems arise, such as what should be done about the soluble radionuclide fraction that has migrated away from the particles for many years? According to experimental data, it is a comparatively small part of the total particle activity. Sampling and analysis to a depth of 0.5 to 1.0 m can eliminate these latter uncertainties.

An analogous calculation for the Chernobyl fallout pattern, based on this model and using archived meteorological data, has been repeatedly applied to other examples of nuclear-explosion patterns by Izrael et al. (1990) and Petkevich et al. (1994).

Figure 6.7 shows the gamma-field distribution on the territory adjacent to the CNPS accident zone, at dose rate isolevels of 0.05 and 0.2 mR/hr ($\approx$ 0.5 and 2.0 μGy/hr) on June 10, 1986. In addition, the deposition fields, calculated according to the model at distances of hundreds of kilometers from the source, are presented (Izrael et al., 1989b). Parameters for the normal logarithmic distribution of particles were chosen in the model in such a way that the distribution areas prescribed by the isolines were nearest to the measured ones. As a whole, good agreement between the measured and calculated data does exist, although considerable discrepancies do arise in certain cases. On average, the calculated and measured values of the total deposition differed by not more than three-fold.

It should be noted, with this model, that close correspondence to the actual data does, in fact, exist but without strict concurrence with respect to location. Even minor errors in the meteorological data (which, as a rule, are insufficient) can move the calculated fallout pattern away from its real location and other uncontaminated areas may then be included in the study zone.

An especially interesting challenge is to reconstruct the contamination source on the basis of various data, taking into account highly dissimilar circumstances. This problem is of primary importance for nuclear accidents (in cases of test explosions, the available data on the source are used) but it became especially pressing for the Chernobyl accident, for the initial time period of hours and days when the dose characteristics were not recorded clearly enough and were, as a result, extremely uncertain. It seems that the most reliable information that can be used to reconstruct the contamination source for the Chernobyl accident, from the viewpoint of the subsequent prolonged exposure, are the data on measured dose rates and the concentrations of individual radionuclides in the atmosphere and on the ground at different locations, coupled with our understanding of certain physical concepts (Izrael et al., 1990, 1994a; Abagyan et al., 1986a & b; Sivintsev and Khrulev, 1995).

However, the problem of the reconstruction of the source of contamination on the basis of measurement data at specific points is a unique issue. Its solution is of primary importance so as to facilitate various predictions for different types of accidents. Highly reliable calculations of doses to the population after a specific accident may be obtained (and actually have been obtained for the Chernobyl and Urals accidents) by carrying out the most detailed measurements of the actual contamination of the atmosphere, the lithosphere and hydrosphere.

In summary, it may be stated again that:

– The reconstruction of fallout patterns from old nuclear explosions and accidents where radioactivity releases occur is a real problem, especially the aftermath of the Chernobyl accident, when people wished to have data on the past and present radiation situations in their own particular regions;

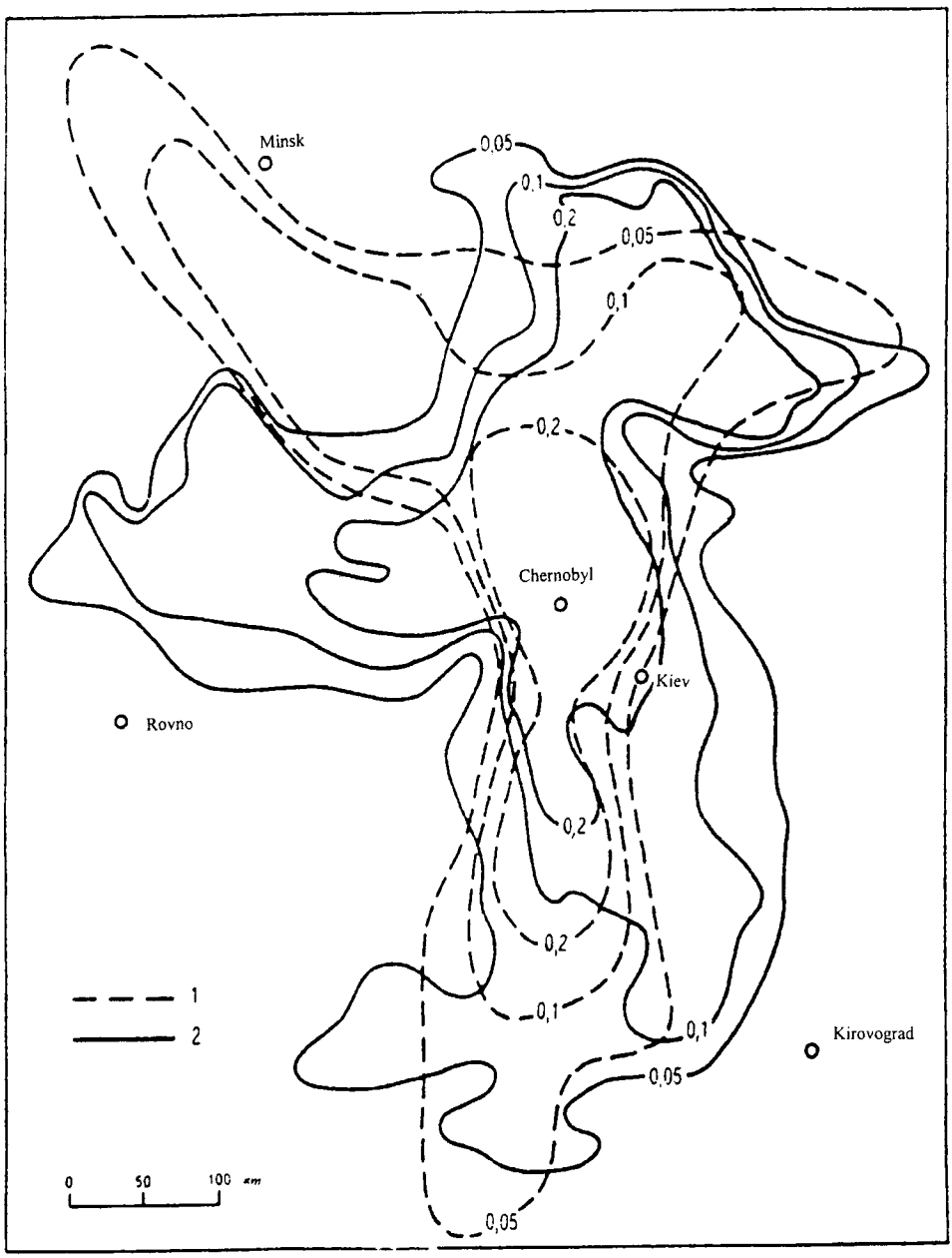

Fig. 6.7. Calculated (1) and measured (2) distribution of radiation levels (mR/hr) on the ground after the Chernobyl accident (on June 10, 1986) (1 mR/hr $\approx$ 10 μGy/hr).

– The reconstruction (if only partial) is most effective when reliable actual data on individual radionuclide densities are available (even if only on one individual nuclide if we are sure it belongs to the particular source in question);

– In the situation where completely reliable data on the range of fission product radionuclides are not available, one should at least have information on one additional radionuclide that characterizes the given explosion (or on the activity ratio of two radionuclides);

– When proceeding with the reconstruction, one should carefully analyze all the available information on contamination levels, geometrical configuration of the existing fallout pattern (together with the archived data), the depth of radionuclide penetration in the soil, etc.;

– In the situation where reliable factual data are deficient, or not available, it is still possible to model the radioactivity distribution. However, one should use extreme caution, because errors in the geographical location of the fallout pattern are possible during the modeling due to deficiencies in the archived meteorological information (at various heights and along the path of the fallout pattern);

– If accidents occur with a concurrent release of radioactivity, then an extensive data base must be compiled (as has been done for Chernobyl and Tomsk-7). This permits the reconstruction of crucial data on the contamination density of different environments and/or the dose characteristics.

This Page Intentionally Left Blank

Chapter 7

GAMMA-RADIATION FIELD ABOVE THE FALLOUT PATTERNS OF A NUCLEAR EXPLOSION

Contents

1. Calculation of the Surface γ-Radiation Exposure Dose Rate 231
2. Influence of Natural Environmental Conditions on the Surface γ-Field 233
3. Aerial γ-survey. Determination of the Total Surface Density of the Terrestrial Contamination from the Measured Dose Rate 236
4. Aerial γ-survey. Estimation of the Surface Density of the Terrestrial Contamination by Individual Nuclides 239

1. Calculation of the Surface γ-Radiation Exposure Dose Rate

Radioactive fallout (both close-in and distant) results in the surface contamination of the land. During the first weeks or months, the radioactive constituents of the fallout, under the influence of different processes, gradually start to penetrate deep into the soil. The radionuclides are transported to depth either with particle-carriers or, separately, as a result of being washed out or following particle destruction. This results in the contamination of the upper layers of the soil down to several centimeters depth. Different authors have indicated that, during the first several months, the upper (5–6 cm) layer contains 80–95% of the total radioactivity and it is only after several decades that part of the radioactivity penetrates deeper, to 0.5 m or more. An exception occurs in ground bulk at the epicentral zone, formed after an underground cratering explosion, where the radioactivity is dispersed immediately throughout the accumulations of rocks, etc.

It is logical to assume that, during the early periods after fallout is deposited, the gamma-field over a plain forestless surface (e.g., a desert, as typically found, for example, at the Semipalatinsk Test Site), is practically identical to the gamma-field of a planar isotropic source. If we take into account multiple scattering of the γ-radiation and use the analytical form for dose factor presentation, then the dose rate P at a height h above an infinite isotropic source of monochromatic radiation, according to Izrael and Stukin (1967), is

$$P(h)_\infty = \frac{k\sigma\sigma_a}{2}\left[E_1(\mu h) + \frac{e^{-\mu h}}{7E^{2.4}}\left(1 + 7E^{2.4} + \mu h\right)\right], \tag{7.1}$$

where σ is the surface density of the contamination, k is a constant, depending on the measurement units, σ_a and μ are, respectively, linear coefficients for γ-radiation absorption and attenuation in air and E is the energy of the initial γ-radiation; $E_1(x)$ is an integral exponential function such that

$$E_1(x) = -E_i(-x) = \int_x^\infty \frac{e^{-t}}{t}\,dt. \tag{7.2}$$

The dose factor arising from scattered radiation is approximated by the expression

$$B_0(\mu r, E) = 1 + \mu r + \frac{(\mu r)^2}{7E^{2.4}}. \tag{7.3}$$

Note that the numerical value of k for the fallout patterns of nuclear explosions is taken to be 5.09×10^{-2} (R/hr)/(MeV·cm^3·s) (for the average energy of the γ-radiation in the fallout). Below are the average values of the recalculated altitude coefficients $K_H(h) = P(h)/P(H)$ for energies within the range 0.225–2 MeV and H from 1 to 100 m:

h (m)	1	10	25	50	100	200
$K_1(h)$	1	0.57	0.41	0.29	0.17	0.07
$K_{100}(h)$	5.8	3.3	2.4	1.7	1.0	0.40

Within the range of energies of nuclear contamination, the altitude-recalculated coefficients do not change significantly (by less than 20%) (Izrael, 1964). The dependence of $P(h)_R/P(h)_\infty$ on the radius of the sites R for different heights h and energy 0.7 MeV (the average energy of the γ-radiation of a nuclear explosion) was analyzed by Izrael and Stukin (1967). With this analysis, the fraction $\alpha = P(h)_R/P(h)_\infty$ of the dose rate contributed by a site with any radius R to the total dose rate from a site with infinite radius can be evaluated.

Note that, up to a height and radius of ~200 m at sites contributing similar fractions of the total dose at the observation point, the dose rates do not differ by more than 20% over the energy range 0.5 MeV $< E <$ 1.5 MeV at $\alpha < 0.8$ and depend only to a slight degree on the initial energy of the γ-radiation. Up to $h = 200$ m, for energies of 0.5–2.5 MeV and for contaminated sites with radii larger than 500 m, one can use Eq. (7.1) which was developed for a site of infinite radius. Using this approach, the error does not exceed 10%.

Table 7.1 shows the results of calculation of the dose rate at a height of 1 m from a planar isotropic source covered with the radionuclides that are the most common in global fallout (surface concentration of radiation is taken to be 100 mCi/km^2 (= 3.7 GBq/km^2)).

The intensity of non-scattered γ-radiation above the planar isotropic source covered by monochromatic radiation is as follows:

$$I(h) = \frac{\sigma E_1(\mu h)}{2} \tag{7.4}$$

Table 7.1
The dose rate above a planar source of contamination by different radionuclides

Radionuclides	σ [MeV/(cm^2 s)]	Calculated dose rate (mR/hr) (Izrael, 1964)
^{95}Zn + ^{95}Nb	0.28	1.40
^{103}Ru	0.164	0.83
^{106}Ru (^{106}Rh)	0.070	0.36
^{137}Cs + ^{137m}Ba	0.20	1.00

1 mR/hr ≈ 10 μGy/hr.

and

$$\sigma = 2\mu \int_0^\infty I(h)\,\mathrm{d}h. \tag{7.5}$$

Integrating the spectral-angular function of radiation from the planar isotropic source with respect to either direction or energy, one can easily obtain the angular or spectral distribution of the radiation. Izrael and Stukin (1967) and Kogan and Fridman (1960) have presented data on these distributions.

The dose rate $P^V(h)$ at height h above an infinite layer of radiation, which concentration of contamination $\sigma_V(z)$ decreases exponentially with depth z (e.g., contamination of soil by radioactive products after a nuclear explosion), can be written in the following form (Izrael and Stukin, 1967):

$$P^V(h) = \frac{k\sigma_{V_0}\sigma_a}{2m}\left\{E_1(\mu h) - \mathrm{e}^{-(\beta-1)\mu h}E_1(\beta\mu h) + \frac{\beta-1}{\beta}\mathrm{e}^{-\mu h}\left[1 + \frac{1}{7E^{2.4}}\left(1 + \mu h + \frac{1}{\beta}\right)\right]\right\}, \tag{7.6}$$

where $\sigma_V(z) = \sigma_{V_0}\mathrm{e}^{-mz}$, σ_{V_0} is the contamination concentration in the near-surface layer, $\beta = 1 + m/\mu_0$; μ_0, μ are linear coefficients for absorption of gamma energy E by the ground and the air, respectively. In this case, the intensity of the non-scattered radiation is expressed as

$$I_V = \frac{\sigma_{V_0}}{2m}\left[E_1(\mu h - \mathrm{e}^{-(\beta-1)\mu h}E_1(\beta\mu h))\right]. \tag{7.7}$$

2. Influence of Natural Environmental Conditions on the Surface γ-Field

The γ-radiation field above a ground surface actually contaminated by radionuclides differs from that of an idealized planar isotropic source located in infinite atmospheric surroundings. The differences are conditioned by:

(i) the influence of substances in the underlying surface, being distinguishable from the air by its density and atomic composition;
(ii) irregularities/roughness in the underlying surface;
(iii) the presence of vegetation;
(iv) any change in air density depending on temperature, pressure and humidity under real conditions as well as by the occurrence of precipitation (rain and snow).

The influence of these factors on the γ-radiation field above a contaminated land surface under natural conditions has been considered by Izrael (1963, 1964 and 1974) and Izrael et al. (1962), Izrael and Stukin (1967), and by others based on the assumption that the source remains only at the surface. The results obtained are briefly presented below.

Experimental and calculated data show that the dissimilarity between the atomic number of the ground and that of the water/air does not have a practical effect on the distribution

of the γ-radiation dose rate in the air from a planar isotropic source that is located at the interface between these media. The influence of micro-relief on the γ-radiation field of the surface contamination leads to screening/shielding by soil undulations and thus a part of the radiation is not seen at the observation point. A detailed experimental investigation of the influence of micro-relief on the γ-radiation field of the surface contamination has been carried out (Izrael, 1963). The results showed that micro-relief only influences the γ-radiation field at low heights and that, at levels above 10 m, its influence can be neglected. When making measurements at a height of 1 m, we can, for practical calculations, take the following correction coefficients for the decrease in radiation levels: 0.75–0.80 for even surface sites, 0.7 for steppe and 0.5–0.6 for arable lands.

If the radioactive products were deposited in a region covered with vegetation, then, at some time later, the surface source of contamination is transported beneath the vegetation cover because of the influence of wind and rain. In this case, the vegetation cover screens the γ-radiation from the terrestrial contamination. This screening is especially noticeable in a forest stand zone.

The absorption properties of plants are mainly determined by the biomass distribution. For a given type of planting, the amount of forest biomass, calculated per unit area, depends on the conditions of growth, the completeness of cover and the age. Izrael (1974) has described the biomass storage factor, q, for the most widespread types of plantings. In connection with the fact that wood consists mainly of organic compounds, the whole system of absorbing media (soil, forest biomass, air) can be considered in terms of an air-equivalent medium. If we neglect the anisotropy of the absorbing medium in our calculations (this does not result in great error), then, according to Izrael and Stukin (1967), the coefficient of screening of the γ-radiation dose rate amounts to

$$f(q) = \frac{P(\mu_1 H)}{P[\mu_1 H + (\mu_2/\kappa)q]} \tag{7.8}$$

for a forest vegetation cover. Here, μ_1 is the linear coefficient of attenuation of the γ-radiation in air; μ_2/κ is a mass coefficient of attenuation in wood, where κ is the wood density; H is the height of measurement ($H > h$, where h is the height of the planting); q is the biomass storage, g/cm^2.

Figure 7.1 shows the relationship between the coefficient $f(q)$ and age T and the estimated productivity for different forest plants (the latter indicated in parentheses where I denotes the best, III is medium and V is the worst). To calculate the screening influence of the forest at $H < h$, it is necessary to substitute in expression (7.8) the amount of biomass enclosed within the layer between the surface and height H.

Usually, the re-calculation of a dose rate from height h of a survey to height $h = 1$ m is performed for a homogeneous atmosphere under standard conditions, i.e., constant density with $\rho = 1.293$ g/l, $t = 0$ °C and pressure 760 mm Hg. It is known that the standard atmospheric density changes with height and is well described by the barometric formula. It is an easy matter to show that, for the standard atmosphere, the coefficient of recalculation of the radiation dose rate from a height of 200 m to the earth's surface, $K_{200}(1)$, is different from that calculated earlier for a homogeneous atmosphere, by a value not greater than 2% (not greater than 4% for non-scattered γ-radiation). At lesser heights, this change is smaller

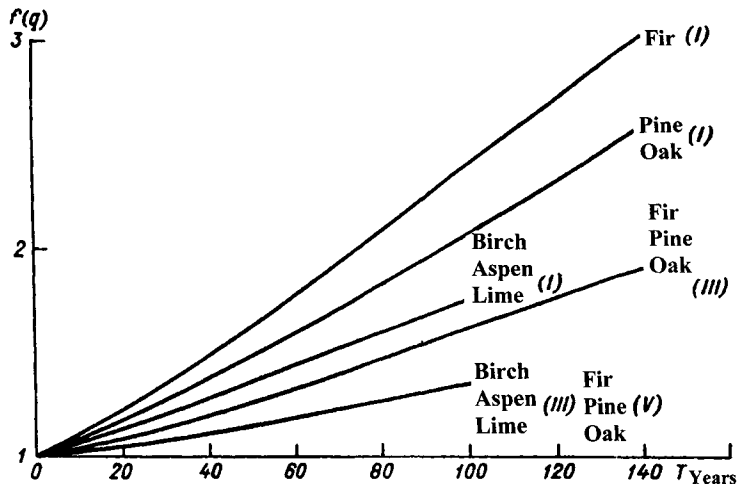

Fig. 7.1. Dependence of the coefficient $f(q)$, for screening the γ-radiation by forest cover, on biomass storage q.

still. Changes in air temperature T, pressure p (but not water content W) affect the values of the recalculation coefficients more so.

$K_{100}(1)$ for the dose rate does not change essentially with variations in the water content of air (the value of 10^{-6} g/cm^3 corresponds to a thick fog, while 4×10^{-6} g/cm^3 is appropriate to a heavy rain). The temperature change from -30 to $+30$ °C results in a $K_{100}(1)$ change of approximately 20%, while a pressure change of 50 mm Hg changes $K_{100}(1)$ by about 5%. For the intensity of the primary γ-radiation, changes of this coefficient are more essential.

Coefficients of recalculation $K_h[H]$ for real conditions are determined by:

$$K_h[H] = K_{h_0}(H_0), \tag{7.9}$$

where

$$h_0 = h\frac{\rho(N, p, W)}{\rho_0} \quad \text{and} \quad H_0 = H\frac{\rho(T, p, W)}{\rho_0}$$

and $K_{h_0}(H_0)$ is the coefficient of recalculation for a homogeneous atmosphere. In addition, it should be noted that, when determining σ from the measured dose rate P, the most widespread source of errors is from the medium absorbing the γ-radiation not being described in "air-equivalent" terms. This effect happened to be the source of error when casual and unprofessional measurements of the dose rate were made using the geological "SRP" instrument in some contaminated areas after the Chernobyl accident (see the introductory Glossary of definitions and units for details of this error source). A "non-equivalent-to air" NaI (T1) crystal was used in this instrument as the γ-radiation detector. Here, the errors were equal to 1.5–2.0 times and larger. The crystal was used to improve the instrument sensitivity in geologic surveys but it was not designed to measure the exposure dose rate of the γ-radiation.

A correction factor η for "non-equivalency-to air" of a Roentgenometric instrument can be determined from the expression (Izrael and Stukin, 1967)

$$\eta(E_0) = \frac{\int_0^{E_0} I(E_0, E)\xi(E)\sigma_a(E)\,dE}{\int_0^{E_0} I(E_0, E)\sigma_a(E)\,dE}, \tag{7.10}$$

where $I(E_0, E)$ is the spectral composition of the γ-radiation at the measurement point, $\xi(E)$ is a change in sensitivity of the dose rate detector with E and E_0 is the primary energy of the γ-radiation.

3. Aerial γ-survey. Determination of the Total Surface Density of the Terrestrial Contamination from the Measured Dose Rate

The dose rate P_H near the earth's surface (at height $H = 1$ m) can be determined from the measured dose rate P at some other height h (for instance, from onboard an aircraft during a gamma-survey):

$$P_H = P(h)K_H(h)\eta_r(h)\eta_f(h)\eta_p(h)\eta_t(h)\eta_w(h), \tag{7.11}$$

where $K_H(h)$ is the altitudinal recalculation coefficient from height H to height h for an ideal even surface and a standard atmosphere; $\eta_i(h)$ are correction coefficients taking into account the influence of real conditions; $\eta_r(h)$ are those for the roughness of the earth's surface, $\eta_f(h)$—for vegetation (mainly forest) cover, $\eta_p(h)$—for pressure, $\eta_t(h)$—for temperature, and $\eta_w(h)$—for air humidity.

As shown in previous sections, the value of $K_H(h)$ for $1\text{ m} \leqslant H \leqslant 200$ m depends only to a slight extent on the primary energy of the γ-radiation within the range of the radiation energies from products of nuclear explosions. Average values have been presented in Section 1 (for $H = 1$ and 100 m). Values of the correction coefficients $\eta_i(h)$ have also been presented in previous sections; for the most part, they (η_p, η_t, η_w) are close to unity.

The mathematical relationships between the surface density of the contamination σ on the surrounding land and the dose rate P are also presented in previous sections. An approximate value for the surface concentration of the γ-radiation σ, expressed in terms of energy units can be determined, with an accuracy of up to 20–25%, from the known dose rate P at height $h \approx 200$ m where the spectral composition of the gamma-radiation is not known but within the limits stated using expression (7.1). Data from surface measurements of the contamination density can be used for the experimental determination of a real numerical value of the coefficient relating P to σ in (7.1). It is possible, however, to dispense with the determination of this coefficient, as shown by Izrael (1964), using the expression:

$$\int_0^{\infty} P(h)\,dh = \frac{k\sigma}{2}. \tag{7.12}$$

From (7.12) and the relationship

$$P(h) = P(H)K_H(h) \tag{7.13}$$

it follows that

$$\sigma = \frac{2}{k}\int_0^\infty P(h)\,\mathrm{d}h = \frac{2P(H)}{k}\int_0^\infty K_H(h)\,\mathrm{d}h. \tag{7.14}$$

Hence, to determine the numerical value of the coefficient relating σ to $P(H)$ in (7.13), it is sufficient to know the dependence of $k_H(h)$ above the radiative plane. On the basis of (7.14), we can write

$$\sigma = L_H P(H), \tag{7.15}$$

where

$$L_H = \frac{2}{k}\int_0^\infty K_H(h)\,\mathrm{d}h. \tag{7.16}$$

The scatter of values for L_H, calculated for different values of E within the range 0.09–3.0 MeV, is smallest when $H = 100$–150 m. Thus the height interval $H = 100$–150 m is optimal for calculations of σ from measured values of $P(h)$ under an unknown spectral composition of the primary γ-radiation, i.e., for the γ-survey of contaminated ground. For $H = 100$ m, $L_H = 1.2 \times 10^6$ MeV/(cm^2 s)/(R/h).

Having written

$$M_H = \int_0^\infty K_H(h)\,\mathrm{d}h \tag{7.17}$$

we obtain, for $H = 100$ m, $M_H = 318$ m (+7%). For $H = 1$ m, $L_H = 2.1 \times 10^5$ MeV/(cm^2 s)/(R/h) and $M_H = 55$ m. In the case of the radioactive fallout pattern, on rather barren, almost plantless, territory, the M_H value would be slightly larger than 55 m. Thus when determining the total amount of a radioactive substance at a contaminated site, one can use the above relationships.

If the radioactive products were distributed irregularly over the area as, for example, in the close-in fallout patterns of nuclear explosions, then, when crossing the contaminated site, one can directly determine the total amount, A of the substance (in energy units) at any selected site just by measuring the dose rates at different levels above the contaminated land. Thus, assuming that about half of the energy radiated by the surface source is in the form of γ-radiation and the integration is performed along the fallout pattern (R is the distance along the pattern axis and l is the distance across the axis), it follows that:

$$A = 2c\int_R\int_l P_H(R,l)\,\mathrm{d}R\,\mathrm{d}l\int_H K_H(h)\,\mathrm{d}h, \tag{7.18}$$

where c depends on the measurement units.

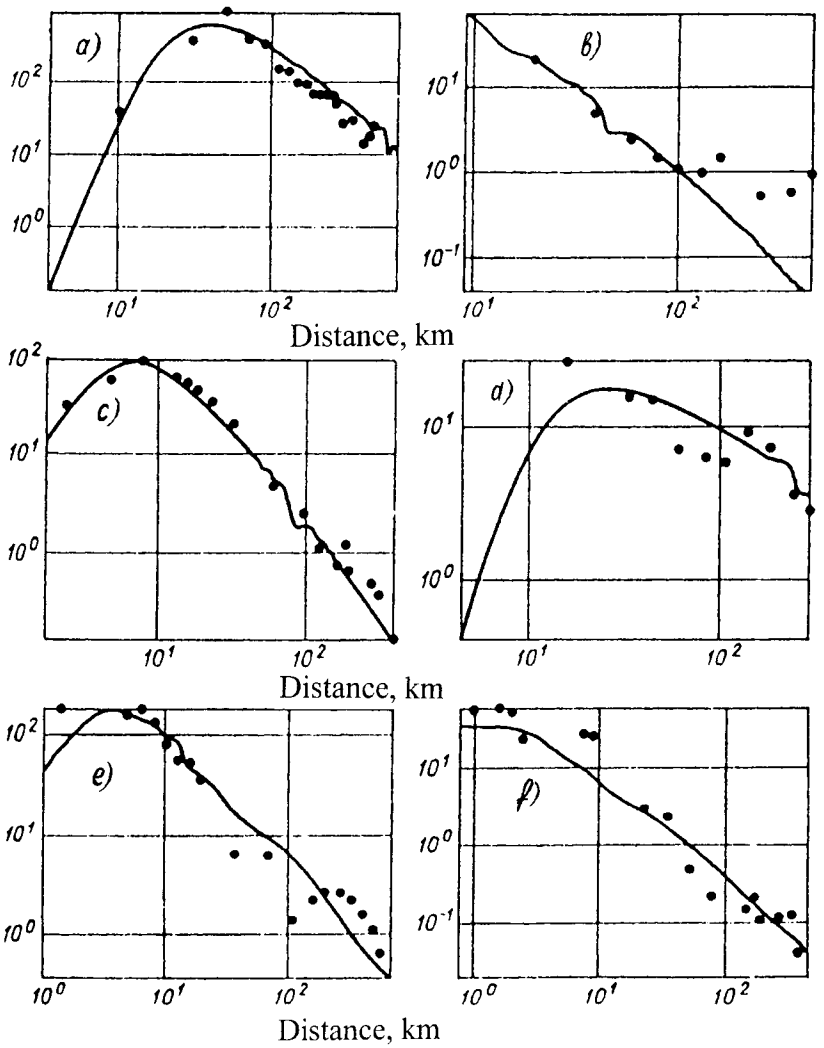

Fig. 7.2. Character of dependence of the quantity of radioactive products $A(R)$ (in conventional units) in the fallout pattern from a different nuclear explosion on distance R from the epicenter.

Integration over the surrounding land can also be performed using the expression:

$$Q_{\text{pat}} = \int_{S_1}^{S_2} P(H)\,\mathrm{d}S \int_H K_H(h)\,\mathrm{d}h, \tag{7.19}$$

where S_1 and S_2 are the areas bounded by the isolines of maximum and minimum dose rates and the integration is performed over the areas enclosed by neighboring isolines; P_H is the dose rate at some fixed height.

The value A is conveniently expressed in units of $P \cdot \text{km}^3/\text{hr}$ or MeV/s. The unit $P \cdot \text{km}^3/\text{hr}$ is equivalent to the rate of absorption of energy in 1 km^3 of air, at each point of which the dose rate amounts to 1 R/hr ($\approx$10 mGy/hr); 1 $P \cdot \text{km}^3/\text{h} = 19.6 \times 10^{15}$ MeV/s. To illustrate the relationship, Fig. 7.2 gives the values of $A(R) = \int_l P(R, l)\, \text{d}l$ (in relative units) for six nuclear explosions that were performed at the Semipalatinsk Test Site during 1953–1962. These data were published by Loborev et al. (1994). We mention in passing that a number of experimental data similar to those shown in Fig. 7.2 (in particular Fig. 7.2b) were obtained personally by the author in 1954 using aerial gamma-survey employing Roentgenometric equipment. Clearly, when performing such a survey, the influence of real conditions were taken into account by introducing the necessary corrections.

In practice, it is best to introduce all of the above correction factors for the determination of the final values of M_H. Thus, for $H = 1$ m, taking into account the micro-relief, a value of $M_h \approx 80$ m resulted, with $L_H \approx 3 \times 10^5$ MeV/(cm^2 s)/(R/hr), compared to an idealized source where $M_H = 55$ m. The M_H value reached 110 m for a terrain that had, as its absorption layer, a covering of grass, the situation that existed for the fallout patterns after the Chernobyl accident (Izrael et al., 1987b).

Calculation of the quantity of a radioactive substance, in energy units, is especially convenient when a portion of the deposited substance (from the whole quantity of the radioactivity formed) is determined in one or other section of the fallout pattern because the quantity of substance in MeV/s, formed in fission of any type, is well known for any moment of time.

When determining the surface density of contamination from a measured dose rate, one should consider possible instrument errors, the most important being those connected with the "non-air equivalency" of the γ-radiation detector. That is why, in aerial gamma-surveys, the most correct approach is to use an air-equivalent detector (for example, an organic crystal or specially designed counter). The use of detectors such as sodium iodide crystals can lead to significant errors since their readings depend strongly on the spectral composition of the radiation and hence on the time after the explosion, the flight altitude, etc. As indicated above, at a height of 1 m, it overestimates the dose rate by 1.5–2 times.

4. Aerial γ-survey. Estimation of the Surface Density of the Terrestrial Contamination by Individual Nuclides

The determination of land contamination by individual radionuclides can be carried out either through laboratory analyses of samples taken from the fallout pattern or by means of gamma-spectrometric equipment installed on board an aeroplane or helicopter. The latter method facilitates the conduct of surveys of contaminated territories quickly and over large areas. Unfortunately, there is a drawback to this method in that it is not possible to obtain reliable data on nuclides having γ-radiation energies less than 0.3 MeV.

A plan for a gamma-spectral survey is as follows: an instrumental gamma-spectrum or a part of the spectrum is measured over a zone of the radioactive fallout for a short time interval, i.e., for several seconds. It is then transformed into a true spectrum through a reciprocal matrix and, from this, the terrestrial contamination by individual nuclides is

calculated. This approach is somewhat complicated due to some uncertainties arising in this method of contamination determination. Usually, a simpler approach is used; a photo-peak, corresponding to the ith radionuclide, is separated in the instrumental gamma-spectrum, then the area or intensity $S(\mu, h, E)$ of the photo-peak is calculated, corresponding to the activity. Using certain recalculation coefficients $b(h_0, E_0)$, the surface density of the terrestrial contamination by a given nuclide is determined. The coefficient $b(h_0, E_0)$ is the ratio of the photo-peak intensity with energy E_0 at height h_0 to the density of the surface contamination of the surrounding land by a nuclide having a gamma-line with energy E_0 and a quantized output equal to unity. So,

$$\sigma = \frac{S(\mu_0, h, E_0)F(h, h_0, E_0)}{K_{iE_0}b(h_0, E_0)}, \tag{7.20}$$

where $F(h, h_0, E_0)$ is the coefficient of reduction of the photo-peak intensity at height h to height h_0, and K_{iE_0} is the quantized output of the gamma-line with energy E_0 of the ith nuclide.

The coefficient $b(h_0, E_0)$ can be determined from measurements over a "reference" site, either artificially created or natural, that simulates the radioactive contamination of the terrain. Izrael and Stukin (1967) has described this procedure for the nuclides ^{51}Cr ($E = 0.32$ MeV), ^{124}Sb ($E = 0.603$; 1.69 and 2.09) and ^{60}Co ($E = 1.17$ and 1.33 MeV) where data on the γ-radiation spectra were obtained above sites that were artificially created from point sources distributed over an area with sufficient spatial resolution.

As gamma-spectrometry systems have improved, the processing and analysis of the spectrometric gamma-survey data have been simplified and become more widely used. Detailed descriptions of such methods have been presented in a number of papers, including for example, the fundamental work by Kogan et al. (1991) and later in Fridman and Nazarov (1994).

In conclusion, it may be of interest here to indicate a means of isolating and examining surface contamination phenomena against a background of radiation from other sources. Such a case arises when surveys of a fallout pattern are being conducted in the presence of radioactive gases and/or a passing radioactive cloud or plume. Certainly, the simplest approach would be to wait for the cloud to move on or for the stream of radioactivity emissions to cease. In some cases, however, the stream of radioactive gases persists over a long period of time (as, for example, after the Chernobyl accident and in certain underground explosions). Usually, in such cases, the aerial gamma-survey of the fallout pattern can be continued even in the presence of other surrounding sources of radioactivity. What is required in this situation is two radiation detectors, one that is isotropic in its detection capabilities and the other directional. The latter is shielded/screened so that only the radiation coming from below can be registered. The radiation contribution originating from the surface contamination can be determined roughly through comparisons of the results of these two detectors.

The monograph by Izrael and Stukin (1967) presents in some detail the problems encountered in the theoretical approaches to the assessment of gamma-fields above planar and volumetric sources and in the experimental data from surveys of the fallout patterns after nuclear explosions. In this book, the methodological basis of using Roentgenometric

equipment is described for the conduct of gamma-surveys of the fallout patterns produced by nuclear explosions. This approach was actually introduced with the participation of the author in the former USSR in 1954 and later in 1957 with the conduct of large-scale gamma-spectral surveys. These approaches were developed in subsequent studies (Izrael, 2000 a & b; Izrael et al., 2000; and Kvasnikova, 2000).

This Page Intentionally Left Blank

Chapter 8

REMEDIATION OF CONTAMINATED AREAS. REHABILITATION OF AREAS SUBJECTED TO RADIOACTIVE CONTAMINATION AND MOBILITY OF RADIONUCLIDES

Contents

1. Fractionation 244
2. Radionuclide Mobility after Nuclear Explosions and Accidents 245
3. Solubility and Biological Accessibility 246
4. Radioactive Contamination of Vegetation and Experimental Data on the Uptake of Radionuclides by Humans and Animals 251
5. Problems of Rehabilitation of Contaminated Areas. Agricultural Radioecology 252
6. Practical Measures for the Restoration of Contaminated Territories 257
   - 6.1. Resumption of Economic Activity after the South Urals Accident (1957) 257
   - 6.2. Urgent Decontamination Efforts after the Chernobyl Accident 258
   - 6.3. Restoration of Agricultural and Industrial Lands after the South Urals and Chernobyl Accidents 258

The large-scale radioactive contamination of territories, mainly by fallout from nuclear explosions and accidents, has led to consideration of possible ways and means of restoring or rehabilitating the land to levels that would be acceptable for human habitation and use for economic purposes. This problem is especially acute in severely contaminated regions that were previously inhabited and used for agricultural and other purposes. Related restoration experience was gained from earlier efforts in regions that were polluted from various usages, e.g., after the exploitation and mining of radioactive minerals, after various small accidents at industrial enterprises and where radioactive substances had been used for medical purposes. The restoration of contaminated territories became a major problem after a series of large-scale accidents, such as that leading to contamination of the South Urals in 1957 and, most certainly, after the Chernobyl accident of 1986, as well as after a number of nuclear tests both on the surface and underground.

It is apparent that, in cases of large-scale contamination of a terrain, vigorous and efficient measures are imperative so that external radiation doses are minimized and the transport of radionuclides by wind or groundwater is controlled. It is especially important in zones where the population or personnel employed by the power stations and enterprises may not be able to leave the area or where the lands are being used for economic purposes (especially for agriculture).

Efficient decontamination is needed to clean the terrain, roads, buildings, and equipment. The territory must also be decontaminated and measures taken to reduce radionuclide mobility through their "fixation". Measures for cleaning, together with the experience gained in a number of different countries, have been summarized in IAEA documents (IAEA, 1998a & b). Obviously, if we are to carry out efficient cleaning and decontamination followed by total or partial rehabilitation of the contaminated territories, it is necessary to have a comprehensive understanding of the character and features of the contamination,

Table 8.1
Scheme of fractionation, mobility, solubility, and biological accessibility of radionuclides in natural environments

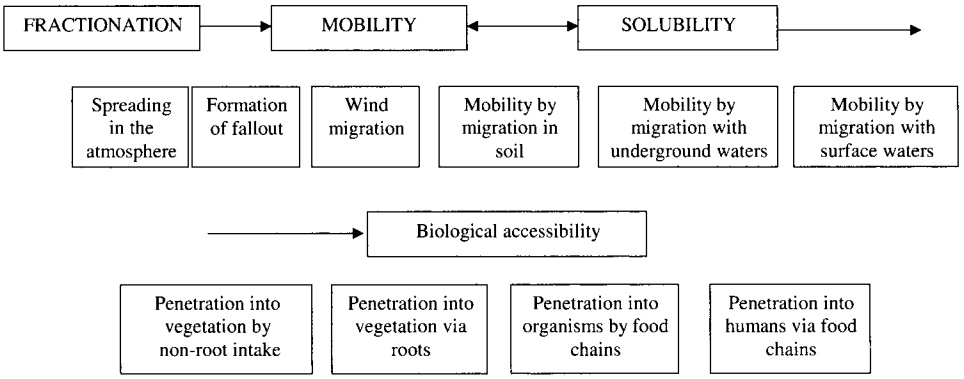

the distribution of the radionuclides in various natural matrices, the radionuclide composition of the contamination, its properties (fractionation) including mobility (migration), solubility and biological accessibility (see Table 8.1).

Radioecological monitoring must be carried out, first of all, including the tracing, estimating and forecasting of the behavior of the radionuclides. The results must be quantitative so as to obtain adequate information on the radionuclides at all stages of their distribution and transformation. Radionuclide behavior and transformation (besides nuclear transformations) characterize the fractionation, mobility, solubility and other possibilities for its transport from one medium to another. Together with biological accessibility, these features constitute the most important factors for our understanding of the ingestion of radionuclides by, and their incorporation into, every living being.

A knowledge of these characteristics, together with the physical properties of the individual radionuclides (rate of decay, type of radiation), makes it possible for us to estimate the degree of hazard associated with the contamination and to take measures for the prevention or reduction of the danger and for the rehabilitation of the contaminated environment to levels suitable for life and the economy. It is also necessary to be well informed as to the location of the population and livestock and the distribution of agricultural lands.

Prior to dealing with the cleaning, restoration and rehabilitation of the contaminated territories, the most important components of Table 8.1 will be examined because knowledge of these factors ultimately determines the approaches that will guarantee a highly efficient result for the clean-up and restoration process.

1. Fractionation

After the radioactive products have been released from their different sources, their fallout on and spread through a terrain begins, along with their migration into different media, mainly as particles derived from the ground surface or from bomb construction materials, destroyed reactors, etc. or in a dissolved state in natural waters. Relationships

between the radionuclides are permanently changed by these processes, fractionation taking place. Freiling (1962), Izrael (1965) and others have outlined the effects of fractionation and Izrael (1996) has published a general summary on the topic. Features of fractionation are described in detail in previous chapters.

In nuclear explosions and reactor accidents, the radionuclide mixture consists of products of nuclear fission, induced activities (by neutron activation of bomb material and/or elements of the ground surface), trans-uranium elements, and, possibly, tritium. The fractionation coefficient of the ith radionuclide is usually expressed as its abundance ratio relative to the radioactive isotope of a refractory chemical element (e.g., ^{95}Zr, ^{99}Mo, ^{144}Ce, etc.). The effects of fractionation, as already mentioned, are described in previous chapters, and therefore we dwell only very briefly here on this part of the problem. A major factor in fractionation is the extent of penetration of different radionuclides into the molten ground matrix or into bomb fragments or, when it occurs at a nuclear power station, into materials used in the construction of the reactor, by the radioactive particles in the fireball of an explosion or in the radioactive cloud. The aerosol particles thus formed spread around, giving rise to the radioactive contamination of natural materials (Izrael, 1973).

Clearly, after a nuclear explosion, when the molten particles of ground-derived material at the test site have not yet hardened (for SiO_2, the melting point temperature is about 1700 K), the refractory radioactive products can penetrate them. Later, they become distributed throughout the molten material and, as the material hardens, the volatile products tend to accumulate on the particle surfaces some several seconds after the explosion. In this situation, the hazardous radionuclides ^{90}Sr and ^{89}Sr that have volatile precursors in their decay chains (i.e., ^{89}Kr and ^{90}Kr, ^{89}Rb and ^{90}Rb) will settle out on particle surfaces (small and fine particles have the largest surface area) and become distributed over great distances. On the other hand, the refractory ^{95}Zr and plutonium isotopes that now form part of the particles (especially the larger ones) fall out mainly within relatively short distances to form the "local" fallout pattern.

If a reactor is destroyed, then the main quantity of ^{89}Sr and ^{90}Sr will be determined by their accumulation over a long period of time before the accident and these radioisotopes will behave as refractory nuclides, falling out in the local areas near to the accident. The cesium isotopes (^{134}Cs, ^{137}Cs), being species of a volatile chemical element, at the time of the explosion/accident will behave as volatile products and consequently spread out over rather large distances. At first, short-lived ^{131}I is very dangerous. The isotopes of Zr and Pu, being refractory, will fall out in the local zone, as has been confirmed experimentally.

2. Radionuclide Mobility after Nuclear Explosions and Accidents

Isotopic fractionation has a significant role to play in the mobility and accessibility of radionuclides in the widest sense. Obviously, radionuclide transport in the atmosphere (at the time of formation of the radioactive fallout) depends mainly on atmospheric properties (e.g., density and meteorological conditions) that determine both the rate of particle dispersion and the composition of fallout on a terrain and also the properties of the particles themselves. Most important is the radioactivity distribution with particle size and hence the rates of fallout deposition.

Extensive experimental data are available on the radioactive contamination of the natural environment. With this comes the experience to create complex models that describe the distribution of the total radioactivity and that of the individual radionuclides in the natural environment such as in the atmosphere, the terrestrial environment, etc. (see previous chapters). Judgments on the degree of radionuclide spreading over different distances and its fallout onto specific areas of the terrain can be made throughout the various stages in the formation of fallout from the first stage of mobility/dispersion in the atmosphere onwards (see Table 8.1). These data are summarized in Izrael (1996b), Aleksakhin and Korneev (1991) and other publications. At this stage, it is already predictable that the refractory nuclides from the nuclear explosions, namely ^{95}Zr, ^{95}Nb, ^{99}Mo, isotopes of plutonium and, after Chernobyl, ^{89}Sr and ^{90}Sr, will fall out in the local or close-in zone, while the volatile elements will spread over great distances, including amongst these, after a weapons explosion, ^{89}Sr and ^{90}Sr. Such conclusions were reached in rather a timely manner in that they were invoked after the Chernobyl accident, where among the volatile and hazardous radionuclides that were spread over long distances, were ^{131}I and the cesium isotopes, particularly ^{137}Cs with its longer half-life, while, in the near-zone, mainly within the 30-km boundary, the main quantities of the strontium and trans-plutonium radioelements were found.

Problems associated with the behavior of these and other radionuclides were especially complicated after the Chernobyl accident. They were investigated experimentally and theoretically for the different directions of spreading of the radioactive debris. Due to the extremely complicated meteorological situations that prevailed and the fact that the radioactivity emissions lasted for ten days, the configurations of both the close-in and distant fallout regimes were very intricate (see Fig. 5.13).

Radionuclide fractionation in different directions of fallout patterns resulting from different radioactivity releases from the reactor differed quite markedly. At the outset, the first portion of the radionuclides was only weakly fractionated, it being similar to that accumulated in the reactor ($f_{137,144} \sim 1.0$) (see Fig. 5.14). In directions other than the areas to the south, the fractionation of the volatile products relative to the refractory nuclides was very large ($f_{137,144}$ reached values of 25–35). In southerly directions, where the fallout occurred between April 30 and May 1, 1986, $f_{137,144}$ again approached unity (Izrael et al., 1990).

At great distances in the north and north-easterly directions (in the Gomel, Mogilev and Tula regions), "cesium hotspots" were formed with a predominant content of the radionuclide ^{137}Cs in the fallout mixture and huge numerical values of the fractionation coefficients of the volatile radionuclides, with values of $f_{i,95}$ for ^{131}I up to 200–290, for ^{110m}Ag up to 100–190, for ^{125}Sb up to 150–250 and for ^{137}Cs up to 170–370 (Izrael et al., 1990). Similar coefficients of fractionation were observed for ^{137}Cs also at very large distances, i.e., for many countries in Europe (De Cort et al., 1998). As is seen from these data, radionuclide mobility was significantly determined by their fractionation.

3. Solubility and Biological Accessibility

As noted above, migration and mobility of radionuclides significantly depend on radionuclide solubility. Here, one should distinguish between the radionuclide solubility,

described as the direct transfer from a radioactive particle or solid sample into an aqueous form, from the "integral" solubility which is the ability of a radionuclide to transfer into the liquid phase (taking into account the time it remains in this phase and also ion-exchange reactions), this latter determining nuclide mobility in the natural environment over large distances, including the migration of radioactive particles, etc. It is obvious that radionuclide solubility determines biological accessibility to a large extent, i.e., transport along food chains and uptake by animals and/or human organisms.

Below we consider the available data on solubility and biological accessibility after certain nuclear explosions and accidents (Izrael, 1996b, 1973; Izrael et al., 1990; Aleksakhin and Korneev, 1991, etc.). If the material that comprises the underlying particles is practically insoluble in water and weak acids (e.g., SiO_2), then, on the basis of the level of surface coverage by particles $N_i^S(t, r)$, an estimate can be made of the fraction of the nuclide that is subject to "leaching". This portion can be considered to be a measure of the magnitude of the biological accessibility and is determined from the quotient of the relative accumulation of this nuclide from the radioactive particles of the explosion by a biological system relative to the relative accumulation of the same nuclide from solution. The magnitude of the biological accessibility for ^{90}Sr on these particles turns out to be practically equal to that portion of the ^{90}Sr that is soluble in 1N HCl, i.e., it approaches the fraction of ^{90}Sr deposited on the surfaces of the particles after they have solidified. So one can imagine that the maximum value of the coefficient of biological accessibility of the ith nuclide coincides qualitatively with the fraction of the nuclide situated on the surfaces of particles of a given size (i.e., that settled after particle solidification) if the underlying substance is practically insoluble in water or weak acids. Thus, the coefficient of biological accessibility for atmospheric nuclear explosions (Izrael, 1973) is

$$b_i(d, t, t_1) = \frac{N_i^S(d, t)}{N_i^S(d, t) + N_i^V(d, t)}, \tag{8.1}$$

where N_i^S, N_i^V are, respectively, the distributions of a radionuclide on the surface and in the volume of a particle of size d, t_i being the time of particle solidification.

^{90}Sr that is associated with large particles is more soluble than the sum of the fission fragments, the latter not being large, and the soluble portion is smaller than that in the fine particles from ground and tower explosions. The solubility of nuclides in particles following the most powerful explosions is the lowest. The solubility of refractory particles from air explosions even in 6N HCl does not exceed several percent. Not more than 2% of the activity enclosed in particles of sizes exceeding 50 μm was present on the surface of vitrified spheres collected at the Nevada test site. Among these particles, the main contributors to the leached activity belonged to nuclides of iodine, cesium, strontium and barium, i.e., the nuclides having volatile (or gaseous) predecessors.

Figures 8.1 and 8.2 show the dependence of $b_i(t, t_i, d)$ on the particle sizes of near fallout after a ground explosion for ^{90}Sr, ^{89}Sr (Fig. 8.1), ^{103}Ru, ^{131}I and ^{132}Te (Fig. 8.2) (for $t_i = 7$ s, i.e., the time of particle hardening after a 20-kt explosion).

The dependence of the average coefficients of fractionation and biological accessibility for a mixture of radioactive products in the local fallout pattern from a nuclear explosion as a function of time is shown in Fig. 8.3. After underground explosions, the nuclides on

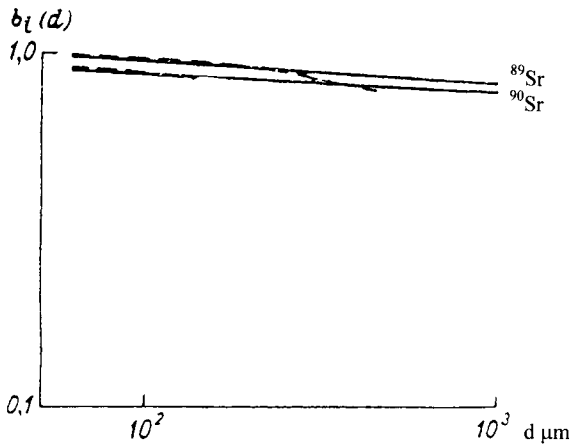

Fig. 8.1. Dependence of coefficients of biological accessibility for ^{89}Sr, ^{90}Sr on particle size for ground explosions.

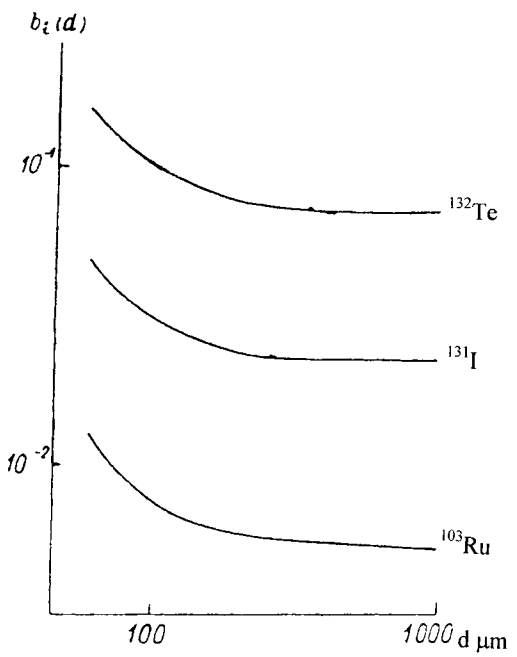

Fig. 8.2. Dependence of coefficients of biological accessibility for ^{103}Ru, ^{131}I and ^{132}Te on particle size for ground explosions.

the particle surfaces (volatile or with volatile predecessors) transfer into solution at the first opportunity. After the "Sary-Uzen 1003" explosion, conducted by the former USSR, several fallout samples taken in the near-zone were treated with distilled water and it was

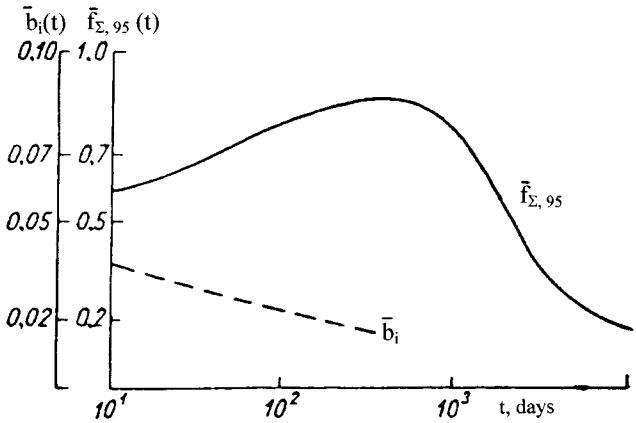

Fig. 8.3. Dependence of integral coefficients of fractionation $f_{\Sigma,95}(t)$ and biological accessibilities $b_i(t)$ of a mixture of radioactive products in the close-in fallout pattern at time t after a ground nuclear explosion.

found that the nuclides ^{89}Sr, ^{90}Sr, ^{140}Ba, ^{103}Ru, ^{106}Ru and ^{125}Sb mainly went into solution (the same was observed for samples taken at the crater). On average, from the data on 20 samples taken from different parts of the fallout from the base surge cloud, it was found that the quantities dissolved in water were, for ^{89}Sr 70–90%, ^{90}Sr 4–6%, ^{140}Ba 0.5–2%, ^{103}Ru and ^{106}Ru 7–20% and ^{125}Sb 1.5–7% at 7 days after the explosion. The solubility of ^{89}Sr and ^{90}Sr increased almost linearly with distance and reached 70–80%, after which it varied only slightly. The behaviors of ^{140}Ba, ^{103}Ru and ^{106}Ru were similar to those of ^{89}Sr and ^{90}Sr; beginning at a certain distance from the epicenter, their solubility was 20–30 and 5–7%, respectively. All nuclides investigated could be arranged in sequence with respect to their solubility (Izrael et al., 1970b):

^{89}Sr >	^{90}Sr >	^{125}Sb >	^{140}Ba >	^{103}Ru >	^{106}Ru >	^{137}Cs >	^{134}Cs, ^{141}Ce >	^{54}Mn, ^{60}Co, ^{144}Ce, ^{91}Y, ^{95}Zr
1.25	1.0	0.3	0.24	0.1	0.04	0.02		0.01–0.001

(the solubility of ^{90}Sr is taken as unity).

It was noticed that the coefficient of dissolution of the nuclides in water decreased with increase in particle size.

The ion-exchange capacity of particles of soil or rock is determined either by the retention of charged ions as a result of surface attraction or by direct internal ion exchange. For many minerals, both mechanisms operate. Using the data on radionuclide solubility and ion-exchange reactions, one can estimate the mobility of the radionuclides in both ground and surface waters.

As early as May 1986, using the above approaches for land contamination after the Chernobyl accident, we were able to obtain preliminary favorable forecasts of the contamination of local rivers and water reservoirs for the subsequent spring flood of 1987. The predictions did not exceed the established norms. For this work, the coefficients obtained earlier for radionuclide migration in ground waters were used (Izrael, 1974). Apparently, the calculation of the runoff of radioactivity from contaminated terrain, based on use of the distribution coefficients for ground waters, can give slightly underestimated results but can, nevertheless, be used for rough estimates.

The possibilities of radioactive product migration in ground waters, after nuclear explosions, were estimated in Izrael (1974). Here, the equations for ion exchange include the constant K_d, termed the distribution coefficient. This relates to the ratio of the ions bound in the solid phase to the number in aqueous solution. The K_d values change for different minerals and nuclides within the range 10^1–10^5. Those with the smallest K_d coefficients are ruthenium followed by strontium, cesium, cerium and plutonium. The average values of K_d for the nuclides (determined in fallout from nuclear explosions) amount to 10^2–10^3, with values for strontium of $10–2 \times 10^3$, for cesium of 10^2–10^4 (sometimes 10^5) and for cerium of 10^4–2×10^5. The average K_d value for fission products after about one year is estimated at 370 (clearly, for tritium, $K_d = 0$).

In accordance with the data in Aleksakhin and Korneev (1991), the K_d values (determined in fallout after the Chernobyl accident) amounted to 2×10^3 for strontium, $10–5 \times 10^4$ for cesium, $6.0–6 \times 10^3$ for cerium and $50–6 \times 10^3$ for zirconium (the lowest K_d values are for the sandy soils). Thus, ion-exchange processes reduce the potential hazards of underground and surface water contamination due to (i) the decrease in ion transport rate compared to water velocity and (ii) the decrease in concentration in the course of migration.

The rate of flow, F_a, of a given substance with underground waters can be expressed by the equation

$$F_a = \frac{F_w}{1 + \rho K_d}, \tag{8.2}$$

where F_w is the flow velocity of the water, ρ is the ratio of the mineral weight to that of water per unit volume of the given mineral; usually $\rho = 4–5$. One can see from this formula that any given ionic flux with groundwater will be hundreds or thousands of times smaller than the water's flow velocity. Even under relatively large velocities of F_w (about 10 m/day), the ^{90}Sr migration over a distance of 1 km will take decades.

After the Chernobyl accident, tens of control boreholes were drilled over distances of several hundred meters (down to the depth of the aquifer). Observations of the ^{90}Sr concentrations in the water of these boreholes, made over a period of one and half years after the accident, did not exceed background (pre-Chernobyl) levels, thus confirming the above estimates (the ^{90}Sr concentration in the boreholes at a distance of 150 m from the cooling basin amounted to 266.4 mBq/l (7.2×10^{-12} Ci/l) when the permissible values are 14.8 Bq/l (4×10^{-10} Ci/l).

Washout of the radionuclides $^{134,137}Cs$, ^{106}Ru, ^{125}Sb and ^{144}Ce by floodwaters after the Chernobyl accident, in comparison with data for nuclear explosions, was investigated during March–April 1987. Five watersheds of different sizes (0.1–60 km^2) and with different landscape and topographic conditions were chosen on the right side of the Dnieper river (the Kiev region). Another three watersheds located on the left side of the Dnieper river (the Gomel region) were also studied (Izrael et al., 1988). The washout coefficients were defined as:

$$m_i = \frac{A_i(t_1, t_2)}{Q_i}, \tag{8.3}$$

Table 8.2
Washout coefficients m_i of radionuclides during the spring flood in 1987 after the Chernobyl accident

No. of watershed	^{134}Cs	^{106}Ru	^{125}Sb	^{144}Ce
1	3×10^{-4}	4×10^{-4}	3×10^{-4}	4×10^{-4}
2	0.09	0.2	0.03	0.1
3	0.05	0.12	0.06	0.05
4	0.1	0.1	0.1	–
5	5×10^{-3}	0.025	–	–
6	0.2	–	–	–
7	0.4	–	–	–
8	0.3	–	–	–

where A_i is the total activity of ith radionuclide carried out of the watershed area by the flood waters for the time period (t_1, t_2); Q_i is the quantity of the ith radionuclide distributed over the watershed area. The resulting washout coefficients are shown in Table 8.2. We should note that, in the Belarussian watersheds, the major part of the runoff activity was attributable to the radioisotopes ^{134}Cs and ^{137}Cs.

The data from Table 8.2 indicate significant scattering of the m_i values in the flood runoff, depending on the landscape-ecology and orographic conditions. The highest values of m_i $(0.1n\%)$ were obtained in the Belarussian watersheds No. 6, 7 and 8 with maximum runoff and at the built-up site No. 4 with its highest antropogenic erosion of soil cover. The lowest value of m_i was on the forested watershed No. 1 (a forest gulch) with its low runoff values and the most favorable conditions for radionuclide fixation by the soil layer. On the watersheds of the Kiev region (Nos. 1–5), ^{106}Ru and ^{125}Sb were the nuclides that migrated most extensively.

4. Radioactive Contamination of Vegetation and Experimental Data on the Uptake of Radionuclides by Humans and Animals

Atmospheric wind transport, the migration in soil materials and hence the redistribution of the radioactive products are of considerable importance in the contamination of vegetation. This problem was investigated earlier for nuclear explosions. The results of investigations of the radionuclide content of vegetation cultivated in a dry steppe zone of the fallout area of an underground cratering nuclear explosion (Sary-Uzen, 1003 explosion, USSR) are presented in Izrael et al. (1970b). The radionuclide composition of the vegetation differed from that in the soil, particularly in the near-zone, where the vegetation was depleted in ^{95}Zr and ^{144}Ce and enriched in ^{90}Sr and ^{105}Ru.

The radionuclide contents of plants depend on the structures of their above-ground features. Plants with strongly dissected and rough surfaces of stems and leaves are contaminated several times more than those with smooth surfaces and low ratios of surface area to biomass. Thus, the contamination of vegetation on pastures is approximately an order of magnitude larger than on haymaking areas. In the zone of dry steppes, the nuclide uptake by plants (in the first year after an accident) is largely through their above-ground

parts; the contribution from the roots and the soil is negligible. Martin (1965) presented the results of investigations of radionuclide uptake by vegetation grown on a soil from the ground bulk of the "Sedan" explosion. The plants strongly concentrated isotopes of tungsten through the root system and to a lesser degree ^{46}Sc, ^{54}Mn and ^{88}Y and the fission debris of ^{89}Sr, ^{90}Sr, ^{95}Zr, ^{106}Ru, ^{125}Sb, ^{137}Cs and ^{144}Ce. Absorption in an acid soil was lower than that in a neutral or alkaline soil.

Wider investigations of the mobility and biological accessibility of radionuclides, especially of iodine-131, cesium-137 and strontium-90, were carried out on the contaminated areas in the vicinity of the South Urals accident of 1957 and again after the Chernobyl accident of 1986 (Aleksakhin and Korneev, 1991; Izrael et al., 1990; and many others). These data are extremely crucial for the proper organization of rehabilitation measures in the contaminated areas, for radiological decontamination, for economic management, especially of the agricultural and industrial sectors, and for civil measures necessary to ensure the safety and well-being of people living in these areas.

5. Problems of Rehabilitation of Contaminated Areas. Agricultural Radioecology

One of the main problems in contaminated areas, next to avoiding high external radiation doses to the population, is the difficulty associated with the safe production of agricultural crops that meet radiological safety standards. The internal radiation dose in such areas, due to the uptake of radionuclides by humans through the food chain, can exceed the total external irradiation dose by as much as 50%. Modification of the external dose (by cleaning the area and changing human behavior) is possible but not to the same degree as through regulation of the internal dose by changes to the economic character and rehabilitation of the contaminated zones. With rehabilitation, it is important to take into account the radiological factors (guaranteeing the radiation safety of human beings), the economic factors (assessments of the expediency of possible expenditures) and the socio-psychological factors (in particular, diminishment or complete removal of the radiophobia of people living on the contaminated territory).

A conceptual scheme for the rehabilitation of agricultural lands exposed to radioactive contamination is shown in Table 8.3 (Aleksakhin et al., 1994). As seen in the scheme, the rehabilitation of the agricultural sector in contaminated areas can be either total or partial. For the partial rehabilitation of agricultural lands, a series of protective and restorative measures was developed and widely used on the territories of the South Urals (Kyshtym accident) and after the Chernobyl accident. In such cases, special attention was given to the effect of temporal change of the biological mobility of radionuclides in the "soil–plant–animal–man" system.

As the radionuclides in fallout accumulate on the land surface, some are absorbed by the soil and, in the situation where they fall on to the surface of a water body, they are ultimately taken up by bottom silts. The absorption fixes the radionuclides in the upper soil horizons, creating a long-lasting source of radioactivity for root uptake and accumulation by plants. On the other hand, this absorption on the soil fixes the radionuclides in such a way that their assimilation through the root systems is limited.

Table 8.3
Conceptual scheme for rehabilitation of agricultural lands exposed to radioactive contamination

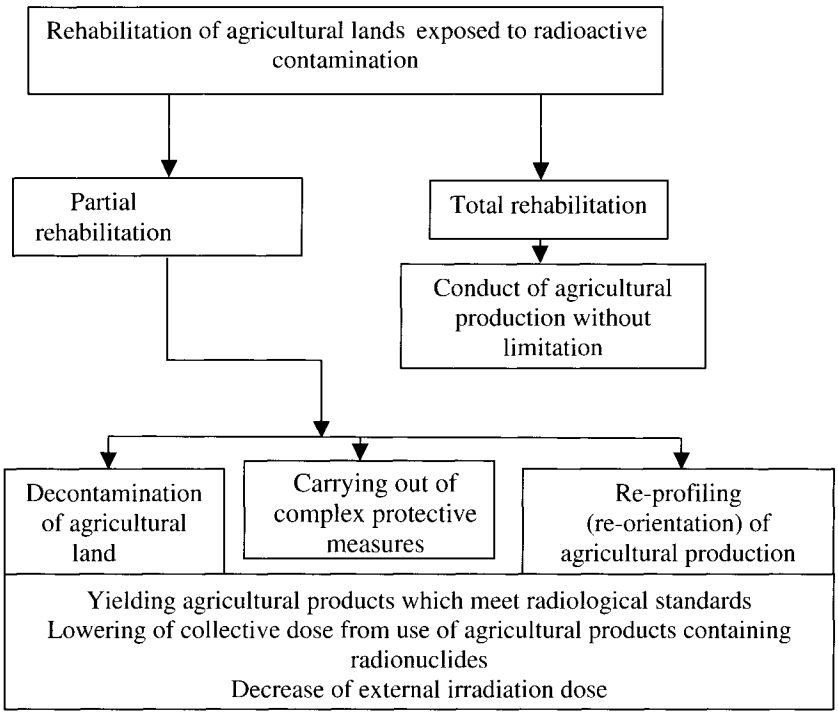

Radionuclide behavior is determined by its distribution between the solid and liquid phases as a result of processes such as the sorption–desorption of the radionuclides and the coagulation–peptization of colloids (Aleksakhin and Korneev, 1991). As noted previously, the radionuclide distribution between the solid and liquid phases is characterized by the distribution coefficient K_d. Certain properties of the soils and the physico-chemical properties of the radionuclides and the chemical elements present, as well as the characteristics of the accompanying micro and macro admixtures, determine the distribution between the solid and liquid phases and their further behavior in the soil and "soil–plant" systems. After complete isotopic exchange in the soil has been attained, then the radionuclides and their stable isotopes behave identically.

The chemical elements examined were divided into four groups: (i) very slow-moving—Zn, Cd and Co; (ii) slow-moving—Y, Ce, Fe, Zr and Nb; (iii) mobile—Na, Rb, Sr and Ru; (iv) highly mobile—S and I anions (Aleksakhin and Korneev, 1991). Some of the behavioral features of the radiologically significant radionuclides along with their stable analogs in soils are presented here (Aleksakhin and Korneev, 1991).

Strontium. The fixing and distribution of ^{89}Sr and ^{90}Sr in soils are determined largely by the regular behavior of stable Sr; the main mechanism for ^{90}Sr absorption by the solid phase of soils is ion exchange. The liming of acid soils and the introduction of potassium phosphates increase the strength of the ^{90}Sr fixation by soils and promote its transition from the water-soluble and exchangeable phases into the non-exchangeable phase.

Cesium. A strong feature of cesium nuclide behavior is its tendency to be non-exchangeably absorbed by the solid soil phase along with a general affinity for ion-exchangeable binding. Absorption of ^{137}Cs by soil is essentially influenced by the potassium content as the replacement of the exchangeable cations of the soil by potassium essentially decreases ^{137}Cs sorption. The higher the content of stable cesium in a soil, the smaller the amount of ^{137}Cs that is absorbed by the soil.

Cerium. In acid soil solutions, ^{144}Ce is in cationic form and is practically totally absorbed by the soil's solid phase. With increase in pH, ^{144}Ce absorption decreases.

Ruthenium. When the pH of the soil solution increases, ^{106}Ru absorption by the soil's solid phase increases also. ^{106}Ru absorbed by soil does not enter into ionic exchange reactions and the anionic forms of ^{106}Ru are more mobile.

Zirconium. Zr is slow moving.

Barium. Ba is related to those elements that are rather mobile in soils.

Lanthanum. In soils, La is in slow-moving form.

Cobalt. In the form of cationic complexes, it is almost totally absorbed by the solid phase of soils; the anionic forms are more mobile.

Trans-uranium radionuclides (TUE). It was noted that microorganisms exert a great influence upon the fixing and distribution of the trans-uranium elements in soils.

Neptunium. Amongst the TUE, Np possesses by far the largest solubility in soils and the highest mobility.

Plutonium. In a soil solution, Pu is mainly present as particles in hydrolyzed forms with wide limits of dispersion. In the "soil–water" system, K_p amounts to $250–4 \times 10^6$.

Americium and curium. The main factor affecting the behavior of these radionuclides in soils is hydrolysis. Hydroxides of Am and Cm have a higher solubility compared to Pu hydroxides and these elements are also characterized by a greater mobility in soils.

It is clear that the problem of biological accessibility of radionuclides can only be solved if the whole chain of radionuclide transitions and transformations is examined, including the most important step of radionuclide uptake by living beings. As far as plant uptake is concerned, the radionuclides can come from the soil or directly through the atmospheric route, i.e., from atmospheric radioactive fallout and/or as a result of wind transportation.

The degree of radionuclide uptake by plants from soils depends on the physico-chemical properties of the radionuclides as well as on the agro-chemical characteristics of the soils, the biological features of the plants and the cultivation methods being employed. It is important to take into account all these factors to be successful in the rehabilitation of contaminated territories. With this knowledge, radionuclide transfer into plants can be minimized, thereby reducing their incorporation into the food chains and their uptake by living organisms. The most accessible radionuclides for assimilation by plants are those that arrive by way of the atmosphere and which tend to reside in the layers of the soils that are available to the plants. With the passage of time, it has been observed for ^{137}Cs that its uptake by plants tends to decrease.

The values of the coefficient of accumulation, K_a, in plants (i.e., the ratio of the radionuclide content per unit mass of the vegetation to that in unit quantity of soil) or the coefficient K_i (the ratio of the radionuclide content in a given mass of the plant (kg) to the density of contamination per unit surface area (m^2)) are highly correlated with the K_d

Table 8.4
Coefficients of radionuclide accumulation in oat grain

Type of soil	^{106}Ru	^{137}Cs	^{144}Ce
Sandy-loam	0.01	1.33	0.014
Loam	0.005	0.29	0.006
Chernozem	0.006	0.06	0.002

distribution coefficients for the soil. This indicates the essential nature of the influence of both the physico-chemical properties of the radionuclides and the soil characteristics.

Depending on the soil properties and the biological features of the plants, ^{89}Sr and ^{90}Sr accumulation fluctuates over a wide range (30–400 times). Thus, for grains/cereals, K_a amounts to 0.6–2.8, while for tubers and potato tops it is 0.7–3.2 and 7.8–48 (Bq ^{90}Sr/kg dry mass of plant/kBq $^{90}Sr/m^2$). The accumulation of ^{137}Cs by plants also changes by factors of 20–30 depending on the soil properties and 10 times according to the biological features of the plants. The value of K_a for ^{137}Cs for agricultural plants changes from $n \times 10^{-3}$ to $n \times 10^{-1}$ (on average, by a factor 5–10 times less than ^{90}Sr).

The fission products ^{91}Y, ^{95}Zr, ^{95}Nb, ^{103}Ru, ^{106}Ru, ^{141}Ce and ^{144}Ce are poorly accumulated in agricultural plants because of their high absorption by soils. ^{106}Ru and, especially, ^{144}Ce are the least accessible to plants. However, the absorption of these radionuclides by plants from derno-podzolic sandy-loam soil ($K_a \sim 0.01$) is much greater than that from a chernozem/black earth ($K_a \sim 2 \times 10^{-3}$–$6 \times 10^{-4}$) (see Table 8.4). Among the induced activities, ^{65}Zn is the most mobile and ^{60}Co the least.

Concentrations of transuranic elements in fruits and grain are 10^2–10^3 times smaller than in leafy plants and vegetables. The accumulation of the transuranic elements by plants decreases in the order: Np > Am > Cm > Pu.

According to laboratory experiments, the coefficients of accumulation of transuranic radionuclides by plants are in the range 10^{-10}–10^{-3}. The retention efficiency of particles by plants from atmospheric uptake increases as particle size decreases. Retention of radionuclides by grassy plants reaches 70–90%. After the radionuclides have settled on the plant surface, their removal by wind and precipitation begins. Maximum losses of the radionuclides occur in the first 2–3 days, with, during the first week, a halfing time of 3–4 days. Over the interval 7–34 days, the halfing time is about 14 days. Up to 70–90% of the losses take place during the first week. Sometimes significant secondary contamination through wind redistribution, etc. occurs. Up to 32–58% of the Cs that is available on the surface of arable land is taken up by the plants, not via the roots but through secondary contamination.

In summary, therefore, it can be stated that the hazards posed by radionuclides derived from nuclear explosions and accidents can be altered in a significant manner following their fractionation, transport and biological uptake. Only a small number of radionuclides hazardous to life then remain. For instance, included among the most dangerous radionuclides (for internal irradiation) released into the atmosphere by the Chernobyl accident were ^{131}I, the isotopes of plutonium (especially ^{241}Pu), ^{144}Ce, ^{106}Ru, ^{90}Sr, ^{140}Ba, ^{137}Cs, ^{132}Te, ^{239}Np and others. After consideration of all the transformations that take place outside the boundaries of the close-in fallout zone, the list of the most

Table 8.5
The main characteristics of the radionuclides released at the Chernobyl accident (note: DK_{Ba} is the permissible concentration in the atmosphere and DK_{Bw} is the same for water)

Radio nuclide	DK_{Ba} (10^{-17}) (Ci/l)	DK_{Bw} (10^{-9}) (Ci/l)	Release (%)	Bk Ai(Σ)	Fractionation near-zone		Fractionation far-zone		A	Distribution coefficient K_d	B	Wind migration
					North	South	North	South				
^{131}I	1.5×10^4	1	50–60	$2.4–3.2 \times 10^{18}$	4–9	0.9	190–290		1.0			Insignificant
^{137}Cs	4.9×10^4	15	23–33	$2.2–3.3 \times 10^{17}$	3–5	0.6	170–370	55	1.0	$10^2–10^4$	< 1%	
^{90}Sr	4×10^3	0.4	4–5	$1.7–2.5 \times 10^{17}$	0.5	0.5–4.0	5.0–7.5	2.5	10	$10^1–2 \times 10^3$		
^{144}Ce	2.2×10^4	12	3.5	$3.2–4.9 \times 10^{18}$	0.9–1.0	1.0	1.4–2.0	1.4	1/20	$10^4–2 \times 10^5$	$\ll 1\%$	
^{106}Ru	1.9×10^4	12	3.5–6.0	$7.9 \times 10^{17}–2.1 \times 10^{18}$	0.6–1.5	0.5–0.75	20–30	7.7	1.0	$10^2–10^3$	< 1%	
^{140}Ba	1.5×10^5	25	3.5	$4.8–5.7 \times 10^{18}$	1–1.6	0.8–1.0	10–15			$10^2–10^4$		
^{239}Pu	3.0	2.2	2–3	$8.0–9.6 \times 10^{14}$	0.9–1.0	1.0	1.4–2.0	1.4	Insignificant	$10^2–10^4$		
^{241}Pu	160	110	2–3	$1.7–1.9 \times 10^{17}$	0.9–1.0	1.0	1.4–2.0	1.4		$10^2–10^4$		

A — Transfer into vegetation from soil relative to ^{137}Cs (average);
B — Migration with surface and underground waters (coefficient of mobility).
1 Ci = 37 GBq.

Table 8.6
Relative danger of radionuclides released after nuclear explosions and the Chernobyl accident with regard to their fractionation, mobility and biological accessibility

	Release	Relative DK_{ba}/DK_{bw}	Relative fractionation	Transition into vegetation (relative)	Migration	Danger (relative)
			All nuclear explosions			
^{90}Sr	19 MCi	1.0	1.0	1.0	Insignificant	1.0
^{137}Cs	35 MCi	10–30	1.0–3.5	0.1	Insignificant	0.01–0.1 +external dose
			Chernobyl			
^{90}Sr	0.2 MCi	1.0	1.0	1.0	Insignificant	1.0
^{137}Cs	2.0 MCi	10–30	50–500	0.1–1.0	Insignificant	~30 +external dose

Note: DK_{ba} is the permissible concentration for the atmosphere; DK_{bw} is the permissible concentration for water.

hazardous radionuclides then includes: for the Chernobyl accident—^{131}I and ^{137}Cs; for nuclear explosions—^{131}I, ^{90}Sr and ^{137}Cs and for the accident in the South Urals (Kyshtym)—^{90}Sr (Tables 8.5 and 8.6). It is seen from Table 8.6 that, after nuclear explosions, ^{90}Sr is the most dangerous nuclide over long distances while, in the Chernobyl long-distance patterns, it is ^{137}Cs (a ten-fold danger).

6. Practical Measures for the Restoration of Contaminated Territories

6.1. *Resumption of Economic Activity after the South Urals Accident (1957)*

For the first time ever, a restoration project on contaminated land was performed on a large scale after the accident in the South Urals (1957). Decontamination of productive agricultural areas and human settlements was pursued over a period of 1–1.5 years after the accident (Sokolov and Krivolutsky, 1993). Special troops equipped with specialized machinery including soil-tilling equipment were involved.

In 1958, after conducting a survey of the boundaries of the contaminated regions and the level of contamination within them, about 106×10^3 hectares of land (55% agricultural, 30% arable) were removed from economic use. One of the acute challenges that arose was to rehabilitate the land and return it to renewed economic use at levels of ^{90}Sr that would no longer be considered hazardous (^{90}Sr was the principal contaminating radionuclide released by this accident). It was found that ^{90}Sr accumulation in plants is crucially dependent on the agrochemical characteristics of the soil, especially the amount of exchangeable non-radioactive calcium.

The accumulation of ^{90}Sr in a harvest was predicted by means of a general-purpose index, I_k, the index of Klechkovsky (Aleksakhin and Korneev, 1991), which is equal to the ratio of the ^{90}Sr concentration in a plant (per unit concentration of calcium) to the

same function for the soil contamination (i.e., the ratio of the contamination density to the content of exchangeable calcium in the soil):

$$I_k = \frac{^{90}Sr_{veg}(Ci/kg)/Ca_{veg}(g/kg)}{^{90}Sr_s(Ci/km^2)/Ca_s(mg-eq/100g)}. \quad (8.4)$$

It was found that, under similar concentrations of radioactive contamination, grass (hay) was the most affected of all agricultural products. ^{90}Sr is accumulated to the least extent in potatoes and root-crops (other crops and beans are intermediate). The main principles for the reuse of the contaminated lands were formulated taking these features into consideration.

6.2. *Urgent Decontamination Efforts after the Chernobyl Accident*

As already noted, the first step to be taken in the restoration of an area is its decontamination, i.e., the removal and burial of the radioactive material. Urgent deactivation and cleaning of contaminated zones after the accident at Chernobyl were carried out during the period May–September 1986 (Kuntsevich, 1993). Included in these endeavors were:

- Removal of the upper layer of contaminated ground;
- Shielding of the radiation by paving the area with concrete or asphalt as well as covering the soil with gravel, rock-debris, sand or clean earth;
- Localization of radionuclides through dust cementation/binding using special agents;
- Demolition of the most contaminated buildings and burial of the ensuing radioactive waste.

Deactivation of transport equipment, vehicles and machinery is not discussed here.

The efficiencies of the different means of decontamination during the early period after the Chernobyl accident are indicated in the data shown in Table 8.7. During this decontamination period, ~200 km of roads were cleaned, 34×10^3 m^2 of concrete were laid, more than 20×10^3 t of asphalt were laid, an area larger than 10^6 m^2 was covered with rock-debris and more than 2×10^6 m^3 of contaminated ground were removed and buried in special waste sites.

A proposal was made to cut a layer of soil 5–10 cm thick within the close-in zone for the purpose of burying the most hazardous radionuclides, the ^{239}Pu, first of all, being placed in special trenches, excavated at a distance of about 100 m from each other. Because the soils in this area (Polesje) are sandy and their active layer is very thin, this proposal was shelved. Actually, this disposal option would have resulted in the deprivation of the whole zone of its soil cover, thereby transforming it into a sandy zone completely open to sand and dust storms and hence to transport of the radioactive materials that would have been buried there.

6.3. *Restoration of Agricultural and Industrial Lands after the South Urals and Chernobyl Accidents*

When applying land improvement techniques to reduce the ^{90}Sr content in agricultural products, the technique of initial decontamination by burial of the upper layer of soil turned

Table 8.7
Efficiency of deactivation methods

Object of deactivation	Means of deactivation	Coefficient of deactivation
Highly contaminated land with radiation level larger than 1 R/hr*	Removal of the upper layer of ground, laying of concrete screens	10–100
Dirt roads	Grading	10–100
Settlements and roads with a hard covering	Single processing with washing solution	1.2–1.5
	Multi-stage processing by the same agent or clays	2–3
Coastal zone	Prevention of radionuclide transition into water by processing with sorbents	10.5
	Prevention of silt transport from inter-stream area between rivers Pripyat' and Dnieper by building dams and filtering coffer-dams	10.5
Agricultural lands	Reploughing, introduction of sorbents, fertilizers and potassium salts	2–5
Dusty sites on land, territory of nuclear power stations, roads	Localization of radionuclides on the dusty sites using special agents	10.0

*1 R/hr $\approx$ 10 mGy/hr.

out to be the most efficient. After the accident in the South Urals, the use of special ploughs made it possible to bury the contaminated layer down to a depth of 30–40 cm and even 30–70 cm (with a reduction in the ^{90}Sr concentration in the ploughed layer of up to 5–50 times). In this case, the accumulation level of ^{90}Sr in wheat decreased by 75% and in potatoes by 99%.

The desired effect in the reduction of the uptake of radioactivity was intensified by applying mineral fertilizers to the soil's arable layer and by lime pretreatment of acid soils. The zoological approach to the control of ^{90}Sr accumulation in the stock-breeding production program was through selection of the forage ration of minimum ^{90}Sr content and by increasing mineral additions of calcium to the fodder.

The process of restoration of contaminated lands for economic use takes many years (in the South Urals, it has been possible in twenty five years to return an area of more than 50×10^3 hectares to economic use). Serious measures have been taken to restore contaminated lands for the re-establishment of forestry and fishery activities. More than 80% of the land in the South Urals fallout areas where ^{90}Sr contamination levels were less than 74 GBq/km^2 (20 Ci/km^2) have been restored.

Restoration of agricultural lands and industrial complexes to their normal state is the most important element of rehabilitation since it is exactly in these endeavors that the major portion of the radiation dose to the population occurs after contamination from a nuclear accident. The work of Korneev et al. (1993) was amongst the first published on this problem, presented at the 1st All-Union Conference on "Radiation aspects of the

Chernobyl accident" (June 22–25, 1988 in Obninsk, in the former USSR). Several periods in the organization of agricultural–industrial practices were recognized during the post-accident period, viz.,

- Operational organization of radiation control, sorting, grading and rejection of highly contaminated agricultural products and forage (10–12 days);
- Radiological mapping of contaminated lands, start of land improvement measures, special technical processing of contaminated agricultural products (2–3 months);
- Transition from the use of the sorting concept to zonal food production; scientific substantiation for a programme of management of the agricultural-industrial complex on the contaminated territory (1.5–2 years).

Later, a permanent program for "clean" production was brought into being along with reorientation of the agricultural–industrial complex, where necessary. Obviously, in addition to the features of the radionuclide contamination, the biogeochemical parameters of the agricultural and industrial practices in the contaminated areas were also studied.

It should be emphasized that the Chernobyl accident took place in an agricultural area within forested lowlands where forest sandy sod-podzolic soils are prevalent. Migration of ^{90}Sr and ^{137}Cs in the "soil–plant" chain proceeds rather intensively in such soils; and, from an agricultural viewpoint, the release of radioactivity took place in a most unfavorable period, i.e., the end of April and beginning of May. As we know, rather significant quantities of mobile radionuclides, i.e., ^{131}I, ^{134}Cs, ^{137}Cs and ^{90}Sr, found their way into the environment as a result of this accident.

Investigations have demonstrated that contamination of agricultural–industrial products (over and above the external gamma-radiation and possible impact of ^{131}I and ^{239}Pu) is the most hazardous of effects. Direct radiation affects on animals and plants played a secondary role. Hence, the main efforts for rehabilitation and use of contaminated lands were directed towards limiting radionuclide transfer into these agricultural–industrial products (first of all with respect to ^{137}Cs since radiological analysis had shown that the cesium isotopes presented the greatest hazard). The reclamation of natural grasslands and pastures were amongst the leading actions that provided the maximum possible reduction of radionuclide transfer to plants from the soil. The radical amelioration of meadows (i.e., reploughing with turn-over of strips, followed by liming and application of minerals fertilizers) secured a reduction of 10–15 times in the radionuclide content of the grass. Here, the experience gained from the South Urals accident was used to the maximum degree.

As, for the Chernobyl accident, ^{137}Cs was predominant in the mixture of long-lived radionuclides, potassium fertilizer played a major role in the reduction of its uptake by plants. The liming of acid soils and the addition of nitrogen, potassium and phosphorous fertilizers resulted in a decrease of the ^{137}Cs in the plants by 1.5–3 times. Certainly, the radionuclide accumulation in plants depends on soil type and the biological features of plants and these should be taken into account in rehabilitation measures.

The restoration of meadows and pastures is a high priority since it favors a decrease in the ^{137}Cs content of milk (next in importance is meat). An efficient approach to this problem is to convert the milk into butter as well as feeding the animals with clean forage in the pre-slaughter period. The measures undertaken during the first two years after the accident in the agricultural–industrial fields resulted in a reduction in the dose to the

population from internal exposure by a factor of ten. More and more new means have appeared in recent years, some of which have been presented at a number of conferences (Izrael, 2000a & b; Zeevaert et al., 1997). Their use has resulted in even greater efficiencies in the rehabilitation measures used for contaminated lands, particularly in the industrial agricultural sector.

Conclusions

In conclusion, it should be noted once again that a huge amount of experimental material has been collected, analyzed and generalized in preparing this book and this material has been supplemented by theoretical studies of the processes of radioactive fallout formation and behavior subsequent to atomic explosions and accidents.

Material that has appeared in the scientific literature since the 1950s has been carefully collected in this book. These are data that have never become outdated, as they are actual data obtained after the different nuclear weapons' tests. We should keep in mind, however, that, for the most part, these data were secret at the beginning. The data contained here were collected as a result of the use of both theoretical and laboratory methods of investigation including aerial gamma-surveys of contamination of the atmosphere and surrounding land. Very fine methods of analysis of micro- and macro-objects were applied here (including investigations of the aerosol particles of fractions of microns). These data were necessary for the understanding of the processes of formation of aerosol particles, their distribution, for prediction of both the radiation situations and the radiological consequences of nuclear weapons' testing (both within the boundaries of test sites and beyond) in the atmosphere (including surface/ground explosions) and underground (including cratering).

The great "break-through" in exchange of information on environmental contamination happened during the Soviet–American meetings and talks (1969–1971) devoted to the peaceful uses of nuclear energy. It then became clear that both Soviet and U.S. scientists, using similar methods, had obtained very similar data on radioactive contamination. At that time, U.S. specialists were able to gain access to additional data on the transfer of radionuclides into aqueous media under natural conditions, i.e., data that could never have been obtained from investigations in the dry desert soils of the Nevada test site.

The book also contains important material on the radioactive contamination of natural environments after the accidents in the South Urals (especially in 1957) and at the Chernobyl nuclear power station in 1986.

The basic contents of this book have been devoted to the behavior of radionuclides from the moment of their generation to their entry into all natural media and, then, along the food chains into animals and human beings. Emphasis was given to the fractionation of radionuclides and their mobility—starting from their distribution on aerosol particle-carriers to their solubility and biological accessibility. All these data are needed to understand and predict their transport and for the forecasting of both external and internal radiation doses to man. The last chapter was devoted to the deactivation and rehabilitation of contaminated territories for which the best information available about radionuclide mobility is especially necessary.

During recent years (in particular, after the Chernobyl accident), several international conferences and symposia were held where the radiological aspects of the consequences of nuclear explosions and accidents were discussed in detail. We should note here the conferences devoted to the Chernobyl accident, especially those in Minsk (Belorussia) and Vienna, Austria (10 years after Chernobyl), a series of conferences on the RADTEST and RADLEG projects and conferences that were supported by NATO. The proceedings of these meetings (actually collections of papers on nuclear energy related problems) present interesting data on radiological consequences. Important contributions to the information regarding the radiation situation after the Chernobyl accident have been presented in two detailed atlases—European and Russian contamination of the lands by ^{137}Cs and other radionuclides. These atlases were published in 1998. In April 2000, the International Conference "Radioactivity after Nuclear Explosions and Accidents" was held in Moscow, assembling many participants and attracting great interest. The first volume, out of a total of three (published in October 2000 and edited by Yu.A. Izrael), contains new material about the current radiation situation in the environment.

The current publication, however, is the only monograph available that summarizes the substantial material on radioactive fallout after nuclear explosions and accidents. Thus, in the book "Nuclear Test Explosions. Environmental and Human Impacts", published by J.W. Wiley (2000) and edited by Sir Frederick Warner and Prof. Rene J.C. Kirschmann, only one chapter is devoted to the radiation situation (with participation of the author). This book is translated from the Russian volume of the same title, published in St. Petersburg in 1996, but for this edition it has been supplemented with new data published for the period up to the end of 2000.

References

Abagyan, A. A., Izrael, Yu. A., Ilyin, L. A., Legasov, V. A. & Petrov, V. E. (1986a). Accident at the Chernobyl NPP and its consequences. Information prepared for IAEA experts meeting, 25–29 August, 1986, Vienna. IAEA Technical Document, August 1986 (71 p.).

Abagyan, A. A., Ilyin, L. A., Izrael, Yu. A., Legasov, V. A. & Petrov, V. E. (1986b). Information on the Chernobyl NPP accident and its consequences prepared for IAEA. *Atomic Energy*, *61* (5), 301–320.

Abramovich, G. N. (1948). *Turbulent Free Jets of Liquids and Gases* [in Russian]. Moscow: Gosenergoizdat.

Adams, C. E., Farlow, N. H. & Schell, W. R. (1960). The compositions, structures and origins of radioactive fallout particles. *Geochemica et Cosmochemica Acta*, *18* (1/2), 42–56.

Adushkin, V. V. (2000). Influence of geological factors upon dissipation of radioactive products after underground nuclear explosions. In: *Proceedings of an International Conference on "Radioactivity after Nuclear Explosions and Accidents"*, Moscow, April 2000 (Vol. 1, pp. 585–593).

Adushkin, V. V. & Spivak, A. A. (2000). Characteristics of radioactive product yields into the atmosphere from an underground explosion. In: *Proceedings of an International Conference on "Radioactivity after Nuclear Explosions and Accidents"*, Moscow, 24–26 April, 2000 (Vol. 1, pp. 601–615). St.-Petersburg: Hydrometeoizdat.

Akopyan, A. A. (1955). *General Thermodynamics* [in Russian]. Moscow: Energoizdat.

Alekin, O. A. (1952). *Hydrochemistry* [in Russian]. Leningrad: Hydrometeoizdat.

Aleksakhin, R. M. & Korneev, N. A. (Eds.) (1991). *Agricultural Radioecology* [in Russian] (p. 397). Moscow: Ecology.

Aleksakhin, R. M., Fesenko, S. V., Kryshev, I. I. & Romanov, G. N. (1993). Establishing of scientific investigation on radioecology on East-Urals radioactive pattern. In: *Ecological Consequences of Radioactive Contamination in the Southern Urals* (p. 6–12). Moscow: Nauka.

Aleksakhin, R. M., Kozmin, G. V., Santerova, N. I. & Fesenko, S. V. (1994). About rehabilitation of territories prone to radioactive contamination. *Herald of the Russian Academy of Sciences*, *64* (2), 28–30.

Aleksakhin, R. M., Romanov, G. N., Tikhomirov, F. A. & Kryshev, I. I. (2000). Radiologic situations related to the large-scale contamination of the environment (River Techa, accidents in the South Urals and at the Chernobyl NPS): agricultural and ecological aspects. In: *Proceedings of an International Conference on "Radioactivity after Nuclear Explosions and Accidents"*, Moscow, 24–26 April, 2000 (Vol. 1, pp. 48–58). St.-Petersburg: Hydrometeoizdat.

Anderson, A. D. (1961). A theory for close-in fallout from land-surface nuclear bursts, *J. Meteorol.*, *18* (4), 431–442.

Andryushin, I. A., Chernyshev, A. K. & Logachev, V. A. (1996). Modern interpretation of data of aerial and ground surveys of the pattern from the first nuclear test in the USSR. In: *Bulletin of Scientific Program "Semipalatinsk polygon – Altai"*, No. 2, pp. 102–108.

Anttila, M. (1987). Studies on reactor physics, dynamics, ECCS reliability and containment related to the Chernobyl accident. VTT Technical Report, TSHERNO-6/87.

Anwera, L. & Vanlierde, R. (1986). Application of a trajectory model to the Chernobyl accident. Institute Royal Meteorologique de Belgique.

Arnold, E. D. (1958). Effect of uranium recycling on transuranic element buildup. *Nucl. Sci. Eng.*, *3*, 707–725.

Artemjev, O. I., Akhmetov, M. A. & Ptitskaya, L. D. (2000). Radiation heritage of the atmospheric nuclear tests carried out at the Semipalatinsk polygon (SIP). In: *Proceedings of an International Conference on "Radioactivity after Nuclear Explosions and Accidents"*, Moscow, April 2000 (Vol. 1, 318 p.).

Batzel, R. E. (1960). Radioactivity associated with underground nuclear explosions. *J. Geophys. Res.*, *65* (9), 2897–2902.

Begichev, S. N. (1990). Radioactive releases due to the Chernobyl accident. In: J. T. Rogers (Ed.), *Fission Product Transport Processes in Reactor Accidents*. Hemisphere.

Benson, P., Gleit, K. & Levental, L. (1965a). Physical characteristics of individual particles after powerful explosions. In: *Proceedings of the Second Conference "Radioactive Fallout from Nuclear Weapon Tests"*, Germantown, Maryland, November 3–6, 1964 (pp. 82–89).

Benson, P., Gleit, K. & Levental, L. (1965b). Characteristics of radiochemical fractionation of radioisotopes in individual particles after powerful air explosions. In: *Proceedings of the Second Conference "Radioactive Fallout from Nuclear Weapon Tests"*, Germantown, Maryland, November 3–6, 1964 (pp. 90–100).

Bethe, H. A. (1950). The hydrogen bomb. *Bull. Atomic Scientists*, *6* (4), 99–104.

Bjornerstedt, R. (1960). Health hazards from fission products and fallout. *Arkiv for Fysik*, *16* (29), 293–313.

Bolsunovsky, A. (1995). On reviewing the official value of radionuclides released as a result of the Chernobyl accident. Information [in Russian]. Krasnoyarsk.

Boltneva, L. I., Izrael, Yu. A. & Nazarov, I. M. et al. (1977). Global contamination with ^{137}Cs and ^{90}Sr and doses of external irradiation on the USSR territory. *Atomic Energy*, *42*, 355.

Bonner, N. A. & Miskel, J. A. (1965). Radioactivity: distribution from cratering on basalt, UCRL-14211. *Science*, *150* (3695), 489.

Borisov, N. B., Ogorodnikov, B. I., Kachanova, N. I., Kaurov, G. A., Borisova, L. I., Churkin, S. L., Skitovich, V. I., Verbov, V. V., Polevov, V. N., Najdenov, Yu. A. & Budyka, A. K. (1993). Observations of gas-aerosol components of radioiodine and radioruthenium during the first weeks after the CNPP accident [in Russian]. In: *Proceedings of the 1st All-Union Conference "Radiation Aspects of the Chernobyl Accident"* (Vol. 1, pp. 132–137). St.-Petersburg: Hydrometeoizdat.

Bracher, D. (1954). Birmingham branch activities in weapon development. *Atomic Scientists J.*, *3* (5), 292–300.

Budyko, A. K. & Ogorodnikov, B. I. (2000). Radioactive aerosols of the Chernobyl genesis. In: *Proceedings of an International Conference on "Radioactivity after Nuclear Explosions and Accidents"*, Moscow, April 2000 (Vol. 1, 231 p.).

Butkovich, T. R. (1965). Calculation of the shock wave from an underground nuclear explosion in granite. *J. Geophys. Res.*, *70* (4), 885.

Buzulukov, Yu. P. & Dobrynin, Yu. L. (1993). Release of radionuclides during the Chernobyl accident. In: *The Chernobyl Papers. Doses to the Soviet Population and Early Health Effect Studies* (Vol. 1). Richland, WA: Research Enterprises Publishing Segment.

Cameron, A. G. W. (1959). Multiple neutron capture in the Mike fusion explosion. *Can. J. Phys.*, *3*, 322–333.

Carslow, G. & Eger, D. (1964). Thermal Conductivity of Solids [in Russian]. Moscow: Nauka.

Central Institute of Forecasts (1962). *Synoptic Bulletin for October 1961*. Northern Hemisphere.

Cherepnin, Yu. S. (2000). The present-day radiation situation at the former Semipalatinsk testing polygon. In: *Proceedings of an International Conference on "Radioactivity after Nuclear Explosions and Accidents"*, Moscow, 24–26 April, 2000 (pp. 92–100). St.-Petersburg: Hydrometeoizdat.

Cherry, J. T. (1967). Computer calculations of explosion-produced craters. *J. Rock. Mech. Min. Sci.*, *1*.

Chiorso, A., Thompson, S. G. & Higgins, G. H. et al. (1955). New elements einsteinium and fermium, atomic numbers 99 and 100. *Phys. Rev.*, *99* (3), 1048–1049.

Chirkin, V. S. (1968). Thermal-Physical Properties of Nuclear Engineering Materials [in Russian]. Moscow: Atomizdat.

Cockroft, S. J. (1955). Radiological hazards from nuclear explosions and nuclear power. *Nature*, *175* (4464), 873–875.

Cray, F. & Freed, R. (1965). Radioactive fallout at large distances from the explosions Sedan and Small Boy. In: *Proceedings of the Second Conference "Radioactive Fallout from Nuclear Weapon Tests"*, Germantown, Maryland, November 3–6, 1964 (pp. 64–82).

Crocer, G. R., O'Connor, J. D. & Freiling, E. C. (1966). Physical and radiochemical properties of fallout particles. *Health Physics*, *12* (8), 1099–1104.

Davitaya, F. F. (Ed.) (1960). *Climate Atlas of the USSR* [in Russian] (Vol. 1, 181 p.). Moscow: Hydrometeoizdat.

De Cort, M. Fridman, Sh. D., Izrael, Yu. A. (Scientific Direction), Jones, A. R., Kelly, G. N., Kvasnikova, E. V., Matveenko, I. I., Nazarov, I. M., Stukin, E. D., Tabachny, L. Ya. & Tsaturov, Yu. S. (Editorial Panel) (1998). *Atlas of Caesium Deposition on Europe after the Chernobyl Accident*. Luxembourg Office for Official Publications of the European Communities. ISBN 92-828-3140-X, Catalogue number CG-NA-16-733-29-C, EN, RU.

Devell, L., Guntay, S. & Powers, D. (1996). The Chernobyl reactor accident source term. Development of a consensus view. In: *Proceedings of an International Conference on "One Decade after Chernobyl* (Vol. 1), 8–12 April, 1996. IAEA-CN-63/155.

Dokuchaev, M. M., Rodionov, V. N. & Romanov, A. N. (1963). *Explosion for Ejection* [in Russian]. Moscow: Publishing office of AN SSSR (Academy of Sciences of the USSR).

Drevinsky, R. J., Wasson, J. N., Couble, E. C. & Dymond, N. A. (1964). ^{7}Be, ^{32}P, ^{33}P and ^{35}S: stratospheric concentrations and artificial production. *J. Geophys. Res., 69* (8), 1457–1467.

Dubasov, Yu. V. & Tukhvatulin, Sh. T. (2000). Radiation situation at the Semipalatinsk polygon 10 years after cessation of underground nuclear tests. In: *Proceedings of an International Conference on "Radioactivity after Nuclear Explosions and Accidents"*, Moscow, April 2000 (Vol. 1, 150 p.).

Dunning, G. M. (1959). Fallout from nuclear tests at the Nevada test site. In: *Fallout from Nuclear Weapons Tests.* (Vol. 3, pp. 2021–2113). Washington: Government Printing Office.

Edvarson, K., Low Kerstin & Sisefsky, J. (1959). Fractionation phenomena in nuclear weapons debris. *Nature, 184* (4701), 1771–1774.

Emeljanov, V. S. (Ed.) (1958). *Atomic Energy (A Brief Encyclopedia)* [in Russian]. Moscow.

Essington, E. H., Nishita, H. & Steen, J. (1965). Release and movement of radionuclides in soils contaminated with fallout material from an underground thermonuclear detonation. *Health Physics, 11* (8), 689–698.

Fedorov, E. K. (Ed.) (1959). *Meteorology and Atomic Energy* [translated from English]. Moscow: Inostrannaya Literatura (Foreign Literature).

Feely, H. W. & Bazan, F. (1965). Stratospheric distribution of radioactive debris. In: *Proceedings of the Second Conference "Radioactive Fallout from Nuclear Weapon Tests"*, Germantown, Maryland, November 3–6, 1964 (pp. 135–158).

Ferber, G. (1965). Distribution of radioactive substances with height in the cloud of a nuclear explosion. In: *Proceedings of the Second Conference "Radioactive Fallout after Nuclear Explosions"*, Germantown, Maryland, November 3–6, 1964 (pp. 265–283).

Ferber, G. J. & List, R. J. (1969). Prediction of external gamma dose from nuclear excavation of a sea-level canal. *Bio-Science, 19* (3), 234–236.

Fesenko, S. V., Aleksakhin, P. M., Santzerova, N. I. & Lisyansky, B. G. (1998). Analysis of strategies of application of protective measures in agriculture after the Chernobyl accident. *Radiation Biology, Radioecology, 28* (5), 721–736.

Fleming Jr., E. H. (1967). The fission product decay chains (^{239}Pu, with fission spectrum neutrons). LRL, Livermore, University of California, USA.

Freiling, E. C. (1961). Radionuclide fractionation in bomb debris. *Science, 133* (3469), 1991–1998.

Freiling, E. C. (1962). *Radioactive Fallout from Nuclear Weapon Tests* (Vol. 1, pp. 25–47). TID-7632, Washington, USA.

Freiling, E. C. (1963). Theoretical basis for logarithmic correlation of fractionated radionuclide compositions. *Science, 139* (3559), 1058–1069.

Freiling, E. C. & Kay, M. A. (1966). Radionuclide fractionation in air-burst debris. *Nature, 209* (5020), 236–238.

Freiling, E. R., Crocer, G. & Adams, C. (1965). Formation of particle-debris of a nuclear explosion. In: *Proceedings of the Second Conference "Radioactive Fallout after Nuclear Explosions"*, Germantown, Maryland, November 3–6, 1964 (pp. 11–53).

Friedlander, S. & Pasery, R. (1965). Study of size particle distribution of the tropospheric aerosols by a sampler with rotating disk. In: *Proceedings of the Second Conference "Radioactive Fallout after Nuclear Explosions"*, Germantown, Maryland, November 3–6, 1964 (pp. 108–118).

Fridman, A. N. & Nazarov, I. M. (Eds.) (1994). *Methods and Some Results of Aerial Gamma-Survey of the Radioactive Contamination of the European Territory of the USSR. Collection of Papers.* St.-Petersburg: Hydrometeoizdat.

Fuks, N. (1934). About a rate of drop evaporation in the gas atmosphere. *Journal of Experimental and Theoretical Physics, 4* (7), 747–759.

Gaglione, P. & Ravera, O. (1964). Manganese-54 concentration in fallout, water and unio mussels of lake Maggiore. *Nature, 204* (4964), 1215–1216.

Garkusha, I. F. (1954). *Pedology* [in Russian]. Moscow: Sel'khozgiz.

Gaziev, Ya. I. (1965). Aerosol dispersibility of the global radioactive contamination of the atmosphere. In: *Proceedings of the Conference on Nuclear Meteorology "Radioactive Isotopes in the Atmosphere and Their Use in Meteorology"*, Obninsk, 3–6 February, 1964 (pp. 53–83). Moscow: Atomizdat.

Gaziev, Ya. I., Malakhov, S. G. & Nazarov, L. E. (1965). Fractionation of radioactive isotopes in hot particles. *Atomic Energy, 18* (5), 535–537.

Gaziev, Ya. I., Nazarov, L. E. & Lachikhin, N. K. (1993). Study of physical characteristics of radioactive gas-aerosol products from the CNPP accident and power estimation of sources of the technogenic release of these products into the atmosphere. In: *Proc. of the 1st All-Union Conference "Radiation Aspects of the Chernobyl Accident"* (Vol. 1, pp. 98–103). St.-Petersburg: Hydrometeoizdat.

Glesston, E. (Ed.) (1966). *Effect of Nuclear Weapons* [in Russian]. Moscow: Voenizdat.

Glushko, V. P. (Ed.) (1962). *Thermodynamic Properties of Individual Substances (Materials)* [in Russian]. Moscow: Academy of Sciences.

Godt, K. J. (1961). Neubestimm und der Halbwertszeit des Wolframisotops ^{181}W mit Fallout- und Labaratoriumspraparaten. Atomkernenergie, Bd 6, H. 7/8, s. 318–323.

Goldstein, G. (1961). *Fundamentals of Reactor Protection* [in Russian]. Moscow: Gosatomizdat.

Grechushkina, M. P. (1964). *Tables on Composition of Instantaneous Fission Products ^{235}U, ^{238}U, and ^{239}Pu by Ast Neutrons* [in Russian]. Moscow: Atomizdat.

Grechushkina, M. P. & Izrael, Yu. A. (1965). Fractionation of radioactive products from a nuclear explosion. In: *Radioactive Isotopes in the Atmosphere and Their Use in Meteorology* (pp. 164–180). Moscow: Atomizdat.

Gustafson, P., Muniak, S. E. & Brar, S. S. (1964). Concentrations of caesium-137, rhodium-102 and manganese-54 in surface air. *Nature, 203* (4944), 470–472.

Heft, R. E., Phillips, W. & Steele, W. (1971). Radionuclide distribution in the particle population produced by the Schooner cratering detonation. *Nuclear Technology, 11* (3), 413–443.

Higgins, G. (1970). Nuclear explosion data for underground engineering applications. TECDOC, IAEA-PL-388/1.

Higgins, G. H. & Butkovich, T. R. (1967). Effect of water content, yield, medium and depth of burst on cavity radii. UCRL-50203.

Hohenemser, C. & Renn, O. (1988), Chernobyl's kernel legacy. *Environment, 30* (3), 4–11, 40–45.

Hunter, H. F. & Ballou, N. E. (1951). Fission product decay rates. *Nucleonics, 9* (5), C-2–C-7.

IAEA (1986). Summary report on the post-accident review meeting on the Chernobyl accident. IAEA Technical Document, 75-INSAG-1, International Atomic Energy Agency, Vienna, Austria.

IAEA (1998a). Characterization of radioactively contaminated sites for remediation purposes. IAEA-TECDOC-1017, Vienna.

IAEA (1998b). Factors for formulating strategies for environmental restoration. IAEA-TECDOC-1032, Vienna.

IAEA (1998c). Radiological Conditions at Bikini Atoll: Prospects for Resettlement. Radiological Assessment Series, International Atomic Energy Agency (IAEA), Vienna (1998).

Izrael, Yu. A. (1963). Influence of a micro-relief of the Earth's surface on the gamma-radiation distribution within the atmosphere ground layer. *Izvestija AN SSSR, ser. Geophys., 5*, 818.

Izrael, Yu. A. (1964). Gamma-radiation field of the surface radioactive contamination of a terrain within the atmosphere ground layer. *Izvestija AN SSSR, ser. Geophys., 7*, p. 1103.

Izrael, Yu. A. (1965). Determination of fractionation coefficients (factors) and biological accessibility of the nuclear test products in radioactive fallout. *Doklady of Academy Nauk SSSR, 149* (2), 343.

Izrael, Yu. A. (1966). Conditions of formation of radioactive fallout particles and fractionation of isotopes in an underground nuclear explosion with ground ejection. *Doklady of Academy Nauk SSSR, 169* (3), 573–576.

Izrael, Yu. A. (1968). Fractionation of isotopes in radioactive fallout at large distances from the explosion site. In: *Study of Processes of Atmosphere Self-cleaning from Radioactive Isotopes* (pp. 57–63). Vilnyus: Mintis.

Izrael, Yu. A. (1969). Calculation of effects of fractionation in atmospheric nuclear explosions. *Trudy IEM* (Proceedings of the Institute of Experimental Meteorology), *21*, 97.

Izrael, Yu. A. (1970a). Radioactivity in camouflet underground explosions, IAEA-PL-3888/22. In: *Proceedings of a Panel "Peaceful Nuclear Explosions"*, IAEA, Vienna, 2–6 March, 1970 (pp. 231–240).

Izrael, Yu. A. (1970b). Tungston isotopes in "fresh" radioactive fallout in December 1968. *Atomic Energy, 30* (9), 377.

Izrael, Yu. A. (1971). *Tritium Fallout and Estimation of Possible Doses of Internal Irradiation from Tritium in the Zone of a Far Trace at an Underground Explosion with an Ejection* [in Russian]. Moscow: Hydrometeoizdat.

Izrael, Yu. A. (1973). *Isotope Composition of Radioactive Fallout* [in Russian] (108 p.). Leningrad: Hydrometeoizdat.

Izrael, Yu. A. (1974). *Peaceful Nuclear Explosions and the Environment* [in Russian] (135 p.). Leningrad: Hydrometeoizdat.

Izrael, Yu. A. (1984). *Ecology and Environmental Control* [in Russian] (560 p.). Moscow: Hydrometeoizdat.

Izrael, Yu. A. (1989). Chernobyl: past and forecast. *Pravda* (newspaper), 1989, 20 March.

Izrael, Yu. A. (1990). Chernobyl echo. *Science and Life*, *9*, 28–29.

Izrael, Yu. A. (Ed.) (1993). In: *Proceedings of the 1st All-Union Conference "Radiation Aspects of the Chernobyl Accident"* (Vol. 1, p. 408). St.-Petersburg: Hydrometeoizdat.

Izrael, Yu. A. (1996a). On assessment of the radiation situation and radioactive contamination of the environment from the Chernobyl NPP accident. *Meteorology and Hydrology*, *4*, 5–7.

Izrael, Yu. A. (1996b). *Radioactive Fallout after Nuclear Explosions and Accidents* [in Russian] (355 p.). St.-Petersburg: Progress-POGODA.

Izrael, Yu. A. (Chief Ed.) (1998). *Atlas of Radioactive Contamination of the European Part of Russia, Belarus and Ukraine*. St.-Petersburg: Cartographical Factory VSEGEI (355 p.).

Izrael, Yu. A. (Ed.) (2000a). *Proceedings of International Conference "Radioactivity after Nuclear Explosions and Accidents"*, Moscow, 24–26 April, 2000 (Vols. 1–3). St.-Petersburg: Hydrometeoizdat.

Izrael, Yu. A. (2000b). Radioactive contamination after nuclear explosions and accidents: general approach. In: *Proceedings of an International Conference on "Radioactivity after Nuclear Explosions and Accidents"*, Moscow, 24–26 April, 2000 (Vol. 1, pp. 26–47). St.-Petersburg: Hydrometeoizdat.

Izrael, Yu. A., Kogan, R. M. & Fridman, A. D. (1962). Deformation of the gamma-field in the atmospheric ground layer caused by forest cover. *Izvestija AN SSSR, ser. Geophys.*, *8*, 1126.

Izrael, Yu. A. & Stukin, E. D. (1967). *Gamma-Radiation of Radioactive Fallout* [in Russian]. Moscow: Hydrometeoizdat (224 p.).

Izrael, Yu. A., Ter-Saakov, A. A. & Schetinin, N. N. (1968). Modeling of radioactive fallout particles. *Atomic Energy*, *24* (6), 584–586.

Izrael, Yu. A. & Petrov, V. N. (1970). Spreading of the radioactive products after underground nuclear explosions over great distances. In: *Nuclear Explosions for Peaceful Uses* [in Russian]. Moscow: Atomizdat (pp. 87–93).

Izrael, Yu. A., Kazakov, Yu. E. & Ter-Saakov, A. A. (1970a). Characteristics of the radioactive contamination of the atmosphere and terrain after single and group underground nuclear explosions with ejection of ground. In: *Nuclear Explosions for Peaceful Uses* [in Russian] (pp. 103–132). Moscow: Atomizdat.

Izrael, Yu. A., Petrov, V. N., Pressman, A. Ya., Rovinsky, F. Ya., Stukin, E. D. & Ter-Saakov, A. A. (1970b). Radioactive Contamination of Natural Environments from Underground Nuclear Explosions and Prediction Methods [in Russian]. Leningrad: Hydrometeoizdat.

Izrael, Yu. A., Ter-Saakov, A. A., Malakhov, S. G., Kurganskaya, V. M., Rovinsky, F. Ya., Iokhelson, S. B., Stukin, E. D., Churkin, V. N. & Shulepko, Z. S. (1971). Tungsten isotopes in fresh radioactive fallout in December 1969. *Atomic Energy*, *30* (4), 377–380.

Izrael, Yu. A. & Petrov, V. N. (1975). Diffusion and fallout of radioactive products from the cloud of an underground nuclear explosion. IAEA TECHDOC—Peaceful Nuclear Explosions IV. Vienna: IAEA.

Izrael, Yu. A., Petrov, V. N. & Severov, D. A. (1987a). Modelling of radioactive fallout in the close-in zone from the Chernobyl nuclear power plant. *Meteorology and Hydrology*, *7*, 5–12.

Izrael, Yu. A., Petrov, V. N., Avdyushin, S. N., Gasilina, N. K., Rovincki, F. Ya., Vetrov, V. A. & Vakulovski, S. M. (1987b). Radioactive contamination of the environment in the Chernobyl NPS accident zone. *Meteorology and Hydrology*, *2*, 5–18.

Izrael, Yu. A., Vetrov, V. A., Alekseenko, V. A., Poslovin, A. L., Kozorezov, E. V. & Stukin, E. D. (1988). Washout of radionuclides with flood waters from natural catchments and migration with underground waters. In: *"Radioactive Contamination of Natural Environments in the Zone of the Chernobyl Accident"* [in Russian], N3. Moscow: Goscomgidromet.

Izrael, Yu. A., Nazarov, I. M., Pressman, A. Ya., Rovinsky, F. Ya., Ryaboshapko, A. G. & Filippova, L. M (1989a). Acid Rains [in Russian] (269 p.). Leningrad: Hydrometeoizdat.

Izrael, Yu. A., Petrov, V. N. & Severov, D. A. (1989b). Regional model of radionuclide transport and deposition from the Chernobyl nuclear power plant accident. *Meteorology and Hydrology*, *6*, 5–14.

Izrael, Yu. A., Vakulovsky, S. M., Vetrov, V. A., Petrov, V. N., Rovinckii, F. Ya. & Stukin, E. D. (1990). *Chernobyl: Radioactive Contamination of Natural Environments* [in Russian] (296 p.). Izrael, Yu. A. (Chief Ed.). Leningrad: Hydrometeoizdat.

Izrael, Yu. A., Nazarov, I. M., Fridman, Sh. D., Avdyuschin, S. I., Kvasnikova, E. V., Kontarovich, R. S., Imshennik, E. V. & Shusharina, N. M. (1992). Radiation situation on the territory of the CIS European part and Urals in 1991. *Meteorology and Hydrology, 4*.

Izrael, Yu. A., Artemov, E. M., Nazarov, I. M., Fridman, Sh. D., Zinenko, V. I., Krivotanko, A. I., Lyaschenko, N. G., Pakholov, V. G., Tchirkov, V. A. & Stukin, E. D. (1993a). Radioactive terrain contamination resulting from the accident at the radiochemical plant in Tomsk-7. *Meteorology and Hydrology, 6*, 5–8.

Izrael, Yu. A., Tsaturov, Yu. S., Nazarov, I. M., Petrov, V. N., Stukin, E. D., Fridman, Sh. D., Kontarovich, P. S., Fedonkin, A. F. & Kertsmen, V. M. (1993b). Reconstruction of the real pattern of terrain radioactive contamination from accidents and nuclear tests based on present-day and other data. In: *Proceedings of an International Symposium on "Remediation and Restoration of Radioactive-Contaminated Sites in Europe"*. Antwerp (Vol. 1, pp. 325–350), DOC XI-5027/94.

Izrael, Yu. A., Kvasnikova, E. V., Nazarov, I. M. & Fridman, Sh. D. (1994a). Caesium-137 global and regional radioactive contamination over the European part of the former USSR. *Meteorology and Hydrology, 5*, 5–9.

Izrael, Yu. A., Stukin, E. D. & Tsaturov, Yu. S. (1994b). On the possibility to identify radioactive patterns from nuclear explosions and reconstruct exposure doses of the population using long-lived radionuclide analysis. *Meteorology and Hydrology, 12*, 5–14.

Izrael, Yu. A., Tsaturov, Yu. S., Nazarov, I. M., Petrov, V. N., Stukin, E. D., Fridman, Sh. D., Kontarovich, P. S., Fedonkin, A. F. & Kertsmen, V. M. (1994c). Reconstruction of the actual features of radioactive terrain contamination resulting from accidents and nuclear tests. *Meteorology and Hydrology, 8*, 5–18.

Izrael, Yu. A. & Stukin, E. D. (1995). Comments on the problem of the radionuclide release scale resulting from the Chernobyl accident (preprint). Moscow: Roshydromet.

Izrael, Yu. A., Volkov, A. S. & Kovalev, A. F. (1995). Radioactive contamination of the territory of the former USSR after nuclear explosions at Novaya Zemlya in autumn 1961. *Meteorology and Hydrology, 5*, 5–12.

Izrael, Yu. A., De Cort, M., Jones, A. R., Nasarov, I. M., Fridman, Sh. D., Kvasnikova, E. V., Stukin, E. D., Kelly, J. N., Matvienko, I. I., Pokuleiko, Yu. P., Tabachnai, L. Ya. & Tsaturov, Yu. S. (1996). The atlas of caesium-137 Contamination of Europe after the Chernobyl accident. In: *1st Intern. Conference of the European Community, Belarus, Russian Federation and Ukraine on the Radiological Consequences of the Chernobyl Accident*. Minsk, March 1996, *Meteorology and Hydrology, 4*, 8–17.

Izrael, Yu. A., Imshennik, E. V., Kvasnikova, E. V., Nazarov, I. M., Stukin, E. D. & Tsaturov, Yu. S. (1998). Long-term forecasting of a change of radioactive contamination of Russian territory by caesium-137 after the Chernobyl accident. *Meteorology and Hydrology, 4*, 5–17.

Izrael, Yu. A., Nazarov, I. M., Petrov, V. N., Stukin, E. D. & Tsaturov, Yu. S. (2000a). Implementation of radiation monitoring in the USSR and Russian Federation: the half century of experience. In: *Proceedings of an International Conference on "Radioactivity after Nuclear Explosions and Accidents"*, Moscow, 24–26 April, 2000 (pp. 107–115). St.-Petersburg: Hydrometeoizdat.

Izrael, Yu. A., Nazarov, I. M., Vasilenko, V. N., Artemov, E. M., Nakhutin, A. I., Uspin, A. A. & Kyamkin, A. M. (2000b). Radioactive contamination of the Urals region by the industrial enterprise "Mayak". In: *Proceedings of an International Conference on "Radioactivity after Nuclear Explosions and Accidents"*, Moscow, 24–26 April, 2000 (pp. 411–424). St.-Petersburg: Hydrometeoizdat.

Japan Society for the Promotion of Science (1956). *Research on the Effects and Influences of the Nuclear Bomb Test Explosions*. Tokyo: Yeno.

Johnson, G. W. (1963). Excavation with nuclear explosives: promise and problems. *Physics Today, 16* (11), 38–44.

Johnson, G. W. & Higgins, G. H. (1965). Engineering applications of nuclear explosives: project Plowshare. *Rev. Geophys., 13* (3), 365–385.

Johnson, G. W., Higgins, G. H. & Violet, C. E. (1959). Underground nuclear detonations. *J. Geophys. Res., 6* (10), 1457–1470.

Johnson, J. E., Ward, G. M. & Stewart, H. F. (1966). Interpretation of gamma-ray spectra of environmental forage samples. *Health Phys., 12* (1), 37–42.

Kadyrzhanov, K. K., Rofer, Ch., Khatekber, S., Kazachevsky, I. V. & Lukashenko, S. N. (2000). Systematization of radionuclide contamination of SIP by a specific features of nuclear tests. In: *Proceedings of an International Conference on "Radioactivity after Nuclear Explosions and Accidents"*, Moscow, April 2000 (Vol. 1, 465 p.).

Kalkstein, M. I. (1962). Rhodium-102 high-altitude tracer experiment. *Science, 137* (3531), 645–652.

Kalkstein, M., Tomassien, A. & Nikula, D. (1965). Results of the cadmium-109 measurements at altitudes below 20 km. In: *Proceedings of the Second Conference "Radioactive Fallout from Nuclear Weapon Tests"*, Germantown, Maryland, November 3–6, 1964 (pp. 211–214).

Karol, I. L. (1972). *Radioactive Isotopes and Global Transport in the Atmosphere* [in Russian] (365 p.). Leningrad: Hydrometeoizdat.

Katcoff, S. (1960). Fission-product yields from neutron-induced fission. *Nucleonics, 18* (11), 201–208.

Kauranen, P. (1964). Radioactive antimony isotopes in the atmosphere. *J. Geophys. Res., 69* (23), 5075–5080.

Kedrovsky, O. L. (1970). The application of contained nuclear explosions in industry and civil engineering. IAEA-PL-388/19, 20,21. In: *Proceedings of a Panel "Peaceful Nuclear Explosions"*, Vienna, 2–6 March, 1970 (pp. 17–21, 163–184, 377–404).

Kellog, W. W. & Rapp, R. R. (1957). Greenfield. Close-in fallout. *J. Meteorol., 14* (1), 1–8.

Khodakovsky, I. L., Dorofeeva, V. A., Morinenko, M. V. & Semenov, Yu. V. (1993). Estimates of chemical forms of radionuclides in release from the CNPP accident using methods of thermodynamics. In: *Proc. of the 1st All-Union Conference "Radiation Aspects of the Chernobyl Accident"* (Vol. 1, pp. 108–114). St.-Petersburg: Hydrometeoizdat.

Kirchner, G. & Noack, C. C. (1988). Core history and nuclide inventory of the Chernobyl core at the time of the accident. *Nuclear Safety, 29*.

Klechkovsky, V. M. (Ed.) (1971). *Radioecology* [in Russian] (141 p.). Moscow: Atomizdat.

Knox, J. B. (1965). Prediction of radioactive fallout from underground nuclear explosions. In: *Proceedings of the Second Conference "Radioactive Fallout from Nuclear Weapon Tests"*, Germantown, Maryland, November 3–6, 1964 (pp. 187–195).

Knox, J. B. & Terhune, R. W. (1965). Calculation of explosion—produced craters—high-explosive sources. *J. Geophys. Res., 70* (10), 2377.

Kogan, R. M. & Fridman, Sh. D. (1960). Gamma-quantum energy distribution in the atmosphere's surface layer. *Izvestija AN USSR, ser. Geophys., 4*, 530–547.

Kogan, R. M., Nazarov, I. M. & Fridman, Sh. D. (1969). *Basis of the Gamma Spectrometry of Natural Media* [in Russian]. Moscow: Atomizdat.

Kogan, R. M., Nazarov, I. M. & Fridman, Sh. D. (1991). *Basis of the Gamma-Spectrometry of Natural Media* (3rd edition). Moscow: Energoatomizdat.

Kolobashkin, V. M. (Ed.) (1983). *Radiation Characteristics of Radiated Nuclear Fuel* (382 p.). Moscow: Energoatomizdat.

Korneev, N. A., Aleksakhin, P. M., Annenkov, V. N., Loschilov, N. A. & Firsakova, S. A. (1993). Scientific basis for agriculture-industry in regions prone to contamination from nuclear accidents. In: *Proceedings of 1st All-Union Conference "Radiation Aspects of Chernobyl Accident"*, Obninsk, June, 1988. St.-Petersburg: Hydrometeoizdat.

Krey, F. & Freid, R. (1965). Radioactive fallout at large distances from the explosions Sedan and Small Boy. In: *Proceedings of the Second Conference "Radioactive Fallout from Nuclear Weapon Tests"*, Germantown, Maryland, November 3–6, 1964 (pp. 64–82).

Krieger, H. L. (1965). The measurements of long-lived activation products in soil by gamma-spectroscopy. *Health Physics, 11* (7), 653–658.

Krieger, H. L. & Groche, D. (1960). Occurrence of scandium-46 and cesium-134 in radioactive fallout. *Science, 131* (3392), 40–41.

Kroker, G., Kavakhara, Ph. & Freiling, E. (1965). Correlation of results of the radiochemical determination of radioactive products after explosions in silicate rocks. In: *Proceedings of the Second Conference "Radioactive Fallout from Nuclear Weapon Tests"*, Germantown, Maryland, November 3–6, 1964 (pp. 54–63).

Kuntsevich, A. D. (1993). Features of radioactive contamination in the region of the Chernobyl NPS and estimate of efficiency of measures for reduction of irradiation level. In: *Proceedings of 1st All-Union Conference "Radiation Aspects of the Chernobyl Accident"* [in Russian], Obninsk, June 1988. St.-Petersburg: Hydrometeoizdat.

Kurchatov, B. V., Lavrenchik, V. N. & Shubko, V. M. (1962). Radioactive wolfram in the atmosphere. *Atomic Energy, 13* (6), 576–580.

Kuroda, P., Kauranen, P., Palmer, B., Melon, K. & Fraij, L. (1965). Fission products in the atmosphere and rain. In: *Proceedings of the Second Conference "Radioactive Fallout from Nuclear Weapon Tests"*, Germantown, Maryland, November 3–6, 1964 (pp. 252–264).

Kvasnikova, E. V. (2000). Theory and practice of radioactive contamination mapping. In: *Proceedings of an International Conference on "Radioactivity after Nuclear Explosions and Accidents"*, Moscow, 24–26 April, 2000 (pp. 153–159). St.-Petersburg: Hydrometeoizdat.

Lane, W. B. (1962). Some Radiochemical and Physical Measurements of Debris from an Underground Nuclear Explosion. NRDL-PNE-229F, Project Sedan, Vol. 17, August, 1962, NSA.

Lapp, R. E. (1955). Radioactive fallout III. *Bull. Atomic Scientists, 11* (6), 206–209.

Lapp, R. E. (1959). Local fallout radioactivity. *Bull. Atomic Scientists, 15* (5), 181–186.

Lavrenchik, V. N. (1965). *Global Fallout of Nuclear Test (Explosion) Products* [in Russian]. Moscow: Atomizdat.

Lehto, J. (Ed.) (1994). Cleanup of large radioactive contaminated areas and disposal of generated waste. Final report of the KAN-2 project, Tema Nord, Copenhagen.

Leipunsky, O. I. (1959). Gamma-Radiation of the Nuclear Explosions [in Russian]. Moscow: Atomizdat.

List, R. J., Hardy, A., Machta, L., Aleksander, T., Allen, J., Majer, M. & Velassis, V. (1965). Strontium-90 on the Earth's surface. III. In: *Proceedings of the Second Conference "Radioactive Fallout from Nuclear Weapon Tests"*, Germantown, Maryland, November 3–6, 1964 (pp. 187–195).

Loborev, V. M., Sudakov, V. V. & Bocharov, M. V. (1994). Dose reconstruction of the population irradiation of the Altai region after the nuclear explosion of 29 August 1949. Report on scientific program "Semipalatinsk Test Site—Altai" (No. 1, pp. 27–56).

Logachev, V. A. & Logacheva, L. A. (2000). Evaluation of radiation consequences after nuclear tests carried out on the world polygons. In: *Proceedings of an International Conference on "Radioactivity after Nuclear Explosions and Accidents"*, Moscow, April 24–26, 2000 (pp. 218–230). St.-Petersburg: Hydrometeoizdat.

Low, K. & Bjornerstedt, R. (1958). Health hazards from fission product and fallout. *Arkiv for Fys., 13* (1), 85–90.

Machta, L., List, R. J. & Telegadas, K. (1962). A survey of radioactive fallout from nuclear tests. *J. Geophys. Res., 67* (4), 1389–1396.

Makhon'ko, K. P. (1971). Problems of Meteorology. *Trudy IEM (Proceedings of Institute of Experimental Meteorology), 7*, 56–65.

Maly, J., Kutzendorfer, J., Machacek, V., Kourim, V. & Jerabek, V. (1957). Temporal dependence of the fission products of ^{233}U, ^{235}U and ^{239}Pu. *Czech. J. Phys., 7* (1), 45–56.

Mamuro, T. & Matsunami, T. (1965). Annual Report. Radiation Center, Osaka Prefecture (Vol. 5, p. 23).

Mamuro, T., Seiyama, T., Matsunami, T., Fujita, A. & Yoshikawa, K. (1963a). Electron microscopic examination of highly radioactive fallout particles. *Nature, 197* (4866), 478–479.

Mamuro, T., Yoshikawa, K., Matsunami, T., Fujita, A. & Azuma, T. (1963b). Fractionation phenomena in highly radioactive fallout particles. *Nature, 197* (4871), 964–966.

Mamuro, T., Yoshikawa, K. & Maki, N. (1965a). Radionuclide fractionation in fallout particles. *Health Phys., 11* (3), 199–209.

Mamuro, T., Fujita, A. & Matsunami, T. (1965b). Microscope examination of highly radioactive fallout particles from the first Chinese nuclear test explosion. *Health Phys., 11* (10), 1097–1101.

Martin, U. (1965). Kinetics of initial food chains for radioisotopes of close-in radioactive fallout from a single nuclear explosion. In: *Proceedings of the Second Conference "Radioactive Fallout from Nuclear Weapon Tests"*, Germantown, Maryland, November 3–6, 1964 (pp. 187–195).

Mikhailov, V. N. (Ed.) (1996). *Nuclear Weapon Tests and Nuclear Explosions for Peaceful Purposes in the USSR, 1949–1990* [in Russian] (66 p.). Sarov: Russian Federal Nuclear Center (RFYaC-VNIIF).

Miskel, L. A. (1966). Release of radioactivity from nuclear cratering. URCL-14778.

Morokhov, I. D. (1970). *Nuclear Explosions for Peaceful Uses* [in Russian]. Moscow: Atomizdat.

Mostovaya, G. A. (1961). Triple fission of nuclei ^{233}U, ^{235}U, ^{239}U and ^{241}Pu. *Atomic Energy, 10* (4), 372–373.

Musikhin, V. I. & Esin, O. A. (1962). Physical chemistry of melted salts and slags. In: *Trans. of All-Union Symposium on Physical Chemistry of Melted Salts and Slags* (p. 383). Moscow: Metallurgizdat.

Myasnikov, K. V., Kasatkin, V. V., Il'ichev, V. A. & Akhunov, V. D. (2000). Emergency situations at objects of peaceful nuclear explosions in Russia. In: *Proceedings of an International Conference on "Radioactivity*

after Nuclear Explosions and Accidents", Moscow, 24–26 April, 2000 (Vol. 1, pp. 594–600). St.-Petersburg: Hydrometeoizdat.

Namburger, R. (1970). United States of America, Statements on National Programs, IAEA-PL-388/13. In: *Proceedings of a Panel "Peaceful Nuclear Explosions"*, Vienna, 2–6 March 1970 (pp. 27–34).

Nifontov, B. I. (1965). *Underground Nuclear Explosions* [in Russian]. Moscow: Atomizdat.

Nishita, H. (1965). Decay characteristics of neutron-induced radioactivity in snails. *Health Phys., 11* (12), 1527–1541.

Nishiwaki, I. (1954). Bikini Ash. *Atomic Scientists J., 4* (2), 97–109.

Nordyke, M. (1970). Peaceful Uses of Nuclear Explosions. IAEA-Pl-388/12. In: *Proceedings of a Panel "Peaceful Nuclear Explosions"*, Vienna, 2–6 March, 1970 (pp. 49–107).

Nordyke, M. D. & Wray, W. (1964). Cratering and radioactivity results from a nuclear cratering detonation in basalt. *J. Geophys. Res., 69* (4675).

Nydal, R. (1963). Increase in radiocarbon from the most recent series of thermonuclear tests. *Nature, 200* (4903), 212.

Nydal, R. & Lovseth, K. (1965). Distribution of radiocarbon from nuclear tests. *Nature, 206* (4988), 1029–1031.

Olsen, C. W. (1967). Time history of the cavity pressure and temperature following a nuclear detonation in alluvium. *J. Geophys. Res., 72* (20), 5037.

Onufriev, A. T. (1967). Theory of a vortex ring motion under gravity action. *Journal of Applied Mechanics and Technical Physics, 2*, 3–15.

Pavlotskaya, R. I., Tyuryukanova, E. B. & Baranov, V. I. (1970). *Global Distribution of Radioactive Strontium over the Earth's Surface*. Moscow: Nauka.

Petrov, V. N. & Pressman, A. Ya. (1962). Estimation of the influence of turbulent scattering along the vertical and windward on propagation of a polydispersed admixture. *Doklady of Akademy Nauk SSSR, 146* (1), 86–88.

Pitkevich, V. A., Duba, V. V., Ivanov, V. K., Shershakov, V. M., Borodin, R. V. & Kosykh, V. S. (1994). Techniques of reconstructing absorbed doses of external irradiation of the population living on Russian territory contaminated by the Chernobyl accident. *J. of Radiation Risk, 4*, 95–112.

Powers, D. A. et al. (1987). The Chernobyl source. *Nuclear Safety, 28* (1), 10–28.

RADLEG-2000. In: *Abstracts of the International Conference on Radiation Legacy of the 20th Century: Environmental Restoration*, Moscow, October 2000.

Ridenour, L. N. (1950). The physics of the H-bomb. *Bull. Atomic Scientists, 6* (4), 105.

Rodionov, V. N. (1970). Methods of modeling the ejection with consideration for gravity, IAEA-PL-388/23. In: *Proceedings of a Panel "Peaceful Nuclear Explosions"*, IAEA, Vienna, 2–6 March, 1970 (pp. 405–414).

Rotblat, J. (1955). The hydrogen-uranium bomb. *Atomic Scientists' J., 4* (4), 224–228.

Ryabinin, Yu. N. (1959). *Gases at Large Densities and High Temperatures* [in Russian]. Moscow: Mir.

Sadovsky, M. A. (Ed.) (1971). *Mechanical Effect of Underground Explosions* [in Russian]. Leningrad: Nedra.

Salter, L. P. (1965). Stratospheric radioactivity in the southern hemisphere. In: *Proceedings of the Second Conference "Radioactive Fallout from Nuclear Weapon Tests"*, Germantown, Maryland, November 3–6, 1964, pp. 215–228.

Salter, L. P. & Harley, J. H. (1965). "Trinity": cobalt-60, cesium-137 and europium-152. *Science, 148* (3671), 954–955.

Scherbov, B. L., Strakhovenko, V. D., Malikova, I. N., Sukhorukov, F. V., Budashkina, V. V. & Osipova, L. P. (2000). The present-day radioactive contamination of the West Siberia regions being suffered as a result of explosions on Semipalatinsk and Hovozemelsky polygons. In: *Proceedings of an International Conference on "Radioactivity after Nuclear Explosions and Accidents"*, Moscow, April 24–26, 2000 (Vol. 1, pp. 579–585). St.-Petersburg: Hydrometeoizdat.

Schumann, G. & Storppler, M. (1963). Beryllium-7 in the atmosphere. *J. Geophys. Res., 68* (13), 3827–3830.

Sedunov, Yu. S., Borzilov, V. A., Klepikova, N. V., Chernokozhin, E. V. & Troyanova, N. I. (1989). Physical-mathematical modelling of regional transport of radioactive products in the atmosphere resulting from the Chernobyl NPP accident. *Meteorology and Hydrology, 9*, 5–10.

Shapiro, C. S. (Ed.) (1988). Atmospheric Nuclear Tests. Environmental and Human Consequences. NATO ASI Series, Vol. 35.

Shipman, W. H., Simone, P. & Weiss, H. V. (1957). Detection of manganese-54 in radioactive fallout. *Science, 126* (3273), 971–972.

Sich, A. R. (1994). The Chernobyl accident revisited: Source term analysis and reconstruction of events during the active phase. Massachussets Institute of Technology, USA.

Sivintsev, Yu. V. & Khrulev, A. A. (1995). Estimation of radioactive release during the accident of 1986 at Unit 4 of the Chernobyl NPP. *Atomic Energy*, *78* (6), 403–417.

Skitovich, V. I., Budyka, A. K. & Ogorodnikov, V. I. (1993). Results of two-years of observations of radioactive particle dimensions within the CNPP 30-km zone. In: *Proceedings of the 1st All-Union Conference "Radiation Aspects of the Chernobyl Accident"* (Vol. 1, pp. 115–121). St.-Petersburg: Hydrometeoizdat.

Sokolov, V. E. & Krivolutsky, D. A. (Eds.) (1993). *Ecological Consequences of Radioactive Contamination in the South Urals* [in Russian]. Moscow: Nauka.

Stehn, J. R. (1960). Table of the radioactive nuclides. *Nucleonics*, *18* (11), 186–193.

Stewart, B. K. (1956). The condensation of a vapor to an assembly of droplets or particles. *Transactions of the Faraday Society*, *52* (397), 161–173.

Storebo, P. (1960a). Orographic and climatological influences on deposition of nuclear-bomb debris. *J. Meteorol.*, *16* (6), 600–608.

Storebo, P. (1960b). Meteorological fractionation of nuclear bomb debris. *Tellus*, *12* (3), 293.

Storebo, P. B. (1964). On particle formation in nuclear bomb debris. Discussion of Meteorological Problems with WMO experts, Thirteenth session of UNSCEAR.

Stratton, J. H. (1965). Sea-level canal: how and where. *Foreign Affairs*, *43* (3), 513–518.

Strom, P. O., MacKin, J. L., MacDonald, D. & Zigman, P. E. (1958). Long-lived cobalt isotopes observed in fallout. *Science*, *128* (3316), 417–419.

Stukin, E. D., Kvasnikova, E. V., Ziborov, A. M., Kryukov, E. V., Levshin, E. B. & Fedotkin, A. F. (2000). Research results of radionuclide contamination in the 60-km zone of the Chernobyl NPS obtained by the use of aerial gamma-spectrometry and reference network of deposition collectors. In: *Proceedings of an International Conference on "Radioactivity after Nuclear Explosions and Accidents"*, Moscow, 24–26 April, 2000 (pp. 349–360). St.-Petersburg: Hydrometeoizdat.

Sutton, O. G. (1947). The problem of diffusion in the lower atmosphere. *Quart. J. Roy. Meteorol. Soc.*, *73*, 257.

Telegadas, K. (1959). Announced Nuclear Detonations, US, UK, USSR. Fallout from Nuclear Tests, US Government Print Office, Washington, Vols. 1–3.

Teller, E., Telley, W., Higgins, G. & Johnson, G. (1968). *The Constructive Uses of Nuclear Explosives*. McGraw-Hill.

Terhune, R. W., Stubbs, T. F. & Cherry, J. T. (1970). Nuclear cratering from a digital computer, IAEA-PL-388/17. In: *Proceedings of a Panel "Peaceful Nuclear Explosions"*, IAEA, Vienna, 2–6 March, 1970 (pp. 415–440).

Tetcher, L., Payne, B. & Cameron, J. (1965). Tendency of the global distribution of tritium beginning with 1961. In: *Proceedings of the Second Conference "Radioactive Fallout from Nuclear Weapon Tests"*, Germantown, Maryland, November 3–6, 1964 (pp. 284–308).

Tewes, H. A. (1969). Results of the cabriolet excavation experiment: Toman I. Project Buggy: a nuclear row-excavation experiment. *Nuclear Applications and Technology*, *7*, 232–252.

Thomas, C. W. & Perkins, R. W. (1975). Transuranium Elements in the Atmosphere. HASL-291. New York.

Tikhomirov, F. V. (1993). Radionuclide distribution and migration in the forests of EURP by radioactive fallout. In: *Ecological Consequences of Radioactive Contamination in the Southern Urals* (pp. 21–39). Moscow: Nauka.

Toman, J. (1970). Results of cratering experiments, IAEA-PL-388/16. In: *Proceedings of a Panel "Peaceful Nuclear Explosions"*, IAEA, Vienna, March 2–6, 1970 (pp. 345–375).

Trifonov, V. A. & Dubasov, Yu. V. (2000). Current radiation situation in a region of Totsk military training with the use of nuclear weapon in 1954. In: *Proceedings of an International Conference on "Radioactivity after Nuclear Explosions and Accidents"*, Moscow, April 2000 (Vol. 1, pp. 500–506).

UCRL (1960). Chemical Reactions Induced by Underground Nuclear Explosions, Report of UCRL-5882, USA.

UNSCEAR (1962). Report of the UN Scientific Committee on the Effects of Atomic Radiation. A/5216, 19 April, 1962. Vol. II, Appendix F.

UNSCEAR (1982). Ionizing Radiation: Sources and Biological Effects. *United Nations Sci. Committee on the Effects of Atomic Radiation*. Report to General Assembly, UN, New York.

US Atomic Energy Congress (1959). Hearings before the Special Subcommittee on Atomic Energy, Congress of the United States, 86th Congress, First Session on Fallout from Nuclear weapons Tests, Vols. 1–3, US Government Print Office, Washington.

US Department of Energy (1994). United States Nuclear Tests: July 1945 through September 1992, DOE/NV-209 (Rev. 14), December 1994.

Vorgaphnik, N. B. (1963). *Reference Book on Thermal Physical Properties of Gases and Liquids* [in Russian]. Moscow: Fizmatgiz.

Wahl, A. C., Ferguson, R. L., Nethaway, D. R., Troutner, D. E. & Wolfsberg, K. (1962). Nuclear-charge distribution in low-energy fission. *Phys. Rev., 126* (3), 1112–1127.

Warman, E. A. (1987). Soviet and far-field radiation measurements and an inferred source term from Chernobyl. TP87-13, Stone and Webster Engineering Corp., Boston, MA.

Warner, F. & Kirschmann, R. J. C. (2000). *Nuclear Test Explosions. Environmental and Human Impacts*. J. W. Willey Publ.

Way, K. & Wigner, E. P. (1946). Radiation from fission products. *Phys. Rev., 70* (1–2), 115–116.

Way, K. & Wigner, E. P. (1948). The rate of decay of fission products. *Phys. Rev., 73* (11), 1318–1330.

Weiss, H. V. & Shipman, W. H. (1957). Biological concentration by killer clams of cobalt-60 from radioactive fallout. *Science, 125* (3249), 695.

Yablokov, A. V. (1995). Atomic mythology: ecologist's sketch of atomic industry. *Bulletin of Commission on Developing Academician V.I. Vernadsky's Scientific Legacy, 13*. Moscow: Nauka.

Yampolskii, P. A. (1961). *Neutrons from an Atomic Explosion* [in Russian]. Moscow: Gosatomizdat.

Yunge, Kh. (1965). In: Izrael, Yu. A. (Ed.), *Chemical Composition and Radioactivity of the Atmosphere* [in Russian] (transl. from English). Moscow: Mir.

Zeevaert, Th., Vanmarcke, V. & Govaerts, P. (1997). Status of the Restoration of Contaminated Sites in Europe, EC L2920, Luxembourg.

Zeldovich, Ya. B. & Raizer, Yu. P. (1966). *Physics of Shock Waves and High-Temperature Hydrodynamic Phenomena* [in Russian]. Moscow: Nauka.

Zvyagintsev, O. E. & Avtokratova, T. D. (1965). *Analytical Chemistry of Ruthenium* [in Russian] (78 p.). Moscow: Nauka.

Zysin, Yu. A., Lbov, A. A. & Selchenkov, L. A. (1963). *Fission Product Yields and Their Mass Distribution. Reference Book* [in Russian] (118 p.). Moscow: Gosatomizdat.

This Page Intentionally Left Blank

Subject Index

absorption
– γ-radiation, 231
– radionuclides by plants and soil, 255
acceleration, 68–70
– phase of gas, 64, 68–70
activation, 88, 101
– fast, 45
– isotopes by neutrons, 25, 101
– particles, 2, 7, 35, 36, 45, 88, 90
activity, xxii, 186, 187, 189
– accumulated, 196, 197
– induced (neutron-induced), 13, 20, 22–26, 75, 101, 127, 150
– particles, 51, 77, 78, 99
– total, 58, 74, 78, 137, 139, 226
agglomeration, 36
amelioration, 260
assimilation (by plant), 254
atlas, 172, 216

background level of radiation, 240, 250
base surge, 64, 71–74, 78, 82, 85, 87, 94, 97, 119, 120, 123, 126, 129, 141, 249
behavior of radionuclides, 165, 194, 244, 252, 254
biological accessibility, 61, 82, 97, 244, 246–248, 252, 254
Bikini Atoll, 22, 116
bomb
– fission–fusion–fission, 12, 22
– "pure", 13
– thermonuclear, 12, 13, 22

capacity
– absorption, 137
– filtering, 125
– heat, 5
cavity, 2, 66, 71, 91, 92
– explosion, 2, 63, 65, 70
– formation, 65
– radius, 63, 67
– spherical, 91
– venting, 63, 71, 72
– volume, 70, 89
chain
– mass, 2, 26–28, 53, 88
– mass decay, 61, 134
– soil–plant, 260
Chernobyl accident, xxiv, 227, Chapter 5, 239, 243
cloud
– ascent, 71
– base surge, 64, 75, 94, 119
– explosion, 80
– formation, 93
– main, 64, 72, 75, 94, 97, 136, 141
– pattern, 83, 85, 134
– radioactive, 2, 3, 73, 78, 80, 119, 123, 156
– stabilization, 3, 71, 93
coefficient
– absorption, 233
– accumulation, 254
– biological accessibility, 247
– condensation, 36, 43, 47
– distribution, 250, 253
– diffusion, 43, 143
– enrichment, 117, 124, 125
– fractionation, 80, 82–85, 87, 99, 101, 111, 138, 139, 148, 246, 249
– mobility, 256
– solubility, 92
– surface tension, 36
– transition, 183
– washout, 96, 250, 251
composition, 88
– average nuclide, 139
– highly volatile, 152
– isotopic, 123
– non-fractionated, 153
– radioactive fallout, 87, 138, 139
– radionuclide, 1, 2, 52, 75, 78, 80, 87, 93, 117, 123–125, 135, 138, 145, 150, 161, 168, 188, 244
concentration
– activity, 25, 127
– β-activity, 127, 128
– radioactive products, 96, 126, 127
– radionuclide, 186
– tritium, 117
concretion
– pumice, 91
– slag, 91
condition
– landscape-ecology, 251
– orographic, 251
– oxidation–reduction, 152

contamination
– atmospheric, 72, 158
– characteristics, 105, 107
– density, 106, 112, 113, 116
– global, 102, 103
– environmental, 140
– local, 112
– radioactive, 1, 13, 64, 73, 74, 125, 134, 141, 153, 177
– regional, 102
– residual, 200
– resulting, 178
– secondary, 255
– soil (surrounding land), 72, 258
– terrestrial, 52, 149, 156–158, 169, 170, 208, 215, 239
– vegetation, 251
control of borehole, 250
coral substrate, 8, 100
core
– graphite, 151
– inactive, 8
– reactor, 152
crater, 120, 140
– negative, 125
cross-section of neutrons, 26
cut-off value, 53–56

deactivation, 258
debris
– fallout pattern, 130, 131
– fission, 14, 20, 74, 131
decay, 155, 191
– constant, 25, 27, 42, 53, 214
– radioactive, 151
– schemes, 13, 19
density
– contamination, xxii, 137, 147, 179, 213, 221, 236
– deposition, 203
– radioactive fallout, 148
– terrestrial contamination, 208
deposition
– close-in, 149
– diffusive, 138
– dry, 96
– gravitational, 48, 96, 203
– kinematic, 138
– local, 222
– monodispersed, 203
– moist (wet), 96
depth
– burial, 66
– scaled, 72, 75, 80
dissipation (of the explosion products), 1, 183
distribution
– activity, 141, 143
– angular, 233
– contamination, 103
– depth, 127–129
– dose rate, 204, 210
– fission product, 187
– gamma-field, 202
– log-normal, 37, 124
– mass of particles, 9
– particle-size, 45, 76, 79, 95, 111, 133, 141, 205
– radiation, 165, 233
– radioactive material, 129, 165, 201, 229, 244
– radionuclides, 244
– spatial, 164, 213
– spectral, 233
– temporal, 179, 213
dolomite decarbonization, 152
dose
– absorbed, xxi
– accumulated, 217
– equivalent, xxii
– exposure, xxi, 221
– external γ-radiation, 126, 168, 217, 252, 253
– γ-radiation, 123, 126, 164
– internal, 217
– radiation, xxi
– total, 232
dose to population, 117, 118, 182, 227, 252, 259
dose rate, xxii, xxiv, 107, 110, 116, 129, 130, 131, 136, 142, 143, 147, 162, 168, 204, 213, 234
– external γ-radiation, 130, 132–134, 147, 157, 162, 164, 170, 179, 219, 231, 252
– exposure, 160, 196, 222
– internal, 179, 252
– total, 15–17
dosimetry, xxiv
dust column, 9, 64, 72, 73, 82, 123–125

effect
– fractionation, 41, 52, 55, 90, 188, 245
– latitudinal, 103
– synergistic, 182
– Thomson, 36, 45
effective time, 88
electron conversion, 13
elements
– environmental, 20
– intermediate, 28
– long-lived transuranium, 191
– refractory, 2, 27, 28, 80, 90, 151, 152
– volatile, 27, 28, 152, 187
energy of dissociation, 5
enrichment, 80, 139
enterprise

– Aerogeophisika, 217
– Mayak, 216
– Tomsk chemical, 208
epicenter, 98, 124, 135, 249
equation
– Einstein, 45
– Fuchsian, 43
equivalency
– air, 239
– non-air, 239
equivalent of Roentgen
– biological, xxiv
– physical, xxii
equivalent of explosion, 20, 23, 48, 53
evacuation of the population, 158
explosion
– air, 61
– atmospheric nuclear, 1, 2, 23, 57, 61, 63, 78, 80, 93, 101, 102, 142, 247
– balloon, 99, 100
– Blanka, 73
– Bravo, 22
– Buggy, 120, 121, 129, 130, 131
– Cabriolet, 120, 121, 129, 130, 131
– Chagan, 76, 77, 80–83, 85, 86, 90, 94, 118, 120, 123–125, 127, 128, 130, 135–138
– Crystal, 64, 121, 125
– contained, 64–67, 73, 91
– cratering, 2, 53, 64, 71–74, 91, 118, 119, 123, 129, 136, 140
– Danny Boy, 74, 80, 83, 84, 87, 120, 121, 124, 125, 129, 130, 132, 142, 144
– Dominic, 59, 100
– Ess, 74, 142
– gaseous, 151
– Gnome, 68
– group, 2, 72, 120, 130, 132, 145
– ground-level nuclear, 2, 9, 23, 36, 37, 50, 61, 97, 98, 116, 129, 141, 247
– Hardtack, 23
– high-altitude atmospheric, 112
– high-yield, 90, 102, 110, 112, 120, 126
– Jungle-S, 141
– Jungle-U, 141
– Lasurite, 121
– local, 97
– low-yield, 61, 119, 120, 126, 137, 138
– marine, 26
– medium-yield, 119, 120
– near-surface, 2, 13, 23, 99, 100
– near-water, 23, 100
– Neptune, 74, 129, 144, 145
– nominal, 36
– non-nuclear, 150
– Palanquin, 81
– Plumbob, 100, 125
– Rainier, 66, 67
– Sary-Uzen, 71–74, 77, 80–83, 85, 87, 91, 120, 121, 123, 124, 127–131, 134–138, 144, 145, 248, 251
– Schooner, 73, 76, 78, 81, 86–90, 94, 112, 120, 121, 134, 138, 140
– Scooter, 69
– Sedan, 70, 72–74, 78, 84, 87, 95, 120, 123, 124, 129, 133, 134, 139, 142, 144, 145, 218
– single, 132, 145
– Small Boy, 61, 94
– Sulky, 64, 80, 81, 120, 125, 126
– surface, 63, 97
– Taiga, 219, 220
– Telkem-1, 1, 76, 77, 80–82, 85, 86, 120, 121, 123, 127, 128, 136, 138, 139
– Telkem-2, 2, 76, 77, 80–82, 85, 86, 120, 121, 123, 125, 126, 130, 132, 133, 136–138
– thermal, 150, 205
– thermonuclear, 20, 22
– tower, 23, 99, 102, 223, 247
– tropospheric nuclear, 1, 93
– underground nuclear, 1, 2, 9, 13, 23, 63–66, 72, 74, 78, 80, 88, 90–93, 112, 119, 120, 126, 129, 136, 137, 138, 140, 141, 179, 249
– underwater, 1, 23
– upper atmosphere (stratosphere), 2
– very low-yield, 119, 120
exposure
– external, 260
– internal, 260

factor
– build-up, 232
– condensation, 36
– fractionation, 52, 55, 57, 59, 138, 139, 154, 165, 167, 174, 187, 194
– screening, 131
fallout, 75, 78, 112
– area, 213
– close-in radioactive, 99, 100, 139, 203, 246
– debris, 156
– distant, 85, 137, 139, 140, 246
– dry, 117
– dry and wet, 117
– global, 97, 100–102, 105, 110, 111, 118, 221, 222
– intermediate, 97, 100–102
– local, 98, 99
– long-distance, 97, 101, 102, 110, 111
– radioactive, 63, 88, 97, 119, 123, 129, 139
– stratospheric, 97, 111
– tritium, 118

– wet, 118
fireball, 2, 3, 8, 9, 37, 61
fission, 55, 131, 245
– nuclear, 1, 12
– process, 88, 101, 186
– products, 12, 134
– thermonuclear, 13, 227
formation, 88
– cloud, 72, 93
– fallout, 93
– funnel, 72, 69, 72, 75, 85
– radioactive particles, 63, 87, 90, 150
– slag-like, 73, 86, 87, 94, 133, 137, 138
fractionation, 80, 93, 110, 138, 244, 246
– inverse, 101, 111, 116
– nuclides, 1, 2, 52, 58, 61, 63, 64, 74, 79, 83, 85, 87, 93, 96, 117, 168
– radioactive fallout, 139
– specific, 102
front
– hydrodynamic, 3
– irradiation, 3
fusion of light nuclei, 1, 12

gamma-field, Chapter 7
gamma-quanta, 66
– average energy, 18
– numerical intensity, 18
gamma-spectrometer, 113, 153, 169, 225, 240
gamma-survey, 112, 156, 157, 164, 217, 239–241
– aerial, 107, 126, 158, 160, 205, 208, 216, 220, 236, 239
gas outburst, 73
graphite
– ash, 151, 153
– burning, 150
ground, 75
– bulk, 69, 79, 80, 85, 92, 94, 97, 119, 124–129, 132, 136, 140, 231
– dome, 73
– heaped, 125
– pattern, 83
– zero, 75

half-life, 27, 28, 61, 102, 223, 224
heat
– evaporation, 5
– melting, 5
Hillendal formulae, 3
hot-spot of radioactivity, 103, 161, 167, 246

index of Klechkovsky, 257
inventory
– radionuclide, 169
– total, 195, 208
internal irradiation, 255
isobar, 26, 38
isotope
– long-lived, 151, 194
– short-lived, 198
isomer, 23

kinetic theory, 42

law
– Gauss, 27
– Henry, 88, 89, 91
– Hopkinson, 64
– Raoult, 12
– Stokes, 48

map (mapping), 113, 260
– dose rate, 158
– global contamination, 103
– radiological, 260
– radionuclide contamination, 171–177, 180, 210, 215
median
– diameter, 78, 156
– size, 36
medium
– absorbing, 234
– air-equivalent, 234
melted rock, 77
migration, 256
– into soil, 61
– radioactive particles, 97, 247, 256
– wind, 244
mitigation of consequences, 213
– in ground waters, 250
mixture
– fission debris, 14, 18, 245
– non-fractionated, 80, 117
– polydispersed, 203
mobility of radionuclides, 243–245, 247, 252
model
– elasticity–plasticity, 69
– semi-empirical forecast, 55
modeling, 149, 194, 200
molecular aggregation, 36, 92
moment of venting, 90
motion
– Brownian, 10
– toroidal, 93

network
– reference observation, 215
neutron, 12
– capture, 25, 26

– cross-section, 26
– fast, 12
– flux, 23
– momentary, 66
– slow, 25
– thermal, 14, 27
– thermonuclear, 15
nuclear power station, 149
– Tree-Mile-Island, 149, 184
– Chernobyl, Chapter 5
nuclei
– heavy, 13
– radioactive, 2
nuclide
– anthropogenic, 211
– Chernobyl-derived, 172
– enrichment, 80
– fractionation, 64
– induced, 150
– intermediate, 38, 42, 46, 47, 134
– long-lived, 13, 53, 101, 150, 168, 169, 194, 225
– most hazardous, 169
– natural, 211
– radioactive, 25
– reference, 55
– refractory, 2, 35, 36, 38, 42, 47, 50, 58, 59, 73, 77, 87, 88, 124, 134, 137
– short-lived, 134, 150, 199
– volatile, 38, 42, 47, 73, 101, 117, 124, 134, 167

particle(s), 8
– activation, 2, 7, 87
– activity–size relationship, 52
– angular, 8
– daughter, 134
– drop-like, 8, 77
– fused radioactive, 7, 151
– glass-like, 76, 77, 86, 87, 133, 151, 223
– glassy slag, 225
– hot, 59, 153
– insoluble, 247
– irregular form, 8, 73, 123, 133
– large, 139
– liquid, 2
– melted, 7, 133, 223
– non-volatile, 92
– porous, 76
– radioactive, 1, 7, 8, 50, 63, 79, 87, 124
– slag-like, 76, 77
– solidification, 2, 5, 10, 38, 88
– spherical, 8, 76, 77
– sub-micron, 47, 155
– sugar-like, 76
– transparent, 86, 133
– volatile, 2, 66, 75, 83, 92, 100, 123
particle-carriers, 2, 7, 10, 26, 50, 63, 77, 93, 98, 133, 231
pattern
– Chernobyl fallout, 215, 227
– cloud, 82, 85, 134
– close-in radioactive fallout, 85, 87, 94, 100, 131, 136–139, 141, 145–147, 156, 157, 159, 161, 167, 217, 237
– deposition, 59, 131
– ground, 82
– long-distance fallout, 111
– old nuclear explosion, 219, 222, 223
– reconstructed, 221
– Urals fallout, 150, 216
penetration, 244
– molecular, 37
– radionuclides into soil, 61, 245
period
– activation, 50
– decay, 25, 27, 155, 191
– delay, 5
phase
– boiling, 91
– condensed, 12
– exchangeable, 253
– gas acceleration, 64, 69
– gaseous, 10, 28
– graphite-burning, 151
– liquid, 6, 10, 28
– non-exchangeable, 253
– solid, 6, 10, 28, 37, 254
– solid soil, 254
plasma, 50
plume, 69, 151, 156, 163, 164, 200
precursors
– gaseous, 2, 74, 75, 78, 80, 83, 92, 124, 136–140
– long-lived gaseous, 85, 87, 137
– volatile, 2, 73, 84, 92, 124, 245
prediction, 119, 141, 145, 188, 249
process
– agglomeration, 36
– coagulation, 36
– ion-exchange, 250
– nuclear, 2
– physico-chemical, 2
products
– activation, 192
– anthropogenic radioactive, 140, 205, 211
– fission, 12, 13, 17, 26, 150, 192
– gamma-active, 205
– gaseous, 149
– non-volatile, 92

– radioactive, 1, 72, 80
– refractory, 79, 90, 91, 156, 196
– volatile, 92, 156, 167, 186

radiation
– α, 164
– β, 12, 164
– γ, xxii, xxiv, 12, 14, 94, 107, 116, 123, 124, 144, 164, Chapter 7
– instantaneous γ, 12
– ionizing, xxi, xxii
– monochromatic, 232
– non-scattered, 233
radioecological consequence, 206
radiological decontamination, 252, 253, 257
radionuclide, 245
– Chernobyl-derived, 171
– distribution, 253
– hazardous, 245, 257
– long-lived, 206, 220, 223, 225
– mobile, 260
– short-lived, 194
– transuranic, 22, 224
– volatile, 165
rate
– accumulation, 171
– air entrainment, 4
– condensation, 12
– decay, 191
– fireball cooling, 10
– ion transport, 250
– particle washout, 96, 97
– total dose, 15, 18
reaction threshold, 23
reconstruction, 180, 213, Chapter 6
– fallout pattern, 217, 227
– source of contamination, 227
"Red" forest, 154
regime
– close-in, 246
– distant fallout, 246
rehabilitation, 243, 252, 253, 261
release
– daily activity, 187, 191, 198
– energy, 159–161, 180
– fission product, 190
– hot, 202
– initial, 199
– instantaneous, 202
– iodine, 187
– radioactivity, 150, 180, 187
– total, 181, 190, 195, 199
remediation, 243, 244
re-orientation of human activity, 253
restoration, 243, 244, 257
retarc, 125
ridge
– bulk, 126, 127
– dam-like, 121
Roentgen, xxi, xxiv
roughness
– ground, 127, 217
– surface, 131, 217
runoff of radioactivity, 249

sample (sampling), 114, 115, 226
– air, 203
– soil, 158, 159, 164, 165, 216
shielding, screening of the radiation, 116, 131, 235, 258
solidification, 2, 37, 71, 90
– particle, 5, 10, 38, 45
solubility, 244
– radionuclides, 246
– refractory particles, 247
source of radioactivity, 93
– infinite, 231, 232
– planar isotropic, 231, 232
South Urals, 205, 208, 216, 243, 259
spectra
– differential γ, 19
– fission debris, 29
– line, 19
structure
– glass-like, 76, 77
– porous, 76
– slag-like, 76
– sugar-like, 76
superposition of pattern, 222
system
– liquid–vapor, 12
– soil, 253
– soil–plant, 253

Test Site
– Nevada, 112, 140
– Novaya Zemlya, 102, 112, 116
– Semipalatinsk, 50, 97, 98, 101, 112, 121, 144, 218, 219, 223
– Totsk, 101
toroid 4, 7, 9, 10
tracer, 23
trajectory of particle transport, 202, 203
transformation
– elements, 48
– nuclear, xxiii
– radioactive, 26

uptake
– radioactivity, 251, 254, 259
– plant, 254
– root, 252

vapor
– partial pressure, 12
– saturated, 12
venting
– cavity, 72
– gases, 68
– moment, 88
– occurrence, 91
volatile species, 167
volatility
– mean, 152
– oxide, 194
– radionuclide, 165

washout, 117, 211
wave
– compression, 68
– rarefaction, 65, 68
– shock, 3, 64, 65, 68, 91

yield
– accumulated fission, 28
– energy, 211
– fission, 13
– independent, 27, 28
– mean γ-radiation, 18

Zhukovsky force, 7
zone
– activity, 119
– base surge, 94
– base surge fallout, 85
– close-in fallout, 77, 119, 146, 165, 170, 188, 194, 195, 202, 255
– combined fallout, 97
– contamination, 59, 83, 158
– crater, 119, 134
– crushed rock, 137
– dry steppe, 251
– emergency, 202
– epicenter, 82, 129, 130, 137, 231
– fallout, xxiii, 93, 119, 126
– forest-stand, 234
– ground bulk, 83, 119, 126
– high contamination, 158
– local contamination, 191
– long-distance, 117, 119, 195
– restriction, 170
– sanitary protective, 184
– vast contamination, 116, 164
– 30-km of Chernobyl accident, 158, 174

This Page Intentionally Left Blank